ALTAIR

ONLY FORWARD

Altair Radioss 2022

Theory Manual

Updated: 03/17/2022

altair.com

Contents

Intellectual Property Rights Notice ... iii
Technical Support ... vii

Theory Manual ... 9

Large Displacement Finite Element Analysis Theory Manual ... 10
Introduction ... 10
Basic Equations ... 18
Finite Element Formulation ... 37
Dynamic Analysis ... 48
Element Library ... 80
Kinematic Constraints ... 210
Linear Stability ... 227
Interfaces ... 231
Material Laws ... 288
Monitored Volume ... 382
Static ... 404
Radioss Parallelization ... 417
ALE, CFD and SPH Theory Manual ... 423
ALE Formulation ... 423
Computational Aero-Acoustic ... 436
Smooth Particle Hydrodynamics ... 440
Appendix A: Basic Relations of Elasticity ... 450

Index ... 454

Intellectual Property Rights Notice

This Intellectual Property Rights Notice is exemplary, and therefore not exhaustive, of intellectual property rights held by Altair Engineering Inc. or its affiliates. Software, other products, and materials of Altair Engineering Inc. or its affiliates are protected under laws of the United States and laws of other jurisdictions. In addition to intellectual property rights indicated herein, such software, other products, and materials of Altair Engineering Inc. or its affiliates may be further protected by patents, additional copyrights, additional trademarks, trade secrets, and additional other intellectual property rights. For avoidance of doubt, copyright notice does not imply publication. Copyrights in the below are held by Altair Engineering Inc. except where otherwise explicitly stated. Additionally, all non-Altair marks are the property of their respective owners.

This Intellectual Property Rights Notice does not give you any right to any product, such as software, or underlying intellectual property rights of Altair Engineering Inc. or its affiliates. Usage, for example, of software of Altair Engineering Inc. or its affiliates is governed by and dependent on a valid license agreement.

Altair Simulation Products

Altair® AcuSolve® ©1997-2022

Altair Activate® ©1989-2022

Altair® BatteryDesigner™ ©2019-2022

Altair Compose® ©2007-2022

Altair® ConnectMe™ ©2014-2022

Altair® EDEM™ ©2005-2022 Altair Engineering Limited, ©2019-2022 Altair Engineering Inc.

Altair® ElectroFlo™ ©1992-2022

Altair Embed® ©1989-2022

Altair Embed® SE ©1989-2022

Altair Embed®/Digital Power Designer ©2012-2022

Altair Embed® Viewer ©1996-2022

Altair® ESAComp® ©1992-2022

Altair® Feko® ©1999-2022 Altair Development S.A. (Pty) Ltd., ©1999-2022 Altair Engineering Inc.

Altair® Flow Simulator™ ©2016-2022

Altair® Flux® ©1983-2022

Altair® FluxMotor® ©2017-2022

Altair® HyperCrash® ©2001-2022

Altair® HyperGraph® ©1995-2022

Altair® HyperLife® ©1990-2022

Altair® HyperMesh® ©1990-2022

Altair® WRAP™ ©1998-2022 Altair Engineering AB

Altair® S-FRAME® ©1995-2022 Altair Engineering Canada, Ltd., ©2021-2022 Altair Engineering Inc.

Altair® S-STEEL™ ©1995-2022 Altair Engineering Canada, Ltd., ©2021-2022 Altair Engineering Inc.

Altair® S-PAD™ ©1995-2022 Altair Engineering Canada, Ltd., ©2021-2022 Altair Engineering Inc.

Altair® S-CONCRETE™ ©1995-2022 Altair Engineering Canada, Ltd., ©2021-2022 Altair Engineering Inc.

Altair® S-LINE™ ©1995-2022 Altair Engineering Canada, Ltd., ©2021-2022 Altair Engineering Inc.

Altair® S-TIMBER™ ©1995-2022 Altair Engineering Canada, Ltd., ©2021-2022 Altair Engineering Inc.

Altair® S-FOUNDATION™ ©1995-2022 Altair Engineering Canada, Ltd., ©2021-2022 Altair Engineering Inc.

Altair® S-CALC™ ©1995-2022 Altair Engineering Canada, Ltd., ©2021-2022 Altair Engineering Inc.

Altair Packaged Solution Offerings (PSOs)

Altair® Automated Reporting Director™ ©2008-2022

Altair® e-Motor Director™ ©2019-2022

Altair® Geomechanics Director™ ©2011-2022

Altair® Impact Simulation Director™ ©2010-2022

Altair® Model Mesher Director™ ©2010-2022

Altair® NVH Director™ ©2010-2022

Altair® Squeak and Rattle Director™ ©2012-2022

Altair® Virtual Gauge Director™ ©2012-2022

Altair® Weld Certification Director™ ©2014-2022

Altair® Multi-Disciplinary Optimization Director™ ©2012-2022

Altair HPC & Cloud Products

Altair® PBS Professional® ©1994-2022

Altair® Control™ ©2008-2022

Altair ®Access™ ©2008-2022

Altair® Accelerator™ ©1995-2022

Altair® Accelerator™ Plus©1995-2022

Altair® FlowTracer™ ©1995-2022

Altair® Allocator™ ©1995-2022

Altair® Monitor™ ©1995-2022

Altair® Hero™ ©1995-2022

Altair® Software Asset Optimization (SAO) ©2007-2022

Altair Data Analytics Products

2022

January 10, 2022

Technical Support

Altair provides comprehensive software support via web FAQs, tutorials, training classes, telephone, and e-mail.

Altair One Customer Portal

Altair One (https://altairone.com/) is Altair's customer portal giving you access to product downloads, a Knowledge Base, and customer support. We recommend that all users create an Altair One account and use it as their primary portal for everything Altair.

When your Altair One account is set up, you can access the Altair support page via this link: www.altair.com/customer-support/

Altair Community

Participate in an online community where you can share insights, collaborate with colleagues and peers, and find more ways to take full advantage of Altair's products.

Visit the Altair Community (https://community.altair.com/community) where you can access online discussions, a knowledge base of product information, and an online form to contact Support. These valuable resources help you discover, learn and grow, all while having the opportunity to network with fellow explorers like yourself.

Altair Training Classes

Altair's in-person, online, and self-paced trainings provide hands-on introduction to our products, focusing on overall functionality. Trainings are conducted at our corporate and regional offices or at your facility.

For more information visit: https://learn.altair.com/

If you are interested in training at your facility, contact your account manager for more details. If you do not know who your account manager is, contact your local support office and they will connect you with your account manager.

Telephone and E-mail

If you are unable to contact Altair support via the customer portal, you may reach out to technical support via phone or e-mail. Use the following table as a reference to locate the support office for your region.

When contacting Altair support, specify the product and version number you are using along with a detailed description of the problem. It is beneficial for the support engineer to know what type of workstation, operating system, RAM, and graphics board you have, so include that in your communication.

Location	Telephone	E-mail
Australia	+61 3 9866 5557	anzsupport@altair.com
Brazil	+55 113 884 0414	br_support@altair.com

Location	Telephone	E-mail
Canada	+1 416 447 6463	support@altairengineering.ca
China	+86 400 619 6186	support@altair.com.cn
France	+33 141 33 0992	francesupport@altair.com
Germany	+49 703 162 0822	hwsupport@altair.de
Greece	+30 231 047 3311	eesupport@altair.com
India	+91 806 629 4500 +1 800 425 0234 (toll free)	support@india.altair.com
Israel		israelsupport@altair.com
Italy	+39 800 905 595	support@altairengineering.it
Japan	+81 3 6225 5830	support@altairjp.co.jp
Malaysia	+60 32 742 7890	aseansupport@altair.com
Mexico	+52 55 5658 6808	mx-support@altair.com
New Zealand	+64 9 413 7981	anzsupport@altair.com
South Africa	+27 21 831 1500	support@altair.co.za
South Korea	+82 704 050 9200	support@altair.co.kr
Spain	+34 910 810 080	support-spain@altair.com
Sweden	+46 46 460 2828	support@altair.se
United Kingdom	+44 192 646 8600	support@uk.altair.com
United States	+1 248 614 2425	hwsupport@altair.com

If your company is being serviced by an Altair partner, you can find that information on our web site at https://www.altair.com/PartnerSearch/.

See www.altair.com for complete information on Altair, our team, and our products.

Theory Manual

This chapter covers the following:

- Large Displacement Finite Element Analysis Theory Manual (p. 10)
- ALE, CFD and SPH Theory Manual (p. 423)
- Appendix A: Basic Relations of Elasticity (p. 450)

Large Displacement Finite Element Analysis Theory Manual

Introduction

Nonlinear finite element analyses confront users with many choices. An understanding of the fundamental concepts of nonlinear finite element analysis is necessary if you do not want to use the finite element program as a black box. The purpose of this manual is to describe the numerical methods included in Radioss.

Radioss belongs to the family of hydro-codes, in which the material is considered as a non viscous fluid. These hydro-codes found their origin in the work supported by the American Department of Energy at the end of the 70's and which led to software like DYNA2D/3D, HEMP, PRONTO, STEALTH, HONDO and WHAM.

Radioss’ main features are:

- A 3D Lagrangian formulation for mesh description
- An explicit time integration scheme, leading to small time steps
- Simplicity, under integrated finite element models
- Element by element assembly of nodal forces leading to in memory codes and low I/O requirements as compared to implicit approaches where matrix assembly and inversion is required every time step
- Non-iterative approaches
- Penalty methods based contact
- Highly vectorized implementation.

This first section introduces the notations which will be used throughout the document. An introduction to kinematics is also given.

Basic Equations recalls the basic equations in nonlinear dynamics. Different aspects are covered:

- Material and spatial coordinates
- Mesh description
- Kinematic and kinetic descriptions
- Stress rates and stresses in solids
- Updated and total Lagrangian formulations
- Equations of equilibrium
- Principle of virtual power and the physical names of power terms.

The small strain formulation is also introduced.

The finite element formulation of the virtual power principle is introduced in Finite Element Formulation, leading to the discretized equations of equilibrium.

Dynamic Analysis deals with time discretization and the integration schemes. Stability and time step concepts are also discussed.

Different finite element models are presented in Element Library. Tetrahedral solid elements, hexahedral solid and solid-shell elements, 3 and 4-node shell elements, 2-node truss and beam elements and spring elements are successively presented.

Kinematic Constraints deals with kinematic constraints, that is, constraints placed on nodal velocities.

Linear stability is introduced in Linear Stability.

The very important concept of interfaces is considered in Interfaces. Interfaces allow the solution of contact and impact conditions between two parts of a model. The different interface types available in Radioss are presented.

Material laws are discussed in Material Laws.

In Monitored Volume, the formulations of different kinds of monitored volumes are presented in detail. Airbag theory is also developed.

Static deals with the use of explicit algorithms to model quasi-static or static problems. Different approaches are discussed: slow dynamic computation, dynamic relaxation, viscous relaxation and energy discrete relaxation. The dynamic relaxation approach is developed. The `/DYREL` and `/DAMP` options are introduced in this chapter.

Radioss Parallelization concerns the presentation of the fundamentals in Radioss parallelization.

In the *ALE, CFD and SPH Theory Manual*, the ALE formulation is presented in ALE Formulation.

Finally, the last sections are respectively dedicated to the Computational Aero-Acoustic and the Smooth Particle Hydrodynamics formulations.

Notation

Two types of notation are used:

Indicial notation
: Equations of continuum mechanics are usually written in this form.

Matrix notation
: Used for equations pertinent to the finite element implementation.

Index Notation

Components of tensors and matrices are given explicitly. A vector, which is a first order tensor, is denoted in indicial notation by x_i. The range of the index is the dimension of the vector.

To avoid confusion with nodal values, coordinates will be written as x, y or z rather than using subscripts. Similarly, for a vector such as the velocity v_i, numerical subscripts are avoided so as to avoid confusion with node numbers. So, $x_1 = x, \quad x_2 = y, \quad x_3 = z$ and $v_1 = v_x, \quad v_2 = v_y$ and $v_3 = v_2$.

Indices repeated twice in a list are summed. Indices which refer to components of tensors are always written in lower case. Nodal indices are always indicated by upper case Latin letters. For instance, v_{iI} is the i-component of the velocity vector at node I. Upper case indices repeated twice are summed over their range.

A second order tensor is indicated by two subscripts. For example, E_{ij} is a second order tensor whose components are E_{xx}, E_{xy}, ...

Matrix Notation

Matrix notation is used in the implementation of finite element models. For instance, equation

$$r^2 = x_i \cdot x_i = x_1 \cdot x_1 + x_2 \cdot x_2 + x_3 \cdot x_3 \qquad (1)$$

is written in matrix notation as:

$$r^2 = x^T x \qquad (2)$$

All vectors such as the velocity vector v will be denoted by lower case letters. Rectangular matrices will be denoted by upper case letters.

Particle Kinematics

Kinematics deals with position in space as a function of time and is often referred to as the "*geometry of motion*". [1] The motion of particles may be described through the specification of both linear and angular coordinates and their time derivatives. Particle motion on straight lines is termed *rectilinear* motion, whereas motion on curved paths is called *curvilinear* motion. Although the rectilinear motion of particles and rigid bodies is well-known and used by engineers, the space curvilinear motion needs some feed-back, which is described in the following section.

Space Curvelinear Motion

The motion of a particle along a curved path in space is called *space curvilinear* motion. The position vector R, the velocity v, and the acceleration of a particle along a curve are:

$$\mathrm{R} = x\hat{\mathrm{i}} + y\hat{\mathrm{j}} + z\hat{\mathrm{k}} \qquad (3)$$

$$\mathrm{v} = \dot{\mathrm{R}} = \dot{x}\hat{\mathrm{i}} + \dot{y}\hat{\mathrm{j}} + \dot{z}\hat{\mathrm{k}} \qquad (4)$$

$$\mathrm{a} = \ddot{\mathrm{R}} = \ddot{x}\hat{\mathrm{i}} + \ddot{y}\hat{\mathrm{j}} + \ddot{z}\hat{\mathrm{k}} \qquad (5)$$

Where x, y and z are the coordinates of the particle and $\hat{\mathrm{i}}$, $\hat{\mathrm{j}}$ and $\hat{\mathrm{k}}$ the unit vectors in the rectangular reference. In the cylindrical reference (r, θ, z), the description of space motion calls merely for the polar coordinate expression:

$$\mathrm{v} = \mathrm{v_r} + \mathrm{v}_\theta + \mathrm{v_z} \qquad (6)$$

Where,

$v_r = \dot{r}$

$v_\theta = r\dot{\theta}$

$v_z = \dot{z}$

Also, for acceleration:

$$\mathrm{a} = \mathrm{a_r} + \mathrm{a}_\theta + \mathrm{a_z} \qquad (7)$$

Where,

$a_r = \ddot{r} - r\dot{\theta}^2$

$a_\theta = r\ddot{\theta} + 2\dot{r}\dot{\theta}$

$a_z = \ddot{z}$

The vector location of a particle may also be described by spherical coordinates as shown in Figure 1.

$$\mathrm{v} = \mathrm{v_R} + \mathrm{v}_\theta + \mathrm{v}_\varphi \tag{8}$$

Where,

$v_R = \dot{R}$

$v_\theta = R\dot{\theta}\cos\varphi$

$v_\varphi = R\dot{\varphi}$

Using the previous expressions, the acceleration and its components can be computed:

$$\mathrm{a} = \mathrm{a_R} + \mathrm{a}_\theta + \mathrm{a}_\varphi \tag{9}$$

Where,

$a_R = \ddot{R} - R\dot{\varphi}^2 - R\dot{\theta}^2\cos^2\varphi$

$a_\theta = \dfrac{\cos\varphi}{R}\dfrac{d}{dt}\left(R^2\dot{\theta}\right) - 2R\dot{\theta}\dot{\varphi}\sin\varphi$

$a_\varphi = \dfrac{1}{R}\dfrac{d}{dt}\left(R^2\dot{\varphi}\right) + R\dot{\theta}^2\sin\varphi\cos\varphi$

The choice of the coordinate system simplifies the measurement and the understanding of the problem.

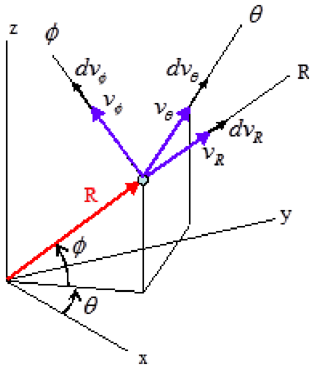

Figure 1: Vector Location of a Particle in Rectangular, Cylindrical and Spherical Coordinates

Coordinate Transformation

It is frequently necessary to transform vector quantities from a given reference to another. This transformation may be accomplished with the aid of matrix algebra. The quantities to transform might be the velocity or acceleration of a particle. It could be its momentum or merely its position, considering the transformation of a velocity vector when changing from rectangular to cylindrical coordinates:

$$\begin{Bmatrix} V_r \\ V_\theta \\ V_z \end{Bmatrix} = \begin{bmatrix} \cos\theta & \sin\theta & 0 \\ -\sin\theta & \cos\theta & 0 \\ 0 & 0 & 1 \end{bmatrix} \begin{Bmatrix} V_x \\ V_y \\ V_z \end{Bmatrix} \tag{10}$$

or $\{V_{r\theta z}\} = [T_\theta]\{V_{xyz}\}$

The change from cylindrical to spherical coordinates is accomplished by a single rotation ϕ of the axes around the θ-axis. The transfer matrix can be written directly from the previous equation where the rotation ϕ occurs in the $R-\phi$ plane:

$$\begin{Bmatrix} V_R \\ V_\theta \\ V_\phi \end{Bmatrix} = \begin{bmatrix} \cos\phi & 0 & \sin\phi \\ 0 & 1 & 0 \\ -\sin\phi & 0 & \cos\phi \end{bmatrix} \begin{Bmatrix} V_r \\ V_\theta \\ V_z \end{Bmatrix} \tag{11}$$

or $\{V_{R\theta\phi}\} = [T_\phi]\{V_{r\theta z}\}$

Direct transfer from rectangular to spherical coordinates may be accomplished by combining Equation 10 and Equation 11:

$$\{V_{R\theta\phi}\} = [T_\phi][T_\theta]\{V_{xyz}\} \tag{12}$$

with: $[T_\phi][T_\theta] = \begin{bmatrix} \cos\phi\cos\theta & \cos\phi\sin\theta & \sin\phi \\ -\sin\theta & \cos\theta & 0 \\ -\sin\phi\cos\theta & -\sin\phi\sin\theta & \cos\phi \end{bmatrix}$

Reference Axes Transformation

Consider now the curvilinear motion of two particles A and B in space. Study at first the translation of a reference without rotation. The motion of A is observed from a translating frame of reference x-y-z moving with the origin B (Figure 2). The position vector of A relative to B is:

$$\mathrm{r}_{A/B} = x\,\hat{\mathrm{i}} + y\,\hat{\mathrm{j}} + \mathrm{z}\,\hat{\mathrm{k}} \tag{13}$$

Where $\hat{\mathrm{i}}$, $\hat{\mathrm{j}}$ and $\hat{\mathrm{k}}$ are the unit vectors in the moving x-y-z system. As there is no change of unit vectors in time, the velocity and the acceleration are derived as:

$$\mathrm{v}_{A/B} = \dot{x}\,\hat{\mathrm{i}} + \dot{y}\,\hat{\mathrm{j}} + \dot{\mathrm{z}}\,\hat{\mathrm{k}} \tag{14}$$

$$\mathrm{a}_{A/B} = \ddot{x}\,\hat{\mathrm{i}} + \ddot{y}\,\hat{\mathrm{j}} + \ddot{\mathrm{z}}\,\hat{\mathrm{k}} \tag{15}$$

The absolute position, velocity and acceleration of A are then:

$$\begin{gathered} \mathrm{r_A} = \mathrm{r_B} + \mathrm{r_{A/B}} \\ \mathrm{v_A} = \mathrm{v_B} + \mathrm{v_{A/B}} \\ \mathrm{a_A} = \mathrm{a_B} + \mathrm{a_{A/B}} \end{gathered} \tag{16}$$

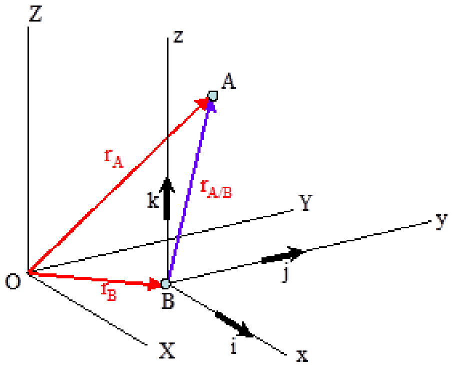

Figure 2: Vector Location with a Moving Reference

In the case of rotation reference, it is proved that the angular velocity of the reference axes x-y-z may be represented by the vector:

$$\omega = \omega_x \hat{\mathrm{i}} + \omega_y \hat{\mathrm{j}} + \omega_z \hat{\mathrm{k}} \tag{17}$$

The time derivatives of the unit vectors $\hat{\mathrm{i}}$, $\hat{\mathrm{j}}$ and $\hat{\mathrm{k}}$ due to the rotation of reference axes x-y-z about ω, can be studied by applying an infinitesimal rotation ωdt. You can write:

$$\frac{d}{dt}(\hat{\mathrm{i}}) = \omega \times \hat{\mathrm{i}} \quad ; \frac{d}{dt}(\hat{\mathrm{j}}) = \omega \times \hat{\mathrm{j}} \quad ; \frac{d}{dt}(\hat{\mathrm{k}}) = \omega \times \hat{\mathrm{k}} \tag{18}$$

Attention should be turned to the meaning of the time derivatives of any vector quantity $V = V_x \mathrm{i} + V_y \mathrm{j} + V_z \mathrm{k}$ in the rotating system. The derivative of V with respect to time as measured in the fixed frame X-Y-Z is:

$$\left(\frac{d\mathrm{V}}{dt}\right)_{XYZ} = \frac{d}{dt}\left(V_x \hat{\mathrm{i}} + V_y \hat{\mathrm{j}} + V_z \hat{\mathrm{k}}\right) \tag{19}$$

$$= \left(V_x \frac{d}{dt}(\hat{\mathrm{i}}) + V_y \frac{d}{dt}(\hat{\mathrm{j}}) + V_z \frac{d}{dt}(\hat{\mathrm{k}})\right) + \left(\dot{V}_x \hat{\mathrm{i}} + \dot{V}_y \hat{\mathrm{j}} + \dot{V}_z \hat{\mathrm{k}}\right)$$

With the substitution of Equation 18, the terms in the first parentheses becomes $\omega \times \mathrm{V}$. The terms in the second parentheses represent the components of time derivatives $\left(\frac{d\mathrm{V}}{dt}\right)_{xyz}$ as measured relative to the moving x-y-z reference axes. Thus:

$$\left(\frac{d\mathrm{V}}{dt}\right)_{XYZ} = \omega \times \mathrm{V} + \left(\frac{d\mathrm{V}}{dt}\right)_{xyz} \tag{20}$$

This equation establishes the relation between the time derivative of a vector quantity in a fixed system and the time derivative of the vector as observed in the rotating system.

Consider now the space motion of a particle A, as observed both from a rotating system x-y-z and a fixed system X-Y-Z (Figure 3).

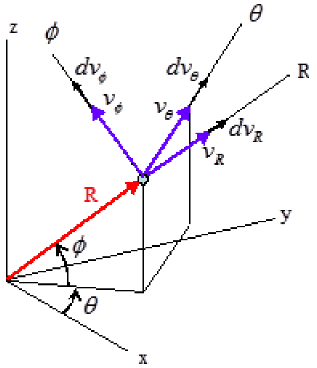

Figure 3: Vector Location with a Rotating Reference

The origin of the rotating system coincides with the position of a second reference particle B, and the system has an angular velocity ω. Standing r for $\mathrm{r}_{A/B}$, the time derivative of the vector position gives:

$$\mathrm{r}_A = \mathrm{r}_B + \mathrm{r} \quad \Rightarrow \quad \mathrm{v}_A = \mathrm{v}_B + \mathrm{r} \tag{21}$$

From Equation 20

$$\dot{\mathrm{r}} = \left(\frac{d\mathrm{r}}{dt}\right)_{XYZ} = \omega \times \mathrm{r} + \mathrm{v}_{\mathrm{rel}} \tag{22}$$

Where, $\mathrm{v}_{\mathrm{rel}}$ denotes the relative velocity measured in x-y-z, that is:

$$\mathrm{v}_{\mathrm{rel}} = (d\mathrm{r}/\mathrm{dt})_{xyz} = \dot{x}\,\hat{\mathrm{i}} + \dot{y}\,\hat{\mathrm{j}} + \dot{z}\,\hat{\mathrm{k}} \tag{23}$$

Thus, the relative velocity equation becomes:

$$\mathrm{v}_A = \mathrm{v}_B + \omega \times \mathrm{r} + \mathrm{v}_{\mathrm{rel}} \tag{24}$$

The relative acceleration equation is the time derivative of Equation 24 which gives:

$$\mathrm{a}_A = \mathrm{a}_B + \dot{\omega} \times \mathrm{r} + \omega \times \dot{\mathrm{r}} + \dot{\mathrm{v}}_{\mathrm{rel}} \tag{25}$$

Where, the last term can be obtained from Equation 20:

$$\dot{\mathrm{v}}_{\mathrm{rel}} = \left(\frac{d\mathrm{v}_{\mathrm{rel}}}{dt}\right)_{XYZ} = \omega \times \mathrm{v}_{\mathrm{rel}} + \mathrm{a}_{\mathrm{rel}} \tag{26}$$

and

$$\mathrm{a}_{\mathrm{rel}} = \left(\frac{d\mathrm{v}_{\mathrm{rel}}}{dt}\right)_{xyz} = \ddot{x}\,\hat{\mathrm{i}} + \ddot{y}\,\hat{\mathrm{j}} + \ddot{\mathrm{z}}\,\hat{\mathrm{k}} \tag{27}$$

Combining Equation 25 to Equation 27, you obtain upon collection of terms:

$$\mathrm{a}_A = \mathrm{a}_B + \dot{\omega} \times \mathrm{r} + \omega \times (\omega \times \mathrm{r}) + 2\omega \times \mathrm{v}_{\mathrm{rel}} + \mathrm{a}_{\mathrm{rel}} \tag{28}$$

Where, the term $2\omega \times \mathrm{v}_{\mathrm{rel}}$ constitutes Coriolis acceleration.

Skew and Frame Notations

Two kinds of reference definition are available in Radioss:

Skew Reference

A projection reference to define the local quantities with respect to the global reference. In fact the origin of skew remains at the initial position during the motion even though a moving skew is defined. In this case, a simple projection matrix is used to compute the kinematic quantities in the reference.

Frame Reference

A mobile or fixed reference. The quantities are computed with respect to the origin of the frame which may be in motion or not depending to the kind of reference frame. For a moving reference frame, the position and the orientation of the reference vary in time during the motion. The origin of the frame defined by a node position is tied to the node. Equation 24 and Equation 28 are used to compute the accelerations and velocities in the frame.

[1] Meriam J.L., “Dynamics”, John Wiley & Sons, Second edition, 1975.

Basic Equations

The continuum mechanics summarized here is based on References. [2] [3] [4]

Three basic choices need to be made in the development of a large deformation semi discretization scheme:

- Mesh description
- Kinematic description, that is, how the deformation is measured
- Kinetic description, that is, how the stresses are measured

Usually, the kinematic description implies the kinetic description as kinetic and kinematic measures should be energetically conjugated.

To go further in to the theory, two sets of coordinates are introduced:

- Spatial or Eulerian coordinates
- Material or Lagrangian coordinates

Material and Spatial Coordinates

In a Cartesian coordinates system, the coordinates of a material point in a reference or initial configuration are denoted by X. The coordinates of the same point in the deformed or final configuration are denoted by x.

The motion or deformation of a body can thus be described by a function $\phi(X, t)$ where the material coordinates X and the time t are considered as independent variables:

$$x = \phi(X, t) \tag{29}$$

The function ϕ gives the spatial positions of material points as a function of time.

The displacement of a material point is the difference between its original and final positions:

$$u(X, t) = \phi(X, t) - X \tag{30}$$

It is possible to consider displacements and, as a consequence final coordinates x, as functions of initial coordinates X. The initial configuration is assumed to be perfectly known and each coordinate X identifies a specific material point. For this reason, the initial coordinates are called *material coordinates*.

[2] Belytschko T. and Hughes T.J.R., “Computational Methods for Transient Analysis”, North-Holland, 1983.

[3] Belytschko T., Wing Kam Liu, and Moran B., “Finite Elements for Nonlinear Continua and Structures”, John Wiley, 1999.

[4] Geradin M., “Structural Dynamics ”, Masson, 1993.

On the other hand, the final coordinates x identify a point of space which can be occupied by different material points according to the different analyzed configurations. For these reasons, the x is called *spatial coordinates*.

In solid mechanics, material coordinates are usually called *Lagrangian coordinates*. In their general definition, they are given by the values of the integration constants of the differential equations of particle trajectories. A particular definition consists in using the coordinates X of the particle in the initial configuration. This point of view corresponds to the definition of material coordinates in solid mechanics.

Use of material coordinates is well suited for solid mechanics as we seek to analyze the evolution of a set of points for which we search the final configuration and properties. Integration can be performed in the initial configuration for which geometric properties are usually simple.

In fluid mechanics however, the engineer is more interested in the evolution of a situation in a region defined by fixed boundaries in space. Boundaries are eventually crossed by fluid particles. It is the spatial configuration which is important while the set of particles may vary. This is the reason why fluid mechanics is usually developed using spatial or Eulerian coordinates.

In solid mechanics, the Eulerian formulation consists in considering displacements and initial coordinates as function of spatial coordinates x. A problem for using Eulerian coordinates in solids mechanics is the difficulty of formulating constitutive equations, such as the relationship between stresses and strains that can take into account change of orientation. For this reason solid mechanics are principally developed using the Lagrangian point of view.

The reason for using the Lagrangian form for solids is primarily due to the need for accurate boundary modeling.

Mesh Definition

In *Lagrangian meshes*, mesh points remain coincident with material points and the elements deform with the material. Since element accuracy and time step degrade with element distortion, the magnitude of deformation that can be simulated with Lagrangian meshes is limited.

In *Eulerian meshes*, the coordinates of the element nodes are fixed. This means that the nodes remain coincident with spatial points. Since elements are not changed by the deformation of the material, no degradation in accuracy occurs because of material deformation. On the other hand, in Eulerian meshes, boundary nodes do not always remain coincident with the boundaries of the domain. Boundary conditions must be applied at points which are not nodes. This leads to severe complications in multi-dimensional problems.

A third type of mesh is an *Arbitrary Lagrangian Eulerian* mesh (ALE). In this case, nodes are programmed to move arbitrarily. Usually, nodes on the boundaries are moved to remain on boundaries. Interior nodes are moved to minimize element distortion.

The selection of an appropriate mesh description, whether a Lagrangian, Eulerian or ALE mesh is very important, especially in the solution of the large deformation problems encountered in process simulation or fluid-structure interaction.

A by-product of the choice of mesh description is the establishment of the independent variables. For a Lagrangian mesh, the independent variable is X. At a quadrature point used to evaluate the internal forces, the coordinate X remains invariant regardless of the deformation of the structure. Therefore, the stress has to be defined as a function of the material coordinate X. This is natural in a solid since the stress in a path-dependent material depends on the history observed by a material point. On the other hand, for an Eulerian mesh, the stress will be treated as a function of x, which means that the history of the point will need to be convected throughout the computation.

Vicinity Transformation

Central to the computation of stresses and strains is the Jacobian matrix which relates the initial and deformed configuration:

$$dx_i = \frac{\partial x_i}{\partial X_j} dX_j = D_j x_i dX_j = F_{ij} dX_j \tag{31}$$

$$D_j = \frac{\partial}{\partial X_j} \tag{32}$$

The transformation is fully described by the elements of the Jacobian matrix F:

$$F_{ij} \equiv D_j x_i \tag{33}$$

So that Equation 31 can be written in matrix notation:

$$dx = F dX \tag{34}$$

The Jacobian, or determinant of the Jacobian matrix, measures the relation between the initial volume $d\Omega$ and the volume in the initial configuration containing the same points:

$$d\Omega = |F| d\Omega^0 \tag{35}$$

Physically, the value of the Jacobian cannot take the zero value without cancelling the volume of a set of material points. So the Jacobian must not become negative whatever the final configuration. This property insures the existence and uniqueness of the inverse transformation:

$$dX = F^{-1} dx \tag{36}$$

At a regular point whereby definition of the field $u(X)$ is differentiable, the vicinity transformation is defined by:

$$F_{ij} = D_j x_i = D_j\left(X_i + u_i(X, t)\right) = \delta_{ij} + D_j u_i \tag{37}$$

or in matrix form:

$$F = 1 + A \tag{38}$$

So, the Jacobian matrix F can be obtained from the matrix of gradients of displacements:

$$A \equiv D_j u_i \tag{39}$$

Kinematic Description

For geometrically nonlinear problems, that is, problems in which rigid body rotations and deformation are large, a large number of measures of deformation are possible but most theoretical work and computer software employ the following three measures:

- The velocity strain (or rate of deformation)

$$D_{ij} = \frac{1}{2}\left(\frac{\partial v_i}{\partial x_j} + \frac{\partial v_j}{\partial x_i}\right) \tag{40}$$

- The Green strain tensor (Lagrangian strain tensor) measured with respect to initial configuration

$$E_{ij} = \frac{1}{2}\left(\frac{\partial u_i}{\partial X_j} + \frac{\partial u_j}{\partial X_i} + \frac{\partial u_k}{\partial X_i}\frac{\partial u_k}{\partial X_j}\right) \tag{41}$$

- The Almansi strain tensor (Eulerian strain tensor) measured with respect to deformed configuration

$$E^A{}_{ij} = \frac{1}{2}\left(\frac{\partial u_i}{\partial x_j} + \frac{\partial u_j}{\partial x_i} - \frac{\partial u_k}{\partial x_i}\frac{\partial u_k}{\partial x_j}\right) \tag{42}$$

All three measures of strains can be related to each other and can be used with any type of mesh.

Velocity Strain or Deformation Rate

The strain rate is derived from the spatial velocity derivative:

$$\dot{\varepsilon}_{ij} = \frac{d\varepsilon_{ij}}{dt} = D_{ij} = \frac{1}{2}\left(\frac{\partial v_i}{\partial x_j} + \frac{\partial v_j}{\partial x_i}\right) \tag{43}$$

or in matrix form:

$$\dot{\varepsilon} = D = \frac{1}{2}\left(L + L^T\right) \tag{44}$$

Where, the velocity gradient in the current configuration is:

$$L_{ij} = \frac{\partial v_i}{\partial x_j} \tag{45}$$

The velocity of a material particle is:

$$v_i = \frac{\partial x_i}{\partial t} \tag{46}$$

Where, the partial differentiation with respect to time t means the rate of change of the spatial position x of a given particle. The velocity difference between two particles in the current configuration is given by:

$$dv_i = \frac{\partial v_i}{\partial x_j}dx_j = L_{ij}dx_j = L_{ij}F_{jk}dX_k \tag{47}$$

In matrix form:

$$dv = Ldx = LFdX \tag{48}$$

On the other hand, it is possible to write the velocity difference directly as:

$$dv = \frac{\partial}{\partial t}(FdX) = \dot{F}dX \tag{49}$$

Where,

$$\dot{F} = \frac{\partial F}{\partial t} \tag{50}$$

One has as a result:

$$L = \dot{F}F^{-1} \tag{51}$$

Now, L is composed of a rate of deformation and a rate of rotation or spin:

$$L = D + \Omega \tag{52}$$

Since these are rate quantities, the spin can be treated as a vector. It is thus possible to decompose L into a symmetric strain rate matrix and an anti symmetric rotation rate matrix just as in the small motion theory the infinitesimal displacement gradient is decomposed into an infinitesimal strain and an infinitesimal rotation. The symmetric part of the decomposition is the strain rate or the rate of deformation and is:

$$\dot{\varepsilon} = D = \frac{1}{2}\left(\dot{F}F^{-1} + F^{-T}\dot{F}^{T}\right) \tag{53}$$

The anti symmetric part of the decomposition is the spin matrix:

$$\Omega = \frac{1}{2}\left(\dot{F}F^{-1} - F^{-T}\dot{F}^{T}\right) \tag{54}$$

The velocity-strain measures the current rate of deformation, but it gives no information about the total deformation of the continuum. In general, Equation 52 is not integral analytically; except in the unidimensional case, where one obtains the true strain:

$$\varepsilon = In(l/L) \tag{55}$$

l and L are respectively the dimensions in the deformed and initial configurations. Furthermore, the integral in time for a material point does not yield a well-defined, path-independent tensor so that information about phenomena such as total stretching is not available in an algorithm that employs only the strain velocity. Therefore, to obtain a measure of total deformation, the strain velocity has to be transformed to some other strain rate.

The volumetric strain is calculated from density. For one dimensional deformation:

$$\mu = \frac{\rho}{\rho_0} - 1 = \frac{-\delta\Omega}{\Omega} = \frac{-\delta l}{l} \tag{56}$$

Green Strain Tensor

The square of the distance which separates two points in the final configuration is given in matrix form by:

$$dx^T dx = dX^T F^T F dX \tag{57}$$

Subtracting the square or the initial distance, you have:

$$dx^T dx - dX^T dX = dX^T \left(F^T F - \mathrm{I} \right) dX = 2E dX^T dX \tag{58}$$

$$E = \frac{1}{2} \left(F^T F^T - \mathrm{I} \right) \tag{59}$$

$C = F^T F$ and $B = F F^T$ are called respectively right and left Cauchy-Green tensor.

Using Equation 38 in Vicinity Transformation:

$$E = \frac{1}{2} \left(A + A^T + A^T A \right) \tag{60}$$

$$E_{ij} = \frac{1}{2} \left(\frac{\partial u_i}{\partial X_j} + \frac{\partial u_j}{\partial X_i} + \frac{\partial u_k}{\partial X_i} \frac{\partial u_k}{\partial X_j} \right) \tag{61}$$

In the unidimensional case, the value of the strain is:

$$E = \left(l^2 - L^2 \right) / \left(2L^2 \right) \tag{62}$$

Where, l and L are respectively the dimensions in the deformed and initial configurations.

It can be shown that any motion F can always be represented as a pure rigid body rotation followed by a pure stretch of three orthogonal directions:

$$F = RU = R \left(I + H \right) \tag{63}$$

with the rotation matrix R satisfying the orthogonality condition:

$$R^T R = I \tag{64}$$

and H symmetric.

The polar decomposition theorem is important because it will enable to distinguish the straining part of the motion from the rigid body rotation.

From Equation 59 and Equation 63:

$$E = H + \frac{H^2}{2} = \frac{1}{2} \left(F^T F - I \right) \tag{65}$$

$$R = F \left(I + H \right)^{-1} \tag{66}$$

Equation 65 allows the computation of H, and Equation 66 of R.

As the decomposition of the Jacobian matrix F exists and is unique, H is a new measure of strain which is sometimes called the *Jaumann strain*. Jaumann strain requires the calculation of principal directions.

If rotations are small,

$$R = I + \Omega \tag{67}$$

$$R^T R = (I + \Omega)^T (I + \Omega) \tag{68}$$

$$\Omega^T + \Omega = 0 \tag{69}$$

if second order terms are neglected.

As a result, for the Jacobian matrix:

$$F = I + A = (I + \Omega)(I + H) \tag{70}$$

leading, if the second order terms are neglected, to the classical linear relationships:

$$A = \Omega + H \tag{71}$$

$$H = \frac{1}{2}(A^T + A) \tag{72}$$

$$\Omega = \frac{1}{2}(A - A^T) \tag{73}$$

So for Equation 71 and Equation 72, when rigid body rotations are large, the linear strain tensor becomes non-zero even in the absence of deformation.

The preceding developments show that the linear strain measure is appropriate if rotations can be neglected; that means if they are of the same magnitude as the strains and if these are of the order of 10^{-2} or less. It is also worth noticing that linear strains can be used for moderately large strains of the order of 10^{-1} provided that the rotations are small. On the other hand, for slender structures which are quite in extensible, nonlinear kinematics must be used even when the rotations are order of 10^{-2} because, if you are interested in strains of 10^{-3} - 10^{-4}, using linear strain the error due to the rotations would be greater than the error due to the strains.

Large deformation problems in which nonlinear kinematics is necessary, are those in which rigid body rotation and deformation are large.

Kinetic Description

The virtual power principle in Virtual Power Principle will state equilibrium in terms of Cauchy true stresses and the conjugate virtual strain rate, the rate of deformation. It is worth noticing that, from the engineer's point of view, the Cauchy true stress is probably the only measure of practical interest because it is a direct measure of the traction being carried per unit area of any internal surface in the body under study. This is the reason why Radioss reports the stress as the Cauchy stress. The second Piola-Kirchhoff stress is, however, introduced here because it is frequently mentioned in standard textbooks.

The relationship between the Piola-Kirchhoff stress and the Cauchy stress is obtained as follows. Starting from the definition of Green's strain as explained in Kinematic Description, Equation 59 ,

$$E = \frac{1}{2}(F^T F - I) \tag{74}$$

the strain rate is given by:

$$\dot{E} = \frac{1}{2}\left(\dot{F}^T F + F^T \dot{F}\right) \tag{75}$$

The power per unit reference volume is:

$$P = \dot{E}S \tag{76}$$

Where S represents the tensor of second Piola-Kirchhoff stresses. On the other hand, for Cauchy stresses:

$$P = \dot{\varepsilon}\sigma|F| \tag{77}$$

$$\left(\dot{F}^T F + F^T F\right)S = \left(\dot{F}F^{-1} + F^{-T}\dot{F}^T\right)\sigma|F| \tag{78}$$

You immediately have:

$$FSF^T = \sigma|F| \tag{79}$$

Second Piola-Kirchhoff stresses have a simple physical interpretation. They correspond to a decomposition of forces in the frame coordinate systems convected by the deformation of the body. However, the stress measure is still performed with respect to the initial surface.

Stress Rates

In practice, the true stress (or Cauchy stress) for any time interval will be computed using the stress rate in an explicit time integration:

$$\sigma_{ij}(t + \delta t) = \sigma_{ij}(t) + \dot{\sigma}_{ij}\delta t \tag{80}$$

$\dot{\sigma}_{ij}$ is not simply the time derivative of the Cauchy stress tensor as Cauchy stress components are associated with spatial directions in the current configuration. So, the derivatives will be nonzero in the case of a pure rigid body rotation, even if from the constitutive point of view the material is unchanged. The stress rate is a function of element average rigid body rotation and of strain rate.

For this reason, it is necessary to separate $\dot{\sigma}_{ij}$ into two parts; one related to the rigid body motion and the remainder associated with the rate form of the stress-strain law. Objective stress rate is used, meaning that the stress tensor follows the rigid body rotation of the material. [5]

A stress law will be objective if it is independent of the space frame. To each definition of the rigid body rotation, corresponds a definition of the objective stress rate. The Jaumann objective stress tensor derivative will be associated with the rigid body rotation defined in Kinematic Description, Equation 53:

$$\dot{\sigma}^v{}_{ij} = \dot{\sigma}_{ij} - \dot{\sigma}^r{}_{ij} \tag{81}$$

Where:

$\dot{\sigma}^v{}_{ij}$	Jaumann objective stress tensor derivative
$\dot{\sigma}^r{}_{ij}$	Stress rate due to the rigid body rotational velocity

The correction for stress rotation is given by:

$$\dot{\sigma}^{r}{}_{ij} = \sigma_{ik}\Omega_{kj} + \sigma_{jk}\Omega_{ki} \tag{82}$$

and Ω_{kj}defined in Kinematic Description, Equation 53 (Isotropic Linear Elastic Stress Calculation).

Stresses in Solids

Principal Stresses

Since the stress tensor is symmetric, you can always find a proper orthogonal matrix, that is, a coordinate system that diagonalizes it:

$$R^{T}\sigma R = \begin{bmatrix} \sigma_1 & 0 & 0 \\ 0 & \sigma_2 & 0 \\ 0 & 0 & \sigma_3 \end{bmatrix} \tag{83}$$

The diagonal components are called the principal stresses and allow a 3D representation of the state of stress at a point.

Stress Invariants

Many of the constitutive models in Radioss are formulated in terms of invariants of the stress tensor. The most important are the first and second invariants, called *pressure* and *von Mises stress* after Richard von Mises.

$$p = -\frac{\sigma_{xx} + \sigma_{yy} + \sigma_{zz}}{3} \tag{84}$$

$$\sigma_{vm} = \sqrt{\frac{3}{2}\left(\left(\sigma_{xx} + p\right)^2 + \left(\sigma_{yy} + p\right)^2 + \left(\sigma_{zz} + p\right)^2 + 2\sigma^2{}_{xy} + 2\sigma^2{}_{zy} + 2\sigma^2{}_{xz}\right)} \tag{85}$$

The values of these functions remain invariant under transformation by a proper orthogonal matrix. If,

$\sigma = R^{\mathrm{T}}\sigma_0 R$

then,

$p = p_0$

$\sigma_{vm} = \sigma_{vm0}$

Invariant Space

It is useful to plot the state of stress as a point in a diagram of pressure and von Mises stress:

[5] Halphen B., "On the velocity field in thermoplasticity finished", Laboratoire de Mécanique des Solides, Ecole Polytechnique, International Journal of Solids and Structures, Vol.11, pp 947-960, 1975.

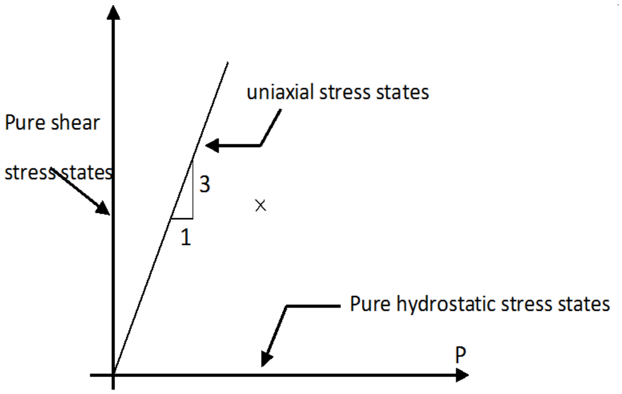

Figure 4:

The horizontal axis corresponds to the hydrostatic loading, the vertical axes to pure shear. The line with tangent 1/3 is uniaxial compression. The line with tangent -1/3 is uniaxial tension.

Deviatoric Stresses

The pressure or first invariant is related to the change in volume of the solid. The deviation from a hydrostatic state of stress is linked to the change in shape. The stress deviator is defined as:

$$S = \sigma + pI$$

The second invariant becomes, in terms of the deviators:

$$\sigma_{vm} = \sqrt{\frac{3}{2}\left(s2_{xx} + s2_{yy} + s2_{zz} + 2s2_{xy} + 2s2_{yz} + 2s2_{xz}\right)} \quad (86)$$

A surface of constant von Mises stress in deviatoric space or principal deviatoric space is a sphere (in stress space it is a cylinder).

Lagrangian and Corotational Formulations

Finite element discretizations with Lagrangian meshes are commonly classified as either an updated Lagrangian formulation or a total Lagrangian formulation. Both formulations use a Lagrangian description. That means that the dependent variables are functions of the material (Lagrangian) coordinates and time. In the geometrically nonlinear structural analysis the configuration of the structure must be tracked in time. This tracking process necessary involves a kinematic description with respect to a reference state. Three choices called "*kinematic descriptions*" have been extensively used:

Total Lagrangian description (TL)	The FEM equations are formulated with respect to a fixed reference configuration which is not changed throughout the analysis. The initial configuration is often used; but in special cases the reference could be an artificial base configuration.
Updated Lagrangian description (UL)	The reference is the last known (accepted) solution. It is kept fixed over a step and updated at the end of each step.
Corotational description (CR)	The FEM equations of each element are referred to two systems. A fixed or base configuration is used as in TL to compute the rigid

body motion of the element. Then the deformed current state is referred to the corotated configuration obtained by the rigid body motion of the initial reference.

The updated Lagrangian and corotational formulations are the approaches used in Radioss. These two approaches are schematically presented in Figure 5.

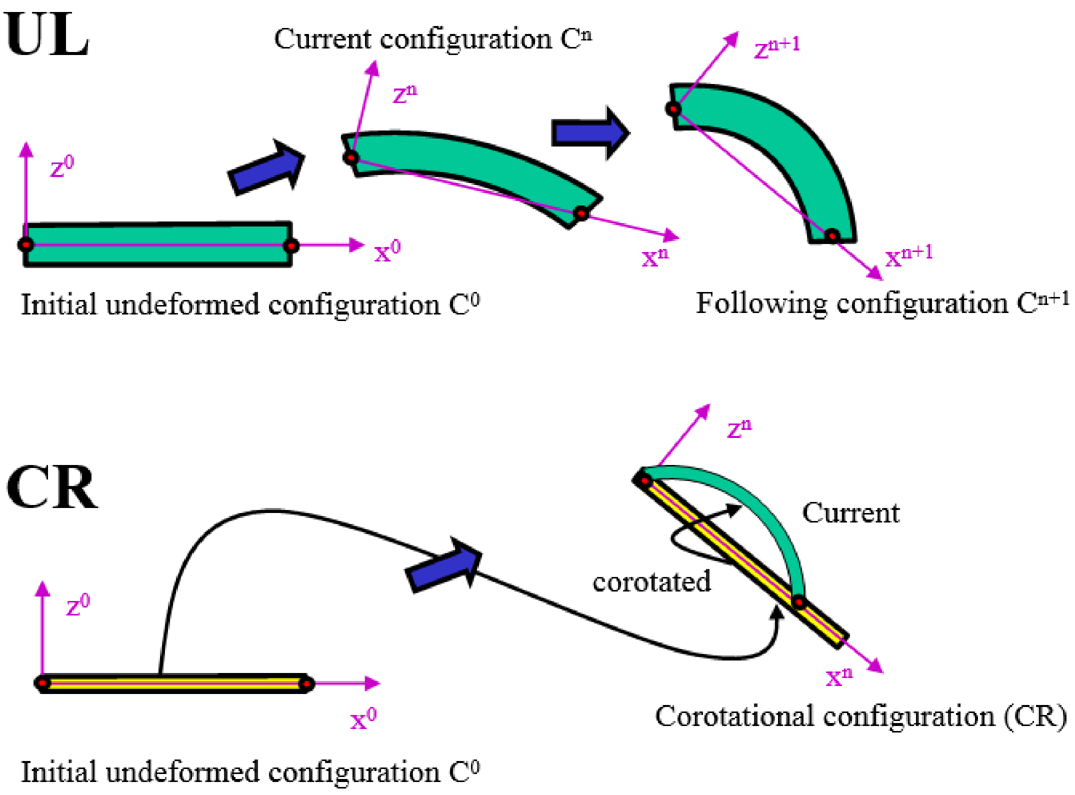
UL
Current configuration C^n
z^{n+1}
z^n
z^0
x^0
x^n
x^{n+1}
Initial undeformed configuration C^0
Following configuration C^{n+1}
CR
z^n
Current
corotated
z^0
x^n
x^0
Corotational configuration (CR)
Initial undeformed configuration C^0

Figure 5: Updated Lagrangian and Corotational Descriptions

By default, Radioss uses a large strain, large displacement formulation with explicit time integration. The large displacement formulation is obtained by computing the derivative of the shape functions at each cycle. The large strain formulation is derived from the incremental strain computation. Hence, stress and strains are true stresses and true strains.

In the updated Lagrangian formulation, the Lagrangian coordinates are considered instantaneously coincident with the Eulerian spatial x coordinates. This leads to the following simplifications:

$$\frac{\partial x_i}{\partial X_j} = \frac{\partial X_j}{\partial x_i} = \delta_{ij} \tag{87}$$

$$d\Omega = d\Omega_0 \tag{88}$$

The derivatives are with respect to the spatial (Eulerian) coordinates. The weak form involves integrals over the deformed or current configuration. In the total Lagrangian formulation, the weak form involves integrals over the initial (reference configuration and derivatives are taken with respect to the material coordinates.

The corotational kinematic description is the most recent of the formulations in geometrically nonlinear structural analysis. It decouples small strain material nonlinearities from geometric nonlinearities and handles naturally the question of frame indifference of anisotropic behavior due to fabrication or material nonlinearities. Several important works outline the various versions of CR formulation.[6] [7] [8] [9] [10]

Some new generation of Radioss elements are based on this approach. Refer to Element Library for more details.

> **Note:** A similar approach to CR description using convected-coordinates is used in some branches of fluid mechanics and theology. However, the CR description maintains orthogonality of the moving frames. This will allow achieving an exact decomposition of rigid body motion and deformational modes. On the other hand, convected coordinates form a curvilinear system that fits the change of metric as the body deforms. The difference tends to disappear as the mesh becomes finer. However, in general case the CR approach is more convenient in structural mechanics.

Equilibrium Equations

Let Ω be a volume occupied by a part of the body in the current configuration, and Γ the boundary of the body. In the Lagrangian formulation, Ω is the volume of space occupied by the material at the current time, which is different from the Eulerian approach where a volume of space through which the material passes is examined. τ is the traction surface on Γ and b are the body forces.

Force equilibrium for the volume is then:

$$\int_{\Gamma} \tau_i d\Gamma + \int_{\Omega} \rho b_i d\Omega = \int_{\Omega} \rho \frac{\partial v_i}{\partial t} d\Omega \tag{89}$$

Where,

ρ
Material density

[6] Belytschko T. and Hsieh B.H., “Nonlinear Transient Finite Element Analysis with convected coordinates”, Int. Journal Num. Methods in Engineering, 7 255-271, 1973.

[7] Argyris J.H., “An excursion into the large rotations”, Computer Methods in Applied Mechanics and Engineering, 32, 85-155, 1982.

[8] Crisfield M.A., “A consistent corotational formulation for nonlinear three-dimensional beam element”, Computer Methods in Applied Mechanics and Engineering, 81, 131-150, 1990.

[9] Simo J.C., “A finite strain beam formulation, Part I: The three-dimensional dynamic problem”, Computer Methods in Applied Mechanics and Engineering, 49, 55-70, 1985.

[10] Wempner G.A., “F.E., finite rotations and small strains of flexible shells”, IJSS, 5, 117-153, 1969.

The Cauchy true stress matrix at a point of Γ is defined by:

$$\tau_i = n_j \sigma_{ji} \tag{90}$$

Where, n is the outward normal to Γ at that point. Using this definition, Equation 89 is written:

$$\int_{\Gamma} n_j \sigma_{ji} d\Gamma + \int_{\Omega} \rho b_i d\Omega = \int_{\Omega} \rho \frac{\partial v_i}{\partial t} d\Omega \tag{91}$$

Gauss' theorem allows the rewrite of the surface integral as a volume integral so that:

$$\int_{\Gamma} n_j \sigma_{ji} d\Gamma = \int_{\Omega} \frac{\partial \sigma_{ij}}{\partial x_j} d\Omega \tag{92}$$

As the volume is arbitrary, the expression can be applied at any point in the body providing the differential equation of translation equilibrium:

$$\frac{\partial \sigma_{ij}}{\partial x_j} + \rho b_i = \rho \frac{\partial v_i}{\partial t} \tag{93}$$

Use of Gauss' theorem with this equation leads to the result that the true Cauchy stress matrix must be symmetric:

$$\sigma = \sigma^T \tag{94}$$

So that at each point there are only six independent components of stress. As a result, moment equilibrium equations are automatically satisfied, thus only the translational equations of equilibrium need to be considered.

Virtual Power Principle

The basis for the development of a displacement finite element model is the introduction of some locally based spatial approximation to parts of the solution. The first step to develop such an approximation is to replace the equilibrium equations by an equivalent weak form. This is obtained by multiplying the local differential equation by an arbitrary vector valued test function defined with suitable continuity over the entire volume and integrating over the current configuration.

$$\int_{\Omega} \left(\delta v_i \left(\frac{\partial \sigma_{ji}}{\partial x_j} + \rho b_i - \rho \dot{v}_i \right) \right) d\Omega = 0 \tag{95}$$

The first term in Equation 95 is then expanded.

$$\int_{\Omega} \left(\delta v_i \frac{\partial \sigma_{ji}}{\partial x_j} \right) d\Omega = \int_{\Omega} \left[\frac{\partial}{\partial x_j} \left((\delta v_i) \sigma_{ji} \right) - \frac{\partial (\delta v_i)}{\partial x_j} \sigma_{ji} \right] d\Omega \tag{96}$$

Taking into account that stresses vanish on the complement of the traction boundaries, use the Gauss's theorem.

$$\int_{\Omega}\left(\frac{\partial}{\partial x_j}\left((\delta v_i)\sigma_{ji}\right)\right)d\Omega=\int_{\Gamma_\sigma}\left[(\delta v_i)n_j\sigma_{ji}\right]d\Gamma \tag{97}$$

Replacing Equation 97 in Equation 96 gives:

$$\int_{\Omega}\left(\delta v_i\frac{\partial\sigma_{ji}}{\partial x_j}\right)d\Omega=\int_{\Gamma}(\delta v_i)\tau_i d\Gamma-\int_{\Omega}\frac{\partial(\delta v_i)}{\partial x_j}\sigma_{ji}d\Omega \tag{98}$$

If this last equation is then substituted in Equation 95, you obtain:

$$\int_{\Omega}\left(\frac{\partial(\delta v_i)}{\partial x_j}\right)\sigma_{ji}d\Omega-\int_{\Omega}\delta v_i\rho b_i d\Omega-\int_{\Gamma}(\delta v_i)\tau_i d\Gamma+\int_{\Omega}\delta v_i\rho\dot{v}_i d\Omega=0 \tag{99}$$

The preceding expression is the weak form for the equilibrium equations, traction boundary conditions and interior continuity conditions. It is known as the principle of virtual power.

Virtual Power Term Names

It is possible to give a physical name to each of the terms in the virtual power equation. This will be useful in the development of finite element equations. The nodal forces in the finite element equations will be identified according to the same physical names.

The first term can be successively written:

$$\frac{\partial(\delta v_i)}{\partial x_j}\sigma_{ji}=(\delta L_{ij})\sigma_{ji}=(\delta D_{ij}+\delta W_{ij})\sigma_{ji}=\delta D_{ij}\sigma_{ji} \tag{100}$$

You have used the decomposition of the velocity gradient L into its symmetric and skew symmetric parts and that $\delta W_{ij}\sigma_{ji}=0$ since δW_{ij} is skew symmetric and σ_{ji} is symmetric.

The latter relation suggests that $\delta D_{ij}\sigma_{ji}$ can be interpreted as the rate of internal virtual work or virtual internal power per unit volume. The total internal power δP^{int} is defined by the integral of $\delta D_{ij}\sigma_{ji}$:

$$\delta P^{\text{int}}=\int_{\Omega}\delta D_{ij}\sigma_{ji}d\Omega=\int_{\Omega}\frac{\partial(\delta v_i)}{\delta x_j}\sigma_{ji}d\Omega\equiv\int_{\Omega}\delta L_{ij}\sigma_{ji}d\Omega \tag{101}$$

The second and third terms in Virtual Power Principle, Equation 99 are the virtual external power:

$$\delta P^{ext}=\int_{\Omega}\delta v_i\rho b_i d\Omega+\int_{\Gamma_\sigma}(\delta v_i)\tau_i d\Gamma \tag{102}$$

The last term is the virtual inertial power:

$$\delta P^{inert}=\int\delta v_i\rho\dot{v}_i d\Omega \tag{103}$$

Inserting Equation 101, Equation 102 and Equation 103 into Equation 104, the principle of virtual power can be written as:

$$\delta P = \delta P^{\mathrm{int}} - \delta P^{ext} + \delta P^{inert} \tag{104}$$

for all δv_i admissible.

We can show that virtual power principle implies strong equations of equilibrium. So it is possible to use the virtual power principle with a suitable test function as a statement of equilibrium.

The virtual power principle has a simple physical interpretation. The rate of work done by the external forces subjected to any virtual velocity field is equal to the rate of work done by the equilibrating stresses on the rate of deformation of the same virtual velocity field. The principle is the weak form of the equilibrium equations and is used as the basic equilibrium statement for the finite element formulation. Its advantage in this regard is that it can be stated in the form of an integral over the volume of the body. It is possible to introduce approximations by choosing test functions for the virtual velocity field whose variation is restricted to a few nodal values.

Small Strain Formulation

Radioss uses two different methods to calculate stress and strain. The method used depends on the type of simulation. The two types are Large strain and Small strain.

The large strain formulation has been discussed before and is used by default. Small strain analysis is best used when the deformation is known to be small, for example, linear elastic problems.

Large strain is better suited to nonlinear, elastoplastic behavior where large deformation is known to occur. However, large mesh deformation and distortion can create problems with the time step. If an element is deformed excessively, the time step will decrease too much, increasing the CPU time. If the element reaches a negative volume, the computation will stop or the element will have to be removed. Using small strain can eliminate these problems.

Using a small strain formulation for part of a large deformation process introduces of course errors. These errors depend on the specific case, but they can provide a better solution than element deletion.

On the other side, materials like honeycomb, which have no Poisson's effect, can have the small strain limitations corrected by using adjusted stress-strain curves.

A small strain, small displacement formulation can thus be specified for some specific material behavior, like honeycomb, or can be implemented when the time step with a large strain formulation reaches a minimum value that is defined by the user. This allows the computation to proceed at an acceptable rate.

The small displacement formulation is, however, not recommended for some simulations, for example, crash analysis.

Small Strain Option

Assuming a constant Jacobian matrix during time and also a constant volume, previous equations degenerate into a small strain and small displacement formulation. All spatial variables are then values defined at time t=0 (or at the time the small strain formulation is initiated).

Time step then becomes constant:

$$\Delta t = \frac{l_0}{c} \tag{105}$$

and the effective negative volume has no effect on the computation (only the initial volume is used.

The Jacobian matrix time transformation is dependent upon element deformation and element rigid body rotation (Kinematic Description, Equation 63 and Equation 64). On the other hand, rigid body translation has no effect on the Jacobian matrix.

A small strain formulation is achieved if the element deformation is not taken into account. Likewise, a small displacement formulation is obtained if the element rigid body rotation is ignored.

From a practical point of view, small strain formulation will be obtained if, instead of recomputing the Jacobian matrix at each cycle, the initial matrix is updated taking into account element rigid body rotation:

$$F(t+\delta t) = F(t)\Omega \tag{106}$$

Where,

Ω	Rigid body angular velocity

An alternative solution that accounts for element rigid body rotation consists in computing the internal forces in a local reference frame attached to the element. This solution is used for shell elements and convected brick elements.

Unlike the large strain formulation, the small strain formulation uses values based on the initial configuration. This is either at the beginning of the simulation or at the beginning of the small strain implementation.

Hence, the strain rate is calculated using:

$$\dot{\varepsilon}_{ij} = \left(\frac{\partial \Phi_I}{\partial x_j}\right)_{t=0} v_{iI} \tag{107}$$

with Φ_I the interpolating shape functions and v_{iI} the components of velocity at node I.

The strain in an arbitrary x direction is calculated by:

$$\varepsilon_x = \sum \dot{\varepsilon}_x dt = \sum \left(\frac{\Delta \delta x}{x_0}\right) = \frac{\Delta x}{x_0} \tag{108}$$

Thus, the strain is the engineering strain.

The stress is calculated using the strain rate and the material law provided by the user. The later is integrated over the element volume to produce the internal force vector, which is summed over the elements to obtain the overall force vector:

$$f_{iI}^{\text{int}} = \int_{\Omega} \sigma_{ij} \left(\frac{\partial \varphi_I}{\partial x_j}\right)_{t=0} d\Omega \tag{109}$$

The stress is the engineering stress.

The volumetric strain using the small strain formulation is independent of density. For one dimensional deformation, one has:

$$\mu = -\left(\varepsilon_{xx} + \varepsilon_{yy} + \varepsilon_{zz}\right) = -\frac{\delta l}{l_0} \tag{110}$$

The small strain formulation for solid elements was developed for specific material, like honeycomb. In the crushing direction, honeycomb has no Poisson's effect and stress integration over the initial surface is acceptable. The effect on strain is small during elastic deformation and can be corrected in the plastic phase by using a modified engineering stress-engineering strain material curve.

For materials like crushable foam, with a small Poisson's ratio, this formulation can be applied successfully in certain situations. However, for other materials, this formulation has to be used very carefully.

Shell elements have fewer limitations than solid elements. For crash applications, the main shell deformation is bending. The small strain formulation has no effect on the bending description if membrane deformation is small.

The small strain formulation can be applied to some elements for which the time step is reaching a user specified value.

If the critical time step is small, compared to the initial one, this formulation gives acceptable results and is more accurate than removing the deformed elements.

Large Strain Option

By default Radioss uses a large strain large displacement formulation with explicit time integration. By computing the derivative of shape functions at each cycle, large displacement formulation is obtained. The large strain formulation results from incremental strain computation. Stresses and strains are therefore true stresses and true strains.

The spatial derivatives of isoparametric brick shape functions are given by:

$$\frac{\partial \Phi_I}{\partial x_j} = F(t)^{-1} \frac{\partial \Phi_I}{\partial r} \tag{111}$$

Where,

$F(t)$ Jacobian matrix

For each element the internal forces are integrated over the volume with one integration point:

$$f_{iI}^{\text{int}} = \int_{\Omega} \left(\sigma_{ij} \left(\frac{\partial \Phi_I}{\partial x_i} \right)_{t=0} d\Omega = \sigma_{ij} \frac{\partial \Phi_I}{\partial x_i} \Omega \right) \tag{112}$$

Time integration of Cauchy stress (true stress):

$$\sigma_{ij}(t + \delta t) = \sigma_{ij}(t) + \frac{d\sigma_{ij}(t)}{dt} dt \tag{113}$$

uses objective stress rate, meaning that the stress tensor follows the rigid body rotation of the material. Stress rate is a function of element average rigid body rotation and of strain rate. Strain rate is obtained from spatial velocity derivative:

$$\frac{d\varepsilon_{ij}}{dt} = \frac{1}{2}\left[\frac{\partial v_i}{\partial x_j} + \frac{\partial v_j}{\partial x_i}\right] \tag{114}$$

Where,

$$\frac{\partial v_i}{\partial x_j} = \frac{\partial \Phi_I}{\partial x_j v_i} \tag{115}$$

Stability of explicit scheme is given by the Courant condition:

$$\Delta t < \frac{l}{c} \tag{116}$$

with

l	Element characteristic length
c	Sound speed

The time step is computed at each cycle.

Large element deformation can give a large time step decrease. For overly large deformations a negative volume can be reached and it then becomes impossible to invert the Jacobian matrix and to integrate the stresses over the volume.

Stress and Strain Definition

With large strain formulation, stresses are true stresses and strains are true strains:

$$\varepsilon = \sum \Delta\Delta l \Big/ l \equiv \ln\frac{l}{l_0} \tag{117}$$

$$\sigma = \frac{F}{S} \tag{118}$$

With small strain formulation stresses become engineering stresses and strains engineering strains:

$$\varepsilon = \sum \Delta\Delta l \Big/ l_0 \equiv \frac{\Delta l}{l_0} \tag{119}$$

$$\sigma = \frac{F}{S_0} \tag{120}$$

The definition of volumic strain is also modified. For large strain Radioss uses a volumic strain computed from density:

$$\mu = \left(\frac{\rho}{\rho_0} - 1\right) = \frac{\Delta V}{V} = \frac{\Delta l}{l} \tag{121}$$

For small strain you have:

$$\mu = -\left(\varepsilon_x + \varepsilon_y + \varepsilon_z\right) = -\frac{\Delta l}{l_0} \tag{122}$$

Finite Element Formulation

Finite Element Approximation

In the finite element method, the motion $x(X, t)$ is approximated by:

$$x_i(X, t) = \Phi_I(X) x_{iI}(t) \tag{123}$$

Where,

$\Phi_I(X)$	Interpolating shape functions
x_{iI}	Position vector of node I

Summation over repeated indices is implied. In the case of lower indices, summation is over the number of space dimensions. For upper case indices, summation is over the number of nodes. The nodes in the sum depend on the type of entity considered. When the volume is considered, the summation is over all the nodes in the domain. When an element is considered, the sum is over the nodes of the element.

Similarly, nodal displacements are defined using Material and Spatial Coordinates, Equation 30 at nodes:

$$u_{iI}(X, t) = x_{iI}(t) - X_{iI} \tag{124}$$

The displacement field is:

$$u_i(X, t) = \Phi_I(X) u_{iI}(t) \tag{125}$$

The velocities are obtained by taking the material time derivative of the displacement giving:

$$v_i(X, t) = \frac{\partial u_i(X, t)}{\partial t} = \Phi_I(X) v_{iI}(t) \tag{126}$$

It is worth pointing out that the velocity is a material time derivative of displacements, that is, the partial derivative with respect to time with the material coordinate fixed.

Finally, accelerations are similarly given by the material time derivative of velocities:

$$\dot{v}_i(X, t) = \Phi_I(X) \dot{v}_{iI}(t)$$ (127

Emphasis is placed on the fact that shapes functions are functions of the material coordinates whatever the updated or the total Lagrangian formulation is used. All the dependency in the finite element approximation of the motion is taken into account in the values of the nodal variables.

From Kinematic Description, Equation 47, the velocity gradient is given by:

$$L_{ij} = \frac{\partial v_i}{\partial x_j} = v_{iI} \frac{\partial \Phi_I}{\partial x_j} = v_{iI} \Phi_{I,j} \tag{128}$$

and the rate of deformation (Kinematic Description, Equation 53) by:

$$D_{ij} = \frac{1}{2}\left(L_{ij} + L_{ji}\right) = \frac{1}{2}\left(v_{iI}\Phi_{I,j} + v_{jI}\Phi_{I,i}\right) \tag{129}$$

Similarly, the test functions are approximated as:

$$\delta v_i(X) = \Phi_I(X)\delta v_{iI} \tag{130}$$

Where, δv_{iI} are the virtual nodal velocities.

The test functions are next substituted into the principle of virtual power (Virtual Power Principle, Equation 99 giving:

$$\delta v_{iI}\int_{\Omega} \frac{\partial \Phi_I}{\partial x_j}\sigma_{ji} d\Omega - \delta v_{iI}\int_{\Omega} \Phi_I \rho b_i d\Omega - \delta v_{iI}\int_{\Gamma_\sigma} \Phi_I \tau_i d\Gamma + \delta v_{iI}\int_{\Omega} \Phi_I \rho \dot{v}_i d\Omega = 0 \tag{131}$$

The virtual velocities must be kinematically admissible, that is, satisfy boundary conditions on Γ_u, the part of the boundary where kinematical conditions are specified. Using the arbitrariness of the virtual nodal velocities everywhere except on Γ_u, the weak form of the momentum equation is:

$$\int_{\Omega} \frac{\partial \Phi_I}{\partial x_j}\sigma_{ji} d\Omega - \int_{\Omega} \Phi_I \rho b_i d\Omega - \int_{\Gamma_\sigma} \Phi_I \tau_i d\Gamma + \int_{\Omega} \Phi_I \rho \dot{v}_i d\Omega = 0 \tag{132}$$

with Γ_σ the part of the boundary where traction loads are imposed.

Internal and External Nodal Forces

As in Virtual Power Term Names, you define the nodal forces corresponding to each term in the virtual power equation.

The internal nodal forces are defined by:

$$\delta P^{\text{int}} = \delta v_{iI} f_{iI}^{\text{int}} = \int_{\Omega} \frac{\partial \delta v_i}{\partial x_j}\sigma_{ji} d\Omega = \delta v_{iI}\int_{\Omega} \frac{\partial \Phi_I}{\partial x_j}\sigma_{ji} d\Omega \tag{133}$$

The stress is the true (Cauchy) stress.

$$f_{iI}^{\text{int}} = \int_{\Omega} \sigma_{ji}\left(\frac{\partial \Phi_I}{\partial x_j}\right) d\Omega \tag{134}$$

These nodal forces are called internal because they represent the stresses in the body. The expression applies to both the complete mesh or to any element. It is pointed out that derivatives are taken with respect to spatial coordinates and that integration is taken over the current deformed configuration.

The external forces are similarly defined in terms of the virtual external power:

$$\delta P^{ext} = \delta v_{iI} f_{iI}^{ext} = \delta v_{il}\int_{\Omega} \Phi_I \rho b_i d\Omega + \delta v_{il}\int_{\Gamma_\sigma} \Phi_I \tau_i d\Gamma \tag{135}$$

so that external forces are given by:

$$f_{iI}{}^{ext} = \int_{\Omega} \Phi_I \rho b_i d\Omega + \int_{\Gamma_\sigma} \Phi_I \tau_i d\Gamma \tag{136}$$

Mass Matrix and Inertial Forces

The inertial body forces are defined by:

$$\delta P^{inert} = \delta v_{iI} f_{iI}{}^{inert} = \delta v_{iI} \int_{\Omega} \Phi_I \rho \dot{v}_i d\Omega = \delta v_{iI} \int_{\Omega} \Phi_I \rho \dot{v}_i d\Gamma \tag{137}$$

so that the inertia forces are given by:

$$f_{iI}{}^{inert} = \int_{\Omega} \Phi_I \rho \dot{v}_i d\Omega \tag{138}$$

or using the Finite Element Approximation, Equation 127 for the accelerations:

$$f_{iI}{}^{inert} = \int_{\Omega} \rho \Phi_I \Phi_J d\Omega \dot{v}_{iJ} \tag{139}$$

It is usual to define the inertial nodal forces as the product of a mass matrix and the nodal accelerations. Defining the mass matrix as:

$$M_{ijIJ} = \delta_{ij} \int_{\Omega} \rho \Phi_I \Phi_J d\Omega \tag{140}$$

the inertial forces are given by:

$$f_{iI}{}^{inert} = M_{ijIJ} \dot{v}_{jJ} \tag{141}$$

Discrete Equations

Using the definitions of the internal and external forces, as well as the definition of the inertial forces, it is possible to write the weak form of the virtual power principle as:

$$\delta v_{iI} \left(M_{ijIJ} \dot{v}_{jJ} + f_{iI}{}^{\text{int}} - f_{iI}{}^{ext} \right) = 0 \tag{142}$$

or taking into account the arbitrariness of the virtual velocities:

$$M_{ijIJ} \dot{v}_{jJ} + f_{iI}{}^{\text{int}} = f_{iI}{}^{ext} \tag{143}$$

Equation of Motion for Translational Velocities

Discrete Equations, Equation 143 is written in matrix notation as:

$$M\frac{dv}{dt}=f^{ext}-f^{\text{int}} \tag{144}$$

This is Newton's equation, where the mass matrix is:

$$M=\int\limits_{\Omega}\rho\Phi^{T}\Phi d\Omega \tag{145}$$

Radioss uses a lumped mass approach, that is, each node represents a discrete mass of zero size. This creates a diagonal mass matrix M, eliminating, as you will see in Dynamic Analysis, the need to solve simultaneous equations for the solution of nodal accelerations.

$$f^{ext}=\int\limits_{\Gamma}\Phi^{T}\tau d\Gamma+\int\limits_{\Omega}\rho\Phi^{T}bd\Omega \tag{146}$$

is the externally applied load vector, and the internal force vector is:

$$f_{iI}{}^{\text{int}}=\int\limits_{\Omega}\sigma_{ij}\frac{\partial\Phi_I}{\partial x_j}d\Omega \tag{147}$$

Adding to the internal and external forces the anti-hourglass force vector and the contact force vector which will be described in the following sections, you obtain the overall equation of motion:

$$M\frac{dv}{dt}=f^{ext}-f^{\text{int}}+f^{hgr}+f^{cont} \tag{148}$$

Equation of Motion for Angular Velocities

Shell, beam and rigid body theory introduces nodal rotational degrees of freedom. The equations of motion for rotational degrees of freedom are complicated if written in the global reference frame. They are much simpler if written for each node in the principal reference frame attached to the node. The resulting equations are the standard Euler equations. They are completely analogous to Newton's law governing translational degrees of freedom and are stated as:

$$l_1\alpha_1+(I_3-I_2)\omega_2\omega_3=m_{1ext}-m_{1\text{int}} \tag{149}$$

$$l_2\alpha_2+(I_1-I_3)\omega_1\omega_3=m_{2ext}-m_{2\text{int}} \tag{150}$$

$$l_3\alpha_3+(I_2-I_1)\omega_1\omega_2=m_{3ext}-m_{3\text{int}} \tag{151}$$

Where,

I_1, I_2, I_3	Principal moments of inertia about the x, y and z axes, respectively
$\alpha 1,\ \alpha 2, \alpha 3$	Angular accelerations expressed in the principal reference frame
$\omega 1,\ \omega 2, \omega 3$	Angular velocities
$m_1^{ext}, m_2^{ext}, m_3^{ext}$	Principal externally applied moments

$m_1^{\text{int}}, m_2^{\text{int}}, m_3^{\text{int}}$ Principal internal moments

The equation of motion for rotational degrees of freedom is thus very similar to that for translational degrees of freedom. In matrix notation and in the nodal principal reference frame:

$$I\frac{d\omega}{dt} = M^{ext} - M^{\text{int}} + F(\omega) \tag{152}$$

The vector function $F(\omega)$ is computed for a value of ω at $t - \delta t/2$. Equation 152 is used for rigid body motion.

For shell, beam and spring using a spherical inertia, the equation of motion becomes:

$$I\frac{d\omega}{dt} = M^{ext} - M^{\text{int}} + M^{hgr} \tag{153}$$

Where,

$I = \sum_{elements} I_e$ Diagonal inertia matrix

$M^{ext} = \sum_{elements} m^{ext}$ Externally applied moment vector

$M^{\text{int}} = \sum_{elements} m^{\text{int}}$ Internal moment vector

$M^{hgr} = \sum_{shells} m^{hgr}$ Anti-hourglass shell moment vector

Element Coordinates

Finite elements are usually developed with shape functions expressed in terms of an intrinsic coordinates system ξ, η, ζ. It is shown hereafter that expressing the shape functions in terms of intrinsic coordinates is equivalent to using material coordinates.

When an element is treated in terms of intrinsic coordinates, we are concerned with three domains that correspond to this element:

- The domain in the intrinsic coordinates system
- The current element domain
- The initial reference element domain

ξ is associated with the direction u.

η is associated with the direction v.

ς is associated with the direction w.

The motion in each element can thus be described by the composition of three maps (the reasoning is described only for the direction u):

- The map from the intrinsic coordinates system to the initial configuration:

$$X(\xi) \tag{154}$$

- The map from the intrinsic coordinates system to the current configuration:

$$x(\xi, t) \tag{155}$$

- The map from the initial to the current configuration:

$$x = \phi(X, t) \tag{156}$$

So, it is possible to approximate the motion in an element by:

$$x_i(\xi, t) = \Phi_I(\xi) x_{iI}(t) \tag{157}$$

Shape functions $\Phi_I(\xi)$ have no dimensions. They simply relate coordinates in the physical world to the intrinsic coordinates system. Writing Equation 157 at t=0, you obtain:

$$x_i(\xi) = x_i(\xi, 0) = \Phi_I(\xi) x_{iI}(0) = \Phi_I(\xi) x_{iI} \tag{158}$$

So, it can be seen from the last equation that the material coordinates system and the intrinsic coordinates system are invariant in a Lagrangian element. As a result, as intrinsic coordinates are time invariant and it is possible to write displacements, velocities and accelerations in terms of intrinsic coordinates (one coordinate system, the two other coordinates have similar shape functions):

$$u_i(\zeta, t) = \Phi_I(\xi) u_{iI}(t) \tag{159}$$

$$\dot{u}_i(\zeta, t) = \Phi_I(\xi) \dot{u}_{iI}(t) \tag{160}$$

$$\dot{v}_i(\zeta, t) = \Phi_I(\xi) \dot{v}_{iI}(t) \tag{161}$$

Isoparametric elements use the same shape functions for the interpolation of x, u, $\dot{u}$ and $\dot{v}$.

Integration and Nodal Forces

In practice, integrals over the current domain in the definition of the internal nodal forces (Equation of Motion for Translational Velocities, Equation 147), of the external nodal forces (Equation of Motion for Translational Velocities, Equation 146) and of the mass matrix have to be transformed into integrals over the domain in the intrinsic coordinate system Δ.

Using Vicinity Transformation, Equation 35, integrals on the current configuration are related to integrals over the reference configuration and over the domain in the intrinsic coordinate system by:

$$\int_{\Omega} g(x) d\Omega = \int_{\Omega^0} g(x) |F| d\Omega_0 = \int_{\Delta} g(\xi) |F_{\xi}| d\Delta \tag{162}$$

and

$$\int_{\Omega_0} g(X) d\Omega_0 = \int_{\Delta} g(\xi) |F_{\xi 0}| d\Delta \tag{163}$$

Where,

$|F|$
The Jacobian determinant of the transformation between the current and the initial configuration

$|F_{\xi}|$
The Jacobian determinant of the transformation between the current configuration and the domain in the intrinsic coordinate system

$|F_{\xi 0}|$
The Jacobian determinant of the transformation between the reference configuration and the intrinsic coordinate system

On the other hand, it comes from Vicinity Transformation, Equation 32 and Element Coordinates, Equation 157:

$$F_{\xi kj} = \frac{\partial x_k}{\partial \xi_j} = \frac{\partial \Phi_I(\xi)}{\partial \xi_j} x_{kl} \tag{164}$$

So, using Equation 162, internal forces computed by integration over the current domain will be obtained by the following quadrature:

$$f_{iI}^{\text{int}} = \int_{\Omega} \sigma_{ij} \frac{\partial \Phi_I}{\partial x_j} d\Omega = \int_{\Delta} \sigma_{ij} \frac{\partial \Phi_I}{\partial x_j} |F_{\xi}| d\Delta \tag{165}$$

and $|F_{\xi}|$ obtained from Equation 164.

External forces and the mass matrix can similarly be integrated over the domain in the intrinsic coordinate system.

Function Derivatives

The definition of internal forces also shows that derivatives of the form:

$$\frac{\partial}{\partial x_j} \tag{166}$$

need to be computed. These spatial derivatives are obtained by implicit differentiation. Considering the velocity gradient such as:

$$L_{ij} = \frac{\partial v_i}{\partial x_j} \tag{167}$$

one has:

$$L_{ij} = \frac{\partial v_i}{\partial \xi_k} \frac{\partial \xi_k}{\partial x_j} = \frac{\partial v_i}{\partial \xi_k} F_{\xi kj}^{-1} = v_{iI} \frac{\partial \Phi_I}{\partial \xi_k} F_{\xi kj}^{-1} \tag{168}$$

Where, the Jacobian matrix of the map between the current coordinates and the intrinsic coordinates is:

$$F_{\xi kj} = \frac{\partial x_k}{\partial \xi_j} = \frac{\partial \Phi_I(\xi)}{\partial \xi_j} x_{kI} \tag{169}$$

Usually, it is not possible to have closed form expression of the Jacobian matrix. As a result the inversion will be performed numerically and numerical quadrature will be necessary for the evaluation of nodal forces.

Numerical Quadrature: Reduced Integration

All elements in Radioss are integrated numerically. Hence, the integrals for nodal forces are replaced by a summation:

$$\int f(\xi) d\xi = \sum_{j=1}^{n} w_j f\left(\xi_j\right) \tag{170}$$

Where,

n
: Number of integration points in the element

w_j
: Eeight associated to the integration point j

Values of w_j and locations of ξ_j are given in tables according to the numerical quadrature approach. Radioss uses either full or reduced integration schemes.

For full integration, the number of integration points is sufficient for the exact integration of the virtual work expression. The full integration scheme is often used in programs for static or dynamic problems with implicit time integration. It presents no problem for stability, but sometimes involves *locking* and the computation is often expensive.

Reduced integration can also be used. In this case, the number of integration points is sufficient for the exact integration of the contributions of the strain field that are one order less than the order of the shape functions. The incomplete higher order contributions to the strain field present in these elements are not integrated.

The reduced integration scheme, especially with one-point quadrature is widely used in programs with explicit time integration to compute the force vectors. It drastically decreases the computation time, and is very competitive if the spurious singular modes (often called *hourglass modes* which result from the reduced integration scheme) are properly stabilized. In two dimensions, a one point integration scheme will be almost four times less expensive than a four point integration scheme. The savings are even greater in three dimensions. The use of one integration point is recommended to save CPU time, but also to avoid "locking" problems, for example, *shear locking* or *volume locking*.

Shear locking is related to bending behavior. In the stress analysis of relatively thin members subjected to bending, the strain variation through the thickness must be at least linear, so constant strain first order elements are not well suited to represent this variation, leading to shear locking. Fully integrated first-order isoparametric elements (tetrahedron) also suffer from shear locking in the geometries where they cannot provide the pure bending solution because they must shear at the numerical integration points to represent the bending kinematic behavior. This shearing then locks the element, that is, the response is far too stiff.

On the other hand, most fully integrated solid elements are unsuitable for the analysis of approximately incompressible material behavior (*volume locking*. The reason for this is that the material behavior forces the material to deform approximately without volume changes. Fully-integrated solid elements, and in particular low-order elements do not allow such deformations. This is another reason for using selectively reduced integration. Reduced integration is used for volume strain and full integration is used for the deviatoric strains.

However, as mentioned above, the disadvantage of reduced integration is that the element can admit deformation modes that are not causing stresses at the integration points. These zero-energy modes make the element rank-deficient which causes a phenomenon called *hour-glassing*; the zero-energy modes start propagating through the mesh, leading to inaccurate solutions. This problem is particularly severe in first-order quadrilaterals and hexahedra.

To prevent these excessive deformations, a small artificial stiffness or viscosity associated with the zero-energy deformation modes is added, leading in Equation of Motion for Translational Velocities, Equation 144 and Equation of Motion for Angular Velocities, Equation 152 to anti-hourglass force and moment vectors:

$$M\frac{dv}{dt} = f^{ext} - f^{\text{int}} + f^{hgr} \tag{171}$$

$$I\frac{d\omega}{dt} = M^{ext} - M^{\text{int}} + M^{hgr} \tag{172}$$

Zero-energy or hourglass modes are controlled using a perturbation stabilization as described by Flanagan-Belytschko [11], or physical stabilization as described in [12] (Element Library).

So, for isoparametric elements, reduced integration allows simple and cost effective computation of the volume integrals, in particular on vectorized supercomputers, and furnishes a simple way to cope with locking aspects, but at the cost of allowing hour-glassing.

Numerical Procedures

The Radioss numerical solver can be summarized by the flow chart in Figure 6. For each time step in a particular analysis, the algorithm used to compute results is:

1. For the displacement, velocity and acceleration at a particular time step, the external force vector is constructed and applied.
2. A loop over element is performed, in which the internal and hourglass forces are computed, along with the size of the next time step. The procedure for this loop is:

[11] Flanagan D. and Belytschko T., “A Uniform Strain Hexahedron and Quadrilateral with Orthogonal Hourglass Control”, Int. Journal Num. Methods in Engineering, 17 679-706, 1981.

[12] Zeng Q. and Combescure A., “A New One-point Quadrature, General Nonlinear Quadrilateral Shell Element with Physical Stabilization”, Int. Journal Num. Methods in Engineering 42, 1307-1338, 1998.

a. The Jacobian matrix is used to relate displacements in the intrinsic coordinates system to the physical space:

$$\left.\frac{\partial \Phi}{\partial x_j}\right|_t = F_\xi^{-1}\left.\frac{\partial \Phi}{\partial \xi}\right|_t \tag{173}$$

b. The strain rate is calculated:

$$\dot{\varepsilon}_{ij} = \left(\frac{\partial \Phi_I}{\partial x_j}\right)\dot{x} = \frac{1}{2}\left(\frac{\partial v_i}{\partial x_j} + \frac{\partial v_j}{\partial x_i}\right) \tag{174}$$

c. The stress rate is calculated:

$$\dot{\sigma}_{ij} = f(\dot{\varepsilon}, material - law) \tag{175}$$

d. Cauchy stresses are computed using explicit time integration:

$$\sigma(t + \Delta t) = \sigma(t) + \dot{\sigma}\Delta t \tag{176}$$

e. The internal and hourglass force vectors are computed.

f. The next time step size is computed, using element or nodal time step methods (Dynamic Analysis)

3. After the internal and hourglass forces are calculated for each element, the algorithm proceeds by computing the contact forces between any interfaces.
4. With all forces known, the new accelerations are calculated using the mass matrix and the external and internal force vectors:

$$\dot{v}_i = M^{-1}\left(f_{ext_i} - f_{\text{int}_i}\right) \tag{177}$$

5. Finally, time integration of velocity and displacement is performed using the new value.

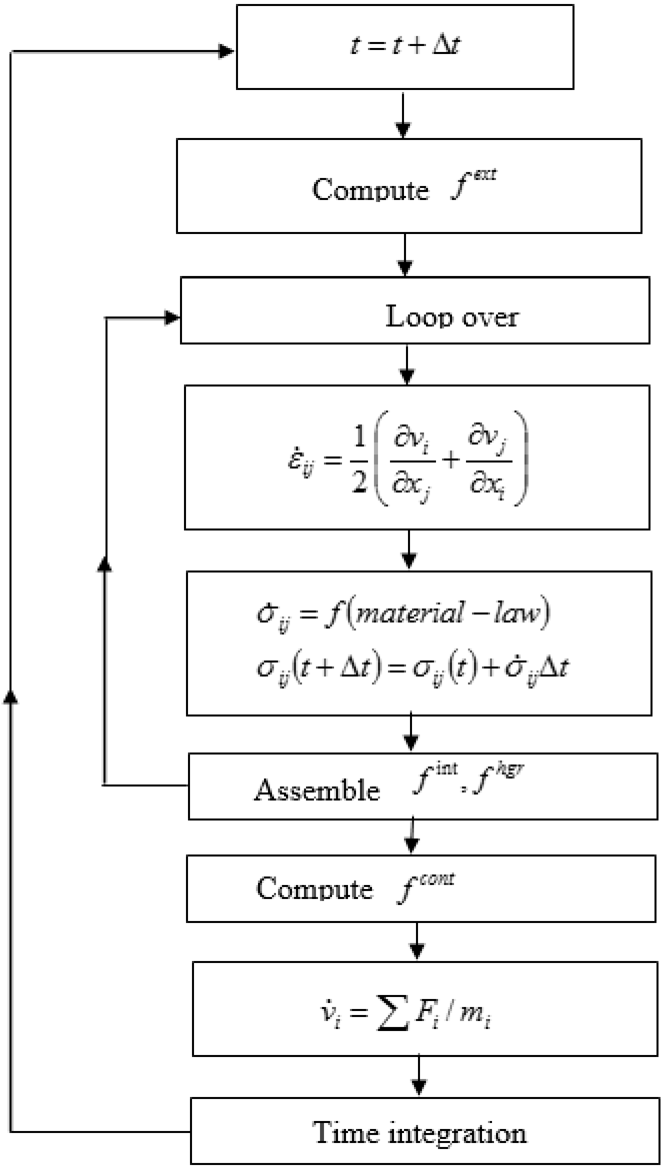
$t = t + \Delta t$
Compute f^{ext}
Loop over
$\dot{\varepsilon}_{ij} = \frac{1}{2}\left(\frac{\partial v_i}{\partial x_j} + \frac{\partial v_j}{\partial x_i}\right)$
$\dot{\sigma}_{ij} = f(material - law)$
$\sigma_{ij}(t + \Delta t) = \sigma_{ij}(t) + \dot{\sigma}_{ij}\Delta t$
Assemble f^{int}, f^{hgr}
Compute f^{cont}
$\dot{v}_i = \sum F_i / m_i$
Time integration

Figure 6: Numerical Procedure

Dynamic Analysis

The discrete form of the equation of motion given in Equation of Motion for Translational Velocities represents a system of linear differential equations of second order and, in principal the solution to the equations can be obtained by standard procedures for the solution of differential equations with constant coefficients. However, in practical finite element analysis, a few effective methods are used. The procedures are generally divided into two methods of solution: direct integration method and mode superposition. Although the two techniques may at first look to be quite different, in fact they are closely related, and the choice for one method or the other is determined only by their numerical effectiveness.

In *direct integration* the equations of motion are directly integrated using a numerical step-by-step procedure. In this method no transformation of the equations into another basis is carried out. The dynamic equilibrium equation written at discrete time points includes the effect of inertia and damping forces. The variation of displacements, velocities and accelerations is assumed with each time interval Δt. As the solution is obtained by a step-by-step procedure, the diverse system nonlinearities as geometric, material, contact and large deformation nonlinearity are taken into account in a natural way even if the resolution in each step remains linear.

The *mode superposition* method generally consists of transforming the equilibrium equation into the *generalized displacement* modes. An eigen value problem is resolved. The eigen vectors are the free vibration mode shapes of the finite element assemblage. The superposition of the response of each eigen vector leads to the global response. As the method is based on the superposition rule, the linear response of dynamically loaded of the structure is generally developed.

In the following, first the resolution procedure in direct integration method when using an explicit time discretization scheme is described. Then, the procedures of modal analysis are briefly presented. The implicit method will be detailed in Radioss Parallelization.

Direct Integration Method: Explicit Scheme

In transient dynamic analysis, the direct integration method is usually chosen. A few commonly used integration methods exist in the literature. [13] The method used in Radioss is derived from Newmark time integration scheme.

This section deals with time integration of accelerations, velocities and displacements. The general algorithm for computing accelerations, velocities and displacements is given. Stability and time step aspects are then discussed.

Newarks Method

Newmark's method is a one step integration method. The state of the system at a given time $t_{n+1} = t_n + h$ is computed using Taylor's formula:

$$f(t_n + h) = f(t_n) + hf'(t_n) + \frac{h^2}{2} f^{(2)}(t_n) + \ldots + \frac{h^s}{s!} f^{(s)}(t_n) + R_s \tag{178}$$

[13] Bathe K.J., “Finite Element Procedures”, Prentice Hall, 1996.

$$R_s = \frac{1}{s!} \int_{t_n}^{t_n+h} f^{(s+1)}(\tau)[t_n + h - \tau]^s d\tau \tag{179}$$

The preceding formula allows the computation of displacements and velocities of the system at time t_{n+1}:

$$\dot{u}_{n+1} = \dot{u}_n + \int_{t_n}^{t_{n+1}} \ddot{u}(\tau) d\tau \tag{180}$$

$$u_{n+1} = u_n + h\dot{u}_n + \int_{t_n}^{t_{n+1}} (t_{n+1} - \tau)\ddot{u}(\tau) d\tau \tag{181}$$

The approximation consists in computing the integrals for acceleration in Equation 180 and in Equation 181 by numerical quadrature:

$$\int_{t_n}^{t_{n+1}} \ddot{u}(\tau) d\tau = (1 - \gamma)h\ddot{u}_n + \gamma h\ddot{u}_{n+1} + r_n \tag{182}$$

$$\int_{t_n}^{t_{n+1}} (t_{n+1} - \tau)\ddot{u}(\tau) d\tau = \left(\frac{1}{2} - \beta\right)h^2\ddot{u}_n + \beta h^2\ddot{u}_{n+1} + r'_n \tag{183}$$

By replacing Equation 180 and Equation 181, you have:

$$\dot{u}_{n+1} = \dot{u}_n + (1 - \gamma)h\ddot{u}_n + \gamma h\ddot{u}_{n+1} \tag{184}$$

$$u_{n+1} = u_n + h\dot{u}_n + \left(\frac{1}{2} - \beta\right)h^2\ddot{u}_n + \beta h^2\ddot{u}_{n+1} + r'_n \tag{185}$$

According to the values of γ and β, different algorithms can be derived:

- $\gamma = 0, \beta = 0$: pure explicit algorithm. It can be shown that it is always unstable. An integration scheme is stable if a critical time step exists so that, for a value of the time step lower or equal to this critical value, a finite perturbation at a given time does not lead to a growing modification at future time steps.
- $\gamma = 1/2, \beta = 0$: central difference algorithm. It can be shown that it is conditionally stable.
- $\gamma = 1/2, \beta = 1/2$: Fox & Goodwin algorithm.
- $\gamma = 1/2, \beta = 1/6$: linear acceleration.
- $\gamma = 1/2, \beta = 1/4$: mean acceleration. This integration scheme is the unconditionally stable algorithm of maximum accuracy.

Central Difference Algorithm

The central difference algorithm corresponds to the Newmark algorithm $\gamma=\frac{1}{2}$ and $\beta=0$ so that with Newarks Method, Equation 184 and Equation 185 become:

$$\dot{u}_{n+1}=\dot{u}_n+\frac{1}{2}h_{n+1}\left(\ddot{u}_n+\ddot{u}_{n+1}\right) \tag{186}$$

$$u_{n+1}=u_n+h_{n+1}\dot{u}_n+\frac{1}{2}h_{n+1}^2\ddot{u}_n \tag{187}$$

with h_{n+1} the time step between t_n and t_{n+1}.

It is easy to show that the central difference algorithm [14] can be changed to an equivalent form with 3 time steps, if the time step is constant.

$$\ddot{u}_n=\frac{u_{n+1}-2u_n+u_{n-1}}{h^2} \tag{188}$$

From the algorithmic point of view, it is, however, more efficient to use velocities at half of the time step:

$$\dot{u}_{n+\frac{1}{2}}=\dot{u}\left(t_{n+\frac{1}{2}}\right)=\frac{1}{h_{n+1}}\left(u_{n+1}-u_n\right) \tag{189}$$

so that:

$$\ddot{u}_n=\frac{1}{h_{n+\frac{1}{2}}}\left(\dot{u}_{n+\frac{1}{2}}-\dot{u}_{n-\frac{1}{2}}\right) \tag{190}$$

$$h_{n+\frac{1}{2}}=\left(h_n+h_{n+1}\right)/2 \tag{191}$$

Time integration is explicit, in that if acceleration $\ddot{u}_n$ is known (Combine Modal Reduction), the future velocities and displacements are calculated from past (known values in time:

- $\dot{u}_{n+\frac{1}{2}}$ is obtained from Equation 190:

$$\dot{u}_{n+\frac{1}{2}}=\dot{u}_{n-\frac{1}{2}}+h_{n+\frac{1}{2}}\ddot{u}_n \tag{192}$$

The same formulation is used for rotational velocities.

- u_{n+1} is obtained from Equation 189:

$$u_{n+1}=u_n+h_{n+1}\dot{u}_{n+\frac{1}{2}} \tag{193}$$

The accuracy of the scheme is of h^2 order, that is, if the time step is halved, the amount of error in the calculation is one quarter of the original. The time step h may be variable from one cycle to another. It is recalculated after internal forces have been computed.

[14] Ahmad S., Irons B.M., and Zienkiewicz O.C., "Analysis of thick and thin shell structures by curved finite elements", Computer Methods in Applied Mechanics and Engineering, 2:419-451, 1970.

Numerical Starting Procedure

At time $t = 0$, the displacement u and velocity $\dot{u}_0$ are known from initial conditions. The acceleration $\ddot{u}_0$ and time step h_1 are found from solving the equations of motion. The initial time step h_0 is set to zero:

$$h_0 = 0 \quad ; \quad h_{\frac{1}{2}} = \frac{h_1}{2} \tag{194}$$

$$\dot{u}_{-\frac{1}{2}} = \dot{u}_0 \tag{195}$$

$$\dot{u}_{\frac{1}{2}} = \dot{u}_0 + h_{\frac{1}{2}} \ddot{u}_0 \tag{196}$$

Algorithm Flow Chart

The flow chart of the central difference algorithm can be summarized as in Figure 7. It is pointed out that the solution of the linear system to compute accelerations is immediate if the mass matrix is diagonal.

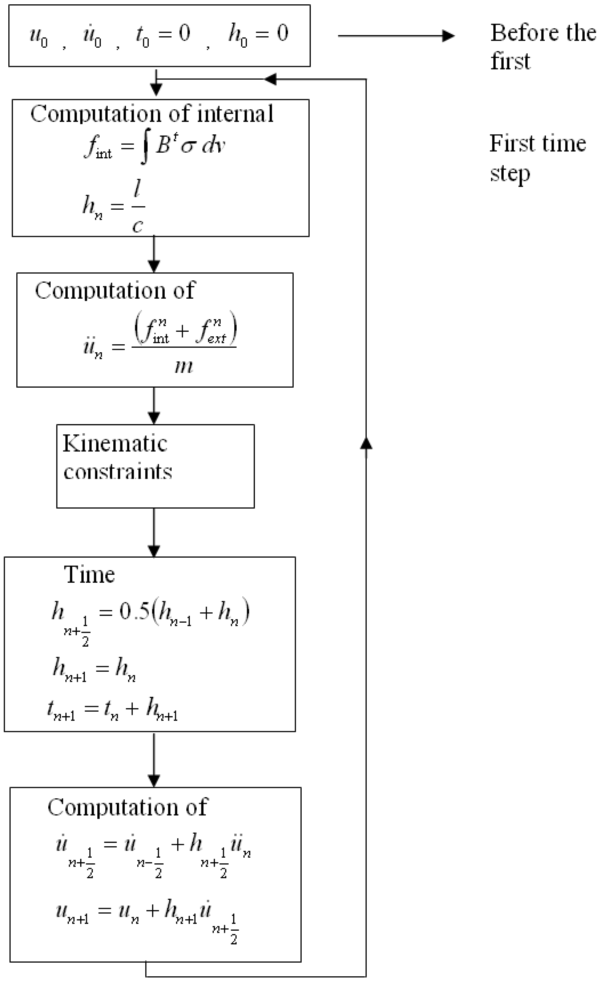
u_0 , $\dot{u}_0$, $t_0 = 0$, $h_0 = 0$
Before the first
Computation of internal
$f_{\text{int}} = \int B^t \sigma \, dv$
$h_n = \frac{l}{c}$
First time step
Computation of
$\ddot{u}_n = \frac{(f^n_{\text{int}} + f^n_{ext})}{m}$
Kinematic constraints
Time
$h_{n+\frac{1}{2}} = 0.5(h_{n-1} + h_n)$
$h_{n+1} = h_n$
$t_{n+1} = t_n + h_{n+1}$
Computation of
$\dot{u}_{n+\frac{1}{2}} = \dot{u}_{n-\frac{1}{2}} + h_{n+\frac{1}{2}} \ddot{u}_n$
$u_{n+1} = u_n + h_{n+1} \dot{u}_{n+\frac{1}{2}}$

Figure 7: Numerical Procedure

Body Drop Example

The question "how far can a body be dropped without incurring damage?" is frequently asked in the packaging manufacturing for transportation of particles. The problem is similar in landing of aircrafts. It can be studied by an analytical approach where the dropping body is modeled by a simple mass-spring system (Figure 8). If h is the dropping height, m and k the mass of the body and the stiffness representing the contact between the body and the ground, the equation of the motion can be represented by a simple one DOF differential equation as long as the spring remains in contact with floor:

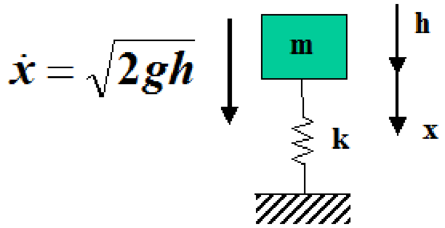

Figure 8: Model for a Dropping Body

$$m\ddot{x} + kx = mg \tag{197}$$

In this equation the damping effects are neglected to simplify the solution. The general solution of the differential equation is written as:

$$x = A\,Sin\omega t + B\,Cos\omega t + C \tag{198}$$

Where, the constants A, B and C are determined by the initial conditions:

$$\text{At t=0} \geq x = 0,\ \dot{x} = \sqrt{2gh},\ \ddot{x} = g \tag{199}$$

Where, ω is the natural frequency of the system:

$$\omega = \sqrt{\frac{k}{m}} \tag{200}$$

Introducing these initial solutions into Equation 199, the following result are obtained:

$$x = \frac{\sqrt{2gh}}{\omega}\,Sin\omega t + \frac{g}{\omega^2}\left(1 - Cos\omega t\right) \tag{201}$$

The same problem can be resolved by the numerical procedure explained in this section. Considering at first the following numerical values for the mass, the stiffness, the dropping height and the gravity:

$$m = 1,\ k = 20,\ h = 1,\ g = 10 \tag{202}$$

From Equation 197, the dynamic equilibrium equation or equation of motion is obtained as:

$$\ddot{x} + 20x = 10 \tag{203}$$

Using a step-by-step time discretization method with a central difference algorithm, for a given known step t_n the unknown kinematic variables for the next step are given by Equation 203, Central Difference Algorithm, Equation 189 and Central Difference Algorithm, Equation 190:

$$\begin{aligned} \ddot{x}_n &= 10 - 20x_n \\ \dot{x}_{n+1} &= \ddot{x}_n \Delta t + \dot{x}_n \\ x_{n+1} &= \dot{x}_n \Delta t + x_n \end{aligned} \tag{204}$$

For the first time step the initial conditions are defined by Equation 199. Using a constant time step $\Delta t = 0.1$ the mass motion can be computed. It is compared to the analytical solution given by Equation 201 in Figure 9. The difference between the two results shows the time discretization error.

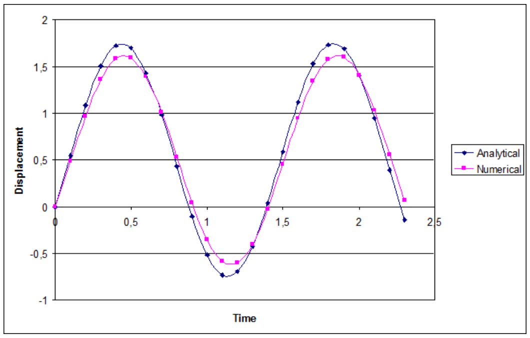

Figure 9: Obtained Results for the Example

Numerical Stability

The definition of numerically stability is similar to the stability of mechanical systems. A numerical procedure is stable if small perturbations of initial data result in small changes in the numerical solution.

It is worthwhile to comment the difference between physical stability and numerical stability. Numerical instabilities arise from the discretization of the governing equations of the system, whereas physical instabilities are instabilities in the solutions of the governing equations independent of the numerical discretization. Usually numerical stability is only examined for physically stable cases. For this reason in the simulation of the physically unstable processes, it is not guaranteed to track accurately the numerical instabilities. Numerical stability of a physically unstable process cannot be examined by the definition given above. You establish the numerical stability criteria on the physically stable system and suppose that any stable algorithm for a stable system remains stable on an unstable system. [15]

On the other hand, the numerical stability of time integrators discussed in the literature concerns generally linear systems and extrapolated to nonlinear cases by examining linearized models of nonlinear systems. The philosophy is: if a numerical method is unstable for a linear system, it will be certainly unstable for nonlinear systems as linear cases are subsets of the nonlinear cases. Therefore, the stability of numerical procedures for linear systems provides a useful guide to explore their behavior in a general nonlinear case.

To study the stability of the central difference time integration scheme, you establish the necessary conditions to ensure that the solution of equations is not amplified artificially during the step-by-step procedure. Stability also means that the errors due to round-off in the computer, do not grow in the integration. It is assured if the time step is small enough to accurately integrate the response in the highest frequency component.

Explicit Scheme Stability

In direct integration method, at time t_n the solutions for the prior steps are known and the solution for the time $t_{n+1} = t_n + \Delta t$ is required next. The equations to relate displacements, velocities and accelerations in a discrete time scale using the central difference time integration algorithm are given in Central Difference Algorithm. They can be rewritten as:

$$\begin{aligned} \dot{u}^{n+1} &= \dot{u}^n + \frac{\Delta t}{2}\left(\ddot{u}^n + \ddot{u}^{n+1}\right) = \dot{u}^{n+\frac{1}{2}} + \frac{\Delta t}{2}\ddot{u}^{n+1} \\ u^{n+1} &= u^n + \Delta t.\dot{u}^n + \frac{\Delta t^2}{2}.\ddot{u}^n = u^n + \Delta t.\dot{u}^{n+\frac{1}{2}} \end{aligned} \tag{205}$$

For stability studies, aim to establish a recursive relationship to link the displacements at three consecutive time steps:

$$\begin{bmatrix} u^{n+1} \\ u^n \end{bmatrix} = [\mathrm{A}]\begin{bmatrix} u^n \\ u^{n-1} \end{bmatrix} + [\mathrm{L}] \tag{206}$$

Where, $[\mathrm{A}]$ is amplification matrix. A spectral analysis of this matrix highlights the stability of the integration scheme.

The numerical algorithm is stable if and only if the radius spectral of $[\mathrm{A}]$ is less than unity. In other words, when the module of all eigen values of $[\mathrm{A}]$ are smaller than unity, the numerical stability is ensured.

The stability of a numerical scheme can be studied using the general form of the 2x2 matrix $[\mathrm{A}]$:

$$[\mathrm{A}] = \begin{bmatrix} A_{11} & A_{12} \\ A_{21} & A_{22} \end{bmatrix} \tag{207}$$

Then, the equations are developed for the systems with or without damping. [16]

The eigen values of $[\mathrm{A}]$ are computed from the characteristic polynomial equation:

$$\begin{aligned} &\det[\mathrm{A} - \lambda \mathrm{I}] = 0 \\ &\lambda^2 - 2A_1\lambda + A_2 = 0 \end{aligned} \tag{208}$$

Where,

$$A_1 = \frac{1}{2}tr[\mathrm{A}] = \frac{1}{2}\left(A_{11} + A_{22}\right)$$

$$A_2 = \det[\mathrm{A}] = A_{11}A_{22} - A_{12}A_{21}$$

The eigen values are then obtained as:

[15] Belytschko T., Wing Kam Liu, and Moran B., "Finite Elements for Nonlinear Continua and Structures", John Wiley, 1999.

$$\lambda_{1,2} = A_1 \pm \sqrt{A_1^2 - A_2} \tag{209}$$

If $A_1^2 < A_2$, eigen values are complex conjugate; if $A_1^2 = A_2$, they are real and identical; if $A_1^2 > A_2$, they are real and distinct. You intend to define a stability domain in the (A_1, A_2) -space, where the spectral radius $\rho([\mathrm{A}]) = \max(|\lambda_i(A_1, A_2)|) \leq 1$. The boundary of this domain is given by couples (A_1, A_2) such as $\rho([\mathrm{A}]) = 1$. Three cases are to be considered:

1. Roots are real and one of them is equal to 1:

   You then have:

   $$1 - 2A_1 + A_2 = 0 \tag{210}$$

   This yields:

   $$\begin{aligned} &A_2 = 2A_1 - 1 \\ &\lambda_1 = 1 \\ &\lambda_2 = A_2 \end{aligned} \tag{211}$$

   The corresponding part of the boundary of the stability domain is the segment analytically defined by $1 - 2A_1 + A_2 = 0$ and $-1 \leq A_2 \leq 1$.

2. Roots are real and one of them is equal to -1:

   You then have:

   $$1 + 2A_1 + A_2 = 0 \tag{212}$$

   This yields:

   $$\begin{aligned} &A_2 = -2A_1 - 1 \\ &\lambda_1 = -1 \\ &\lambda_2 = -A_2 \end{aligned} \tag{213}$$

   In this case, the corresponding part of the boundary is the segment given by $1 + 2A_1 + A_2 = 0$ and $-1 \leq A_2 \leq 1$.

3. Roots are complex conjugate:

   Their modulus is equal to 1. You then have, using $\lambda_{1,2} = e^{\pm i\alpha}$:

   $$\begin{aligned} 0 &= e^{2i\alpha} - 2A_1 e^{i\alpha} + A_2 \\ &= (\cos 2\alpha - 2A_1 \cos\alpha + A_2) + i(\sin 2\alpha - 2A_1 \sin\alpha) \\ &= (2\cos\alpha(\cos\alpha - A_1) + A_2 - 1) + i(2\sin\alpha(\cos\alpha - A_1)) \end{aligned} \tag{214}$$

   This yields:

   $$\begin{aligned} &2\cos\alpha(\cos\alpha - A_1) + A_2 - 1 = 0 \\ &2\sin\alpha(\cos\alpha - A_1) = 0 \end{aligned} \tag{215}$$

   Since $\sin\alpha \neq 0$, you obtain:

$$
\begin{aligned}
&A_1 = \cos\alpha \\
&A_2 = 1
\end{aligned}
\tag{216}
$$

The corresponding part of the boundary is thus the segment given by $A_2 = 1$ and $-1 \leq A_2 \leq 1$.

The 3 segments introduced above define a closed contour. Point $A_1 = A_2 = 0$ is located inside this contour and in this case, $\rho([A]) = 0$. Since $\rho([A])$ varies continuously with respect to A_1 and A_2, you can conclude that the stability domain corresponds to the interior of the contour. To precisely define the stability domain, you must also have points leading to double eigen value of modulus 1, that is, the intersections between the parabola $A_1^2 = A_2$ and the boundary of the domain. This corresponds to Points $(A_1, A_2) = (\pm 1, 1)$.

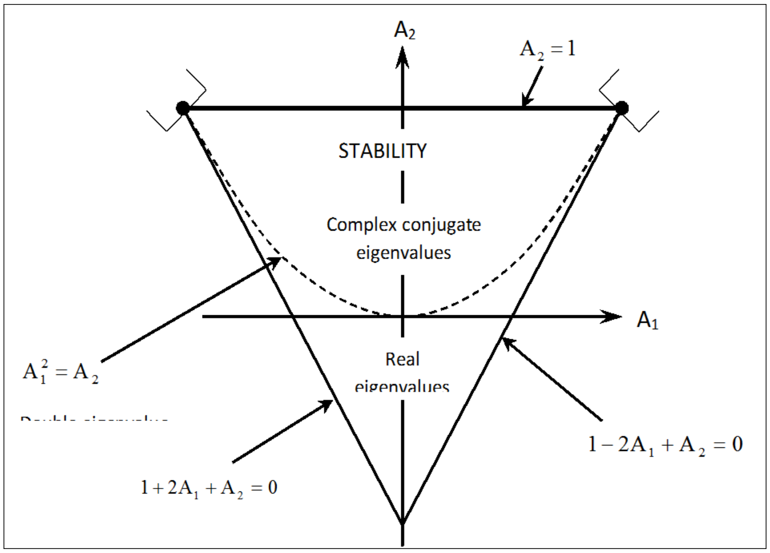

Figure 10: Stability Domain

You can analytically summarize the description of the stability by means of the following two sets of conditions:

$$
\begin{aligned}
&(1) \quad -\frac{(A_2+1)}{2} \leq A_1 \leq \frac{(A_2+1)}{2}, \qquad -1 \leq A_2 < 1 \\
&(2) \quad -1 < A_1 < 1, \qquad A_2 = 1
\end{aligned}
\tag{217}
$$

Numerical Stability of Undamped Systems

The stability conditions developed in the previous section can be applied to a one degree-of-freedom of a system without damping. The dynamic equilibrium equation at time t_n is given by:

$$
m\ddot{u}^n + ku^n = f^n \tag{218}
$$

Where, m and k are respectively the nodal mass and stiffness. f^n is the external force at time t_n. Rewriting the central difference time integration equations from Equation 205, you obtain:

$$u^{n+1} = u^n + \Delta t.\dot{u}^{n+\frac{1}{2}} = u^n + \Delta t.\dot{u}^{n-\frac{1}{2}} + \Delta t^2.\ddot{u}^n$$
$$u^n = u^{n-1} + \Delta t.\dot{u}^{n-\frac{1}{2}} \tag{219}$$

and:

$$\ddot{u}^n = \frac{u^{n+1} - 2u^n + u^{n-1}}{\Delta t^2} \tag{220}$$

Substituting these equations into Equation 218, it yields:

$$m\frac{u^{n+1} - 2u^n + u^{n-1}}{\Delta t^2} + ku^n = f^n \tag{221}$$

This equation can be written as Equation 206. Then the amplification matrix takes the expression:

$$[\mathrm{A}] = \begin{bmatrix} 2 - \omega^2\Delta t^2 & -1 \\ 1 & 0 \end{bmatrix} \tag{222}$$

Where, $\omega = \sqrt{\frac{k}{m}}$ is the angular frequency of the considered mode.

Comparing with Equation 207, you have $A_1 = 1 - \frac{\omega^2\Delta t^2}{2}$ and $A_2 = 1$. Stability is then given by:

$$-1 < 1 - \frac{\omega^2\Delta t^2}{2} < 1 \tag{223}$$

The right inequality is always true if $\omega \neq 0$. For, the particular case of $\omega = 0$, the scheme is unstable. However, the analytical solution for a system with $\omega = 0$ leads to an unbounded solution. The left inequality implies:

$$\Delta t < \frac{2}{\omega} \tag{224}$$

Numerical Stability with Viscous Damping: Velocities at Time Steps

The dynamic equilibrium equation at time step n is written as:

$$m\ddot{u}^n + c\dot{u}^n + ku^n = f^n \tag{225}$$

Using the equations:

$$u^{n+1} = u^n + \Delta t.\dot{u}^{n+\frac{1}{2}}$$
$$u^n = u^{n-1} + \Delta t.\dot{u}^{n-\frac{1}{2}} \tag{226}$$

Results in:

$$u^{n+1} - u^{n-1} = \Delta t\left(\dot{u}^{n+\frac{1}{2}} + \dot{u}^{n-\frac{1}{2}}\right) \tag{227}$$

For the velocity, write the equations:

$$\dot{u}^n = \dot{u}^{n-\frac{1}{2}} + \frac{\Delta t}{2}\ddot{u}^n$$
$$\dot{u}^{n+\frac{1}{2}} = \dot{u}^n + \frac{\Delta t}{2}\ddot{u}^n \tag{228}$$

to obtain:

$$\dot{u}^n = \frac{1}{2}\left(\dot{u}^{n-\frac{1}{2}} + \dot{u}^{n+\frac{1}{2}}\right) = \frac{1}{2\Delta t}\left(u^{n+1} - u^{n-1}\right) \tag{229}$$

Substituting these equations into Equation 225, the recurring continuation equation on the displacement is written in the form:

$$m\frac{u^{n+1} - 2u^n + u^{n-1}}{\Delta t^2} + \frac{c}{2\Delta t}\left(u^{n+1} - u^{n-1}\right) + ku^n = f^n \tag{230}$$

The equation can be rearranged to obtain the expression of the amplification matrix:

$$[\mathrm{A}] = \begin{bmatrix} \frac{2-\omega^2\Delta t^2}{1+\frac{c\Delta t}{2m}} & \frac{-1+\frac{c\Delta t}{2m}}{1+\frac{c\Delta t}{2m}} \\ 1 & 0 \end{bmatrix} \tag{231}$$

This yields $A_1 = \dfrac{1-\frac{\omega^2\Delta t^2}{2}}{1+\frac{c\Delta t}{2m}}$ and $A_2 = \dfrac{1-\frac{c\Delta t}{2m}}{1+\frac{c\Delta t}{2m}}$.

Stability is given by the set of conditions from Equation 217:

$$\begin{gathered} -\frac{1}{1+\frac{c\Delta t}{2m}} \le \frac{1-\frac{\omega^2\Delta t^2}{2}}{1+\frac{c\Delta t}{2m}} \le \frac{1}{1+\frac{c\Delta t}{2m}} \\ -1 \le \frac{1-\frac{c\Delta t}{2m}}{1+\frac{c\Delta t}{2m}} < 1 \end{gathered} \tag{232}$$

The second expression is always verified for $c > 0$. It is the same for the right inequality of the first expression. The left inequality of the first expression leads to the condition on the time step:

$$\Delta t \le \frac{2}{\omega} \tag{233}$$

You find the same condition as in the undamped case, which echoes a conclusion given in [16]. You may yet remark that damping has changed the strict inequality into a large inequality, preventing from weak instability due to a double eigen value of modulus unity.

It is important to note that the relation Equation 233 is obtained by using the expression Equation 229 to compute nodal velocities at time steps. However, in an explicit scheme generally the mid-step velocities $\dot{u}^{n+\frac{1}{2}}$ and $\dot{u}^{n-\frac{1}{2}}$ are used. This will be studied in the next section.

Numerical Stability with Viscous Damping: Velocities at Mid Steps

Considering the case in which damping effects cannot be neglected, you still would like to deal with decoupled equilibrium equations to be able to use essentially the same computational procedure. Except for the case of full modal projection which is a very expensive technique and practically unused, the damping matrix $[\mathrm{C}]$ is not diagonal, contrary to $[\mathrm{M}]$. The computation of the viscous forces with the exact velocity given by the integration algorithm requires the matrix $[\mathrm{M}] + \frac{\Delta t}{2}[\mathrm{C}]$ to be inverted, which can harm the numerical performances. You therefore often compute the viscous forces using the velocities at the preceding mid-step, which are explicit. This leads to an equilibrium at step n in the form:

$$m\ddot{u}^n + c.\dot{u}^{n-\frac{1}{2}} + ku^n = f^n \tag{234}$$

The integration algorithm immediately yields:

$$\dot{u}^{n-\frac{1}{2}} = \frac{1}{\Delta t}\left(u^n - u^{n-1}\right) \tag{235}$$

The recurring continuation becomes:

$$m\frac{u^{n+1} - 2u^n + u^{n-1}}{\Delta t^2} + \frac{c}{\Delta t}\left(u^n - u^{n-1}\right) + ku^n = f^n \tag{236}$$

As above, you obtain the amplification matrix:

$$[\mathrm{A}] = \begin{bmatrix} 2 - \omega^2\Delta t^2 - \frac{c\Delta t}{m} & -1 + \frac{c\Delta t}{m} \\ 1 & 0 \end{bmatrix} \tag{237}$$

You have in this case $A_1 = 1 - \frac{\omega^2\Delta t^2}{2} - \frac{c\Delta t}{2m}$ and $A_2 = 1 - \frac{c\Delta t}{m}$.

Stability is again given by the set of conditions Equation 217:

$$\begin{aligned} &-1 + \tfrac{c\Delta t}{2m} \le 1 - \tfrac{\omega^2\Delta t^2}{2} - \tfrac{c\Delta t}{2m} \le 1 - \tfrac{c\Delta t}{2m} \\ &-1 \le 1 - \tfrac{c\Delta t}{m} < 1 \end{aligned} \tag{238}$$

Right inequalities are always verified in both preceding expressions. Left inequalities now lead to two conditions on the time step:

$$\Delta t \le \frac{-\frac{c}{m} + \sqrt{\frac{c^2}{m^2} + 4\omega^2}}{\omega^2}, \quad \Delta t \le \frac{2m}{c} \tag{239}$$

Therefore, the critical time step depends not only to ω but also to the mass and the damping. However, the critical time step depends only to ω when using the exact velocities to compute the viscous forces as described in the previous section.

Numerical Stability with Rayleigh Damping

The linearized equations of equilibrium governing the dynamic response of a finite element system can derived from the equations of motion given in Equation of Motion for Translational Velocities and Equation of Motion for Angular Velocities:

$$[M]\{\ddot{U}\} + [C]\{\dot{U}\} + [K]\{U\} = \{F\} \tag{240}$$

In the case of direct step-by-step time integration, it is necessary to evaluate the damping matrix $[\mathrm{C}]$ explicitly. The Rayleigh damping method assumes that the matrix $[\mathrm{C}]$ is computed by the following equation:

$$[\mathrm{C}] = \alpha[\mathrm{M}] + \beta[\mathrm{K}] \tag{241}$$

Where,

$[\mathrm{C}]$
Viscous damping matrix of the system

$[\mathrm{M}]$
Mass matrix

$[\mathrm{K}]$
Stiffness matrix

As described in the preceding sections, the computation of the viscous forces by using velocities at time steps leads to obtain a non-diagonal matrix $[\mathrm{C}]$ which should be inverted in the resolution procedure. To avoid the high cost operations, generally the simplifications are made to obtain a diagonal matrix. Substituting the Rayleigh equation into Equation 240 and using the mid-step velocities for $\beta[K]$ terms and at step nodal velocities for $\alpha[\mathrm{M}]$ terms, the following expression is obtained:

$$[M]\{\ddot{u}^n\} + \alpha[M]\{\dot{u}^n\} + \beta[K]\left\{\dot{u}^{n-\frac{1}{2}}\right\} + [K]\{u^n\} = \{f^n\} \tag{242}$$

Studying the equilibrium of a node to obtain a one dimensional equation of motion, write:

$$m\ddot{u} + c\dot{u} + ku = f \tag{243}$$

Where,

m
Modal mass

c
Associated modal damping

k
Nodal stiffness

This leads to the following recurring continuation on the displacement:

$$m\frac{u^{n+1} - 2u^n + u^{n-1}}{\Delta t^2} + \frac{\alpha m}{2\Delta t}\left(u^{n+1} - u^{n-1}\right) + \frac{\beta k}{\Delta t}\left(u^n - u^{n-1}\right) + ku^n = f^n \tag{244}$$

The amplification matrix is then:

$$[\mathrm{A}] = \begin{bmatrix} \dfrac{2-\omega^2\Delta t^2-\beta\omega^2\Delta t}{1+\frac{\alpha\Delta t}{2}} & \dfrac{-1+\frac{\alpha\Delta t}{2}+\beta\omega^2\Delta t}{1+\frac{\alpha\Delta t}{2}} \\ 1 & 0 \end{bmatrix} \tag{245}$$

In this case, $A_1 = \dfrac{1-\frac{\omega^2\Delta t^2}{2}-\frac{\beta\omega^2\Delta t}{2}}{1+\frac{\alpha\Delta t}{2}}$ and $A_2 = \dfrac{1-\frac{\alpha\Delta t}{2}-\beta\omega^2\Delta t}{1+\frac{\alpha\Delta t}{2}}$.

Stability is obtained as before by means of the set of conditions from Equation 217:

$$\frac{-1+\frac{\beta\omega^2\Delta t}{2}}{1+\frac{\alpha\Delta t}{2}} \le \frac{1-\frac{\omega^2\Delta t^2}{2}-\frac{\beta\omega^2\Delta t}{2}}{1+\frac{\alpha\Delta t}{2}} \le \frac{1-\frac{\beta\omega^2\Delta t}{2}}{1+\frac{\alpha\Delta t}{2}} \tag{246}$$

$$-1 \le \frac{1-\frac{\alpha\Delta t}{2}-\beta\omega^2\Delta t}{1+\frac{\alpha\Delta t}{2}} < 1$$

This again yields two conditions on the time step, coming from the left inequalities in both expressions:

$$\Delta t \le \frac{-\beta\omega + \sqrt{\beta^2\omega^2 + 4}}{\omega}, \quad \Delta t \le \frac{2}{\beta\omega^2} \tag{247}$$

It is equivalent to consider only the $\beta[\mathrm{K}]$ contribution in the damping for the computation of the time step, which appears to be logical since the $\alpha[\mathrm{M}]$ contribution is used with the exact velocity. It is advantageous to separate the two contributions, restrictions of the time step then becoming lighter. It can be shown that for the complete treatment of the Rayleigh damping using mid-step velocities, the stability conditions can be given by:

$$\Delta t \le \frac{-\alpha - \beta\omega^2 + \sqrt{(\alpha + \beta\omega^2)^2 + 4\omega^2}}{\omega}, \quad \Delta t \le \frac{2}{\alpha + \beta\omega^2} \tag{248}$$

Example: Critical Time Step for a Mass-Spring System

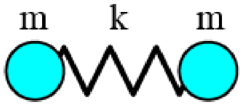

Figure 11:

Consider a free mass-spring system without damping. The governing differential equation can be written as:

$$M\ddot{X} + KX = 0 \tag{a}$$

The element matrix expressions are given as:

$$[M] = m\begin{bmatrix} 1 & 0 \\ 0 & 1 \end{bmatrix}; \ [K] = k\begin{bmatrix} 1 & -1 \\ -1 & 1 \end{bmatrix}$$

The general solution is assumed in the form of:

$$X = Cos(\omega t - \alpha)[I]\Psi \tag{b}$$

Where, the angular frequency ω and the phase angle α are common for all X_i. α and Ψ_i are the constants of integration to be determined from the initial conditions of the motion and ω is a characteristic value (eigen value) of the system. Substituting (b) into (a) yields:

$$(K - \omega^2 M)\Psi Cos(\omega t - \alpha) = 0 \qquad (c)$$

The consistency of (c) for $\Psi Cos(\omega t - \alpha) \neq 0$ requires that:

$$\det(K - \omega^2 M) = 0 => \omega^2 = \frac{2k}{m} \qquad (d)$$

Assuming the following numerical values $m = 1$ and $k = 10$, you have $\omega = \sqrt{\frac{2k}{m}} = 4.472136$.

The critical time step of the system is given by Equation 224:

$$\Delta t \leq \frac{2}{\omega} \quad \Rightarrow \quad \Delta t \leq \frac{2}{4.472136} \quad \Rightarrow \quad \Delta t \leq 0.4472$$

Example: Critical Time Step for Dropping Body

A dropping body is studied in Body Drop Example with analytical and numerical approaches. As shown in Figure 14, the numerical results are closed to the analytical solution if you use a step-by-step time discretization method with a constant time step $\Delta t = 0.1$. This value is less than the critical time step obtained by:

$$\Delta t_{cr} = \frac{2}{\omega_{\max}}$$

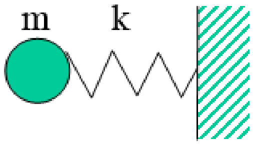

Figure 12:

which may be computed as:

$$\omega = \sqrt{\frac{k}{m}} = \sqrt{20} \Rightarrow \quad \Delta t_{cr} = \frac{2}{4.472136} \quad \Rightarrow \quad \Delta t_{cr} = 0.4472$$

Therefore, the used time step in the Body Drop Example ensures the stability of the numerical scheme as it is less than the critical value. Now using the values higher than or equal to the critical time step, the solution diverges towards the infinity as shown in Figure 13.

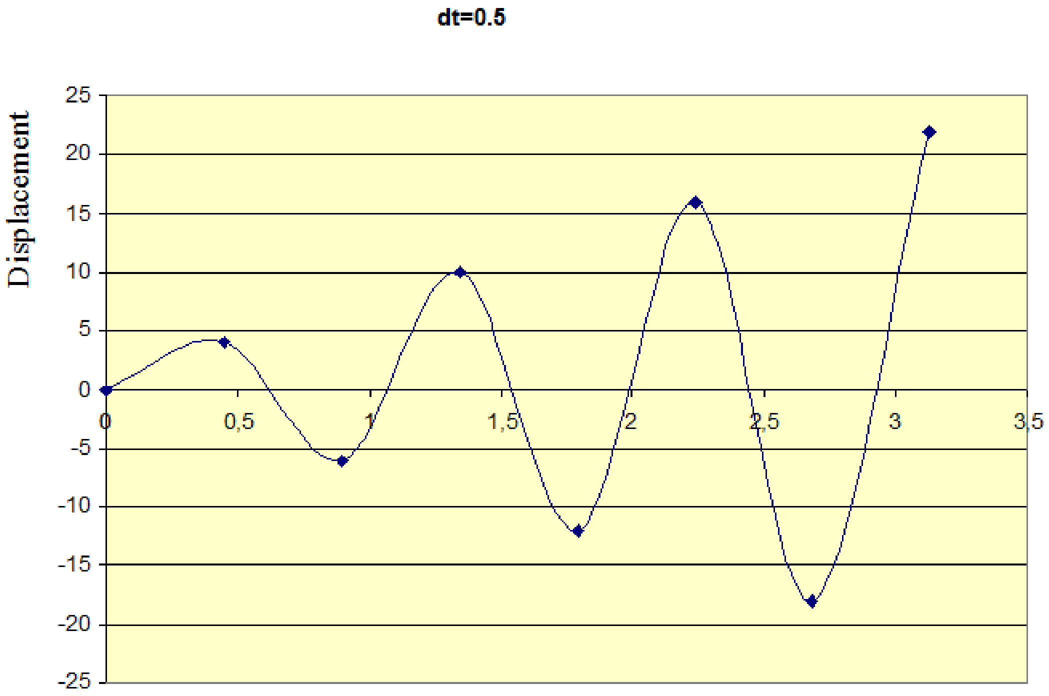

Figure 13: Numerical instability for Example Using Over Critical Time Steps

It is worthwhile to comment that in a general explicit finite element program as Radioss, the critical time step is computed for an entire element (two nodal masses and stiffness for spring element). In the case of dropping body example, the mass-spring system can be compared by analogy to a two-node mass-spring system where the global stiffness is twice softer. The critical time step is then computed using the nodal time step of the entire element (refer to the following sections [16] for more details on the computation of nodal time step).

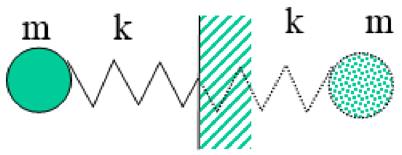

Figure 14:

[16] Hughes T.J.R., "Analysis of Transient Algorithms with Particular Reference to Stability Behavior", Computational Methods for Transient Analysis, eds. T. Belytschko and T.J.R. Hugues, 67-155, North Holland, 1983.

Courant Condition Stability

Radioss uses elements with a lumped mass approach. This reduces computational time considerably as no matrix inversion is necessary to compute accelerations.

The integration scheme used by Radioss is based on the central difference integration scheme which is conditionally stable, that is, the time step must be small enough to assure that the solution does not grow boundlessly.

The stability condition is given in the last sections. For a system without damping, it can be written in a closed form:

$$\Delta t \leq \frac{2}{\omega_{\max}} \tag{249}$$

Where, $\omega_{\max}$ is the highest angular frequency in the system:

$$\det\left(K - \omega^2 M\right) = 0 \tag{250}$$

Where, K and M are respectively the stiffness and the mass matrices of the system.

The time step restriction given by Equation 249 was derived considering a linear system (Explicit Scheme Stability), but the result is also applicable to nonlinear analysis since on a given step the resolution is linear. However, in nonlinear analysis the stiffness properties change during the response calculation. These changes in the material and the geometry influence the value of $\omega_{\max}$ and in this way the critical value of the time step.

The above point can be easily pointed out by using a nonlinear spring with increasing stiffness in Body Drop Example. It can be shown that the critical time step decreases when the spring becomes stiffer. Therefore, if a constant time step close to the initial critical value is considered, a significant solution error is accumulated over steps when the explicit central difference method is used.

Another consideration in the time integration stability concerns the type of problem which is analyzed. For example in the analysis of wave propagation, a large number of frequencies are excited in the system. That is not always the case of structural dynamic problems. In a wave shock propagation problem, the time step must be small enough in order to excite all frequencies in the finite element mesh. This requires short time step so that the shock wave does not miss any node when traveling through the mesh. It follows that the time step should be limited by the following relation:

$$\Delta t \leq \frac{l_c}{c} \tag{251}$$

Where,

l_c
: Characteristic element length, representing the shortest road for a wave arriving on a node to cross the element

c
: Speed of sound in the material

Δt
: Time step

The condition Equation 251 gives a severe time step restriction with respect to stability time step, that is, $\Delta t < \frac{2}{\omega}$. It can easily be shown that for a simple case of a bar element, the two expressions Equation 251 and Equation 249 are equivalent.

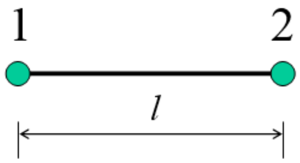

Figure 15: Bar Element

If a uniform linear-displacement bar element is considered, (Figure 16), and a lumped mass formulation at the nodes is used, the highest frequency of this element can be obtained by a resolution of an eigen value problem:

$$[K]\{X\} = \omega^2[M]\{X\} \tag{252}$$

$$\det([K] - \omega^2[M]) = 0 \tag{253}$$

For a lumped mass bar, you have:

$$[K] = k\begin{bmatrix} 1 & -1 \\ -1 & 1 \end{bmatrix} \tag{254}$$

$$[M] = m\begin{bmatrix} 1 & 0 \\ 0 & 1 \end{bmatrix} \tag{255}$$

Where, m and k are respectively the nodal mass and stiffness of the bar:

$$k = \frac{EA}{l} \quad ; \quad m = \frac{A\rho l}{2} \tag{256}$$

Equation Equation 253 yields:

$$\left(k - m\omega^2\right)^2 - k^2 = 0 \tag{257}$$

then:

$$\omega = \sqrt{\frac{2k}{m}} \tag{258}$$

which can be simplified with Equation 256 to obtain:

$$\omega = \frac{2}{l}\sqrt{\frac{E}{\rho}} = \frac{2c}{l} \tag{259}$$

Where, c is the speed of sound in the material and its expression is given as:

$$c = \sqrt{\frac{E}{\rho}} \tag{260}$$

with ρ the material density and the Young's modulus. Combining Equation 259 and Equation 249, you obtain:

$$\Delta t \leq \frac{l}{c} \tag{261}$$

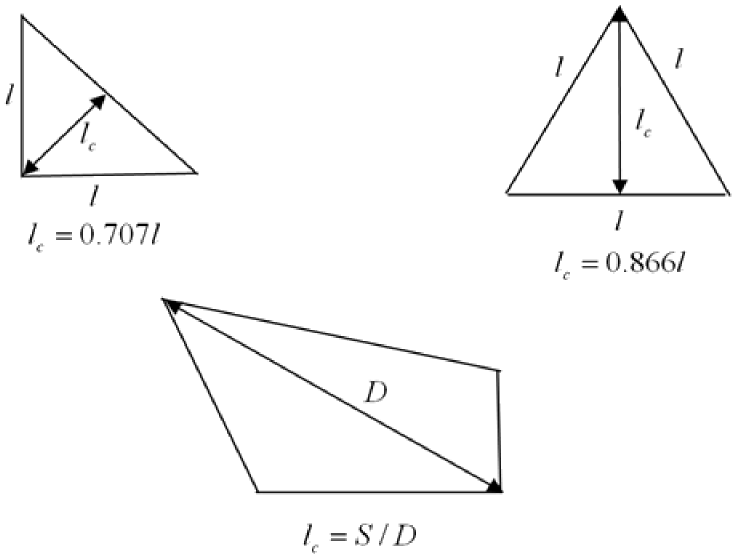

Figure 16: Element Characteristic Lengths

This relation is that of Equation 251 and shows that the critical time step value in the explicit time integration of dynamic equation of motion can be carried out by the interpretation of shock wave propagation in the material. This is shown for the first time by Courant. [17] In spite of their works are limited to simple cases, the same procedure can be used for different kinds of finite elements. The characteristic lengths of the elements are found and Equation 251 is written for all elements to find the most critical time step over a mesh. Regarding to the type (shape) of element, the expression of characteristic length is different. Figure 16 shows some typical cases for elements with one integration point.

Time Step Control

The time incrementation in Radioss is fully automatic and *a priori* requires no user intervention. The step used for time integration (or moving forward in time) can be calculated using two different methods. The method used depends on the type of simulation being performed.

- Element time step
- Nodal time step

[17] Courant R., Friedrichs K.O., and Levy H., "About the partial Differenzensleichungen Bogdanova of Physics", Math. A nn., Vol. 100, 32, 1928.

The time step used by the solver is the largest possible time step, as determined by the Courant condition that will maintain stability. If the default large strain formulation is used, the time step is computed at each cycle. Large element deformation can give a large time step decrease. If the deformation is too large, negative volumes can result, which make it impossible to invert the Jacobian matrix and to integrate the stress over the volume. If the small strain formulation is used, assuming a constant Jacobian matrix during time and also a constant volume, all spatial variables are defined at $t = 0$. This is either the beginning of the analysis or the time at which the small strain formulation is initiated. If the sound speed is constant, the time step thus becomes constant. Using this formulation, the time step has no effect on the computation since the initial volume is used.

Element Time Step Control

The stable element time step was detailed in Courant Condition Stability and is restated as:

$$\Delta t = \min_{Elements}\left(\frac{l}{c}\right) \tag{262}$$

Where,

l
: Element characteristic length

c
: Speed of sound in the material

This is the default setting.

The element time step is computed at the same time as the internal forces. The characteristic length and the sound speed are computed for each element in every cycle.

The computed time step is compared to a minimum time step value and a scale factor is applied to ensure a conservative bound. Different minimum time step values can be given to different element types by using the option: `/DT/Keyword`.

Where,

Keyword
: Defined in the user manual as the element type

If deformation is large enough for the time step to reach the minimum defined value, there are 3 user-defined options possible:

- Stop the analysis when the minimum time step value is reached. This is the default for brick and quadrilateral elements.
- Delete the element(s) defining the time step. This is the default for shell elements.
- Implement small strain formulation using a constant time step. This only works for shell and brick elements.

These options are defined using a third keyword: STOP, DEL, CST, AMS or SET

Nodal Time Step Control

The nodal time step is calculated after the computation of all the internal forces at each node using:

$$\Delta t = \min_{Nodes}\sqrt{\frac{2m}{k}} \tag{263}$$

Where,

m	Nodal mass
k	Equivalent nodal stiffness

The nodal stiffness is one half of eigen value from element stiffness matrix; for a truss element this value is equal to the diagonal term of the stiffness matrix. It is computed from the accumulation of element and interface stiffness'. These stiffness' are obtained during internal force computation.

For a regular mesh, the element time step and nodal time step conditions are identical. Consider the element time step condition for a truss element.

$$\Delta t_{element} = \frac{l}{c} = \frac{l}{\sqrt{\frac{E}{\rho}}} \tag{264}$$

The nodal time step condition is written as:

$$\Delta t_{nodal} = \sqrt{\frac{2m}{k}} \tag{265}$$

with

$$m = \frac{1}{2}\rho Al \quad \text{and} \quad k = \frac{EA}{l} \tag{266}$$

Therefore:

$$\Delta t_{nodal} = \sqrt{\frac{\rho Al}{EA/l}} = \frac{l}{\sqrt{\frac{E}{\rho}}} = \frac{l}{c} = \Delta t_{element} \tag{267}$$

To select the nodal time step when running Radioss the option `/DT/NODA` has to be used.

As for the element time step, minimum time step and scale factors are required. The default value for the scale factor is 0.9. If the minimum time step is reached, the analysis can either be stopped or a mass scaling formulation can be applied. In the latter case, mass is added to the affected nodes so that the time step remains constant at the minimum value. This option can be enabled using the same third keyword as used in the element time step control. It must be checked that added masses do not affect the accuracy of results. If one uses the nodal time step, the element time step is ignored.

Interface Time Step Control

Finally, the time step is influenced by existence of interfaces. The interface time step control depends on the type of interface being used.

For the interfaces in which the contact conditions are defined by applying kinematic conditions, no time step restriction is required. This is the case of interface TYPE 2 of Radioss.

In addition, for the interfaces TYPES 3, 4, 5, and 8 in Radioss a small stiffness is used. Therefore, the interfaces are stable if a time step scale factor less than or equal to 0.9 is used.

TYPES 7, 10 and 11 interfaces use a variable stiffness and if this stiffness is not small compared to the element stiffness, a stability condition must be adhered to.

For interfaces 3, 4, 5, 7, 8, and 10, there are three possibilities that can be selected, shown in Table 1.

Table 1: Interface Time Step Cases

Default (element) time step without interfaces TYPES 7, 10 or 11	Element time step is computed and a scaling factor of 0.9 (default) is applied.
Option /DT/NODA is used with or without interface TYPES 7 and/or 10, 11	Nodal time step is computed and a scaling factor of 0.9 (default) is applied.
Default time step with interface TYPES 7 or 10, 11	Nodal and element time steps are computed and the smallest is used.

If the deletion option is applied with the /DT/INTER/DEL interface time step control, the node controlling the minimum time step is deleted from the interface.

Mass scaling, where mass is added to an interface node, can be enabled using the option /DT/INTER/CST.

Time Step Control Limitations

Many of the time step control options influence the solution results. The solution of the nonlinear dynamic response of a finite element system accurate is the numerical model correctly represents the physical model. The critical time step given for finite element system is determined by a theoretical approach in which the highest frequency of the discretized system controls this value. Therefore, the time step limitations are related to the model and cannot be changed without incidence on the quality of results.

Using the DEL option can significantly alter the model, since elements and nodes are removed without replacement. In fact, mass and/or volume is lost. Using either /DT/NODA/CST or /DT/INTER/CST will add mass to the model to allow mathematical solution. The added mass will increase the kinetic energy. This should be checked by the user to see if there is a significant effect. Switching to a small strain option using brick or shell elements also introduces errors as it was seen in Small Strain Formulation.

Generally, in the study of the nonlinear dynamic response of a system, three physical laws have to be respected:

- Conservation of mass
- Conservation of energy
- Conservation of momentum dynamic equilibrium

The last one is generally respected as the equation of motion is resolved at each resolution cycle. However, in the case of adding masses especially when using /DT/NODA/CST option, it is useful to verify the momentum variation. The two other conservation laws are not explicitly satisfied. They should be checked a posteriori after computation to ensure the validity of the numerical model with respect to the physical problem.

Example: Time Step

Explicit Scheme Stability Condition

$$M\ddot{X} + KX = 0 \tag{268}$$

$$\ddot{X} = M^{-1}KX \tag{269}$$

$$\dot{X}_{n+\frac{1}{2}} = \dot{X}_{n-\frac{1}{2}} + dt\ddot{X}_n \tag{270}$$

$$X_n = X_{n-1} + dt\dot{X}_{n-\frac{1}{2}} \tag{271}$$

Equation 269 and n Equation 270 are added:

$$\dot{X}_{n+\frac{1}{2}} = \dot{X}_{n-\frac{1}{2}} + dtM^{-1}KX_n \tag{272}$$

The following equation is obtained:

$$\dot{X}_{n-\frac{1}{2}} = \dot{X}_{n-\frac{1}{2}-1} + dtM^{-1}KX_{n-1} \tag{273}$$

When Equation 273 is subtracted from Equation 272, and Equation 271 is used:

$$\dot{X}_{n+\frac{1}{2}} = A\dot{X}_{n-\frac{1}{2}} - X_{n-\frac{1}{2}-1} \tag{274}$$

Where,

$A = 2I + dt^2M^{-1}K$

For non-divergence of Equation 274:

≥ λ: largest eigen value of $A - I$ is smaller than 1

≥ $\det\left(\lambda I + I + dt^2M^{-1}K\right) = 0$

≥ $\det\left(I\left((\lambda + 1)/dt^2\right) + M^{-1}K\right) = 0$

≥ $2dt^2 >$ largest eigen value of $M^{-1}K$

≥ $2dt^2$ < smallest eigen value of $2K^{-1}M$

Application

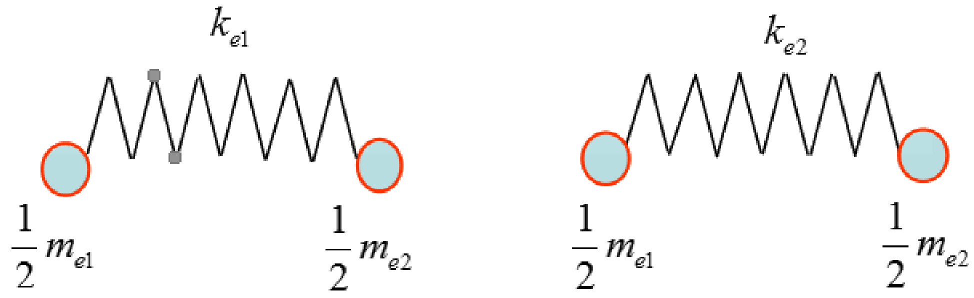

Figure 17:

$$dt_1 = \sqrt{\frac{2m_{el}}{k_{el}}}$$

$$dt_2 = \sqrt{\frac{2m_{e2}}{k_{e2}}}$$

$$dt_e = \min(dt_1, dt_2)$$

$$dt_n = \sqrt{\frac{m_{e1}+m_{e2}}{k_{el}+k_{e2}}}$$

Interface

Interfaces have stiffness but no mass: $dt_e = 0$

Solution 1: (interface TYPE3, TYPE4, TYPE5)

$$k_{\mathrm{inter}face} < < k_{elements}$$

Solution 2: nodal time step (interface TYPE7 and TYPE10)

$$dt_n = \sqrt{\frac{2m}{k}} \quad k = \sum k_{\mathrm{interface}} + \sum k_{\mathrm{elements}}$$

Kinematic time step (interface TYPE7):

$$dt < \frac{(gap - pene)}{2\,V}$$

Where,

V	Impact speed

Large Scale Eigen Value Computation

The numerical solution of large scale algebraic eigen value problems is now available thanks to new methods and software. A class of methods called *Krylov subspace projection methods* is used. The well known Lanczos method is the first one. The Arnoldi method is a generalization of Lanczos method applied to the non-symmetric case. A variant of Arnoldi-Lonczos scheme called the Implicitly Restarted

Arnoldi Method [18] is a part of public domain software package called *ARPACK* which is integrated in Radioss. Restarting is introduced as a way to overcome intractable storage and computational requirements in the original Arnoldi method. Implicit restarting is a variant of restarting which may be considered as a truncated form of the powerful implicitly shifted QR technique that is suitable for large scale problems. It provides a mean to approximate a few eigen values with user specified properties in space proportional to the number of eigen values required. The details of the method are not explained here.

Combine Modal Reduction

A domain decomposition method allowing the combination of nonlinear sub-domains with linear modal sub-domains has been proposed. [19] With this technique, the displacement field in the linear sub-domains is projected on a local basis of reduction modes calculated on the detailed geometry and the kinematic continuity relations are written at the interface in order to recombine the physical kinematic quantities of reduced sub-domains locally. The method yields promising save of computing time in industrial applications. However, the use of modal projection is limited to linear sub-domains. In the case of overall rigid-body motion with small local vibrations, the geometrical nonlinearity of sub-domains must be taken into account. Therefore, the projection cannot be used directly even thought the global displacements may still be described by a small number of unknowns; for example six variables to express motion of local frame plus a set of modal coordinates in this frame. This approach is used in the case of implicit framework. [20] In the case of direct integration with an explicit scheme an efficient approach is presented. [21] One of the main problems is to determine the stability conditions for the explicit integration scheme when the classical rotation parameters as Euler angles or spin vectors are used. A new set of parameters, based on the so-called *frame-mass* concept is introduced to describe the global rigid body motion. The position and the orientation of the local frame are given by four points where the distances between the points are kept constant during the motion. In this way, only the displacement type DOF is dealt and the equations of motion are derived to satisfy perfectly the stability conditions. This approach, which was integrated in Radioss V5, will be presented briefly here.

Linear Modal Reduction

A modal reduction basis is defined on one or more sub-domains of the decomposition. The definition of this basis is completely arbitrary. Any combination of eigen modes and static corrections can be used. All these modes are orthogonalized with respect to the finite element mass matrix in order for the projected mass matrix to be diagonal and suitable for an explicit solver.

Considering the case of a structure divided into two sub-domains, assume that modal reduction is used for linear Sub-domain 1. Thus, the displacement field of this sub-domain is projected onto the reduction vectors:

$$\mathrm{U}_1(t) = \sum_1^n \alpha_{1i}(t)\,\Phi_{1i} = \Phi_1 \alpha_1(t) \tag{275}$$

[18] Sorensen D.C., “Implicit application of polynomial filters in a k-step Arnoldi method”, SIAM J. Matrix Anal. Appl., Vol. 13, pp. 357-385, 1992.

with U_1 vector of discretized displacements in Sub-domain 1, α_1 vector of modal participations. This naturally yields:

$$\dot{U}_1 = \Phi_1 \dot{\alpha}_1 \\ \ddot{U}_1 = \Phi_1 \ddot{\alpha}_1 \tag{276}$$

The number of modal unknowns α_1 chosen is much smaller than the original number of degrees of freedom of Sub-domain 1.

In order to obtain the new coupled system, the dynamic equilibrium of sub-domain 1 must be projected onto the reduction basis and the velocities involved in the kinematic relations must be expressed in terms of the modal coordinates. Thus, write the new matrix system for a single time scale as:

$$\begin{bmatrix} \frac{\Delta t}{2}\hat{M}_1 & 0 & -\frac{\Delta t}{2}\hat{C}_1 T \\ 0 & \frac{\Delta t}{2}\mathrm{M}_2 & -\frac{\Delta t}{2}\mathrm{C}_2 T \\ -\frac{\Delta t}{2}\hat{C}_1 & -\frac{\Delta t}{2}\mathrm{C}_2 & 0 \end{bmatrix} \begin{bmatrix} \ddot{\alpha}_1^{n+1} \\ \ddot{U}_2^{n+1} \\ \Lambda \end{bmatrix} = \begin{bmatrix} \frac{\Delta t}{2}\hat{F}_1^{n+1} \\ \frac{\Delta t}{2}\mathrm{F}_2^{n+1} \\ \hat{C}_1{}^P \dot{\alpha}_1^{n+1} + \mathrm{C}_2{}^P \dot{U}_2^{n+1} \end{bmatrix} \tag{277}$$

Where,

$$\hat{M}_1 = \Phi_1 T \mathrm{M}_1 \Phi_1 \\ \hat{F}_1 = \Phi_1 T \mathrm{F}_{ext1} - \hat{K}_1 \alpha_1 \\ \hat{K}_1 = \Phi_1 T \mathrm{K}_1 \Phi_1 \\ \hat{C}_1 = \mathrm{C}_1 \Phi_1 \tag{278}$$

The structure of this system is strictly identical to that which existed before reduction. Therefore, use exactly the same resolution process and apply the multi-time-step algorithm.

The time step for a reduced sub-domain is deduced from the highest eigen frequency of the projected system in order to preserve the stability of the explicit time integration. This time step is often larger than that given by the Courant condition with the finite element model before reduction.

Model Reduction with Finite Overall Rotation

Since large rotations are highly nonlinear [22], the displacement field in a sub-domain undergoing finite rotations cannot be expressed as a linear combination of constant modes. However, the rigid contribution to the displacement field creates no strain. In the case of small strains and linear behavior, the local vibrating system can still be projected onto a basis of local reduction modes. Then, take into account the rotation matrix from the initial global coordinate system to the local coordinate system and its time derivatives. A classical parameterization of this rotation, for example, Euler angles, would introduce nonlinear terms involving velocities. Since these quantities, in the central difference scheme, are implicit, this would require internal iterations in order to solve the equilibrium problem, a situation you clearly want to reduce the computation time due to the reduction.

Classically, the displacement field of a rotating and vibrating sub-domain is decomposed into a finite rigid-body contribution and a small-amplitude vibratory contribution measured in a local frame. The large rigid motion is represented using the so-called *four-mass* approach. [21]

Four points (O, A, B, C) in space are arbitrarily chosen to represent the position of a local frame attached to the sub-domain. In order to simplify the local equations, choose these points so that they constitute an ortho-normal frame.

> **Note:** The four points defining the local frame do not have to coincide with nodes of the mesh.

Displacement Field Decomposition

The global displacements of these four points are the unknowns describing the rigid motion of the sub-domain. These are classical displacement-type parameters. The relative distances between these points are kept constant during the dynamic calculation through external links. This enables us to express the total continuous displacement field of the sub-domain as:

$$\mathrm{u} = X\mathrm{u}_A + Y\mathrm{u}_B + Z\mathrm{u}_C + (1 - X - Y - Z)\mathrm{u}_O + \mathrm{P}\mathrm{u}_L = \mathrm{u}_E + \mathrm{P}\mathrm{u}_L \tag{279}$$

Where,

X, Y, Z
: Coordinates in the local frame $[O, A, B, C]$

P
: Rotation matrix expressing the transformation from the local to the global coordinates: since $(\overrightarrow{OA}, \overrightarrow{OB}, \overrightarrow{OC})$ are unit vectors, $\mathrm{P} = [\overrightarrow{OA}; \overrightarrow{OB}; \overrightarrow{OC}]$.

In order to express the dynamic equilibrium, Equation 278 must be derived with respect to time to yield velocities and accelerations.

$$\begin{aligned}\dot{u} &= X\dot{u}_A + Y\dot{u}_B + Z\dot{u}_C + (1 - X - Y - Z)\dot{u}_O + \dot{\mathrm{P}}\mathrm{u}_L + \mathrm{P}\dot{\mathrm{u}}_L\\ \ddot{\mathrm{u}} &= X\ddot{\mathrm{u}}_A + Y\ddot{\mathrm{u}}_B + Z\ddot{\mathrm{u}}_C + (1 - X - Y - Z)\ddot{\mathrm{u}}_O + \ddot{\mathrm{P}}\mathrm{u}_L + \mathrm{P}\ddot{\mathrm{u}}_L + 2\dot{\mathrm{P}}\dot{\mathrm{u}}_L\end{aligned} \tag{280}$$

The time derivatives of the rotation matrix are given by:

$$\begin{aligned}\dot{\mathrm{P}} &= [\dot{\mathrm{u}}_A - \dot{\mathrm{u}}_O; \dot{\mathrm{u}}_B - \dot{\mathrm{u}}_O; \dot{\mathrm{u}}_C - \dot{\mathrm{u}}_O]\\ \ddot{\mathrm{P}} &= [\ddot{\mathrm{u}}_A - \ddot{\mathrm{u}}_O; \ddot{\mathrm{u}}_B - \ddot{\mathrm{u}}_O; \ddot{\mathrm{u}}_C - \ddot{\mathrm{u}}_O]\end{aligned} \tag{281}$$

Thus, the fields in Equation 280 have the following expression:

$$\begin{aligned}\dot{u} &= (X + \mathrm{u_L}X)\dot{u}_\mathrm{A} + (Y + \mathrm{u_L Y})\dot{u}_\mathrm{B} + (Z + \mathrm{u}_L Z)\dot{u}_C + [1 - (X + \mathrm{u_L}X) - (Y + \mathrm{u_L Y}) - (Z + \mathrm{u}_L Z)]\dot{u}_O + \mathrm{P}\dot{u}_L\\ \ddot{u} &= (X + \mathrm{u_L}X)\ddot{u}_\mathrm{A} + (Y + \mathrm{u_L Y})\ddot{u}_\mathrm{B} + (Z + \mathrm{u}_L Z)\ddot{u}_C + [1 - (X + \mathrm{u_L}X) - (Y + \mathrm{u_L Y}) - (Z + \mathrm{u}_L Z)]\ddot{u}_O + \mathrm{P}\ddot{u}_L + 2\dot{P}\dot{u}_L\end{aligned} \tag{282}$$

Where, $\mathrm{u}_L X, \mathrm{u}_L Y, \mathrm{u}_L Z$ are the components of the local displacement in the local frame. The assumption of small perturbations in the local frame enables us to consider that the rigid and the deformed configurations are the same, that is, you can neglect $\mathrm{u}_L X, \mathrm{u}_L Y, \mathrm{u}_L Z$ compared to the local coordinates, X, Y, Z. Thus, you get simplified expressions of the velocity and acceleration fields:

$$\begin{aligned}\dot{\mathrm{u}} &= X\ddot{\mathrm{u}}_A + Y\ddot{\mathrm{u}}_B + Z\ddot{\mathrm{u}}_C + (1 - X - Y - Z)\ddot{\mathrm{u}}_O + \dot{\mathrm{P}}\mathrm{u}_L\\ \ddot{\mathrm{u}} &= X\ddot{\mathrm{u}}_A + Y\ddot{\mathrm{u}}_B + Z\ddot{\mathrm{u}}_C + (1 - X - Y - Z)\ddot{\mathrm{u}}_O + \mathrm{P}\ddot{\mathrm{u}}_L + 2\dot{\mathrm{P}}\dot{\mathrm{u}}_L\end{aligned} \tag{283}$$

To express the weak form of the dynamic equilibrium, you also need the variation δu of the displacement field:

$$\delta\mathbf{u} = X\delta\mathbf{u}_A + Y\delta\mathbf{u}_B + Z\delta\mathbf{u}_C + (1 - X - Y - Z)\delta\mathbf{u}_O + \delta\mathbf{P}\mathbf{u}_L + \mathbf{P}\delta\mathbf{u}_L \tag{284}$$

Where, $\delta\mathbf{P} = [\delta\mathbf{u}_A - \delta\mathbf{u}_O; \delta\mathbf{u}_B - \delta\mathbf{u}_O; \delta\mathbf{u}_C - \delta\mathbf{u}_O]$

Again, the same assumption as above allows us to simplify this expression:

$$\delta u = X\delta u_A + Y\delta u_B + Z\delta u_C + (1 - X\text{-}Y\text{-}Z)\delta u_O + P\delta u_L \tag{285}$$

Local Reduced Dynamic System

The local dynamic equilibrium of the sub-domain is given by:

$$\rho\ddot{u} - f_{\text{int}}(u) = 0 \tag{286}$$

The principle of virtual work yields a weak form of this equilibrium, taking into account, Dirichlet-type boundary conditions:

$$\int_{\Omega} \rho\delta u^T \ddot{u}\, d\Omega - \int_{\Omega} \delta u^T f_{\text{int}}(u)\, d\Omega = 0 \tag{287}$$

Where,

$\forall\ \delta u$
: Verifies the kinematic boundary conditions

Ω
: Volume of the sub-domain

To introduce Equation 278 into this weak form of the equilibrium, you must express with the new parameterization the virtual works of both the internal and external forces and the virtual work, due to the rigid links among the points defining the local frame.

The internal forces can be calculated from the local part of the displacement, using Equation 279 and taking into account the rigid links, for example, the fact that displacement u_E creates no strain.

$$\mathbf{f}_{\text{int}}(\mathbf{u}) = \mathbf{P}\mathbf{f}_{\text{intL}}(\mathbf{u}_L) = \mathbf{P}\,div_L[\boldsymbol{\sigma}_L(\mathbf{u}_L)] \tag{288}$$

Where, index L expresses that the coordinates and the spatial derivatives are taken in the local frame.

The virtual work of the internal forces is then:

$$\delta W_{\text{int}} = \int_{\Omega} \delta u^T P\, div_L[\sigma_L(u_L)]\, d\Omega \tag{289}$$

The integration by parts in the local frame introduces external surface forces f_{ext}:

$$\begin{aligned} \delta W_{\text{int}} &= -\int_{\Omega} \sigma_L(u_L) : \varepsilon_L(P^T\delta u)\, d\Omega + \int_{\Gamma} \delta u^T P \sigma_L(u_L).n_L\, d\Omega \\ &= -\int_{\Omega} \sigma_L(u_L) : \varepsilon_L(P^T\delta u)\, d\Omega + \int_{\Gamma} \delta u^T f_{\text{ext}}\, dS \end{aligned} \tag{290}$$

Where,

Γ
: The boundary of Ω

n_L
: The normal to Γ expressed in the local frame

To compute forces associated to the rigid links, first, new Lagrange multipliers are introduced to express the energy of a link:

$$W_{links} = \sum_{\substack{(I,J)\in(O,A,B,C)^2 \\ J>I}} \Lambda_{IJ} \mathrm{D_{IJ}}(u_I, u_J) \tag{291}$$

Where, $\mathrm{D}_{IJ} = \| (\mathrm{x}_I^0 + \mathrm{u}_I) - (\mathrm{x}_J^0 + \mathrm{u}_J) \| - \| \mathrm{x}_I^0 - \mathrm{x}_J^0 \|$ and x_I^0 are the initial coordinates of point I and the rigid link between points I and J is given by: $\mathrm{D}_{IJ}(\mathrm{u}_I, \mathrm{u}_J) = 0$.

Then, the differentiation of this energy is used to obtain the virtual work to be introduced into the weak form of the equilibrium:

$$\delta W_{links} = -\sum_{\substack{(I,J)\in(O,A,B,C)^2 \\ J>I}} \delta\Lambda_{IJ} \mathrm{D}_{IJ}(u_I, u_j) - \sum_{I\in(O,A,B,C)} \delta u_I \sum_{\substack{J\in(O,A,B,C) \\ J\neq I}} \delta\Lambda_{IJ} \frac{\mathrm{D}_{IJ}(u_I, u_j)}{\partial u_I} \tag{292}$$

$$\forall\ \delta \mathrm{u_I} \quad \mathrm{I}\in(O, A, B, C) \tag{293}$$

> **Note:** The quantity $\sum_{\substack{J\in(O,A,B,C) \\ J\neq I}} \Lambda_{IJ} \frac{\partial \mathrm{D}_{IJ}(\mathrm{u}_I, \mathrm{u}_J)}{\partial \mathrm{u}_I} = \mathrm{F}_{linksIJ}$ can be viewed as the resisting force applied to point I to preserve the distances from this point to the other points of the local frame.

Weak Form of Equilibrium

Now, express the displacement field using Equation 279 and the local field projected on a Ritz basis:

$$\begin{aligned} \mathrm{u} &= \sum_{\mathrm{i=1}}^{3} \mathrm{u_A^i \varphi_X^i + u_B^i \varphi_Y^i + u_C^i \varphi_Z^i + u_O^i \varphi_{1-X\text{-}Y\text{-}Z}^i + y^i P \varphi_L^i} \\ &= \Phi_{\mathrm{P}} \widehat{U} \end{aligned} \tag{294}$$

where $\varphi_X^i = X\mathrm{e}_i$, $\varphi_Y^i = Y\mathrm{e}_i$, $\varphi_Z^i = Z\mathrm{e}_i$, $\varphi_{1-X-Y-Z}^i = (1 - X - Y - Z)\mathrm{e}_i$, $(\mathrm{e}_1, \mathrm{e}_2, \mathrm{e}_3)$ is a basis of the global frame, $\{\varphi_L^i\}$ is a basis of local Ritz vectors obtained, for example, by finite element discretization or by modal analysis, $\widehat{\mathrm{U}}$ is the vector of the discrete unknowns:

$$\hat{\mathrm{U}}=\begin{bmatrix}\left[\mathrm{u}_A^i\right]\\ \left[\mathrm{u}_B^i\right]\\ \left[\mathrm{u}_C^i\right]\\ \left[\mathrm{u}_O^i\right]\\ \left[\mathrm{y}^i\right]\end{bmatrix}=\begin{bmatrix}\hat{\mathrm{U}}_E\\ \hat{\mathrm{U}}_L\end{bmatrix}$$, with $\hat{\mathrm{U}}_E=\begin{bmatrix}\left[\mathrm{u}_A^i\right]\\ \left[\mathrm{u}_B^i\right]\\ \left[\mathrm{u}_C^i\right]\\ \left[\mathrm{u}_O^i\right]\end{bmatrix}$ and $\hat{\mathrm{U}}_L=\left[\mathrm{y}^i\right]$,

Φ_P is the projection basis: $\Phi_P=\left[\left\{\varphi_X^i\right\},\left\{\varphi_Y^i\right\},\left\{\varphi_Z^i\right\},\left\{\varphi_{1-X-Y-Z}^i\right\},\left\{\mathrm{P}\varphi_L^i\right\}\right]=\left[\Phi_E,\,\mathrm{P}\Phi_L\right]$.

Equation 283 and Equation 285 yield:

$$\begin{aligned}\dot{\mathrm{u}}&=\Phi_P\dot{\hat{\mathrm{U}}}\\ \ddot{\mathrm{u}}&=\Phi_P\ddot{\hat{\mathrm{U}}}+\mathrm{G}\left(\dot{\hat{\mathrm{U}}}\right)\\ \delta\mathrm{u}&=\Phi_P\delta\hat{\mathrm{U}}\end{aligned}\tag{295}$$

Where, $\mathrm{G}\left(\dot{\hat{\mathrm{U}}}\right)$ is the gyroscopic contribution to the acceleration, given by:

$$\mathrm{G}\left(\dot{\hat{\mathrm{U}}}\right)=2\dot{\mathrm{P}}\left(\left[\dot{\mathrm{u}}_A^i\right],\left[\dot{\mathrm{u}}_B^i\right],\left[\dot{\mathrm{u}}_C^i\right],\left[\dot{\mathrm{u}}_O^i\right]\right)\Phi_L\dot{\hat{\mathrm{U}}}_L$$

The final expression of the complete weak form of the dynamic equilibrium is obtained as:

$$\begin{aligned}&\int_\Omega\delta\hat{\mathrm{U}}^T\left(\Phi_{PT}\right)\Phi_P\ddot{\hat{\mathrm{U}}}\rho d\Omega+\int_\Omega\delta\hat{\mathrm{U}}^T\left(\Phi_{PT}\right)\mathrm{G}\left(\dot{\hat{\mathrm{U}}}\right)\rho d\Omega+\int_\Omega\sigma_L\left(\Phi_L\hat{\mathrm{U}}_L\right):\varepsilon_L\left(\Psi_P\delta\hat{\mathrm{U}}\right)d\Omega\\ &\qquad-\delta\Lambda^T\mathrm{D}\left(\hat{\mathrm{U}}_E\right)-\delta\hat{\mathrm{U}}_{ET}\mathrm{F}_{links}\left(\Lambda,\,\hat{\mathrm{U}}_E\right)=\int_\Gamma\delta\hat{\mathrm{U}}^T\left(\Phi_{PT}\right)\mathrm{f}_{ext}d\mathrm{S}\end{aligned}\tag{296}$$

Where,

$$\Phi_L=\left\{\phi_L^i\right\}$$

$$\psi_P=\left[\left\{P^T\phi_X^i\right\},\left\{P^T\phi_Y^i\right\},\left\{P^T\phi_Z^i\right\},\left\{P^T\phi_{1-X-Y-Z}^i\right\},\left\{\phi_L^i\right\}\right]=\left[P^T\Phi_E,\,\Phi_L\right]$$

D
: Vector formed by the 6 relations preserving the relative distances of points $(O,\,A,\,B,\,C)$

Λ
: Vector of the Lagrange multipliers corresponding to each rigid link

F_{links}
: Vector of the link forces given by Equation 293

Equation 296 can be rewritten using classical matrix and vector operators obtained by finite element discretization:

$$\delta\hat{\mathrm{U}}^T\mathrm{M}_P\ddot{\hat{\mathrm{U}}}+\delta\hat{\mathrm{U}}^T\mathrm{F}_{gyr}\left(\dot{\hat{\mathrm{U}}}\right)+\delta\hat{\mathrm{U}}^T\mathrm{K}_L\hat{\mathrm{U}}_L-\delta\Lambda^T\mathrm{D}\left(\hat{\mathrm{U}}_E\right)-\delta\hat{\mathrm{U}}_{ET}\mathrm{F}_{links}\left(\Lambda,\,\hat{\mathrm{U}}_E\right)=\delta\hat{\mathrm{U}}^T\mathrm{F}_{extP}\tag{297}$$

Where,

$$\mathrm{M}_P = \bar{\Phi}_{PT}\mathrm{M}\bar{\Phi}_P$$

M

Classical mass matrix of sub-domain

$\bar{\Phi}_P$

Projection matrix consisting of vectors of Φ_P discretized on the nodes of the mesh.

$$F_{gyr}\left(\dot{\hat{U}}\right) = \int_{\Omega} (\Phi_P^T) G\left(\dot{\hat{U}}\right) \rho d\Omega \tag{298}$$

$\mathrm{K}_L = \bar{\Psi}_{PT}\mathrm{K}\bar{\Phi}_L$, with K being the sub-domain's local stiffness matrix and $\bar{\Psi}_P$ and $\bar{\Phi}_L$ deduced (as was $\bar{\Phi}_L$) from $\bar{\Psi}_P$, $\bar{\Phi}_L$ and the mesh, $\mathrm{F}_{extP} = \bar{\Phi}_{PT}\mathrm{F}_{ext}$, with F_{ext} being the classical vector of the external forces assembled on the sub-domain.

Now, you are able to reduce the number of unknowns on the sub-domain drastically by choosing as the Ritz vectors, instead of classical finite element shape functions, an appropriate (and small) family of local reduction vectors. The modal vibration problem is purely local and guidelines found in the literature for the proper choice of the projection basis apply here.

Note: As far as inertia coupling with local vibration and overall large motion is concerned, two separate contributions must be considered. The first contribution appears in the projected mass matrix, which as now the following form:

$$\mathrm{M_P} = \begin{bmatrix} \mathrm{M_E} & \mathrm{M_C^T} \\ \mathrm{M_C} & \mathrm{M_V} \end{bmatrix} \tag{299}$$

Where, $\mathrm{M_E}$ is the constant mass matrix corresponding only to the global displacement field given by $X\ddot{\mathrm{u}}_\mathrm{A} + Y\ddot{\mathrm{u}}_\mathrm{B} + Z\ddot{\mathrm{u}}_\mathrm{C} + (1 - X - Y - Z)\ddot{\mathrm{u}}_\mathrm{O}$, $\mathrm{M_V}$ is the constant mass matrix corresponding to the local vibration given by $\mathrm{u_L}$, $\mathrm{M_C}$ is a coupling matrix, variable with overall rotation, arising from the interaction between the local vibratory acceleration field expressed in the global frame $\mathrm{P}\ddot{\mathrm{u}}_L$ and the overall virtual displacement field $X\delta u_\mathrm{A} + Y\delta u_\mathrm{B} + Z\delta u_\mathrm{C} + (1 - X - Y - Z)\delta u_\mathrm{O}$; $\mathrm{M_C^T}$ naturally comes from the symmetric interaction between virtual local displacement field and the overall acceleration field.

The second contribution to the inertia coupling is the gyroscopic forces.

Note: In Radioss a special procedure is used to linearize the rigid links. [21]

The rigid body motion component of the displacement increment is computed in unconditionally stable way by the use of Lagrange Multiplier to impose the rigid links. The deforming part is generated by the local vibration modes retained in the reduction basis. Therefore, you can conclude that the stability condition is the same as that given by the local vibrating system. The critical time step is constant throughout the calculation and can be derived from the highest eigen frequency of the local reduced stiffness matrix with respect to the local reduced mass matrix.

The highest eigen frequency $\mathrm{f_{max}}$ is given by the system:

$$\Phi_L^T K \Phi_L V = \omega^2 \Phi_L^T M \Phi_L V \tag{300}$$

Where, $\Phi_L = \left\{\phi_L^i\right\}$ and $\mathrm{f} = \frac{\omega}{2\pi}$.

Having determined $\mathrm{f}_{\max}$, the maximum time step which can be used on the reduced sub-domain while ensuring the stability of the time integration is:

$$\Delta t_{\max} = \frac{1}{\pi f_{\max}} \tag{301}$$

[19] Faucher V. and Combescure A., “A time and space mortar method for coupling linear modal subdomains and nonlinear subdomains in explicit structural dynamics”, Computer Methods in Applied Mechanics and Engineering, Vol. 192, pp. 509-533, 2002.

[20] Cardona A. and Géradin M., “A superelement formulation for mechanism analysis”, Computer Methods in Applied Mechanics and Engineering, Vol. 100, pp. 1-29, 1992.

[21] Faucher V. and Combescure A., “Local modal reduction in explicit dynamics with domain decomposition. Part 1: extension to subdomains undergoing finite rigid rotations”, Int. Journal Num. Methods in Engineering, Vol. 60, pp. 2531-2560, 2004.

[22] Argyris J.H., “An excursion into the large rotations”, Computer Methods in Applied Mechanics and Engineering, 32, 85-155, 1982.

Element Library

Radioss element library contains elements for one, two or three dimensional problems.

Some new elements have been developed and implemented in recent versions. Most of them use the assumed strain method to avoid some locking problems. For the elements using reduced integration schema, the physical stabilization method is used to control efficiently the hourglass deformations. Another point in these new elements is the use of co-rotational coordinate system. For the new solid elements, as the assumed strains are often defined in the specific directions, the use of global system combined with Jaumman's stress derivation contributes to commutative error especially when solid undergoes large shear strains.

The Radioss finite element library can be classified into the following categories of elements:

Solid elements	8- and 20-node bricks, 4- and 10-node tetrahedrons
Solid-shells	8- , 16- and 20-node hexahedrons, 6-node pentahedral element
2 dimensional elements	4-node quadrilaterals for plane strain and axisymmetrical analysis
Shell elements	4-node quadrilaterals and 3-node triangles
One dimensional elements	rivet, springs, bar and beams

The implementation of these elements will now be detailed. Expression of nodal forces will be developed as, for explicit codes they represent the discretization of the momentum equations. Stiffness matrices, which are central to implicit finite element approaches, are not developed here.

Solid Hexahedron Elements

Radioss brick elements have the following properties:

BRICK8	8-node linear element with reduced or full integration
HA8	8-node linear element with various number of integration points going from 2x2x2 to 9x9x9
HEPH	8-node linear element with reduced integration point and physical stabilization of hourglass modes
BRICK20	20-node quadratic element with reduced or full integration schemes

For all elements, a lumped mass approach is used and the elements are isoparametric, that is, the same shape functions are used to define element geometry and element displacements.

The fundamental theory of each element is described in this chapter.

Linear Brick Shape Functions

Shape functions define the geometry of an element in its computational (intrinsic) domain. As was seen in Finite Element Formulation, physical coordinates are transformed into simpler computational intrinsic coordinates so that integration of values is numerically more efficient.

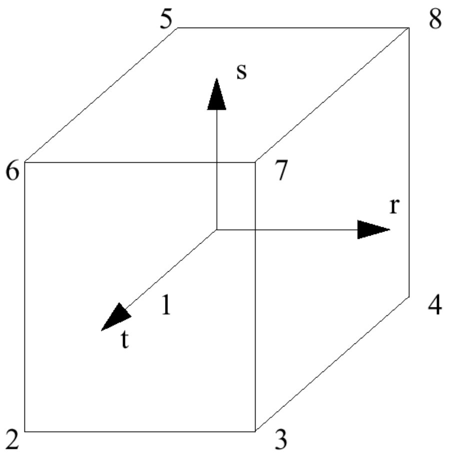

Figure 18: Node Brick Element

Where, $r \equiv \xi$, $s \equiv \eta$, and $t \equiv \zeta$.

The shape functions of an 8 node brick element, shown in Figure 18, are given by:

$$\Phi_1 = \frac{1}{8}(1-\xi)(1-\eta)(1-\zeta) \tag{302}$$

$$\Phi_2 = \frac{1}{8}(1-\xi)(1-\eta)(1+\zeta) \tag{303}$$

$$\Phi_3 = \frac{1}{8}(1+\xi)(1-\eta)(1+\zeta) \tag{304}$$

$$\Phi_4 = \frac{1}{8}(1+\xi)(1-\eta)(1-\zeta) \tag{305}$$

$$\Phi_5 = \frac{1}{8}(1-\xi)(1+\eta)(1-\zeta) \tag{306}$$

$$\Phi_6 = \frac{1}{8}(1-\xi)(1+\eta)(1+\zeta) \tag{307}$$

$$\Phi_7 = \frac{1}{8}(1+\xi)(1+\eta)(1+\zeta) \tag{308}$$

$$\Phi_8 = \frac{1}{8}(1+\xi)(1+\eta)(1-\zeta) \tag{309}$$

The element velocity field is related by:

$$v_i = \sum_{I=1}^{8} \Phi_I . v_{iI} \tag{310}$$

Where, v_{iI} are the nodal velocities.

Strain Rate

The relationship between the physical coordinate and computational intrinsic coordinates system for a brick element is given by the matrix equation:

$$\begin{bmatrix} \frac{\partial \Phi_I}{\partial \xi} \\ \frac{\partial \Phi_I}{\partial \eta} \\ \frac{\partial \Phi_I}{\partial \zeta} \end{bmatrix} = \begin{bmatrix} \frac{\partial x}{\partial \xi} & \frac{\partial y}{\partial \xi} & \frac{\partial z}{\partial \xi} \\ \frac{\partial x}{\partial \eta} & \frac{\partial y}{\partial \eta} & \frac{\partial z}{\partial \eta} \\ \frac{\partial x}{\partial \zeta} & \frac{\partial y}{\partial \zeta} & \frac{\partial z}{\partial \zeta} \end{bmatrix} \cdot \begin{bmatrix} \frac{\partial \Phi_I}{\partial x} \\ \frac{\partial \Phi_I}{\partial y} \\ \frac{\partial \Phi_I}{\partial z} \end{bmatrix} = F_\xi \cdot \begin{bmatrix} \frac{\partial \Phi_I}{\partial x} \\ \frac{\partial \Phi_I}{\partial y} \\ \frac{\partial \Phi_I}{\partial z} \end{bmatrix} \tag{311}$$

Hence:

$$\left[\frac{\partial \Phi_I}{\partial x_i}\right] = F_\xi^{-1} \cdot \left[\frac{\partial \Phi_I}{\partial \xi}\right] \tag{312}$$

Where, F_ξ is Jacobian matrix.

The element strain rate is defined as:

$$\dot{\varepsilon}_{ij} = \frac{1}{2}\left(\frac{\partial v_i}{\partial x_j} + \frac{\partial v_j}{\partial x_i}\right) \tag{313}$$

Relating the element velocity field to its shape function gives:

$$\frac{\partial v_i}{\partial x_j} = \sum_{I=1}^{8} \frac{\partial \Phi_I}{\partial x_j} \cdot v_{iI} \tag{314}$$

Hence, the strain rate can be described directly in terms of the shape function:

$$\dot{\varepsilon}_{ij} = \frac{1}{2}\left(\frac{\partial v_i}{\partial x_j} + \frac{\partial v_j}{\partial x_i}\right) = \sum_{I=1}^{8} \frac{\partial \Phi_I}{\partial x_j} \cdot v_{iI} \tag{315}$$

As was seen in Velocity Strain or Deformation Rate, volumetric strain rate is calculated separately by volume variation.

For one integration point:

$$\frac{\partial \Phi_1}{\partial x_j} = -\frac{\partial \Phi_7}{\partial x_j}; \quad \frac{\partial \Phi_2}{\partial x_j} = -\frac{\partial \Phi_8}{\partial x_j}; \quad \frac{\partial \Phi_3}{\partial x_j} = -\frac{\partial \Phi_5}{\partial x_j}; \quad \frac{\partial \Phi_4}{\partial x_j} = -\frac{\partial \Phi_6}{\partial x_j} \tag{316}$$

F.E Method is used only for deviatoric strain rate calculation in A.L.E and Euler formulation.

Volumetric strain rate is computed separately by transport of density and volume variation.

Assumed Strain Rate

Using Voigt convention, the strain rate of Strain Rate, Equation 315 can be written as:

$$\{\dot{\varepsilon}\} = [B]\{v\} = \sum_{I=1}^{8} [B_I]\{v_I\} \tag{317}$$

With,

$$\{\dot{\varepsilon}\} = \langle \dot{\varepsilon}_{xx} \quad \dot{\varepsilon}_{yy} \quad \dot{\varepsilon}_{zz} \quad 2\dot{\varepsilon}_{xy} \quad 2\dot{\varepsilon}_{yz} \quad 2\dot{\varepsilon}_{xz} \rangle^t$$

$$[B_I] = \begin{bmatrix} \frac{\partial \Phi_I}{\partial x} & 0 & 0 & 0 & \frac{\partial \Phi_I}{\partial x} & \frac{\partial \Phi_I}{\partial y} \\ 0 & \frac{\partial \Phi_I}{\partial y} & 0 & \frac{\partial \Phi_I}{\partial x} & 0 & \frac{\partial \Phi_I}{\partial z} \\ 0 & 0 & \frac{\partial \Phi_I}{\partial z} & \frac{\partial \Phi_I}{\partial y} & \frac{\partial \Phi_I}{\partial z} & 0 \end{bmatrix}^t$$

It is useful to take the Belytschko-Bachrach's mix form [23] of the shape functions written by:

$$\Phi_I(x, y, z, \xi, \eta, \zeta) = \Delta_I + b_{xI} \cdot x + b_{yI} \cdot y + b_{zI} \cdot z + \sum_{\alpha=1}^{4} \gamma_I^{\alpha} \phi_{\alpha} \tag{318}$$

Where,

$$b_{iI} = \frac{\partial \Phi_I}{\partial x_i}(\xi = \eta = \zeta = 0);$$

$$\gamma_I^{\alpha} = \tfrac{1}{8}\left[\Gamma_I^{\alpha} - \left(\sum_{J=1}^{8} \Gamma_J^{\alpha} x_J \right) b_{xI} - \left(\sum_{J=1}^{8} \Gamma_J^{\alpha} y_J \right) b_{yI} - \left(\sum_{J=1}^{8} \Gamma_J^{\alpha} z_J \right) b_{zI} \right];$$

$$\langle \phi \rangle = \langle \eta\zeta \quad \xi\zeta \quad \xi\eta \quad \xi\eta\zeta \rangle$$

The derivation of the shape functions is given by:

$$\frac{\partial \Phi_I}{\partial x_i} = b_{iI} + \sum_{\alpha=1}^{4} \gamma_I^{\alpha} \frac{\partial \phi_{\alpha}}{\partial x_i} \tag{319}$$

It is decomposed by a constant part which is directly formulated with the Cartesian coordinates, and a non-constant part which is to be approached separately. For the strain rate, only the non-constant part is modified by the assumed strain. You can see in the following that the non-constant part or the high order part is just the hourglass terms.

You now have the decomposition of the strain rate:

$$\{\dot{\varepsilon}\} = \sum_{I=1}^{8} [B_I]\{v_I\} = \sum_{I=1}^{8} \left([B_I]^0 + [B_I]^H \right)\{v_I\} = \{\dot{\varepsilon}\}^0 + \{\dot{\varepsilon}\}^H \tag{320}$$

with:

$$[B_I]^0 = \begin{bmatrix} b_{xI} & 0 & 0 \\ 0 & b_{yxI} & 0 \\ 0 & 0 & b_{zI} \\ b_{yxI} & b_{xI} & 0 \\ b_{zI} & 0 & b_{xI} \\ 0 & b_{zI} & b_{yxI} \end{bmatrix}; \; [B_I]^H = \begin{bmatrix} \sum_{\alpha=1}^{4} \gamma_I^\alpha \frac{\partial \phi_\alpha}{\partial x} & 0 & 0 & 0 & \sum_{\alpha=1}^{4} \gamma_I^\alpha \frac{\partial \phi_\alpha}{\partial x} & \sum_{\alpha=1}^{4} \gamma_I^\alpha \frac{\partial \phi_\alpha}{\partial y} \\ 0 & \sum_{\alpha=1}^{4} \gamma_I^\alpha \frac{\partial \phi_\alpha}{\partial y} & 0 & \sum_{\alpha=1}^{4} \gamma_I^\alpha \frac{\partial \phi_\alpha}{\partial x} & 0 & \sum_{\alpha=1}^{4} \gamma_I^\alpha \frac{\partial \phi_\alpha}{\partial z} \\ 0 & 0 & \sum_{\alpha=1}^{4} \gamma_I^\alpha \frac{\partial \phi_\alpha}{\partial z} & \sum_{\alpha=1}^{4} \gamma_I^\alpha \frac{\partial \phi_\alpha}{\partial y} & \sum_{\alpha=1}^{4} \gamma_I^\alpha \frac{\partial \phi_\alpha}{\partial z} & 0 \end{bmatrix}^t$$

Belvtschko and Bindeman [24] ASQBI assumed strain is used:

$$\{\dot{\varepsilon}\} = \sum_{I=1}^{8} \left([B_I]^0 + [\bar{B}_I]^H \right) \{v_I\} \tag{321}$$

with $[\bar{B}_I]^H = \begin{bmatrix} X_I^{1234} & -\bar{v} Y_I^3 - v Y_I^{24} & -\bar{v} Z_I^2 - v Z_I^{34} \\ -\bar{v} X_I^3 - v X_I^{14} & Y_I^{1234} & -\bar{v} Z_I^1 - v Z_I^{34} \\ -\bar{v} X_I^2 - v X_I^{14} & -\bar{v} Y_I^1 - v Y_I^{24} & Z_I^{1234} \\ Y_I^{12} & X_I^{12} & 0 \\ Z_I^{13} & 0 & X_I^{13} \\ 0 & Z_I^{23} & Y_I^{23} \end{bmatrix}$

Where, $X_I^{13} = \gamma_I^1 \frac{\partial \varphi_1}{\partial x} + \gamma_I^3 \frac{\partial \varphi_3}{\partial x}$; $Y_I^{13} = \gamma_I^1 \frac{\partial \varphi_1}{\partial y} + \gamma_I^3 \frac{\partial \varphi_3}{\partial y}$; and $\bar{v} = \frac{v}{1-v}$; .

To avoid shear locking, some hourglass modes are eliminated in the terms associated with shear so that no shear strain occurs during pure bending. That is, Y_I^3, X_I^3 in $\dot{\varepsilon}_{xy}$ terms and all fourth hourglass modes in shear terms are also removed since this mode is non-physical and is stabilized by other terms in $[\bar{B}_I]^H$.

The terms with Poisson coefficient are added to obtain an isochoric assumed strain field when the nodal velocity is equivoluminal. This avoids volumetric locking as $v = 0.5$. In addition, these terms enable the element to capture transverse strains which occurs in a beam or plate in bending. The plane strain expressions are used since this prevents incompatibility of the velocity associated with the assumed strains.

Incompressible or Quasi-incompressible Cases

Flag for new solid element: I_{cpre} =1,2,3

For incompressible or quasi- incompressible materials, the new solid elements have no volume locking problem due to the assumed strain. Another way to deal with this problem is to decompose the stress field into the spherical part and the deviatory part and use reduced integration for spherical part so that the pressure is constant. This method has the advantage on the computation time, especially for the full integrated element. For some materials which the incompressibility can be changed during computation (for example: elastoplastic material, which becomes incompressible as the growth of plasticity), the treatment is more complicated. Since the elastoplastic material with large strain is the most frequently used, the constant pressure method has been chosen for Radioss usual solid elements. The flag I_{cpre} has been introduced for new solid elements.

$\boldsymbol{I_{cpre}}$

=0
Assumed strain with v terms is used.

=1
Assumed strain without v terms and with a constant pressure method is used. The method is recommended for incompressible (initial) materials.

=2
Assumed strain with v terms is used, where v is variable in function of the plasticity state. The formulation is recommended for elastoplastic materials.

=3
Assumed strain with v terms is used.

Internal Force Calculation

Internal forces are computed using the generalized relation:

$$f_{iI}^{\text{int}} = \int_{\Omega} \sigma_{ij} \frac{\partial \Phi_I}{\partial x_j} d\Omega \tag{322}$$

However, to increase the computational speed of the process, some simplifications are applied.

Reduced Integration Method

This is the default method for computing internal forces. A one point integration scheme with constant stress in the element is used. Due to the nature of the shape functions, the amount of computation can be substantially reduced:

$$\frac{\partial \Phi_1}{\partial x_j} = -\frac{\partial \Phi_7}{\partial x_j}; \quad \frac{\partial \Phi_2}{\partial x_j} = -\frac{\partial \Phi_8}{\partial x_j}; \quad \frac{\partial \Phi_3}{\partial x_j} = -\frac{\partial \Phi_5}{\partial x_j}; \quad \frac{\partial \Phi_4}{\partial x_j} = -\frac{\partial \Phi_6}{\partial x_j} \tag{323}$$

Hence, the value $\frac{\partial \Phi_I}{\partial x_j}$ is taken at the integration point and the internal force is computed using the relation:

$$F_{iI} = \sigma_{ij} \left(\frac{\partial \Phi_I}{\partial x_j} \right)_0 \Omega \tag{324}$$

The force calculation is exact for the special case of the element being a parallelepiped.

[23] Belytschko T. and Bachrach W.E., "Efficient implementation of quadrilaterals with high coarse-mesh accuracy", Computer Methods in Applied Mechanics and Engineering, 54:279-301, 1986.

[24] Belytschko Ted and Bindeman Lee P., "Assumed strain stabilization of the eight node hexahedral element", Computer Methods in Applied Mechanics and Engineering, vol.105, 225-260, 1993.

Full Integration Method

The final approach that can be used is the full generalized formulation found in Equation 322. A classical eight point integration scheme, with non-constant stress, but constant pressure is used to avoid locking problems. This is computationally expensive, having eight deviatoric stress tensors, but will produce accurate results with no hourglass.

When assumed strains are used with full integration (HA8 element), the reduced integration of pressure is no more necessary, as the assumed strain is then a free locking problem.

ALE Improved Integration Method

This is an ALE method for computing internal forces (flag *INTEG*). A constant stress in the element is used.

The value $\int_{\Omega} \frac{\partial \Phi_I}{\partial x_j} d\Omega$ is computed with Gauss points.

Hourglass Modes

Hourglass modes are element distortions that have zero strain energy. Thus, no stresses are created within the element. There are 12 hourglass modes for a brick element, 4 modes for each of the 3 coordinate directions. Γ represents the hourglass mode vector, as defined by Flanagan-Belytschko. [25] They produce linear strain modes, which cannot be accounted for using a standard one point integration scheme.

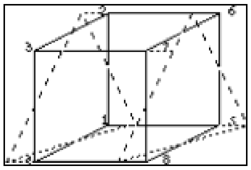

Figure 19:

$$\Gamma^1 = (+1, -1, +1, -1, +1, -1, +1, -1)$$

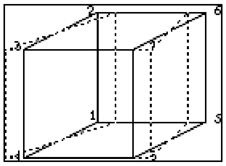

Figure 20:

$$\Gamma^2 = (+1, +1, -1, -1, -1, -1, +1, +1)$$

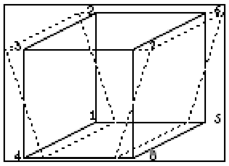

Figure 21:

$$\Gamma^{3} = \left(+1,\ -1,\ -1,\ +1,\ -1,\ +1,\ +1,\ -1\right)$$

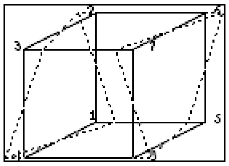

Figure 22:

$$\Gamma^{4} = \left(+1,\ -1,\ +1,\ -1,\ -1,\ +1,\ -1,\ +1\right)$$

To correct this phenomenon, it is necessary to introduce anti-hourglass forces and moments. Two possible formulations are presented hereafter.

Kosloff and Frasier Formulation

The Kosloff-Frasier hourglass formulation [26] uses a simplified hourglass vector. The hourglass velocity rates are defined as:

$$\frac{\partial q_i^{\alpha}}{\partial t} = \sum_{I=1}^{8} \Gamma_I^{\alpha} \cdot v_{iI} \tag{325}$$

Where,

Γ	Non-orthogonal hourglass mode shape vector
v	Node velocity vector
i	Direction index, running from 1 to 3
I	Node index, from 1 to 8
α	Hourglass mode index, from 1 to 4

This vector is not perfectly orthogonal to the rigid body and deformation modes.

All hourglass formulations except the physical stabilization formulation for solid elements in Radioss use a viscous damping technique. This allows the hourglass resisting forces to be given by:

$$f_{iI}^{hgr} = \frac{1}{4} \rho c h \left(\sqrt[3]{\Omega}\right)^{2} \sum_{\alpha} \frac{\partial q_i^{\alpha}}{\partial t} \cdot \Gamma_I^{\alpha} \tag{326}$$

Where,

ρ	Material density
c	Sound speed
h	Dimensional scaling coefficient defined in the input
Ω	Volume

Flanagan-Belytschko Formulation

In the Kosloff-Frasier formulation seen in Kosloff and Frasier Formulation, the hourglass base vector Γ_I^α is not perfectly orthogonal to the rigid body and deformation modes that are taken into account by the one point integration scheme. The mean stress/strain formulation of a one point integration scheme only considers a fully linear velocity field, so that the physical element modes generally contribute to the hourglass energy. To avoid this, the idea in the Flanagan-Belytschko formulation is to build an hourglass velocity field which always remains orthogonal to the physical element modes. This can be written as:

$$v_{iI}^{Hour} = v_{iI} - v_{iI}^{Lin} \tag{327}$$

The linear portion of the velocity field can be expanded to give:

$$v_{iI}^{Hour} = v_{iI} - \left(\overline{v_{iI}} + \frac{\partial v_{iI}}{\partial x_j} \cdot \left(x_j - \overline{x_j} \right) \right) \tag{328}$$

Decomposition on the hourglass vectors base gives [25]:

$$\frac{\partial q_i^\alpha}{\partial t} = \Gamma_I^\alpha \cdot v_{iI}^{Hour} = \left(v_{iI} - \frac{\partial v_{il}}{\partial x_j} \cdot x_j \right) \cdot \Gamma_I^\alpha \tag{329}$$

Where,

$\frac{\partial q_i^\alpha}{\partial t}$	Hourglass modal velocities
Γ_I^α	Hourglass vectors base

Remembering that $\frac{\partial v_i}{\partial x_j} = \frac{\partial \Phi_j}{\partial x_j} \cdot v_{iJ}$ and factorizing Equation 329 gives:

$$\frac{\partial q_i^\alpha}{\partial t} = v_{iI} \cdot \left(\Gamma_I^\alpha - \frac{\partial \Phi_j}{\partial x_j} x_j \Gamma_I^\alpha \right) \tag{330}$$

$$\gamma_I^\alpha = \Gamma_I^\alpha - \frac{\partial \Phi_j}{\partial x_j} x_j \Gamma_J^\alpha \tag{331}$$

is the hourglass shape vector used in place of Γ_I^α in Equation 326.

Physical Hourglass Formulation

You also try to decompose the internal force vector as:

$$\left\{f_I^{\text{int}}\right\} = \left\{\left(f_I^{\text{int}}\right)^0\right\} + \left\{\left(f_I^{\text{int}}\right)^H\right\} \tag{332}$$

In elastic case, you have:

$$\begin{aligned}\left\{f_I^{\text{int}}\right\} &= \int_\Omega [B_I]^t [C] \sum_{j=1}^{8} [B_J] \{v^J\} d\Omega \\ &= \int_\Omega \left([B_I]^0 + [\bar{B}_I]^H\right)^t [C] \sum_{j=1}^{8} \left([B_J]^0 + [\bar{B}_J]^H\right) \{v^J\} d\Omega\end{aligned} \tag{333}$$

The constant part $\left\{\left(f_I^{\text{int}}\right)^0\right\} = \int_\Omega \left([B_I]^0\right)^t [C] \sum_{j=1}^{8} [B_J]^0 \{v^J\} d\Omega$ is evaluated at the quadrature point just like other one-point integration formulations mentioned before, and the non-constant part (Hourglass) will be calculated as:

Taking the simplification of $\frac{\partial x_i}{\partial \xi_j} = 0; (i \neq j)$(that is the Jacobian matrix of Strain Rate, Equation 311 is diagonal), you have:

$$\left(f_{iI}^{\text{int}}\right)^H = \sum_{\alpha=1}^{4} Q_{i\alpha} \gamma_I^\alpha \tag{334}$$

with 12 generalized hourglass stress rates $\dot{Q}_{i\alpha}$ calculated by:

$$\begin{aligned}\dot{Q}_{ii} &= \mu\left[\left(H_{jj} + H_{kk}\right)\dot{q}_i^i + H_{ij}\dot{q}_j^j + H_{ik}\dot{q}_k^k\right] \\ \dot{Q}_{jj} &= \mu\left[\frac{1}{1-v} H_{ii}\dot{q}_i^j + \bar{v} H_{ij}\dot{q}_j^i\right] \\ \dot{Q}_{i4} &= 2\mu\frac{1+v}{3} H_{ii}\dot{q}_j^4\end{aligned} \tag{335}$$

and

$$\begin{aligned}H_{ii} &= \int_\Omega \left(\frac{\partial \phi_j}{\partial x_i}\right)^2 d\Omega = \int_\Omega \left(\frac{\partial \phi_k}{\partial x_i}\right)^2 d\Omega = 3\int_\Omega \left(\frac{\partial \phi_4}{\partial x_i}\right)^2 d\Omega \\ H_{ij} &= \int_\Omega \frac{\partial \phi_i}{\partial x_j}\frac{\partial \phi_j}{\partial x_i} d\Omega\end{aligned} \tag{336}$$

Where, i, j, k are permuted between 1 to 3 and $\dot{q}_i^\alpha$ has the same definition than in Equation 330.

Extension to nonlinear materials has been done simply by replacing shear modulus μ by its effective tangent values which is evaluated at the quadrature point. For the usual elastoplastic materials, use a more sophistic procedure which is described in Advanced Elasto-plastic Hourglass Control.

Advanced Elasto-plastic Hourglass Control

With one-point integration formulation, if the non-constant part follows exactly the state of constant part for the case of elasto-plastic calculation, the plasticity will be under-estimated due to the fact that the constant equivalent stress is often the smallest one in the element and element will be stiffer. Therefore, defining a yield criterion for the non-constant part seems to be a good idea to overcome this drawback.

Plastic yield criterion

The von Mises type of criterion is written by:

$$f = \sigma_{eq}^2(\xi, \eta, \zeta) - \sigma_y^2 = 0 \tag{337}$$

for any point in the solid element, where σ_y is evaluated at the quadrature point.

As only one criterion is used for the non-constant part, two choices are possible:

1. taking the mean value, that is, $f = f(\bar{\sigma}_{eq}); \bar{\sigma}_{eq} = \frac{1}{\Omega}\int_{\Omega} \sigma_{eq} d\Omega$
2. taking the value by some representative points, for example: eight Gauss points

The second choice has been used in this element.

Elastro-plastic hourglass stress calculation

The incremental hourglass stress is computed by:

- Elastic increment

$$(\sigma_i)_{n+1}^{trH} = (\sigma_i)_n^H + [C]\{\dot{\varepsilon}\}^H \Delta t$$

- Check the yield criterion
- If $f \geq 0$, the hourglass stress correction will be done by un radial return

$$(\sigma_i)_{n+1}^H = P\left((\sigma_i)_{n+1}^{trH}, f\right)$$

Stability

The stability of the numerical algorithm depends on the size of the time step used for time integration . For brick elements, Radioss uses the following equation to calculate the size of the time step:

$$h \leq k \frac{l}{c\left(\alpha + \sqrt{\alpha^2 + 1}\right)} \tag{338}$$

This is the same form as the Courant condition for damped materials. The characteristic length of a particular element is computed using:

[25] Flanagan D. and Belytschko T., "A Uniform Strain Hexahedron and Quadrilateral with Orthogonal Hourglass Control", Int. Journal Num. Methods in Engineering, 17 679-706, 1981.

[26] Kosloff D. and Frazier G., "Treatment of hourglass pattern in low order finite element code", International Journal for Numerical and Analytical Methods in Geomechanics, 1978.

$$l = \frac{Element\ Volume}{Largest\ Side\ Surface} \tag{339}$$

For a 6-sided brick, this length is equal to the smallest distance between two opposite faces.

The terms inside the parentheses in the denominator are specific values for the damping of the material:

- $\alpha = \frac{2v}{\rho c l}$
- v effective kinematic viscosity
- $c = \sqrt{\frac{1 \partial p}{\rho \partial \rho}}$ for fluid materials
- $c = \sqrt{\frac{K}{\rho} + \frac{4}{3}\frac{\mu}{\rho}} = \sqrt{\frac{\lambda + 2\mu}{\rho}}$ for a solid elastic material
- K is the bulk modulus
- λ, μ are Lame moduli

The scaling factor $k = 0.90$, is used to prevent strange results that may occur when the time step is equal to the Courant condition. This value can be altered by the user.

Shock Waves

Shocks are non-isentropic phenomena, that is, entropy is not conserved, and necessitates a special formulation.

The missing energy is generated by an artificial bulk viscosity q as derived by von Neumann and Richtmeyer. [27] This value is added to the pressure and is computed by:

$$q = q_a 2\rho l^2 \left(\frac{\partial \varepsilon_{kk}}{\partial t}\right)^2 - q_b \rho l c \frac{\partial \varepsilon_{kk}}{\partial t} \tag{340}$$

Where,

l	Is equal to $\sqrt[3]{\Omega}$ or to the characteristic length
Ω	Volume
$\frac{\partial \varepsilon_{kk}}{\partial t}$	Volumetric compression strain rate tensor
c	Speed of sound in the medium

The values of q_a and q_b are adimensional scalar factors defined as:

- q_a is a scalar factor on the quadratic viscosity to be adjusted so that the Hugoniot equations are verified. This value is defined by the user. The default value is 1.10.
- q_b is a scalar factor on the linear viscosity that damps out the oscillations behind the shock. This is user specified. The default value is 0.05.

Default values are adapted for velocities lower than Mach 2. However, for viscoelastic materials (LAW34, LAW35, LAW38) or honeycomb (LAW28), very small values are recommended, that is, 10^{-20}.

Element Degeneration

Element degeneration is the collapsing of an element by one or more edges. For example: making an eight node element into a seven node element by giving nodes 7 and 8 the same node number.

The use of degenerated elements for fluid applications is not recommended. The use of degenerated elements for assumed strain formulation is not recommended. If they cannot be avoided, any two nodes belonging to a same edge can be collapsed, with examples shown below.

For solid elements, it is recommended that element symmetry be maintained.

For 4 node elements, it is recommended that the special tetrahedron element be used.

Brick elements can be degenerated into other 3D solid elements by repeating nodes numbers in the *node_ID* input to combine brick corners to together to form another shape. The most common example is a triangular prism pentahedra element, as shown in the next two images but other shapes are shown if needed to connect a complex mesh.

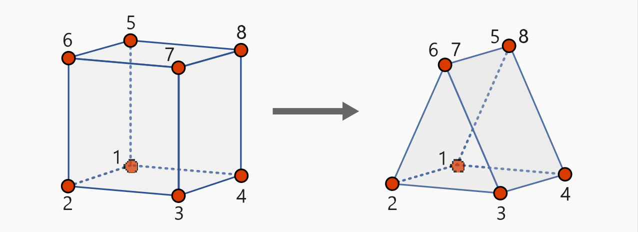

Connectivity:
1 2 3 4 5 6 7 8

Connectivity:
1 2 3 4 5 6 6 5
(7 = 6 and 8 = 5)

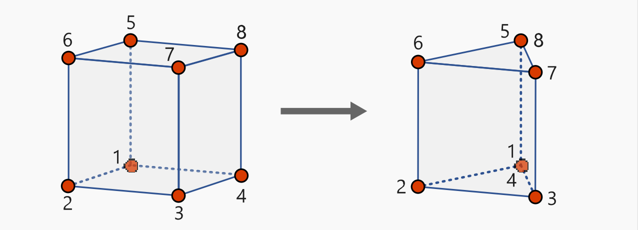

Connectivity:
1 2 3 4 5 6 7 8

Connectivity:
1 2 3 1 5 6 7 5
(4 = 1 and 8 = 5)

[27] Von Neumann J. and Richtmeyer R., “A method for the numerical calculation of hydrodynamical shocks”, Journal of applied physics, 1950.

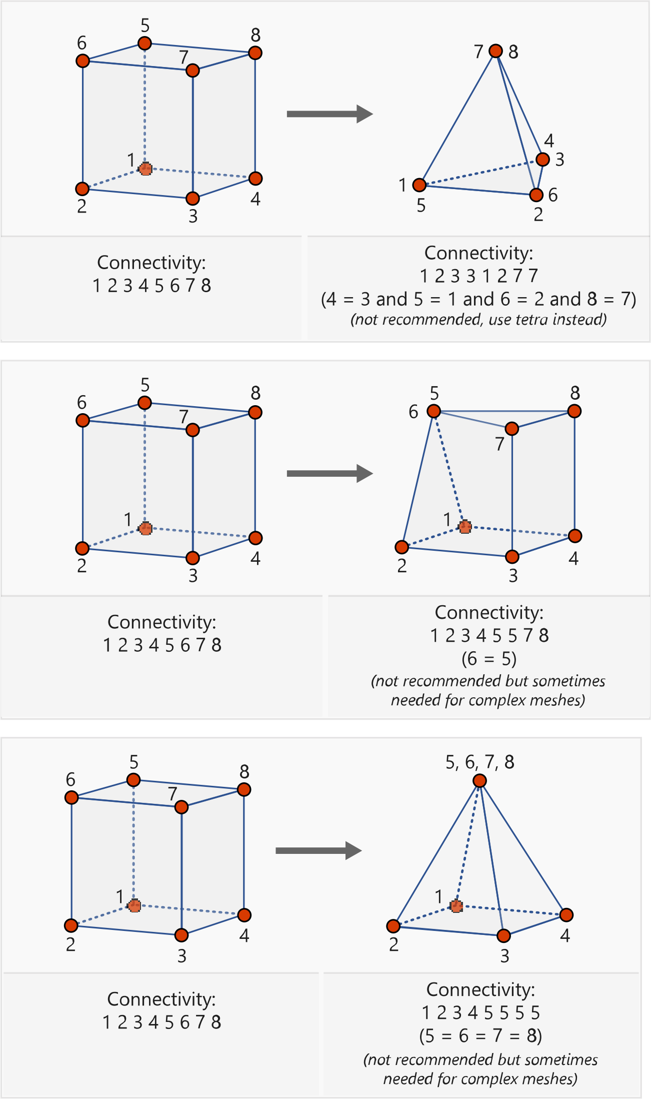

Figure 23: Degenerated 3D Solid Element Examples

Internal Stress Calculation

Global Formulation

The time integration of stresses has been stated earlier (Stress Rates) as:

$$\sigma_{ij}(t+\Delta t)=\sigma_{ij}(t)+\dot{\sigma}_{ij}\Delta t \tag{341}$$

The stress rate is comprised of two components:

$$\dot{\sigma}_{ij}=\dot{\sigma}_{ij}^{v}+\dot{\sigma}_{ij}^{r} \tag{342}$$

Where,

$\dot{\sigma}_{ij}^{r}$
Stress rate due to the rigid body rotational velocity

$\dot{\sigma}_{ij}^{v}$	Jaumann objective stress tensor derivative

The correction for stress rotation from time t to time $t+\Delta t$ is given by [28]:

$$\dot{\sigma}_{ij}^{r}=\sigma_{ik}\Omega_{kj}+\sigma_{jk}\Omega_{ki} \tag{343}$$

Where, Ω is the rigid body rotational velocity tensor (Kinematic Description, Equation 53).

The Jaumann objective stress tensor derivative $\dot{\sigma}_{ij}^{v}$ is the corrected true stress rate tensor without rotational effects. The constitutive law is directly applied to the Jaumann stress rate tensor.

Deviatoric stresses and pressure (Stresses in Solids) are computed separately and related by:

$$\sigma_{ij}=s_{ij}-p\delta_{ij} \tag{344}$$

Where,

s_{ij}	Deviatoric stress tensor
p	Pressure or mean stress - defined as positive in compression
δ_{ij}	Substitution tensor or unit matrix

Co-rotational Formulation

A co-rotational formulation for bricks is a formulation where rigid body rotations are directly computed from the element's node positions. Objective stress and strain tensors are computed in the local (co-rotational) frame. Internal forces are computed in the local frame and then rotated to the global system.

So, when co-rotational formulation is used, Deviatoric Stress Calculation, Equation 356 $\dot{\sigma}_{ij}=\dot{\sigma}_{ij}^{v}+\dot{\sigma}_{ij}^{r}$ reduces to:

$$\dot{\sigma}_{ij}=\dot{\sigma}_{ij}^{v} \tag{345}$$

Where,

$\dot{\sigma}_{ij}^{v}$	Jaumann objective stress tensor derivative expressed in the co-rotational frame

Figure 24 orthogonalization, when one of the r, s, t directions is orthogonal to the two other directions.

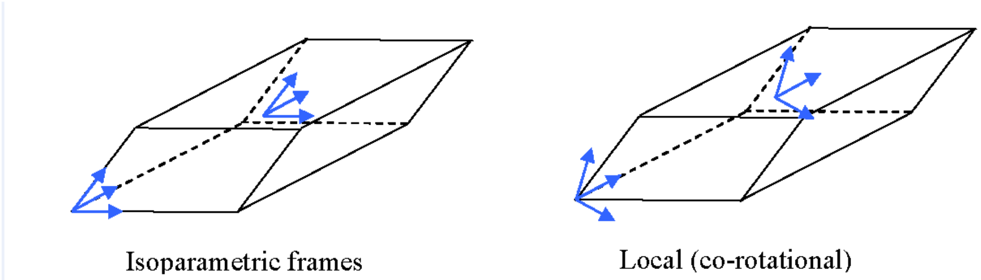

Figure 24:

When large rotations occur, this formulation is more accurate than the global formulation, for which the stress rotation due to rigid body rotational velocity is computed in an incremental way.

Co-rotational formulation avoids this kind of problem. Consider this test:

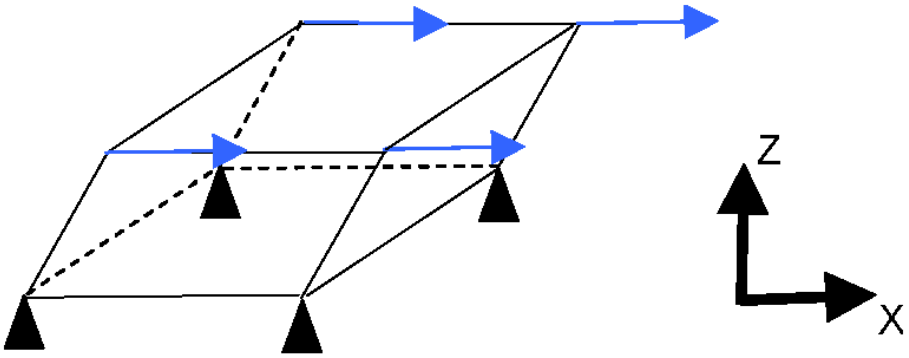

Figure 25:

The increment of the rigid body rotation vector during time step Δt is:

$$\Delta\Omega = \Delta t \Big/ 2 \cdot \begin{cases} \left(\partial v_x / \partial y - \partial v_y / \partial x\right) = 0 \\ \left(\partial v_x / \partial z - \partial v_z / \partial x\right) = \partial v_x \, \rule[0.5ex]{10em}{0.8pt} \, \partial z \\ \left(\partial v_y / \partial x - \partial v_x / \partial y\right) = 0 \end{cases} \tag{346}$$

So, $\Delta\Omega_y = \alpha\Delta T / 2$

Where, $\alpha = v / h$ equals the imposed velocity on the top of the brick divided by the height of the brick (constant value).

Due to first order approximation, the increment of stress σ_{xx} due to the rigid body motion is:

$$\Delta\sigma_{xx}^r = \Delta\Omega_y\left(\tau_{xz} + \tau_{zx}\right) = 2\Delta\Omega_y\tau_{xz} = \alpha\Delta T\tau_{xz} \tag{347}$$

Increment of stress σ_{zz} due to the rigid body motion:

$$\Delta\sigma_{zz}^r = -\Delta\Omega_y\left(\tau_{xz} + \tau_{zx}\right) = -2\Delta\Omega_y\tau_{xz} = -\alpha\Delta T\tau_{xz} \tag{348}$$

Increment of shear stress τ_{xz} due to the rigid body motion:

$$\Delta\tau_{xz}^{r} = \Delta\Omega_y(\sigma_{zz} - \sigma_{xx}) = 2\Delta\Omega_y\sigma_{zz} = \alpha\Delta T\sigma_{zz} \tag{349}$$

Increment of shear strain:

$$\Delta\gamma_{xz} = \Delta T(\partial v_x / \partial z + \partial v_z / \partial x) = \alpha\Delta T \tag{350}$$

Increment of stress σ_{zz} due to strain:

$$\Delta\sigma_{zz}^{v} = 0 \tag{351}$$

and increment of shear stress due to strain is:

$$\Delta\tau_{xz}^{v} = G\Delta\gamma_{xz} = G\alpha\Delta T \tag{352}$$

Where, G is the shear modulus (material is linear elastic).

From Equation 348 to Equation 352, you have:

$$\begin{bmatrix} \Delta\tau_{xz} = \alpha\Delta T\sigma_{zz} + G\alpha\Delta T \\ \Delta\sigma_{zz} = -\alpha\Delta\tau_{xz} \end{bmatrix} \tag{353}$$

System Equation 353 leads to:

$$\Delta\tau_{xz} / \Delta T^2 = -\alpha^2\tau_{xz} \tag{354}$$

So, shear stress is sinusoidal and is not strictly increasing.

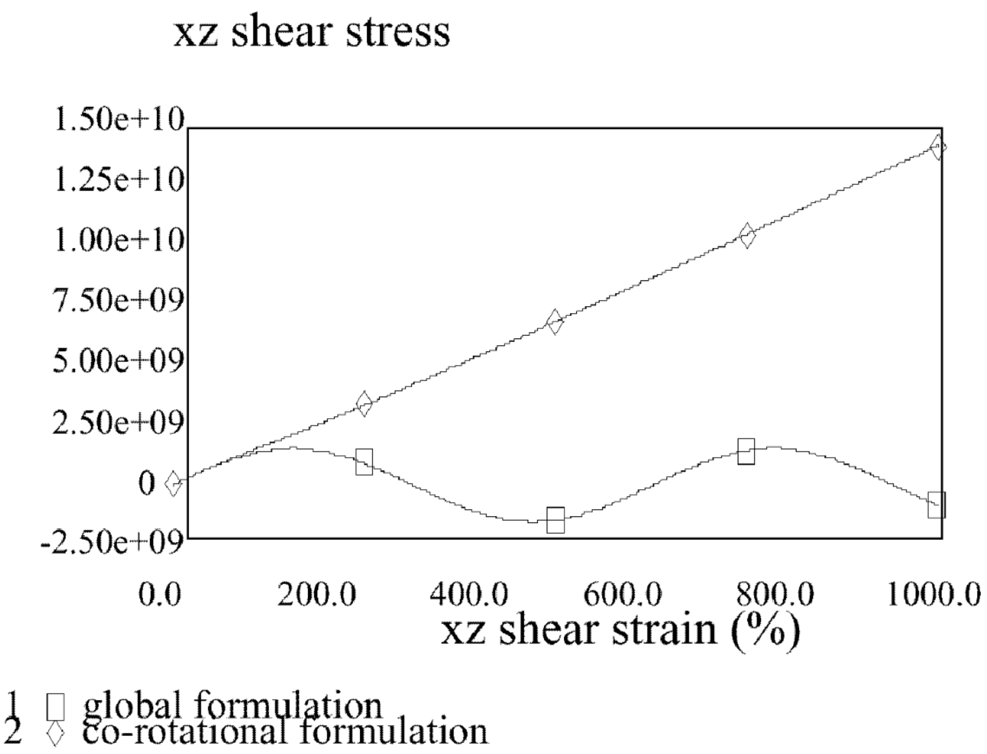

Figure 26:

So, it is recommended to use co-rotational formulation, especially for visco-elastic materials such as foams, even if this formulation is more time consuming than the global one.

Co-rotational Formulation and Orthotropic Material

When orthotropic material and global formulation are used, the fiber is attached to the first direction of the isoparametric frame and the fiber rotates a different way depending on the element numbering.

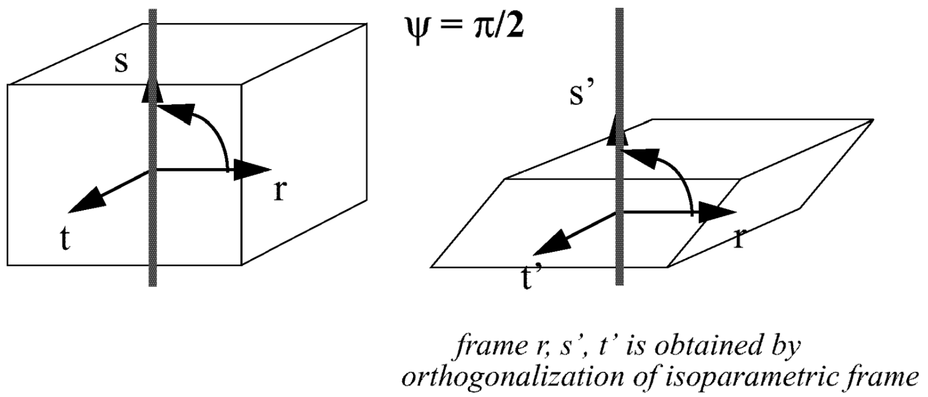
s
r
t
ψ = π/2
s'
r
t'
frame r, s', t' is obtained by
orthogonalization of isoparametric frame

Figure 27:

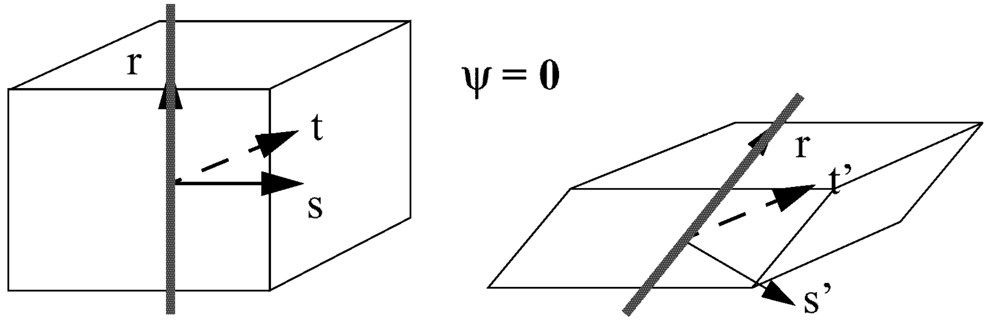

Figure 28:

On the other hand, when the co-rotational formulation is used, the orthotropic frame keeps the same orientation with respect to the local (co-rotating) frame, and is therefore also co-rotating.

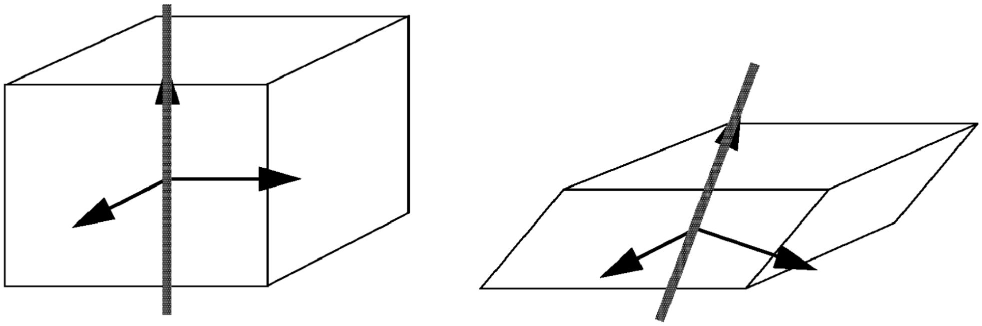

Figure 29:

Deviatoric Stress Calculation

With the stress being separated into deviatoric and pressure (hydrostatic) stress (Stresses in Solids), it is the deviatoric stress that is responsible for the plastic deformation of the material. The hydrostatic stress will either shrink or expand the volume uniformly, that is, with proportional change in shape. The determination of the deviatoric stress tensor and whether the material will plastically deform requires a number of steps.

Perform an Elastic Calculation

The deviatoric stress is time integrated from the previous known value using the strain rate to compute an elastic trial stress:

$$s_{ij}^{el}(t+\Delta t) = s_{ij}(t) + \dot{s}_{ij}^{r}\Delta t + 2G\left(\dot{\varepsilon}_{ij} - \frac{1}{3}\dot{\varepsilon}_{kk}\delta_{ij}\right)\Delta t \tag{355}$$

Where,

G Shear modulus

This relationship is Hooke's Law, where the strain rate is multiplied by time to give strain.

Compute von Mises Equivalent Stress and Current Yield Stress

Depending on the type of material being modeled, the method by which yielding or failure is determined will vary. The following explanation relates to an elastoplastic material (LAW2).

The von Mises equivalent stress relates a three dimensional state of stress back to a simple case of uniaxial tension where material properties for yield and plasticity are well known and easily computed.

The von Mises stress, which is strain rate dependent, is calculated using the equation:

$$\sigma_{vm}^{e} = \sqrt{\frac{3}{2}s_{ij}^{el}s_{ij}^{el}} \tag{356}$$

The flow stress is calculated from the previous plastic strain:

[28] Wilkins M., "Calculation of elastic plastic flow" LLNL, University of California UCRL-7322, 1981.

$$\sigma_y(t) = a + b\varepsilon^{p^n}(t) \tag{357}$$

For material laws 3, 4, 10, 21, 22, 23 and 36, Equation 357 is modified according to the different modeling of the material curves.

Plasticity Check

The state of the deformation must be checked.

$$\sigma_{vm}^e - \sigma_y \leq 0 \tag{358}$$

If this equation is satisfied, the state of stress is elastic. Otherwise, the flow stress has been exceeded and a plasticity rule must be used (Figure 30).

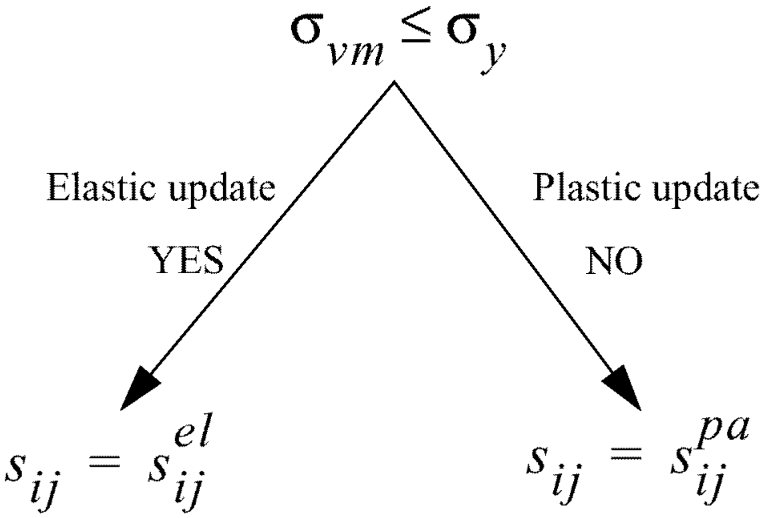

Figure 30: Plasticity Check

The plasticity algorithm used is due to Mendelson. [29]

Compute Hardening Parameter

The hardening parameter is defined as the slope of the strain-hardening part of the stress-strain curve:

$$H = \frac{d\sigma_y}{d\varepsilon^p} \tag{359}$$

This is used to compute the plastic strain at time t:

$$\dot{\varepsilon}^p \Delta t = \frac{\sigma_{vm} - \sigma_y}{3G + H} \tag{360}$$

This plastic strain is time integrated to determine the plastic strain at time $t + \Delta t$:

$$\varepsilon^p(t + \Delta t) = \varepsilon^p(t) + \dot{\varepsilon}^p \Delta t \tag{361}$$

The new flow stress is found using:

$$\sigma_y(t+\Delta t) = a + b\varepsilon^{p^n}(t+\Delta t) \tag{362}$$

Radial Return

There are many possible methods for obtaining s_{ij}^{pa} from the trial stress. The most popular method involves a simple projection to the nearest point on the flow surface, which results in the radial return method.

The radial return calculation is given in Equation 363. Figure 31 is a graphic representation of radial return.

$$s_{ij}^{pa} = \frac{\sigma_y}{\sigma_{vm}} s_{ij}^{el} \tag{363}$$

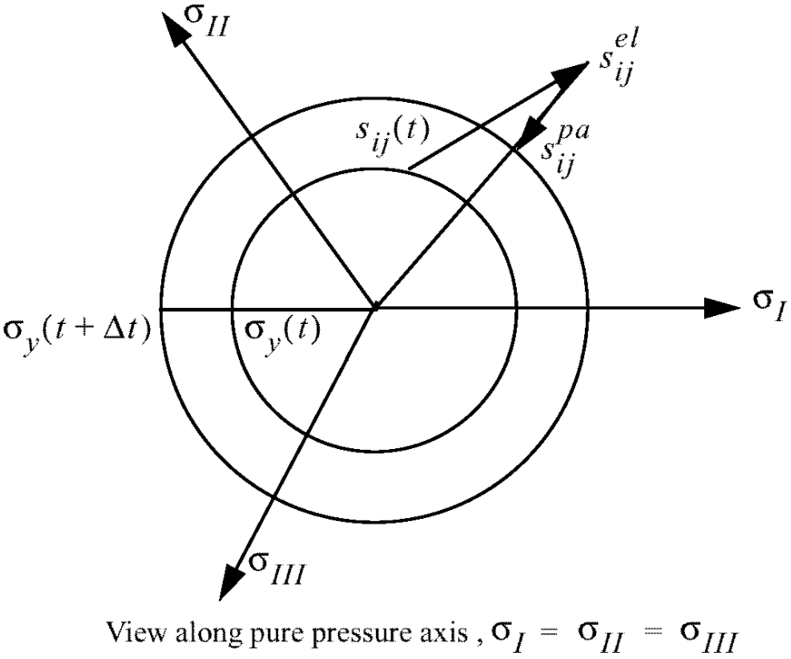

Figure 31: Radial Return

29. Mendelson A., "Plasticity: Theory and Application", MacMillan Co., New York, 1968.

Solid Tetrahedron Elements

4-Node Solid Tetrahedron

The Radioss solid tetrahedron element is a 4 node element with one integration point and a linear shape function.

This element has no hourglass. But the drawbacks are the low convergence and the shear locking.

10-Node Solid Tetrahedron

The Radioss solid tetrahedron element is a 10 nodes element with 4 integration points and a quadratic shape function as shown in Figure 32.

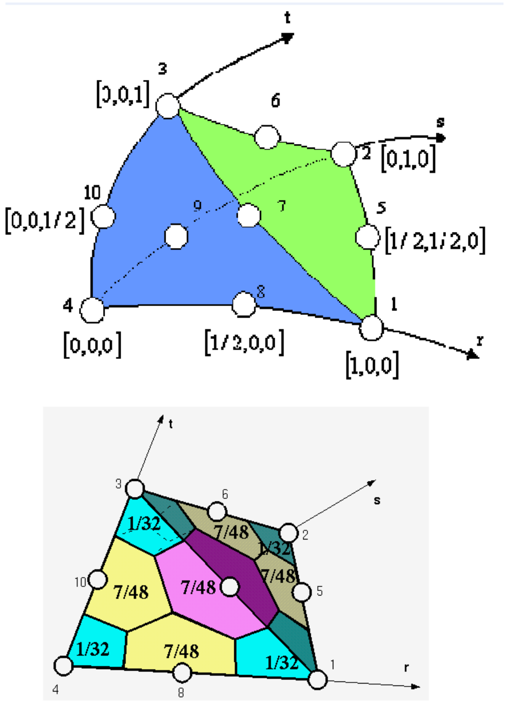

Figure 32: (a) Isoparametric 10 Node Tetrahedron; (b) Nodal Mass Distribution

Introducing volume coordinates in an isoparametric frame:

$L_1 = r$

$L_2 = s$

$L_3 = t$

$L_4 = 1 - L_1 - L_2 - L_3$

The shape functions are expressed by:

$$\Phi_1 = (2L_1 - 1)L_1 \tag{364}$$

$$\Phi_2 = (2L_2 - 1)L_2 \tag{365}$$

$$\Phi_3 = (2L_3 - 1)L_3 \tag{366}$$

$$\Phi_4 = (2L_4 - 1)L_4 \tag{367}$$

$$\Phi_5 = 4L_1L_2 \tag{368}$$

$$\Phi_6 = 4L_2L_3 \tag{369}$$

$$\Phi_7 = 4L_3L_1 \tag{370}$$

$$\Phi_8 = 4L_1L_4 \tag{371}$$

$$\Phi_9 = 4L_2L_4 \tag{372}$$

$$\Phi_{10} = 4L_3L_4 \tag{373}$$

Location of the 4 integration points is expressed by [30].

	L_1	L_2	L_3	L_4
a	ɑ	β	β	β
b	β	ɑ	β	β
c	β	β	ɑ	β
d	β	β	β	ɑ

With,

$\alpha = 0 \cdot 58541020$ and $\beta = 0 \cdot 13819660$.

a, b, c, and d are the 4 integration points.

Advantages and Limitations

This element has various advantages:

- No hourglass
- Compatible with powerful mesh generators
- Fast convergence
- No shear locking.

But there are some drawbacks too:

- Low time step
- Not compatible with ALE formulation

Time Step

The time step for a regular tetrahedron is computed as:

$$dt = \frac{L_c}{c} \tag{374}$$

Where, L_c is the characteristic length of element depending on tetra type. The different types are:

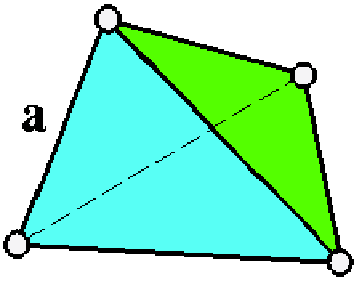

Figure 33: Regular 4 Nodes Tetra

$$L_c = a\sqrt{\frac{2}{3}}\,; L_c = 0.816a \tag{375}$$

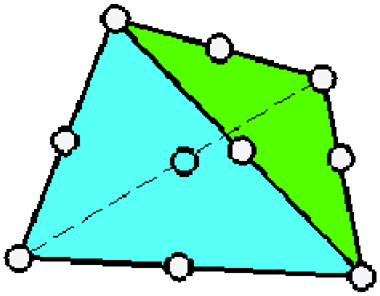

Figure 34: Regular 10 Nodes Tetra

$$L_c = a\sqrt{\frac{5/2}{6}}\,; L_c = 0.264a \tag{376}$$

For another regular tetra obtained by the assemblage of four hexa as shown in Figure 35, the characteristic length is:

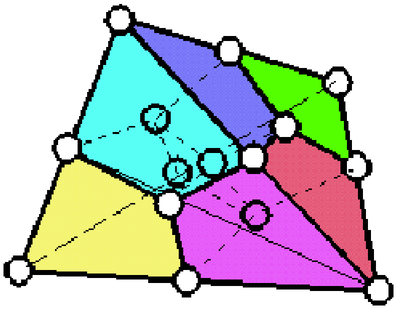

Figure 35: Other Regular Tetra

$$L_c = a\frac{\sqrt{2/3}}{4}; L_c = 0.204a \tag{377}$$

CPU Cost and Time/Element/Cycle

The CPU cost is shown in Figure 36:

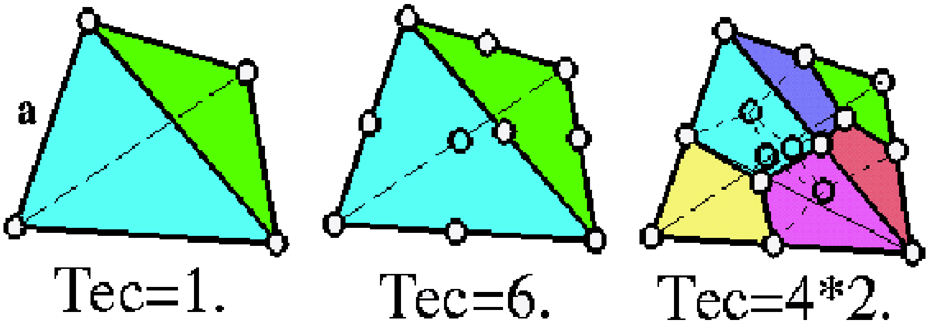

Figure 36: CPU Cost in TEC

Example: Comparison

Below is a comparison of the 3 types of elements (8-nodes brick, 10-nodes tetra and 20-nodes brick). The results are shown in Figure 37 for a plastic strain contour.

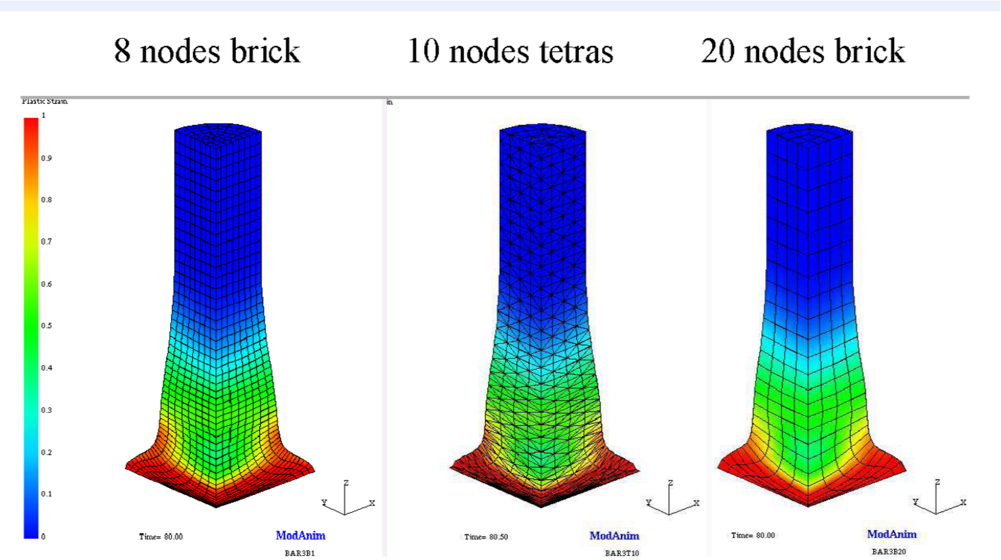

Figure 37: Comparison (plastic strain max = 60%)

[30] Hammet P.C., Marlowe O.P. and Stroud A.H., "Numerical integration over simplexes and cones", Math. Tables Aids Comp, 10, 130-7, 1956.

Shell Elements

Since the degenerated continuum shell element formulation was introduced by Ahmad et al. [31], it has become dominant in commercial Finite Element codes due to its advantage of being independent of any particular shell theory, versatile and cost effective, and applicable in a reliable manner to both thin and thick shells.

In the standard 4-node shell element, full integration and reduced integration schemes have been used to compute the stiffness matrices and force vectors:

- The full integration scheme is often used in programs for static or dynamic problems with implicit time integration. It presents no problem for stability, but sometimes involves "locking" and computations are often more expensive.
- The reduced integration scheme, especially with one-point quadrature (in the mid-surface), is widely used in programs with explicit time integration such as Radioss and other programs applied essentially in crashworthiness studies. These elements dramatically decrease the computation time, and are very competitive if the hourglass modes (which result from the reduced integration scheme) are "well" stabilized.

Shell Elements Overview

The historical shell element in Radioss is a simple bilinear Mindlin plate element coupled with a reduced integration scheme using one integration point. It is applicable in a reliable manner to both thin and moderately thick shells.

This element is very efficient if the spurious singular modes, called "*hourglass modes*", which result from the reduced integration are stabilized.

The stabilization approach consists of providing additional stiffness so that the spurious singular modes are suppressed. Also, it offers the possibility of avoiding some locking problems. One of the first solutions was to generalize the formulation of Kosloff and Frazier [32] for brick element to shell element. It can be shown that the element produces accurate flexural response (thus, free from the membrane shear locking) and is equivalent to the incompatible model element of Wilson et al. [33] without the static condensation procedure. Taylor [34] extended this work to shell elements. Hughes and Liu [35] employed a similar approach and extended it to nonlinear problems.

Belytschko and Tsay [36] developed a stabilized flat element based on the γ projections developed by Flanagan and Belytschko [37]. Its essential feature is that hourglass control is orthogonal to any linear field, thus preserving consistency. The stabilized stiffness is approached by a diagonal matrix and scaled by the perturbation parameters h_i which are introduced as a regulator of the stiffness for nonlinear problems. The parameters h_i are generally chosen to be as small as possible, so this approach is often called, *perturbation stabilization*.

The elements with perturbation stabilization have two major drawbacks:

- The parameters h_i are user-inputs and are generally problem-dependent.

[31] Ahmad S., Irons B.M., and Zienkiewicz O.C., "Analysis of thick and thin shell structures by curved finite elements", Computer Methods in Applied Mechanics and Engineering, 2:419-451, 1970.

- Poor behavior with irregular geometries (in-plane, out-of-plane). The stabilized stiffness (or stabilized forces) is often evaluated based on a regular flat geometry, so they generally do not pass either the Patch-test or the Twisted beam test.

Belytschko [38] extended this perturbation stabilization to the 4-node shell element which has become widely used in explicit programs.

Belytschko [39] improved the poor behavior exhibited in the warped configuration by adding a coupling curvature-translation term, and a particular nodal projection for the transverse shear calculation analogous to that developed by Hughes and Tezduyar [37], and MacNeal [41]. This element passes the Kirchhoff patch test and the Twisted Beam test, but it cannot be extended to a general 6 DOF element due to the particular projection.

Belytschko and Bachrach [42] used a new method called *physical stabilization* to overcome the first drawback of the quadrilateral plane element. This method consists of explicitly evaluating the stabilized stiffness with the help of 'assumed strains', so that no arbitrary parameters need to be prescribed. Engelmann and Whirley [43] have applied it to the 4-node shell element. An alternative way to evaluate the stabilized stiffness explicitly is given by Liu et al. [44] based on Hughes and Liu's 4-node selected reduced integration scheme element [35], in which the strain field is expressed explicitly in terms of natural coordinates by a Taylor-series expansion. A remarkable improvement in the one-point quadrature shell element with physical stabilization has been performed by Belytschko and Leviathan [45]. The element performs superbly for both flat and warped elements especially in linear cases, even in comparison with a similar element under a full integration scheme, and is only 20% slower than the Belytschko and Tsay element. More recently, based on Belytschko and Leviathan's element, Zhu and Zacharia [46] implemented the drilling rotation DOF in their one-point quadrature shell element; the drilling rotation is independently interpolated by the Allman function [47] based on Hughes and Brezzi's [48] mixed variational formulation.

The physical stabilization with assumed strain method seems to offer a rational way of developing a cost effective shell element with a reduced integration scheme. The use of the assumed strains based on the mixed variational principles, is powerful, not only in avoiding the locking problems (volumetric locking, membrane shear locking, as in Belytschko and Bindeman [49]; transverse shear locking, as in Dvorkin and Bathe [50]), but also in providing a new way to compute stiffness. However, as highlighted by Stolarski et al. [51], assumed strain elements generally do not have rigorous foundations; there is almost no constraint for the independent assumed strains interpolation. Therefore, a sound theoretical understanding and numerous tests are needed in order to prove the legitimacy of the assumed strain elements.

The greatest uncertainty of the one-point quadrature shell elements with physical stabilization is with respect to the nonlinear problems. All of these elements with physical stabilization mentioned above rely on the assumptions that the spin and the material properties are constant within the element. The first assumption is necessary to ensure the objectivity principle in geometrical nonlinear problems. The second was adapted in order to extend the explicit evaluation of stabilized stiffness for elastic problems to the physical nonlinear problems. It is found that the second assumption leads to a theoretical contradiction in the case of an elastoplastic problem (a classic physical nonlinear problem), and results in poor behavior in case of certain crash computations.

Zeng and Combescure [52] have proposed an improved 4-node shell element named QPPS with one-point quadrature based on the physical stabilization which is valid for the whole range of its applications (see Shell Formulations). The formulation is based largely on that of Belytschko and Leviathan.

Based on the QPPS element, Zeng and Winkelmuller have developed a new improved element named QEPH which is integrated in Radioss 44 version (see 3-Node Shell Elements).

[32] Kosloff D. and Frazier G., “Treatment of hourglass pattern in low order finite element code”, International Journal for Numerical and Analytical Methods in Geomechanics, 1978.

[33] Wilson L.T., “Incompatible displacement models”, page 43. Academi Press, New York, 1973.

[34] Taylor R.L., “Finite element for general shell analysis”, 1979.

[35] Hughes T.J.R. and Liu W.K., “Nonlinear finite element analysis of shells: Part I: Three-dimensional shells”, Computer Methods in Applied Mechanics and Engineering, 26:331-362, 1981.

[36] Belytschko T. and Tsay C.S., “A stabilization procedure for the quadrilateral plate element with one-point quadrature”, Computer Methods in Applied Mechanics and Engineering, 55:259-300, 1986.

[37] Flanagan D. and Belytschko T., “A Uniform Strain Hexahedron and Quadrilateral with Orthogonal Hourglass Control”, Int. Journal Num. Methods in Engineering, 17 679-706, 1981.

[38] Belytschko T. and Leviathan I., “Physical stabilization of the 4-node shell element with one-point quadrature”, Computer Methods in Applied Mechanics and Engineering, 113:321-350, 1992.

[39] Belytschko T., Wong B.L. and Chiang H.Y. “Advances in one-point quadrature shell elements”, Computer Methods in Applied Mechanics and Engineering, 96:93-107, 1989.

[40] Hughes T.J.R. and Tezduyar T.E., “Finite elements based upon Mindlin plate theory with particular reference to the four-node bilinear isoparametric element”, J. of Applied Mechanics, 48:587-596, 1981.

[41] MacNeal R.H., “Derivation of element stiffness matrices by assumed strain distributions”, Nuclear Engrg. Des., 70:3-12, 1982.

[42] Belytschko T. and Bachrach W.E., “Efficient implementation of quadrilaterals with high coarse-mesh accuracy”, Computer Methods in Applied Mechanics and Engineering, 54:279-301, 1986.

[43] Engelmann B.E. and Whirley R.G., “A new elastoplastic shell element formulation for DYNA3D”, Report ugrl-jc-104826, Lawrence Livermore National Laboratory, 1990.

[44] Liu W.K., Law E.S., Lam D. and Belytschko T., “Resultant-stress degenerated-shell element”, Int. Journal Num. Methods in Engineering, 19:405-419, 1983.

[45] Belytschko T. and Leviathan I., “Projection schemes for one-point quadrature shell elements”, Computer Methods in Applied Mechanics and Engineering, 115:277-286, 1993.

[46] Zhu Y. and Zacharia T., “A new one-point quadrature, quadrilateral shell element with drilling degree of freedom”, Computer Methods in Applied Mechanics and Engineering, 136:165-203, 1996.

[47] Allman D.J., “A quadrilateral finite element including vertex rotations for plane elasticity problems”, Int. Journal Num. Methods in Engineering, 26:717-739, 1988.

[48] Hughes T.J.R. and Brezzi F., “On drilling degrees of freedom”, Computer Methods in Applied Mechanics and Engineering, 72:105-121, 1989.

[49] Belytschko T. and Bindeman L., “Assumed strain stabilization of the 4-node quadrilateral with 1-point quadrature for nonlinear problems”, Computer Methods in Applied Mechanics and Engineering, 88:311-340, 1991.

[50] Dvorkin E. and Bathe K.J. “A continuum mechanics four-node shell element for 35 general nonlinear analysis”, Engrg Comput, 1:77-88, 1984.

Bilinear Mindlin Plate Element

Most of the following explanation concerns four node plate elements, Figure 38. 3-Node Shell Elements explains the three node plate element, shown in Figure 39.

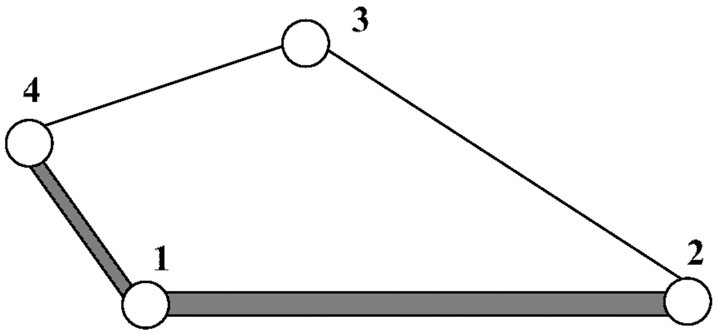

Figure 38: Four Node Plate Element

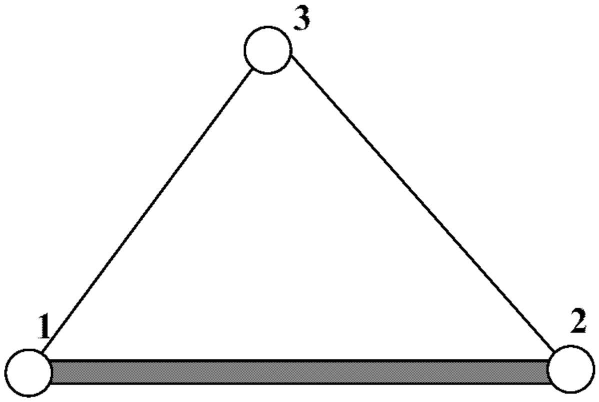

Figure 39: Three Node Plate Element

Plate theory assumes that one dimension (the thickness, z) of the structure is small compared to the other dimensions. Hence, the 3D continuum theory is reduced to a 2D theory. Nodal unknowns are the velocities (v_x, v_y, v_z) of the midplane and the nodal rotation rates $\left(\omega_x, \omega_y\right)$ as a consequence of the suppressed z direction. The thickness of elements can be kept constant, or allowed to be variable. This is user defined. The elements are always in a state of plane stress, that is $\sigma_{zz} = 0$, or there is no stress acting perpendicular to the plane of the element. A plane orthogonal to the midplane remains a plane, but not necessarily orthogonal as in Kirchhoff theory, (where $\varepsilon_{xz} = \varepsilon_{yz} = 0$) leading to the rotations rates $\omega_x = -\frac{\partial v_z}{\partial y}$ and $\omega_y = \frac{\partial v_z}{\partial x}$. In Mindlin plate theory, the rotations are independent variables.

[51] Stolarski H., Belytschko T. and Lee S.H., "A review of shell finite elements and corotational theories", Computational Mechanics Advances, 2:125-212, 1995.

[52] Zeng Q. and Combescure A., "A New One-point Quadrature, General Nonlinear Quadrilateral Shell Element with Physical Stabilization", Int. Journal Num. Methods in Engineering 42, 1307-1338, 1998.

Stability Time Step

The characteristic length, L, for computing the critical time step, referring back to Figure 40, is defined by:

$$L_1 = \frac{area}{\max\left(\overline{13}, \overline{42}\right)} \tag{378}$$

$$L_2 = \min\left(\overline{12}, \overline{23}, \overline{34}, \overline{41}, \overline{13}, \overline{42}\right) \tag{379}$$

$$L_c = \max\left(L_1, L_2\right) \tag{380}$$

When the orthogonalized mode of the hourglass perturbation formulation is used, the characteristic length is defined as:

$$L_3 = \max\left(L_1, L_2\right) \tag{381}$$

$$L_4 = 0.5\frac{\left(L_1 + L_2\right)}{\max\left(h_m, h_f\right)} \tag{382}$$

$$L_c = \min\left(L_3, L_4\right) \tag{383}$$

Where, h_m is the shell membrane hourglass coefficient and h_f is the shell out of plane hourglass coefficient, as mentioned in Hourglass Modes.

Local Reference Frame

Three coordinate systems are introduced in the formulation:

- Global Cartesian fixed system $X = \left(X\vec{i} + Y\vec{j} + Z\vec{k}\right)$
- Natural system $\left(\xi, \eta, \zeta\right)$, covariant axes x,y
- Local systems (x, y, z) defined by an orthogonal set of unit base vectors (t_1, t_2, n). n is taken to be normal to the mid-surface coinciding with ζ, and (t_1, t_2) are taken in the tangent plane of the mid-surface.

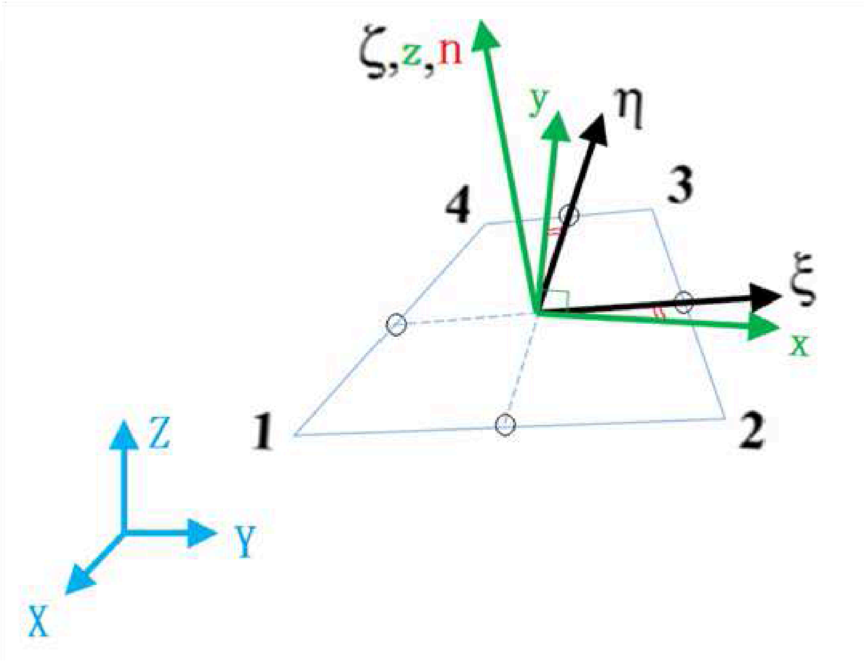

Figure 40: Local Reference Frame

The vector normal to the plane of the element at the mid point is defined as:

$$n = \frac{x \times y}{\| x \times y \|} \tag{384}$$

The vector defining the local direction is:

$$t_1 = \frac{x}{\| x \|} \tag{385}$$

Hence, the vector defining the local direction is found from the cross product of the two previous vectors:

$$t_2 = n \times t_1 \tag{386}$$

Bilinear Shape Functions

The shape functions defining the bilinear element used in the Mindlin plate are:

$$\Phi_I(\xi, \eta) = \frac{1}{4}(1 + \xi_I \xi)(1 + \eta_I \eta) \tag{387}$$

or, in terms of local coordinates:

$$\Phi_I(x, y) = a_I + b_I x + c_I y + d_I xy \tag{388}$$

It is also useful to write the shape functions in the Belytschko-Bachrach [53] mix form:

$$\Phi_I(x, y, \xi\eta) = \Delta_I + b_{xI} x + b_{yI} y + \gamma_I \xi\eta \tag{389}$$

with

$$\Delta_I = \left[t_I - (t_I x^I) b_{xI} - (t_I y^I) b_{yI}\right];\ t = (1, 1, 1, 1)$$

$$b_{xI} = \left(y_{24} y_{31} y_{42} y_{13}\right) / A; \quad \left(f_{ij} = \left(f_i - f_j\right)/2\right)$$

$$b_{yI} = \left(x_{42} x_{13} x_{24} x_{31}\right) / A$$

$$\gamma_I = \left[\Gamma_I - (\Gamma_J x^J) b_{xI} - (\Gamma_J y^J) b_{xI}\right] / 4; \quad \Gamma = (1, -1, 1, -1)$$

A is the area of the element.

The velocity of the element at the mid-plane reference point is found using the relations:

$$v_x = \sum_{I=1}^{4} \Phi_I v_{xI} \tag{390}$$

$$v_y = \sum_{I=1}^{4} \Phi_I v_{yI} \tag{391}$$

$$v_z = \sum_{I=1}^{4} \Phi_I v_{zI} \tag{392}$$

Where, v_{xI}, v_{yI}, v_{zI} are the nodal velocities in the x, y, z directions.

In a similar fashion, the element rotations are found by:

$$\omega_x = \sum_{I=1}^{4} \Phi_I \omega_{xI} \tag{393}$$

$$\omega_y = \sum_{I=1}^{4} \Phi_I \omega_{yI} \tag{394}$$

Where, ω_{xI} and ω_{yI} are the nodal rotational velocities about the x and y reference axes.

The velocity change with respect to the coordinate change is given by:

$$\frac{\partial v_x}{\partial x} = \sum_{I=1}^{4} \frac{\partial \Phi_I}{\partial x} v_{xI} \tag{395}$$

$$\frac{\partial v_x}{\partial y} = \sum_{I=1}^{4} \frac{\partial \Phi_I}{\partial y} v_{xI} \tag{396}$$

[53] Belytschko T. and Bachrach W.E., "Efficient implementation of quadrilaterals with high coarse-mesh accuracy", Computer Methods in Applied Mechanics and Engineering, 54:279-301, 1986.

Mechanical Properties

Shell elements behave in two ways, either membrane or bending behavior. The Mindlin plate elements that are used by Radioss account for bending and transverse shear deformation. Hence, they can be used to model thick and thin plates.

Membrane Behavior

The membrane strain rates for Mindlin plate elements are defined as:

$$\dot{e}_{xx} = \frac{\partial v_x}{\partial x} \tag{397}$$

$$\dot{e}_{yy} = \frac{\partial v_y}{\partial y} \tag{398}$$

$$\dot{e}_{xy} = \frac{1}{2}\left(\frac{\partial v_x}{\partial y} + \frac{\partial v_y}{\partial x}\right) \tag{399}$$

$$\dot{e}_{xz} = \frac{1}{2}\left(\frac{\partial v_x}{\partial z} + \frac{\partial v_z}{\partial x}\right) = \frac{1}{2}\left(\omega_y + \frac{\partial v_z}{\partial x}\right) \tag{400}$$

$$\dot{e}_{yz} = \frac{1}{2}\left(\frac{\partial v_y}{\partial z} + \frac{\partial v_z}{\partial y}\right) = \frac{1}{2}\left(-\omega_x + \frac{\partial v_z}{\partial y}\right) \tag{401}$$

Where,

$\dot{e}_{ij}$ Membrane strain rate

Bending Behavior

The bending behavior in plate elements is described using the amount of curvature. The curvature rates of the Mindlin plate elements are defined as:

$$\dot{\chi}_x = \frac{\partial \omega_y}{\partial x} \tag{402}$$

$$\dot{\chi}_y = -\frac{\partial \omega_x}{\partial y} \tag{403}$$

$$\dot{\chi}_{\mathrm{xy}} = \frac{1}{2}\left(\frac{\partial \omega_y}{\partial y} - \frac{\partial \omega_x}{\partial x}\right) \tag{404}$$

Where,

$\dot{\chi}_{ij}$ Curvature rate

Strain Rate Calculation

The calculation of the strain rate of an individual element is divided into two parts, membrane and bending strain rates.

Membrane Strain Rate

The vector defining the membrane strain rate is:

$$\{\dot{e}\}_m = \{\dot{e}_x, \dot{e}_y, 2\dot{e}_{xy}\} \tag{405}$$

This vector is computed from the velocity field vector $\{v\}_m$ and the shape function gradient $\{B\}_m$:

$$\{\dot{e}\}_m = \{B\}_m \{v\}_m \tag{406}$$

Where,

$$\{v\}_m = \{v_x^1, v_y^1, v_x^2, v_y^2, v_x^3, v_y^3, v_x^4, v_y^4\} \tag{407}$$

$$[B]_m = \begin{bmatrix} \frac{\partial \Phi_1}{\partial x} & 0 & \frac{\partial \Phi_2}{\partial x} & 0 & \frac{\partial \Phi_3}{\partial x} & 0 & \frac{\partial \Phi_4}{\partial x} & 0 \\ 0 & \frac{\partial \Phi_1}{\partial y} & 0 & \frac{\partial \Phi_2}{\partial y} & 0 & \frac{\partial \Phi_3}{\partial y} & 0 & \frac{\partial \Phi_4}{\partial y} \\ \frac{\partial \Phi_1}{\partial y} & \frac{\partial \Phi_1}{\partial x} & \frac{\partial \Phi_2}{\partial y} & \frac{\partial \Phi_2}{\partial x} & \frac{\partial \Phi_3}{\partial y} & \frac{\partial \Phi_3}{\partial x} & \frac{\partial \Phi_4}{\partial y} & \frac{\partial \Phi_4}{\partial x} \end{bmatrix} \tag{408}$$

Bending Strain Rate

The vector defining the bending strain rate is:

$$\{\dot{e}\}_b = \{\dot{\chi}_x, \dot{\chi}_y, 2\dot{\chi}_{xy}, 2\dot{e}_{zx}, 2\dot{e}_{yz}\} \tag{409}$$

As with the membrane strain rate, the bending strain rate is computed from the velocity field vector. However, the velocity field vector for the bending strain rate contains rotational velocities, as well as translations:

$$\{\dot{e}\}_b = \{B\}_b \{v\}_b \tag{410}$$

Where,

$$\{v\}_b = \{\omega_y^1, -\omega_x^1, \omega_y^2, -\omega_x^2, \omega_y^3, -\omega_x^3, \omega_y^4, -\omega_x^4, v_z^1, v_z^2, v_z^3, v_z^4\} \tag{411}$$

$$[B]_b = \begin{bmatrix} \frac{\partial \Phi_1}{\partial x} & 0 & \frac{\partial \Phi_2}{\partial x} & 0 & \frac{\partial \Phi_3}{\partial x} & 0 & \frac{\partial \Phi_4}{\partial x} & 0 & 0 & 0 & 0 & 0 \\ 0 & \frac{\partial \Phi_1}{\partial y} & 0 & \frac{\partial \Phi_2}{\partial y} & 0 & \frac{\partial \Phi_3}{\partial y} & 0 & \frac{\partial \Phi_4}{\partial y} & 0 & 0 & 0 & 0 \\ \frac{\partial \Phi_1}{\partial y} & \frac{\partial \Phi_1}{\partial x} & \frac{\partial \Phi_2}{\partial y} & \frac{\partial \Phi_2}{\partial x} & \frac{\partial \Phi_3}{\partial y} & \frac{\partial \Phi_3}{\partial x} & \frac{\partial \Phi_4}{\partial y} & \frac{\partial \Phi_4}{\partial x} & 0 & 0 & 0 & 0 \\ \Phi_1 & 0 & \Phi_2 & 0 & \Phi_3 & 0 & \Phi_4 & 0 & \frac{\partial \Phi_1}{\partial x} & \frac{\partial \Phi_2}{\partial x} & \frac{\partial \Phi_3}{\partial x} & \frac{\partial \Phi_4}{\partial x} \\ 0 & \Phi_1 & 0 & \Phi_2 & 0 & \Phi_3 & 0 & \Phi_4 & \frac{\partial \Phi_1}{\partial y} & \frac{\partial \Phi_2}{\partial y} & \frac{\partial \Phi_3}{\partial y} & \frac{\partial \Phi_4}{\partial y} \end{bmatrix} \tag{412}$$

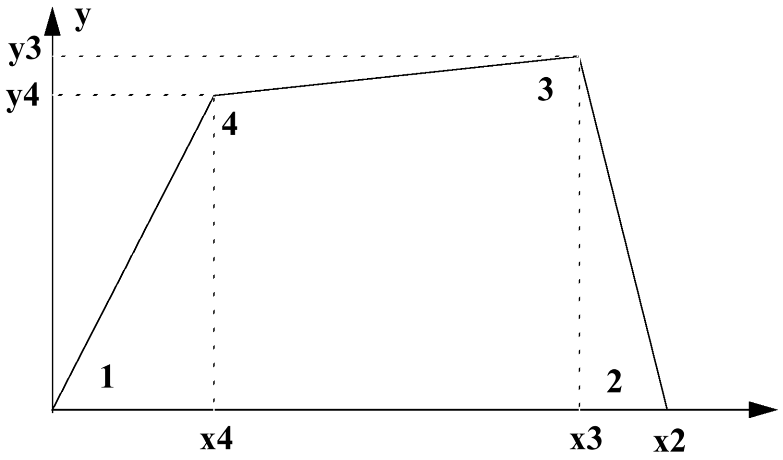

$$Px_1 = \frac{1}{2}(y_2 - y_4) \qquad Px_2 = \frac{1}{2}y_3$$

$$Py_1 = \frac{1}{2}(x_4 - x_2) \qquad Py_2 = -\frac{1}{2}x_3$$

$$\frac{\partial\Phi_1}{\partial x} = \frac{1}{S}Px_1 \qquad \frac{\partial\Phi_2}{\partial x} = \frac{1}{S}Px_2 \qquad \frac{\partial\Phi_3}{\partial x} = -\frac{1}{S}Px_1 \qquad \frac{\partial\Phi_4}{\partial x} = -\frac{1}{S}Px_2$$

$$\frac{\partial\Phi_1}{\partial y} = \frac{1}{S}Py_1 \qquad \frac{\partial\Phi_2}{\partial y} = \frac{1}{S}Py_2 \qquad \frac{\partial\Phi_3}{\partial y} = -\frac{1}{S}Py_1 \qquad \frac{\partial\Phi_4}{\partial y} = -\frac{1}{S}Py_2$$

$$\Phi_1 = \Phi_2 = \Phi_3 = \Phi_4 = \frac{1}{4}$$

Figure 41: Strain Rate Calculation

Mass and Inertia

Consider a rectangular plate with sides of length a and b, surface area $A = ab$ and thickness t, as shown in Figure 42.

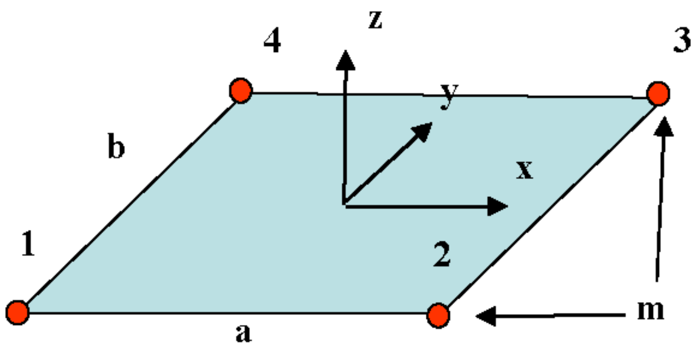

Figure 42: Mass distribution

Due to the lumped mass formulation used by Radioss, the lumped mass at a particular node is:

$$m = \frac{1}{4}\rho At \tag{413}$$

The mass moments of inertia, with respect to local element reference frame, are calculated at node i by:

$$I_{xx} = m\left(\frac{b^2 + t^2}{12}\right) \tag{414}$$

$$I_{yy} = m\left(\frac{a^2 + t^2}{12}\right) \tag{415}$$

$$I_{zz} = m\left(\frac{a^2 + b^2}{12}\right) \tag{416}$$

$$I_{xy} = -m\frac{ab}{16} \tag{417}$$

Inertia Stability

With the exact formula for inertia (Equation 414 to Equation 417), the solution tends to diverge for large rotation rates. Belytschko proposed a way to stabilize the solution by setting I_{xx} =I_{yy}, that is, to consider the rectangle as a square with respect to the inertia calculation only. This introduces an error into the formulation. However, if the aspect ratio is small the error will be minimal. In Radioss a better stabilization is obtained by:

$$I_{xx} = m\left(\frac{A}{f} + \frac{t^2}{12}\right) \tag{418}$$

$$I_{zz} = I_{yy} = I_{xx} \tag{419}$$

$$I_{xy} = 0 \tag{420}$$

Where, f is a regulator factor with default value f=12 for QBAT element and f=9 for other quadrilateral elements.

Internal Forces

The internal force vector is given by:

$$f^{\text{int}} = \int_{\Omega e} B^t \sigma d\Omega^e \tag{421}$$

In elasticity it becomes:

$$f^{\text{int}} = \int_{\Omega e} B^t C B v d\Omega^e \tag{422}$$

It can be written as:

$$f^{\text{int}} = f^{\text{int}}{}_0 + f^{\text{int}^{hgr}} \tag{423}$$

with the constant part f^{int_0} being computed with one-point quadrature and the non constant part or hourglass part $f^{\text{int}^{hgr}}$ being computed by perturbation stabilization (I_{shell} = 1, 2 ,3 ...) or by physical stabilization (I_{shell} = 22).

Hourglass Modes

Hourglass modes are element distortions that have zero strain energy. The 4 node shell element has 12 translational modes, 3 rigid body modes (1, 2, 9), 6 deformation modes (3, 4, 5, 6, 10, 11) and 3 hourglass modes (7, 8, 12).

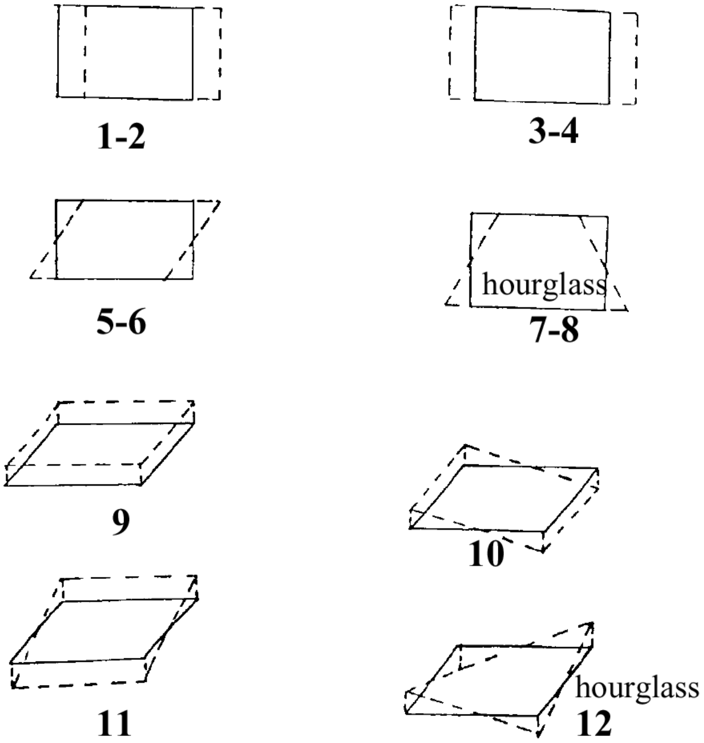

Figure 43: Translational Modes of Shell

Along with the translational modes, the 4 node shell has 12 rotational modes: 4 out of plane rotation modes (1, 2, 3, 4), 2 deformation modes (5, 6), 2 rigid body or deformation modes (7, 8) and 4 hourglass modes (9, 10, 11, 12).

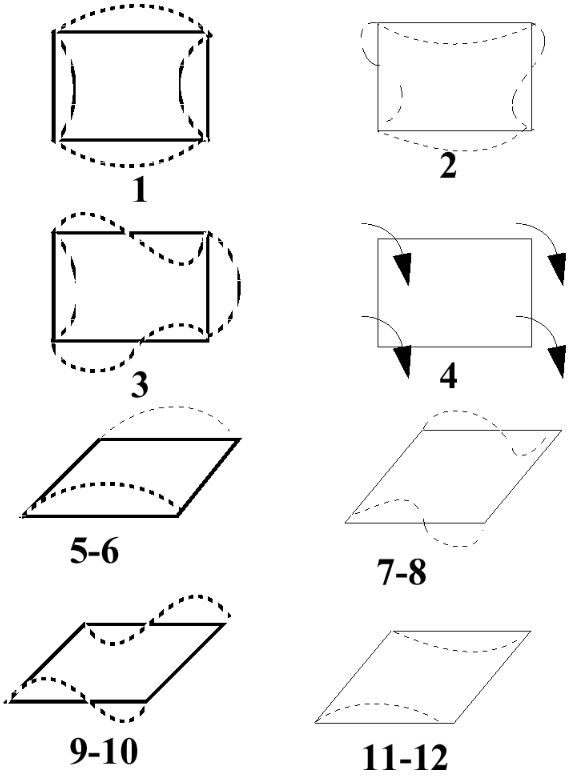

Figure 44: Rotational Modes of Shell

Hourglass Viscous Forces

Hourglass resistance forces are usually either viscous or stiffness related. The viscous forces relate to the rate of displacement or velocity of the elemental nodes, as if the material was a highly viscous fluid. The viscous formulation used by Radioss is the same as that outlined by Kosloff and Frasier [54]. Refer to Hourglass Modes. An hourglass normalized vector is defined as:

$$\Gamma = (1, \ -1, \ 1, \ -1) \tag{424}$$

The hourglass velocity rate for the above vector is defined as:

$$\frac{\partial q_i}{\partial t} = \Gamma_I v_{iI} = v_{iI} - v_{i2} + v_{i3} - v_{i4} \tag{425}$$

The hourglass resisting forces at node I for in-plane modes are:

$$f_{iI}^{hgr} = \frac{1}{4} \rho c t \sqrt{h_m} \frac{A}{2} \frac{\partial q_i}{\partial t} \Gamma_I \tag{426}$$

For out of plane mode, the resisting forces are:

$$f_{iI}^{hgr} = \frac{1}{4} \rho c t^2 \sqrt{\frac{h_f}{10}} \tag{427}$$

Where,

i	Direction index
I	Node index
t	Element thickness
c	Sound propagation speed
A	Element area
ρ	Material density
h_m	Shell membrane hourglass coefficient
h_f	Shell out of plane hourglass coefficient

Hourglass Elastic Stiffness Forces

Radioss can apply a stiffness force to resist hourglass modes. This acts in a similar fashion to the viscous resistance, but uses the elastic material stiffness and node displacement to determine the size of the force. The formulation is the same as that outlined by Flanagan et al. [55] Refer to Flanagan-Belytschko Formulation. The hourglass resultant forces are defined as:

$$f_{iI}^{hgr} = f_i^{hgr} \Gamma_I \tag{428}$$

For membrane modes:

$$f_i^{hgr}(t+\Delta t) = f_i^{hgr}(t) + \frac{1}{8} h_m E t \frac{\partial q_i}{\partial t} \Delta t \tag{429}$$

For out of plane modes:

$$f_i^{hgr}(t+\Delta t) = f_i^{hgr}(t) + \frac{1}{40} h_f E t^3 \frac{\partial q_i}{\partial t} \Delta t \tag{430}$$

Where,

t	Element thickness
Δt	Time step
E	Young's modulus

Hourglass Viscous Moments

This formulation is analogous to the hourglass viscous force scheme. The hourglass angular velocity rate is defined for the main hourglass modes as:

$$\frac{\partial r_i}{\partial t} = \Gamma_I \omega_{iI}^I = \omega_{i1} - \omega_{i2} + \omega_{i3} - \omega_{i4} \tag{431}$$

The hourglass resisting moments at node I are given by:

$$m_{iI}^{hgr} = \frac{1}{50}\sqrt{\frac{h_r}{2}}\,\rho c A t^2 \frac{\partial r_i}{\partial t}\Gamma_I \tag{432}$$

Where, h_r is the shell rotation hourglass coefficient.

Hourglass Resistance

To correct this phenomenon, it is necessary to introduce anti-hourglass forces and moments. Two possible formulations are presented hereafter.

Flanagan-Belytschko Formulation

I_{shell}=1[56]

In the Kosloff-Frasier formulation seen in Kosloff and Frasier Formulation, the hourglass base vector $\Gamma_{I\alpha}$ is not perfectly orthogonal to the rigid body and deformation modes that are taken into account by the one point integration scheme. The mean stress/strain formulation of a one point integration scheme only considers a fully linear velocity field, so that the physical element modes generally contribute to the hourglass energy. To avoid this, the idea in the Flanagan-Belytschko formulation is to build an hourglass velocity field which always remains orthogonal to the physical element modes. This can be written as:

$$v_{iI}^{Hour} = v_{iI} - v_{iI}^{Lin} \tag{433}$$

The linear portion of the velocity field can be expanded to give:

$$v_{iI}^{Hour} = v_{iI} - \left(\overline{v_{iI}} + \frac{\partial v_{iI}}{\partial x_j}\cdot\left(x_j - \overline{x_j}\right)\right) \tag{434}$$

Decomposition on the hourglass base vectors gives [56]:

$$\frac{\partial q_i^\alpha}{\partial t} = \Gamma_I^\alpha \cdot v_{iI}^{Hour} = \left(v_{iI} - \frac{\partial v_{iI}}{\partial x_j}\cdot x_j\right)\cdot\Gamma_I^\alpha \tag{435}$$

Where,

$\frac{\partial q_i^\alpha}{\partial t}$	Hourglass modal velocities
Γ_I^α	Hourglass vectors, base

Remembering that $\frac{\partial v_i}{\partial x_j} = \frac{\partial \Phi_j}{\partial x_j}\cdot v_{i,J}$and factorizing Hourglass Modes, Equation 329 gives:

[54] Kosloff D. and Frazier G., “Treatment of hourglass pattern in low order finite element code”, International Journal for Numerical and Analytical Methods in Geomechanics, 1978.

[55] Flanagan D. and Belytschko T., “A Uniform Strain Hexahedron and Quadrilateral with Orthogonal Hourglass Control”, Int. Journal Num. Methods in Engineering, 17 679-706, 1981.

$$\frac{\partial q_i^\alpha}{\partial t} = v_{iI} \cdot \left(\Gamma_I^\alpha - \frac{\partial \Phi_J}{\partial x_j} x_j \Gamma_J^\alpha \right) \tag{436}$$

$$\gamma_I^\alpha = \Gamma_I^\alpha - \frac{\partial \Phi_J}{\partial x_j} x_j \Gamma_J^\alpha \tag{437}$$

is the hourglass shape vector used in place of Γ_I^αin Hourglass Modes, Equation 326.

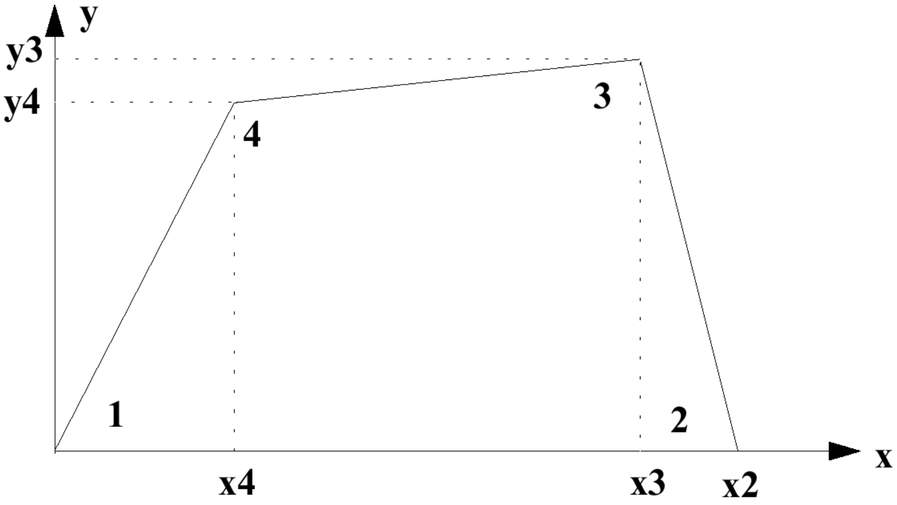

Figure 45: Flanagan Belytschko Hourglass Formulation

$$Px_1 = \frac{1}{2}(y_2 - y_4) \qquad Px_2 = \frac{1}{2}y_3$$

$$Py_1 = \frac{1}{2}(x_4 - x_2) \qquad Py_2 = -\frac{1}{2}x_3$$

$$hx = \frac{(-x_2 + x_3 - x_4)}{S} \qquad hy = \frac{(-y_2 + y_3 - y_4)}{S}$$

$$\Gamma_1 = 1 - Px_1 hx - Py_1 hy$$

$$\Gamma_2 = -1 + Px_2 hx + Py_2 hy$$

$$\Gamma_3 = 1 - Px_1 hx - Py_1 hy$$

$$\Gamma_4 = -1 + Px_2 hx + Py_2 hy$$

Elastoplastic Hourglass Forces

I_{shell}=3

The same formulation as elastic hourglass forces is used (Hourglass Elastic Stiffness Forces and Flanagan et al. [56]) but the forces are bounded with a maximum force depending on the current element mean yield stress. The hourglass forces are defined as:

$$f_{iI}^{hgr} = f_i^{hgr} \Gamma_I \tag{438}$$

For in plane mode:

$$f_i^{hgr}(t+\Delta t) = f_i^{hgr}(t) + \frac{1}{8} h_m E t \frac{\partial q_i}{\partial t} \Delta t \tag{439}$$

$$f_i^{hgr}(t+\Delta t) = \min\left(f_i^{hgr}(t+\Delta t), \quad \frac{1}{2} h_m \sigma_y t \sqrt{A}\right) \tag{440}$$

For out of plane mode:

$$f_i^{hgr}(t+\Delta t) = f_i^{hgr}(t) + \frac{1}{40} h_f E t^3 \frac{\partial q_i}{\partial t} \Delta t \tag{441}$$

$$f_i^{hgr}(t+\Delta t) = \min\left(f_i^{hgr}(t+\Delta t), \frac{1}{4} h_f \sigma_y t^2\right) \tag{442}$$

Where,

t	Element thickness
σ_y	Yield stress
A	Element area

Physical Hourglass Forces

I_{shell}=22, 24

The hourglass forces are given by:

$$f^{\text{int}^{hgr}} = \int_{\Omega e} B^{Ht} C B^H v d\Omega^e \tag{443}$$

For in-plane membrane rate-of-deformation, with $\Phi = \xi\eta$ and $\gamma_I$defined in Bilinear Shape Functions, Equation 389:

$$\left[\left(B_I^m\right)^H\right] = \begin{bmatrix} \gamma_I \phi, x & 0 & 0 \\ 0 & \gamma_I \phi, y & 0 \\ \gamma_I \phi, y & \gamma_I \phi, x & 0 \end{bmatrix} \tag{444}$$

For bending:

$$\left[\left(B_I^b\right)^H\right]=\begin{bmatrix} 0 & \gamma_I\phi,x \\ -\gamma_I\phi,y & 0 \\ -\gamma_I\phi,x & \gamma_I\phi,y \end{bmatrix} \tag{445}$$

It is shown in [57] that the non-constant part of the membrane strain rate does not vanish when a warped element undergoes a rigid body rotation. Thus, a modified matrix $[\left(B_I^m\right)^H]$ is chosen using $z_\gamma=\gamma_I z^I$ as a measure of the warping:

$$\left[\left(B_I^m\right)^H\right]=\begin{bmatrix} \gamma_I\phi_{,x} & 0 & z_\gamma b_{xI}\phi_{,x} \\ 0 & \gamma_I\phi_{,y} & z_\gamma b_{yI}\phi_{,y} \\ \gamma_I\phi_{,y} & \gamma_I\phi_{,x} & z_\gamma\left(b_{xI}\phi_{,y}+b_{yI}\phi_{,x}\right) \end{bmatrix} \tag{446}$$

This matrix is different from the Belytschko-Leviathan [58] correction term added at rotational positions, which couples translations to curvatures as:

$$\left[\left(B_I^m\right)^H\right]=\begin{bmatrix} \gamma_I\phi_{,x} & 0 & 0 & 0 & -\frac{1}{4}z_\gamma\phi_{,x} \\ 0 & \gamma_I\phi_{,y} & 0 & \frac{1}{4}z_\gamma\phi_{,y} & 0 \\ \gamma_I\phi_{,y} & \gamma_I\phi_{,x} & 0 & \frac{1}{4}z_\gamma\phi_{,x} & -\frac{1}{4}z_\gamma\phi_{,y} \end{bmatrix} \tag{447}$$

This will lead to *membrane locking* (the membrane strain will not vanish under a constant bending loading). According to the general formulation, the coupling is presented in terms of bending and not in terms of membrane, yet the normal translation components in (B_I^m) do not vanish for a warped element due to the tangent vectors $t_i(\xi,\eta)$ which differ from $t_i(0,0)$.

Fully Integrated Formulation

I_{shell}=12

The element is based on the Q4γ24 shell element developed in [59] by Batoz and Dhatt. The element has 4 nodes with 5 local degrees-of-freedom per node. Its formulation is based on the Cartesian shell approach where the middle surface is curved. The shell surface is fully integrated with four Gauss points. Due to an in-plane reduced integration for shear, the element shear locking problems are avoided. The element without hourglass deformations is based on Mindlin-Reissner plate theory where the transversal shear deformation is taken into account in the expression of the internal energy. Consult the reference for more details.

Shell Membrane Damping

The shell membrane damping, *dm*, is only used for LAWS 25, 27, 19, 32 and 36. The Shell membrane damping factor is a factor on the numerical VISCOSITY and not a physical viscosity. Its effect is shown in the formula of the calculation of forces in a shell element:

$dm=dm$ read in `D00` input (Shell membrane damping factor parameter) then:

$$dm = \sqrt{2} \cdot dm_{D00} \cdot \rho_0 \cdot c \cdot \sqrt{AREA} \tag{448}$$

Effect in the force vector (F) calculation:

$$F_{1new} = F_{1old} + dm\left(\dot{\varepsilon}_{11} + \frac{\dot{\varepsilon}_{22}}{2}\right) \tag{449}$$

$$F_{2new} = F_{2old} + dm\left(\dot{\varepsilon}_{22} + \frac{\dot{\varepsilon}_{11}}{2}\right) \tag{450}$$

$$F_{3new} = F_{3old} + dm\frac{\dot{\varepsilon}_{12}}{3} \tag{451}$$

Where,

ρ_0	Density
$AREA$	Area of the shell element surface
dt	Time step
c	Sound speed

In order to calibrate the dm value so that it represents the physical viscosity, one should obtain the same size for all shell elements (Cf. $AREA$ factor), then scale the physical viscosity value to the element size.

Stress and Strain Calculation

The stress and strain for a shell element can be written in vector notation. Each component is a stress or strain feature of the element.

The generalized strain ε can be written as:

$$\{\varepsilon\} = \{e_x, e_y, e_{xy}, k_x, k_y, k_{xy}\} \tag{452}$$

Where,

e_{ij}	Membrane strain

[56] Flanagan D. and Belytschko T., "A Uniform Strain Hexahedron and Quadrilateral with Orthogonal Hourglass Control", Int. Journal Num. Methods in Engineering, 17 679-706, 1981.

[57] Belytschko T., Lin J.L. and Tsay C.S., "Explicit algorithms for the nonlinear dynamics of shells", Computer Methods in Applied Mechanics and Engineering, 42:225-251, 1984.

[58] Belytschko T. and Leviathan I., "Physical stabilization of the 4-node shell element with one-point quadrature", Computer Methods in Applied Mechanics and Engineering, 113:321-350, 1992.

[59] Batoz J.L. and Dhatt G., "Modeling of Structures by finite element", volume 3, Hermes, 1992.

χ_{ij} Bending strain or curvature

The generalized stress $\sum$ can be written as:

$$\left\{\sum\right\}=\left\{N_x, N_y, N_{xy}, M_x, M_y, M_{xy}\right\} \tag{453}$$

Where,

$$N_x = \int_{-t/2}^{t/2} \sigma_x dz \qquad M_x = -\int_{-t/2}^{t/2} \sigma_x z dz$$

$$N_y = \int_{-t/2}^{t/2} \sigma_y dz \qquad M_y = -\int_{-t/2}^{t/2} \sigma_y z dz$$

$$N_{xy} = \int_{-t/2}^{t/2} \sigma_{xy} dz \qquad M_{xy} = -\int_{-t/2}^{t/2} \sigma_{xy} z dz$$

$$N_{yz} = \int_{-t/2}^{t/2} \sigma_{yz} dz \qquad N_{xz} = \int_{-t/2}^{t/2} \sigma_{xz} dz$$

Isotropic Linear Elastic Stress Calculation

The stress for an isotropic linear elastic shell for each time increment is computed using:

$$\left\{\sum^{el}(t+\Delta t)\right\}=\left\{\sum(t)\right\}+\mathrm{L}\{\dot{\varepsilon}\}\Delta t \tag{454}$$

Where,

$$\mathrm{L}=\begin{bmatrix} L_m & 0 \\ 0 & L_b \end{bmatrix} \tag{455}$$

$$L_m=\begin{bmatrix} \frac{Et}{1-v2} & \frac{-vEt}{1-v2} & 0 \\ \frac{-vEt}{1-v2} & \frac{Et}{1-v2} & 0 \\ 0 & 0 & \frac{Et}{1+v} \end{bmatrix} \tag{456}$$

$$L_b = \begin{bmatrix} \frac{Et^3}{12(1-v2)} & \frac{-vEt^3}{12(1-v2)} & 0 \\ \frac{-vEt^3}{12(1-v2)} & \frac{Et^3}{12(1-v2)} & 0 \\ 0 & 0 & \frac{Et^3}{12(1+v)} \end{bmatrix} \tag{457}$$

E	Young's or Elastic modulus
υ	Poisson's ratio
t	Shell thickness

Isotropic Linear Elastic-Plastic Stress Calculation

An incremental step-by-step method is usually used to resolve the nonlinear problems due to elasto-plastic material behavior. The problem is presented by the resolution of the following equation:

$$\dot{\sigma} = C : \left(\dot{\varepsilon} - \dot{\varepsilon}_p\right) \tag{458}$$

$$f\left(\sigma, \sigma_y\right) = \sigma_{eq}^2 - \sigma_y^2 = 0 \quad ; \quad \dot{\sigma}_y = H\dot{\varepsilon}^p \tag{459}$$

$$\dot{f} = 0 \tag{460}$$

and

$$\dot{\varepsilon}_p = \frac{\partial f}{\partial \sigma}\dot{\lambda} \tag{461}$$

f is the yield surface function for plasticity for associative hardening. The equivalent stress σ_{eq} may be expressed in form:

$$\sigma_{eq}^2 = \{\sigma\}^t [A] \{\sigma\} \tag{462}$$

with $\{\sigma\} = \begin{Bmatrix} \sigma_{xx} \\ \sigma_{yy} \\ \sigma_{xy} \end{Bmatrix}$ and $[A] = \begin{bmatrix} 1 & -\frac{1}{2} & 0 \\ -\frac{1}{2} & 1 & 0 \\ 0 & 0 & 3 \end{bmatrix}$ for von Mises criteria.

The normality law (Stress and Strain Calculation, Equation 461) for associated plasticity is written as:

$$\{\dot{\varepsilon}_p\} = \frac{\partial f}{\partial(\sigma)}\dot{\lambda} = 2[A]\{\sigma\}\dot{\lambda} = \frac{\dot{\varepsilon}^p}{\sigma_y}[A]\{\sigma\} \tag{463}$$

Where,

$\dot{\varepsilon}^p$	Equivalent plastic deformation

Stress and Strain Calculation, Equation 458 is written in an incremental form:

$$\{\sigma\}_{n+1} = \{\sigma\}_n + \{d\sigma\} = \{\sigma\}_n + [C](\{d\varepsilon\} - \{d\varepsilon_p\}) = \{\sigma^*\} - \frac{d\varepsilon^p}{\sigma_y^{n+1}}[C][A]\{\sigma\}_{n+1} \tag{464}$$

Where, $\{\sigma^*\}$ represents stress components obtained by an elastic increment and $[C]$ the elastic matrix in plane stress. The equations in Stress and Strain Calculation, Equation 458 to Equation 464 lead to obtain the nonlinear equation:

$$f(d\varepsilon^p) = 0 \tag{465}$$

that can be resolved by an iterative algorithm as Newton-Raphson method.

To determine the elastic-plastic state of a shell element, a number of steps have to be performed to check for yielding and defining a plasticity relationship. Stress-strain and force-displacement curves for a particular ductile material are shown in Figure 46.

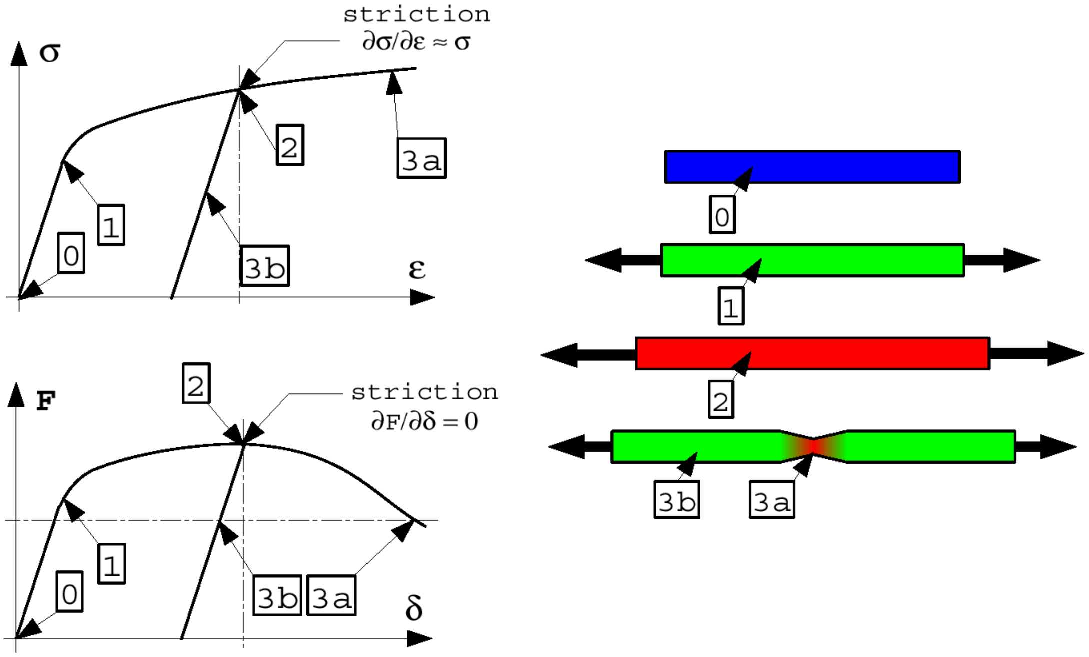

Figure 46: Material Curve

The steps involved in the stress calculation are:

1. Strain calculation at integration point z

   The overall strain on an element due to both membrane and bending forces is:

$$\varepsilon_x = e_x - z\chi_x \tag{466}$$

$$\varepsilon_y = e_y - z\chi_y \tag{467}$$

$$\varepsilon_{xy} = e_{xy} - z\chi_{xy} \tag{468}$$

$$\{\varepsilon\} = \{\varepsilon_x, \varepsilon_y, \varepsilon_{xy}\} \tag{469}$$

2. Elastic stress calculation

   The stress is defined as:

$$\{\sigma\} = \{\sigma_x, \sigma_y, \sigma_{xy}\} \tag{470}$$

   It is calculated using explicit time integration and the strain rate:

$$\{\sigma^{el}(t+\Delta t)\} = \{\sigma(t)\} + \mathrm{L}\{\dot{\varepsilon}\}\Delta t \tag{471}$$

$$\mathrm{L} = \begin{bmatrix} \frac{E}{1-v2} & \frac{vE}{1-v2} & 0 \\ \frac{vE}{1-v2} & \frac{E}{1-v2} & 0 \\ 0 & 0 & \frac{E}{1+v} \end{bmatrix}$$

   The two shear stresses acting across the thickness of the element are calculated by:

$$\begin{aligned} \sigma_{yz}^{el}(t+\Delta t) &= \sigma_{yz}(t) + \alpha\frac{E}{1+v}\dot{e}_{yz}\Delta t \\ \sigma_{xz}^{el}(t+\Delta t) &= \sigma_{xz}(t) + \alpha\frac{E}{1+v}\dot{e}_{xz}\Delta t \end{aligned} \tag{472}$$

   Where, α is the shear factor. Default is Reissner's value of 5/6.

3. von Mises yield criterion

   The von Mises yield criterion for shell elements is defined as:

$$\sigma_{vm}^2 = \sigma_x^2 + \sigma_y^2 - \sigma_x\sigma_y + 3\sigma_{xy}^2 \tag{473}$$

   For type 2 simple elastic-plastic material, the yield stress is calculated using:

$$\sigma_{yield}(t) = a + b\varepsilon^{p^n}(t) \tag{474}$$

4. Plasticity Check

   The element's state of stress must be checked to see if it has yielded. These values are compared with the von Mises and Yield stresses calculated in the previous step. If the von Mises stress is greater than the yield stress, then the material will be said to be in the plastic range of the stress-strain curve.

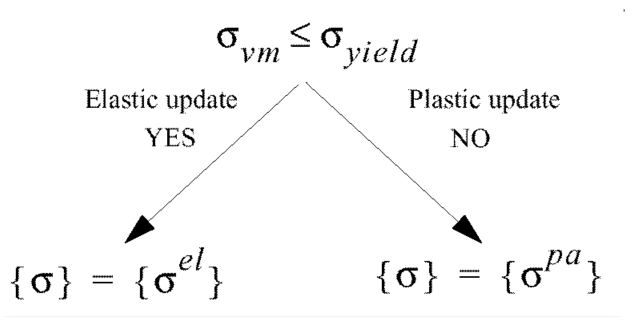
$\sigma_{vm} \le \sigma_{yield}$
Elastic update
YES
Plastic update
NO
$\{\sigma\} = \{\sigma^{el}\}$
$\{\sigma\} = \{\sigma^{pa}\}$

Figure 47: Plasticity Check

5. Compute plastically admissible stresses

If the state of stress of the element is in the plastic region, there are two different analyses that can be used as described in the next paragraph. The scheme used is defined in the shell property set, card 2 of the input.

6. Compute thickness change

The necking of the shells undergoing large strains in hardening phase can be taken into account by computing normal strain ε_{zz} in an incremental process. The incompressibility hypothesis in plasticity gives:

$$d\varepsilon_{zz}^{p} = -\left(d\varepsilon_{xx}^{p} + d\varepsilon_{yy}^{p}\right) \tag{475}$$

Where, the components of membrane strain $d\varepsilon_{xx}^{p}$ and $d\varepsilon_{yy}^{p}$ are computed by Equation 463 as:

$$\begin{Bmatrix} d\varepsilon_{xx}^{p} \\ d\varepsilon_{yy}^{p} \end{Bmatrix} = \frac{d\varepsilon^{p}}{\sigma_{y}}[A]_{2x2}\begin{Bmatrix} \sigma_{xx} \\ \sigma_{yy} \end{Bmatrix} \tag{476}$$

7. The plan stress condition $d\sigma_{zz} = 0$ allows to resolve for $d\varepsilon_{zz}$:

$$d\varepsilon_{zz} = -\frac{\upsilon}{1-\upsilon}\left(d\varepsilon_{xx} + d\varepsilon_{yy}\right) + \frac{1-2\upsilon}{1-\upsilon}d\varepsilon_{zz}^{p} \tag{477}$$

Plastically Admissible Stresses

Radial return

I_{plas}=2

When the shell plane stress plasticity flag is set to 0 on card 1 of the shell property type definition, a radial return plasticity analysis is performed. Thus, Step 5 of the stress computation is:

The hardening parameter is calculated using the material stress-strain curve:

$$\sigma_{yield}(t) = a + b\varepsilon^{p^{n}}(t) \tag{478}$$

$$\dot{\varepsilon}^{p}\Delta t = \frac{\sigma_{vm} - \sigma_{yield}}{E}$$

Where, ε^{p} is the plastic strain rate.

The plastic strain, or hardening parameter, is found by explicit time integration:

$$\varepsilon^{p}(t+\Delta t) = \varepsilon^{p}(t) + \dot{\varepsilon}^{p}\Delta t \tag{479}$$

Finally, the plastic stress is found by the method of radial return. In case of plane stress this method is approximated because it cannot verify simultaneously the plane stress condition and the flow rule. The following return gives a plane stress state:

$$\sigma_{ij}^{pa} = \frac{\sigma_{yield}}{\sigma_{vm}}\sigma_{ij}^{el} \tag{480}$$

Iterative algorithm

I_{plas}=1

If flag 1 is used on card 1 of the shell property type definition, an incremental method is used.

Step 5 is performed using the incremental method described by Mendelson. [60] It has been extended to plane stress situations. This method is more computationally expensive, but provides high accuracy on stress distribution, especially when one is interested in residual stress or elastic return. This method is also recommended when variable thickness is being used. After some calculations, the plastic stresses are defined as:

$$\sigma_x^{pa} = \frac{\sigma_x^{el} + \sigma_y^{el}}{2\left(1+\frac{\Delta r}{1-v}\right)} + \frac{\sigma_x^{el} - \sigma_y^{el}}{2\left(1+\frac{3\Delta r}{1+v}\right)} \tag{481}$$

$$\sigma_y^{pa} = \frac{\sigma_x^{el} + \sigma_y^{el}}{2\left(1+\frac{\Delta r}{1-v}\right)} - \frac{\sigma_x^{el} - \sigma_y^{el}}{2\left(1+\frac{3\Delta r}{1+v}\right)} \tag{482}$$

$$\sigma_{xy}^{pa} = \frac{\sigma_{xy}^{el}}{1+\frac{3\Delta r}{1+v}} \tag{483}$$

Where,

$$\Delta r = \frac{E\Delta\varepsilon^p}{2\sigma_{yield}(t+\Delta t)} \tag{484}$$

The value of $\Delta\varepsilon^P$ must be computed to determine the state of plastic stress. This is done by an iterative method. To calculate the value of $\Delta\varepsilon^P$, the von Mises yield criterion for the case of plane stress is introduced:

$$\sigma_x^2 + \sigma_y^2 - \sigma_x\sigma_y + 3\sigma_{xy}^2 = \sigma_{yield}^2(t+\Delta t) \tag{485}$$

and the values of σ_x, σ_y, σ_{xy} and σ_{yield} are replaced by their expression as a function of $\Delta\varepsilon^P$ (Hourglass Modes, Equation 424 to Hourglass Modes, Equation 427), with for example:

$$\sigma_{yield}(t+\Delta t) = a + b\varepsilon^{p^n}(t+\Delta t) \tag{486}$$

and:

$$\varepsilon^p(t+\Delta t) = \varepsilon^p(t) + \Delta\varepsilon^p \tag{487}$$

The nonlinear equation Equation 485 is solved iteratively for $\Delta\varepsilon^P$ by Newton's method using three iterations. This is sufficient to obtain $\Delta\varepsilon^P$ accurately.

Plastic Plane Stress with Hill's Criterion

In the case of Hill's orthotropic criterion, the equivalent stress is given by:

$$\sigma_{eq}^2 = A_1\sigma_{xx}^2 + A_2\sigma_{yy}^2 - A_3\sigma_{xx}\sigma_{yy} + A_{12}\sigma_{xy}^2 \tag{488}$$

with $[A] = \begin{bmatrix} A_1 & -\frac{A_3}{2} & 0 \\ & A_2 & 0 \\ sym & & A_{12} \end{bmatrix}$

Equation 464 is then written as:

$$[B]\{\sigma\}_{n+1} = \{\sigma^*\} \tag{489}$$

$$[B]=\begin{bmatrix} 1+\left(A_1-\frac{A_3}{2}\upsilon\right)dR & \left(A_2\upsilon-\frac{A_3}{2}\right)dR & 0 \\ \left(A_1\upsilon-\frac{A_3}{2}\right)dR & 1+\left(A_2-\frac{A_3}{2}\upsilon\right)dR & 0 \\ 0 & 0 & 1+\frac{1-\upsilon}{2}A_{12}dR \end{bmatrix};\ dR=\frac{d\varepsilon^p}{\sigma_y}\frac{E}{1-\upsilon^2}$$

Changing the stress variables to $\{\overline{\sigma}\}$:

$$\{\overline{\sigma}\}=[Q]\{\sigma\} \tag{490}$$

with:

$$[Q]=\begin{bmatrix} 1 & \frac{A_1-A_2+C}{-2\left(A_2\upsilon-\frac{A_3}{2}\right)} & 0 \\ \frac{A_1-A_2+C}{2\left(A_1\upsilon-\frac{A_3}{2}\right)} & 1 & 0 \\ 0 & 0 & 1 \end{bmatrix};\ C=\sqrt{(1-\upsilon^2)(A_1-A_2)^2+[A_3-(A_1+A_2)\upsilon]^2}$$

The matrix $[\overline{B}]=[Q][B][Q]^{-1}$ is diagonal:

$$[\overline{B}]=\begin{bmatrix} 1+dR\left(A_2-\frac{A_3\upsilon}{2}-\frac{C}{J_Q}\right) & 0 & 0 \\ 0 & 1+dR\left(A_1-\frac{A_3\upsilon}{2}+\frac{C}{J_Q}\right) & 0 \\ 0 & 0 & 1+dR.A_{12}\left(\frac{1-\upsilon}{2}\right) \end{bmatrix} \tag{491}$$

Where, $J_Q=1+\frac{(A_1-A_2+C)^2}{4\left(A_1\upsilon-\frac{A_3}{2}\right)\left(A_2\upsilon-\frac{A_3}{2}\right)}$ is the Jacobian of $[Q]$. Equation 490 is now written as:

$$[\overline{B}]\{\overline{\sigma}\}_{n-1}=\{\overline{\sigma}^*\} \tag{492}$$

This will enable to give explicitly the expression of the yield surface Equation 465:

$$\begin{aligned} f_{n+1}&=\left(\sigma_{eq}^{n+1}\right)^2-\left(\sigma_y^{n+1}\right)^2=\{\overline{\sigma}^*\}^t[\overline{B}]^{-t}[\overline{A}][\overline{B}]^{-1}\{\overline{\sigma}^*\}-\left(\sigma_y^{n+1}\right)^2 \\ &=\frac{\overline{A}_{11}}{\overline{B}_1^2}\overline{\sigma}_{xx}^2+\frac{\overline{A}_{22}}{\overline{B}_2^2}\overline{\sigma}_{yy}^2+\frac{A_{12}}{\overline{B}_3^2}\overline{\sigma}_{xy}^2+\frac{\overline{A}_{12}}{\overline{B}_1\overline{B}_2}\overline{\sigma}_{xx}\overline{\sigma}_{yy}-\left(\sigma_y^{n+1}\right)^2 \end{aligned} \tag{493}$$

With $[\overline{A}]_{2\times2}=[Q]_{2\times2}^{-t}[A]_{2\times2}[Q]_{2\times2}^{-1}$.

The derivative of f_{n+1} is carried out in order to use the Newton-Raphson method:

$$\Delta\varepsilon_{n+1}^p=\Delta\varepsilon_n^p-\frac{f_{n+1}}{f'_{n+1}} \tag{494}$$

60. Mendelson A., "Plasticity: Theory and Application", MacMillan Co., New York, 1968.

Forces and Moments Calculation

Integration Points Throughout the Thickness

The integration is performed using n equally spaced integration points throughout the thickness. The method used assumes a linear variation of stresses between integrations points:

$$N_x = t\sum_{k=1}^{n} w_k^N \sigma_{xk}^{pa} \tag{495}$$

$$M_x = t^2\sum_{k=1}^{n} w_k^M \sigma_{xk}^{pa} \tag{496}$$

Table 2 compares the coefficients used to the classical Newton quadrature in case of 3 integration points.

Table 2: w^N for 3 Integration Points

Coefficients	w_1	w_2	w_3
Radioss	0.250	0.500	0.250
Simpson	0.166	0.666	0.166

Table 3: w^M for 3 Integration Points

Coefficients	w_1	w_2	w_3
Radioss	-0.083	0.	0.083
Simpson	-0.083	0.	0.083

Table 4: Gauss Integration Scheme

Number of Points	Position	Weight
1	±0.0000	2.0000
2	±0.5774	1.0000
3	0.0000 ±0.7746	0.8889 0.5556
4	±0.8611	0.6521

Number of Points	Position	Weight
	±0.3400	0.3479
5	±0.9062 ±0.5385 0.0000	0.2369 0.4786 0.5689
6	±0.9325 ±0.6612 ±0.2386	0.1713 0.3608 0.4679
7	±0.9491 ±0.7415 ±0.4058 0.0000	0.1295 0.2797 0.3818 0.4180
8	±0.9603 ±0.7967 ±0.5255 ±0.1834	0.1012 0.2224 0.3137 0.3627
9	±0.9681 ±0.8360 ±0.6134 ±0.3243 0.0000	0.0813 0.1806 0.2606 0.3123 0.3302
10	±0.9739 ±0.8650 ±0.6794 ±0.4334 ±0.1489	0.0667 0.1495 0.2191 0.2693 0.2955

Table 5: Lobatto Integratin Scheme

Number of Points	Position	Weight for Membrane w^N	Weight for Bending w^M
1	0.0000	1.0000	0.0000
2	±0.5000	0.5000	±0.0833
3	±0.5000 0.0000	0.2500 0.5000	±0.0833 0.0000
4	±0.5000 ±0.1667	0.1667 0.3333	±0.0648 ±0.0556
5	±0.5000 ±0.2500 0.0000	0.1250 0.2500 0.2500	±0.0521 ±0.0625 0.0000
6	±0.5000 ±0.3000 ±0.1000	0.1000 0.2000 0.2000	±0.0433 ±0.0600 ±0.0200
7	±0.500 ±0.3333 ±0.1667 0.0000	0.0833 0.1667 0.1667 0.1667	±0.0370 ±0.0556 ±0.0278 0.0000
8	±0.5000 ±0.3750 ±0.2500 ±0.1250	0.0714 0.1429 0.1429 0.1429	±0.0323 ±0.0510 ±0.0306 ±0.0102
9	±0.5000 ±0.3750 ±0.2500 ±0.1250 0.0000	0.0625 0.1250 0.1250 0.1250 0.1250	±0.086 ±0.0469 ±0.0313 ±0.0156 0.0000

Number of Points	Position	Weight for Membrane w^N	Weight for Bending w^M
10	±0.5000	0.0556	±0.0257
	±0.3889	0.1111	±0.0432
	±0.2778	0.1111	±0.0309
	±0.1667	0.1111	±0.0185
	±0.0555	0.1111	±0.0062

For shell elements, integration points through the thickness are almost Lobatto points.

Global Plasticity Algorithm

In the case of global plasticity, the forces and moments are computed directly. The algorithm is activated by specifying the number of integration points through the thickness as zero. The first step is an obvious elastic calculation:

$$\left\{\sum^{el}\right\} = \left\{\sum(t)\right\} + \mathrm{L}\{\dot{E}\}\Delta t \tag{497}$$

The yield criterion used is the uncoupled Iliouchine [61] form:

$$F = \frac{\bar{N}^2}{t^2} + \frac{16\bar{M}^2}{t^4} - \sigma_{yield}^2 \leq 0 \tag{498}$$

with

$$\bar{N}^2 = N_x^2 + N_y^2 - N_x N_y + 3N_{xy}^2 \tag{499}$$

$$\bar{M}^2 = M_x^2 + M_y^2 - M_x M_y + 3M_{xy}^2 \tag{500}$$

Where,

$$N_x = \int_{-t/2}^{t/2} \sigma_x^{pa} dz \qquad M_x = \int_{-t/2}^{t/2} \sigma_x^{pa} z dz$$

$$N_y = \int_{-t/2}^{t/2} \sigma_y^{pa} dz \qquad M_y = \int_{-t/2}^{t/2} \sigma_y^{pa} z dz$$

$$N_{xy} = \int_{-t/2}^{t/2} \sigma_{xy}^{pa} dz \qquad M_{xy} = \int_{-t/2}^{t/2} \sigma_{xy}^{pa} z dz$$

An extension of Iliouchine criterion for isotropic hardening is developed here. The yield surface can be expressed as:

$$f = \begin{Bmatrix} \{N\} \\ \{M\} \end{Bmatrix}^t [F] \begin{Bmatrix} \{N\} \\ \{M\} \end{Bmatrix} - \left(\sigma_y^0 \beta\right)^2 = 0 \tag{501}$$

with

$$[F] = \begin{bmatrix} \frac{1}{h^2}[A] & \frac{1}{2\sqrt{3}\left(s\gamma h \frac{h^2}{6}\right)}[A] \\ sym & \frac{1}{\left(\gamma \frac{h^2}{6}\right)^2}[A] \end{bmatrix} \tag{502}$$

and

$$s = \frac{\left|\{N\}^t [A] \{M\}\right|}{\{N\}^t [A] \{M\}} \tag{503}$$

Where, β and γ are scalar material characteristic constants, function of plastic deformation. They can be identified by the material hardening law in pure traction and pure bending.

In pure traction:

$$f = \frac{N^2}{h^2} - \left(\sigma_y^0 \beta\right)^2 = 0 \rightarrow \beta = \frac{\sigma_y\left(\varepsilon^p\right)}{\sigma_y^0} \tag{504}$$

In pure bending:

$$f = \frac{M^2}{\left(\gamma h^2 / 6\right)^2} - \left(\sigma_y^0 \beta\right)^2 = 0 \rightarrow \gamma = \frac{M}{\sigma_y h^2 / 6} \tag{505}$$

If no hardening law in pure bending is used, γ is simply computed by $\gamma = \frac{\sigma_y / E + \frac{3}{2}\varepsilon^p}{\sigma_y / E + \varepsilon^p}$ varying between 1.0 and 1.5.

The plasticity flow is written using the normality law:

$$\begin{Bmatrix} \{d\varepsilon_p\} \\ \{dX_p\} \end{Bmatrix} = d\lambda \frac{\partial f}{\partial \begin{Bmatrix} \{N\} \\ \{M\} \end{Bmatrix}} = 2 d\lambda [F] \begin{Bmatrix} \{N\} \\ \{M\} \end{Bmatrix} \tag{506}$$

The equivalent plastic deformation ε^P is proportional to the plastic work. Its expression is the same as in the case of traction:

$$\sigma_y^0 \beta d\varepsilon^p = \begin{Bmatrix} \{d\varepsilon_p\} \\ \{d\chi_p\} \end{Bmatrix}^t \begin{Bmatrix} \{N\} \\ \{M\} \end{Bmatrix} = 2d\lambda\left(\sigma_y^0 \beta\right)^2 \tag{507}$$

This leads to:

$$d\varepsilon^p = 2d\lambda\sigma_y^0\beta \quad \text{and} \quad d\beta = \frac{H}{\sigma_y^0} d\varepsilon^p \tag{508}$$

Where, H is the plastic module. The derivative of function f in Equation 501 is discontinuous when $\{N\}^t \{A\}\{M\}$ =0. This can be treated when small steps are used by putting s=0 as explained in [62].

Then the derivative of f with respect to $d\varepsilon^P$ ($\frac{\partial f}{\partial d\varepsilon^P}$) is carried out. The derived equation is nonlinear in internal efforts and is resolved by Newton-Raphson:

$$\begin{Bmatrix} \{N\} \\ \{M\} \end{Bmatrix}_{n+1} = \begin{Bmatrix} \{N\} \\ \{M\} \end{Bmatrix}_{*} - 2d\lambda[D][F]\begin{Bmatrix} \{N\} \\ \{M\} \end{Bmatrix}_{n+1} \tag{509}$$

Where, $[D]$ is the elastic stiffness matrix and:

$$\begin{Bmatrix} \{N\} \\ \{M\} \end{Bmatrix}_{*} = \begin{Bmatrix} \{N\} \\ \{M\} \end{Bmatrix}_{n} - [D]\begin{Bmatrix} \{d\varepsilon\} \\ \{d\chi\} \end{Bmatrix} \tag{510}$$

Shell Formulations

QPH shell is the Belytschko Leviathan [63] shell for linear models or quasi-static analysis is identical to a QPPS shell analysis, only one difference being explained in Fully-integrated Shell Element QBAT.

The QPPS shell is a new One-point Quadrature, General Nonlinear Quadrilateral Shell Element with Physical Stabilization. This shell is a Belytschko Leviathan [63] shell modified by Zeng and Combescure.[64]

The physical stabilization is applied which enables the explicit evaluation of the stabilizing forces based on the general degenerated shell formulation and which does not require any input parameters. An optimized choice of the moduli is made in order to compute the stabilized forces for nonlinear material so that element's behavior is improved with respect to similar physical stabilization elements. The cost efficiency of the element is demonstrated by numerical examples, as compared with a fully-integrated 4-node element.

[61] Iliouchine A., “Plasticity”, Edition Eyrolles Paris, 1956.

[62] Crisfield M.A., “Nonlinear finite element analysis of solids and structures”, J. Wiley, Vol. 2, 1997.

The QEPH shell is a new improved element with respect to QPH,QPPS. The improvements will be explained in Fully-integrated Shell Element QBAT. As the QEPH is very efficient, it replaces QPH,QPPS in the applications.

The QBAT shell is a new fully-integrated 4-node element based γ 24 shell of Batoz and Dhatt [66] on Q4 as discussed in Fully Integrated Formulation.

The general formulation of the degenerated continuum quadrilateral shell (for which all these elements used) is given in General Degenerated 4-Node Shell Formulations. The difficulties in evaluating the stabilized stiffness are also described. Fully-integrated Shell Element QBAT presents the detailed formulations for the one-point quadrature shell element based on the general formulation, and compares it with that of Belytschko and Leviathan.

General Degenerated 4-Node Shell Formulations

The following formulations of degenerated quadrilateral shells are based on the successful full integration element MITC4 developed by Dvorkin-Bathe [65] and Q4γ24 developed by Batoz and Dhatt [66]; they are suitable for both thin and thick shells and are applicable to linear and nonlinear problems. Their main feature is that a classical displacement method is used to interpolate the in-plane strains (membrane, bending), and a mix/collocation (or assumed strain) method is used to interpolate the out-plane strains (transverse shear). Certain conditions are also specified:

- They are based on the Reissner-Mindlin model,
- In-plane strains are linear, out-plane strains (transverse shear) are constant throughout the thickness,
- Thickness is constant in the element (the normal and the fiber directions are coincident),
- 5 DOF in the local system (that is, the nodal normal vectors are not constant from one element to another).

Notational Conventions

- A bold letter denotes a vector or a tensor.
- An upper case index denotes a node number; a lower case index denotes a component of vector or tensor.
- The Einstein convention applies only for the repeated index where one is subscript and another is superscript, e.g.:

  $$N_I x^I = \sum N_I x^I$$
- {} denotes a vector and [ ] denotes a matrix.

[63] Belytschko T. and Leviathan I., “Physical stabilization of the 4-node shell element with one-point quadrature”, Computer Methods in Applied Mechanics and Engineering, 113:321-350, 1992.

[64] Zeng Q. and Combescure A., “A New One-point Quadrature, General Nonlinear Quadrilateral Shell Element with Physical Stabilization”, Int. Journal Num. Methods in Engineering 42, 1307-1338, 1998.

Geometry and Kinematics

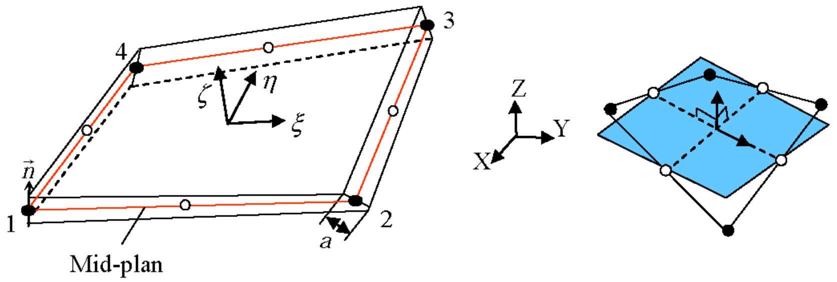

Figure 48: Coordinate Systems

The geometry of the 4-node degenerated shell element, as shown in Figure 48, is defined by its mid-surface with coordinates denoted by Xp interpolated by the node coordinates X^I (I=1,4):

$$Xp(\xi,\eta)=N_I X^I \tag{511}$$

Where, $N_I(\xi,\eta)$ are the bilinear isoparametric shape functions, given by:

$$N_I(\xi,\eta)=\left(1+\xi_I\xi\right)\left(1+\eta_I\eta\right)/4 \tag{512}$$

A generic point q within the shell is derived from point p on the mid-surface and its coordinate along the normal (fiber):

$$Xq(\xi,\eta,\zeta)=Xp+z\cdot n \tag{513}$$

with $z=\frac{a\zeta}{2}$

Where,

a Shell thickness

The transformation between the Cartesian system and the Natural system is given by the differential relation (in matrix form):

$$\{dXq\}=\left([F_0]+z\left[\{n_{,\xi}\}\quad\{n_{,\eta}\}\quad\{0\}\right]\right)\{d\xi\}=[F]\{d\xi\} \tag{514}$$

with $[F_0]=\left[\{g_1\}\{g_2\}\frac{a}{2}\{n\}\right]$; $g_1(\xi,\eta)=X_{p,\xi}=N_{I,\xi}X^I$, $g_2(\xi,\eta)=X_{p,\eta}=N_{I,\eta}X^I$

F is the gradient tensor which is related to the Jacobian tensor $[J]=[F]^t$.

With 5 DOF at each node I (three translational velocities $v^I\rightarrow v_i^I$ and two rotational velocities $\left(\omega^I\rightarrow\omega_i^I\right)$, the velocity interpolation is given by the Mindlin model:

$$v_q(\xi,\eta,\zeta)=v_p+z\beta=N_I(\xi,\eta)\left(v^I+z\beta^I\right) \tag{515}$$

$$\beta=\omega\times n$$

Where, β and ω are the rotational velocity vectors of the normal: $\beta=\beta_1 t_1+\beta_2 t_2=\omega_2 t_1-\omega_1 t_2$

and (t_1, t_2, n) is base of the local coordinate system.

Equation 515 can be written also by:

$v_i = N_I v_i^I + z\left(- N_I \omega_1^I t_{2i}^I + N_I \omega_2^I t_{1i}^I\right); \quad i = 1, 3$

This velocity interpolation is expressed in the global system, but ω^I must be defined first in the local nodal coordinate system to ensure Mindlin's kinematic condition.

Strain-Rate Construction

The in-plane rate-of-deformation is interpolated by the usual displacement method.

The rate-of-deformation tensor (or velocity-strains) $D = \left(L_t + L_{\mathrm{t}}^{\mathrm{T}}\right)/2$ is defined by the velocity gradient tensor L:

$$\{dv_q\} = [L_\zeta]\{d\xi\} = [L_\zeta][F]^{-1}\{dXq\} = [L]\{dXq\} = [Q][L_t][Q]^T\{dXq\} \tag{516}$$

with $[Q] = [\{t_1\}\{t_2\}\{n\}]$.

The Reissner-Mindlin conditions $\varepsilon_\zeta = 0$ and $\sigma_\zeta = 0$ requires that the strain and stress tensors are computed in the local coordinate system (at each quadrature point).

After the linearization of L_t with respect to z, the in-plane rate-of-deformation terms are given by:

$[L_t]_{2\times 2} = [L_{s0}] + z[L_{s1}]$

with the membrane terms:

$[L_{s0}] = [C_1][C_0]$

the bending terms:

$$[L_{s1}] = 2H[L_{s0}] + [C_1]\begin{bmatrix} g^2 \cdot n_{,\eta} & - g^1 \cdot n_{,\eta} \\ - g^2 \cdot n_{,\xi} & g^1 \cdot n_{,\xi} \end{bmatrix}[C_0] + \begin{bmatrix} t_1 \cdot \beta_{,\xi} & t_1 \cdot \beta_{,\eta} \\ t_1 \cdot \beta_{,\xi} & t_1 \cdot \beta_{,\eta} \end{bmatrix} \tag{517}$$

Where, the contravariant vectors $g^\alpha(\alpha = 1, 2)$, dual to g_α, satisfy the orthogonality condition: $g^\alpha.\, g_\beta = \delta_\beta^\alpha$ (Kronecker delta symbol); $H(\xi, \eta)$ is the average curvature: $2H = -\left(g^1 n_{,\xi} + g^2 n_{,\eta}\right)$

$$[C_0] = \begin{bmatrix} t_1 \cdot g^1 & t_2 \cdot g^1 \\ t_1 \cdot g^2 & t_2 \cdot g^2 \end{bmatrix} \quad \text{and} \quad [C_1] = \begin{bmatrix} t_1 \cdot v_{p,\xi} & t_1 \cdot v_{p,\eta} \\ t_2 \cdot v_{p,\xi} & t_2 \cdot v_{p,\eta} \end{bmatrix} \tag{518}$$

The curvature-translation coupling is presented in the bending terms for a warped element (the first two terms in the last equation.)

The out-plane rate-of-deformation (transverse shear) is interpolated by the "assumed strain" method, which is based on the Hu-Washizu variation principle.

If the out-plane rate-of-deformation is interpolated in the same manner for a full integration scheme, it will lead to *shear locking*. It is known that the transverse shear strains energy cannot vanish when it is subjected to a constant bending moment. Dvorkin-Bathe's [65] mix/collocation method has been proved very efficient in overcoming this problem. This method consists in interpolating the transverse shear from the values of the covariant components of the transverse shear strains at 4 mid-side points. That is:

$$\gamma_\xi = \left[(1-\eta)\gamma_{\xi A1} + (1+\eta)\gamma_{\xi A2} \right] / 2 \tag{519}$$

$$\gamma_\eta = \left[(1-\xi)\gamma_{\eta B1} + (1+\xi)\gamma_{\eta B2} \right] / 2 \tag{520}$$

Where, $\gamma_{\xi A\alpha}, \gamma_{\eta B\alpha}$ are the values of the covariant components at 4 mid-side points which vanish under a constant bending moment (Figure 49).

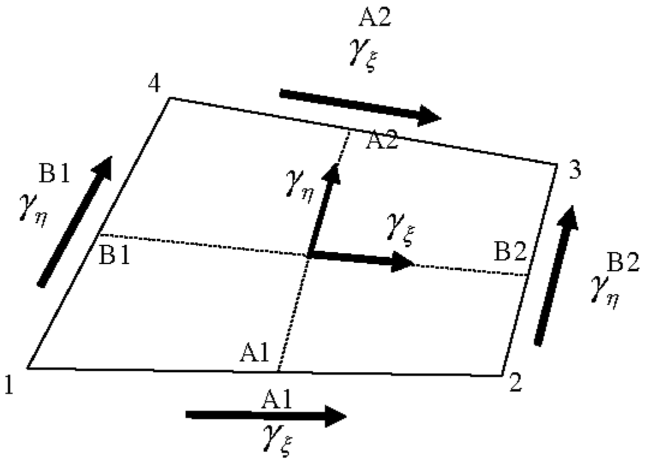

Figure 49: Covariant Components at 4 Mid-Side

Special Case for One-point Quadrature and the Difficulties in Stabilization

The formulations described above are general for both the full integration and reduced integration schemes. For a one-point quadrature element, you have the following particularities:

The quadrature point is often chosen at $(\xi = 0, \eta = 0)$. The derivatives of the shape functions are:

$$N_{I,\xi} = (\xi_I + h_I \eta)/4$$
$$N_{I,\eta} = (\eta_I + h_I \xi)/4 \tag{521}$$

Where, $h_I = (1 \quad -1 \quad 1 \quad -1)$.

This implies that all the terms computed at the quadrature point are the constant parts with respect to (ξ, η), and the stabilizing terms (hourglass) are the non-constant parts.

The constant parts can be derived directly from the general formulations at the quadrature point without difficulty. The difficulties in stabilization lie in correctly computing the internal force vector (or stiffness matrices):

$$f^{\text{int}} = \int_\Omega \bar{B}^t \cdot \sigma \quad d\Omega = f^{\text{int}}(\xi = \eta = 0) + f^{\text{int}}_{stab} \tag{522}$$

It would be ideal if the integration term f_{stab}^{int} could be evaluated explicitly. But such is not the case, and the main obstacles are the following:

For a non-coplanar element, the normal varies at each point so that it is difficult to write the non-constant part of strains explicitly. For a physically nonlinear problem, the non-constant part of stress is not generally in an explicit form. Thus, simplification becomes necessary.

Fully-integrated Shell Element QBAT

QBAT is a fully-integrated shell element based on the general formulation described above. In the surface of each element, 4 Gauss points are used to evaluate the nodal forces.

The main modifications with respect to Q4γ24 shell element [66] are:

- Reduced integration for in-plane shear (constant) to avoid locking.
- Co-rotational coordinate system is used and the stresses are evaluated in 4 local systems at each Gauss points.

One-Point Quadrature Shell Element

In this section, a one-point quadrature shell element formulation will be developed from the general formulation described in the previous section. It is based on the Physical Stabilization method which explicitly computes the stabilization terms in making some simplifications.

The following formulations will be written in the local coordinate system $[\mathbf{t}_1\ \mathbf{t}_2\ \mathbf{n}]$ (the circumflex in the co-rotational system notation has been omitted for convenience).

Kinematic Approximation

The velocity interpolation using the nodal tangent vectors (t_1^I, t_2^I) complicates the strain computation, especially for transverse shear which is used mainly as a penalty function. To be consistent with the one-point quadrature approach, the kinematic approximation is performed by:

$$v_i = N_I\left[v_i^I + z\left(-\delta_{i2}\varpi_1^I + \delta_{i1}\varpi_2^I\right)\right] \tag{523}$$

Where, ϖ_i^I (i=1,2) is the nodal rotation velocity around t_i^I. ϖ_i^I can be computed by a projection scheme by:

$$\varpi^I = \omega^I - \left(\omega^I \cdot n^I\right)n^I = P\left(n^I\right)\omega^I \tag{524}$$

The projection consists in eliminating the nodal drilling rotations in order to reinforce Mindlin's kinematic condition at the nodes. It has been pointed out [67] that without this projection, the element is too flexible and cannot pass the Twisted Beam test.

[65] Dvorkin E. and Bathe K.J. "A continuum mechanics four-node shell element for 35 general nonlinear analysis", Engrg Comput, 1:77-88, 1984.

[66] Batoz J.L. and Dhatt G., "Modeling of Structures by finite element", volume 3, Hermes, 1992.

This projection has a drawback of changing the invariance property to rigid body motion, that is, a warped element being invariant to rigid body rotation will now strains under to rigid body rotation if the drill projection is applied. To overcome this problem, a full projection proposed by Belytschko-Leviathan [68] which free either drilling rotation or rigid motion should be used. This full projection is only used for QEPH element.

In-plane Strain-rate Construction

Constant part

It is useful to write the shape functions in Belytschko-Bachrach's mixed form:

$$N_I(x, y, \xi\eta) = \Delta_I + b_{xI}^{x} + b_{yI}^{y} + \gamma_I \phi \tag{525}$$

with:

$$\Delta_I = \left[t_I - \left(t_I x^I\right) b_{xI} - \left(t_I y^I\right) b_{yI}\right]; \quad t_I = (1, 1, 1, 1)$$

$$b_{xI} = \left(y_{24} y_{31} y_{42} y_{13}\right) / A; \, b_{yI} = \left(x_{42} x_{13} x_{24} x_{31}\right) / A \quad \left(f i j = (f i - f j) / 2\right)$$

$$\gamma_I = \left[h_I - \left(h_J x^J\right) b_{xI} - \left(h_J y^J\right) b_{yI}\right] / 4; \phi = \xi\eta \quad ;$$

A is the area of element.

The derivation of the shape functions is given by:

$$N_{I,\alpha} = b_{\alpha I} + \gamma_I \phi_{,\alpha} (\alpha = x, y)$$

Where,

$$\begin{aligned} \phi_{,x} &= \eta \xi_{,x} + \xi \eta_{,x} = J_{11}^{-1} \eta + J_{12}^{-1} \xi \\ \phi_{,y} &= \eta \xi_{,y} + \xi \eta_{,y} = J_{21}^{-1} \eta + J_{22}^{-1} \xi \end{aligned} \tag{526}$$

The advantage of this shape function form is that a linear field expressed with Cartesian coordinates and a bilinear field expressed with Natural coordinates is decomposed so that the constant part is directly formulated with the Cartesian coordinates, and the non-constant part is to be approached separately.

The in-plane rate-of-deformation (decomposed on membrane and bending) is given by:

$$\{D\} = \{D^m\} + z\{D^b\} = [B_I]\{v_n^I\} \tag{527}$$

with:

[67] Belytschko T. and Leviathan I., "Projection schemes for one-point quadrature shell elements", Computer Methods in Applied Mechanics and Engineering, 115:277-286, 1993.

[68] Belytschko Ted and Leviathan Itai, "Projection schemes for one-point quadrature shell elements", Computer Methods in Applied Mechanics and Engineering, Vol. 115, 227-286, 1994.

$$[B_I]=[B_I^m]+z[B_I^b]; \quad < v_n^I > \; = \; < v_x^I v_y^I v_z^I \varpi_x^I \varpi_y^I > .$$

The development of the general formulations leads to the constant part, denoted by superscript 0, of the matrix $[B_I]$:

$$\left[(B_I^m)^0\right]=\begin{bmatrix} b_{xI} & 0 & 0 \\ 0 & b_{yI} & 0 \\ b_{yI} & b_{xI} & 0 \end{bmatrix} \tag{528}$$

$$\left[(B^b)^0\right]=2H\left[(B_I^m)^0\right]+\begin{bmatrix} b_{xI}^c & 0 & 0 & 0 & b_{xI} \\ 0 & b_{yI}^c & 0 & -b_{yI} & 0 \\ b_{yI}^c & b_{xI}^c & 0 & -b_{xI} & b_{yI} \end{bmatrix}$$

with

$$< b_{xI}^c > \; = 4z_\gamma / A^2 < b_{y2};\; b_{y1};\; b_{y4};\; b_{y3} >$$

$$< b_{yI}^c > \; = 4z_\gamma / A^2 < b_{x4};\; b_{x3};\; b_{x2};\; b_{x1} >$$

The parameter $z_\gamma = \gamma_I z^I$ is a measure of the warping of the element.

The first term $2H\left[(B_I^m)^0\right]$ is neglectable. You have verified that the order of $2H\left[(B_I^m)^0\right]$ is ε times the second term of $\left[(B^b)^0\right]$ with $\varepsilon = 2\bar{x}_{34} / \bar{y}_{34} \quad \left(\bar{f}_{ij} = \left(f_i + f_j\right)/2\right)$, which vanishes when the element is rectangular. Thus, this term is not used in the program.

The constant part of the in-plane rate-of-deformation formulation without the H term is consistent with the result of Belytschko's family shell element [70], [72]though this part has been obtained in a very different manner. Letellier has given the same result in his thesis [71], and studies were also made of the quadratic terms with respect to z.

Non-constant Part

The main simplification for the non-constant part formulation, in order to overcome the difficulties described above, is:

The element is considered to be flat.

In this case, the Jacobian matrix is written as:

$$[J]=[F_0]^t=\begin{bmatrix} x,_\xi & y,_\xi & 0 \\ x,_\eta & y,_\eta & 0 \\ 0 & 0 & a\bar{J}_0/2\bar{J} \end{bmatrix}=\begin{bmatrix} [\bar{J}] & 0 \\ 0 & a\bar{J}_0/2\bar{J} \end{bmatrix} \tag{529}$$

with the determinant $\bar{J}$ of the in-plane Jacobian:

$$\bar{J}=\det[\bar{J}]=\bar{J}_0+\bar{J}_1\xi+\bar{J}_2\eta \tag{530}$$

and:

$$\bar{J}_0 = \left[\left(\xi_I x^I\right)\left(\eta_I y^I\right) - \left(\eta_I x^I\right)\left(\xi_I y^I\right)\right] / 16 = A/4$$

$$\bar{J}_1 = \left[\left(\xi_I x^I\right)\left(h_I y^I\right) - \left(h_I x^I\right)\left(\xi_I y^I\right)\right] / 16$$

$$\bar{J}_2 = \left[\left(h_I x^I\right)\left(\eta_I y^I\right) - \left(\eta_I x^I\right)\left(h_I y^I\right)\right] / 16$$

The inverse of the in-plane Jacobian matrix can be expressed explicitly:

$$[J] = \begin{bmatrix} \xi_{,x} & \eta_{,x} \\ \xi_{,y} & \eta_{,y} \end{bmatrix} = \frac{1}{J}\begin{bmatrix} y_{,\eta} & -y_{,\xi} \\ -x_{,\eta} & x_{,\xi} \end{bmatrix} = \frac{1}{4J}\begin{bmatrix} \left(\eta_I + h_I\xi\right)y^I & \left(\xi_I + h_I\eta\right)y^I \\ \left(\eta_I + h_I\xi\right)x^I & \left(\xi_I + h_I\eta\right)x^I \end{bmatrix} \tag{531}$$

You can now write the non-constant part, denoted by superscript H, of the matrix $[B_I]$ for in-plane rate-of-deformation:

$$\left[\left(B_I^m\right)^H\right] = \begin{bmatrix} \gamma_I\phi_{,x} & 0 & 0 \\ 0 & \gamma_I\phi_{,y} & 0 \\ \gamma_I\phi_{,y} & \gamma_I\phi_{,x} & 0 \end{bmatrix}; \quad \left[\left(B_I^b\right)^H\right] = \begin{bmatrix} 0 & \gamma_I\phi_{,x} \\ -\gamma_I\phi_{,y} & 0 \\ -\gamma_I\phi_{,x} & \gamma_I\phi_{,y} \end{bmatrix} \tag{532}$$

It is shown in [69] that the non-constant part of membrane rate-strain does not vanish when a warped element undergoes a rigid body rotation. Thus, a modified matrix $\left[\left(B_I^m\right)^H\right]$ is chosen:

$$\left[\left(B_I^m\right)^H\right] = \begin{bmatrix} \gamma_I\phi_{,x} & 0 & z_\gamma b_{xI}\phi_{,x} \\ 0 & \gamma_I\phi_{,y} & z_\gamma b_{yI}\phi_{,y} \\ \gamma_I\phi_{,y} & \gamma_I\phi_{,x} & z_\gamma\left(b_{xI}\phi_{,y} + b_{yI}\phi_{,x}\right) \end{bmatrix} \tag{533}$$

This matrix is different from the Belytschko-Leviathan correction term added at rotational positions, which couples translations to curvatures:

$$\left[\left(B_I^m\right)^H\right] = \begin{bmatrix} \gamma_I\phi_{,x} & 0 & 0 & 0 & -\frac{1}{4}z_\gamma\phi_{,x} \\ 0 & \gamma_I\phi_{,y} & 0 & \frac{1}{4}z_\gamma\phi_{,y} & 0 \\ \gamma_I\phi_{,y} & \gamma_I\phi_{,x} & 0 & \frac{1}{4}z_\gamma\phi_{,x} & -\frac{1}{4}z_\gamma\phi_{,y} \end{bmatrix} \tag{534}$$

This will lead to '*membrane locking*' (the membrane strain will not vanish under a constant bending loading). According to the general formulation, the coupling is presented in the bending terms not in the membrane terms, yet the normal translation components in $\left(B_I^m\right)_{i3}$ do not vanish for a warped element due to the tangent vectors $\mathbf{t}_i\,(\xi, \eta)$ which differ from $\mathbf{t}_i$ (0,0).

[69] Belytschko T., Lin J.L. and Tsay C.S., "Explicit algorithms for the nonlinear dynamics of shells", Computer Methods in Applied Mechanics and Engineering, 42:225-251, 1984.

[70] Belytschko T., Wong B.L. and Chiang H.Y. "Advances in one-point quadrature shell elements", Computer Methods in Applied Mechanics and Engineering, 96:93-107, 1989.

Out-plane Strain-rate Construction

The out-plane rate-of-deformation (transverse shear) is interpolated by the Dvorkin-Bathe method, whose closed form is given by Belytschko-Leviathan:

$$\begin{Bmatrix} D_{xz} \\ D_{yz} \end{Bmatrix} = [B_{Ic}] \begin{Bmatrix} v_z^I \\ \varpi_x^I \\ \varpi_y^I \end{Bmatrix} \tag{535}$$

Where, $[B_{Ic}](\zeta, \eta) = [B_{Ic\eta}](\eta) + [B_{Ic\xi}](\xi)$

$$\left(B_{Ic}^{\eta}\right)^0 = \frac{1}{16A} \begin{bmatrix} 4\eta_I y^I \xi_I & -\left(\xi_J + h_J \eta_I\right)\eta_k y^k y^J & \left(\xi_J + h_J \eta_I\right)\eta_k y^k x^J \\ -4\eta_I x^I \xi_I & \left(\xi_J + h_J \eta_I\right)\eta_k x^k y^J & -\left(\xi_J + h_J \eta_I\right)\eta_k x^k x^J \end{bmatrix} \tag{536}$$

$$\left(B_{Ic}^{\xi}\right)^0 = \frac{1}{16A} \begin{bmatrix} -4\xi_I y^I \eta_I & \left(\eta_J + h_J \xi_I\right)\xi_k y^k y^J & -\left(\eta_J + h_J \xi_I\right)\xi_k y^k x^J \\ 4\xi_I y^I \eta_I & -\left(\eta_J + h_J \xi_I\right)\xi_k x^k y^J & \left(\eta_J + h_J \xi_I\right)\xi_k x^k x^J \end{bmatrix}$$

$$\text{and} \quad \left(B_{Ic\eta}\right)^H = \eta_I \left(B_{Ic\eta}\right)^0 \eta; \left(B_{Ic\xi}\right)^H = \xi_I \left(B_{Ic\xi}\right)^0 \xi$$

The straightforward form of $[B_{\mathrm{Ic}}]$ is obtained using one additional simplification:

$$\xi_{,x}(\xi, \eta) = \xi_{,x}(0, 0) \eta_{,x}(\xi, \eta) = \eta_{,x}(0, 0)$$

which is true for a parallelogram element. Although this simplification is not necessary, it is justified by the fact that the transverse shear terms serve mainly as a penalty function.

Explicit Integration of the Nodal Internal Force Vector

Elastic Case

The elementary nodal force vector is computed by:

$$\left\{f_I^{\mathrm{int}}\right\} = \int_{ve} [B_I]^t [C][B_J]\{v_n^J\} dv^e$$

Taking advantage of substantial orthogonality between the:

- Constant in-plane fields along with the non-constant ones
- Membrane and the bending
- In-plane fields and the out-plane fields
- Decomposed non-constant out-plane fields

Resulting in:

$$\left\{f_I^{\mathrm{int}}\right\} = \left\{\left(f_I^{\mathrm{int}}\right)^0\right\} + \left\{\left(f_I^{\mathrm{int}}\right)^H\right\}$$

[71] Letellier Antoine, “Contribution to the modeling of impacts of birds on the blades of aircraft engines”, PhD thesis, University d'Evry, 1996.

With $\left\{\left(f_I^{\text{int}}\right)^0\right\}$ the constant part being computed with one-point quadrature, and

$$\left\{\left(f_I^{\text{int}}\right)^H\right\}=\int_{ve}\left[\left(B_I\right)^H\right]^t\left[C\right]\left[\left(B_J\right)^H\right]\left\{v_n^J\right\}dv^e$$

It can be shown in the last equation that only the following scalar functions need to be integrated:

$$H_{xx}=\int A_e\phi_{,x}\phi_{,x}dA_e,\ H_{xy}=\int A_e\phi_{,x}\phi_{,y}dA_e,\ H_{yy}=\int A_e\phi_{,y}\phi_{,y}dA_e \tag{537}$$

These can be evaluated explicitly.

Defining 6 hourglass generalized rate-of-deformation $\dot{q}$ by:

$$\text{membrane}:\begin{cases}\dot{q}_x^m=\gamma_I v_x^I+z^1 b_{xI}v_z^I\\ \dot{q}_y^m=\gamma_I v_y^I+z^1 b_{yI}v_z^I\end{cases} \tag{538}$$

$$\text{bending}:\begin{cases}\dot{q}_x^b=\gamma_I\varpi_y^I\\ \dot{q}_y^b=\gamma_I\varpi_x^I\end{cases} \tag{539}$$

$$\text{shear}:\begin{cases}\dot{q}_x^s=4h_I v_z^I-\left[\left(\xi_I y^I\right)\eta_I+\left(h_I y^I\right)t_I\right]\varpi_x^I+\left[\left(\xi_I x^I\right)\eta_I+\left(h_I x^I\right)t_I\right]\varpi_y^I\\ \dot{q}_y^s=4h_I v_z^I-\left[\left(\eta_I y^I\right)\xi_I+\left(h_I y^I\right)t_I\right]\varpi_x^I+\left[\left(\eta_I x^I\right)\xi_I+\left(h_I x^I\right)t_I\right]\varpi_y^I\end{cases} \tag{540}$$

The rate-of-deformations will be written explicitly.

The rate form of the constitutive relation is written as (stress plane for in-plane terms):

$\dot{\sigma}=C:D$

With the assumption: *the spin is constant within the element*, the objectivity principle will be satisfied. The incremental computation is performed with the hourglass generalized rate-of-deformation $\dot{q}$:

$$(q)_{n+1}=(q)_n+\dot{q}_{n+\frac{1}{2}}\Delta t$$

Noting that if $\phi_{,\alpha}$ is considered as constant over a time step, it is equivalent to the incremental stress computation.

Physical Nonlinear Case

Now consider an elastoplastic problem.

The elementary nodal internal force vector is now computed by:

$$\left\{f_I^{\text{int}}\right\}=\int_{ve}\left[B_I\right]^t\{\sigma\}dv^e$$

The constitutive relation is written by either a tangent form: $\dot{\sigma}=C^t:D$, or a projection form: $\sigma=P\left(\sigma^e,\ \ldots\right)$

Where, $C^t(\sigma,\ \ldots)$ is the history-dependent tangent tensor; $\left\{\sigma_{n+1}^e\right\}=\left\{\sigma_n\right\}+\left[C\right]\left\{D_{n+1/2}\right\}\Delta t$ is the trial stress, and the function P consists of projecting the trial stress on the updated yield surface.

The decomposed form of the last equation is written:

$$\left\{f_I^{\text{int}}\right\}=\left\{\left(f_I^{\text{int}}\right)^0\right\}+\left\{\left(f_I^{\text{int}}\right)^H\right\}$$

The constant part is computed by integration at each integration point through the thickness.

The stabilization part will be approached by relying on two hypotheses:

- Keep the same orthogonalities as in the elastic case, and
- Use the unidimensional tangent modulus $E_t(\zeta)$ to evaluate the non-constant rate-stress, that is,

  $$\{\dot{\sigma}\}^H=\left(E_t(\zeta)/E\right)[C]\{D\}^H \tag{541}$$

  Where,

  E
  : Young's modulus

  $[C]$
  : Matrix of elastic moduli

Thus, the elastic case easily extends to the nonlinear case.

The incremental computation with the hourglass generalized rate-of-deformation $\dot{q}$ becomes:

$$membrane:\left(q^m\right)_{n+1}=\left(q^m\right)_n+\lambda_m\dot{q}^m_{n+1/2}\Delta t \tag{542}$$

$$bending:\left(q^b\right)_{n+1}=\left(q^b\right)_n+\lambda_b\dot{q}^b_{n+1/2}\Delta t \tag{543}$$

$$shear:\left(q^s\right)_{n+1}=\left(q^s\right)_n+\dot{q}^s_{n+1/2}\Delta t \tag{544}$$

Where, $E_t(\zeta)$ is obtained by the constant stress incremental computation along the thickness and $E_t(\zeta)=E$ in the elastic zone, and $\lambda_m=\bar{E}_t/E$; $\bar{E}_t$ is the average value of $E_t(\zeta)$ and $\lambda_b=\min E_t(\zeta)/E$.

For the QPH shell, λ_m= 1

The key orthogonalities has been maintained without any significant deterioration in performance, although the first two orthogonalities might have been slightly violated. In fact, it is simply due to these orthogonalities that a one-point quadrature element dramatically reduces the computation cost; otherwise you return to the full integration scheme.

Most of the physical stabilization elements have incorporated the following assumption.

The material response is constant within the element.

There are two alternatives to this assumption:

- Take the elastic matrix $[C]$ directly:

  $$\{\dot{\sigma}\}=\{\dot{\sigma}\}^0+[C]\left\{\left(\dot{\varepsilon}-\dot{\varepsilon}^P\right)^H\right\}=\{\dot{\sigma}\}^0+[C]\left\{\left(\dot{\varepsilon}\right)^H\right\}\rightarrow\left\{\left(\dot{\varepsilon}^P\right)^H\right\}=0$$

  which means that the plastic rate-of-deformation $\{\dot{\varepsilon}^P\}$ is constant within the element; or
- Take the tangent matrix [$\mathbf{C}^{\mathbf{t}}$] ($\xi=\eta=0$, $\zeta=$ constant).

Since the components of $[\mathbf{C}^{\mathbf{t}}]$ are generally functions of the updated stress (precisely, the stress deviator for an elastoplastic problem with an associative flow rule, which means that the stress is constant within the element.

Neither of these alternatives is theoretically perfect. Note that the $[C]$ option results in a contradiction with the stress computation (which yields different results for the constant part and the non-constant part); it is more expensive and the tangent form is not generally used for constant stress computations within an explicit program. Hence, the approximation based on the above assumption is not necessary.

The choice of the moduli for the nonlinear case has not been studied for Belytschko-Leviathan's element [72], and it has been shown that this choice has little effect on the result of the "Cylindrical panel test". In [73], the elastic tangent matrix has been used for the evaluation of the stabilizing forces.

QPH,QPPS have shown often stiffer behaviors and sometimes have certain numerical problems in crash simulations.

Advanced Elasto-plastic Hourglass Control

QEPH (Quadrilateral ElastoPlastic Physical Hourglass Control) Element

With one-point integration formulation, if the non-constant part follows exactly the state of constant part for the case of elasto-plastic calculation, the plasticity will be under-estimated due to the fact that the constant equivalent stress is often the smallest one in the element and element will be stiffer. Therefore, defining a yield criterion for the non-constant part seems to be a good idea to overcome this drawback.

From In-plane Strain-rate Construction, Equation 526 and Equation 531, you have the rate of stresses of non-constant part:

$$\{\dot{\sigma}_i\}^H = [C]\{\dot{\varepsilon}\}^H = [C]\begin{Bmatrix} \phi_{,x}\dot{q}_x^{\alpha} \\ \phi_{,y}\dot{q}_y^{\alpha} \\ 0 \end{Bmatrix} = \eta\begin{Bmatrix} \dot{\sigma}_{x\eta}^{\alpha} \\ \dot{\sigma}_{y\eta}^{\alpha} \\ 0 \end{Bmatrix} + \xi\begin{Bmatrix} \dot{\sigma}_{x\xi}^{\alpha} \\ \dot{\sigma}_{y\xi}^{\alpha} \\ 0 \end{Bmatrix} \tag{545}$$

Where, $\alpha = m, b$ corresponds to the membrane and bending terms respectively.

> **Note:** The shear terms are eliminated to avoid shear locking.

The transverse shear terms can also be written as the same way:

$$\{\dot{\tau}_i\}^H = \eta\begin{Bmatrix} \dot{\tau}_{x\eta} \\ \dot{\tau}_{y\eta} \end{Bmatrix} + \xi\begin{Bmatrix} \dot{\tau}_{x\xi} \\ \dot{\tau}_{y\xi} \end{Bmatrix} \tag{546}$$

[72] Belytschko T. and Leviathan I., "Physical stabilization of the 4-node shell element with one-point quadrature", Computer Methods in Applied Mechanics and Engineering, 113:321-350, 1992.

[73] Zhu Y. and Zacharia T., "A new one-point quadrature, quadrilateral shell element with drilling degree of freedom", Computer Methods in Applied Mechanics and Engineering, 136:165-203, 1996.

You can now redefine 12 generalized hourglass stresses by integrating their rate ones, and the stress field can be expressed by:

Membrane, bending

$$\left\{\sigma_i^\alpha\right\} = \left\{\sigma_i^\alpha\right\}^0 + \left\{\sigma_i^\alpha\right\}^H = \left\{\sigma_i^\alpha\right\}^0 + \eta\begin{Bmatrix}\sigma_{x\eta}^\alpha \\ \sigma_{y\eta}^\alpha \\ 0\end{Bmatrix} + \xi\begin{Bmatrix}\sigma_{x\xi}^\alpha \\ \sigma_{y\xi}^\alpha \\ 0\end{Bmatrix}$$

Shear

$$\left\{\tau_i\right\} = \left\{\tau_i\right\}^0 + \left\{\tau_i\right\}^H = \left\{\tau_i\right\}^0 + \eta\begin{Bmatrix}\dot{\tau}_{x\eta} \\ \dot{\tau}_{y\eta}\end{Bmatrix} + \xi\begin{Bmatrix}\dot{\tau}_{x\xi} \\ \dot{\tau}_{y\xi}\end{Bmatrix}$$

Even the redefinition for shear is not necessary as it is not included in the plastic yield criterion, but the same stress calculation as the constant part with the updated Lagrangian formulation is always useful when large strain is involved.

Plastic Yield Criterion

The von Mises type of criterion for any point in the solid element is written by:

$$f = \sigma_{eq}^2(\xi, \eta, \zeta) - \sigma_y^2 = 0 \tag{547}$$

Where, σ_y is evaluated at the quadrature point.

As only one criterion is used for the non-constant part, two choices are possible:

- taking the mean value, that is: $f = f\left(\bar{\sigma}_{eq}\right); \bar{\sigma}_{eq} = \frac{1}{\Omega}\int_\Omega \sigma_{eq} d\Omega$
- taking the value by some representative points, such as eight Gauss points

The second choice has been used in this element.

Elasto-plastic Hourglass Stress Calculation

The incremental hourglass stress is computed by:

- Elastic increment

$$\left(\sigma_i\right)_{n+1}^{trH} = \left(\sigma_i\right)_n^H + [C]\{\dot{\varepsilon}\}^H \Delta t$$

- Check the yield criterion
- If $f \geq 0$, the hourglass stress correction will be done by unradial return

$$\left(\sigma_i\right)_{n+1}^H = P\left(\left(\sigma_i\right)_{n+1}^{trH}, f\right)$$

3-Node Shell Elements

As for the four node shell element, a simple linear Mindlin Plate element formulation is used. Likewise, the use of one integration point and rigid body motion given by the time evolution of the local reference frame is applied. There is no hourglass mode in case of one integration point.

Local Reference Frame

The local reference frame for the three node shell element is shown in Figure 50.

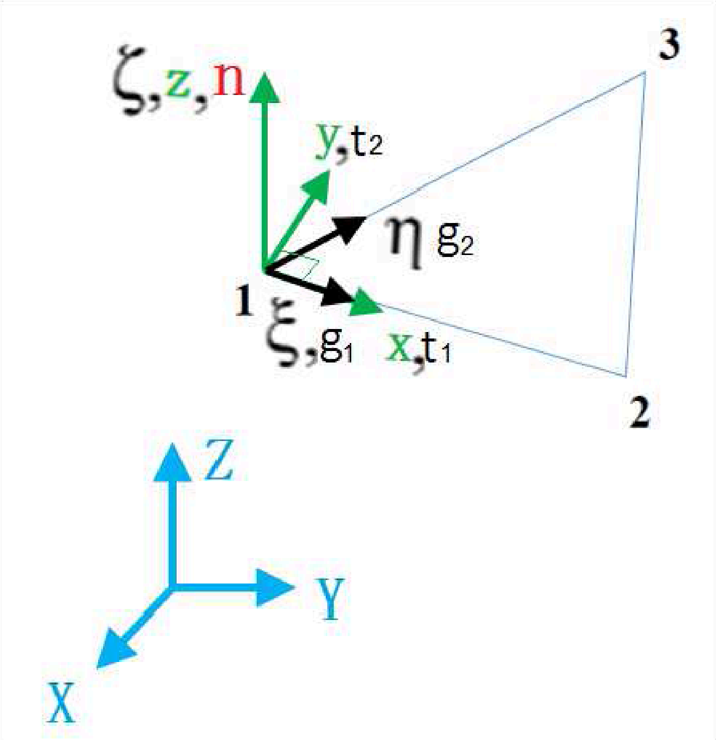

Figure 50: Node Shell Local Reference Frame

The vector normal to the plane of the element is defined as:

$$n = \frac{g_1 \times g_2}{\| g_1 \times g_2 \|} \tag{548}$$

The vector defining the local x direction is defined as edge 1-2:

$$t_1 = \frac{g_1}{\| g_1 \|} \tag{549}$$

Hence, the vector defining the local y direction is found from the cross product of the two previous vectors:

$$t_2 = n \times t_1 \tag{550}$$

Time Step

The characteristic length for computing the critical time step is defined by:

$$L = \frac{2area}{\max(\overline{12}, \overline{23}, \overline{31})} \tag{551}$$

Three Node Shell Shape Functions

The three node shell has a linear shape functions defined as:

$$\phi_1 = a_1 + b_1 x + c_1 y \tag{552}$$

$$\phi_2 = a_2 + b_2 x + c_2 y \tag{553}$$

$$\phi_3 = a_3 + b_3 x + c_3 y \tag{554}$$

These shape functions are used to determine the velocity field in the element:

$$v_x = \sum_{I=1}^{3} \phi_I v_{xI} \tag{555}$$

$$v_y = \sum_{I=1}^{3} \phi_I v_{yI} \tag{556}$$

$$v_z = \sum_{I=1}^{3} \phi_I v_{zI} \tag{557}$$

$$\omega_x = \sum_{I=1}^{3} \phi_I \omega_{xI} \tag{558}$$

$$\omega_y = \sum_{I=1}^{3} \phi_I \omega_{yI} \tag{559}$$

$$\frac{\partial v_x}{\partial x} = \sum_{I=1}^{3} \frac{\partial \phi_I}{\partial x} v_{xI} \tag{560}$$

$$\frac{\partial v_x}{\partial y} = \sum_{I=1}^{3} \frac{\partial \phi_I}{\partial y} v_{xI} \tag{561}$$

Membrane Behavior

The method used to calculate the membrane behavior and the membrane strain rates is exactly the same as that used for four node shell elements (Membrane Behavior).

Bending Behavior

The bending behavior and calculation of the bending strain rates (or curvature rates) is the exact same method used for four node shell elements (Bending Behavior).

Strain Rate Calculation

The strain rate calculation for the three node shell is the same as the method used for the four node shell. However, only three nodes are accounted for. This makes the vectors and matrices smaller. The overall membrane strain rate is calculated by:

$$\{\dot{e}\}_m = \{\dot{e}_x, \dot{e}_y, 2\dot{e}_{xy}\} \tag{562}$$

$$\{v\}_m = \{v_x^1, v_y^1, v_x^2, v_y^2, v_x^3, v_y^3\} \tag{563}$$

$$\{\dot{e}\}_m = [B]_m \{v\}_m \tag{564}$$

Where the $[B]_m$ matrix of shape function gradients is defined as:

$$[B]_m = \begin{bmatrix} \frac{\partial \phi_1}{\partial x} & 0 & \frac{\partial \phi_2}{\partial x} & 0 & 0 & 0 \\ 0 & \frac{\partial \phi_1}{\partial y} & 0 & \frac{\partial \phi_2}{\partial y} & 0 & \frac{\partial \phi_3}{\partial y} \\ \frac{\partial \phi_1}{\partial y} & \frac{\partial \phi_1}{\partial x} & \frac{\partial \phi_2}{\partial y} & \frac{\partial \phi_2}{\partial x} & \frac{\partial \phi_3}{\partial y} & \frac{\partial \phi_3}{\partial x} \end{bmatrix} \tag{565}$$

Where $\frac{\partial \phi_3}{\partial x} = 0$ for a shell element.

The overall bending strain or curvature rate is computed by:

$$\{\dot{e}\}_b = \{\dot{k}_x, k_y, 2\dot{k}_{xy}, 2\dot{e}_{zx}, 2\dot{e}_{yz}\} \tag{566}$$

$$\{v\}_b = \{\omega_y^1, -\omega_x^1, \omega_y^2, -\omega_{\dot{x}}^2 \omega_y^3, -\omega_x^3, v_z^1, v_z^2, v_z^3\} \tag{567}$$

$$\{\dot{e}\}_b = [B]_b \{v\}_{bm} \tag{568}$$

Where,

$$[B] = \begin{bmatrix} \frac{\partial \phi_1}{\partial x} & 0 & \frac{\partial \phi_2}{\partial x} & 0 & 0 & 0 & 0 & 0 & 0 \\ 0 & \frac{\partial \phi_1}{\partial y} & 0 & \frac{\partial \phi_2}{\partial y} & 0 & \frac{\partial \phi_3}{\partial y} & 0 & 0 & 0 \\ \frac{\partial \phi_1}{\partial y} & \frac{\partial \phi_1}{\partial x} & \frac{\partial \phi_2}{\partial y} & \frac{\partial \phi_2}{\partial x} & \frac{\partial \phi_3}{\partial y} & \frac{\partial \phi_3}{\partial x} & 0 & 0 & 0 \\ \phi_1 & 0 & \phi_2 & 0 & \phi_3 & 0 & \frac{\partial \phi_1}{\partial x} & \frac{\partial \phi_2}{\partial x} & \frac{\partial \phi_3}{\partial x} \\ 0 & \phi_1 & 0 & \phi_2 & 0 & \phi_3 & \frac{\partial \phi_1}{\partial y} & \frac{\partial \phi_2}{\partial y} & \frac{\partial \phi_3}{\partial y} \end{bmatrix} \tag{569}$$

Mass and Inertia

The three node shell element is considered as an element with a lumped mass. Its mass is defined as:

$$m = \rho A t \tag{570}$$

Where,

ρ
Material density

t
Shell thickness

A
Reference plane surface area

The mass moment of inertia about all axes is the same:

$$I_{xx} = m\left(\frac{2A}{6} + \frac{t^2}{12}\right) \tag{571}$$

$$I_{zz} = I_{yy} = I_{xx} \tag{572}$$

$$I_{xy} = 0 \tag{573}$$

When nodal masses need to be calculated, the distribution is determined by the shape of the element as shown in Figure 51.

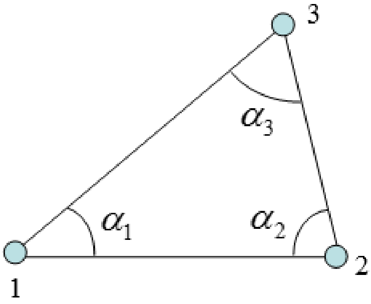

Figure 51: Mass Distribution

The mass and inertia at node i are given by:

$$m_i = \frac{\alpha_i}{\pi} m \quad ; \quad I_i = \frac{\alpha_i}{\pi} I \tag{574}$$

Composite Shell Elements

There are three different element types that can be used for modeling composites.

- `TYPE9` Element Property - Orthotropic Shell
- `TYPE10` Element Property - Composite Shell
- `TYPE11` Element Property - Composite Shell with variable layers

These elements are primarily used with the Tsai-Wu model (material `LAW25`). They allow one global behavior or varying characteristics per layer, with varying orthotropic orientations, varying thickness and/or varying material properties, depending on which element is used. Elastic, plastic and failure modeling can be undertaken.

Transformation Matrix: Global to Orthotropic Skew

If the element reference is defined by the axes X, Y and the orthotropy directions by axes 1-2, write:

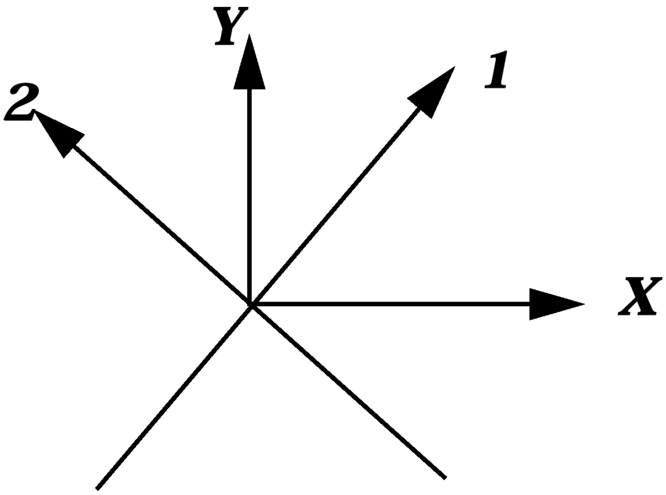

Figure 52: Fiber Orientation

$\begin{bmatrix} c & -s \\ s & c \end{bmatrix}$ with $c = \cos\theta$ and $s = \sin\theta$.

$$\begin{bmatrix} \varepsilon_{11} & \varepsilon_{12} \\ \varepsilon_{12} & \varepsilon_{22} \end{bmatrix} = \begin{bmatrix} c & s \\ -s & c \end{bmatrix} \cdot \begin{bmatrix} \varepsilon_X & \varepsilon_{XY} \\ \varepsilon_{XY} & \varepsilon_Y \end{bmatrix} \cdot \begin{bmatrix} c & -s \\ s & c \end{bmatrix} \tag{575}$$

$$\begin{bmatrix} \varepsilon_{11} & \varepsilon_{12} \\ \varepsilon_{12} & \varepsilon_{22} \end{bmatrix} = \begin{bmatrix} c & s \\ -s & c \end{bmatrix} \cdot \begin{bmatrix} c \cdot \varepsilon_X + s\varepsilon_{XY} & -s \cdot \varepsilon_X + c\varepsilon_{XY} \\ c \cdot \varepsilon_{XY} + s\varepsilon_Y & -s \cdot \varepsilon_{XY} + c\varepsilon_Y \end{bmatrix} \tag{576}$$

$$\begin{bmatrix} \varepsilon_{11} & \varepsilon_{12} \\ \varepsilon_{12} & \varepsilon_{22} \end{bmatrix} = \begin{bmatrix} c^2 \cdot \varepsilon_X + 2cs\varepsilon_{XY} + s^2\varepsilon_Y & -cs \cdot \varepsilon_X + \left(c^2 - s^2\right)\varepsilon_{XY} + cs\varepsilon_Y \\ -cs \cdot \varepsilon_X + \left(c^2 - s^2\right)\varepsilon_{XY} + cs\varepsilon_Y & s^2\varepsilon_X - 2cs\varepsilon_{XY} + c^2\varepsilon_Y \end{bmatrix} \tag{577}$$

The strain-stress relation in orthotropy directions is written as:

$$\{\sigma\} = [C]\{\varepsilon\} \tag{578}$$

$$[C]^{-1} = \begin{bmatrix} \frac{1}{E_{11}} & \frac{-\nu_{21}}{E_{22}} & 0 \\ \frac{-\nu_{12}}{E_{11}} & \frac{1}{E_{22}} & 0 \\ 0 & 0 & \frac{1}{G_{12}} \end{bmatrix} \tag{579}$$

$$\langle\sigma\rangle = \langle\sigma_{11} \quad \sigma_{22} \quad \sigma_{12}\rangle \qquad ; \qquad \langle\varepsilon\rangle = \langle\varepsilon_{11} \quad \varepsilon_{22} \quad \varepsilon_{12}\rangle \tag{580}$$

The computed stresses are then projected to the element reference:

$$\begin{bmatrix} \sigma_{XX} & \sigma_{XY} \\ \sigma_{XY} & \sigma_{YY} \end{bmatrix} = \begin{bmatrix} c & -s \\ s & c \end{bmatrix} \cdot \begin{bmatrix} \sigma_{11} & \sigma_{12} \\ \sigma_{12} & \sigma_{22} \end{bmatrix} \cdot \begin{bmatrix} c & s \\ -s & c \end{bmatrix} \tag{581}$$

Composite Modeling

Radioss has been successfully used to predict the behavior of composite structures for crash and impact simulations in the automotive, rail and aeronautical industries.

The purpose of this chapter is to present the various options available in Radioss to model composites, as well as some modeling methods.

Modeling Composites with Shell Elements

Composite materials with up to 100 layers may be modeled, each with different material properties, thickness, and fiber directions.

Lamina plasticity is taken into account using the Tsai-Wu criteria, which may also consider strain rate effects. Plastic work is used as a plasticity as well as rupture criterion.

Fiber brittle rupture may be taken into account in both orthotropic directions.

Delamination may be taken into account through a damage parameter in shear direction.

Modeling Composites with Solid Elements

Solid elements may be used for composites.

Two material laws are available:

- Solid composite materials: one layer of composite is modeled with one solid element. Orthotropic characteristics and yield criteria are the same as shell elements (Modeling Composites with Shell Elements).
- A honeycomb material law is also available, featuring user defined yield curves for all components of the stress tensor and rupture strain.

Solid + Shell Elements

For sandwich plates, if the foam or the honeycomb is very thick, it is possible to combine composite shells for the plates and solid elements for the sandwich.

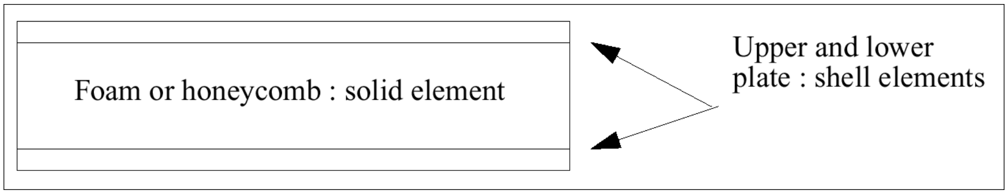
Foam or honeycomb : solid element
Upper and lower plate : shell elements

Figure 53:

Element Orientation

A global reference vector $\mathbf{V}$ is used to define the fiber direction. The direction in which the material properties (or fiber direction) lay is known as the direction 1 of the local coordinate system of orthotropy. It is defined by the ϕ angle, which is the angle between the local direction 1 (fiber direction) and the projection of the global vector $\mathbf{V}$ as shown in Figure 54.

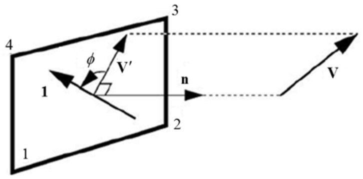

Figure 54: Fiber Direction Orientation

The shell normal defines the positive direction for ϕ. For elements with more than one layer, multiple ϕ angles can be defined.

The fiber direction orientation may be updated by two different ways:

1. Constant orientation in local corotational reference frame constant orientation in local isoparametric frame. The first formulation may lead to unstable models especially in the case of very thin shells (airbag modeling). In Figure 55 the difference between the two formulations is illustrated for the case of element traction and shearing.

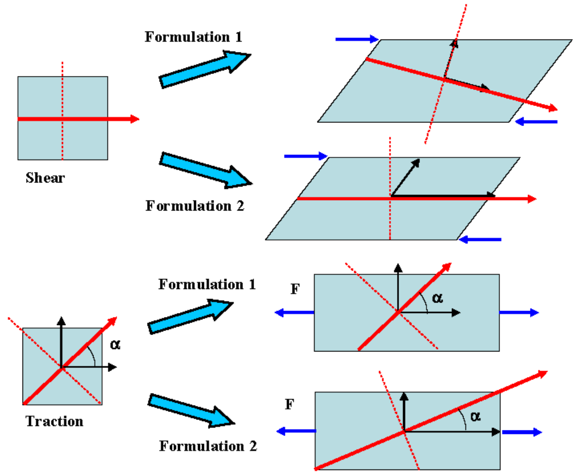

Figure 55: Fiber Direction Updating

Orthotropic Shells

The TYPE9 element property set defines orthotropic shell elements. They have the following properties:

1. Only one layer
2. Can have up to 5 integration points[1] through the thickness
3. One orientation
4. One material property

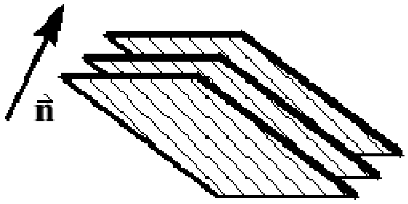

Figure 56:

Composite Shells

The TYPE10 element property set defines composite shell elements. They have the following properties:

1. Up to 100 layers can be modeled
2. Constant layer thickness
3. Constant reference vector
4. Variable layer orientation
5. Constant material properties

Integration is performed with constant stress distribution for each layer.

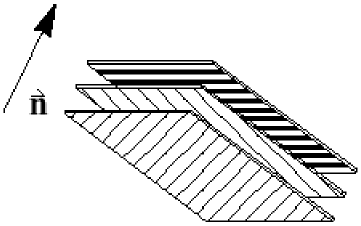

Figure 57:

Composite Shells with Variable Layers

The TYPE11 element property set defines composite shell elements that allow variable layer thicknesses and materials. They have the following properties:

1. Up to 100 layers can be modeled
2. Variable layer thicknesses
3. Constant reference vector
4. Variable layer orientation
5. Variable material properties, $m_i^{2,3}$

Integration is performed with constant stress distribution for each layer.

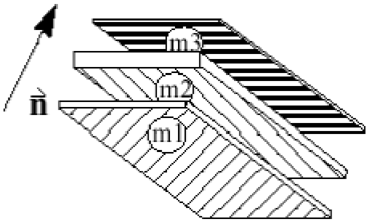

Figure 58:

Limitations

When modeling a composite material, there are two strategies that may be applied. The first, and simplest, is to model the material in a laminate behavior. This involves using TYPE9 property shell elements. The second is to model each ply of the laminate using one integration point. This requires either a TYPE10 or TYPE11 element.

Modeling using the TYPE9 element allows global behavior to be modeled. Input is simple, with only the reference vector as the extra information. A Tsai-Wu yield criterion and hardening law is easily obtained from the manufacturer or a test of the whole material.

Using the TYPE10 or TYPE11 element, one model's each ply in detail, with one integration point per ply and tensile failure is described in detail for each ply. However, the input requirements are complex, especially for the TYPE11 element.

Delamination is the separation of the various layers in a composite material. It can occur in situations of large deformation and fatigue. This phenomenon cannot be modeled in detail using shell theory. A global criterion is available in material LAW25. Delamination can affect the material by reducing the bending stiffness and buckling force.

3-Node Triangle without Rotational DOF

The need of simple and efficient element in nonlinear analysis of shells undergoing large rotations is evident in crash and sheet metal forming simulations. The constant-moment plate elements fit this need. One of the famous concepts in this field is that of Batoz et al. [77] known under DKT elements where DKT stands for Discrete Kirchhoff Triangle. The DKT12 element [77], [78] has a total of 12 DOFs. The discrete Kirchhoff plate conditions are imposed at three mid-point of each side. The element makes use of rotational DOF. at each edge to take into account the bending effects. A simplified three-node element without rotational DOF is presented in [79]. The rotational DOF is computed with the help of out-of-plane translational DOF in the neighbor elements. This attractive approach is used in Radioss in the development of element SH3N6 which based on DKT12.

[74] Same integration rule as shells.

[75] Material number m_i must be defined as LAW25 or LAW27 (not both) in material input cards.

[76] Material given in the shell definition is only used for memory allocation, time step computation and interface stiffness. It must also be defined as LAW25.

Strain Computation

Consider two adjacent coplanar elements with a common edge i-j as shown in Figure 60. Due to out-of-plane displacements of nodes m and k, the elements rotate around the side i-j. The angles between final and initial positions of the elements are respectively α_m and α_k for corresponding opposite nodes m and k. Assuming, a constant curvature for both of elements, the rotation angles θ_m and θ_k related to the bending of each element around the common side are obtained by:

$$\theta_k = \frac{h_k}{2R} \qquad \text{and} \qquad \theta_m = \frac{h_m}{2R} \tag{582}$$

However, for total rotation you have:

$$\theta_k + \theta_m = \alpha_k + \alpha_m \tag{583}$$

which leads to:

$$\theta_k = \frac{(\alpha_k + \alpha_m)h_k}{(h_k + h_m)} \qquad \text{and} \qquad \theta_m = \frac{(\alpha_k + \alpha_m)h_m}{(h_k + h_m)} \tag{584}$$

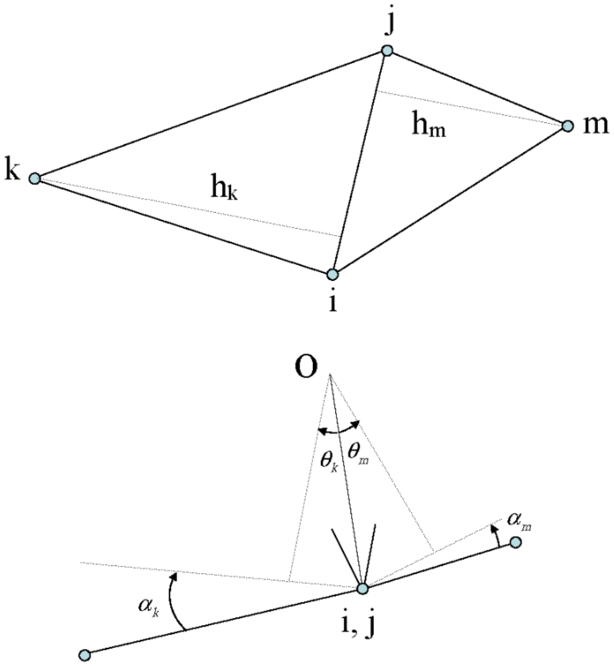

Figure 59: Computation of Rotational DOF in SH3N6

Consider the triangle element in Figure 60. The outward normal vectors at the three sides are defined and denoted $n1$, $n2$ and $n3$. The normal component strain due to the bending around the element side is obtained using plate assumption:

$$\begin{Bmatrix} \varepsilon_{n1} \\ \varepsilon_{n2} \\ \gamma_{n3} \end{Bmatrix} = \begin{bmatrix} \frac{2}{(h_1+h_5)} & 0 & 0 & 0 & \frac{2}{(h_1+h_5)} & 0 \\ 0 & \frac{2}{(h_2+h_6)} & 0 & 0 & 0 & \frac{2}{(h_2+h_6)} \\ 0 & 0 & \frac{2}{(h_3+h_4)} & \frac{2}{(h_3+h_4)} & 0 & 0 \end{bmatrix} \begin{Bmatrix} \alpha_1 \\ \alpha_2 \\ \alpha_3 \\ \alpha_4 \\ \alpha_5 \\ \alpha_6 \end{Bmatrix} \tag{585}$$

The six mid-side rotations α_i are related to the out-of-plane displacements of the six apex nodes as shown in Figure 61 by the following relation:

$$\begin{Bmatrix} \alpha_1 \\ \alpha_2 \\ \alpha_3 \\ \alpha_4 \\ \alpha_5 \\ \alpha_6 \end{Bmatrix} = \begin{bmatrix} \frac{1}{h_1} & -\frac{\cos\beta_3}{h_2} & -\frac{\cos\beta_2}{h_3} & 0 & 0 & 0 \\ -\frac{\cos\beta_3}{h_1} & \frac{1}{h_2} & -\frac{\cos\beta_1}{h_3} & 0 & 0 & 0 \\ -\frac{\cos\beta_2}{h_1} & -\frac{\cos\beta_1}{h_2} & \frac{1}{h_3} & 0 & 0 & 0 \\ -\frac{\cos\gamma_2}{q_1} & -\frac{\cos\gamma_1}{q_2} & 0 & \frac{1}{h_4} & 0 & 0 \\ 0 & -\frac{\cos\psi_3}{r_2} & -\frac{\cos\psi_2}{r_3} & 0 & \frac{1}{h_5} & 0 \\ -\frac{\cos\varphi_2}{s_1} & 0 & -\frac{\cos\varphi_1}{s_3} & 0 & 0 & \frac{1}{h_6} \end{bmatrix} \begin{Bmatrix} w_1 \\ w_2 \\ w_3 \\ w_4 \\ w_5 \\ w_6 \end{Bmatrix} \tag{586}$$

Where, $(h_1 \;\; h_2 \;\; h_3)$, $(q_1 \;\; h_4 \;\; q_2)$, $(r_2 \;\; h_5 \;\; r_3)$ and $(s_3 \;\; h_6 \;\; s_1)$ are respectively the heights of the triangles (1,2,3), (1,4,2), (2,5,3) and (3,6,1).

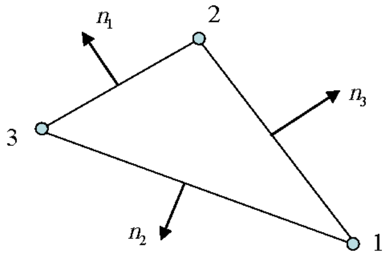

Figure 60: Normal Vectors Definition

The non-null components of strain tensor in the local element reference are related to the normal components of strain by the following relation: [77] [79]

$$\begin{Bmatrix} \varepsilon_{xx} \\ \varepsilon_{yy} \\ \gamma_{xy} \end{Bmatrix} = \begin{bmatrix} \left(\frac{y_3-y_2}{l_1}\right)^2 & \left(\frac{y_1-y_3}{l_2}\right)^2 & \left(\frac{y_2-y_1}{l_3}\right)^2 \\ \left(\frac{x_2-x_3}{l_1}\right)^2 & \left(\frac{x_3-x_1}{l_2}\right)^2 & \left(\frac{x_1-x_2}{l_3}\right)^2 \\ 2\left(\frac{y_3-y_2}{l_1}\right)\left(\frac{x_2-x_3}{l_1}\right) & 2\left(\frac{y_1-y_3}{l_2}\right)\left(\frac{x_3-x_1}{l_2}\right) & 2\left(\frac{y_2-y_1}{l_3}\right)\left(\frac{x_1-x_2}{l_3}\right) \end{bmatrix} \begin{Bmatrix} \varepsilon_{n1} \\ \varepsilon_{n2} \\ \gamma_{n3} \end{Bmatrix} \tag{587}$$

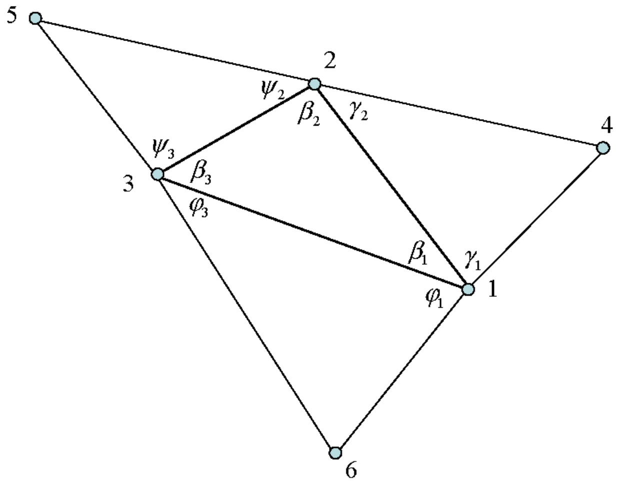

Figure 61: Neighbor Elements for a Triangle

Boundary Conditions Application

As the side rotation of the element is computed using the out-of-plane displacement of the neighbor elements, the application of clamped or free boundary conditions needs a particular attention. It is natural to consider the boundary conditions on the edges by introducing a virtual and symmetric element outside of the edge as described in Figure 62. In the case of free rotation at the edge, the normal strain ε_{nk} is vanished. From Equation 585, this leads to:

$$\alpha_k = -\alpha_m \tag{588}$$

In Equation 586 the fourth row of the matrix is then changed to:

$$\left[\frac{\cos\beta_2}{h_1} \quad \frac{\cos\beta_1}{h_2} \quad -\frac{1}{h_3} \quad 0 \quad 0 \quad 0\right] \tag{589}$$

The clamped condition is introduced by the symmetry in out-of-plane displacement, that is, $w_m = w_k$. This implies $\alpha_k = \alpha_m$. The fourth row of the matrix in Equation 586 is then changed to:

$$\left[-\frac{\cos\beta_2}{h_1} \quad -\frac{\cos\beta_1}{h_2} \quad -\frac{1}{h_3} \quad 0 \quad 0 \quad 0\right] \tag{590}$$

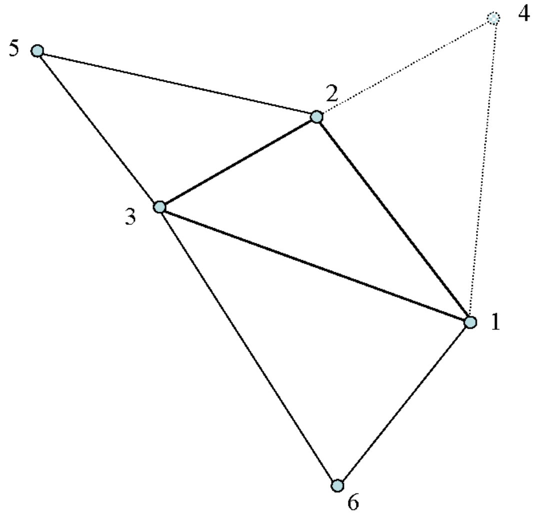

Figure 62: Virtual Element Definition for Boundary Conditions Application

77. Batoz J.L. and Dhatt G., "Modeling of Structures by finite element", volume 3, Hermes, 1992.

78. Batoz J.L., Guo Y.Q., Shakourzadeh H., "Nonlinear Analysis of thin shells with elasto-plastic element DKT12", Revue Europénne des Eléments Finis, Vol. 7, N° 1-2-3, pp. 223-239. 1998.

79. Sabourin F. and Brunet M., "Analysis of plates and shells with a simplified three-node triangle element", Thin-walled Structures, Vol. 21, pp. 209-223, Elsevier, 1995.

Solid-Shell Elements

Solid-shell elements form a class of finite element models intermediate between thin shell and conventional solid elements. From geometrical point of view, they are represented by solid meshes with two nodes through the thickness and generally without rotational degree-of-freedom. On the other hand, they account for shell-like behavior in the thickness direction. They are useful for modeling shell-like portions of a 3D structure without the need to connect solid element nodes to shell nodes (Figure 63).

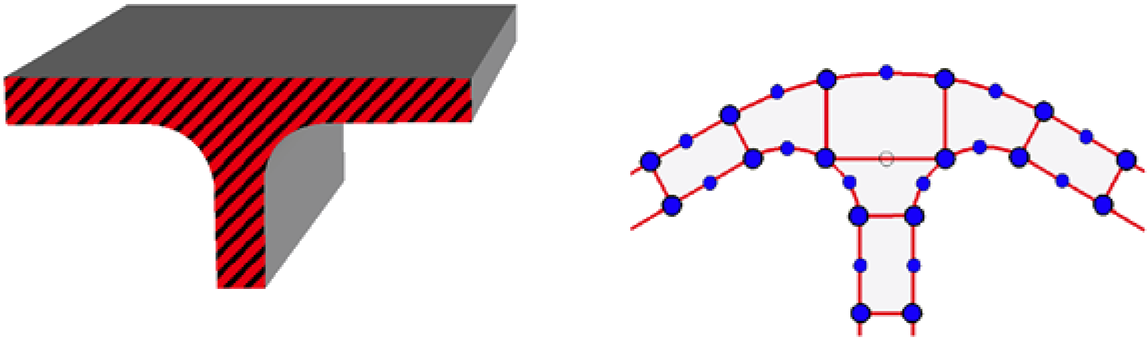

Figure 63: Solid-Shell Elements Application

The derivation of solid-shell elements is more complicated than that of standard solid elements since they are prone to the following problems:

- Shear and membrane locking with the hybrid strain formulation [80 81], the hybrid stress [82], and the Assumed and Enhanced Natural Strain formulations. [83 84 85 86]
- Trapezoidal locking caused by deviation of mid-plane from rectangular shape [87].
- Thickness locking due to Poisson's ratio coupling of the in-plane and transverse normal stresses. [80 81 83 85]

Solid shell elements in Radioss are the solid elements with a treatment of the normal stresses in the thickness direction. This treatment consists of ensuring constant normal stresses in the thickness by a penalty method. Advantage of this approach with respect to the plane-stress treatment is that it can simulate the normal deformability and exhibits no discernible locking problems. The disadvantage is its possible small time step since it is computed as solid element and the characteristic length is determined often using the thickness.

The solid-shell elements of Radioss are:

- HA8: 8-node linear solid and solid-shell with or without reduced integration scheme,
- HSEPH: 8-node linear thick shell with reduced integration scheme and physical stabilization of hourglass modes,
- PA6: Linear pentahedral element for thick shells,
- SHELL16: 16-node quadratic thick shell.

The thick shell elements HA8 and HSEPH are respectively the solid elements HA8 and HEPH in which the hypothesis of constant normal stress through the thickness is applied by penalty method. The theoretical features of these elements are explained in Solid Hexahedron Elements. The thick shell element SHELL16 is described hereby.

Thick Shell Elements SHELL16

The element can be used to model thick-walled structures situated between 3D solids and thin shells. The element is presented in Figure 64. It has 16 nodes with three translational DOFs per each node. The element is quadratic in plane and linear through the thickness. The numerical integration through the thickness is carried out by Gauss-Lobatto schemes rise up to 9 integrations to enhance the quality of elasto-plastic behavior. The in-plane integration may be done by a reduced 2x2 scheme or a fully integrated 3x3 points (Figure 65). A reduced integration method is applied to the normal stress in order to avoid locking problems.

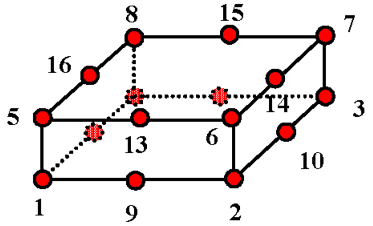

Figure 64: Thick Shell Element SHELL16

The distribution of mass is not homogenous over the nodes. The internal nodes receive three times more mass than the corner nodes as shown in Figure 66.

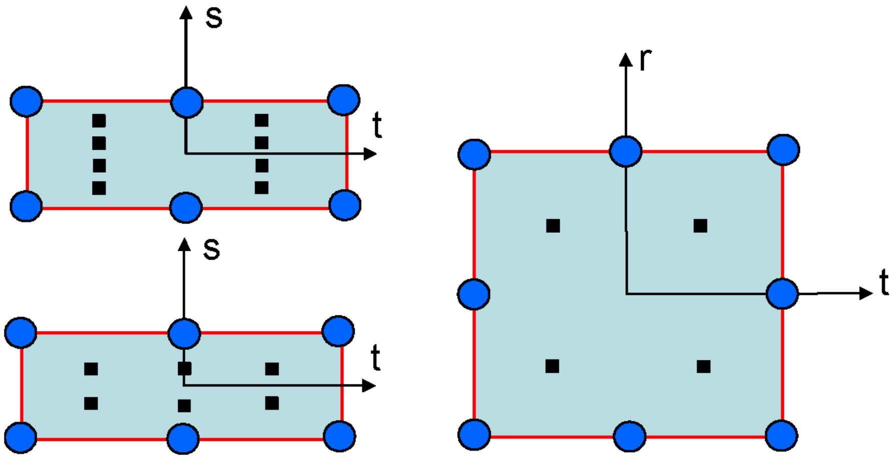

(a) Two to nine integration points through the thickness

(b) In-plane 2x2 and 3x3 integration schemes

Figure 65: Integration Points for SHELL16

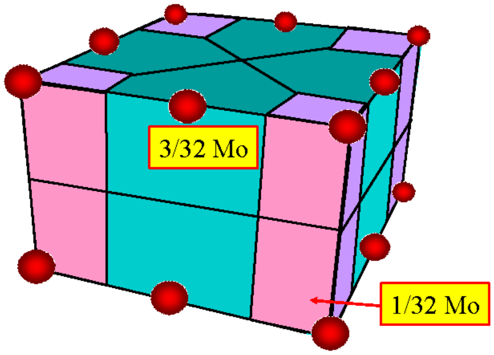

Figure 66: Mass Distribution for SHELL16 Element

80. Ausserer M.F. and Lee S.W., "An eighteen node solid element for thin shell analysis",Int. Journal Num. Methods in Engineering, Vol. 26, pp. 1345, 1364, 1988.

81. Park H.C., Cho C. and Lee S.W., "An efficient assumed strain element model with six dof per node for geometrically nonlinear shells", Int. Journal Num. Methods in Engineering, Vol. 38, pp. 4101-4122, 1995.

82. Sze K.Y. and Ghali A., "A hexahedral element for plates, shells and beam by selective scaling", Int. Journal Num. Methods in Engineering, Vol. 36, pp. 1519-1540, 1993.

83. Betch P. and Stein E., "An assumed strain approach avoiding artificial thickness straining for a nonlinear 4-node shell element", Computer Methods in Applied Mechanics and Engineering, Vol. 11, pp. 899-909, 1997.

84. Bischoff M. and Ramm E., "Shear deformable shell elements for large strains and rotations", Int. Journal Num. Methods in Engineering, Vol. 40, pp. 445-452, 1997.

85. Hauptmann R. and Schweizerhof K., "A systematic development of solid-shell element formulations for linear and nonlinear analysis employing only displacement degrees of freedom", Int. Journal Num. Methods in Engineering, Vol. 42, pp. 49-69, 1988.

86. Simo J.C. and Rifai M.S., "A class of mixed assumed strain methods and the method of incompatible modes", Int. Journal Num. Methods in Engineering, Vol. 9, pp. 1595-1638, 1990.

87. Donea J., "An Arbitary Lagrangian-Eulerian finite element method for transient dynamic fluid-structure interactions", Computer methods in applied mechanics, 1982.

Truss Elements (TYPE2)

Truss elements are simple two node linear members that only take axial extension or compression. Figure 67 shows a truss element.

Figure 67: Truss Element

Property Input

The only property required by a truss element is the cross-sectional area. This value will change as the element is deformed. The cross sectional area is computed using:

$$Area(t) = \frac{Area(t - \Delta t)}{(1 - v\dot{\varepsilon}_x \Delta t)^2} \tag{591}$$

Where,

v Poisson's ratio defined in the material law

Stability

Determining the stability of truss elements is very simple. The characteristic length is defined as the length of the element, that is, the distance between N1 and N2 nodes.

$$\Delta t \le \frac{L(t)}{C} \tag{592}$$

Where,

$L(t)$ Current truss length

$C = \sqrt{\frac{E}{\rho}}$ Sound speed

Rigid Body Motion

The rigid body motion of a truss element as shown in Figure 68 shows the different velocities of nodes 1 and 2. It is the relative velocity difference between the two nodes that produces a strain in the element, namely e_x.

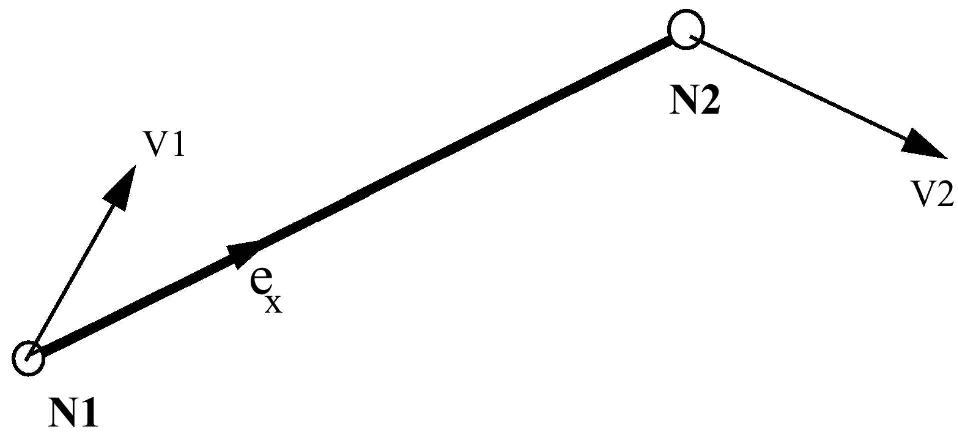

Figure 68: Truss Motion

Strain

The strain rate, as shown in Figure 68, is defined as:

$$\dot{\varepsilon}_x = \frac{\partial v_x}{\partial x} = \frac{\partial\left(\vec{V} \cdot \vec{e}_x\right)}{\partial x} \tag{593}$$

Material Type

A truss element may only be assigned two types of material properties. These are TYPE1 and TYPE2, elastic and elasto-plastic properties, respectively.

Force Calculation

The calculation of forces in a truss element is performed by explicit time integration:

$$Area(t) = \frac{Area(t - \Delta t)}{\left(1 - v\dot{\varepsilon}_x \Delta t\right)^2} \tag{594}$$

A generalized force-strain graph can be seen in Figure 69. The force rate under elastic deformation is given by:

$$\dot{F}_x = EA\dot{\varepsilon}_x \tag{595}$$

Where,

E	Elastic modulus
A	Cross-sectional area

In the plastic region, the force rate is given by:

$$\dot{F}_x = E_t A\dot{\varepsilon}_x \tag{596}$$

Where,

E_t Gradient of the material curve at the deformation point

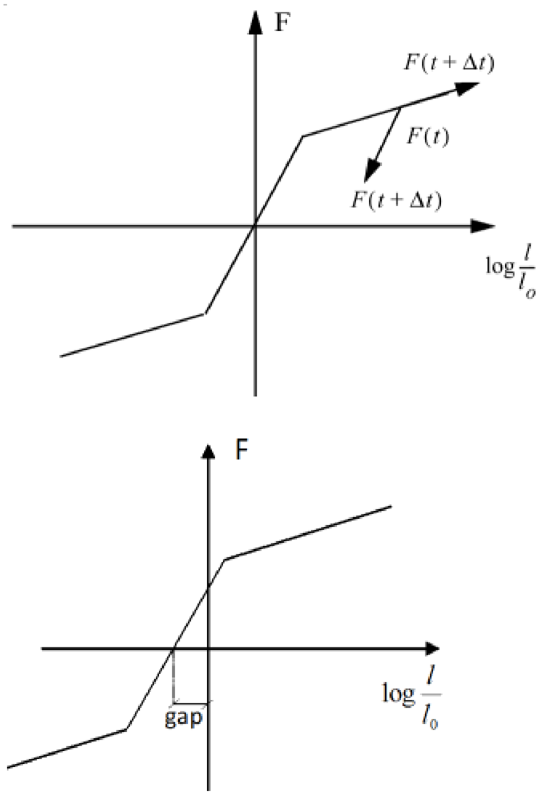

Figure 69: Force-Strain Relationship
(a) without gap; (b) with gap

In a general case, it is possible to introduce a gap distance in the truss definition. If gap is not null, the truss is activated when the length of the element is equal to the initial length minus the gap value. This results a force-strain curve shown in Figure 69(b).

Beam Elements (TYPE3)

Radioss uses a shear beam theory or Timoshenko formulation for its beam elements.

This formulation assumes that the internal virtual work rate is associated with the axial, torsional and shear strains. The other assumptions are:

- No cross-section deformation in its plane.
- No cross-section warping out of its plane.

With these assumptions, transverse shear is taken into account.

This formulation can degenerate into a standard Euler-Bernoulli formulation (the cross section remains normal to the beam axis). This choice is under user control.

Local Coordinate System

The properties describing a beam element are all defined in a local coordinate system.

This coordinate system can be seen in Figure 70. Nodes 1 and 2 of the element are used to define the local X axis, with the origin at node 1. The local Y axis is defined using node 3, which lies in the local XY plane, along with nodes 1 and 2. The Z axis is determined from the vector cross product of the positive X and Y axes.

The local Y direction is first defined at time $t=0$ and its position is corrected at each cycle, taking into account the mean rotation of the X axis. The Z axis is always orthogonal to the X and Y axes.

Deformations are computed with respect to the local coordinate system displaced and rotated to take into account rigid body motion. Translational velocities V and angular velocities Ω with respect to the global reference frame are expressed in the local frame.

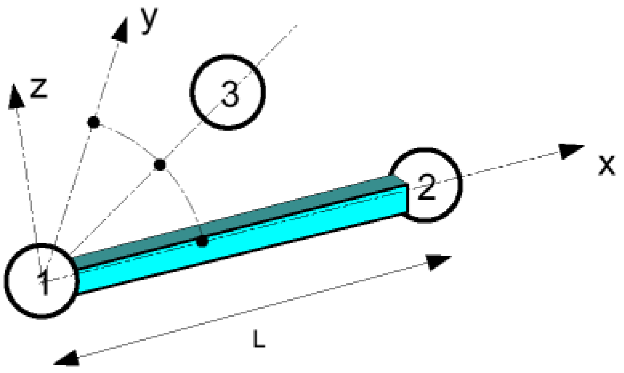

Figure 70: Beam Element Local Axis

Beam Element Geometry

The beam geometry is user-defined by:

A	Cross section area
I_x	Area moment of inertia of cross section about local x axis

I_y	Area moment of inertia of cross section about local y axis
I_z	Area moment of inertia of cross section about local z axis

The area moments of inertia about the y and z axes are concerned with bending. They can be calculated using the relationships:

$$I_y = \iint_A z^2 dydz \tag{597}$$

$$I_z = \iint_A y^2 dydz \tag{598}$$

The area moment of inertia about the x axis concerns torsion. This is simply the summation of the previous two moments of Ontario:

$$I_x = I_y + I_z \tag{599}$$

Minimum Time Step

The minimum time step for a beam element is determined using the following relation:

$$\Delta t = \frac{aL}{c} \tag{600}$$

Where,

c is the speed of sound: $\sqrt{E/\rho}$,

$a = \frac{1}{2}\min\left(\sqrt{\min\left(4,\ 1+\frac{b}{12}\right)} \cdot F_1,\ \sqrt{\frac{b}{3}} \cdot F_2\right)$,

$F_1 = \sqrt{1+2d^2} - \sqrt{2}\,d$

$F_2 = \min\left(F_1,\ \sqrt{1+2d_s2} - \sqrt{2}\,d_s\right)$

$b = \frac{AL^2}{\max(I_y,\ I_z)}$

$d = \max(d_m,\ d_f)$

$d_s = d \cdot \max\left(1,\ \sqrt{\frac{12}{b}} \cdot \sqrt{1+\frac{12E}{\frac{5}{6}Gb}(1-I_{shear})}\right)$

Beam Element Behavior

Radioss beam elements behave in four individual ways:

- Membrane or axial deformation
- Torsion
- Bending about the z axis

- Bending about the y axis

Membrane Behavior

Membrane or axial behavior is the extension or compression of the beam element. The forces acting on an element are shown in Figure 71.

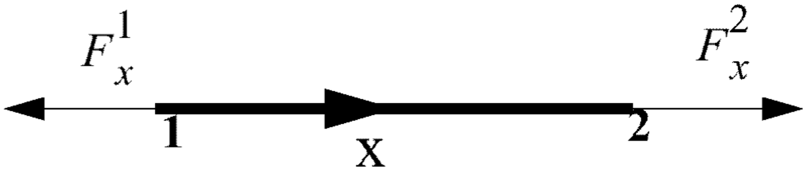

Figure 71: Membrane Forces

The force rate vector for an element is calculated using the relation:

$$\begin{bmatrix}\dot{F}_{x1}\\ \dot{F}_{x2}\end{bmatrix} = \frac{EA}{l}\begin{bmatrix}+1 & -1\\ -1 & +1\end{bmatrix}\begin{bmatrix}\upsilon_{x1}\\ \upsilon_{x2}\end{bmatrix} \tag{601}$$

Where,

E	Elastic modulus
l	Beam element length
υ_x	Nodal velocity in x direction

With the force rate equation, the force vector is determined using explicit time integration:

$$F_x(t+\Delta t) = F_x(t) + \dot{F}_x \Delta t \tag{602}$$

Torsion

Torsional deformation occurs when the beam is loaded with a moment M about the X axis as shown in Figure 72.

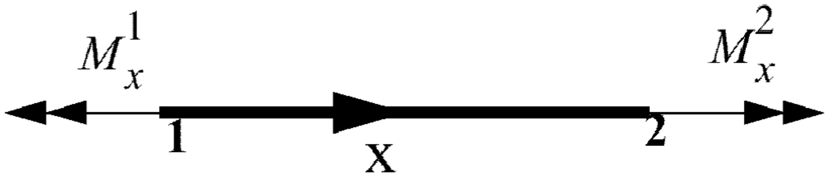

Figure 72: Torsional Loading

The moment rate vector is computed by:

$$\begin{bmatrix}\dot{M}_{x1}\\ \dot{M}_{x2}\end{bmatrix} = \frac{GI_x}{l}\begin{bmatrix}+1 & -1\\ -1 & +1\end{bmatrix}\begin{bmatrix}\dot{\theta}_{x1}\\ \dot{\theta}_{x2}\end{bmatrix} \tag{603}$$

Where,

G	Modulus of rigidity
$\dot{\theta}_x$	Angular rotation rate

The moment about the X axis is found by explicit time integration:

$$M_x(t+\Delta t)=M_x(t)+\dot{M}_x\Delta t \tag{604}$$

Bending About Z-axis

Bending about the z axis involves a force in the y direction and a moment about the z axis as shown in Figure 73.

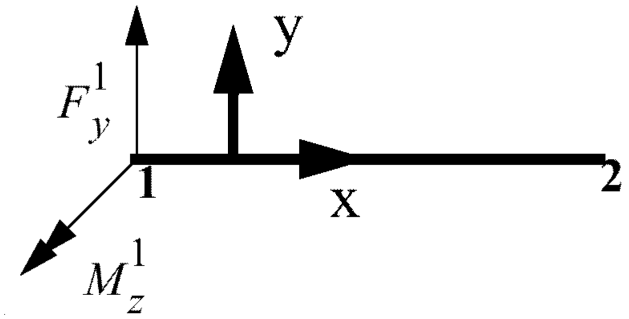

Figure 73: Bending about the Z Axis

Two vector fields must be solved for forces and moments. The rate equations are:

$$\begin{bmatrix}\dot{F}_{y1}\\ \dot{F}_{y2}\end{bmatrix}=\frac{EI_z}{l^3(1+\phi_y)}\begin{bmatrix}+12 & 6l & -12 & +6l\\ -12 & -6l & +12 & -6l\end{bmatrix}\begin{bmatrix}v_{y1}\\ \dot{\theta}_{z1}\\ v_{y2}\\ \dot{\theta}_{z2}\end{bmatrix} \tag{605}$$

$$\begin{bmatrix}\dot{M}_{z1}\\ \dot{M}_{z2}\end{bmatrix}=\frac{EI_z}{l^3(1+\phi_y)}\begin{bmatrix}+6l & (4+\phi_y)l^2 & -6l & (2-\phi_y)l^2\\ +6l & (2-\phi_y)l^2 & -6l & (4+\phi_y)l^2\end{bmatrix}\begin{bmatrix}v_{y1}\\ \dot{\theta}_{z1}\\ v_{y2}\\ \dot{\theta}_{z2}\end{bmatrix} \tag{606}$$

Where,

$\phi_y=\frac{144(1+v)I_z}{5Al^2}$,

υ is the Poisson's ratio.

The factor ϕ_y takes into account transverse shear.

The time integration for both is:

$$F_y(t+\Delta t)=F_y(t)+\dot{F}_y\Delta t \tag{607}$$

$$M_z(t+\Delta t)=M_z(t)+\dot{M}_z\Delta t \tag{608}$$

Bending About Y-axis

Bending about the Y axis is identical to bending about the Z axis. A force in the Y direction and a moment about the Z axis, shown in Figure 74, contribute to the elemental bending.

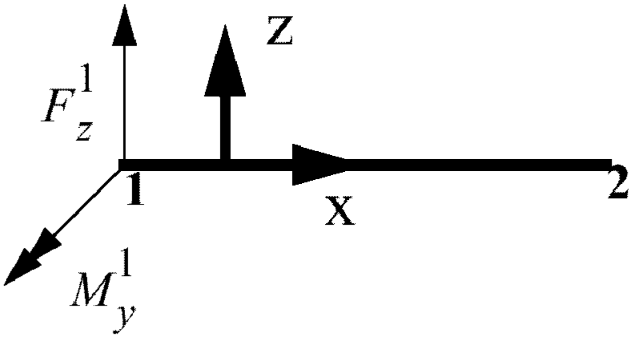

Figure 74: Bending about Y Axis

The rate equations are:

$$\begin{bmatrix}\dot{F}_{z1}\\ \dot{F}_{z2}\end{bmatrix}=\frac{EI_y}{l^3(1+\Phi_z)}\begin{bmatrix}+12 & 6l & -12 & +6l\\ -12 & -6l & +12 & -6l\end{bmatrix}\begin{bmatrix}v_{z1}\\ \dot{\theta}_{y1}\\ v_{z2}\\ \dot{\theta}_{y2}\end{bmatrix} \tag{609}$$

$$\begin{bmatrix}\dot{M}_{y1}\\ \dot{M}_{y2}\end{bmatrix}=\frac{EI_y}{l^3(1+\Phi_z)}\begin{bmatrix}+6l(4+\Phi_z)l^2 & -6l(2-\Phi_z)l^2\\ +6l(2-\Phi_z)l^2 & -6l(4+\Phi_z)l^2\end{bmatrix}\begin{bmatrix}v_{z1}\\ \dot{\theta}_{y1}\\ v_{z2}\\ \dot{\theta}_{y2}\end{bmatrix} \tag{610}$$

Where, $\Phi_z=\dfrac{144(1+v)I_y}{5Al^2}$.

Like bending about the Z axis, the factor Φ_z introduces transverse shear.

With the time integration, the expression is:

$$F_z(t+\Delta t)=F_z(t)+\dot{F}_z\Delta t \tag{611}$$

$$M_y(t+\Delta t)=M_y(t)+\dot{M}_y\Delta t \tag{612}$$

Material Properties

A beam element may have two different types of material property:

- Elastic
- Elasto-plastic

Elastic Behavior

The elastic beam is defined using material LAW1 which is a simple linear material law.

The cross-section of a beam is defined by its area A and three area moments of inertia I_x, I_y and I_z.

An elastic beam can be defined with these four parameters. For accuracy and stability, the following limitations should be respected:

$$L > \sqrt{A} \tag{613}$$

$$0.01A^2 < I_y < 100A^2 \tag{614}$$

$$0.01A^2 < I_z < 100A^2 \tag{615}$$

$$0.1(I_y + I_z) < I_x < 10(I_y + I_z) \tag{616}$$

Elasto-plastic Behavior

A global plasticity model is used.

The main assumption is that the beam cross section is full and rectangular. Optimal relations between sections and section inertia are:

$$12I_yI_z = A^4 \tag{617}$$

$$I_x = I_y + I_z \tag{618}$$

However, this model also gives good results for the circular or ellipsoidal cross-section. For tubular or H cross-sections, plasticity will be approximated.

Recommendations:

$$L > \sqrt{A} \tag{619}$$

$$0.1A^4 < 12I_yI_z < 10A^4 \tag{620}$$

$$0.01 < I_y / I_z < 100 \tag{621}$$

$$0.5(I_y + I_z) < I_x < 2(I_y + I_z) \tag{622}$$

Global Beam Plasticity

The elasto-plastic beam element is defined using material LAW2:

$$\sigma_y = \left(A + B\varepsilon_p^n\right)\left(1 + C\ln\frac{\dot{\varepsilon}}{\dot{\varepsilon}_0}\right) \tag{623}$$

The increment of plastic strain is:

$$\Delta\varepsilon_p = \frac{\Delta W_{plastic}}{\sigma_y} \tag{624}$$

The equivalent strain rate is derived from the total energy rate:

$$\dot{\varepsilon} = \frac{\Delta W_{total}}{\sigma_{eq}\Delta t} \tag{625}$$

Yield stress:

$$\sigma_{eq} = \sqrt{\frac{F_x^2}{A^2} + \frac{3}{A}\left(\frac{M_x^2}{I_{xx}} + \frac{M_y^2}{I_{yy}} + \frac{M_z^2}{I_{zz}}\right)} \tag{626}$$

If $\sigma_{eq} > \sigma_y$, you perform a radial return on the yield surface:

$$F_x^{pa} = F_x\frac{\sigma_y}{\sigma_{eq}} \tag{627}$$

and for i= x, y, z:

$$M_i^{pa} = M_i\frac{\sigma_y}{\sigma_{eq}} \tag{628}$$

Inertia Computation

The computational method of inertia for some kinds of elements as beam is particular as the inertia has to be transferred to the extremities of the beam. The nodal inertias are computed in function of the material density ρ, the cross-section area S, the element length L and the moments of inertia I_{xx}, I_{yy}, I_{zz}:

$$MAX\left(\left(\frac{\rho SL}{2}\right)\left(\frac{L^2}{12}\right) + \left(\frac{\rho L}{2}\right) \bullet MAX\left(I_{yy} \;\; ; \;\; I_{zz}\right) \; ; \; \left(\frac{\rho L}{2}\right) \bullet I_{xx}\right) \tag{629}$$

One Degree of Freedom Spring Elements (TYPE4)

One degree of freedom (DOF) spring elements are defined as a TYPE4 property set. Three variations of the element are possible:

- Spring only
- Dashpot (damper) only
- Spring and dashpot in parallel

These three configurations are shown in Figure 75 to Figure 77.

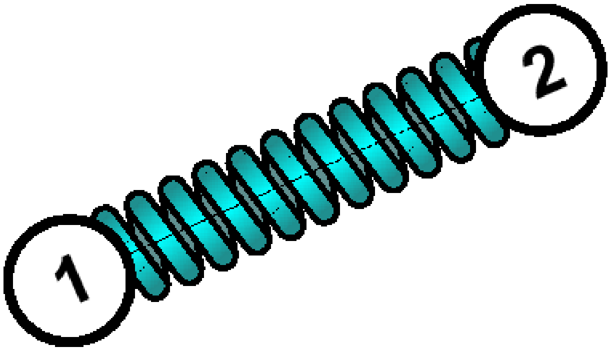

Figure 75: Spring Only

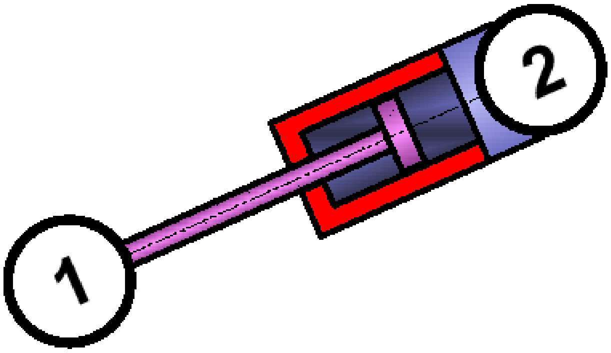

Figure 76: Dashpot Only

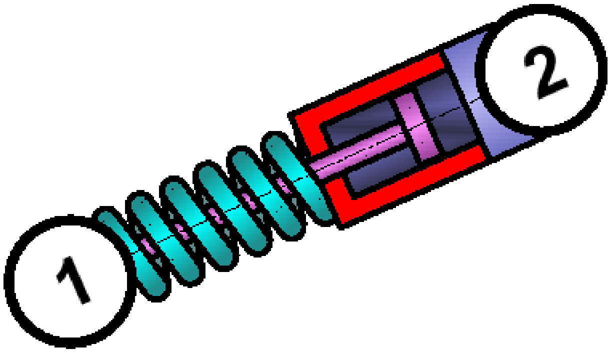

Figure 77: Spring and Dashpot in Parallel

No material data card is required for spring elements. However, the stiffness k and equivalent viscous damping coefficient c are required. The mass m is required if there is any spring translation.

There are three other options defining the type of spring stiffness with the hardening flag:

- Linear Stiffness
- Nonlinear Stiffness
- Nonlinear Elasto-Plastic Stiffness

Likewise, the damping can be either:

- Linear
- Nonlinear

A spring may also have zero length. However, a one DOF spring must have 2 nodes.

The forces applied on the nodes of a one DOF spring are always colinear with direction through both nodes; refer to Figure 78.

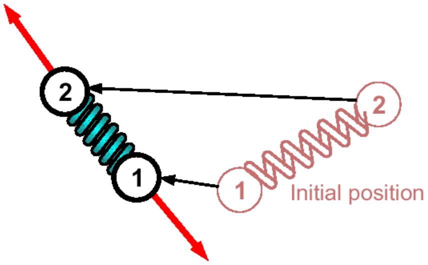

Figure 78: Colinear Forces

Time Step

The time of a spring element depends on the values of stiffness, damping and mass.

For a spring only element:

$$\Delta t = \sqrt{\frac{m}{k}} \tag{630}$$

For a dashpot only element:

$$\Delta t = \frac{m}{2c} \tag{631}$$

For a parallel spring and dashpot element:

$$\Delta t = \frac{\left(\sqrt{mk + c^2}\right) - c}{k} \tag{632}$$

The critical time step ensures that the stability of the explicit time integration is maintained, but it does not ensure high accuracy of spring vibration behavior. Only two time steps are required during one vibration period of a free spring to keep stability. However, if true sinusoidal reproduction is desired, the time step should be reduced by a factor of at least 5.

If the spring is used to connect the two parts, the spring vibration period increases and the default spring time step ensures stability and accuracy.

Linear Spring

Function number defining $\mathbf{f}(\delta)$.

N1=0

The general linear spring is defined by constant mass, stiffness and damping. These are all required in the property type definition. The relationship between force and spring displacement is given by:

$$F = k(l - l_0) + c\frac{dl}{dt} \tag{633}$$

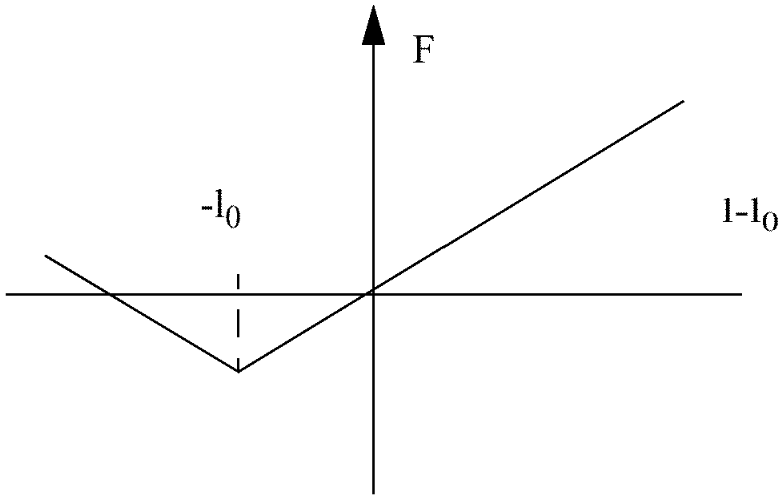

Figure 79: Linear Force-Displacement Curve

The stability condition is given by Equation 632:

$$\Delta t = \frac{\left(\sqrt{c^2 + km}\right) - c}{k} \tag{634}$$

Nonlinear Elastic Spring

Hardening flag

H=0

The hardening flag must be set to 0 for a nonlinear elastic spring. The only difference between linear and nonlinear elastic spring elements is the stiffness definition. The mass and damping are defined as constant. However, a function must be defined that relates the force, F, to the displacement of the spring, $(l - l_0)$. It is defined as:

$$F = f(l - l_0) + c\frac{dl}{dt} \tag{635}$$

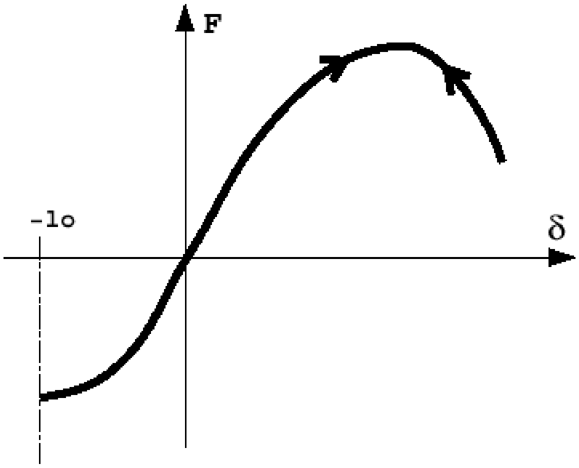

Figure 80: Nonlinear Elastic Force-Displacement Curve

The stability criterion is the same as for the linear spring, but rather than being constant, the stiffness is displacement dependent:

$$\Delta t = \frac{\left(\sqrt{c^2 + k'm}\right) - c}{k'} \tag{636}$$

Where,

$$k' = \max\left[\frac{\partial}{\partial(l - l_0)} f(l - l_0)\right] \tag{637}$$

Nonlinear Elasto-plastic Spring: Isotropic Hardening

H=1

The hardening flag must be set to 1 in this case and $f(l - l_0)$ is defined by a function. Hardening is isotropic if compression behavior is identical to tensile behavior:

$$F = f(l - l_0) + C\frac{dl}{dt} \tag{638}$$

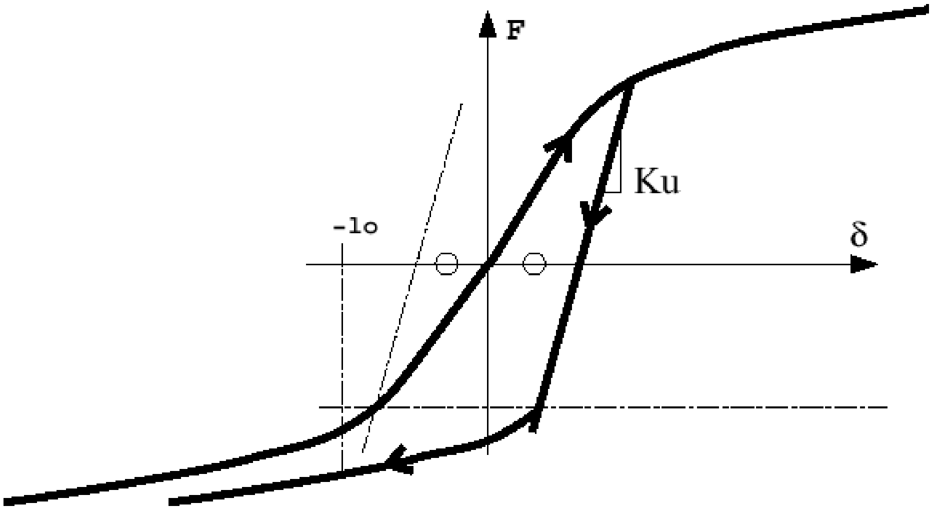

Figure 81: Isotropic Hardening Force-Displacement Curve

Nonlinear Elasto-plastic Spring: Decoupled Hardening

H=2

The hardening flag is set to 2 in this case and f $f(l-l_0)$ is defined by a function. The hardening is decoupled for compression and tensile behavior:

$$F = f(l-l_0) + C\frac{dl}{dt} \tag{639}$$

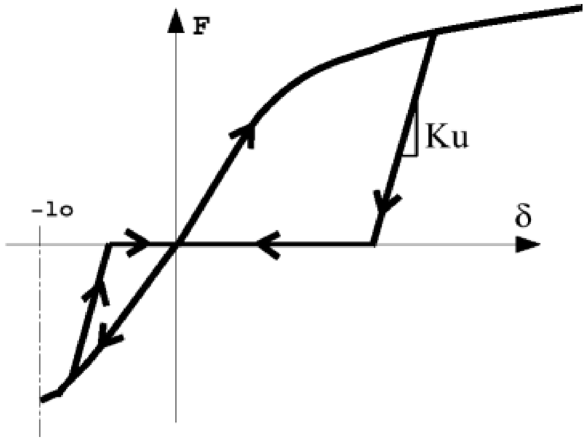

Figure 82: Decoupled Hardening Force-Displacement Curve

Nonlinear Elasto-plastic Spring: Kinematic Hardening

H=4

The hardening flag is set to 4 in this case and $f_1(l-l_0)$ and $f_2(l-l_0)$ (respectively maximum and minimum yield force) are defined by a function. The hardening is kinematic if maximum and minimum yield curves are identical:

$$F = f(l - l_0) + C\frac{dl}{dt} \qquad (640)$$

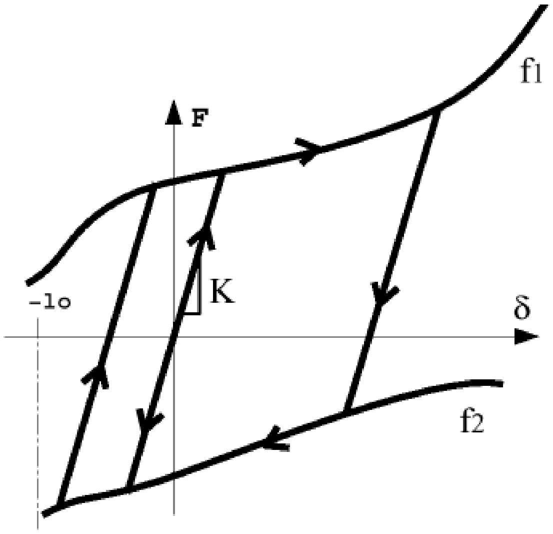

Figure 83: Kinematic Hardening Force-Displacement Curve

Nonlinear Elasto-plastic Spring: Nonlinear Unloading

H=5

The hardening flag is set to 5 in this case and $\mathbf{f}(\delta)$ and $\mathbf{f}2(\delta_{max})$ (maximum yield force and residual deformation, respectively) are defined by a function. Uncoupled hardening in compression and tensile behavior with nonlinear unloading:

$$F = f(l - l_0) + C\frac{dl}{dt} \qquad (641)$$

With $\delta = l - l_0$.

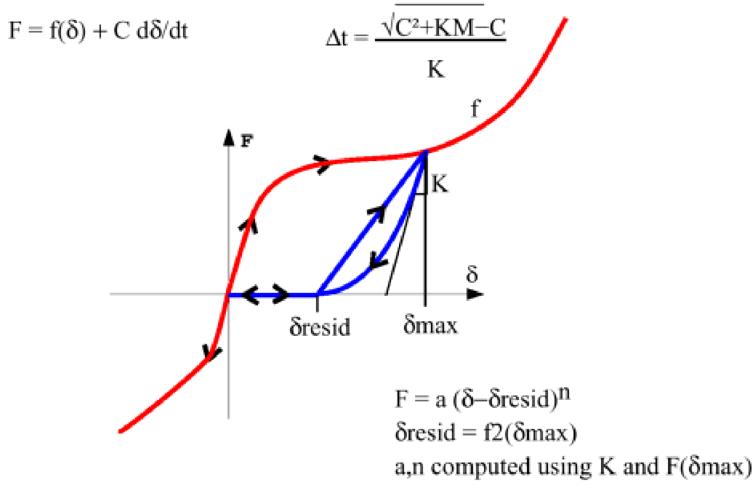

Figure 84: Nonlinear Unloading Force-Displacement Curve

Nonlinear Dashpot

The input properties for a nonlinear dashpot are very close to that of a spring. The required values are:

- Mass, M.
- A function defining the change in force with respect to the spring displacement. This must be equal to unity:

  $f(l - l_0) = 1$
- A function defining the change in force with spring displacement rate,

  $g(dl / dt)$
- The hardening flag in the input must be set to zero.

The relationship between force and spring displacement and displacement rate is:

$$F = f(l - l_0) g\left(\frac{dl}{dt}\right) = g\left(\frac{dl}{dt}\right) \tag{642}$$

A nonlinear dashpot property is shown in Figure 85.

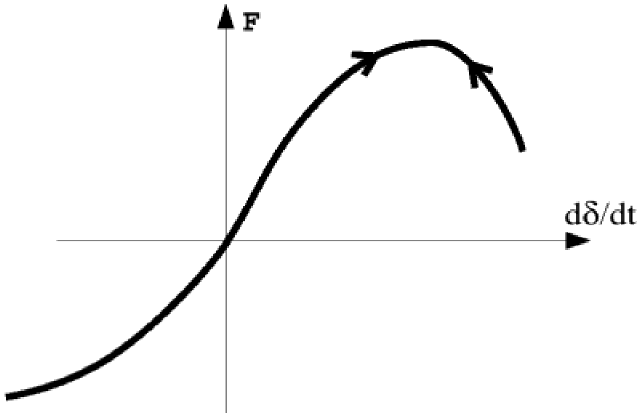

Figure 85: Nonlinear Dashpot Force Curve

The stability condition for a nonlinear dashpot is given by:

$$\Delta t = \sqrt{\frac{M}{C'}} \tag{643}$$

Where,

$$C' = \max\left[\frac{\partial}{\partial(dl / dt)} g(dl / dt)\right] \tag{644}$$

Nonlinear Viscoelastic Spring

The input properties for a nonlinear viscoelastic spring are:

- Mass, M
- Equivalent viscous damping coefficient C
- A function defining the change in force with spring displacement

$f(l-l_0)$

- A function defining the change in force with spring displacement rate

$g(dl/dt)$

The hardening flag in the input must be set to equal zero. The force relationship is given by:

$$F = f(l-l_0)g\left(\frac{dl}{dt}\right) \tag{645}$$

Graphs of this relationship for various values of $g(dl/dt)$ are shown in Figure 86.

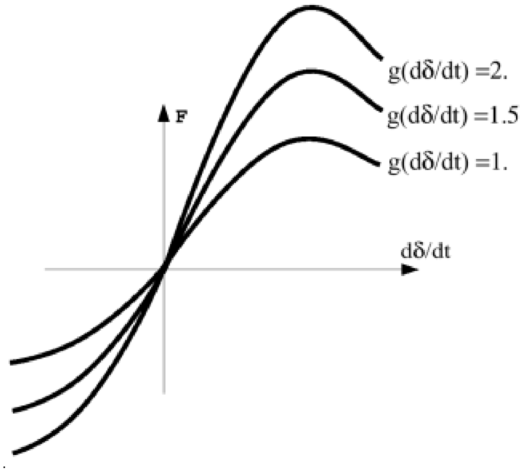

Figure 86: Visco-Elastic Spring Force-Displacement Curves

The stability condition is given by:

$$\Delta t = \frac{\left(\sqrt{C'^2 + k'M}\right) - C'}{k'} \tag{646}$$

Where,

$$K' = \max\left[\frac{\partial}{\partial(l-l_0)} f(l-l_0)\right] \tag{647}$$

$$C' = \max\left[\frac{\partial}{\partial(dl/dt)} g(dl/dt)\right] \tag{648}$$

General Spring Elements (TYPE8)

General spring elements are defined as TYPE8 element property. They are mathematical elements, which have 6 DOF, three translational displacements and three rotational degrees of freedom. Each DOF is completely independent from the others. Spring displacements refer to either spring extension or compression. The stiffness is associated to each DOF. Directions can either be global or local. Local directions are defined with a fixed or moving skew frame. Global force equilibrium is respected, but without global moment equilibrium. Therefore, this type of spring is connected to the laboratory that applies the missing moments, unless the two defining nodes are not coincident.

Time Step

The time step calculation for general spring elements is the same as the calculation of the equivalent TYPE4 spring (Time Step).

Linear Spring

See Linear Spring; the explanation is the same as for spring TYPE4.

Nonlinear Elastic Spring

See Nonlinear Elastic Spring; the explanation is the same as for spring TYPE4.

Nonlinear Elasto-plastic Spring: Isotropic Hardening

See Nonlinear Elasto-plastic Spring: Isotropic Hardening; the explanation is the same as for spring TYPE 4.

Nonlinear Elasto-plastic Spring: Decoupled Hardening

See Nonlinear Elasto-plastic Spring: Decoupled Hardening; the explanation is the same as for spring TYPE4.

Nonlinear Elasto-plastic Spring: Kinematic Hardening

See Nonlinear Elasto-plastic Spring: Kinematic Hardening; the explanation is the same as for spring TYPE4.

Nonlinear Elasto-plastic Spring: Nonlinear Unloading

See Nonlinear Elasto-plastic Spring: Nonlinear Unloading; the explanation is the same as for spring TYPE4.

Nonlinear Dashpot

See Nonlinear Dashpot; the explanation is the same as for spring TYPE4.

Nonlinear Viscoelastic Spring

See Nonlinear Viscoelastic Spring; the explanation is the same as for spring TYPE4.

Skew Frame Properties

To help understand the use of skew frames, the deformation in the local x direction of the spring will be considered. If the skew frame is fixed, deformation in the local X direction is shown in Figure 87:

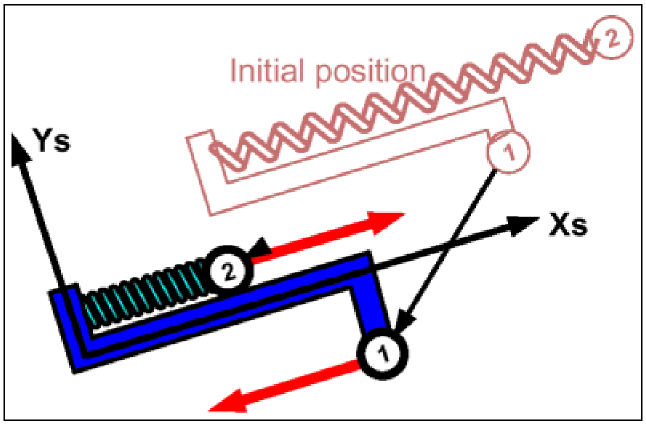

Figure 87: Fixed Skew Frame

The same local x direction deformation, with a moving skew frame, can be seen in Figure 88.

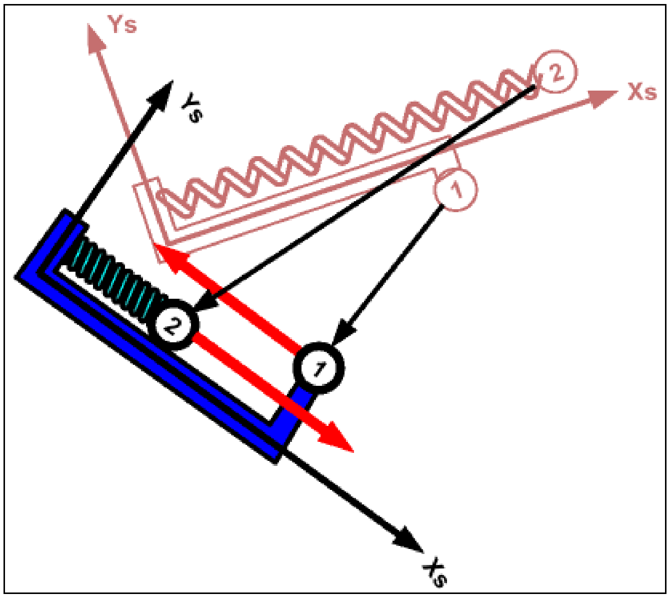

Figure 88: Moving Skew Frame

In both cases, the forces are in equilibrium, but the moments are not. If the first two nodes defining the moving skew system are the same nodes as the two spring element nodes, the behavior becomes exactly the same as that of a TYPE4 spring element. In this case the momentum equilibrium is respected and local Y and Z deformations are always equal to zero.

Fixed Nodes

If one of the two nodes is completely fixed, the momentum equilibrium problem disappears. For example, if node 1 is fixed, the force computation at node 2 is not dependent on the location of node 1. The spring then becomes a spring between node 1 and the laboratory, as shown in Figure 89.

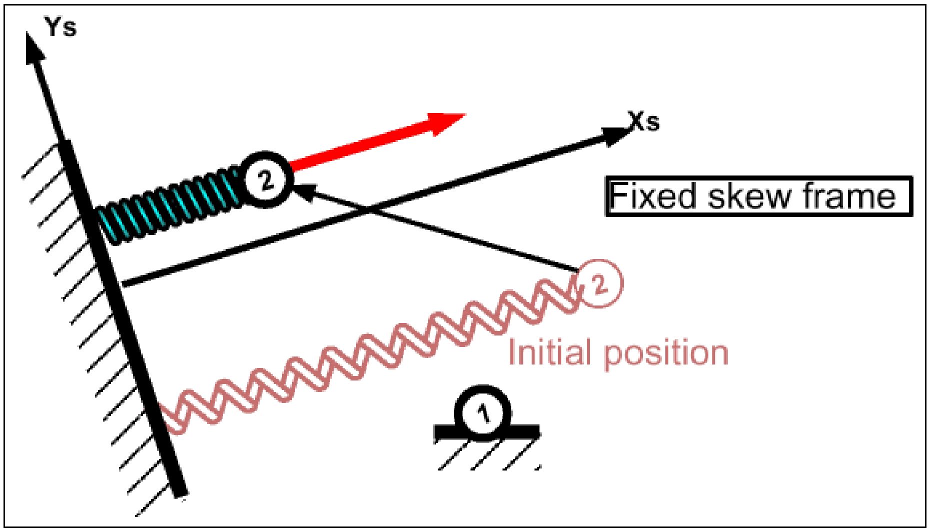

Figure 89: Fixed Node - Fixed Skew Frame

It is generally recommended that a general spring element (TYPE8) be used only if one node is fixed in all directions or if the two nodes are coincident. If the two nodes are coincident, the translational stiffness' have to be large enough to ensure that the nodes remain near coincident during the simulation.

Deformation Sign Convention

Positive and negative spring deformations are not defined with the variation of initial length. The initial length can be equal to zero for all or a given direction. Therefore, it is not possible to define the deformation sign with length variation.

The sign convention used is the following. A deformation is positive if displacement (or rotation) of node 2 minus the displacement of node 1 is positive. The same sign convention is used for all 6 degrees of freedom.

$$u_i = u_{i2} - u_{i1} \tag{649}$$

$$\theta_i = \theta_{i2} - \theta_{i1} \tag{650}$$

Translational Forces

The translational forces that can be applied to a general spring element can be seen in Figure 90. For each DOF (i = x, y, z), the force is calculated by:

$$F_i = f_i(u_i) + C_i\dot{u}_i \tag{651}$$

Where,

C
: Equivalent viscous damping coefficient

$f_i(u_i)$
: Force function related to spring displacement

The value of the displacement function depends on the type of general spring being modeled.

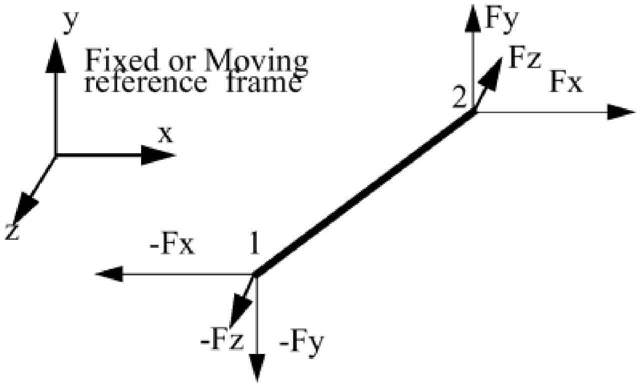

Figure 90: Translational Forces

Linear Spring

If a linear general spring is being modeled, the translation forces are given by:

$$F_i = K_i u_i + C_i \dot{u}_i \tag{652}$$

Where,

K	Stiffness or unloading stiffness (for elasto-plastic spring)

Nonlinear Spring

If a nonlinear general spring is being modeled, the translation forces are given by:

$$F_i = f_i(u_i)\left(A + B\ln\left(\left|\frac{\dot{u}_i}{D}\right|\right) + g(\dot{u}_i)\right) + C_i \dot{u}_i \tag{653}$$

Where,

$f(u_i)$	Function defining the change in force with spring displacement
$g(\dot{u}_i)$	Function defining the change in force with spring displacement rate
A	Coefficient Default = 1
B	Coefficient
D	Coefficient Default = 1

Moments

Moments can be applied to a general spring element, as shown in Figure 91. For each DOF (i = x, y, z), the moment is calculated by:

$$M_i = f_i(\theta_i) + C_i \dot{\theta}_i \tag{654}$$

Where,

C	Equivalent viscous damping coefficient
$f_i(\theta_i)$	Force function related to spring rotation

The value of the rotation function depends on the type of general spring being modeled. Not all functions and coefficients defining moments and rotations are of the same value as that used in the translational force calculation.

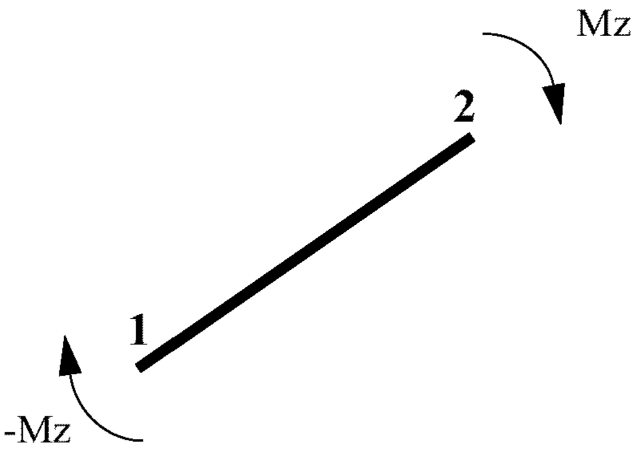

Figure 91: General Spring Moments

Linear Spring

If a linear general spring is being modeled, the translation forces are given by:

$$M_i = K_i\theta_i + C_i\dot{\theta}_i \tag{655}$$

Where,

K	Stiffness or unloading stiffness (for elasto-plastic spring)

Nonlinear Spring

If a nonlinear general spring is being modeled, the translation forces are given by:

$$M_i = f(\theta_i)\left(A + B\ln\left(\left|\frac{\dot{\theta}_i}{D}\right|\right) + g(\dot{\theta}_i)\right) + C_i\dot{\theta}_i \tag{656}$$

Where,

$f(\theta_i)$	Function defining the change in force with spring displacement
$g(\theta_i)$	Function defining the change in force with spring displacement rate
A	Coefficient Default = 1
B	Coefficient

D Coefficient

Default = 1

Multidirectional Failure Criteria

Flag for rupture criteria: I_{fail}

I_{fail}=1

The rupture criteria flag is set to 1 in this case:

$$F^2 = D_x^2 + D_y^2 + D_z^2 + D_{xx}^2 + D_{yy}^2 + D_{zz}^2 \tag{657}$$

Where,

$D_x = D_{xp}$ The rupture displacement in positive x direction if $u_x > 0$

$D_x = D_{xn}$ The rupture displacement in negative x direction if $u_x > 0$

Graphs of this rupture criterion can be seen in Figure 92.

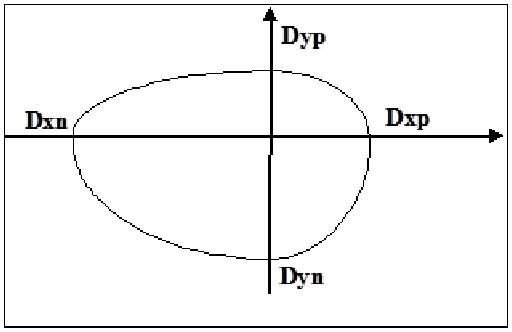

Figure 92: Multi-directional Failure Criteria Curves

Pulley Type Spring Elements (TYPE12)

Pulley type springs are defined by TYPE12 element property. A general representation can be seen in Figure 93. It is defined with three nodes, where node 2 is located at the pulley position. Other properties such as stiffness, damping, nonlinear and plastic effects are the same as for the other spring types, and are defined using the same format.

A deformable "rope" joins the three nodes, with the mass distribution as follows: one quarter at node 1; one quarter at node 3 and one half at node 2.

Coulomb friction can be applied at node 2, which may also take into account the angle between the two rope strands.

The two rope strands have to be long enough to avoid node 1 or node 3 sliding up to node 2 (the pulley). If this occurs, either node 1 or 3 will be stopped at node 2, just as if there were a knot at the end of the rope.

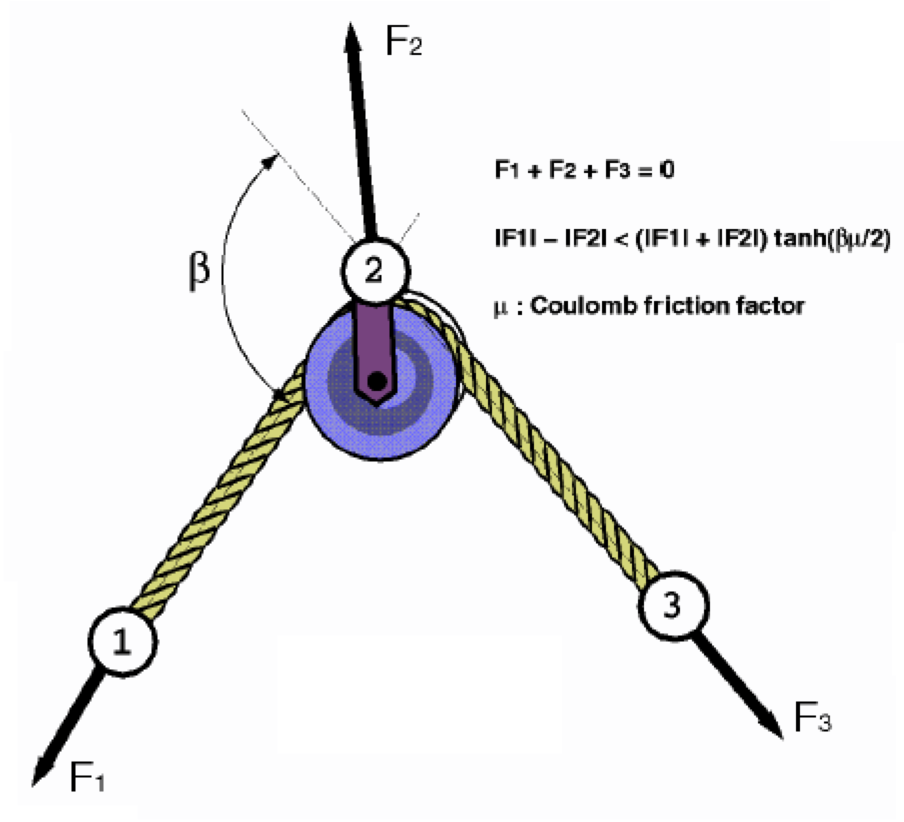
F2
F1 + F2 + F3 = 0
|F1| – |F2| < (|F1| + |F2|) tanh(βμ/2)
μ : Coulomb friction factor
β
2
1
3
F3
F1

Figure 93: Pulley Type Spring Element Representation

Time Step

The time step is calculated using the relation:

$$\Delta t = \frac{\left(\sqrt{KM + C^2}\right) - C}{2K} \tag{658}$$

This is the same as for TYPE4 spring elements, except that the stiffness is replaced with twice the stiffness to ensure stability with high friction coefficients.

Linear Spring

See Linear Spring; the explanation is the same as for spring TYPE4.

Nonlinear Elastic Spring

See Nonlinear Elastic Spring; the explanation is the same as for spring TYPE4.

Nonlinear Elasto-Plastic Spring - Isotropic Hardening

See Nonlinear Elasto-plastic Spring: Isotropic Hardening; the explanation is the same as for spring TYPE4.

Nonlinear Elasto-Plastic Spring - Decoupled Hardening

See Nonlinear Elasto-plastic Spring: Decoupled Hardening; the explanation is the same as for spring TYPE4.

Nonlinear Dashpot

See Nonlinear Dashpot; the explanation is the same as for spring TYPE4.

Friction Effects

Pulley type springs can be modeled with or without Coulomb friction effects.

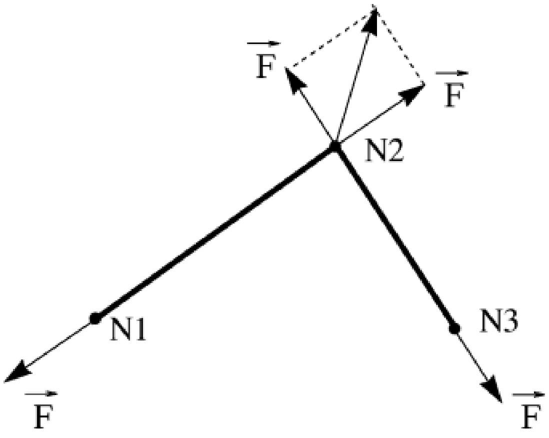

Figure 94:

Forces without Friction

Without friction, the forces are computed using:

$$|F_1| = |F_2| = K\delta + C\frac{d\delta}{dt} \tag{659}$$

Where,

δ Total rope elongation = $l - l_0$ with $l = l_{12} + l_{23}$

K Rope stiffness

C Rope equivalent viscous damping

Forces with Coulomb Friction

If Coulomb friction is used, forces are corrected using:

$$F = K(\delta_1 + \delta_2) + C\left(\frac{d\delta_1}{dt} + \frac{d\delta_2}{dt}\right) \tag{660}$$

$$\Delta F = \max\left(K(\delta_1 + \delta_2) + C\left(\frac{d\delta_1}{dt} + \frac{d\delta_2}{dt}\right), F\tanh\left(\frac{\beta\mu}{2}\right)\right) \tag{661}$$

$$|F_1| = F + \Delta F \tag{662}$$

$$F_2 = -F_1 - F_3 \tag{663}$$

$$|F_3| = F - \Delta F \tag{664}$$

Where,

δ_1 Elongation of strand 1-2

δ_2 Elongation of strand 2-3

Beam Type Spring Elements (TYPE13)

Beam type spring elements are defined as property TYPE13 elements. This type of spring element functions as if it were a beam element. The six independent modes of deformation are:

- Traction / compression
- Torsion
- Bending (two modes)
- Shear (two modes)

Beam type springs only function if their length is not zero. A physical representation of a beam type spring can be seen in Figure 93.

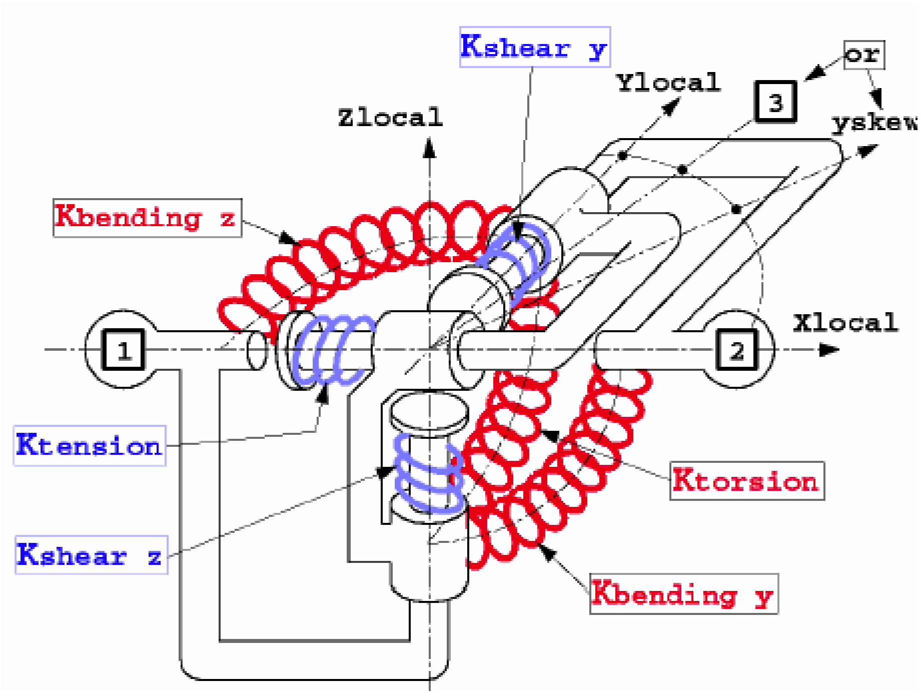

Figure 95: Representation of Beam Type Spring

Time Step

Translational Stiffness Time Step

$$\Delta t_{translational\_stifness} = \frac{\sqrt{mass.\max(Kt)+C_t^2} - C_t}{\max(K_t)}$$

Where,

$\max(Kt)$	Maximum translational stiffness
C_t	Translational damping

Rotational Stiffness Time Step

$$\Delta t_{rotational\_stifness} = \frac{\sqrt{inertia.K'_r + C'^2_r} - C'r}{K'_r}$$

K'_r is the equivalent rotational stiffness: $K'_r = \max(K_t).L^2 + \max(K_r)$

Where,

$\max(K_t)$	Maximum translational stiffness
$\max(K_r)$	Maximum rotational stiffness
$C'r$	Equivalent rotational damping: $C'_r = \max(C_t).L^2 + \max(C_r)$

Where,

$\max(C_t)$	Maximum translational damping
$\max(C_r)$	Maximum rotational damping

Linear Spring

The properties required to define the spring characteristics are stiffness K and damping C. Nonlinear and elasto-plastic properties can also be applied, for all degrees of freedom. The properties are of the same form as simple TYPE4 spring elements (One Degree of Freedom Spring Elements (TYPE4)).

See Linear Spring; the explanation is the same as for spring TYPE4.

Nonlinear Elastic Spring

See Nonlinear Elastic Spring; the explanation is the same as for spring TYPE4.

Nonlinear Elasto-Plastic Spring - Isotropic Hardening

See Nonlinear Elasto-plastic Spring: Isotropic Hardening; the explanation is the same as for spring TYPE4.

Nonlinear Elasto-Plastic Spring - Decoupled Hardening

See Nonlinear Elasto-plastic Spring: Decoupled Hardening; the explanation is the same as for spring TYPE4.

Nonlinear Elasto-Plastic Spring - Kinematic Hardening

See Nonlinear Elasto-plastic Spring: Kinematic Hardening; the explanation is the same as for spring TYPE4.

Nonlinear Elasto-Plastic Spring - Nonlinear Unloading

See Nonlinear Elasto-plastic Spring: Nonlinear Unloading; the explanation is the same as for spring TYPE4.

Nonlinear Dashpot

See Nonlinear Dashpot; the explanation is the same as for spring TYPE4.

Nonlinear Visco-Elastic Spring

See Nonlinear Viscoelastic Spring; the explanation is the same as for spring TYPE4.

Skew Frame Properties

Beam type spring elements are best defined using three nodes (Figure 96). Nodes 1 and 2 are the two ends of the element and define the local X axis. Node 3 allows the local Y and Z axes to be defined. However, this node does not need to be supplied.

If all three nodes are defined, the local reference frame is calculated by:

$$\vec{x} = \overline{n_1 n_2} \tag{665}$$

$$\vec{z} = \vec{x} \times \overline{n_1 n_3} \tag{666}$$

$$\vec{y} = \vec{z} \times \vec{x} \tag{667}$$

If node 3 is not defined, the local skew frame that can be specified for the element is used to define the Z axis. The X and Y axes are defined in the same manner as before.

$$\vec{z} = \vec{x} \times \vec{y}_{skew} \tag{668}$$

If no skew frame and no third node are defined, the global Y axis is used to replace the Y skew axis. If the Y skew axis is collinear with the local X axis, the local Y and Z axes are placed in a totally arbitrary position. The local Y axis is defined at time zero, and is corrected at each cycle, taking into account the mean X axis rotation.

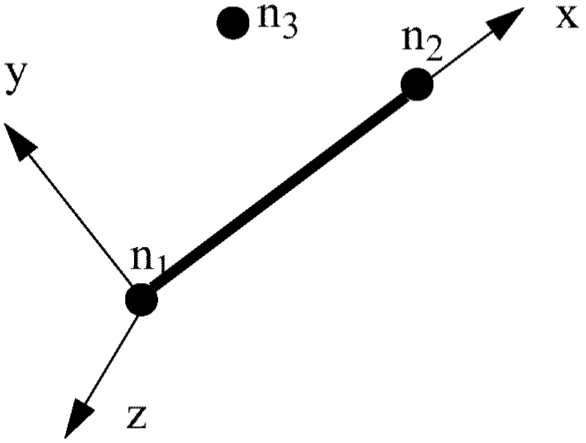

Figure 96: Element Definition

Sign Conventions

The sign convention used for defining positive displacements and forces can be seen in Figure 97.

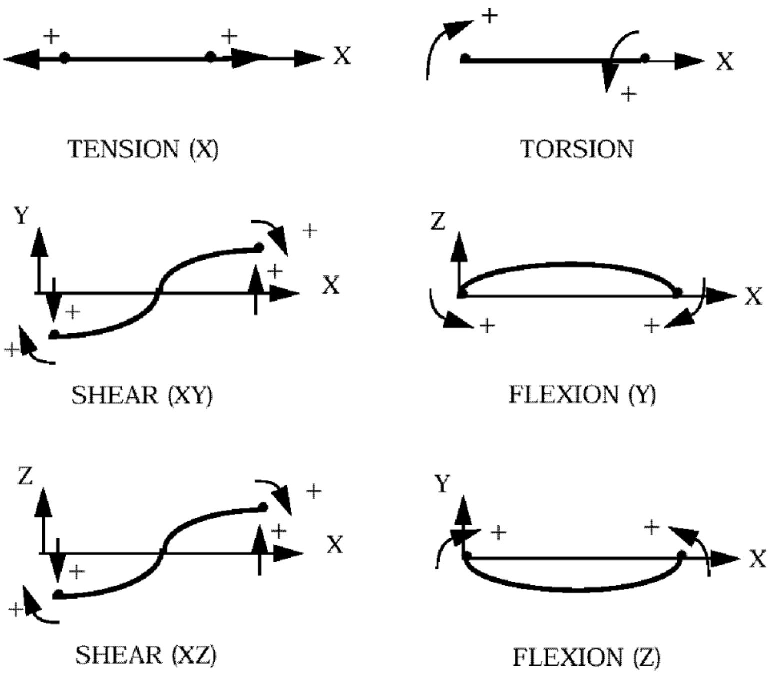

Figure 97: Sign Conventions

Tension

The tension component of the beam type spring element is independent of other forces. It is shown in Figure 98. The tension at each node is computed by:

$$F_{x1} = f_x(u_x) + C_x\dot{u}_x \tag{669}$$

$$F_{x2} = -F_{x1} \tag{670}$$

Where,

$u_x = u_{x2} - u_{x1}$
: Relative displacement of nodes 1 and 2

$f_x(u_x)$
: Function defining the force-displacement relationship

It can be linear or nonlinear (Linear Spring to Nonlinear Elasto-plastic Spring: Decoupled Hardening).

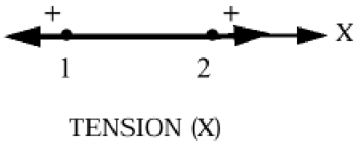

Figure 98: Spring Tension

Shear - XY

Shear in the Y direction along the face perpendicular to the X axis is a combination of forces and moments. This can be seen in Figure 99.

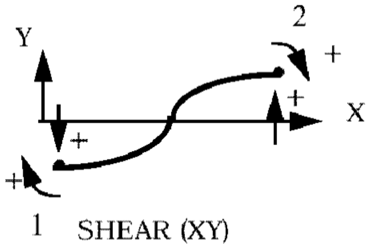

Figure 99: XY Shear Forces and Moments

There are two mechanisms that can cause shear. The first is the beam double bending as shown in Figure 99. The second is shear generated by node displacement, as shown in Figure 100, where node 2 is displaced.

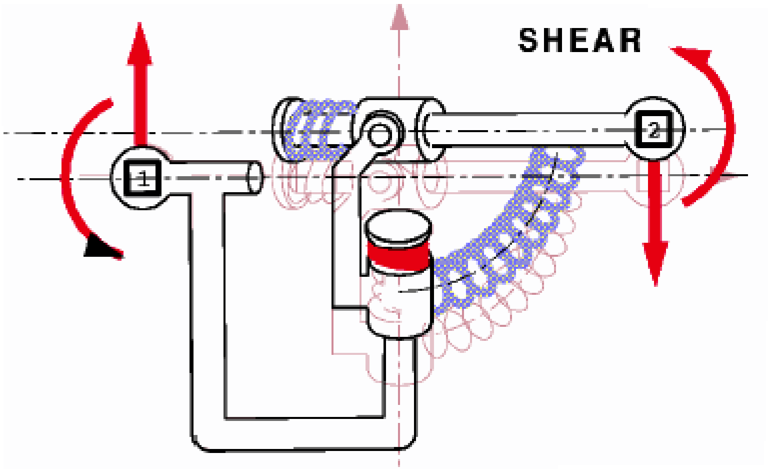

Figure 100: Shear Due to Node Displacement

The forces and moments are calculated by:

$$F_{y1} = f_y(u_y) + C_y \dot{u}_y \tag{671}$$

$$F_{y2} = -F_{y1} \tag{672}$$

$$M_{z1} = -lF_{y2} \tag{673}$$

$$M_{z2} = M_{z1} \tag{674}$$

Where,

$$u_y = u_{y2} - u_{y1} - l\left(\frac{\theta_{z2} + \theta_{z1}}{2}\right)$$

$f_y(u_y)$ is the function defining the force-displacement relationship.

Shear - XZ

The XZ shear is orthogonal to the XY shear described in the previous section. The forces and moments causing the shear can be seen in Figure 101.

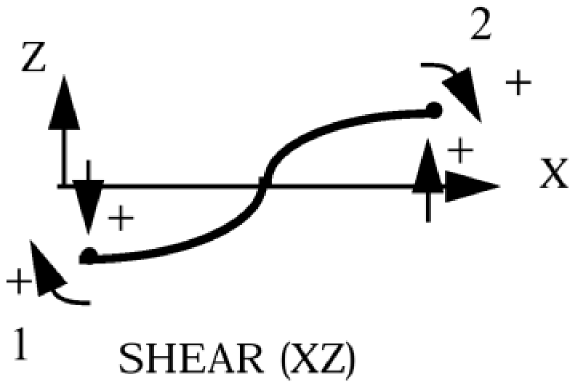

Figure 101: XZ Shear Forces and Moments

The forces and moments are calculated by:

$$F_{z1} = f_z(u_z) + C_z \dot{u}_z \tag{675}$$

$$F_{z2} = -F_{z1} \tag{676}$$

$$M_{y1} = lF_{z2} \tag{677}$$

$$M_{y2} = M_{y1} \tag{678}$$

Where,

$$u_z = u_{z2} - u_{z1} + l\left(\frac{\theta_{y2} + \theta_{y1}}{2}\right)$$

$f_z(u_z)$ is the function defining the force-displacement relationship.

Torsion

Torsional forces, shown in Figure 102, are calculated using the relations:

$$M_{x1} = f_{xx}(\theta_x) + C_{xx}\dot{\theta}_x \tag{679}$$

$$M_{x2} = -M_{x1} \tag{680}$$

Where,

$\theta_x = \theta_{x2} - \theta_{x1}$ is the relative rotation of node 1 and 2.

$f_{xx}(\theta_x)$ is the function defining the force-displacement relationship.

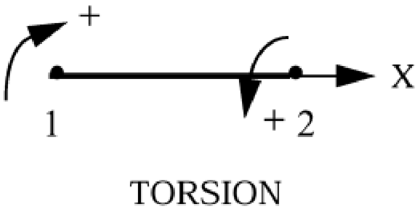

Figure 102: Beam Type Spring Torsion

Bending About the Y Axis

Bending about the Y axis can be seen in Figure 103. The equations relating to the moments being produced are calculated by:

$$M_{y1} = f_{yy}(\theta_y) + C_{yy}\dot{\theta}_y \tag{681}$$

$$M_{y2} = -M_{y1} \tag{682}$$

Where,

$\theta_y = \theta_{y2} - \theta_{y1}$ is the relative rotation of node 1 and 2.

$f_{yy}(\theta_y)$ is the function defining the force-displacement relationship.

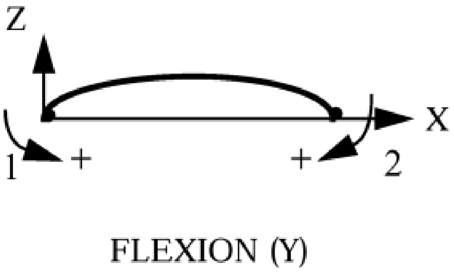

Figure 103: Bending about Y Axis

Bending About the Z Axis

The equations relating to the moment generated in a beam type spring element and the beam's displacement, (Figure 104) is given by:

$$M_{z1} = f_{zz}(\theta_z) + C_{zz}\dot{\theta}_z \tag{683}$$

$$M_{z2} = -M_{z1} \tag{684}$$

Where,

$\theta_z = \theta_{z2} - \theta_{z1}$ is the relative rotation of node 1 and 2.

$f_{zz}(\theta_z)$ is the function defining the force-displacement relationship.

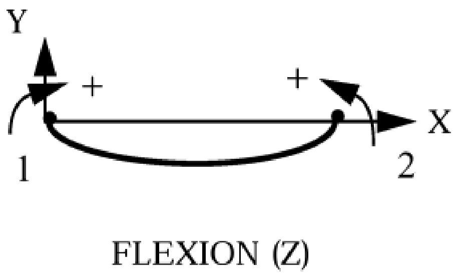

Figure 104: Bending about Z Axis

Multidirectional Failure Criteria

See Multidirectional Failure Criteria; the explanation is the same as for spring TYPE8.

Multistrand Elements (TYPE28)

Multistrand elements are n-node springs where matter is assumed to slide through the nodes.

It could be used for belt modelization by taking nodes upon the dummy. Friction may be defined at all or some nodes. When nodes are taken upon a dummy in order to modelize a belt, this allows friction to be modelized between the belt and the dummy.

Internal Forces Computation

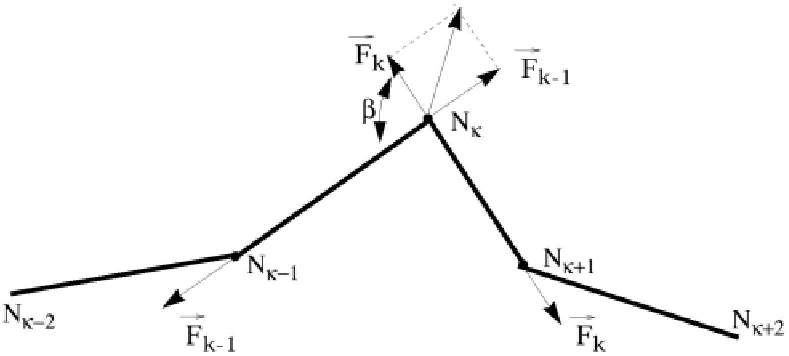

Figure 105: Internal Forces Computation

Nodes are numbered from 1 to n, and strands are numbered from 1 to n-1 (strand k goes from node N_k to node N_{k+1}).

Averaged Force

The averaged force in the multistrand is computed as:

Linear spring $F = \frac{K}{L^0}\delta + \frac{C}{L^0}\dot{\delta}$

Nonlinear spring $F = f(\varepsilon) \cdot g(\dot{\varepsilon}) + \frac{C}{L^0}\dot{\delta}$

or, if g function identifier is 0:

$$F = f(\varepsilon) + \frac{C}{L^0}\dot{\delta} \tag{685}$$

or, if f function identifier is 0:

$$F = g(\dot{\varepsilon}) + \frac{C}{L^0}\dot{\delta} \tag{686}$$

Where,

ε
: Engineering strain: $\varepsilon = \frac{L - L^0}{L^0}$

L^0
: Reference length of element

Force into each Strand

The force into each strand k is computed as:

$F_k = F + \Delta F_k$

Where, ΔF_k is computed an incremental way:

$$\Delta F_k(t) = \Delta F_k(t-1) + \frac{K}{l_k^0}\delta\varepsilon_k - \frac{K}{L^0}\delta\varepsilon \tag{687}$$

with l_k^0 the length of the unconstrained strand k, $\delta\varepsilon = \varepsilon(t) - \varepsilon(t-1)$ and $\delta\varepsilon_k = \delta t u_k \cdot (v_{k+1} - v_k)$.

Where, u_k is the unitary vector from node N_k to node N_{k+1}.

Assuming:

$$\frac{l_k}{l_k^0} = \frac{L}{L^0} \tag{688}$$

Where, l_k is the actual length of strand k.

Therefore, Equation 687 reduces to:

$$\Delta F_k(t) = \Delta F_k(t-1) + \frac{K}{l^0}\left(\delta\varepsilon_k \frac{L}{l_k} - \delta\varepsilon\right) \tag{689}$$

Friction

Friction is expressed at the nodes: if μ is the friction coefficient at node k, the pulley friction at node N_k is expressed as:

$$\left|\Delta F_{k-1} - \Delta F_k\right| \le (2F + \Delta F_{k-1} + \Delta F_k)\tanh\left(\frac{\beta\mu}{2}\right) \tag{690}$$

When equation Equation 690 is not satisfied, $\left|\Delta F_{k-1} - \Delta F_k\right|$ is reset to $(2F + \Delta F_{k-1} + \Delta F_k)\tanh\left(\frac{\beta\mu}{2}\right)$.

All the ΔF_k (k=1, n-1) are modified in order to satisfy all conditions upon $\Delta F_{k-1} - \Delta F_k$ (k=2, n-1), plus the following condition on the force integral along the multistrand element:

$$\sum_{k=1,n-1} l_k(F + \Delta F_k) = LF \tag{691}$$

This process could fail to satisfy Equation 690 after the $\Delta F_k (k = 1, n-1)$ modification, since no iteration is made. However, in such a case one would expect the friction condition to be satisfied after a few time steps.

> **Note:** Friction expressed upon strands (giving a friction coefficient μ along strand k) is related to pulley friction by adding a friction coefficient $\mu/2$ upon each nodes N_k and N_{k+1}.

Time Step

Stability of a multistrand element is expressed as:

$$\Delta t \leq \frac{\sqrt{C_k^2 + \rho l_k K_k} - C_k}{K_k}, \forall\, k \tag{692}$$

with $K_k = \frac{Mass\, of\, the\, multistrand}{L^0}$:

$$K_k = \max\left(\frac{K}{l_k^0}, \frac{F}{l_k - l_k^0}\right) = \max\left(\frac{KL}{l_k L^0}, \frac{FL}{l_k\left(L - L^0\right)}\right) \tag{693}$$

$$C_k = \frac{\left(f(\varepsilon)\frac{dg}{d\dot{\varepsilon}}(\dot{\varepsilon}) + C\right)}{l_k^0} = \left(f(\varepsilon)\frac{dg}{d\varepsilon}(\dot{\varepsilon}) + C\right)\frac{L}{l_k L^0} \tag{694}$$

Internal Forces Computation

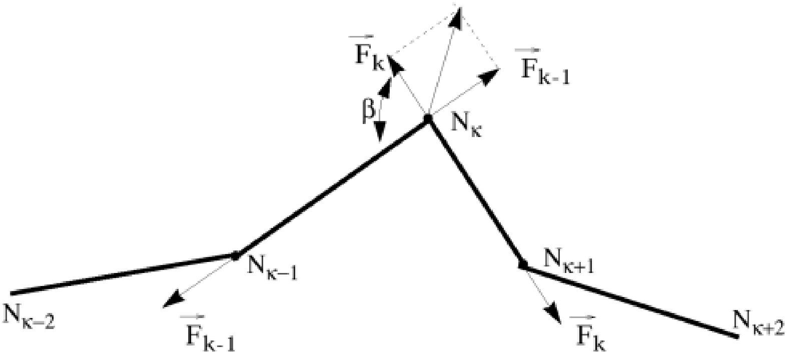

Figure 106:

Nodes are numbered from 1 to n, and strands are numbered from 1 to n-1 (strand k goes from node N_k to node N_{k+1}).

Averaged Force

The averaged force in the multistrand is computed as:

Linear spring $F = \frac{K}{L^0}\delta + \frac{C}{L^0}\dot{\delta}$

Nonlinear spring $F = f(\varepsilon) \cdot g(\dot{\varepsilon}) + \frac{C}{L^0}\dot{\delta}$

or, if g function identifier is 0:

$$F = f(\varepsilon) + \frac{C}{L^0}\dot{\delta} \tag{695}$$

or, if f function identifier is 0:

$$F = g(\dot{\varepsilon}) + \frac{C}{L^0}\dot{\delta} \tag{696}$$

Where, ε is engineering strain $\varepsilon = \frac{L - L^0}{L^0}$.

Where, L^0 is the reference length of element.

Force Into Each Strand

The force into each strand k is computed as:

$F_k = F + \Delta F_k$

Where, ΔF_k is computed an incremental way:

$$\Delta F_k(t) = \Delta F_k(t-1) + \frac{K}{l_k^0}\delta\varepsilon_k - \frac{K}{L^0}\delta\varepsilon \tag{697}$$

with l_k^0 the length of the unconstrained strand k, $\delta\varepsilon = \varepsilon(t) - \varepsilon(t-1)$ and $\delta\varepsilon_k = \delta t u_k \cdot (v_{k+1} - v_k)$.

Where, u_k is the unitary vector from node N_k to node N_{k+1}.

Assuming:

$$\frac{l_k}{l_k^0} = \frac{L}{L^0} \tag{698}$$

Where, l_k is the actual length of strand k.

Therefore, Equation 697 reduces to:

$$\Delta F_k(t) = \Delta F_k(t-1) + \frac{K}{l^0}\left(\delta\varepsilon_k \frac{L}{l_k} - \delta\varepsilon\right) \tag{699}$$

Friction

Friction is expressed at the nodes: if μ is the friction coefficient at node k, the pulley friction at node N_k is expressed as:

$$\Delta F_k(t) = \Delta F_k(t-1) + \frac{K}{l_k^0}\delta\varepsilon_k - \frac{K}{L^0}\delta\varepsilon \tag{700}$$

When equation Equation 700 is not satisfied, $|\Delta F_{k-1} - \Delta F_k|$ is reset to $(2F + \Delta F_{k-1} + \Delta F_k)\tanh\left(\frac{\beta\mu}{2}\right)$.

All the ΔF_k (k=1, n-1) are modified in order to satisfy all conditions upon $\Delta F_{k-1} - \Delta F_k$ (k=2, n-1), plus the following condition on the force integral along the multistrand element:

$$\sum_{k=1,n-1} l_k(F + \Delta F_k) = LF \tag{701}$$

This process could fail to satisfy Equation 700 after the $\Delta F_k(k = 1, n - 1)$ modification, since no iteration is made. However, in such a case one would expect the friction condition to be satisfied after a few time steps.

Note: Friction expressed upon strands (giving a friction coefficient μ along strand k) is related to pulley friction by adding a friction coefficient $\mu/2$ upon each nodes N_k and N_{k+1}.

Time Step

Stability of a multistrand element is expressed as:

$$\Delta t \leq \frac{\sqrt{C_k^2 + \rho l_k K_k} - C_k}{K_k}, \forall\, k \tag{702}$$

with $K_k = \frac{Mass\,of\;the\,multistrand}{L^0}$ and (assuming Equation 698):

$$K_k = \max\left(\frac{K}{l_k^0}, \frac{F}{l_k - l_k^0}\right) = \max\left(\frac{KL}{l_k L^0}, \frac{FL}{l_k\left(L - L^0\right)}\right) \tag{703}$$

$$C_k = \frac{\left(f(\varepsilon)\frac{dg}{d\dot{\varepsilon}}(\dot{\varepsilon}) + C\right)}{l_k^0} = \left(f(\varepsilon)\frac{dg}{d\varepsilon}(\dot{\varepsilon}) + C\right)\frac{L}{l_k L^0} \tag{704}$$

Spring Type Pretensioners (TYPE32)

Pretensioner expected behavior is as follows: before pretensioning, a piston is fixed in its initial position; when activated, the piston is pushed and cannot slide once the piston has reached the end of its slide, it is unable to slide further in any direction in the opposite direction from its actual position.

Pretensioner Model

Linear Model

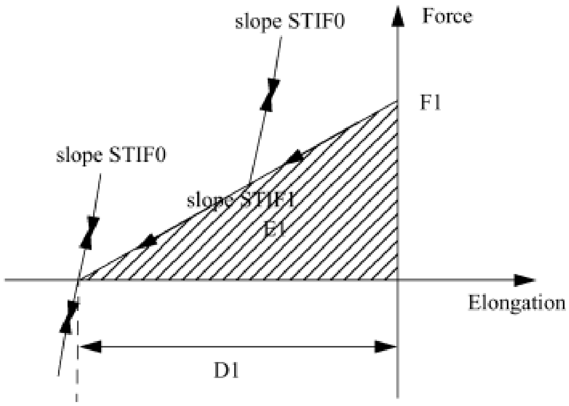

Figure 107:

$STIF_0$ is the spring stiffness before sensor activation. At sensor activation, the 2 input coefficients among D1, STIF1, F1 and E1 determine the pretensioner characteristics. Let us recall the following relations between the 4 coefficients:

$$E_1 = \frac{D_1 \cdot F_1}{2}, K_1 = \frac{F_1}{D_1} \tag{705}$$

$STIF_0$ is also used as unloading stiffness before the end of the piston's slide, and as both loading and unloading stiffness at the end of the piston's slide. $STIF_0$ should be large enough to allow locking.

Nonlinear Model

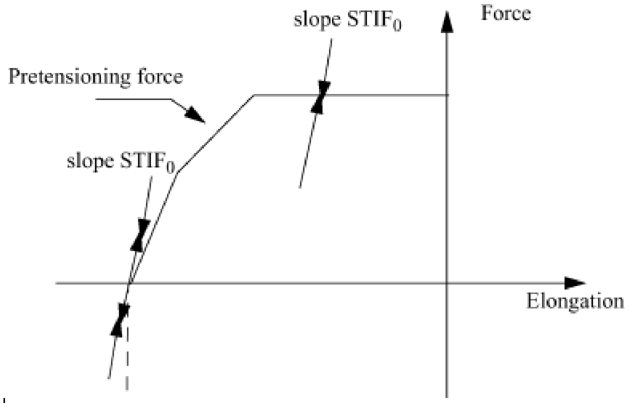

Figure 108:

$STIF_0$ is spring stiffness before sensor activation. Depending on the input, pretensioning force is defined as $f(L-L_0)$, with either $g(t-t_0)$, or $f(L(t)-L_0)\cdot g(t-t_0)$, with L_0 length of the spring at sensor activation time and at t_0 sensor activation time.

Similar use of $STIF_0$ allows piston locking.

Force Computation

Let the pretensioning force $F_p(t)=F_1+STIF_1\cdot(L(t)-L_0)$ for a linear model, and $F_p(t)=f(L(t)-L_0)$ or $g(t-t_0)$ or $f(L(t)-L_0)\cdot g(t-t_0)$ for a nonlinear model.

The force into the pretensioner spring is computed as:

if, $F_p(t+dt)\geq 0$

$$F(t+dt)=Max(F_p(t+dt), F(t)+STIF_0\cdot L(t+dt)-L(t))$$

and $F(t+dt)=F(t)+STIF_0\cdot(L(t+dt)-L(t))$ otherwise.

Kinematic Constraints

Kinematic constraints are boundary conditions that are placed on nodal velocities. They are mutually exclusive for each degree of freedom (DOF), and there can only be one constraint per DOF.

There are seven different types of kinematic constraints that can be applied to a model in Radioss:

1. Rigid Body
2. Initial static equilibrium
3. Boundary Condition
4. Tied Interface (TYPE2)
5. Rigid Wall
6. Rigid Link
7. Cylindrical Joint

Two kinematic conditions applied to the same node may be incompatible.

Rigid Body

A rigid body is defined by a main node and its associated secondary nodes. Mass and inertia may be added to the initial main node location. The main node is then moved to the center of mass, taking into account the main node and all secondary node masses. Figure 109 shows an idealized rigid body.

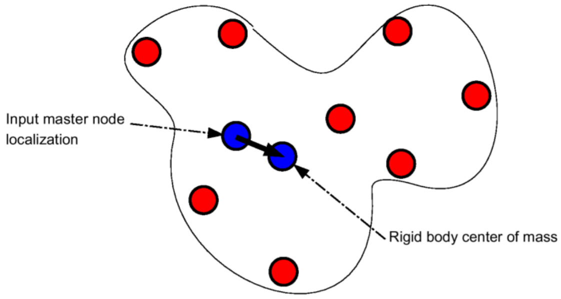

Figure 109: Idealized Rigid Body

Rigid Body Mass

The mass of the rigid body is calculated by:

$$m = m^M + \sum_I m^I \tag{706}$$

The rigid body's center of mass is defined by:

$$x^G = \frac{m^M x^M + \sum m^I x^I}{m} \tag{707}$$

$$y^G = \frac{m^M y^M + \sum m^I y^I}{m} \tag{708}$$

$$z^G = \frac{m^M z^M + \sum m^I z^I}{m} \tag{709}$$

Where,

m^M	Main node mass
m^I	Secondary node masses
x^G, y^G, z^G	Coordinates of the mass center

Rigid Body Inertia

The six components of inertia of a rigid body are computed by:

$$I_{xx} = J_{xx}^M + m^M\left(\left(y_M - y_G\right)^2 + \left(z_M - z_G\right)^2\right) + \sum_i \left(I_{xx}^i + m^i\left(\left(y_i - y_G\right)^2 + \left(z_i - z_G\right)^2\right)\right) \tag{710}$$

$$I_{yy} = J_{yy}^M + m^M\left(\left(x_M - x_G\right)^2 + \left(z_M - z_G\right)^2\right) + \sum_i \left(I_{yy}^i + m^i\left(\left(x_i - x_G\right)^2 + \left(z_i - z_G\right)^2\right)\right) \tag{711}$$

$$I_{zz} = J_{zz}^M + m^M\left(\left(x_M - x_G\right)^2 + \left(y_M - y_G\right)^2\right) + \sum_i \left(I_{zz}^i + m^i\left(\left(x_i - x_G\right)^2 + \left(y_i - y_G\right)^2\right)\right) \tag{712}$$

$$I_{xy} = J_{xy}^M + m^M\left(\left(x_M - x_G\right) + \left(y_M - y_G\right)\right) + \sum_i \left(I_{xy}^i - m^i\left(\left(x_i - x_G\right) + \left(y_i - y_G\right)\right)\right) \tag{713}$$

$$I_{yz} = J_{yz}^M + m^M\left(\left(y_M - y_G\right) + \left(z_M - z_G\right)\right) + \sum_i \left(I_{yz}^i - m^i\left(\left(y_i - y_G\right) + \left(z_i - z_G\right)\right)\right) \tag{714}$$

$$I_{xz} = J_{xz}^M + m^M\left(\left(x_M - x_G\right) + \left(z_M - z_G\right)\right) + \sum_i \left(I_{xz}^i - m^i\left(\left(x_i - x_G\right) + \left(z_i - z_G\right)\right)\right) \tag{715}$$

Where,

I_{ij}	Moment of rotational inertia in the ij direction
J_{ij}^M	Main node added inertia

Rigid Body Force And Moment Computation

The forces and moments acting on the rigid body are calculated by:

$$\vec{F} = \vec{F}^M + \sum_i \vec{F}^i \tag{716}$$

$$\vec{M} = \vec{M}^M + \sum_i \vec{M}^i + \sum_i S_i\vec{G} \times \vec{F}^i \tag{717}$$

Where,

$\vec{F}^M$	Force vector at the main node
$\vec{F}^i$	Force vector at the secondary nodes
$\vec{M}^M$	Moment vector at the main node
$\vec{M}^i$	Moment vector at the secondary nodes
$\vec{G}$	Vector from secondary node to the center of mass

Resolving these into orthogonal components, the linear and rotational acceleration may be computed as:

Linear Acceleration

$$\gamma_i = \frac{F_i}{m} \tag{718}$$

Rotational Acceleration

$$I_1\alpha_1 = M_1 - (I_3 - I_2)\omega_2\omega_3 \tag{719}$$

$$I_2\alpha_2 = M_2 - (I_1 - I_3)\omega_1\omega_3 \tag{720}$$

$$I_3\alpha_3 = M_3 - (I_2 - I_1)\omega_1\omega_2 \tag{721}$$

Where,

I_i	Principal moments of inertia of the rigid body
α_1	Rotational accelerations in the principal inertia frame (reference frame)
ω_i	Rotational velocity in the principal inertia frame (reference frame)
M_i	Moments in the principal inertia frame (reference frame)

Time Integration

Time integration is performed to find velocities of the rigid body at the main node:

$$\vec{v}\left(t + \frac{\Delta t}{2}\right) = \vec{v}\left(t - \frac{\Delta t}{2}\right) + \vec{\gamma}(t)\Delta t \tag{722}$$

$$\vec{\omega}\left(t + \frac{\Delta t}{2}\right) = \vec{\omega}\left(t - \frac{\Delta t}{2}\right) + \vec{\alpha}(t)\Delta t \tag{723}$$

Where, $\vec{v}$ is the linear velocity vector. Rotational velocities are computed in the local reference frame.

The velocities of secondary nodes are computed by:

$$\vec{v}^{i} = \vec{v}^{M} + S_i\vec{G}x\vec{\omega} \tag{724}$$

$$\vec{\omega}^{i} = \vec{\omega}^{M} \tag{725}$$

Boundary Conditions

The boundary conditions given to secondary nodes are ignored. The rigid body has the boundary conditions given to the main node only.

A kinematic condition is applied on each secondary node, for all directions. A secondary node is not allowed to have any other kinematic conditions.

No kinematic condition is applied on the main node. However, the rotational velocities are computed in a local reference frame. This reference frame is not compatible with all options imposing rotation such as imposed velocity, rotational, rigid link.

The only exception concerns the rotational boundary conditions for which a special treatment is carried out. Connecting shell, beam or spring with rotation stiffness to the main node, is not yet allowed either.

Tied Interface (TYPE2)

With a tied interface it is possible to connect rigidly a set of secondary nodes to a main surface.

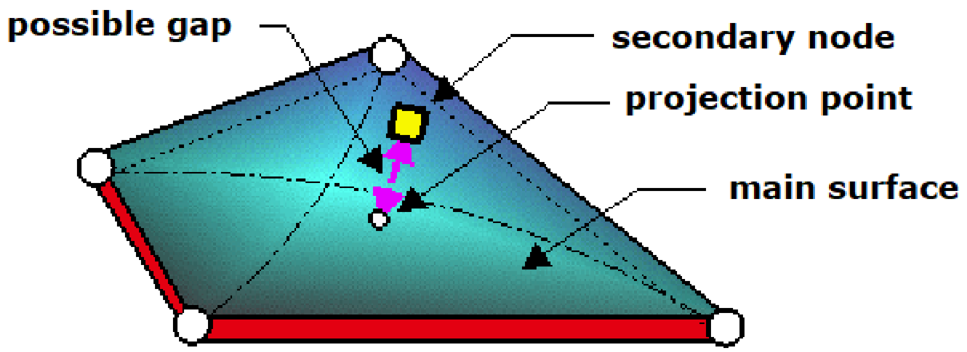

Figure 110:

A tied interface (TYPE2) can be used to connect a fine mesh of Lagrangian elements to a coarse mesh or two different kinds of meshes (for example, spring to shell contacts).

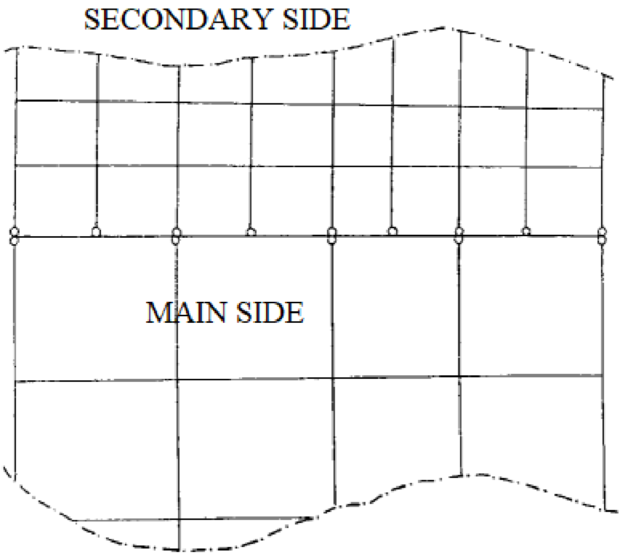

Figure 111: Fine and Coarse Mesh

A main and a secondary surface are defined in the interface input cards. The contact between the two surfaces is tied. No sliding or movement of the secondary nodes is allowed on the main surface. There are no voids present either.

It is recommended that the main surface has a coarser mesh.

Accelerations and velocities of the main nodes are computed with forces and masses added from the secondary nodes.

Kinematic constraint is applied on all secondary nodes. They remain at the same position on their main segments.

Tied interfaces are useful in rivet modeling, where they are used to connect springs to a shell or solid mesh.

Spotweld Formulation

The secondary node is rigidly connected to the main surface. Two formulations are available to describe this connection:

- Default formulation
- Optimized formulation

Default Spotweld Formulation

When $Spot_{flag}$=0, the spotweld formulation is a default formulation:

- Based on element shape functions
- Generating hourglass with under integrated elements
- Providing a connection stiffness function of secondary node localization
- Recommended with full integrated shells (mainr)

- Recommended for connecting brick secondary nodes to brick main segments (mesh transition without rotational freedom)

Forces and moments transfer from secondary to main nodes is described in Figure 112:

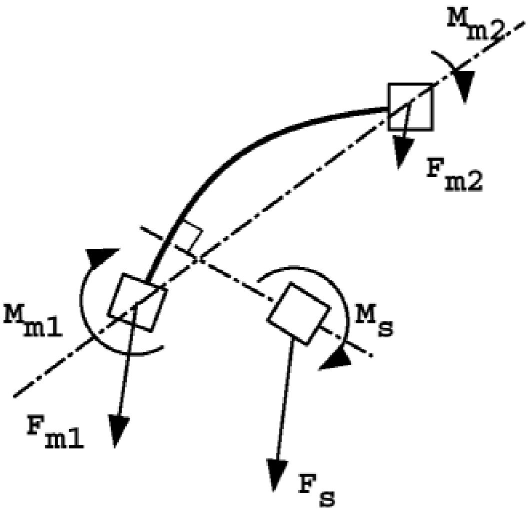

Figure 112: Default Tied Interface (TYPE2)

The mass of the secondary node is transferred to the main nodes using the position of the projection on the segment and linear interpolation functions:

$$\bar{m}^i_{main} = m^i_{main} + m_{secondary} * \Phi_i(p) \tag{726}$$

Where,

p Denotes the position of the secondary point

Φ Weight function obtained by the interpolation equations

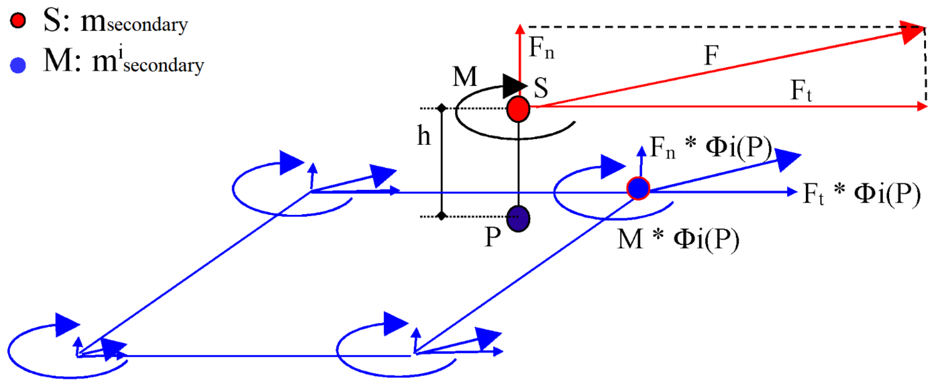

Figure 113: Transfer of Secondary Node Efforts to the Main Nodes ($Spot_{flag}$=0)

The inertia of the secondary node is also transferred to the main nodes by taking into account the distance d between the secondary node and the main surface:

$$\bar{I}^i_{main} = I^i_{main} + \left(I_{secondary} + m_{secondary} * d^2\right) * \Phi_i(\text{p}) \tag{727}$$

The term $m_{secondary} * d^2$ may increase the total inertia of the model especially when the secondary node is far from the main surface.

The stability conditions are written on the main nodes:

$$\begin{aligned} \bar{K}_{main} &= K_{main} + K_{secondary} * \Phi_i(\text{p}) \\ \bar{K}^{rotation}_{main} &= K^{rotation}_{main} + \left(K^{rotation}_{secondary} + K_{secondary} * d^2\right) * \Phi_i(\text{p}) \end{aligned} \tag{728}$$

The dynamic equilibrium of each main node is then studied and the nodal accelerations are computed. Then the velocities at main nodes can be obtained and updated to compute the velocity of the projected point P by:

$$\begin{aligned} V^{translation}_P &= \sum_i V^{translation}_{main\ i} \Phi_i(\text{p}) \\ V^{rotation}_P &= \sum_i V^{rotation}_{main\ i} \Phi_i(\text{p}) \end{aligned} \tag{729}$$

The velocity of the secondary node is then obtained:

$$\begin{aligned} V^{translation}_{secondary} &= V^{translation}_P + V^{rotation}_P \otimes \overrightarrow{PS} \\ V^{rotation}_{secondary} &= V^{rotation}_P \end{aligned} \tag{730}$$

With this formulation, the added inertia may be very large especially when the secondary node is far from the mean plan of the main element.

Optimized Spotweld Formulation

When *Spot*$_{flag}$=1, the spotweld formulation is an optimized formulation:

- Based on element mean rigid motion (that is, without exciting deformation modes)
- Having no hourglass problem
- Having constant connection stiffness
- Recommended with under integrated shells (main)
- Recommended for connecting beam, spring and shell secondary nodes to brick main segments

This spotweld formulation is optimized for spotwelds or rivets.

The secondary node is joined to the main segment barycenter as shown in Figure 114.

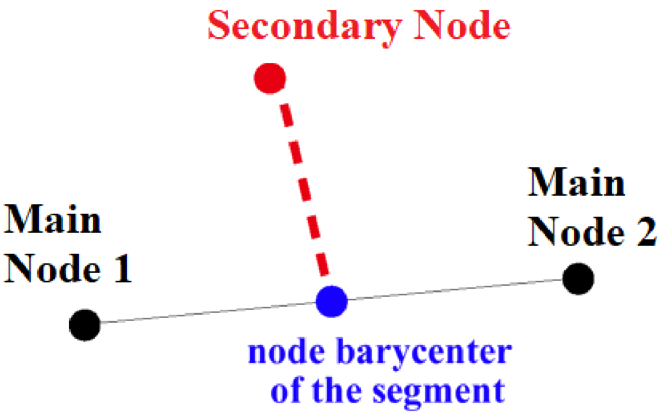

Figure 114: Relation Between Secondary Node and Main Node

Forces and moments transfer from secondary to main nodes is described in Figure 115. The force applied at the secondary node S is redistributed uniformly to the main nodes. In this way, only translational mode is excited. The moment $M + CS \otimes F$ is redistributed to the main nodes by four forces F_i such that:

$$F_i \propto \vec{A} \otimes CM_i$$

$$\sum_i CM_i \otimes F_i = M + CS \otimes F \tag{731}$$

Where,

$\vec{A}$ Normal vector to the segment

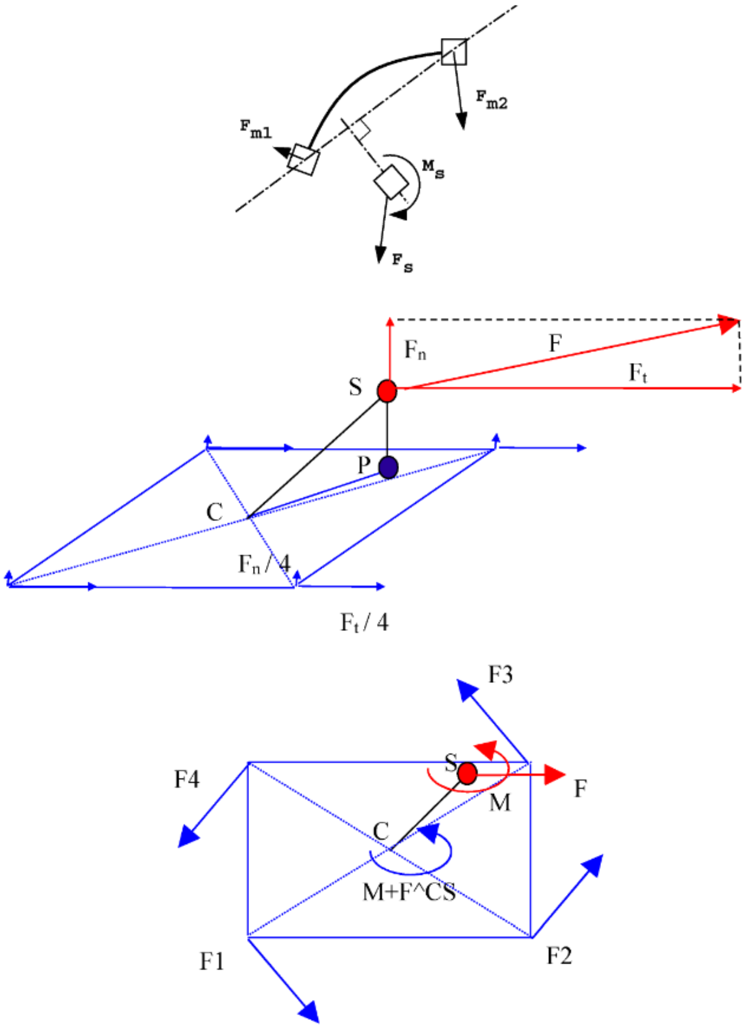

Figure 115: Optimized Tied Interface (TYPE2)

In this formulation the mass of the secondary node is equally distributed to the main nodes. In conformity with effort transmission, the spherical inertia is computed with respect to the center of the main element C:

$$I_C^{Secondary} = I^{Secondary} + m^{Secondary}.d^2 \tag{732}$$

Where, d is distance from the secondary node to the center of element. In order to insure the stability condition without reduction in the time step, the inertia of the secondary node is transferred to the main nodes by an equivalent nodal mass computed by:

$$\Delta m = \frac{I^{Secondary} + \mathrm{m}^{Secondary}.d^2}{\| \bar{I} \|}, with \bar{I} = \sum_{i=1,..4} \begin{pmatrix} Y_i^2 + Z_i^2 & -X_iY_i & -X_iZ_i \\ -X_iY_i & X_i^2 + Z_i^2 & -Y_iZ_i \\ -X_iZ_i & -Y_iZ_i & X_i^2 + Y_i^2 \end{pmatrix} \tag{733}$$

Closest Main Segment Formulation

The main segment is found via 2 formulations:

- Old formulation
- New improved formulation

Old Search of Closest Main Segment Formulation

When I_{search}= 1, the search of closest main segment was based on the old formulation.

A box with a side equal to *dsearch* (input) is built to search the main node contained within this box.

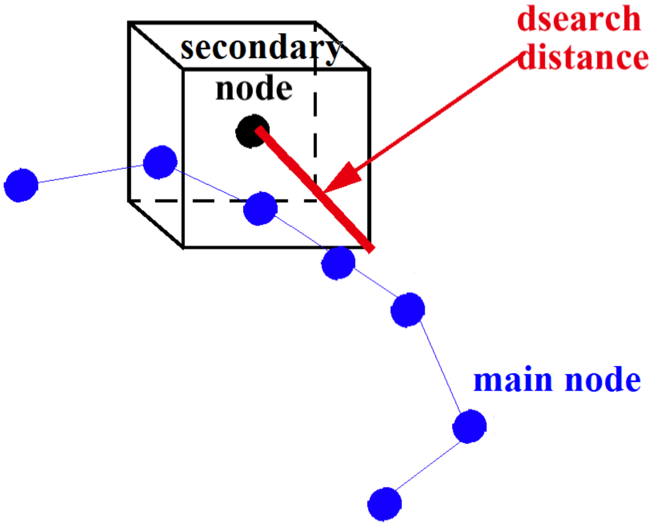

Figure 116: Old Search of Closest Main Segment

The distance between each main node in the box and the secondary node is computed.

The main node giving the minimum distance (*dmin*) is retained.

The segment is chosen with the selected node, (if the selected node belongs to 2 segments, one is selected at random).

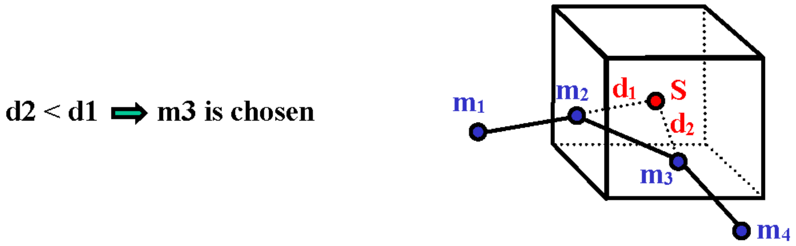

Figure 117: Old Search of Closest Main Segment

New Improved Search of Closest Main Segment Formulation

When I_{search}=2, the search of closest main segment is based on the new improved formulation; a box including the main surface is built.

The dichotomy principle is applied to this box as long as the box contains only one main node and as long as the box side is equal to *dsearch*.

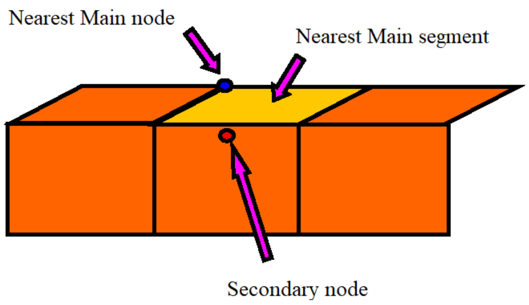

Figure 118: New Improved Search of Closest Main Segment

There are two solutions to compute the minimum distance, *dmin*:

1. The secondary node is an internal node for the main segment, as shown in Figure 119.

   The secondary node is projected orthogonally on the main segment to give a distance that may be compared with other distances. Select the minimum distance:

   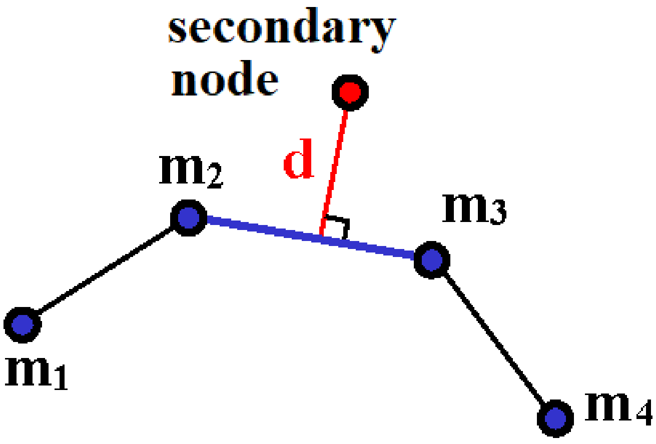

   Figure 119: Orthogonal Projection on the Main Segment

   The segment that provides the minimum distance is chosen for the following computation.
2. The secondary node is a node external to the main segment, as shown in Figure 120.

   The distance selected is that between the secondary node and the nearest main node.

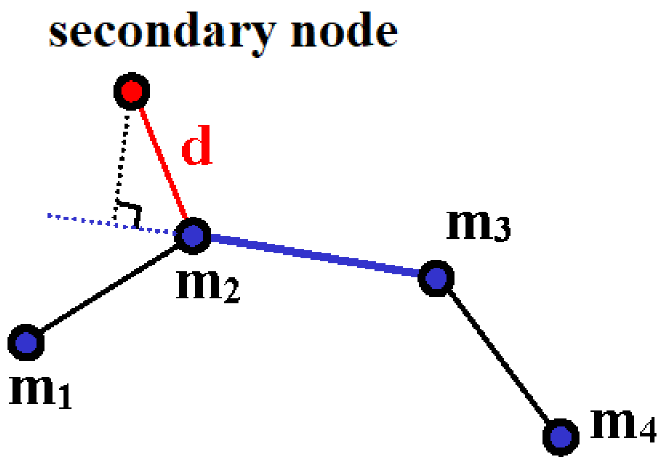

Figure 120: Nearest Main Node

The segment is chosen using the selected node, (if the selected node belongs to 2 segments, one is chosen at random).

Rigid Wall

There are four types of rigid walls available in Radioss:

1. Infinite Plane
2. Infinite Cylinder with Diameter D
3. Sphere with Diameter D
4. Parallelogram

Each wall can be fixed or moving.

A kinematic condition is applied on each impacted secondary node. Therefore, a secondary node cannot have another kinematic condition; unless these conditions are applied in orthogonal directions.

Fixed Rigid Wall

A fixed wall is a pure kinematic option on all impacted secondary nodes. It is defined using two points, M and M1. These define the normal, as shown in Figure 121.

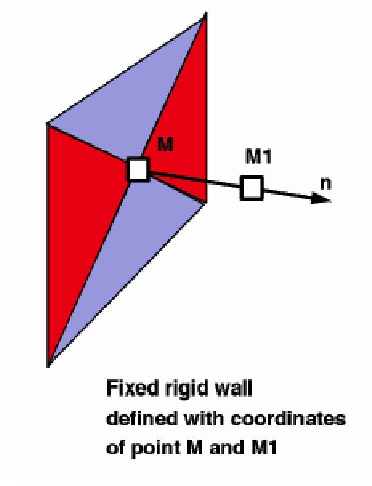

Figure 121: Fixed Rigid Wall Definition

Moving Rigid Wall

A moving rigid wall is defined by a node number, N, and a point, M1. This allows a normal to be calculated, as shown in Figure 122.

The motion of node N can be specified with fixed velocity, or with an initial velocity. For simplification, an initial velocity and a mass may be given at the wall definition level.

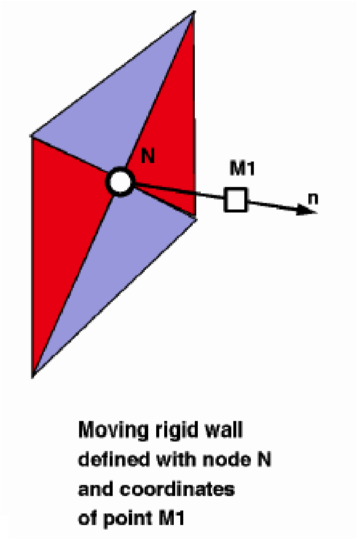

Figure 122: Moving Rigid Wall Definition

A moving wall is a main secondary option. Main node defines the wall position at each time step and imposes velocity on impacted secondary nodes. Impacted secondary node forces are applied to the main node. The secondary node forces are computed with momentum conservation. The mass of the secondary nodes is not transmitted to the main node, assuming a large rigid wall mass compared to the impacted secondary node mass.

Secondary Node Penetration

Secondary node penetration must be checked. Figure 123 shows how penetration is checked.

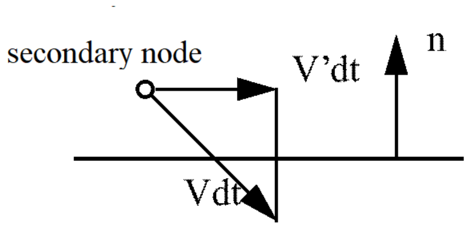

Figure 123: Secondary Node Penetration

If penetration occurs, a new velocity must be computed. This new velocity is computed using one of three possible situations.

1. Sliding
2. Sliding with Friction
3. Tied

For a node which is allowed to slide along the face of the rigid wall, the new velocity $\vec{V}'$ is given by:

$$\vec{V}' = \vec{V} - (\vec{V} \cdot \vec{n})\vec{n} \tag{734}$$

A friction coefficient can be applied between a sliding node and the rigid wall. The friction models are developed in Interface Friction.

For a node that is defined as tied, once the secondary node contacts the rigid wall, its velocity is the same as that of the wall. The node and the wall are tied. Therefore:

$$\vec{V}' = 0 \tag{735}$$

Rigid Wall Impact Force

The force exerted by nodes impacting onto a rigid wall is found by calculating the impulse by:

$$\vec{I} = \sum_{i=I}^{N} \vec{F}_i \Delta t = \sum_{i=I}^{N} \Delta m_i (\vec{V}_i - \vec{W}) \tag{736}$$

Where,

N Number of penetrated secondary nodes

$\vec{W}$ Wall velocity

The force can then be calculated by the rate of change in the impulse:

$$\vec{F} = \frac{d\vec{I}}{dt} \tag{737}$$

Rigid Link

A rigid link imposes the same velocity on all secondary nodes in one or more directions. The directions are defined to a skew or global frame. Figure 124 displays a rigid link.

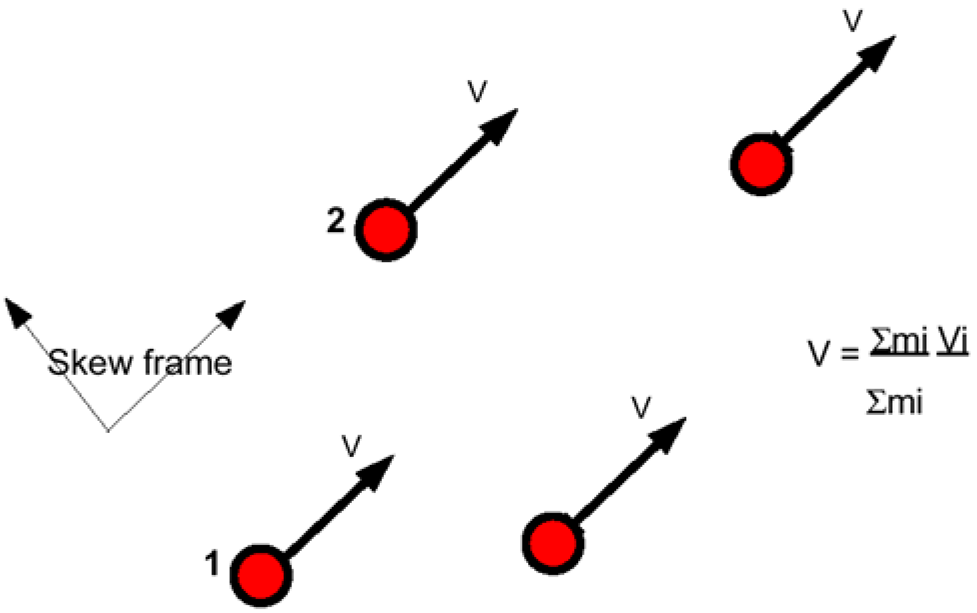

Figure 124: Rigid Link Model

The velocity of the group of nodes rigidly linked together is computed using momentum conservation (Section Definition, Equation 740). However, no global moment equilibrium is respected.

$$V^i = \frac{\sum_{i=i}^{N} m_i v_i}{\sum_{i=i}^{N} m_i} \tag{738}$$

Angular velocity for the ith DOF with respect to the global or a skew reference frame is:

$$\omega^i = \frac{\left(\sum_{j=1}^{n} I_j^i \omega_j^i\right)}{\left(\sum_{j=1}^{N} I_j^i\right)} \tag{739}$$

For non-coincident nodes, no rigid body motion is possible.

A rigid link is equivalent to an infinitely stiff spring TYPE8.

Section Definition

A section is a cut in the structure where forces and moments will be computed and stored in output files.

It is defined by:

- A cutting plane
- A reference point to compute forces
- A direction of the section.

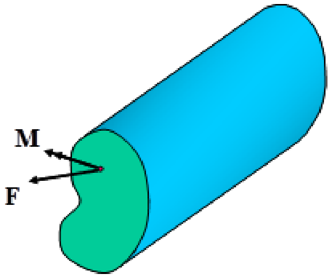

Figure 125: Definition of a Section for an Oriented Solid

In Radioss the cutting plane is defined by a group of elements and its orientation by a group of nodes as shown in Figure 126.

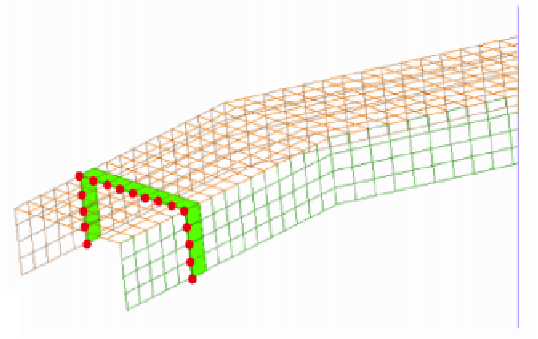

Figure 126: Definition of a Section for a Shell Mesh

Then, a point is defined for the center of rotation of the section and a reference frame is attached to this point to compute the internal efforts.

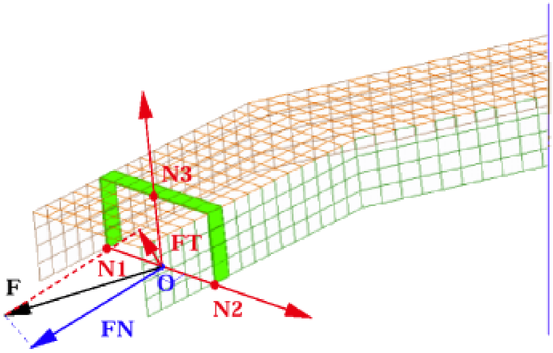

Figure 127: Center of Rotation and its Associated Frame for a Section

The resultant of all forces applied to the elements and its application point are computed by:

$$F = \sum f_i \tag{740}$$

$$M = \sum m_i + \sum ON_i \times f_i \tag{741}$$

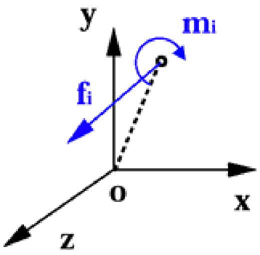

Figure 128: Resultant of Force and Moment for a Node I with the Rotation Point O

Linear Stability

The stability of solution concerns the evolution of a process subjected to small perturbations. A process is considered to be stable if small perturbations of initial data result in small changes in the solution. The theory of stability can be applied to a variety of computational problems.

The numerical stability of the time integration schemes is widely discussed in the *Theory Manual*. Here, the stability of an equilibrium state for an elastic system is studied. The material stability will be presented in an upcoming version of this manual.

The stability of an equilibrium state is of considerable interest. It is determined by examining whether perturbations applied to that equilibrium state grow. A famous example of stable and unstable cases is often given in the literature. It concerns a ball deposited on three kinds of surfaces as shown in Figure 129.

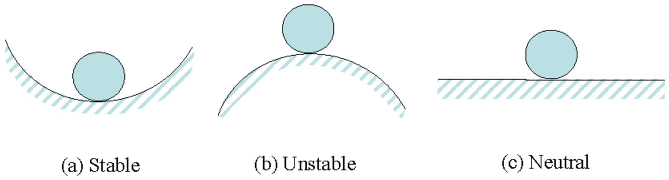

Figure 129: Schematic Presentation of Stability

It is clear that the state (b) represents an unstable case since a small change in the position of the ball results the rolling either to the right or to the left. It is worthwhile to mention here that stability and equilibrium notions are quite different. A system in static equilibrium may be in unstable state and a system in evolution is not necessary unstable.

A good understanding of the stability of equilibrium can be obtained by studying the load-deflection curves. A typical behavior of a structure in buckling is given in Figure 130. The load-deflection curves are slightly different for systems with and without imperfection. In the first case, the structure is loaded until the bifurcation point B corresponding to the first critical load level. Then, two solutions are mathematically acceptable: response without buckling (BA), response after buckling (BC).

In the case of structures with imperfection, no bifurcation point is observed. The behavior before buckling is not linear and the turning point D is the limit point in which the slope of the curve changes sign. If the behavior before buckling is linear or the nonlinearity before the limit point is not high, the linear stability technique can be used to determine the critical load. The method is based on the perturbation of the equilibrium state. As the perturbations are small, the linearized model is used. The method is detailed in the following section.

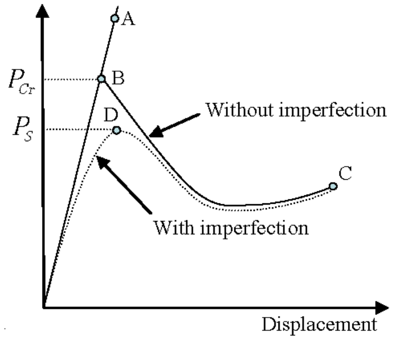

Figure 130: Bifurcation and Limit Points in Load-Deflection Curves for System With and Without Imperfections

B: Bifurcation point, D: Limit point

General Theory of Linear Stability

The principle of virtual power and the minimum of total potential energy are the various mathematical models largely used in Finite Element Method. Under small-perturbations assumption these notions can be applied to the equilibrium state in order to study the stability of the system.

Consider the example of the ball on the three kinds of surfaces as shown in Linear Stability, Figure 129. If Π is the total potential energy, the equilibrium is obtained by:

Static equilibrium

$$\delta\Pi = 0 \tag{742}$$

Applying a small perturbation to the equilibrium state, the variation of the total potential energy can be written as:

$$\delta\Pi(t+\Delta t) = \delta\Pi(t) + \delta^2\Pi \tag{743}$$

Where, $\delta^2\Pi$ is the second variation of the potential energy. Then, the three cases can be distinguished:

Stable (case a)

$$\delta^2\Pi > 0 \tag{744}$$

The energy increases around the equilibrium state.

Unstable (case b)

$$\delta^2\Pi < 0 \tag{745}$$

The energy decreases around the equilibrium state.

Neutral stability (case c)

$$\delta^2\Pi = 0 \tag{746}$$

The energy remains unchanged around the equilibrium state.

The last case is used to compute the critical loads:

$$\delta^2 \Pi = \delta^2 \Pi_{\text{int}} + \delta^2 \Pi_{ext} = 0 \tag{747}$$

Where, the indices int and ext denote the interval and external parts of the total potential energy. After the application of the application of finite element method, the stability equation in a discrete form can be written as:

$$\delta^2 \Pi = \sum_n \delta^2 \Pi^e_{\text{int}} + \sum_n \delta^2 \Pi^e_{ext} = 0 \tag{748}$$

$$\delta^2 \Pi^e_{ext} = \int_{S_e^0} \langle \delta X \rangle \{ \delta f_n \} \, dS_{e0} \tag{749}$$

$$\delta^2 \Pi^e_{\text{int}} = \int_{V_e^0} ([E][S] + [\delta E][\delta S]) \, dV_{e0} \tag{750}$$

Where,

e	Designate element
$\{f_n\}$	Vector of the external forces
$\langle \delta X \rangle$	Virtual displacement vector
$[E]$	Green-Lagrange strain tensor
$[S]$	Piola-Kirchhoff stress tensor

The equation Equation 750 is written as a function of X, the displacement between the initial configuration C^0 and the critical state C^t. If X_L and S_L are the linear response obtained after application the load f_L in the initial configuration C^0, in linear theory of stability suppose that the solution in C^t for the critical load f_{cr} is proportional to the linear response:

$$\{X_{cr}\} = \lambda \{X_L\}$$

$$\{S_{cr}\} = \lambda \{S_L\} \tag{751}$$

$$\{F_{cr}\} = \lambda \{F_L\}$$

If you admit that the loading does not depend on the deformation state, the hypothesis $\delta^2 \Pi_{ext} = 0$ is then true. Using Kinematic Description, Equation 62 and denoting $[e]$ for the linear part of Green-Lagrange strain tensor and $[\eta]$ for the nonlinear part, you have:

$$\{E\} = \{e\} + \{\eta\} \tag{752}$$

Putting this equation in Equation 750, you obtain:

$$\delta^2 \Pi^e{}_{ext} = \int_{V_0^e} \left(\langle \delta e \rangle [C] \{\delta e\} + \lambda \left(\langle \delta \eta_L \rangle [C] \{\delta e\} + \langle \delta e \rangle [C] [\delta \eta_L] + \langle S \rangle \{\delta^2 E\} \right) \right) dV_e^0 \tag{753}$$

Or

$$\delta^2 \Pi^e{}_{ext} = \langle \delta X \rangle \left([k] + \lambda \left([k_u (X_L)] + [k_\sigma] \right) \right) \{\delta X\} \tag{754}$$

Where,

$[k]$	Stiffness matrix
$[k_u]$	Initial displacement matrix
$[k_\sigma]$	Initial stress or geometrical stiffness matrix
$[C]$	Elastic matrix

The linear theory of stability allows estimating the critical loads and their associated modes by resolving an eigenvalue problem:

$$\left([K] + \lambda \left([K_u] + [K_\sigma] \right) \right) \{\delta X\} = 0 \tag{755}$$

Linear stability assumes the linearity of behavior before buckling. If a system is highly nonlinear in the neighborhood of the initial state C^0, moderate perturbations may lead to unstable growth. In addition, in case of path-dependent materials, the use of method is not conclusive from an engineering point of view. However, the method is simple and provides generally good estimations of limit points.

The resolution procedure consists in two main steps. First, the linear solution for the equilibrium of the system under the application of the load $\{F_L\}$ is obtained. Then, Equation 755 is resolved to compute the first desired critical loads and modes. The methods to compute the eigen values are those explained in Large Scale Eigen Value Computation.

Interfaces

Interfaces solve the contact and impact conditions between two parts of a model.

Contact-impact problems are among the most difficult nonlinear problems to solve as they introduce discontinuities in the velocity time histories. Prior to the contact, the normal velocities of the two bodies which come into contact are not equal, while after impact the normal velocities must be consistent with the impenetrability condition. In the same way, the tangential velocities along interfaces are discontinuous when stick-slip behavior occurs in friction models. These discontinuities in time complicate the integration of governing equations and influence performance of numerical methods.

Central to the contact-impact problem is the condition of impenetrability. This condition states that bodies in contact cannot overlap or that their intersection remains empty. The difficulty with the impenetrability condition is that it cannot be expressed in terms of displacements as it is not possible to anticipate which parts of the bodies will come into contact. For this reason, it is convenient to express the impenetrability condition in a rate form at each cycle of the process. This condition can be written as:

$$\gamma_N = v_N^A - v_N^B \leq 0 \tag{756}$$

on the contact surface Γ_C common to the two bodies.

v_N^A and v_N^B are respectively the normal velocities in the two bodies in contact. γ_N is the rate of interpenetration.

Equation 756 simply expresses that when two bodies are in contact, they must either remain in contact and $\gamma_N = 0$, or they must separate and $\gamma_N < 0$.

On the other hand, the tractions must observe the balance of momentum across the contact interface. This requires that the sum of the tractions on the two bodies vanish:

$$t_N^A + t_N^B = 0 \tag{757}$$

Normal tractions are assumed compressive, which can be stated as:

$$t_N = t_N^A = -t_N^B < 0 \tag{758}$$

Equation 756 and Equation 757 can be combined in a single equation stating that, $t_N\gamma_N = 0$. This condition simply expresses that the contact forces do not create work. If the two bodies are in contact, the interpenetration rate vanishes. On the other hand, if the two bodies are separated $\gamma_N < 0$ but the surface tractions vanish. As a result, the product of the surface tractions and the interpenetration rate disappear in all cases.

The impenetrability condition is expressed as an inequality constraint, the condition:

$$t_N\gamma_N = 0 \tag{759}$$

can also be seen as the Kuhn-Tucker condition associated with the optimization problem consisting in minimizing the total energy (Virtual Power Principle, Equation 99) subject to the inequality constraint Lagrange Multiplier Method, Equation 756.

In practice, the solution to a contact problem entails in three steps:

- First, it is necessary to find for each point those points in the opposite body which will possibly come into contact. This is the geometrical recognition phase.
- The second phase is to check whether or not the bodies are in contact and, if the bodies are in contact, if they are sticking or slipping. This step makes use of the geometrical information computed in the first phase.
- The last step will be to compute a satisfactory state of contact.

The geometrical recognition phase is dependent on the type of interface. This will be discussed below in parallel with the description of interfaces. On the other hand, structural problems with contact-impact conditions lead to constrained optimization problems, in which the objective function to be minimized is the virtual power subject to the contact-impact conditions. There are conventionally two approaches to solving such mathematical programming problems:

- the Lagrange multiplier method
- the Penalty method.

Both methods are used in Radioss.

Lagrange Multiplier Method

Lagrange multipliers can be used to find the extreme of a multivariate function $f(x_1, x_2, ..., x_n)$ subject to the constraint $g(x_1, x_2, ..., x_n) = 0$

Where, f and g are functions with continuous first partial derivatives on the open set containing the constraint curve, and $\nabla g \neq 0$ at any point on the curve (where ∇ is the gradient).

To find the extreme, write:

$$df = \frac{\partial f}{\partial x_1} dx_1 + \frac{\partial f}{\partial x_2} dx_2 + ... + \frac{\partial f}{\partial x_n} dx_n = 0 \tag{760}$$

But, because g is being held constant, it is also true that

$$dg = \frac{\partial g}{\partial x_1} dx_1 + \frac{\partial g}{\partial x_2} dx_2 + ... + \frac{\partial g}{\partial x_n} dx_n = 0 \tag{761}$$

So multiply Equation 761 by the as yet undetermined parameter λ and add to Equation 761,

$$\left(\frac{\partial f}{\partial x_1} + \lambda \frac{\partial g}{\partial x_1}\right) dx_1 + \left(\frac{\partial f}{\partial x_2} + \lambda \frac{\partial g}{\partial x_2}\right) dx_2 + ... + \left(\frac{\partial f}{\partial x_n} + \lambda \frac{\partial g}{\partial x_n}\right) dx_n = 0 \tag{762}$$

Note that the differentials are all independent, so any combination of them can be set equal to 0 and the remainder must still give zero. This requires that:

$$\left(\frac{\partial f}{\partial x_k} + \lambda \frac{\partial g}{\partial x_k}\right) dx_k = 0 \tag{763}$$

for all k = 1, ..., n, and the constant λ is called the Lagrange multiplier. For multiple constraints, $g_1 = 0$, $g_2 = 0$, ...,

$$\nabla f = \lambda_1 \nabla g_1 + \lambda_2 \nabla g_2 + \ldots \tag{764}$$

The Lagrange multiplier method can be applied to contact-impact problems. In this case, the multivariate function is the expression of total energy subjected to the contact conditions:

$$f(x_1, x_2, .., x_n) \equiv \Pi(x, \dot{x}, \ddot{x}) \tag{765}$$

$$g(x_1, x_2, .., x_n) \equiv Q(x, \dot{x}, \ddot{x}) = 0 \tag{766}$$

Where, $x, \dot{x}, \ddot{x}$ are the global vectors of DOF. The application of Lagrange multiplier method to the previous equations gives the weak form as:

$$M\ddot{x} + f_{int} - f_{ext} + L\lambda = 0 \tag{767}$$

with

$$Lx = b \tag{768}$$

This leads to:

$$\begin{bmatrix} K & L^T \\ L & 0 \end{bmatrix} \begin{Bmatrix} x \\ \lambda \end{Bmatrix} = \begin{Bmatrix} f \\ 0 \end{Bmatrix} \tag{769}$$

The Lagrange multipliers are physically interpreted as surface tractions. The equivalence of the modified virtual power principle with the momentum equation, the traction boundary conditions and the contact conditions (impenetrability and surface tractions) can be easily demonstrated. [88]

It is emphasized that the above weak form is an inequality. In the discretized form, the Lagrange multiplier fields will be discretized and the restriction of the normal surface traction to be compressive will result from constraints on the trial set of Lagrange multipliers.

Penalty Method

In the solution of constrained optimization problems, penalty methods consist in replacing the constrained optimization problem with a sequence of unconstrained optimization problems. The virtual power continues to be minimized so as to find the stationary condition, but a penalty term is added to Virtual Power Term Names, Equation 99 so as to impose the impenetrability condition:

$$\delta Q = \int_{\Gamma^c} \rho \phi(\gamma_N) d\Gamma \tag{770}$$

Where,

$\phi(\gamma_N) = 0$ if $\gamma_N = 0$

[88] Engelmann B.E. and Whirley R.G., "A new elastoplastic shell element formulation for DYNA3D", Report ugrl-jc-104826, Lawrence Livermore National Laboratory, 1990.

$\phi(\gamma_N) > 0$ if $\gamma_N < 0$

ρ is an arbitrary parameter known as the penalty parameter. The penalty function ϕ is an arbitrary function of the interpenetration and its rate. It is emphasized that the weak form, including the virtual power and the penalty term Penalty Method, Equation 770 is not an inequality form. The penalty function will be defined in the description of interfaces.

Interface Overview

There are several different interface types available in Radioss. A brief overview of the different types and their applications.

TYPE1	Tied contact (boundary) between an ALE part and a Lagrangian part.
TYPE2	Tied contact
TYPE3	Used to simulate impacts and contacts on shell and solid elements. Surfaces should be simply convex.
TYPE5	Used to simulate impacts and contacts between a main surface and a list of secondary nodes. Best suited for beam, truss and spring impacts on a surface.
TYPE6	Used to simulate impacts and contacts between two rigid surfaces.
TYPE7	A general interface that removes the limitations of TYPE3 and TYPE5.
TYPE8	Drawbead contact for stamping applications.
TYPE9	ALE Lagrange with void opening and free surface.
TYPE10	Tied after impact with or without rebound.
TYPE11	Edge to edge or line to line impact.
TYPE12	Connects 2 fluid meshes with free, tied or periodic options. ALE or EULER or LAG/ALE or EULER or LAG.
TYPE14	Ellipsoidal surfaces to nodes contact.
TYPE15	Ellipsoidal surfaces to segments contact.
TYPE18	Coupling between a Lagrangian material and an ALE material.
TYPE19	General contact interface. Node to segment contact and Edge to Edge contact. Equivalent to one interface TYPE7 + one interface TYPE11.

TYPE20

Single surface, surface to surface with optional Edge to Edge contact.

No time step condition with soft penalty

TYPE21

Specific interface between a non-deformable main surface and a secondary surface designed for stamping.

Each of these interfaces was developed for a specific application field. However, this application field is not the only selection criteria. Some limitations of the different algorithms used in each interface can also determine the choice.

The algorithm limitations concern mainly the search of the impacted segment. This search may be performed directly (TYPE7, TYPE10, and TYPE11 interfaces), or via a search of the nearest node (TYPE3, TYPE5, and TYPE6 interfaces).

Apart from the limitation of the nearest node search, some limitations exist for the choice between the segments connected to the nearest node. These limitations are the same for TYPE3, TYPE5 and TYPE6 interfaces.

TYPE3, TYPE5 and TYPE6 interfaces also have some limitations due to the orientation of the normal segment.

TYPE7 interface was written to emulate TYPE3 and TYPE5 interfaces without algorithm limitations. With this interface, each node can impact one or more segments, on both sides, on the edges or on the corners of the segments. The only limitation to this interface concerns high impact speed and/or small gap. For these situations the interface will continue to work properly, but the time step can decrease dramatically.

TYPE3, TYPE5 and TYPE7 interfaces are compatible with all Radioss kinematic options.

TYPE1 interface is a special option used with solid elements to provide mesh transition. TYPE1 interface is used to connect a Lagrangian and an ALE mesh.

TYPE2 interface is used to connect a fine and a coarse Lagrangian mesh.

All other interface types (TYPE3, TYPE4, TYPE5, TYPE6 and TYPE7) are used to simulate impacts and contacts.

A node may belong to several interfaces.

Surface (Segment) Definition

Surfaces or segments may be defined in different ways, depending on the type of element being used. For a four node three dimensional shell element, an element is a segment.

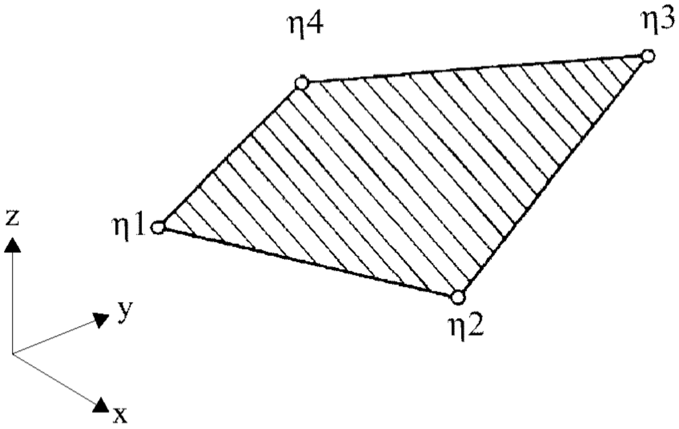

Figure 131: Shell Elements Segment

For a brick element, a segment is one face of the brick.

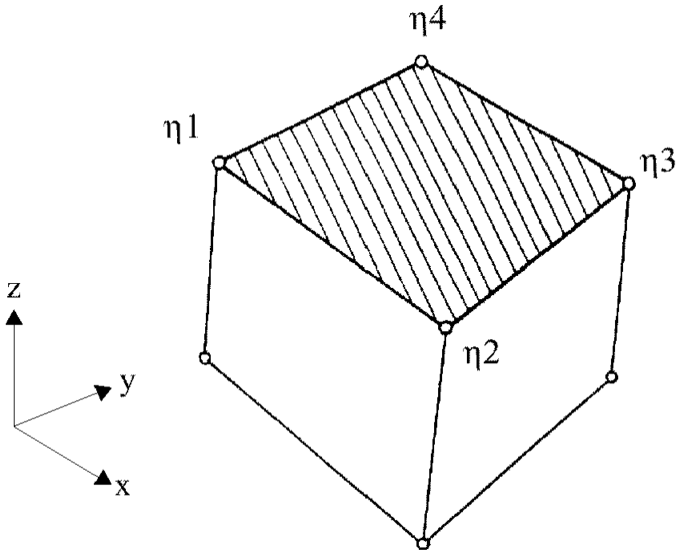

Figure 132: Brick Element Segment

For a two dimensional element, a segment is one side.

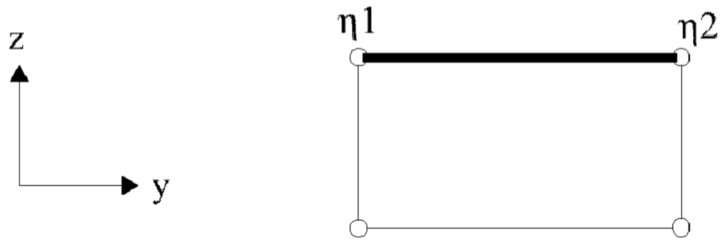

Figure 133: 2D Element Segment

Tied Interface (TYPE2)

Refer to Kinematic Constraints for a detailed description.

Auto Contacts

The physics of contacts is involved in various phenomena, such as the impact of two billiard balls, the contact between two gears, the impact of a missile, the crash of a car, etc. While the physics of the contact itself is the same in all these cases, the main resulting phenomena are not.

In the case of billiard balls, it is the shock itself that is important and it will then be necessary to simulate perfectly the wave propagation. In the case of gears, it is the contact pressure that has to be evaluated precisely.

The quality of these simulations depends mainly on the quality of the models (spatial and temporal discretization) and on the choice of the integration scheme. In structural crash or vehicle crash simulations, the majority of the contacts result from the buckling of tubular structures and metal sheets. Modeling the structure using shell and plate finite elements, the physics of the contact cannot be described in a precise way. The reflection of the waves in the thickness is not captured and the distribution of contact pressures in the thickness is not taken into account. The peculiarity of the contacts occurring during the crash of a structure lies more in the complexity of the structural folding and the important number of contact zones than in the description of the impact or the contact itself.

During a contact between two solid bodies, the surface in contact is usually continuous and only slightly curved. On the other hand, during the buckling of a structure, the contacts, resulting from sheet folding, are many and complex. Globally, the contact is no longer between two identified surfaces, but in a surface impacting on itself. The algorithms able to describe this type of contact are "*auto-impacting*" algorithms. Especially adapted to shell structures, they still can be used to simulate the impact of the external surface of a solid (3D element) on itself.

The main capabilities of the auto-contact can be summarized by the following functionalities:

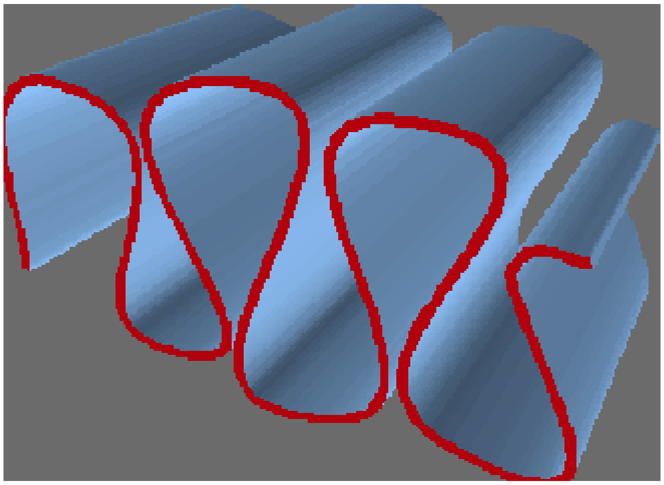

Figure 134:

- Capacity to make each point of the surface impact on itself
- Capacity to impact on both sides of a segment (internal and external)
- Possibility for a point of the surface to be wedged between an upper and a lower part
- Processing of very strong concavities (will complete folding)
- Reversibility of the contact, thereby authorizing unfolding after folding or the simulation of airbag deployment.

Contacts Modeling

The contacts occurring between two surfaces of a finite element mesh can be modeled in different ways:

- Contact nodes to nodes

The contact is detected based on the criteria of distance between the two nodes. After detection of contact, a kinematic condition or penalty formulation method prevents the penetration attaining the rebound point ("pin-ball" formulation).

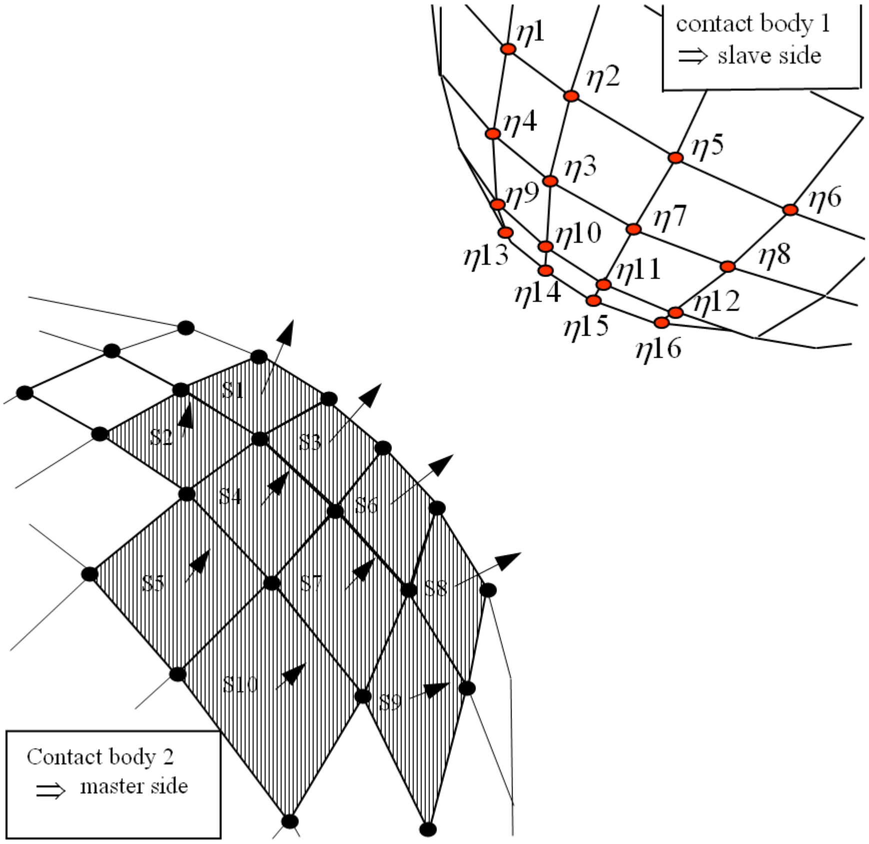

Figure 135: Contact Nodes to Surface

The contact is detected based on the criteria of distance between a group of nodes and a meshed surface. The distance between a node and the surface of a triangular or quadrangular segment is evaluated, locally.

Symmetrized contact nodes to surface

The symmetrization of the previous formulation makes it possible to model a contact between two surfaces, as the group of nodes of the first surface can impact the second group and vice-versa.

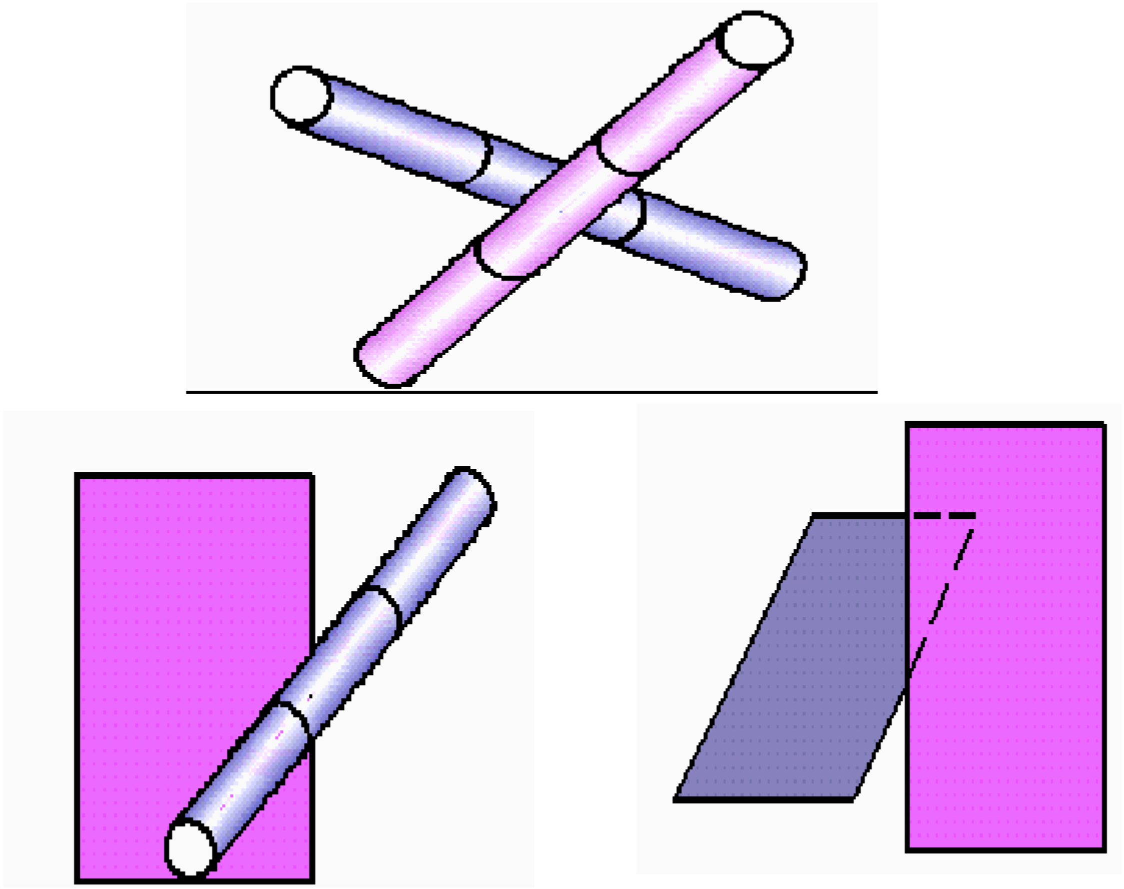

Figure 136: Contact Edges to Edges

This formulation makes it possible to model contacts between wire framed structures or between edges of two-dimensional structures. Contact is detected based on the criteria of distance between two segments. This formulation can also be used to describe in an approximate way the surface to surface contact.

Surface to surface contact

Several approaches can be used to detect the contact between two surfaces. If the two surfaces are quadrangular, the exact calculation of the contact can be complex and quite expensive. An approximate solution may be made by combining the two previous formulations. By evaluating all the contacts of nodes to surface, as well as the edge to edge contacts, the only approximation is the partial consideration of the segment curvature.

Choice of a Formulation for Auto Impact

In the case of a surface impacting on itself, it is possible to use one of the previous formulations if considering certain specificities of the auto-contact. The choice of a formulation will depend on two essential criteria: the quality of the description of the contact and the robustness of the formulation. The selected formulation has to provide results that are as precise as possible in a normal operational situation, while still working in a satisfying way in extreme situations. The node-to-node method provides the best robustness, but the quality of the description is not sufficient enough to simulate in a realistic way those contacts occurring during the buckling of a structure.

The node-to-surface contact is the best compromise. However, it has some limitations, the main one being that it cannot detect contacts occurring on the edges of a segment. The most critical situation occurs when this leads to the locking of a part of one surface to another. This phenomenon, being irreversible, might create irrelevant behavior during the deployment of a structure (example, airbag deployment). An example of a locking situation is shown in the above images. To correct this, it is possible to associate a node-to-surface formulation to an edge-to-edge formulation.

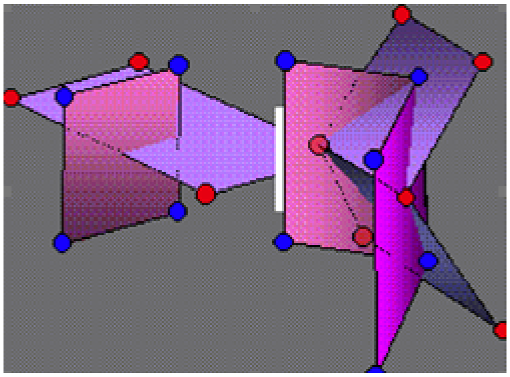

Figure 137:

Algorithms for Impact Candidates

During the impact of one part on another, it is possible to predict which node will impact on a certain segment. In the case of the buckling of a shell structure, such as a tube, it is impossible to predict where different contacts will occur. It is thus necessary to have a fairly general and powerful algorithm that is able to search for impact candidates.

The detail of the formulation of an algorithm, able to search for impact candidates, will depend on the choice of the contact formulation described in the previous chapter. In a node-to-node contact formulation, it is necessary to find for each node the closest node, whose distance is lower than a certain value. In the case of the edge-to-edge formulation, the search for neighboring entities concerns the edges and not the nodes. However, we should note that in some algorithms, the search for neighboring edges or segments is obtained by a node proximity calculation. Moreover, an algorithm designed to search for proximity of nodes can be adapted in order to transform it into a search for proximity of segments or even for a mixed proximity of nodes and segments.

It is possible to distinguish four main types of search for proximity:

- Direct search
- Topologically limited search
- Algorithms of sorting by boxes (bucket sort)
- Algorithms of fast sort (octree, quick sort)

When using direct search, at each cycle the distance is calculated from each entity (node, segment, edge) to all others. The quadratic cost (N*N) of this algorithm makes it unusable in case of auto-contact.

Topologically Limited Search

In a simulation in fast dynamics, geometrical modifications of the structure are not very important during one cycle of calculation. It is then possible to consider neighborhood search algorithms using the information of the previous cycle of computation. If for a node the nearest segment is known at the previous cycle, it is then possible to limit the search for this node to the segments topologically close to the previous one (the segments having at least one common node). Furthermore, if an algorithm based on the search of neighboring nodes is used, then the search may be limited to the nodes of the segments connected to the previous closest node.

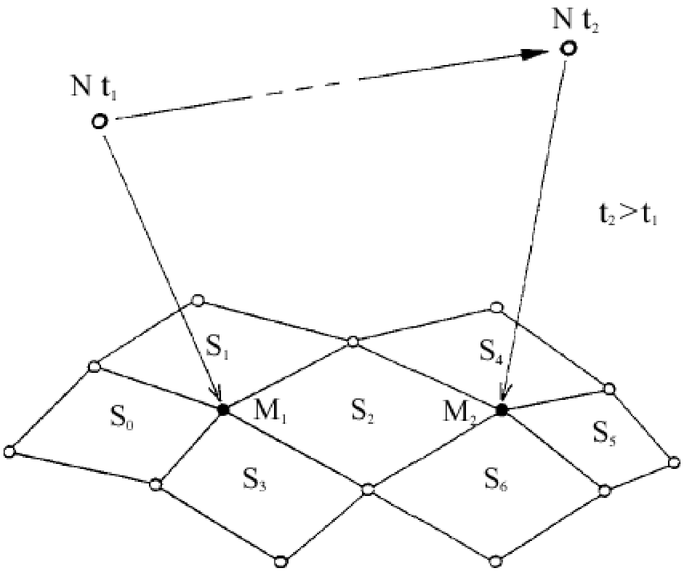

Figure 138:

It remains however necessary to do a complete search before the first cycle of calculation. We will also see that this algorithm presents significant restrictions that limit its use to sliding surfaces (it cannot be used for auto-impacting surfaces).

The cost of this algorithm is linear (N), except at the first cycle of computation, during which it is quadratic (N*N). The combination of this algorithm with one of the following two is also possible.

Bucket Sort

Sorting by boxes consists in dividing space in to steady boxes (not necessarily identical) in which the nodes are placed. The search for closest nodes is limited to one box and the twenty-six neighboring boxes. The cost of this sorting is linear (N) for regular meshes. For irregular meshes, an adaptation is possible but its interest becomes less interesting compared with the next solution. This three-dimensional sorting is of the same kind as one-way sorting with direct addressing or needle sort.

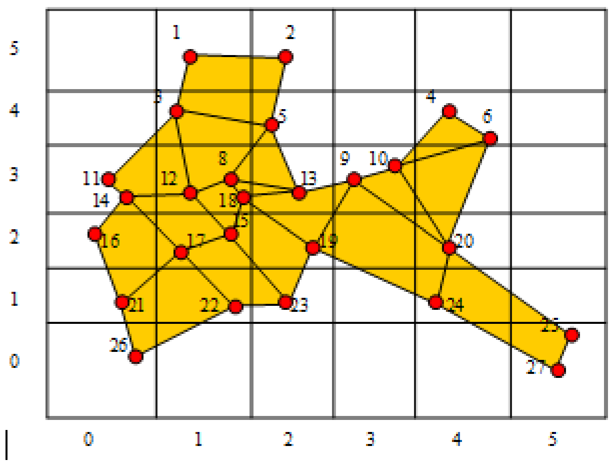

Figure 139:

In order to limit the memory space needed, we first count the number of nodes in each box, thereby making it possible to limit the filling of those boxes that are not empty. In the two-dimensional example shown above, nodes are arranged in the boxes as described in the following table. With this arrangement, the calculation of distances between nodes of the same box is not a problem. On the other hand, taking into account the nodes of neighboring boxes is not straightforward, especially in the horizontal direction (if the arrangement is first made vertically, as in this case). One solution is to consider three columns of boxes at a time. Another solution, more powerful but using more memory, would be for each box to contain the nodes already located there plus those belonging to neighboring boxes. This is shown in the third series of columns in the following table. Once this sorting has been performed, the last step is to calculate the distances between the different nodes of a box, followed by the distance between these nodes and those of the neighboring box. In box 0,3 for example, fifteen distances must be calculated.

11-14, 11-3, 11-8, 11-12, 11-15, 11-16, 11-17, 11-18, 14-3, 14-8,

14-12, 14-15, 14-16, 14-17, 14-18.

Box	Nodes			Nodes of the Neighboring Box										
0,0	26			21										
0,1	21			15	16	17	22	26						
0,2	16			8	11	12	14	15	17	21	22	26		
0,3	11	14		3	8	12	15	16	17	18				
1,1	22			15	16	17	19	21	23	26				
1,2	15	17		8	11	12	13	14	18	16	19	21	22	23
1,3	8	12	18	3	5	11	13	14	15	16	17	19		

Box	Nodes			Nodes of the Neighboring Box										
1,4	3			1	2	5	11	12	13	14	18			
1,5	1			2	3	5								
2,1	23			15	17	19	22							
2,2	19			8	9	10	12	13	15	17	18	22	23	
2,3	13			3	5	8	9	10	12	15	17	18	19	
2,4	5			1	2	3	8	9	10	12	13	18		
2,5	2			1	3	5								
3,3	9	10		4	5	6	13	19	20					
4,1	24			20	25	27								
4,2	20			9	10	24								
4,4	4	6		9	10									
5,0	25	27		24										

In this example you have considered a search based on nodal proximity. It is possible to adapt this algorithm in order to arrange segments or even edges in the boxes. It will be necessary however to reserve more memory, for a segment can overlap several boxes.

Quick Sort

The octree is a three-dimensional adaptation of fast sorting. Space is divided into eight boxes, each one being subdivided into eight boxes. In this way a tree with eight branches per node is obtained. An alternative to the "octree", closer to the quick sort, consists in successively dividing space in two equal parts, according to directions X, Y, or Z. This operation is renewed for each of the two resulting parts as long as some segments or nodes are found in the space concerned. The main advantage to this algorithm, as compared to sorting by boxes, lies in the fact that its performance is affected neither by the irregularity of the mesh, nor by the irregularity of the model. The cost of this algorithm is logarithmic (N*Log(N)).

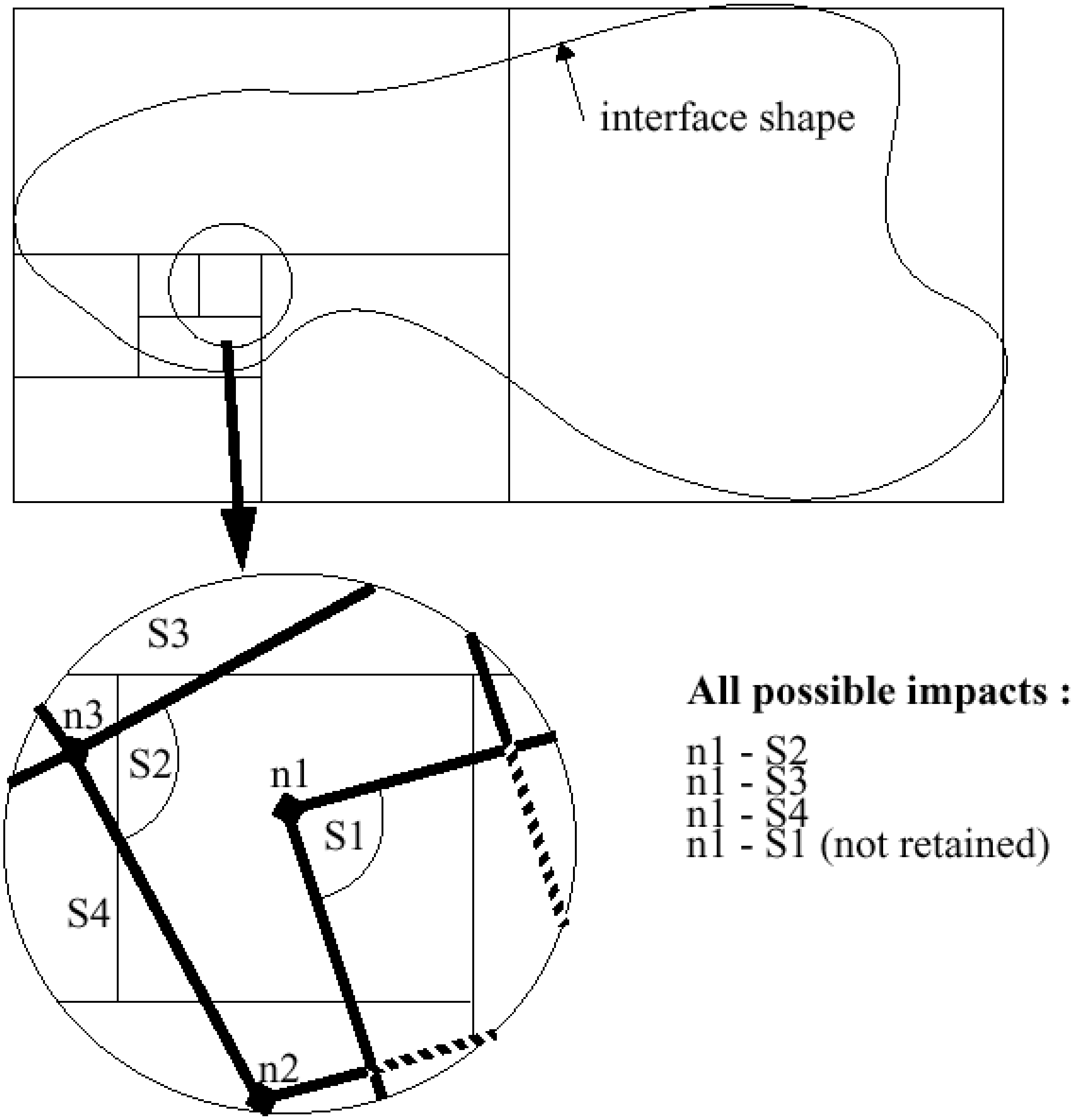

Figure 140: Possible Impact of Node n_1

In order to illustrate the 3D quick sort, consider a search for node-segment proximity. At each step, space is successively divided into two equal parts, according to directions X, Y or Z. The group of nodes is thus separated into two subsets. We thereby obtain a tree organization with two branches per node. After each division, a check is made to determine whether the first of the two boxes must be divided. If so, it will be divided similar to the previous one. If not, the next branch is then checked. This recursive algorithm is identical to the regular fast sorting one.

The segments are also sorted using the spatial pivot. The result of the test can lead to three possibilities: the segment is on the left side of the pivot, on the right side of the pivot or astride the pivot. In the first two cases, the segments are treated similar to the nodes, but in the third situation, the segment is duplicated and placed on both sides.

Among the different criteria that can be used to stop the division are the following situations:

- The box does not contain any nodes
- The box does not contain any segments
- The box contains sufficiently few elements that the calculation of distance of all the couples is more economical
- The dimension of the box is smaller than a threshold

Contact Processing

After the choice of a good sorting algorithm, a formulation for the handling of the contact has to be selected. One can distinguish three techniques ensuring the conditions of continuity during the contact:

- Kinematic formulation of type main/secondary.

  In a contact node to segment, the secondary node transmits its mass and force to the main segment and the segment transmits its speed to the node. This formulation is particularly adapted to an explicit integration scheme, provided that the nodes do not belong to a main segment. A node cannot be at the same time secondary and main. This approach then cannot be used in the case of auto-contact.
- The Lagrange multipliers ensure kinematic continuity at contact.

  There is no restriction as in the previous formulation but the system of equations cannot be solved in an explicit way. The Lagrange multiplier matrix has to be reversed at each cycle of computation. In the case of auto-contact, the number of points in contact can become significant and this formulation then becomes quite expensive.
- Penalty methods do not ensure kinematic contact continuity, but they add springs at the contact spots.

  The first advantage to this formulation is its natural integration in an explicit code. Each contact is treated like an element and integrates itself perfectly into the code architecture, even if the programming is vectorial and parallel. Contrary to the kinematic formulations, the penalty method ensures the conservation of momentum and kinetic energy during impact.

The formulation used in Radioss is a penalty type formulation. The choice of the penalty factor is a major aspect of this method. In order to respect kinematic continuity, the penalty spring must be as rigid as possible. If the impedance of the interface becomes higher than those of the structures in contact, some numerical rebounds (high frequency) can occur. To ensure the stability of the integration diagram, without having additional constraints, this rigidity must be low. With a too low penalty, the penetration of the nodes becomes too strong and the geometrical continuity is no longer ensured.

The compromise selected consists in using a stiffness of the same order of magnitude than the stiffness of the elements in contact. This stiffness is nonlinear and increases with the penetration, so that a node is not allowed to cross the surface.

These choices provide a clear representation of physics, without numerical generation of noise, but require the contact stiffness in the calculation of the criteria of stability of the explicit scheme to be taken into account.

Contact Detection

After identifying the candidates for the impact, it is necessary to determine whether contact takes place and its precise localization. If for a formulation of node to node contact the detection of the contact is quite easy, it becomes more complex in the case of a node to segment or edge to edge contact. In the case of edge-to-edge contacts, a direct solution is possible if the segments are planar. If not, it is better to triangulate one of the segments, which would then turn it into a node-to-segment contact problem.

The search algorithm for candidates is uncoupled from the rest of the processing of the interfaces. This is not the case with regard to the detection, localization and processing of the contact. These last three tasks significantly overlap with each other so we will limit ourselves to the processing of the contact by penalty for simplicity.

In the case of contact between two solid bodies modeled with 3D finite elements, contact can only take place on the segments of the external surface. This external surface has a certain orientation and the impact of a node can come only from the outside. Most of the node-to-surface contact algorithms use this orientation to simplify detection of contact. In the case of impact of a two-dimensional structure modeled with shell or plate finite elements, contact is possible on both sides of the surface.

For an oriented surface, it is necessary to consider contacts of the positive dimension side of the surface on itself, contacts of the negative dimension side on itself, and the contact of the "positive" side on the "negative" one. This last situation, which is quite rare, can occur in the case of a surface rolled up into itself or during the impact of a twisted surface.

Node to Segment Contact

The use of a "gap" surrounding the segment is one way of providing physical thickness to the surface and makes it possible to distinguish the impacts on the top or on the lower part of the segment.
The contact is activated if the node penetrates within the gap or if the distance from the node to the segment becomes smaller than the gap.

To calculate the distance from the node to the segment, we make a projection of this node on the segment and measure the distance between the node and the projected point.

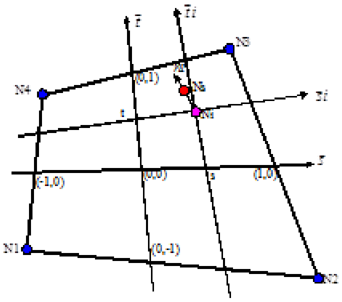

Figure 141:

The projected point is calculated using isoparametric coordinates for a quadrangular segment and barycentric coordinates for a triangular segment. In the case of any quadrangular segment, the exact calculation of these coordinates leads to a system of two quadratic equations that can be solved in an iterative way. The division of the quadrangular segment into four triangular segments makes it possible to work with a barycentric coordinate system and gives equations that can be solved in an analytical way.

From the isoparametric coordinates (s, t) of the projected point (Ni), we have all the necessary information for the detection and the processing of contact. The relations needed for the determination of s and t are: the vector $NiNs$ is normal to the segment at the point Ni; and the normal to the segment is given by the vectorial product of the vectors si and ti.

$$H1=(1-s)(1-t)/4$$
$$H2=(1+s)(1-t)/4$$
$$H3=(1+s)(1+t)/4$$
$$H4=(1-s)(1+t)/4$$
$$\overrightarrow{ONi}= H1\overrightarrow{ON1}+H2\overrightarrow{ON2}+H3\overrightarrow{ON3}+H4\overrightarrow{ON4}$$
$$\vec{s}i=(1-t)\overrightarrow{N1N2}+(1+t)\overrightarrow{N4N3}$$
$$\vec{t}i=(1-s)\overrightarrow{N1N4}+(1+s)\overrightarrow{N2N3}$$
$$\vec{n}i=(\vec{s}i\times\vec{t}i)/\overline{(\vec{s}i\times\vec{t}i)}$$
$$\overrightarrow{NiNs}=a\,\vec{n}i$$

After bounding the isoparametric coordinates between +1 or -1, the distance from the node to the segment and the penetration are calculated:

$$D=\overline{NiNs}$$
$$P=\max(0, Gap-D)$$

A penalty force is deducted from this. It is applied to the node Ns and distributed between the four nodes ($N1$, $N2$, $N3$, $N4$) of the segment according to the following shape functions.

Edge to Edge Contact

The formulation of edge-to-edge contact is similar to that of node-to-segment contact. The gap surrounding each edge defines a cylindrical volume. The contact is detected if the distance between the two edges is smaller than the sum of the gaps of the two edges. The distance is then calculated as:

$$2\overrightarrow{N1Ni}=(1-s)\overrightarrow{N1N3}+(1+s)\overrightarrow{N1N4}$$
$$D=\left|\overrightarrow{N1Ni}-\left(\overrightarrow{N1Ni}\,\overrightarrow{N1N2}/\overline{N1N2}^{2}\right)\overrightarrow{N1N2}\right|$$
$$\partial D/\partial s=0$$

The force of penalty is calculated as in node-to-segment contact. It is applied to the nodes $N1$, $N2$, $N3$, $N4$ and therefore ensures the equilibrium of forces and moments.

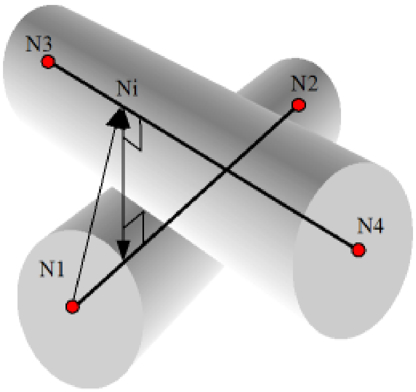

Figure 142:

Solid and Shell Element Contact (TYPE3)

The main use of this interface is with shell or solid plates that are initially in contact.

There are no main and secondary surfaces in this interface. Each surface is considered as if it were a secondary.

Limitations

The main limitations of TYPE3 interfaces are:

- The two surfaces should be simply convex.
- The surface normals must face each other.
- A node may not exist on the main and secondary side of an interface simultaneously.
- Surfaces must consist of either shell or brick elements.

It is recommended that the two surface meshes be regular with a good aspect ratio. The interface gap should be kept small, if not zero.

There are some search problems associated with this interface.

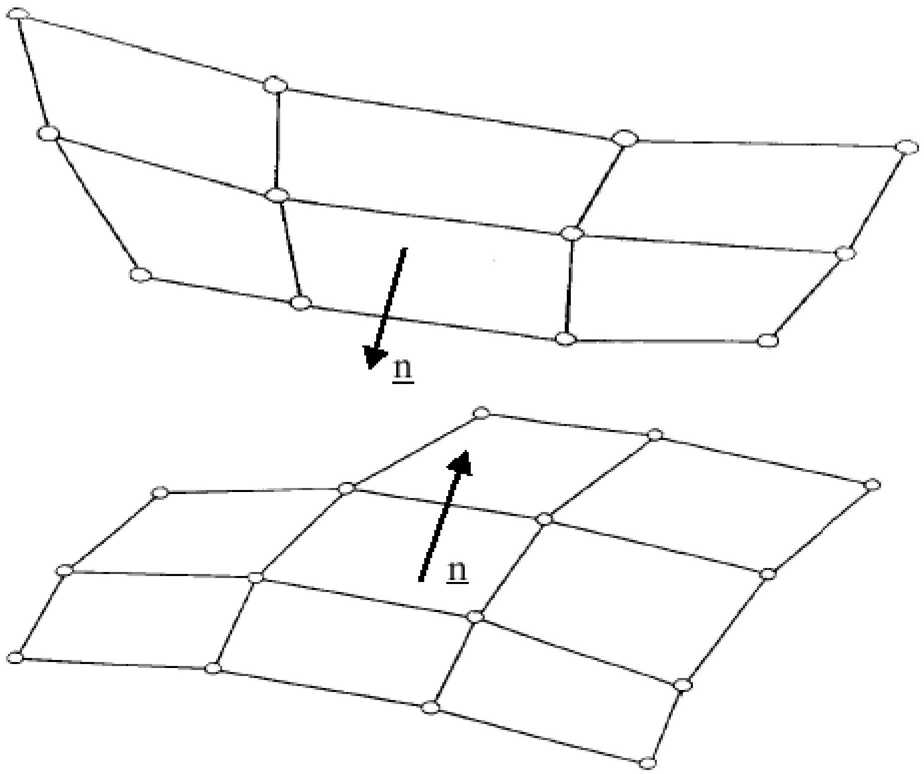

Figure 143: Surfaces 1 and 2 with Facing Normals

Computation Algorithm

The computation and search algorithms used for TYPE3 interface are the same as for TYPE5. However, TYPE3 interface does not have a main surface, so that the algorithms are applied twice, one for each surface.

The surfaces are treated symmetrically, with all nodes allowed to penetrate the opposing surface. The interface spring stiffness applies the opposing penetration reduction force.

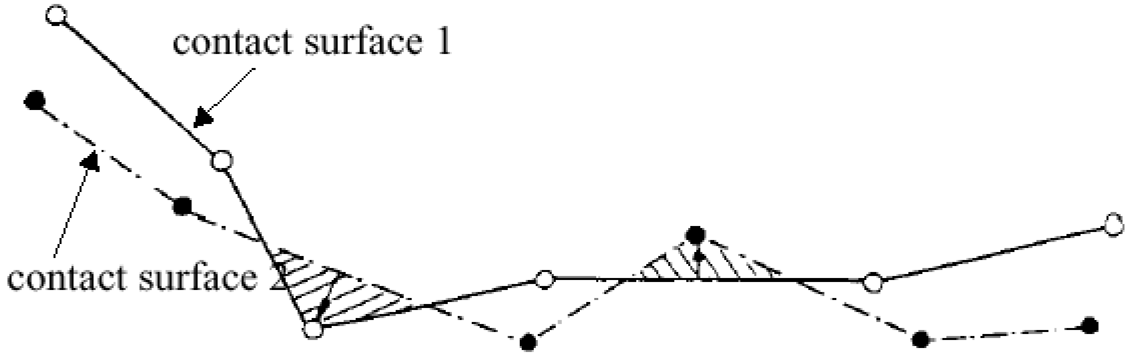

Figure 144: Contact Surfaces Treated Symmetrically

Because the computation algorithm is performed twice, accuracy is improved over a TYPE5 interface. However, the computational cost is increased.

The first pass solution solves the penetration of the nodes on surface 1 with respect to segments on surface 2. The second pass solves surface 2 nodes with respect to surface 1 segments.

Interface Stiffness

When two surfaces contact, a massless stiffness is introduced to reduce the penetration's nodes of the other surface into the surface.

The nature of the stiffness depends on the type of interface and the elements involved.

The introduction of this stiffness may have consequences on the time step, depending on the interface type used.

The TYPE3 interface spring stiffness K is determined by both surfaces. To retain solution stability, stiffness is limited by a scaling factor which is user defined on the input card. The default value (and recommended value) is 0.2.

The overall interface spring stiffness is determined by considering two springs acting in series.

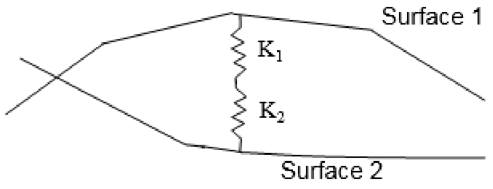

Figure 145: Interface Springs in Series

The equation for the overall interface spring stiffness is:

$$K = s\frac{K_1 K_2}{K_1 + K_2} \tag{771}$$

Where,

s
Stiffness scaling factor. Default is 0.2.

K_1
Surface 1 Stiffness

K_2
Surface 2 Stiffness

K
Overall interface spring stiffness

The scale factor, s, may have to be increased if:

$K_1 << K_2$ or $K_2 << K_1$

The calculation of the spring stiffness for each surface is determined by the type of elements.

For example:

$K_1 = \frac{1}{10} K_2$ implies $K = \frac{s}{11} K_2$ or $K = \frac{10s}{11} K_1$

Shell Element

If the main interface segment is a set of shell elements, the stiffness is calculated by:

$$K = 0.5sEt \tag{772}$$

Where,

E	Modulus of Elasticity
t	Shell Thickness

The stiffness does not depend on the shell size.

Brick Element

If the main interface segment is a set of brick elements, the stiffness is calculated by:

$$K = 0.5\frac{sBA^2}{V} \tag{773}$$

Where,

B	Bulk modulus
A	Segment area
V	Element volume

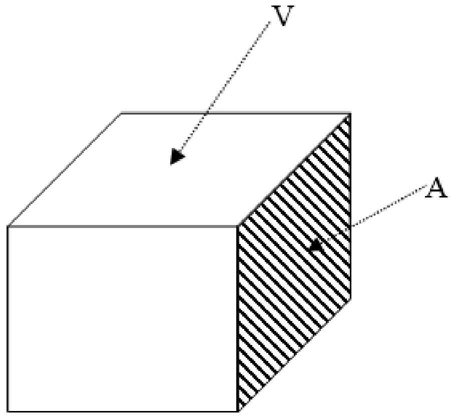

Figure 146: Brick Element

Combined Elements

If a segment is a shell element that is attached to the face of a brick element, the shell stiffness is used.

Interface Friction

TYPE3 interface allows sliding between contact surfaces. Coulomb friction between the surfaces is modeled. The input card requires a friction coefficient. No value (default) defines zero friction between the surfaces.

The friction on a surface is calculated by:

$$\Delta\vec{F}_t = \frac{K}{10}\overrightarrow{C_1C_0} \tag{774}$$

Where,

K
Interface spring stiffness

$\overrightarrow{C_1C_0}$
Contact node displacement vector

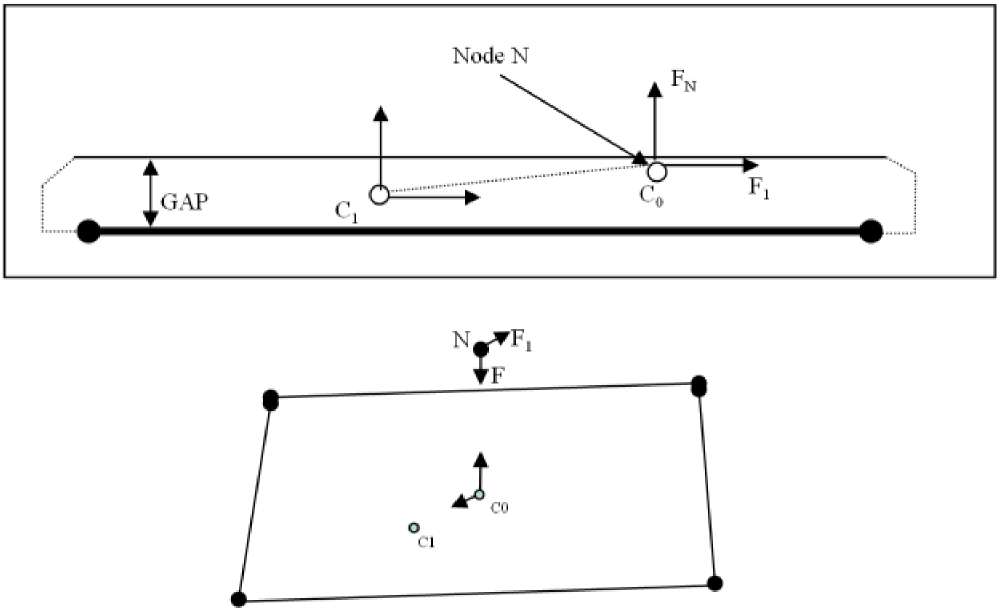

Figure 147: Coulomb Friction

C_0
Contact point at time t

C_1
Contact point at time $t+\Delta t$

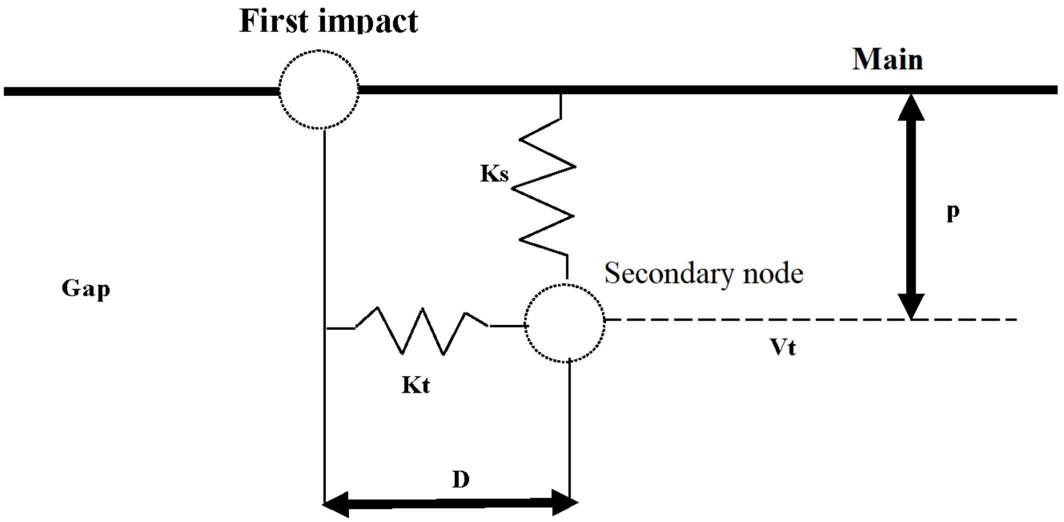

Figure 148: Friction on Interface TYPE3

The normal force computation is given by:

$$F_n = K_s P \tag{775}$$

Where,

$$K_s = K_0\left(\frac{Gap}{Gap - P}\right)$$

K_0
Initial interface spring stiffness (as in TYPE5)

The tangential force computation is given by:

$$F_t = K_t D \tag{776}$$

Where, $K_t = \frac{K_n}{10}$.

If the friction force is greater than the limiting situation, $|F_t| > \mu|F_n|$, the frictional force is reduced to equal the limit, $|F_t| = \mu|F_n|$, and sliding will occur. If the friction is less than the limiting condition, $F_t \le \mu F_n$, the force is unchanged and sticking will occur.

Time integration of the frictional forces is performed by:

$$\vec{F}_t^{new} = \vec{F}_t^{old} + \Delta\vec{F}_t \tag{777}$$

Where,

$\Delta\vec{F}_t$
Result from Equation 774

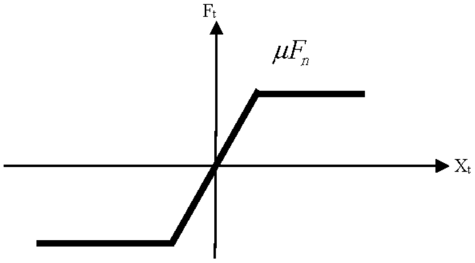

Figure 149: Friction on TYPE3 Interface

Interface Gap

TYPE3 interfaces have a gap that determines when contact between two segments occurs. This gap is user defined, but some interfaces will calculate an automatic default gap.

The gap determines the distance for which the segment interacts with the three nodes. If a node moves within the gap distance, such as nodes 1 and 2, reaction forces act on the nodes.

TYPE3 interface have a gap:

- Only normal to the segment, as shown in Figure 150
- On the contact side of the segments, which is defined by the surface normal. The size of the gap defined for certain interface types is critical. If the gap is too small, the solution time step may be dramatically reduced or a node may move across the entire gap in one time step. However, if the gap is too large, nodes not associated with the direct contact may become involved.

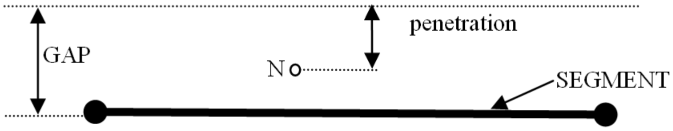

Figure 150: Interface Gap

Examples: Interface Failure

There are a number of situations in which TYPE3 elements may fail. A couple of these are shown below.

Care must be taken when defining contact surfaces with large deformation simulations. If the normal definitions of the contact surfaces are incorrect, node penetration will occur without any reaction from either surface.

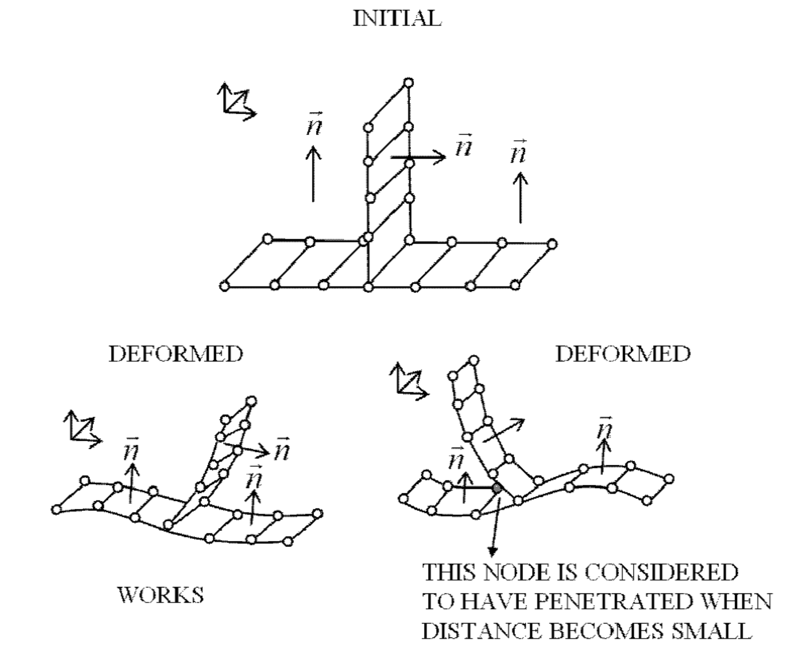

Figure 151: Improper Normal Direction

Referring to Figure 151, the first situation shows the mesh deforming in a way that allows the normals to be facing each other. However, in the second case, the deformation moves two surfaces with normals all facing the same direction, where contact will not be detected. Large rotations can have a similar effect, as shown in Figure 152.

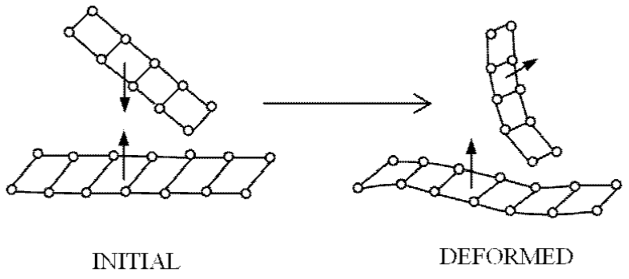

Figure 152: Initial and Deformed Mesh (Before Impact)

Kinematic motion may reposition the mesh so that normals do not correspond. It is recommended that possible impact situations be understood before a simulation is attempted.

General Purpose Contact (TYPE5)

This interface is used to simulate the impact between a main surface and a list of secondary nodes., as shown in Figure 153.

The penetration is reduced by the penalty method.

Another method is possible: Lagrange multipliers. But spatial distribution force is not smooth and induces hourglass deformation.

This interface is mainly used for:

- Simulation of impact between beam, truss and spring nodes on a surface.
- Simulation of impact between a complex fine mesh and a simple convex surface.
- A replacement for a rigid wall.

Limitations

The main limitations of TYPE5 interface are:

- The main segment normals must be oriented from the main surface towards the secondary nodes.
- The main side segments must be connected to solid or shell elements.
- The same node is not allowed to exist on both the main and secondary surfaces.
- In certain situations, the search algorithm does not identify the correct node to surface impacts.

It is recommended that the main surface mesh be regular, with a good aspect ratio and that a small or zero gap be used to detect penetration.

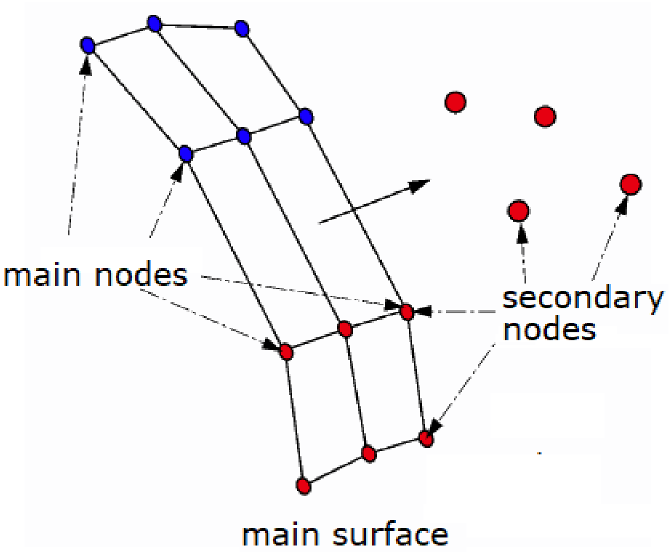

Figure 153: Surface 1 (Nodes) and Surface 2 (Segments)

Computation Algorithm

The computation and search algorithms used for TYPE5 are the same as for TYPE3. Refer to Computation Algorithm.

Interface Stiffness

When two surfaces contact, a massless stiffness is introduced to reduce the penetration's nodes of the other surface into the surface.

The nature of the stiffness depends on the type of interface and the elements involved.

The introduction of this stiffness may have consequences on the time step, depending on the interface type used.

For a TYPE5 interface, the spring stiffness K is determined by main and secondary sides. The stiffness scaling factor default value (and recommended value) is 0.2.

For a soft main surface material and stiff secondary surface, the stiffness scaling factor should be increased by the elastic modulus ratio of the two materials.

The calculation of the spring stiffness' is the same as in a TYPE3 interface.

If a segment is a shell as well as the face of brick element, the shell stiffness is used.

The overall interface spring stiffness is determined by considering two springs acting in series.

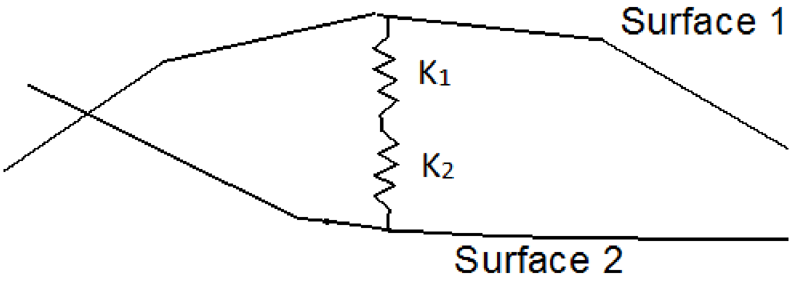

Figure 154: Interface Springs in Series

The equation for the overall interface spring stiffness is:

$$K = s\frac{K_1 K_2}{K_1 + K_2} \tag{778}$$

Where,

s
: Stiffness scaling factor. Default is 0.2.

K_1
: Surface 1 Stiffness

K_2
: Surface 2 Stiffness

K
: Overall interface spring stiffness

The scale factor, s, may have to be increased if:

$K_1 < < K_2$ or $K_2 < < K_1$

The calculation of the spring stiffness for each surface is determined by the type of elements.

For example:

$K_1 = \frac{1}{10} K_2$ implies $K = \frac{s}{11} K_2$ or $K = \frac{10s}{11} K_1$.

Shell Elements

For more information, refer to Shell Element.

Brick Elements

For more information, refer to Brick Element.

Combined Elements

For more information, refer to Combined Elements.

Interface Friction

TYPE5 interface allows sliding between contact surfaces.

Coulomb friction between the surfaces is modeled. The input card requires a friction coefficient. No value (default) defines zero friction between the surfaces.

The friction computation on a surface is the same as for TYPE3 interface. Refer to Interface Friction.

Darmstad and Renard models for friction are also available:

Darmstad Law:

$$\mu = C_1 \cdot e^{(C_2 V)} \cdot p^2 + C_3 \cdot e^{(C_4 V)} \cdot p + C_5 \cdot e^{(C_6 V)} \tag{779}$$

Renard Law:

$$\begin{aligned}
&\mu = C_1 + (C_3 - C_1) \cdot \frac{V}{C_5} \cdot \left(2 - \frac{V}{C_5}\right) && if \quad V \in [0, C_5] \\
&\mu = C_3 - \left((C_3 - C_4) \cdot \left(\frac{V - C_5}{C_6 - C_5}\right)^2 \cdot \left(3 - 2 \cdot \frac{V - C_5}{C_6 - C_5}\right)\right) && if \quad V \in [C_5, C_6] \\
&\mu = C_2 - \frac{1}{\frac{1}{C_2 - C_4} + (V - C_6)} && if \quad V \geq C_6
\end{aligned} \tag{780}$$

Where,

$C_1 = \mu_s, C_2 = \mu_d$

$C_3 = \mu_{\max}, C_4 = \mu_{m:\min}$

$C_5 = V_{cr1}, C_6 = V_{cr2}$

Possibility of smoothing the tangent forces via a filter:

$$4F_T = \alpha \cdot F_T^t + (1 - \alpha) \cdot F_T^{t-1} \tag{781}$$

Where, the coefficient a depends on the I_{filtr} flag value.

Interface Gap

Refer to Interface Gap for TYPE3 interface.

Interface Algorithm

The algorithm used to calculate interface interaction for each secondary node is:

1. Determine the closest main node.
2. Determine the closest main segment.
3. Check if the secondary node has penetrated the main segment.
4. Calculate the contact point.
5. Compute the penetration.
6. Apply forces to reduce penetration.

For more information, refer to Auto Contacts.

Detection of Closest Main Node

The Radioss Starter and Engine use different methods to determine the closest main node to a particular secondary node.

The Starter searches for the main node with the minimum distance to the particular secondary node. The Engine carries out the following algorithm, referring to Figure 155.

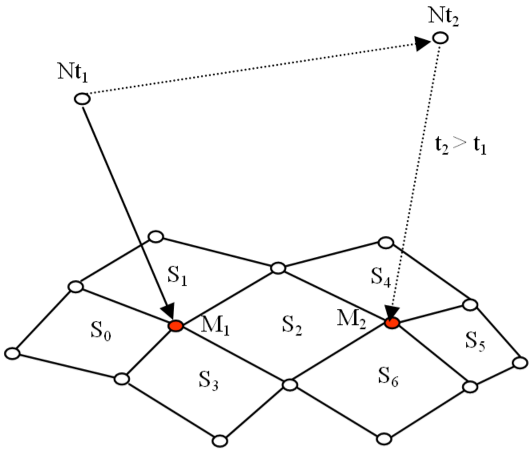

Figure 155: Search Method

1. Get the previous closest segment, S_0, to node N at time t_1.
2. Determine the closest node, M_1, to node N which belongs to segment S_0.
3. Determine the segments connected to node M_1 (S_0, S_1, S_2 and S_3).
4. Determine the new closest main node, M_2, to node N at time t_1. The new main node must belong to one of the segments S_0, S_1, S_2 or S_3.
5. Determine the new closest main segment (S_2, S_4, S_5 and S_6).

The Starter CPU cost is calculated with the following equation:

- CPUstarter = a x Number of Secondary Nodes x Number of Main Nodes

The Engine CPU cost is calculated with the following equation:

- CPUengine = b x Number of Secondary Nodes

The algorithm used in the Engine is less expensive but it does not work in some special cases. In Figure 156, if node N is moving from $N(t_0)$ to $N(t_1)$ and then to $N(t_2)$, the closest main nodes are M_0 and M_1. When the final node movement to $N(t_2)$ is taken, the impact on segment S will not be detected since none of the nodes on this segment are considered as the closest main node.

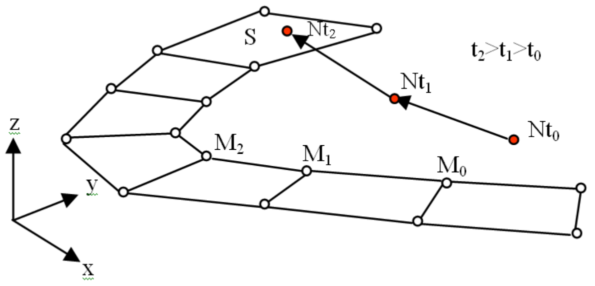

Figure 156: Undetected Impact

Detection of Closest Main Segment

The closest main segment to a secondary node N, shown in Figure 157, is found by determining a reference quantity, A.

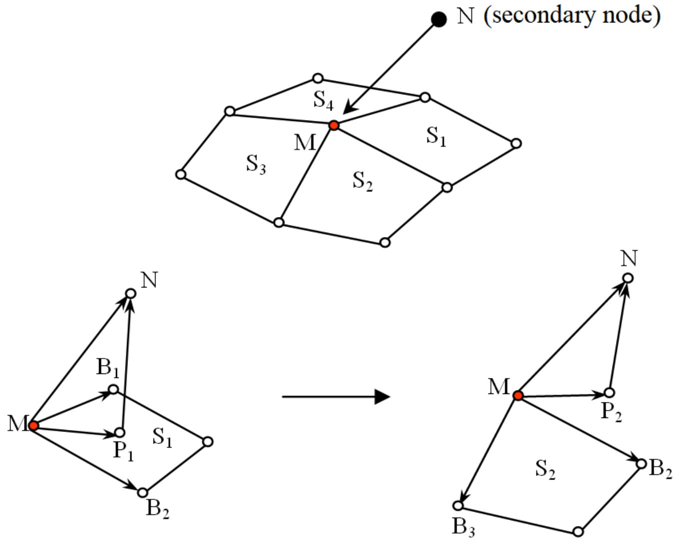

Figure 157: Closest Main Segment Determination Method

The A value for segment S_1 is given by:

$$A = \left(M\vec{B}_2 \times M\vec{P}_1\right)\left(M\vec{B}_1 \times M\vec{P}_1\right) < 0 \tag{782}$$

Where,

P_1
: Projection of N on plane (M, B_1, B_2)

B_1 **and** B_2
: Tangential Surface Vectors along segment S_1 edges.

The A value for segment S_2 is given by:

$$A = \left(M\vec{B}_3 \times M\vec{P}_2\right)\left(M\vec{B}_2 \times M\vec{P}_2\right) > 0 \tag{783}$$

Where,

P_2
: Projection of N on plane (M, B_2, B_3)

The same procedure is carried out for all main segments that node M is connected to.

The closest segment is the segment for which A is a minimum.

In some special cases (curved surfaces), it is possible that:

- All values of A are positive.
- More than one value of A is negative.

Detection of Penetration

Penetration is detected by calculating the volume of the tetrahedron made by secondary node N and the main nodes of the corresponding main segment, as shown in Figure 158.

For a given normal n, the sign of the volume shows if penetration has occurred.

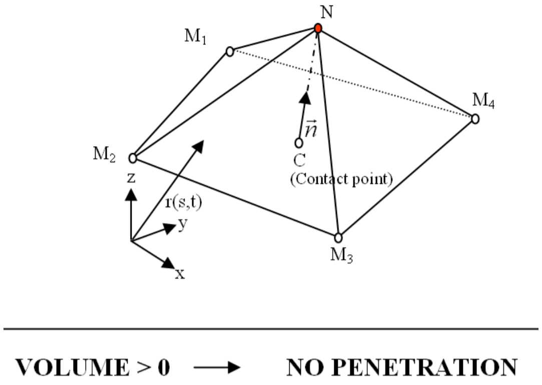

Figure 158: Tetrahedron used for Penetration Detection

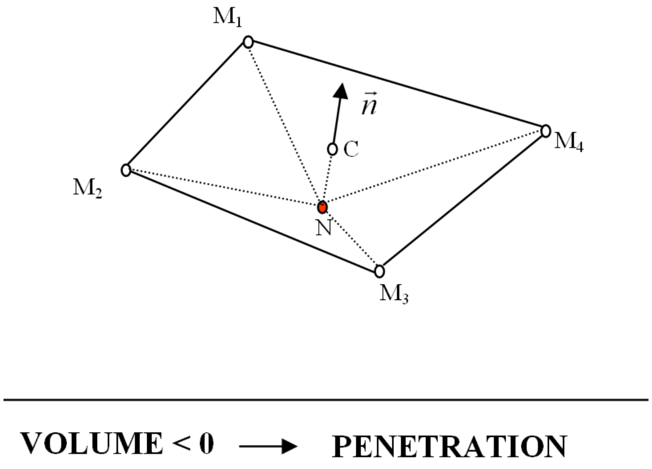

Figure 159: Negative Volume Tetrahedron - Penetrated Node

Reduction of Penetration

The penetration, p, is reduced by the introduction of a massless spring between the node, N, and the contact point, C.

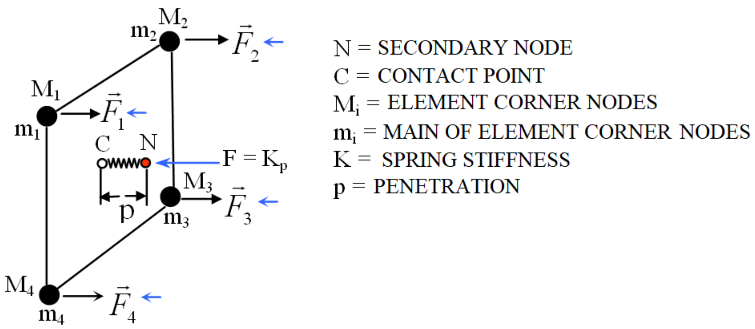

Figure 160: Forces Associated with Penetration

The force applied on node N in direction $\overrightarrow{NC}$ is:

$$F = Kp \tag{784}$$

Where, K is the interface spring stiffness.

Reaction forces F_1, F_2, F_3 and F_4 are applied on each main node (shown in Figure 160) in the opposite direction to the penetration force, such that:

$$F_1 + F_2 + F_3 + F_4 = -F \tag{785}$$

Forces F_i (i = 1, 2, 3, 4) are functions of the position of the contact point, C. They are evaluated by:

$$F_i = \frac{d_i}{\sum_{j=1}^{4} d_j} F \tag{786}$$

Where, $d_i = \frac{Ni(S_c, t_c)}{\sum_{j=1}^{4} N_j^2(S_c, t_c)} m_i$

or more simply:

$$F_i = N_i(S_c, t_c) F \tag{787}$$

Where,

N_i
Standard linear quadralateral interpolation functions

S_c **and** t_c
Isoparametric coordinates contact point

The penalty method is used to reduce the penetration. This provides:

- Accuracy
- Generality
- Efficiency
- Compatibility

Rigid Body Contact (TYPE6)

This interface is used to simulate impacts between two rigid bodies.

It works like TYPE3 interface except that the total interface force is a user defined function of the maximum penetration. The input and computational algorithms are the same as for TYPE3 interfaces. This interface is used extensively in vehicle occupant simulations; example, knee bolsters.

Limitations

Some of the main limitations for this interface type are:

- Surface 1 must be part of one and only one rigid body.
- Surface 2 must be part of one and only one rigid body.
- The interface stiffness (user defined function) can reduce the time step.

Other limitations are the same as for TYPE3 interfaces.

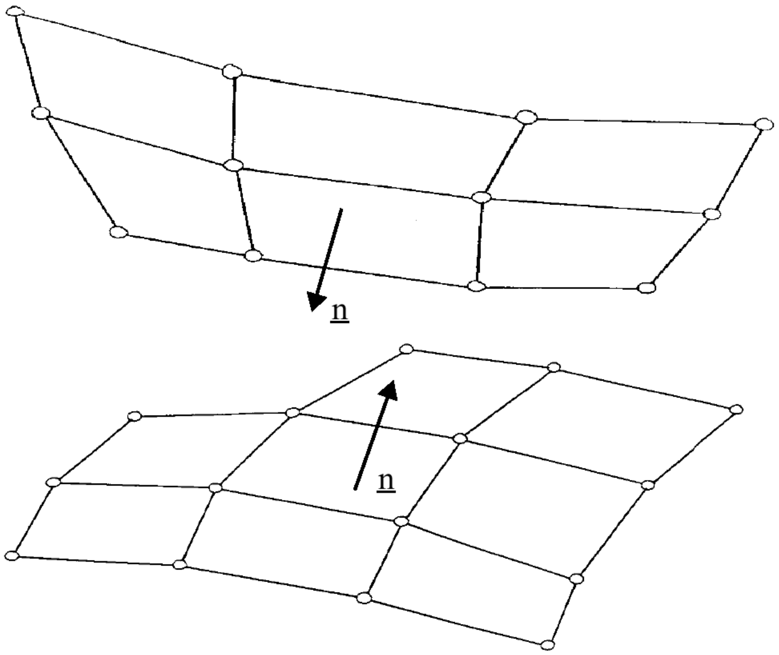

Figure 161: Surfaces 1 and 2 with Facing Normals

Interface Stiffness

When two surfaces contact, a massless stiffness is introduced to reduce the penetration's nodes of the other surface into the surface.

The nature of the stiffness depends on the type of interface and the elements involved.

If a segment is a shell as well as the face of brick element, the shell stiffness is used.

Interface Friction

TYPE6 interface allows sliding between contact surfaces. Coulomb friction between the surfaces is modeled. The input card requires a friction coefficient. No value (default) defines zero friction between the surfaces. The friction computation on a surface is the same as for TYPE3 interface (refer to Contact Processing).

Interface Gap

Refer to Contact Detection for TYPE3 interface.

Time Step Calculation

The stable time step used for time integration equations is computed by:

$$\Delta t = 0.1\sqrt{\frac{M}{K}} \tag{788}$$

Where,

M min(M rigid body 1, M rigid body 2)

K Tangent of user force function

Time step Δt is affected by the actual stiffness derived from function f:

$$\Delta t \leq \sqrt{\frac{M}{f'(p)}} \tag{789}$$

The function f refers to a function number given in input and must be user-defined.

Contact Force

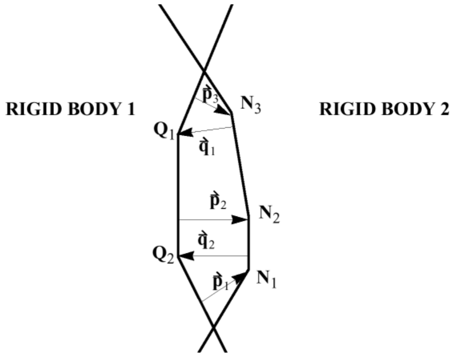

Figure 162: Especially Suited for Rigid Bodies

$$F_{N_i} = \frac{-\vec{p}_i + \vec{q}_{Ni}}{\| \sum \vec{p}_j - \sum \vec{q}_k \|} f\left(MAX\left(\| \vec{p}_k \|, \| \vec{q}_j \|\right)\right) \tag{790}$$

$\vec{q}_{N_i}$ is the contribution to node N_i of vector $\vec{q}_i$ distributed on the segment penetrated by node Q_i.

General Purpose Contact (TYPE7)

This interface simulates the most general type of contacts and impacts. TYPE7 interface has the following properties:

1. Impacts occur between a main surface and a set of secondary nodes, similar to TYPE5 interface.
2. A node can impact on one or more mainr segments.
3. A node can impact on either side of a main surface.
4. Each secondary node can impact each main segment except if it is connected to this segment.
5. A node can belong to a main surface and a set of secondary nodes, as shown in Figure 163.
6. A node can impact on the edge and corners of a main segment. None of the previous interfaces allow this.
7. Edge to edge contacts between main and secondary segments are not solved by this interface.

Limitations

All limitations encountered with interface TYPE3, TYPE4 and TYPE5 are solved with this interface.

It is a fast search algorithm without limitations.

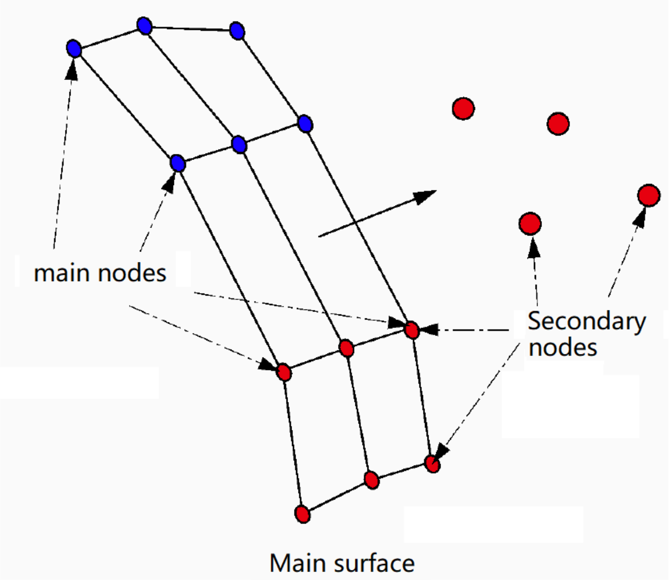

Figure 163: Secondary and Main Node Impact

There are no search limitations with this interface concerning node to surface contacts. All possible contacts are found.

There is no limitation on the use of large and small segments on the same interface. This is recommended to have a good aspect ratio elements or a regular mesh to obtain reasonable results; however, it is not an obligation.

There is no limitation to the size of the spring stiffness factor. The spring stiffness is much greater than interfaces TYPE3 and TYPE5, with the default stiffness factor set to 1.0. This is to avoid node penetrations larger than the gap size, removing problems that were associated with the other interfaces.

Interface Stiffness

When two surfaces contact, a massless stiffness is introduced to reduce the penetration of one surface node to the other surface.

The nature of the stiffness depends on the type of interface and the elements involved.

The introduction of this stiffness may have consequences on the time step, depending on the interface type used.

The interface spring stiffness calculation is not as simple as for TYPE3, TYPE4 and TYPE5. The initial stiffness is calculated using the methods for TYPE3 interfaces. However, after initial penetration, the stiffness is given as a function of the penetration distance and the rate of penetration.

A critical viscous damping coefficient given on the input card (*visc*) allows damping to be applied to the interface stiffness.

$$F = f(p) + visc\sqrt{2KM}\frac{dp}{dt} \tag{791}$$

The stiffness is much larger than the other interfaces to accommodate high speed impacts with minimal crossing of surfaces. The consequence of this is that a stable time step is calculated to maintain solution stability.

Interface Friction

TYPE7 interface allows sliding between contact surfaces.

Coulomb friction between the surfaces is modelled. The input card requires a friction coefficient. No value (default) defines zero friction between the surfaces.

In TYPE7 interface a critical viscous damping coefficient is defined, allowing viscous damped sliding.

The friction on a surface may be calculated by two methods. The first method suitable for contact tangential velocity greater that 1m/s consist in computing a viscous tangential growth by:

$$\Delta\vec{F}_t = C_t\vec{V}_t \tag{792}$$

In the second method an artificial stiffness K_S is input. The change of tangent force F is obtained using:

$$\Delta F_t = K_S\,\delta_t \tag{793}$$

Where,

δ_t Tangent displacement

The normal force computation is given by:

$$F_n = K_s P + C\frac{dP}{dt} \tag{794}$$

Where,

$$K_s = K_0\left(\frac{Gap}{Gap - P}\right)$$

$$C = VIS_s\sqrt{2K_sM}$$

K_0 Initial interface spring stiffness (as in TYPE5)

VIS_s Critical damping coefficient on interface stiffness (input)

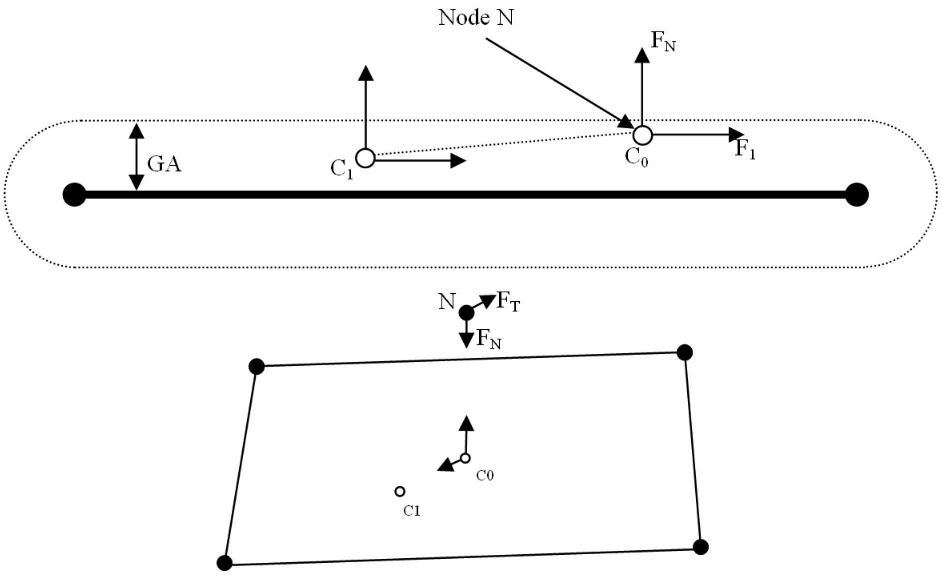

Figure 164: Coulomb Friction

C_0 Contact Point at time t

C_1 Contact Point at time $t = t + \Delta t$

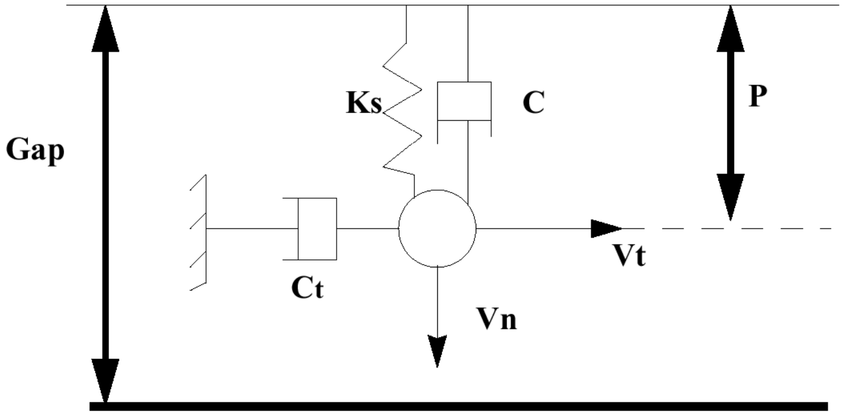

Figure 165: Friction on TYPE7 Interface - Scheme

The tangential force computation is given by:

$$F_t = \min(\mu * F_n, F_{ad}) \quad (795)$$

Where,

$F_{ad} = C_t V_t$ Adhesion force

$C = VIS_F \sqrt{2K_s M}$

V_t Tangential velocity calculated from the movement of the node from c_0 to c_1 in Figure 164.

Note: The friction coefficient μ may be obtained by Coulomb, Darmstad and Renard models as described in Interface Friction.

Time integration of the frictional forces is performed by:

$$\vec{F}_t^{new} = \vec{F}_t^{old} + \Delta\vec{F}_t \tag{796}$$

Where, $\Delta\vec{F}_t$ is obtained from Equation 792 or Equation 793.

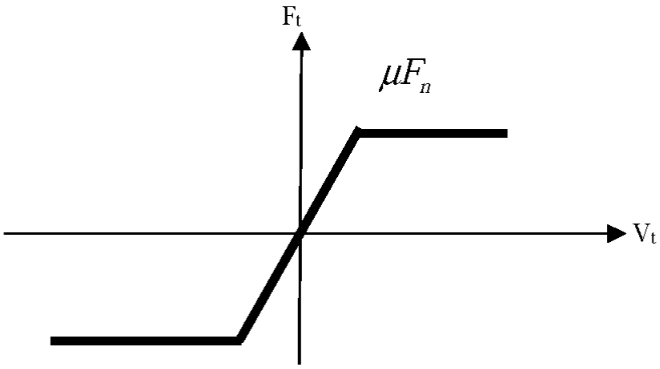

Figure 166: Friction on TYPE7 Interface

Interface Gap

TYPE7 interfaces have a gap that determines when contact between two segments occurs.

This gap is user-defined, but some interfaces will calculate an automatic default gap. Shown in Interface Stiffness, is a segment TYPE7 interface with three nodes in close proximity. The gap, as shown, determines the distance for which the segment interacts with the three nodes. If a node moves within the gap distance, such as nodes 1 and 2, reaction forces act on the nodes.

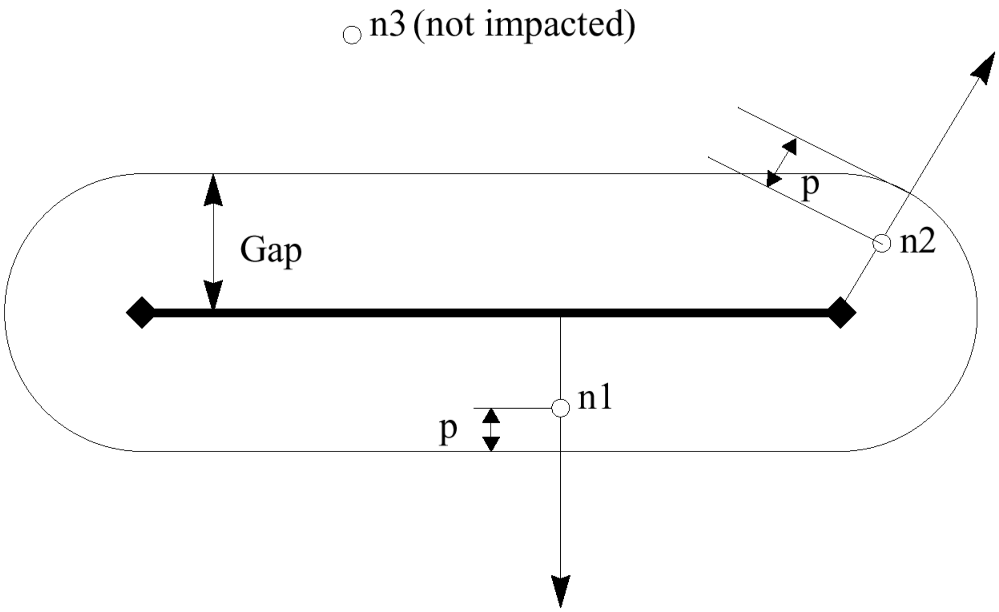

Figure 167: TYPE7 Interface Gap

TYPE7 interface has a gap that covers both edges of the segments, as shown in Figure 167.

Time Step

A time step is calculated to maintain stability when a TYPE7 interface is used.

The kinematic or interface time step is calculated if $\frac{dP}{dt} > 0$ by:

$$\Delta t_{\min} = 0.5\left[\frac{Gap - p}{\frac{dP}{dt}}\right] \tag{797}$$

The stable time step or nodal time step is given by:

$$\Delta t_{nod} = \sqrt{\frac{2M}{K}} \tag{798}$$

Where,

M	Nodal mass
$K = \sum(K_{\text{inter}} + K_{el})$	Nodal stiffness

The time step used for the interface is the smaller of the two. If the interface spring stiffness is too great, the time step can be reduced dramatically. If the two materials involved in the contact are the same, the default interface stiffness factor can be retained. This is the case when modeling sheet metal. However, the stiffness factor may need adjustment if the two materials stiffness' vary too much; for example, steel and foam.

Methods to Increase Time Step

The time step can be altered by two different methods, by altering the size of the gap and by increasing the initial stiffness. Figure 168 shows three force-penetration curves for a TYPE7 interface. Both methods change the nature of the stiffness which affects the time step.

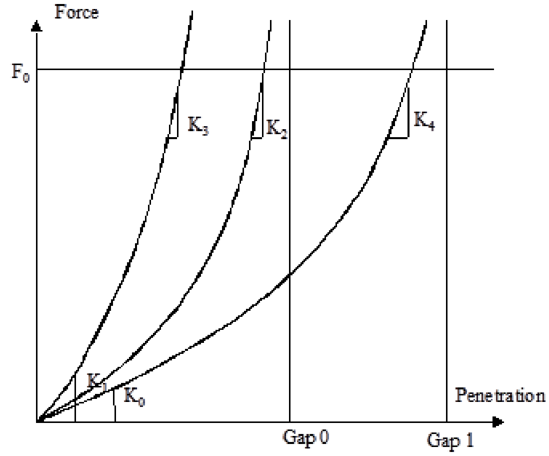

Figure 168: Force - Penetration Curves

Using a larger gap size, curves 1 and 2 keep the same initial stiffness; hence the initial time step remains the same. Since the impact slowing force is applied over a greater distance, the stiffness is not changed as much, but increases.

Increasing the initial interface stiffness, although decreasing the time step initially; will increase the time step if penetration is large.

Detection and Gap Size

A secondary node can be detected near a main segment from all directions, as shown in Figure 169.

The size of the gap can be user defined, but Radioss automatically calculates a default gap size, based on the size of the interface elements. For shell elements, the computed gap is the average thickness. For brick elements it is equal to one tenth of the minimum side length.

Variable Gap

By default the gap is constant on all main segments.

If the variable gap option is activated, a different gap is used for each contact taking into account the physical thickness on the main and secondary sides.

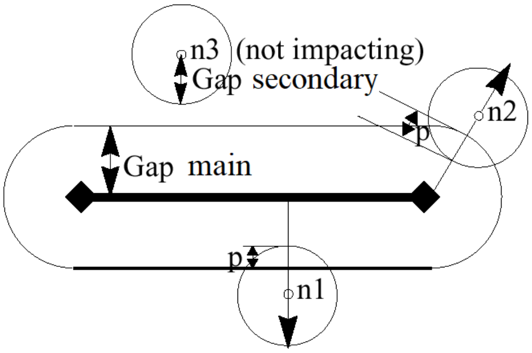

Figure 169: Variable Gap

For shell elements, the main gap is equal to one half of the shell thickness. The secondary gap is equal to one half of the largest thickness of all connected shell elements.

For solid elements, the main gap is zero. If the secondary node is only connected to solid elements, the secondary gap is zero.

For beam or truss elements connected to the secondary node, the secondary gap is one half of the square root of the section area.

If a secondary node is connected to different elements (shell, brick, beam, and truss) the largest gap value is used.

The total gap is the sum of the secondary and main gaps. The total gap cannot be smaller than a minimum gap (user input gap).

Gap Correction

TYPE7 interface is very sensitive to initial penetrations. One method for solving the resulting problems is to use an automatic gap correction (*Inacti* = 5).

With automatic gap correction the effective gap is corrected to take into account the initial penetration. The correction is only applied to the initially penetrated nodes. If the node penetration decreases, the correction is reduced. The computed penetration is illustrated in Figure 170.

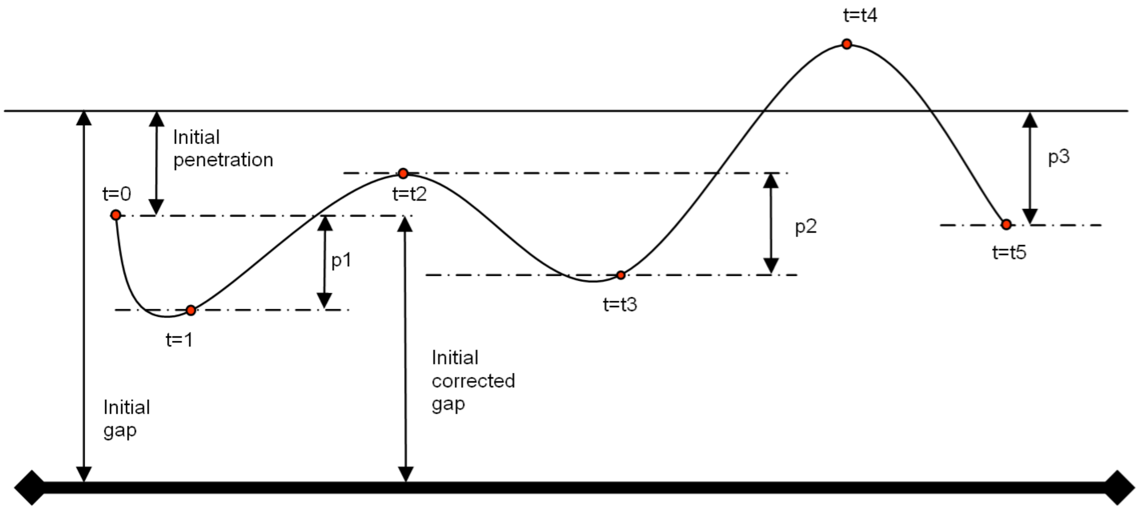

Figure 170: Corrected Gap

Penetration Reaction

Like the other interface types, TYPE7 has a spring stiffness as a secondary node penetrates the interface gap (previous section). However, there are some fundamental differences in the determination of the reaction force. Figure 171 shows a graph of force versus penetration of a node on a main segment. This figure also shows a pictorial diagram of node penetration and the associated forces.

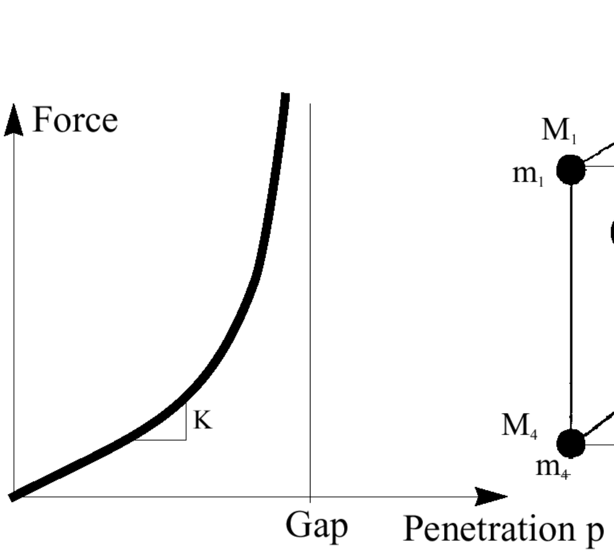

Figure 171: Penetration Reaction Force

The reaction force is not a linear relation like the previous interfaces. There is a viscous damping which acts on the rate of penetration.

The force computation is given by:

$$F = K_s P + C\frac{dP}{dt} \tag{799}$$

Where,

$$K_s = K_0\left(\frac{Gap}{Gap - P}\right)$$

$$C = VIS_s\sqrt{2K_s M}$$

K_0
Initial interface spring stiffness (as in TYPE5)

VIS_s
Critical damping coefficient on interface stiffness (input)

The instantaneous stiffness is given by:

$$K_t = K_0\left(\frac{Gap^2}{(Gap - P)^2}\right) \tag{800}$$

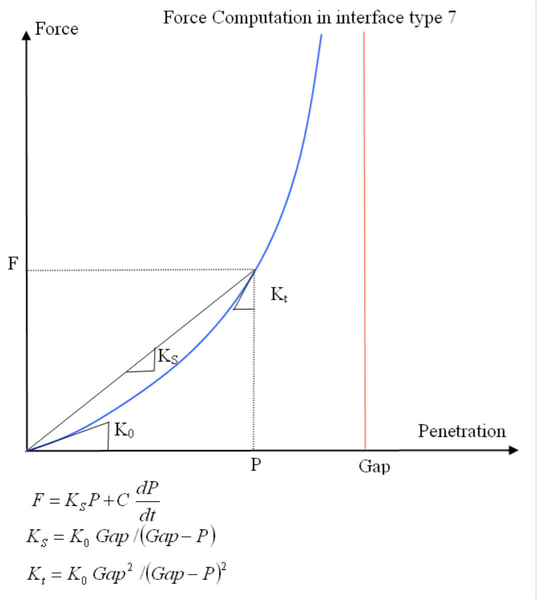

Figure 172: Force - Penetration Graph

A critical viscous damping is required to be defined on the TYPE7 input card for both damping on the spring stiffness and for interface friction damping.

Force Orientation

Due to the gap on a TYPE7 interface extending around the edges of a segment, the reaction forces over a surface will be smooth.

Penetration Reaction, Figure 172 shows the reaction forces on a node at various positions around two adjoining segments.

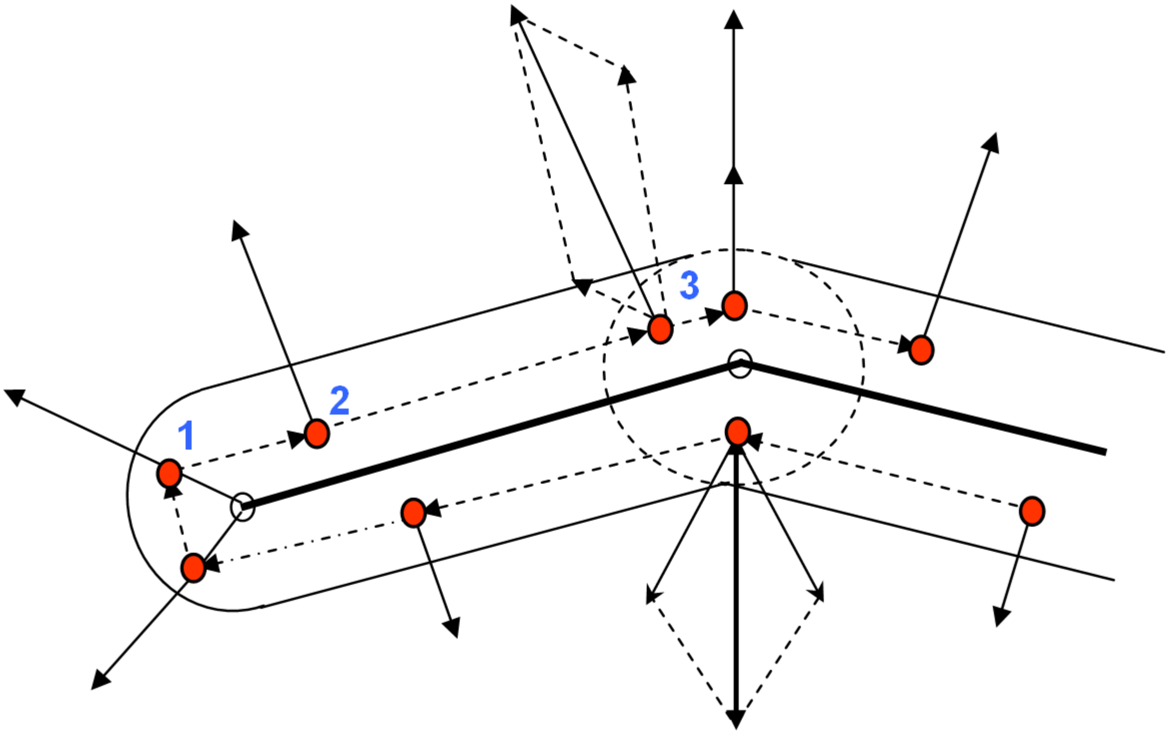

Figure 173: Force Orientation

Position 1 in Figure 173 shows the force acting radially from the edge of the segment. The size of the force depends on the amount of penetration. At position 2 the force is normal to the segment surface. In position 3 two segments intersect and their gaps overlap. The result is that each segment applies a force to the node, normal to the respective segment, this may double the force for the distance of gap overlap.

Interface Hints

Main Problem

One main problem remains namely, deep penetrations are not easily tolerated. They lead to high penalty forces and stiffness', and consequently to a drop-in time step. When such a problem occurs, you may see:

- A very small time step
- A large contact force vector in animation

Deep penetrations (that is, close to gap value) can sometimes occur in most car crash simulations. They occur in the following cases:

- Initial penetrations of adjacent plates
- Edge impacts: wrong side contacts
- Full collapse of one structural region
- Rigid body impact on another rigid body or on fixed nodes or on very stiff structures
- Impact between heavy stiff structures
- High impact speed
- Small gap

The elastic contact force is calculated with the formulation:

$$F = k \cdot \frac{gp}{(g-p)} \tag{801}$$

With $k = 0.5 Stfac * E * t$

The elastic contact energy is calculated with the formulation:

$$CE = kg\left(-p - g \times \ln\left(\frac{(g-p)}{g}\right)\right) \tag{802}$$

Where,

k
: Interface stiffness

g
: Contact gap

p
: Penetration

When node to element mid-plane distance is smaller then 10^{-10} gap, the node is deactivated.

The maximum potential contact energy is:

elastic contact energy CE = 23 kg

Drastic time step dropping is mostly due to cases where node is forced into the gap region.

Remedies to the Main Problem

There are several ways to resolve this problem:

1. Increase Gap

   Increasing the gap is the best remedy, but check that no initial penetrations result from this.
2. Increase Stiffness

   Increase *Stfac* dimensionless stiffness factor or provide an appropriate effective global stiffness value (v23 and up).
3. `/DT/INTER/DEL` (Engine option)

   Some nodes will be allowed to cross the impacted surface freely before penetration reaches $(1\text{-}10^{10}\ )$ gap.
4. `/DT/INTER/CST` (Engine option)

Nodal mass will be modified to maintain time step constant. This option should be avoided when rigid body secondary nodes are secondary of a TYPE7 interface.

The initial penetrations are mostly due to discretization and modelization problems.

They result in high initial forces that should be avoided.

5. Modify geometry

   New coordinates are proposed in the output file for all initially penetrated nodes. These are the coordinates used in the automatic coordinate change option. However, this might not suffice. Several iterations are sometimes necessary. Radioss will create a file `RootD0A` containing the modified geometry.

6. Reduce gap

   When there are only small penetrations with a gap, this should be reduced; otherwise care should be taken as this will reduce potential contact energy.

7. Deactivate node stiffness

   This solution is the simplest. It will generally not unduly affect your results. For sake of precision, use this option only for initial penetrations remaining after geometrical adjustments.

Edge Contact Problem

A special algorithm is developed for this purpose.

Modelization should eventually be adapted to prevent situations where 2 nodes of an element move to opposite sides of a surface.

For solid to solid contacts, the external closed surfaces may be used.

Ellipsoidal Surface to Node Contact (TYPE14)

This interface simulates impacts between a hyper-ellipsoidal rigid main surface and a list of secondary nodes. This interface is used for MADYMO to Radioss coupling.

The hyper-ellipsoidal surface is treated as an analytical surface (hyper-ellipsoidal surfaces are discretized only for post-processing).

The interface allows user-defined behavior:

- User defines total elastic force versus maximum penetration of nodes.
- A local friction coefficient is computed at each impacted node, depending upon elastic force computed at its location by scaling the total elastic force by the following factor: penetration of the node divided by sum of node penetrations.
- A local viscosity coefficient in the normal direction to the surface is computed at each impacted node, depending upon this node's velocity or the computed elastic force at its location.

It is also possible to only define a constant stiffness factor, a constant friction coefficient or a constant viscosity coefficient. A time step is computed to ensure stability.

Interface Hints

As the interface is defined as nodes impacting upon a surface, impact cannot be detected if the mesh is too coarse. In general, use a mesh which size is finer than the lowest semi-axis of the main surface.

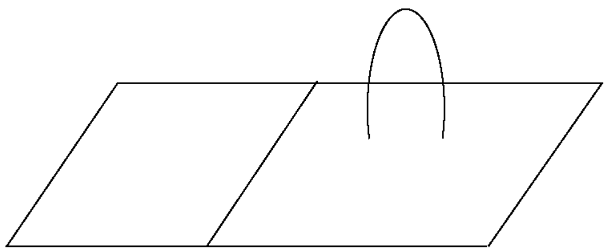

Figure 174: No Impact is Detected

The interface is designed to allow penetration of secondary nodes. However, the contact algorithm does not ensure that a node will not cross the ellipsoid when sliding; nodes may slide along the ellipsoid until they fully cross the ellipsoid, resulting in that the structure itself fully crossing the surface and contact force is no longer applied to it (as shown in Figure 175, where perfect sliding is considered).

Increase interface stiffness or friction to avoid this problem.

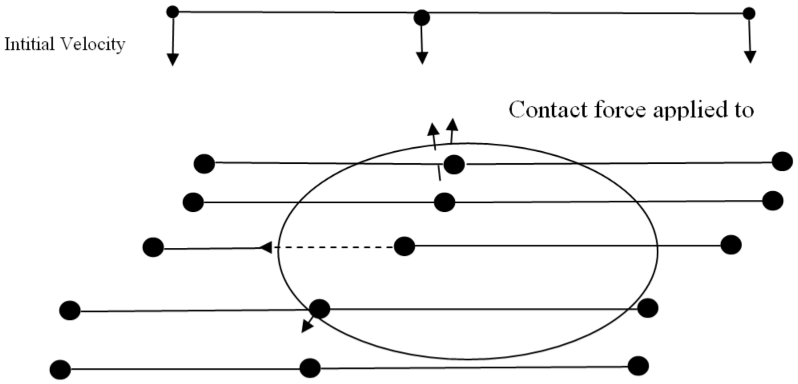

Figure 175: Sliding Until Structure Fully Crosses Surface

Ellipsoidal Surface to Segment Contact (TYPE15)

TYPE15 interface between surfaces made up of 4-node or 3-node segments and hyper-ellipsoids is a penalty contact interface without damping.

It applies to TYPE14 interface, especially when the mesh is coarser than the ellipsoid size. Remember that in such a case, TYPE14 interface is able to compute low quality contact forces even if it fails to find contact.

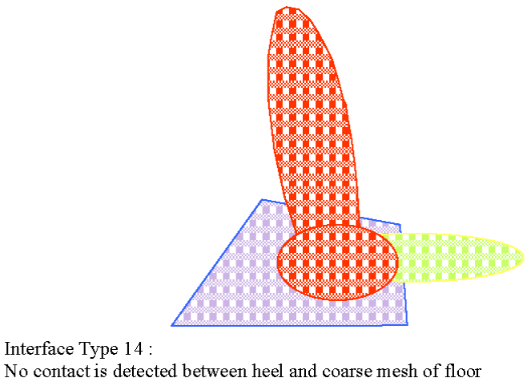
Interface Type 14 :
No contact is detected between heel and coarse mesh of floor

Figure 176: No Contact is Detected

Interface stiffness is a nonlinear increasing function of penetration, computed in order to avoid penetrations up to half the ellipsoid:

$$K = K_0 \left[\frac{Depth}{Depth - Penetration} \right]^2$$

Where,

K_0 Input stiffness factor

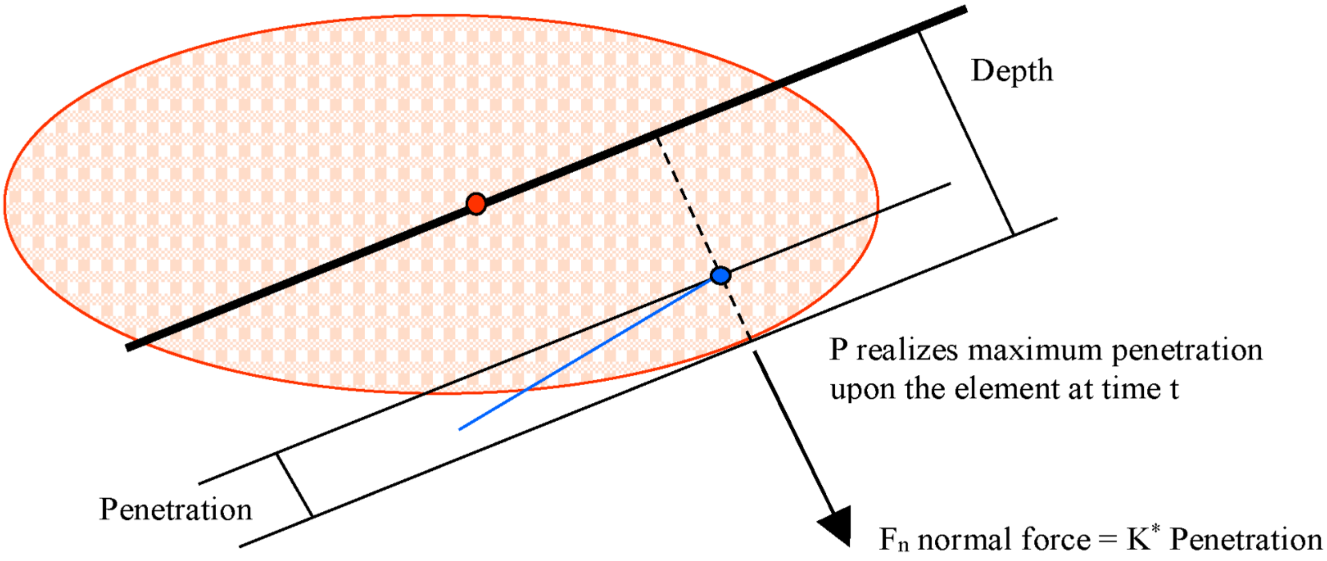
Depth
P realizes maximum penetration upon the element at time t
Penetration
Fn normal force = K* Penetration

Figure 177: Penetration is Detected

A Kinematic Time Step is computed so that the element does not cross the line Lt within one time step.

A friction coefficient m is input.

Interface takes into account sliding/rolling effects.

Coulomb Friction condition is expressed as:

$F_t \leq mF_n$ for each penetrated element

Node to Curved Surface Contact (TYPE16)

Interface TYPE16 will enable to define contact conditions between a group of nodes (secondary) and a curve surface of quadratic elements (main part) as shown in Figure 178 for a symmetric contact. The main part may be made of 16-node thick shells or 20 node-bricks. The Lagrange Multiplier Method (LMM) is used to apply the contact conditions. By the way that the LMM is used, no gap is necessary to be applied. Some applications of this interface are sliding contacts without gaps as in gear box modeling.

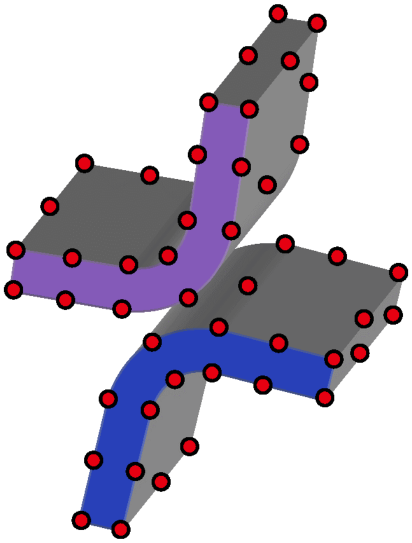

Figure 178: Node to Curved Surface Contact in Interface TYPE16

General Surface to Surface Contact (TYPE17)

The interface is used in the modeling of surface-to-surface contact. It is a generalized form of TYPE16 interface in which the contact on the two quadratic surfaces are directly resolved without needs of gap as the Lagrange Multiplier Method is used (Figure 179). The contact is supposed to be sliding or tied.

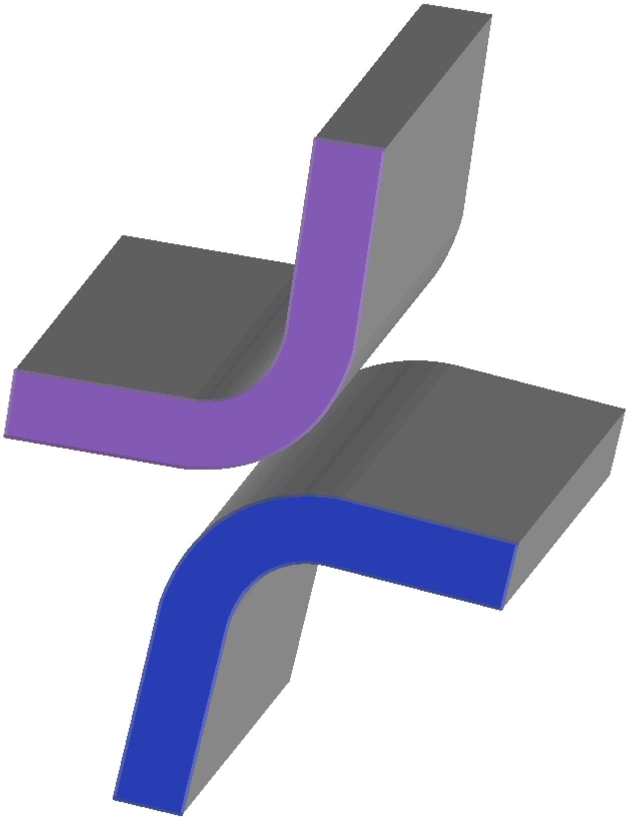

Figure 179: Quadratic Surface to Quadratic Surface Contact

Common Problems

The following sections contain examples of some common problems in the contact interfaces and solutions to overcome them.

Nearest Main Node Found Incorrect

If the interface surface is not simply convex, the simplified main node search may find an incorrect nearest main node.

This problem occurs with interface TYPE3, TYPE6 and TYPE5 (main side only).

The solution to this problem is to use TYPE7 interface.

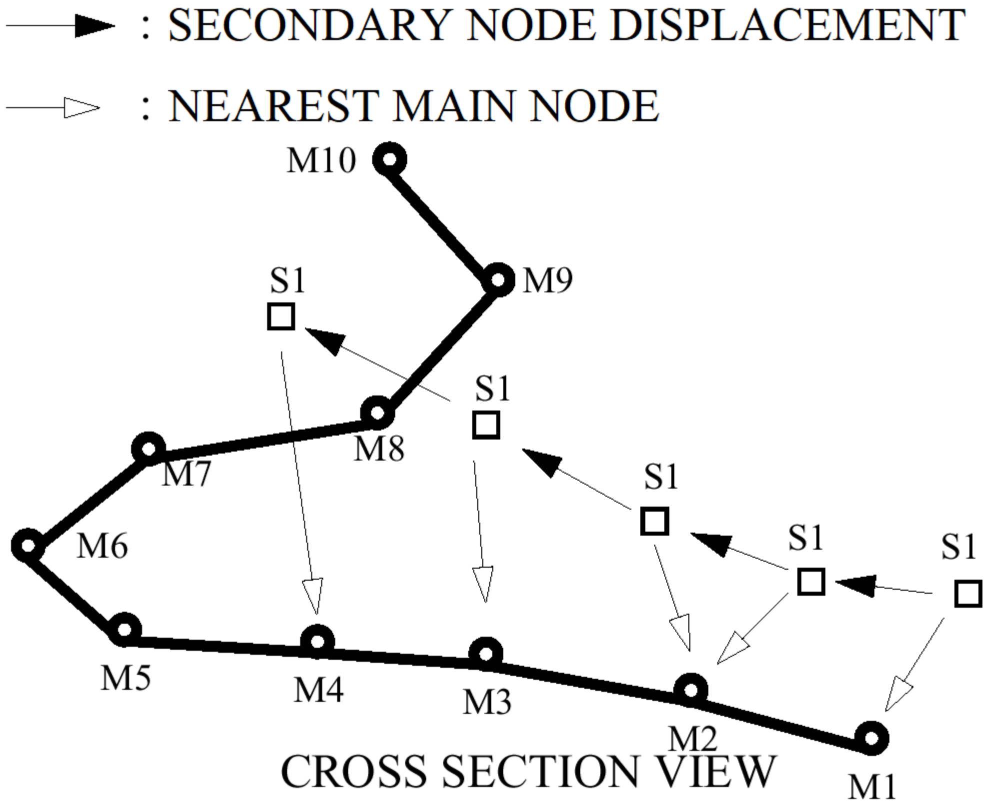

Figure 180: Incorrect Main Node Found

Nearest Main Segment Found Incorrect: B1

In some cases the nearest main node is not connected to the nearest segment.

This problem can occur with interface TYPE3, TYPE6 and TYPE5 (main side only).

The solution is to either use TYPE7 interface or to refine the mesh.

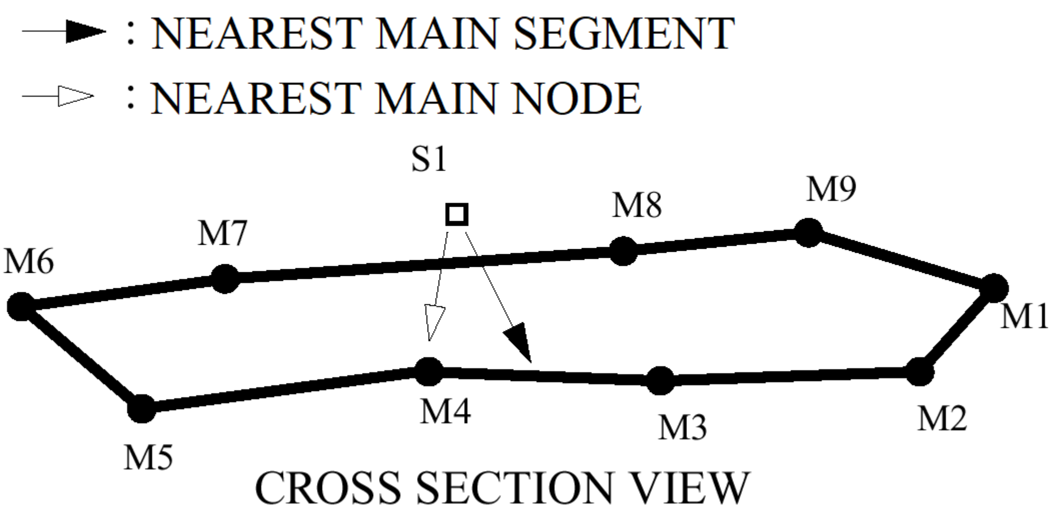

Figure 181: Wrong Nearest Main Segment 1

Nearest Main Segment Found Incorrect: B2

In some cases the nearest main node is not connected to the nearest segment.

This problem can occur with interface TYPE3, TYPE5 and TYPE6 (main side only).

The solution is to either use TYPE7 interface or change the mesh (for initial mesh problem).

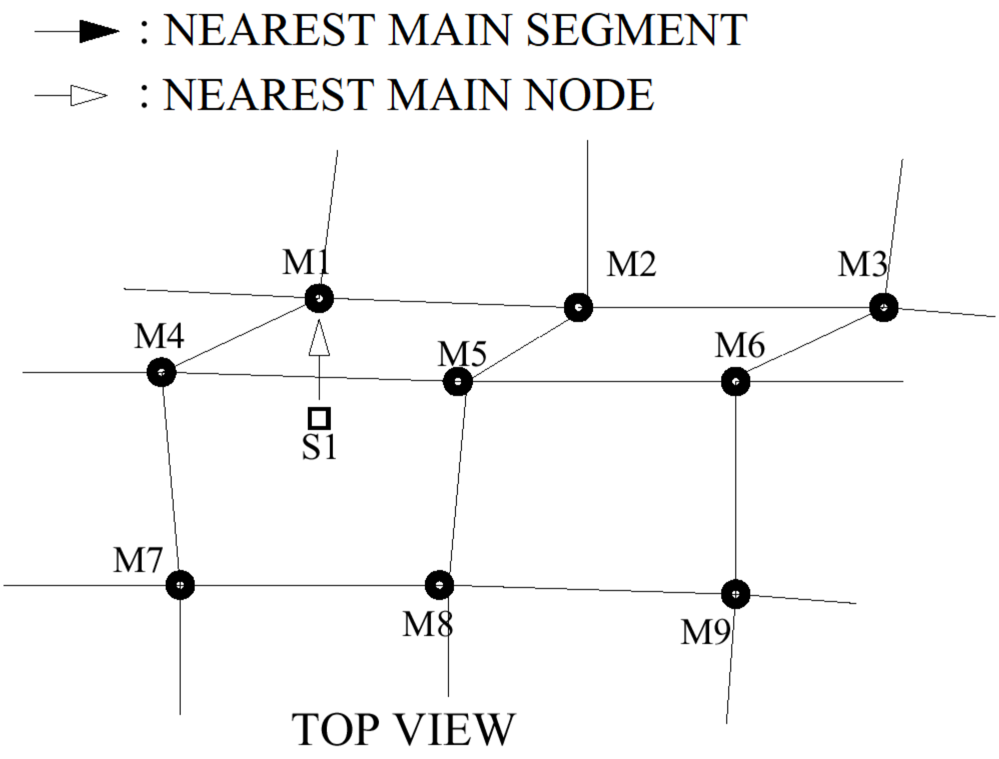

Figure 182: Incorrect Nearest Main Segment 2

Nearest Main Segment Found Incorrect: B3

If the angle between segments is less than 90 degrees, the incorrect nearest segment may sometimes be found, as in Figure 183.

This problem can occur with interface TYPE3, TYPE5 and TYPE6.

The solution is to use a TYPE7 interface or to refine the mesh. With a finer mesh, the shape is smoother.

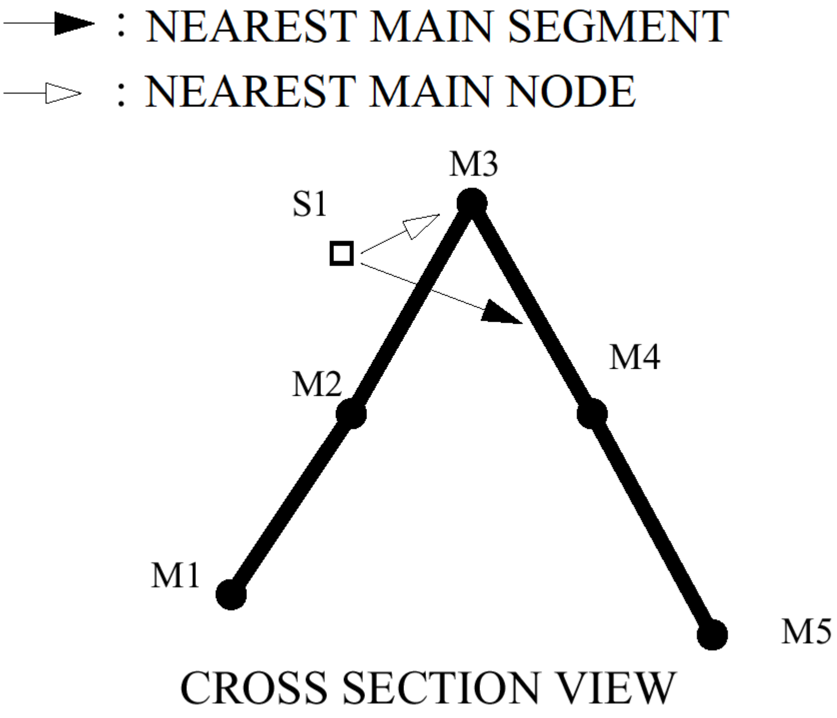

Figure 183: Main Segment Angle to Acute

Impact Side Incorrect: C1

A node can only impact on the positive side of a segment for interface TYPE3, TYPE6, and TYPE5 (main side). The solution is to use a TYPE7 interface.

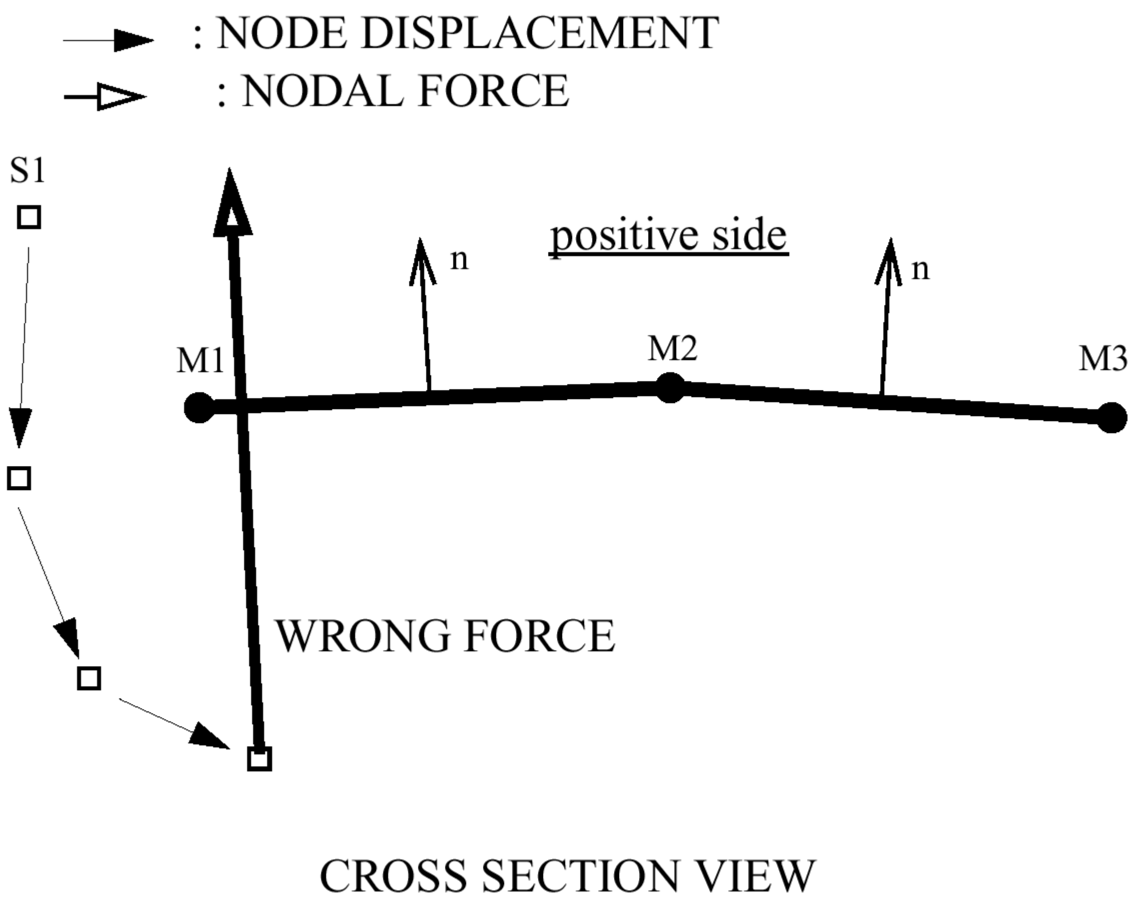

Figure 184: Wrong Normal Direction

No Main Node Impact: D1

With TYPE5 interface, only secondary nodes impact main segments; main nodes cannot impact secondary segments.

This can be solved by either inverting the secondary and main sides, or by changing the type of interface. Interface TYPE3 and TYPE7 will solve this problem adequately.

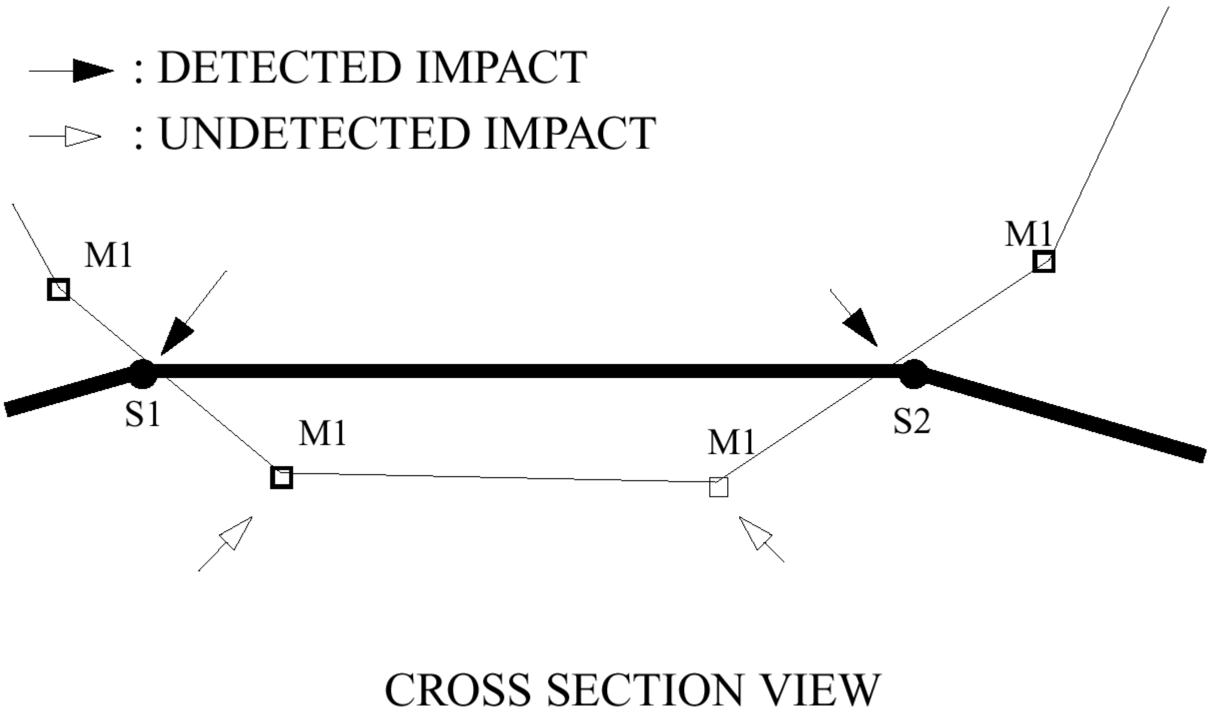

Figure 185: Main Node Penetration

Material Laws

A large variety of materials is used in the structural components and must be modeled in stress analysis problems. For any kind of these materials a range of constitutive laws is available to describe by a mathematical approach the behavior of the material.

The choice of a constitutive law for a given material depends at first to desired quality of the model. For example, for standard steel, the constitutive law may take into account the plasticity, anisotropic hardening, the strain rate, and temperature dependence. However, for a routine design maybe a simple linear elastic law without strain rate and temperature dependence is sufficient to obtain the needed quality of the model. This is the analyst design choice. On the other hand, the software must provide a large constitutive library to provide models for the more commonly encountered materials in practical applications.

Radioss material library contains several distinct material laws. The constitutive laws may be used by the analyst for general applications or a particular type of analysis. You can also program a new material law in Radioss. This is a powerful resource for the analyst to code a complex material model.

Theoretical aspects of the material models that are provided in Radioss are described in this chapter. The available material laws are classified in the table below. This classification is in complementary with those of Radioss input manual. The reader is invited to consult that one for all technical information related to the definition of input data.

Table 6: Material Law Descriptions

Group	Model Description	Law Number in Radioss (MID)
Elasto-plasticity Materials	Johnson-Cook	(2)
	Zerilli-Armstrong	(2)
	von Mises isotropic hardening with polynomial pressure	(3)
	Johnson-Cook	(4)
	Gray model	(16)
	Ductile damage for solids and shells	(22)
	Ductile damage for solids	(23)
	Aluminum, glass, etc.	(27)
	Hill	(32)
	Tabulated piecewise linear	(36)
	Cowper-Symonds	(44)

Group	Model Description	Law Number in Radioss (MID)
	Zhao	(48)
	Steinberg-Guinan	(49)
	Ductile damage for porous materials, Gurson	(52)
	Foam model	(53)
	3-Parameter Barlat	(57)
	Tabulated quadratic in strain rate	(60)
	Hänsel model	(63)
	Ugine and ALZ approach	(64)
	Elastomer	(65)
	Visco-elastic	(66)
	Anisotropic Hill	(72)
	Thermal Hill Orthotropic	(73)
	Thermal Hill Orthotropic 3D	(74)
	Semi-analytical elasto-plastic	(76)
	Yoshida-Uemori	(78)
	Brittle Metal and Glass	(79)
	High strength steel	(80)
	Swift and Voce elastio-plastic Material	(84)
	Barlat YLD2000	(87)
Hyper and Visco-elastic	Closed cell, elasto-plastic foam	(33)
	Boltzman	(34)
	Generalized Kelvin-Voigt	(35)
	Tabulated law	(38)

Group	Model Description	Law Number in Radioss (MID)
	Generalized Maxwell-Kelvin	(40)
	Ogden-Mooney-Rivlin	(42)
	Hyper visco-elastic	(62)
	Tabulated input for Hyper-elastic	(69)
	Tabulated law - hyper visco-elastic	(70)
	Tabulated law - visco-elastic foam	(77)
	Ogden material	(82)
	Simplified hyperelastic material with strain rate effects	(88)
	Tabulated law - visco-elastic foam	(90)
	Arruda-Boyce Hyperelastic Material	(92)
	Yeoh hyperelastic material	(94)
	Bergstrom-Boyce Nonlinear viscoelastic material	(95)
Composite and Fabric	Tsai-Wu formula for solid	(12)
	Composite Solid	(14)
	Composite Shell Chang-Chang	(15)
	Fabric	(19)
	Composite Shell	(25)
	Fabric	(58)
Concrete and Rock	Drücker-Prager for rock or concrete by polynominal	(10)
	Drücker-Prager for rock or concrete	(21)

Group	Model Description	Law Number in Radioss (MID)
	Reinforced concrete	(24)
	Drücker-Prager with cap	(81)
Honeycomb	Honeycomb	(28)
	Crushable foam	(50)
	Cosserat Medium	(68)
Multi-Material, Fluid and Explosive Material	Jones Wilkins Lee model	(5)
	Hydrodynamic viscous	(6)
	Hydrodynamic viscous with k-ε	(6)
	Boundary element	(11)
	Boundary element with k-ε	(11)
	ALE and Euler formulation	(20)
	Hydrodynamic bi-material liquid gas material	(37)
	Lee-Tarver material	(41)
	Viscous fluid with LES subgrid scale viscosity	(46)
	Solid, liquid, gas and explosives	(51)
Connections Materials	Predit rivets	(54)
	Connection material	(59)
	Advanced connection material	(83)
Other Materials	Fictitious	(0)
	Hooke	(1)
	Purely thermal material	(18)
	SESAM tabular EOS, used with a Johnson-Cook yield criterion	(26)

Group	Model Description	Law Number in Radioss (MID)
	Superelastic Law for Shape Memory Alloy	(71)
	Porous material	(75)
	GAS material	GAS (-)
	User material	(29~31)

Isotropic Elastic Material

Two kinds of isotropic elastic materials are considered:

- Linear elastic materials with Hooke’s law,
- Nonlinear elastic materials with Ogden, Mooney-Rivlin and Arruda-Boyce laws.

Linear Elastic Material (LAW1)

This material law is used to model purely elastic materials, or materials that remain in the elastic range. The Hooke's law requires only two values to be defined; the Young's or elastic modulus E, and Poisson's ratio, υ. The law represents a linear relation between stress and strain.

Ogden Materials (LAW42, LAW69 and LAW82)

Ogden's law is applied to slightly compressible materials as rubber or elastomer foams undergoing large deformation with an elastic behavior. The detailed theory for Odgen material models can be found in [89]. The strain energy W is expressed in a general form as a function of $W(\lambda_1, \lambda_2, \lambda_3)$:

$$W(\lambda_1, \lambda_2, \lambda_3) = \sum_{p=1}^{5} \frac{\mu_p}{\alpha_p}\left(\bar{\lambda}_{1\alpha_p} + \bar{\lambda}_{2\alpha_p} + \bar{\lambda}_{3\alpha_p} - 3\right) + \frac{K}{2}(J-1)^2 \tag{803}$$

[89] Ogden R.W., “Nonlinear Elastic Deformations”, Ellis Horwood, 1984.

[90] Arruda, E.M. and Boyce, M.C., “A three-dimensional model for the large stretch behavior of rubber elastic materials”, J. Mech. Phys. Solids, 41(2), pp. 389–412, 1993.

[91] Jo¨rgen Bergstro¨m, “Mechanics of solid polymers: theory and computational modeling”, pp. 250-254, 2015.

[92] Yeoh, O. H., “Some forms of the strain energy function for rubber”, Rubber Chemistry and Technology, Vol. 66, Issue 5, pp. 754-771, November 1993.

[93] Kolling S., Du Bois P.A., Benson D.J., and Feng W.W., "A tabulated formulation of hyperelasticity with rate effects and damage." Computational Mechanics 40, no. 5 (2007).

Where, λ_1, i$_{\text{th}}$ principal stretch

$\lambda_i = 1 + \varepsilon_i$, with ε_i being the i$_{\text{th}}$ principal engineering strain

J is relative volume with:

$$J = \lambda_1 \cdot \lambda_2 \cdot \lambda_3 = \frac{\rho_0}{\rho} \tag{804}$$

$\bar{\lambda}_i$ is the deviatoric stretch

$$\bar{\lambda}_i = J^{-\frac{1}{3}} \lambda_i \tag{805}$$

α_p and μ_p are the material constants.

p is order of Ogden model and defines the number of coefficients pairs $\left(\alpha_p, \mu_p\right)$.

This law is very general due to the choice of coefficient pair $\left(\alpha_p, \mu_p\right)$.

- If p=1, then one pair $\left(\alpha_1, \mu_1\right)$ of material constants is needed andin this case if $\alpha_1 = 2$ then it becomes a Neo-hookean material model.
- If p=2 then two pairs $\left(\alpha_1, \mu_1\right), \left(\alpha_2, \mu_2\right)$ of material constants are needed and in this case if $\alpha_1 = 2$ and $\alpha_1 =$ -2 then it becomes a Mooney-Rivlin material model

For uniform dilitation:

$$\lambda_1 = \lambda_2 = \lambda_3 = \lambda \tag{806}$$

The strain energy function can be decomposed into deviatoric part $\overline{W}(\bar{\lambda}_1, \bar{\lambda}_2, \bar{\lambda}_3)$ and spherical part $U(J)$:

$$W = \overline{W}(\bar{\lambda}_1, \bar{\lambda}_2, \bar{\lambda}_3) + U(J) \tag{807}$$

With:

$$\overline{W}(\bar{\lambda}_1, \bar{\lambda}_2, \bar{\lambda}_3) = \sum_p \frac{\mu_p}{\alpha_p}\left(\bar{\lambda}_{1\alpha_p} + \bar{\lambda}_{2\alpha_p} + \bar{\lambda}_{3\alpha_p} - 3\right)$$

$$U(J) = \tfrac{K}{2}(J-1)^2$$

The stress σ_i corresponding to this strain energy is given by:

$$\sigma_i = \frac{\lambda_i}{J}\frac{\partial W}{\partial \lambda_i} \tag{808}$$

which can be written as:

$$\sigma_i = \frac{\lambda_i}{J}\frac{\partial W}{\partial \lambda_i} = \frac{\lambda_i}{J}\left(\sum_{j=1}^{3} \frac{\partial \overline{W}}{\partial \bar{\lambda}_j}\frac{\partial \bar{\lambda}_j}{\partial \lambda_i} + \frac{\partial U}{\partial J}\frac{\partial J}{\partial \lambda_i}\right) \tag{809}$$

Since $\lambda_1 \frac{\partial J}{\partial \lambda_i} = J$ and $\frac{\partial \bar{\lambda}_j}{\partial \lambda_i} = \frac{2}{3} J^{-\frac{1}{3}}$ for i=j and $\frac{\partial \bar{\lambda}_j}{\partial \lambda_i} = \frac{1}{3} J^{-\frac{1}{3}} \frac{\lambda_j}{\lambda_i}$ for i≠j

Equation 809 is simplified to:

$$\sigma_i = \frac{1}{J}\left(\bar{\lambda}_i \frac{\partial \overline{W}}{\partial \bar{\lambda}_i} - \left(\frac{1}{3}\sum_{j=1}^{3} \bar{\lambda}_j \frac{\partial \overline{W}}{\partial \bar{\lambda}_j} - J\frac{\partial U}{\partial J}\right)\right) \tag{810}$$

For which the deviator of the Cauchy stress tensor s_i, and the pressure P would be:

$$s_i = \frac{1}{J}\left(\bar{\lambda}_i \frac{\partial \overline{W}}{\partial \bar{\lambda}_i} - \frac{1}{3}\sum_{j=1}^{3} \bar{\lambda}_j \frac{\partial \overline{W}}{\partial \bar{\lambda}_j}\right) \tag{811}$$

$$p = -\frac{1}{3}\sum_{j=1}^{3} \sigma_j = -\frac{\partial U}{\partial J} \tag{812}$$

Only the deviatoric stress above is retained, and the pressure is computed independently:

$$P = K \cdot Fscale_{blk} \cdot \mathrm{f}_{blk}(J) \cdot (J-1) \tag{813}$$

Where, $\mathrm{f}_{blk}(J)$ a user-defined function related to the bulk modulus K in LAW42 and LAW69:

$$K = \mu \cdot \frac{2(1+v)}{3(1-2v)} \tag{814}$$

For an imcompressible material $(v \approx 0.5)$, $J = 1$ and no pressure in material.

$$\mu = \frac{\sum_p \mu_p \cdot \alpha_p}{2} \tag{815}$$

With μ being the initial shear modulus, and υ the Poisson's ratio.

Note: For an incompressible material you have $\upsilon \approx 0.5$. However, $\upsilon \approx 0.495$ is a good compromise to avoid too small time steps in explicit codes.

A particular case of the Ogden material model is the Mooney-Rivlin material law which has two basic assumptions:

- The rubber is incompressible and isotropic in unstrained state
- The strain energy expression depends on the invariants of Cauchy tensor

The three invariants of the Cauchy-Green tensor are:

$$I_1 = \lambda_1 2 + \lambda_2 2 + \lambda_3 2 \tag{816}$$

$$I_2 = \lambda_1 2 \lambda_2 2 + \lambda_2 2 \lambda_3 2 + \lambda_3 2 \lambda_1 2 \tag{817}$$

For incompressible material:

$$I_3 = \lambda_1 2\lambda_2 2\lambda_3 2 = 1 \tag{818}$$

The Mooney-Rivlin law gives the closed expression of strain energy as:

$$W = C_{10}(I_1 - 3) + C_{01}(I_2 - 3) \tag{819}$$

with:

$$\mu_1 = 2 \cdot C_{10} \tag{820}$$

$$\mu_2 = -2 \cdot C_{01}$$

$$\alpha_1 = 2$$

$$\alpha_2 = -2$$

The model can be generalized for a compressible material.

Viscous Effects in LAW42

Viscous effects are modeled through the Maxwell model:

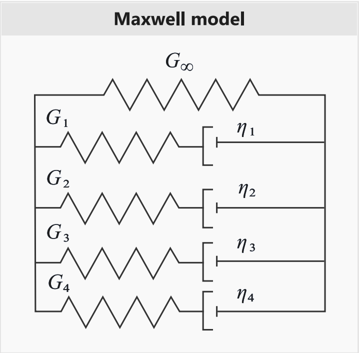

Figure 186: Maxwell Model

Where, the shear modulus of the hyper-elastic law μ is exactly the long-term shear modulus G_∞.

$$\mu = \frac{\sum_p \mu_p \cdot \alpha_p}{2} = G_\infty \tag{821}$$

τ_{i} are relaxation times: $\tau_{\mathrm{i}} = \frac{\eta_i}{G_i}$

Rate effects are modeled through visco-elasticity using convolution integral using Prony series. This corresponds to extension of small deformation theory to finite deformation.

This viscous stress is added to the elastic one.

The visco-Kirchoff stress is given by:

$$\boldsymbol{\tau}^{v}=\sum_{i=1}^{M}G_{i}\int_{0}^{t}e^{-\frac{t-s}{\tau_{i}}}\frac{d}{ds}\left[\mathrm{dev}\left(\overline{\mathbf{F}}\overline{\mathbf{F}}^{T}\right)\right]ds \tag{822}$$

Where,

M	Order of the Maxwell model
$\mathbf{F}$	Deformation gradient matrix
$\overline{\mathbf{F}}=J^{-\frac{1}{3}}\mathbf{F}$	
$\mathrm{dev}\left(\overline{\mathbf{F}}\overline{\mathbf{F}}^{T}\right)$	Denotes the deviatoric part of tensor $\overline{\mathbf{F}}\overline{\mathbf{F}}^{T}$

The viscous-Cauchy stress is written as:

$$\boldsymbol{\sigma}^{v}(t)=\frac{1}{J}\boldsymbol{\tau}^{v}(t) \tag{823}$$

LAW69, Ogden Material Law (Using Test Data as Input)

This law, like `/MAT/LAW42 (OGDEN)` defines a hyperelastic and incompressible material specified using the Ogden or Mooney-Rivlin material models. Unlike LAW42 where the material parameters are input this law computes the material parameters from an input engineering stress-strain curve from a uniaxial tension and compression tests. This material can be used with shell and solid elements.

The strain energy density formulation used depends on the *law_ID*.

law_ID =1, Ogden law (Same as LAW42):

$$W(\lambda_1,\lambda_2,\lambda_3)=\sum_{p=1}^{5}\frac{\mu_p}{\alpha_p}\left(\bar{\lambda}_{1\alpha_p}+\bar{\lambda}_{2\alpha_p}+\bar{\lambda}_{3\alpha_p}-3\right)+\frac{K}{2}(J-1)^2$$

law_ID =2, Mooney-Rivlin law

$$W=C_{10}(I_1-3)+C_{01}(I_2-3)$$

Curve Fitting

After reading the stress-strain curve (*fct_ID*$_1$), Radioss calculates the corresponding material parameter pairs using a nonlinear least-square fitting algorithm. For classic Ogden law, (*law_ID* =1), the calculated material parameter pairs are μ_p and α_p where the value of p is defined via the *N_pair* input. The maximum value of *N_pair* = 5 with a default value of 2.

For the Mooney-Rivlin law (*law_ID* =2), the material parameter C_{10} and C_{01} are calculated remembering that μ_p and α_p for the LAW42 Ogden law can be calculated using this conversion.

$\mu_1=2\cdot C_{10}$, $\mu_2=-2\cdot C_{01}$, $\alpha_1=2$ and $\alpha_2=-2$.

The minimum test data input should be a uniaxial tension engineering stress strain curve. If uniaxial compression data is available, the engineering strain should increate monotonically from a negative value in compression to a positive value in tension. In compression, the engineering strain should not be less than -1.0 since -100% strain is physically not possible.

This material law is stable when (with p=1,…5) is satisfied for parameter pairs for all loading conditions. By default, Radioss tries to fit the curve by accounting for these conditions (I_{check}=2). If a proper fit cannot be found, then Radioss uses a weaker condition (I_{check}=1:) which ensures that the initial shear hyperelastic modulus (μ) is positive.

Once the material parameters are calculated by the Radioss Starter in LAW69, all the calculations done by LAW69 in the simulation are the same as LAW42.

LAW82

The Ogden model used in LAW82 is:

$$W = \sum_{i=1}^{N} \frac{2\mu_i}{\alpha_i^2} \left(\bar{\lambda}_{1\alpha_i} + \bar{\lambda}_{2\alpha_i} + \bar{\lambda}_{3\alpha_i} - 3 \right) + \sum_{i=1}^{N} \frac{1}{D_i} (J-1)^{2i} \tag{824}$$

The Bulk Modulus is calculated as $K = \frac{2}{D_1}$ based on these rules:

- If $v = 0$, D_1 should be entered.
- If $v \neq 0$, D_1 input is ignored and will be recalculated and output in the Starter output using:

$$D_1 = \frac{3(1-2v)}{\mu(1+v)} \tag{825}$$

- If $v = 0$ and D_1=0, a default value of $v = 0.475$ is used and D_1 is calculated using Equation 825

LAW88, A simplified hyperelastic material with strain rate effects

This law utilizes tabulated uniaxial tension and compression engineering stress and strain test data at different strain rates to model incompressible materials. It is only compatible with solid elements. The material is based on Ogden's strain energy density function but does not require curve fitting to extract material constants like most other hyperelastic material models. Strain rate effects can be modeled by including engineering stress strain test data at different strain rates. This can be easier than calculating viscous parameters for traditional hyperelastic material models. The following Ogden strain energy density function is used but instead of extracting material constants via curve fitting this law determines the Ogden function directly from the uniaxial engineering stress strain curve tabulated data. [93]

$$W = \underbrace{\sum_{i=1}^{3} \sum_{j=1}^{m} \frac{\mu_j}{\alpha_j} \left(\bar{\lambda}_{i\alpha_j} - 1 \right)}_{deviatoric\,part} + \underbrace{K(J - 1 - \ln J)}_{spherical\,part} \tag{826}$$

Unloading can be represented using an unloading function, *Fscale_{unL}*, or by providing hysteresis, *Hys* and shape factor, *Shape*, inputs to a damage model based on energy.

When using the damage model, the loading curves are used for both loading and unloading and the unloading stress tensor is reduced by:

$$\boldsymbol{\sigma} = (1 - D)\boldsymbol{\sigma} \tag{827}$$

$$D = (1 - Hys)\left(1 - \left(\frac{W_{cur}}{W_{\max}}\right)^{Shape}\right) \tag{828}$$

If the unloading function, *Fscale$_{unL}$*, is entered, unloading is defined based on the unloading flag, *Tension* and the damage model is not used.

Arruda-Boyce Material (LAW92)

LAW92 describes the Arruda-Boyce material model, which can be used to model hyperelastic behavior. The Arruda-Boyce model is based on the statistical mechanics of a material with a cubic representative volume element containing eight chains along the diagonal directions. It assumes that the chain molecules are located on the average along the diagonals of the cubic in principal stretch space.

The strain energy density function is:

$$W = \underbrace{\mu\sum_{i=1}^{5}\frac{c_i}{(\lambda_m)^{2i-2}}\left(\bar{I}_1^i - 3^i\right)}_{W(\bar{I}_1)} + \underbrace{\frac{1}{D}\left(\frac{J^2 - 1}{2} + \ln(J)\right)}_{U(J)} \tag{829}$$

Where, Material constant c_i are:

$c_1 = \frac{1}{2},\ c_2 = \frac{1}{20},\ c_3 = \frac{11}{1050},\ c_4 = \frac{19}{7000},\ c_5 = \frac{519}{673750}$

μ	Shear modulus
μ_0	Initial shear modulus

$$\mu_0 = \mu\left(1 + \frac{3}{5\lambda_m 2} + \frac{99}{175\lambda_m 4} + \frac{513}{875\lambda_m 6} + \frac{42039}{67375\lambda_m 8}\right) \tag{830}$$

λ_m is the limit of stretch which describes the beginning of hardening phase in tension (locking strain in tension) and so it is also called the *locking stretch*.

Arruda-Boyce is always stable if positive values of the shear modulus, μ, and the locking stretch, λ_m are used.

$\bar{I}_1$ is deviatoric part of first strain invarient I_1

$$\bar{I}_1 = \bar{\lambda}_1 2 + \bar{\lambda}_2 2 + \bar{\lambda}_3 2 = J^{-2/3} I_1 \tag{831}$$

with $\bar{\lambda}_i = J^{-\frac{1}{3}}\lambda_i$

D is a material parameter for the bulk modulus computation given as:

$$D = \frac{2}{K} \tag{832}$$

The Cauchy stress corresponding to above strain energy is:

$$\sigma_i = \frac{\lambda_i}{J}\frac{\partial W}{\partial \lambda_i} \tag{833}$$

For incompressible materials, the Cauchy stress is then given by:

- Uniaxial test

$$\sigma = \lambda\frac{\partial W}{\partial \lambda} = 2\mu\left(\lambda^2 - \frac{1}{\lambda}\right)\sum_{i=1}^{5}\frac{i \cdot c_i}{\lambda_{m2i-2}}\left(\bar{\lambda}_{1}2 + \bar{\lambda}_{2}2 + \bar{\lambda}_{3}2\right)^{i-1} \tag{834}$$

  with $\lambda_1 = \lambda$ and $\lambda_2 = \lambda_3 = \lambda^{-\frac{1}{2}}$, then $\bar{I}_1 = \lambda^2 + \frac{2}{\lambda}$

  and nominal stress is:

$$N^{th} = \frac{\partial W}{\partial \lambda} = 2\mu(\lambda - \lambda^{-2})\sum_{i=1}^{5}\frac{i \cdot c_i}{(\lambda_m)^{2i-2}}\left(\lambda^2 + \frac{2}{\lambda}\right)^{i-1} \tag{835}$$

- Equibiaxial test

$$\sigma = \lambda\frac{\partial W}{\partial \lambda} = 2\mu\left(\lambda^2 - \frac{1}{\lambda^4}\right)\sum_{i=1}^{5}\frac{i \cdot c_i}{\lambda_{m2i-2}}\left(\bar{\lambda}_{1}2 + \bar{\lambda}_{2}2 + \bar{\lambda}_{3}2\right)^{i-1} \tag{836}$$

  with $\lambda_1 = \lambda_2 = \lambda$ and $\lambda_3 = \lambda^{-2}$, then $\bar{I}_1 = 2\lambda^2 + \frac{1}{\lambda^4}$

  and the nominal stress is:

$$N^{th} = \frac{\partial W}{\partial \lambda} = 2\mu(\lambda - \lambda^{-5})\sum_{i=1}^{5}\frac{i \cdot c_i}{(\lambda_m)^{2i-2}}\left(2\lambda^2 + \frac{1}{\lambda^4}\right)^{i-1} \tag{837}$$

- Planar test

$$\sigma = \lambda\frac{\partial W}{\partial \lambda} = 2\mu\left(\lambda^2 - \frac{1}{\lambda^2}\right)\sum_{i=1}^{5}\frac{i \cdot c_i}{\lambda_{m2i-2}}\left(\bar{\lambda}_{1}2 + \bar{\lambda}_{2}2 + \bar{\lambda}_{3}2\right)^{i-1} \tag{838}$$

  with $\lambda_1 = \lambda,\ \lambda_3 = 1$ and $\lambda_2 = \lambda^{-1}$, then $\bar{I}_1 = \lambda^2 + 1 + \lambda^{-2}$

  and nominal stress is:

$$N^{th} = \frac{\partial W}{\partial \lambda} = 2\mu(\lambda - \lambda^{-3})\sum_{i=1}^{5}\frac{ic_i}{(\lambda_m)^{2i-2}}(\lambda^2 + 1 + \lambda^{-2})^{i-1} \tag{839}$$

Additional information about Arruda-Boyce model. [90] [91]

Yeoh Material (LAW94)

The Yeoh model (LAW94) [92]is a hyperelastic material model that can be used to describe incompressible materials. The strain energy density function of LAW94 only depends on the first strain invariant and is computed as:

$$W=\sum_{i=1}^{3}\left[\underbrace{C_{i0}(\bar{I}_1-3)^i}_{W(\bar{I}_1)}+\underbrace{\frac{1}{D_i}(J-1)^{2i}}_{U(J)}\right] \tag{840}$$

Where,

$\bar{I}_1=\bar{\lambda}_1^2+\bar{\lambda}_2^2+\bar{\lambda}_3^2$ First strain invariant

$\bar{\lambda}_i=J^{-\frac{1}{3}}\lambda_i$ Deviatoric stretch

The Cauchy stress is computed as:

$$\sigma_i=\frac{\lambda_i}{J}\frac{\partial W}{\partial \lambda_i} \tag{841}$$

For incompressible materials with i=1 only and D_1 are input and the Yeoh model is reduced to a Neo-Hookean model.

The material constant specify the deviatoric part (shape change) of the material and parameters D_1, D_2, D_3 specify the volumetric change of the material. These six material constants need to be calculated by curve fitting material test data. RD-E: 5600 Hyperelastic Material with Curve Input includes a Yeoh fitting Compose script for uniaxial test data. The Yeoh material model has been shown to model all deformation models even if the curve fit was obtained using only uniaxial test data.

The initial shear modulus and the bulk modulus are computed as:

$\mu=2\cdot C_{10}$ and $K=\frac{2}{D_1}$

LAW94 is available only as an incompressible material model.

If D_1=0, an incompressible material is considered, where $v=0.495$ and D_1 is calculated as:

$$D_1=\frac{3(1-2v)}{\mu(1+v)} \tag{842}$$

Composite and Anisotropic Materials

The orthotropic materials can be classified into following cases:

- Linear elastic orthotropic shells as fabric
- Nonlinear orthotropic pseudo-plastic solids as honeycomb materials
- Elastic-plastic orthotropic shells
- Elastic-plastic orthotropic composites

The purpose of this section is to describe the mathematical models related to composite and orthotropic materials.

Fabric Law for Elastic Orthotropic Shells (LAW19 and LAW58)

Two elastic linear models and a nonlinear model exist in Radioss.

Fabric Linear Law for Elastic Orthotropic Shells (LAW19)

A material is orthotropic if its behavior is symmetrical with respect to two orthogonal plans. The fabric law enables to model this kind of behavior. This law is only available for shell elements and can be used to model an airbag fabric. Many of the concepts for this law are the same as for LAW14 which is appropriate for composite solids. If axes 1 and 2 represent the orthotropy directions, the constitutive matrix C is defined in terms of material properties:

$$C^{-1} = \begin{bmatrix} \frac{1}{E_{11}} & -\frac{\upsilon_{21}}{E_{22}} & 0 & 0 & 0 \\ -\frac{\upsilon_{12}}{E_{11}} & \frac{1}{E_{22}} & 0 & 0 & 0 \\ 0 & 0 & \frac{1}{G_{12}} & 0 & 0 \\ 0 & 0 & 0 & \frac{1}{G_{23}} & 0 \\ 0 & 0 & 0 & 0 & \frac{1}{G_{31}} \end{bmatrix} \tag{843}$$

where the subscripts denote the orthotropy axes. As the matrix C is symmetric:

$$\frac{\upsilon_{12}}{E_{11}} = \frac{\upsilon_{21}}{E_{22}} \tag{844}$$

Therefore, six independent material properties are the input of the material:

E_{11}	Young's modulus in direction 1
E_{22}	Young's modulus in direction 2
$\upsilon_{\mathbf{12}}$	Poisson's ratio
G_{12}, G_{23}, G_{31}	Shear moduli for each direction

The coordinates of a global vector $\vec{V}$ is used to define direction 1 of the local coordinate system of orthotropy.

The angle Φ is the angle between the local direction 1 (fiber direction) and the projection of the global vector $\vec{V}$ as shown in Figure 187.

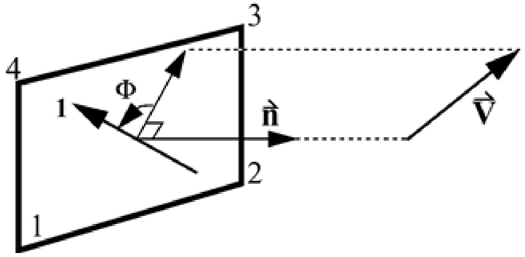

Figure 187: Fiber Direction Orientation

The shell normal defines the positive direction for Φ. Since fabrics have different compression and tension behavior, an elastic modulus reduction factor, R_E, is defined that changes the elastic properties of compression. The formulation for the fabric law has a σ_{11} reduction if σ_{11} < 0 as shown in Figure 188.

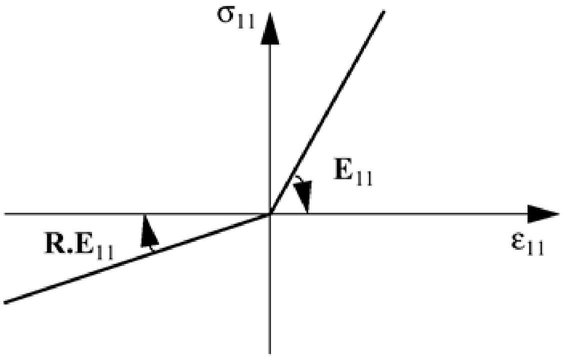

Figure 188: Elastic Compression Modulus Reduction

Fabric Nonlinear Law for Elastic Anisotropic Shells (LAW58)

This law is used with Radioss standard shell elements and anisotropic layered property (TYPE16). The fiber directions (warp and weft) define the local axes of anisotropy. Material characteristics are determined independently in these axes. Fibers are nonlinear elastic and follow the equation:

$$\begin{aligned} \sigma_{ii} &= E_i \varepsilon_{ii} - \frac{(B_i \varepsilon_{ii}{}^2)}{2} \\ \sigma_{ii} &= \max_{\varepsilon_{ii}} \left(E_i \varepsilon_{ii} - \frac{(B_i \varepsilon_{ii}{}^2)}{2} \right) \end{aligned} \quad \text{with} \quad \begin{aligned} \frac{d\sigma}{d\varepsilon} &> 0 \\ \frac{d\sigma}{d\varepsilon} &\le 0 \end{aligned} \quad \text{and } i\text{=1,2} \tag{845}$$

The shear in fabric material is only supposed to be function of the angle between current fiber directions (axes of anisotropy):

$$\begin{aligned} \tau &= G_0 \tan(\alpha) - \tau_0 \quad \text{if} \quad \alpha \le \alpha_T \\ \tau &= G \tan(\alpha) + G_A - \tau_0 \quad \text{if} \quad \alpha > \alpha_T \end{aligned} \tag{846}$$

and

$$G_A = (G_0 - G)\tan(\alpha_T),\ G = \frac{G_T}{1+\tan^2(\alpha_T)} \text{ with } \tau_0 = G_0\tan(\alpha_0)$$

Where, α_T is a shear lock angle, G_T is a tangent shear modulus at α_T, and G_0 is a shear modulus at α = 0. If G_0 = 0, the default value is calculated to avoid shear modulus discontinuity at α_T: G_0 = G.

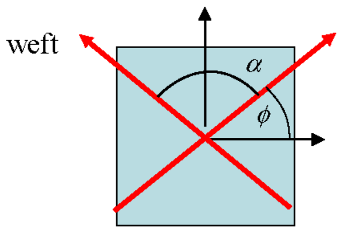

Figure 189: Elastic Compression Modulus Reduction

α_0 is an initial angle between fibers defined in the shell property (TYPE16).

The warp and weft fiber are coupled in tension and uncoupled in compression. But there is no discontinuity between tension and compression. In compression only fiber bending generates global stresses. Figure 190 illustrates the mechanical behavior of the structure.

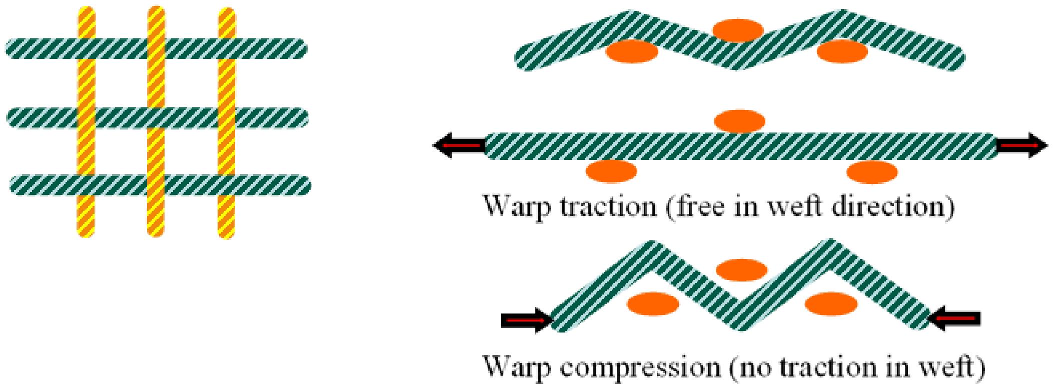
Warp traction (free in weft direction)
Warp compression (no traction in weft)

Figure 190: Local Frame Definition

A local micro model describes the material behavior (Figure 191). This model represents just ¼ of a warp fiber wave length and ¼ of the weft one. Each fiber is described as a nonlinear beam and the two fibers are connected with a contacting spring. These local nonlinear equations are solved with Newton iterations at membrane integration point.

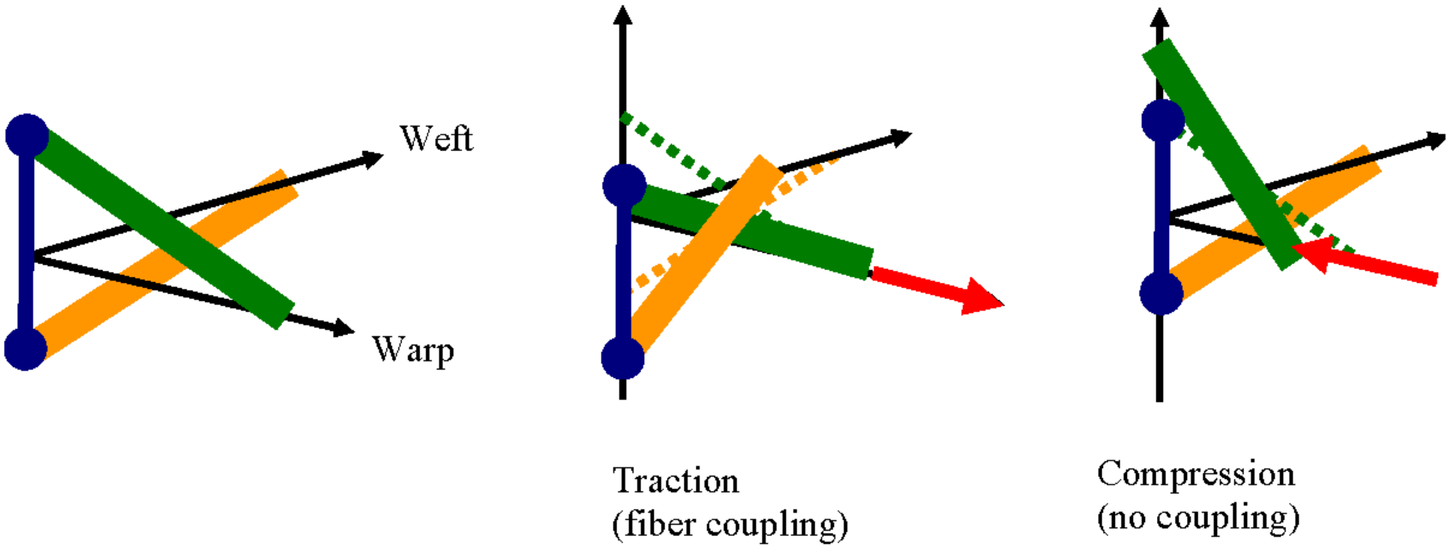

Figure 191: Local Frame Definition

Nonlinear Pseudo-plastic Orthotropic Solids (LAWS28, 50 and 68)

Conventional Nonlinear Pseudo-plastic Orthotropic Solids (LAW28 and LAW50)

These laws are generally used to model honeycomb material structures as crushable foams. The microscopic behavior of this kind of materials can be considered as a system of three independent orthogonal springs. The nonlinear behavior in orthogonal directions can then be determined by experimental tests. The behavior curves are injected directly in the definition of law. Therefore, the physical behavior of the material can be obtained by a simple law. However, the microscopic elasto-plastic behavior of a material point cannot be represented by decoupled unidirectional curves. This is the major drawback of the constitutive laws based on this approach. The cell direction is defined for each element by a local frame in the orthotropic solid property. If no property set is given, the global frame is used.

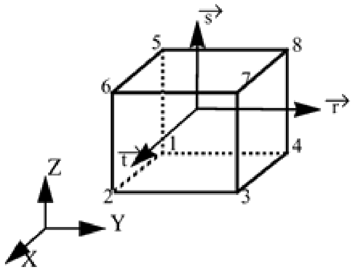

Figure 192: Local Frame Definition

The Hooke matrix defining the relation between the stress and strain tensors is diagonal, as there is no Poisson's effect:

$$\begin{bmatrix}\sigma_{11}\\ \sigma_{22}\\ \sigma_{33}\\ \sigma_{12}\\ \sigma_{23}\\ \sigma_{31}\end{bmatrix}=\begin{bmatrix}E_{11} & 0 & 0 & 0 & 0 & 0\\ 0 & E_{12} & 0 & 0 & 0 & 0\\ 0 & 0 & E_{33} & 0 & 0 & 0\\ 0 & 0 & 0 & G_{12} & 0 & 0\\ 0 & 0 & 0 & 0 & G_{23} & 0\\ 0 & 0 & 0 & 0 & 0 & G_{31}\end{bmatrix}\begin{bmatrix}\varepsilon_{11}\\ \varepsilon_{22}\\ \varepsilon_{33}\\ \varepsilon_{12}\\ \varepsilon_{23}\\ \varepsilon_{31}\end{bmatrix} \tag{847}$$

An isotropic material may be obtained if:

$$E_{11}=E_{22}=E_{33} \quad \text{and} \quad G_{12}=G_{23}=G_{31}=\frac{E_{11}}{2} \tag{848}$$

Plasticity may be defined by a volumic strain or strain dependent yield curve (Figure 193). The input yield stress function is always positive. If the material undergoes plastic deformation, its behavior is always orthotropic, as all curves are independent to each other.

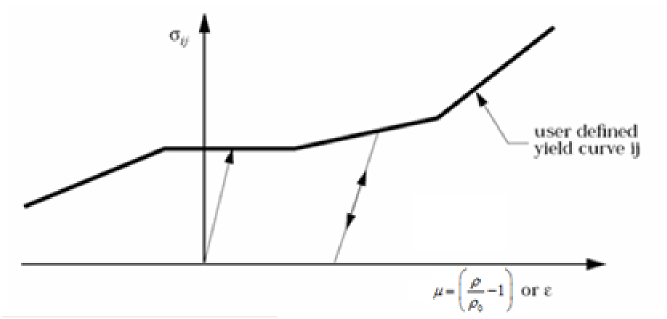

Figure 193: Honeycomb Typical Constitutive Curve

The failure plastic strain may be input for each direction. If the failure plastic strain is reached in one direction, the element is deleted. The material law may include strain rate effects (LAW50) or may not (LAW28).

Cosserat Medium for Nonlinear Pseudo-plastic Orthotropic Solids (LAW68)

Conventional continuum mechanics approaches cannot incorporate any material component length scale. However, a number of important length scales as grains, particles, fibers, and cellular structures must be taken into account in a realistic model of some kinds of materials. To this end, the study of a microstructure material having translational and rotational degrees-of-freedom is underlying. The idea of introducing couple stresses in the continuum modeling of solids is known as Cosserat theory which returns back to the works of brothers Cosserat in the beginning of 20th century. [94] A recent renewal of Cosserat mechanics is presented in several works of Forest [95] [96] [97] [98] A short summary of these publications is presented in this section.

Cosserat effects can arise only if the material is subjected to non-homogeneous straining conditions. A Cosserat medium is a continuous collection of particles that behave like rigid bodies. It is assumed that the transfer of the interaction between two volume elements through surface element dS occurs not only by means of a traction and shear forces, but also by moment vector as shown in Figure 194.

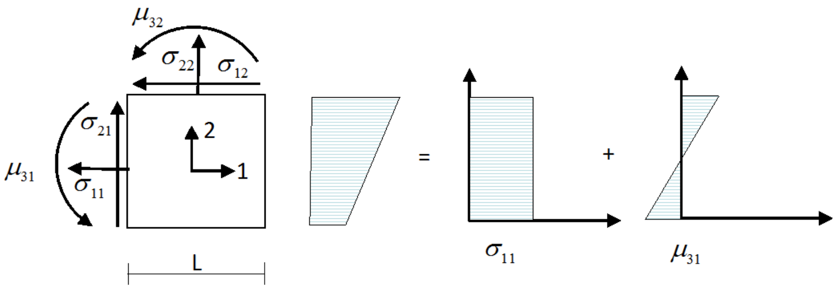

Figure 194: Equilibrium of Cosserat Volume Element

Surface forces and couples are then represented by the generally non-symmetrical force-stress and couple-stress tensors σ_{ij} and μ_{ij} (units MPA and MPa-m):

$$t_i = \sigma_{ij} n_j \quad : \quad m_i = \mu_{ij} n_j \tag{849}$$

The force and couple stress tensors must satisfy the equilibrium of momentums:

$$\begin{gathered} \sigma_{ij,j} + f_i = \rho \ddot{u}_i \\ \mu_{ij,j} - \varepsilon_{ikl}\sigma_{kl} + c_i = I\ddot{\varphi}_i \end{gathered} \tag{850}$$

Where,

f_i
: Volume forces

c_i
: Volume couples

ρ
: Mass density

I
: Isotropic rotational inertia

ε_{ikl}
: Signature of the perturbation (i,k,l)

In the often used couple-stress, the Cosserat micro-rotation is constrained to follow the material rotation given by the skew-symmetric part of the deformation gradient:

$$\varphi_i = -\frac{1}{2}\varepsilon_{ijk} u_{j,k} \tag{851}$$

The associated torsion-curvature and couple stress tensors are then traceless. If a Timoshenko beam is regarded as a one-dimensional Cosserat medium, constraint Equation 851 is then the counterpart of the Euler-Bernoulli conditions.

The resolution of the previous boundary value problem requires constitutive relations linking the deformation and torsion-curvature tensors to the force- and couple-stresses. In the case of linear isotropic elasticity, you have:

$$\sigma_{ij} = \lambda e_{kk}\delta_{ij} + 2\mu\, e_{ij}^{Symm.} + 2\mu_c e_{ij}^{Skew\ Symm.}$$
$$\mu_{ij} = \alpha\, k_{kk}\delta_{ij} + 2\beta\, \kappa_{ij}^{Symm.} + 2\gamma\kappa_{ij}^{Skew\ Symm.} \quad (852)$$

Where, $e_{ij}^{Symm.}$ and $e_{ij}^{Skew\ Symm.}$ are respectively the symmetric and skew-symmetric part of the Cosserat deformation tensor. Four additional elasticity moduli appear in addition to the classical Lamé constants.

Cosserat elastoplasticity theory is also well-established. von Mises classical plasticity can be extended to micropolar continua in a straightforward manner. The yield criterion depends on both force- and couple-stresses:

$$f(\sigma,\mu) = \sqrt{\frac{3}{2}\left(a_1 s_{ij}s_{ij} + a_2 s_{ij}s_{ji} + b_1\mu_{ij}\mu_{ij} + b_2\mu_{ij}\mu_{ji}\right)} - R \quad (853)$$

Where,

s
: Stress deviator

a_i **and** b_i
: Material constants

Cosserat continuum theory can be applied to several classes of materials with microstructures as honeycombs, liquid crystals, rocks and granular media, cellular solids and dislocated crystals.

Hill's Law for Orthotropic Plastic Shells

Hill's law models an anisotropic yield behavior. It can be considered as a generalization of von Mises yield criteria for anisotropic yield behavior.

The yield surface defined by Hill can be written in a general form:

$$F(\sigma_{22}-\sigma_{33})^2 + G(\sigma_{33}-\sigma_{11})^2 + H(\sigma_{11}-\sigma_{22})^2 + 2L\sigma_{23}^2 +$$
$$2M\sigma_{31}^2 + 2N\sigma_{12}^2 - 1 = 0 \quad (854)$$

Where, the coefficients F, G, H, L, M and N are the constants obtained by the material tests in different orientations. The stress components σ_{1j} are expressed in the Cartesian reference parallel to

[94] Cosserat E. and Cosserat F., "Theory of Deformable Bodies", Hermann, Paris, 1909.

[95] Forest S. and Sab K., "Cosserat overall modeling of heterogeneous materials", Mechanics Research Communications, Vol. 25, No. 4, pp. 449-454, 1998.

[96] Forest S., Cailletaud G. and Sievert R., "A Cosserat Theory for Elastoviscoplastic Single Crystals at Finite Deformation", Archives of Mechanics, Vol. 49, pp. 705-736, 1997.

[97] Besson J., Bultel F., and Forest S., "Plasticity Cosserat media. Application to particular composites particles", 4th Symposium Calculation of Structures, CSMA/Teksea, Toulouse, pp. 759-764, 1999.

[98] Forest S., "Cosserat Media", ed. by K.H.J. Buschow, R.W. Cahn, M.C. Flemings, B. Ilschner, E.J. Kramer and S. Mahajan, Encyclopedia of Materials, Science and Technology, Elsevier, 2001.

the three planes of anisotropy. Equation 854 is equivalent to von Mises yield criteria if the material is isotropic.

In a general case, the loading direction is not the orthotropic direction. In addition, we are concerned with the plane stress assumption for shell structures. In planar anisotropy, the anisotropy is characterized by different strengths in different directions in the plane of the sheet. The plane stress assumption will enable to simplify Equation 854, and write the expression of equivalent stress σ_{eq} as:

$$\sigma_{eq} = \sqrt{A_1\sigma_{11}^2 + A_2\sigma_{22}^2 - A_3\sigma_{11}\sigma_{22} + A_{12}\sigma_{12}^2} \tag{855}$$

The coefficients A_1 are determined using Lankford's anisotropy parameter r_α:

$$\begin{aligned} &R = \frac{r_{00}+2r_{45}+r_{90}}{4} \quad ; \quad H = \frac{R}{1+R} \quad ; \quad A_1 = H\left(1+\frac{1}{r_{00}}\right) \\ &A_2 = H\left(1+\frac{1}{r_{90}}\right) \quad ; \quad A_3 = 2H \quad ; \quad A_{12} = 2H\left(r_{45}+0.5\right)\left(\frac{1}{r_{00}}+\frac{1}{r_{90}}\right) \end{aligned} \tag{856}$$

Where, the Lankford's anisotropy parameters r_α are determined by performing a simple tension test at angle α to orthotropic direction 1:

$$r_\alpha = \frac{d\varepsilon_{\alpha+\frac{\pi}{2}}}{d\varepsilon_{33}} = \frac{H + (2N - F - G - 4H)Sin^2\alpha\, Cos^2\alpha}{F\, Sin^2\alpha + G\, Cos^2\alpha} \tag{857}$$

The equivalent stress σ_{eq} is compared to the yield stress σ_y which varies in function of plastic strain ε_p and the strain rate $\dot{\varepsilon}$ (LAW32):

$$\sigma_y = a\left(\varepsilon_0 + \varepsilon_p\right)^n .\max\left(\dot{\varepsilon}, \dot{\varepsilon}_0\right)^m \tag{858}$$

Therefore, the elastic limit is obtained by:

$$\sigma_0 = \mathrm{a}\left(\varepsilon_0\right)^n .\left(\dot{\varepsilon}_0\right)^m \tag{859}$$

The yield stress variation is shown in Figure 195.

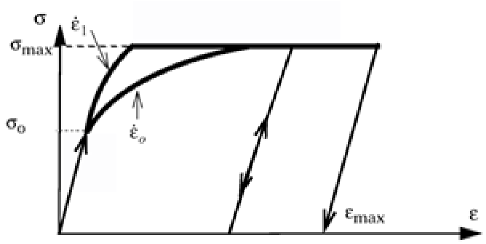

Figure 195: Yield Stress Variation

The strain rates are defined at integration points. The maximum value is taken into account:

$$\frac{d\varepsilon}{dt} = \max\left(\frac{d\varepsilon_x}{dt}, \frac{d\varepsilon_y}{dt}, 2\frac{d}{dt}\left(\varepsilon_{xy}\right)\right) \tag{860}$$

In Radioss, it is also possible to introduce the yield stress variation by a user-defined function (LAW43). Then, several curves are defined to take into account the strain rate effect.

It should be noted that as Hill's law is an orthotropic law, it must be used for elements with orthotropy properties as TYPE9 and TYPE10 in Radioss.

Anistropic Hill Material Law with MMC Fracture Model (LAW72)

This material law uses an anistropic Hill yield function along with an associated flow rule. A simple isotropic hardening model is used coupled with a modified Mohr fracture criteria. The yield condition is written as:

$$\varphi(\sigma, \sigma_y) = \sigma_{Hill} - \sigma_y = 0$$

Where, σ_{Hill} is the Equivalent Hill stress given as:

- For 3D model (Solid)

$$\sigma_{Hill} = \sqrt{F(\sigma_{yy} - \sigma_{zz})^2 + G(\sigma_{zz} - \sigma_{xx})^2 + H(\sigma_{xx} - \sigma_{yy})^2 + 2L\sigma_{yz}^2 + 2M\sigma_{zx}^2 + 2N\sigma_{xy}^2}$$

- For Shell

$$\sigma_{hill} = \sqrt{F\sigma_{yy}2 + G\sigma_{xx}2 + H(\sigma_{xx} - \sigma_{yy})^2 + 2N\sigma_{xy}^2}$$

Where, F, G, H, N, M, and L are six Hill anisotropic parameters.

For the yield surface a modified swift law is employed to describe the isotropic hardening in the application of the plasticity models:

$$\sigma_y = \sigma_y^0(\varepsilon_p^0 + \varepsilon_p)^n$$

Where,

σ_y^0	Initial yield stress
ε_p^0	Initial equivalent plastic strain
ε_p	Equivalent plastic strain
n	Material constant

Modified Mohr fracture criteria

A damage accumulation is computed as:

$$D = \int_0^{\varepsilon_p} \frac{d\varepsilon_p}{\varepsilon_f(\theta, \eta)}$$

Where, ε_f is a plastic strain fracture for the modified Mohr fracture criteria is given by:

- Anisotropic 3D model

$$\varepsilon_f = \left\{ \frac{\sigma_y^0}{C_2}\left[C_3 + \frac{\sqrt{3}}{2-\sqrt{3}}(1 - C_3)\left(\sec(\frac{\theta\pi}{6}) - 1\right) \right]\left[\sqrt{\frac{1+C_1^2}{3}}\cos(\frac{\theta\pi}{6}) + C_1\left(\eta + \frac{1}{3}\sin(\frac{\theta\pi}{6})\right) \right] \right\}^{-\frac{1}{n}}$$

with:

$$\begin{cases} \theta = 1 - \frac{2}{\pi} \arccos \xi \\ \xi = \frac{27}{2} \frac{J_3}{\sigma_{VM}^3} \\ \eta = \frac{\frac{1}{3}(\sigma_{xx}+\sigma_{yy}+\sigma_{zz})}{\sigma_{VM}} \end{cases}$$

Where,

J_3 Third invariant of the deviatoric stress

- 2D Anisotropic Model

$$\varepsilon_f = \left\{ \frac{\sigma_y^0}{C_2} f_3 \left[\left(\sqrt{\frac{1+C_1^2}{3}} f_1 \right) + C_1 \left(\eta + \frac{f_2}{3} \right) \right] \right\}^{-\frac{1}{n}}$$

With:

$$\begin{cases} f_1 = \cos\left\{ \frac{1}{3} \arcsin\left[-\frac{27}{2} \eta \left(\eta^2 - \frac{1}{3} \right) \right] \right\} \\ f_2 = \sin\left\{ \frac{1}{3} \arcsin\left[-\frac{27}{2} \eta \left(\eta^2 - \frac{1}{3} \right) \right] \right\} \\ f_3 = C_3 + \frac{\sqrt{3}}{2-\sqrt{3}} (1 - C_3) \left(\frac{1}{f_1} - 1 \right) \end{cases}$$

Where,

C_1, C_2 **and** C_3 Parameters for MMC fracture model

The fracture initiates when D = 1.
In order to represent realistic process of an element, a softening function β is introduced to reduce the deformation resistance. The yield surface is modified as:

$$\sigma_y = \beta \sigma_y^0 \left(\varepsilon_p^0 + \varepsilon_p \right)^n$$

with $\beta = \left(\frac{D_c - D}{D_c - 1} \right)^m$

Where,

D_c Critical damage

We have crack propagation when $1 < D < D_C$ in this case $0 < \beta < 1$ is considered to reduce the yield surface otherwise the β =1.

The element is deleted if $D \geq D_c$.

Elastic-plastic Orthotropic Composite Shells

Two kinds of composite shells may be considered in the modeling:

- Composite shells with isotropic layers
- Composite shells with at least one orthotropic layer

The first case can be modeled by an isotropic material where the composite property is defined in element property definition as explained in Element Library. However, in the case of composite shell with orthotropic layers the definition of a convenient material law is needed. Two dedicated material laws for composite orthotropic shells exist in Radioss:

- Material law COMPSH (25) with orthotropic elasticity, two plasticity models and brittle tensile failure,
- Material law CHANG (15) with orthotropic elasticity, fully coupled plasticity and failure models.

These laws are described here. The description of elastic-plastic orthotropic composite laws for solids is presented in the next section.

Tensile Behavior

The tensile behavior is shown in Figure 197. The behavior starts with an elastic phase. Then, reached to the yield state, the material may undergo an elastic-plastic work hardening with anisotropic Tsai-Wu yield criteria. It is possible to take into account the material damage. The failure can occur in the elastic stage or after plastification. It is started by a damage phase then conducted by the formation of a crack. The maximum damage factor will allow these two phases to separate. The unloading can happen during the elastic, elastic-plastic or damage phase. The damage factor d varies during deformation as in the case of isotropic material laws (LAW27). However, three damage factors are computed; two damage factors d_1 and d_2 for orthotropy directions and the other d_3 for delamination:

$$\begin{aligned}\sigma_{11} &= E_{11}(1-d_1)\varepsilon_{11}\\ \sigma_{22} &= E_{22}(1-d_2)\varepsilon_{22}\\ \sigma_{12} &= G_{12}(1-d_1)(1-d_2)\gamma_{12}\end{aligned} \tag{861}$$

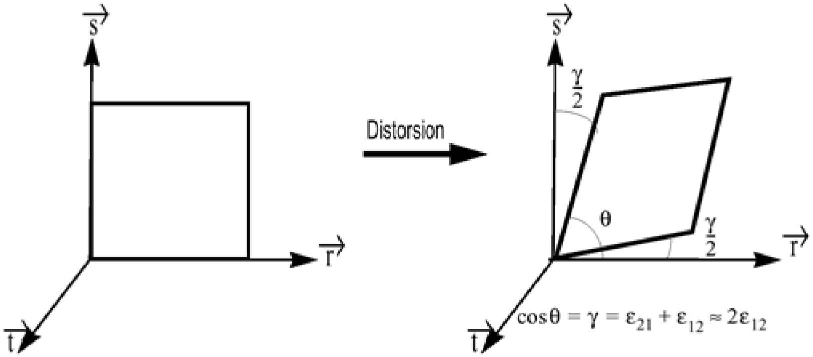

Figure 196: Shear Strain

Where, d_1 and d_2 are the tensile damages factors. The damage and failure behavior is defined by introduction of the following input parameters:

ε_{t1}	Tensile failure strain in direction 1
ε_{m1}	Maximum strain in direction 1
ε_{t2}	Tensile failure strain in direction 2

ε_{m2}	Maximum strain in direction 2
d$_{\max}$	Maximum damage (residual stiffness after failure)

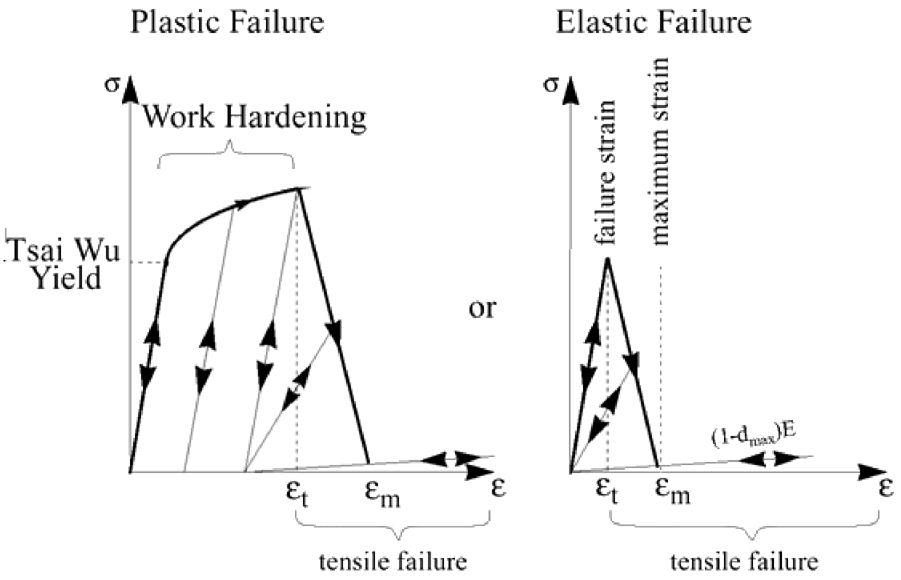

Figure 197: Tensile Behavior of Composite Shells

Delamination

The delamination equations are:

$$\sigma_{31} = G_{31}(1 - d_3)\gamma_{31} \tag{862}$$

$$\sigma_{23} = G_{23}(1 - d_3)\gamma_{23} \tag{863}$$

Where, d_3 is the delamination damage factor. The damage evolution law is linear with respect to the shear strain.

Let $\gamma = \sqrt{\gamma_{31}^2 + \gamma_{23}^2}$ then:

for d_3 # γ=γ_{ini} (864)

for d_3=1 # γ=$\gamma_{\max}$

Plastic Behavior

The plasticity model is based on the Tsai-Wu criterion [99] which enable to model the yield and failure phases.

$$F(\sigma) = F_1\sigma_1 + F_2\sigma_2 + F_{11}\sigma_1^2 + F_{22}\sigma_2^2 + F_{44}\sigma_{12}^2 + 2F_{12}\sigma_1\sigma_2 \tag{865}$$

Where,

$$F_1 = -\frac{1}{\sigma_{1y}^c} + \frac{1}{\sigma_{1y}^t} \tag{866}$$

$$F_{22} = \frac{1}{\sigma_{2y}^c\sigma_{2y}^t} \tag{867}$$

$$F_2 = -\frac{1}{\sigma_{2y}^c} + \frac{1}{\sigma_{2y}^t} \tag{868}$$

$$F_{44} = \frac{1}{\sigma_{12y}^c\sigma_{12y}^t} \tag{869}$$

$$F_{11} = \frac{1}{\sigma_{1y}^c\sigma_{1y}^t} \tag{870}$$

$$F_{12} = -\frac{\alpha}{2}\sqrt{F_{11}F_{22}} \tag{871}$$

Where, α is the reduction factor. The six other parameters are the yield stresses in tension and compression for the orthotropy directions which can be obtained uniaxial loading tests:

σ_{1y}^t	Tension in direction 1 of orthotropy
σ_{2y}^t	Tension in direction 2 of orthotropy
σ_{1y}^c	Compression in direction 1 of orthotropy
σ_{2y}^c	Compression in direction 2 of orthotropy
σ_{12y}^c	Compression in direction 12 of orthotropy
σ_{12y}^t	Tension in direction 12 of orthotropy

The Tsai-Wu criteria are used to determine the material behavior:

- $F(\sigma) < 1$: elastic state
- $F(\sigma) = 1$: plastic admissible state
- $F(\sigma) > 1$: plastically inadmissible stresses

(872)

For $F(\sigma) = 1$ the cross-sections of Tsai-Wu function with the planes of stresses in orthotropic directions is shown in Figure 198.

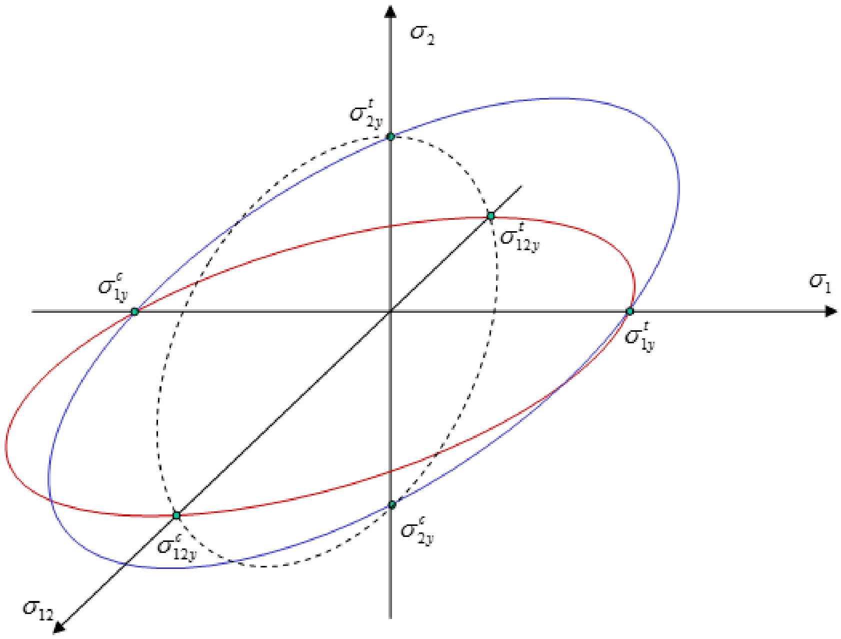

Figure 198:Cross-sections of Tsai-Wu Yield Surface For $F(\sigma) = 1$

If $F(\sigma) > 1$, the stresses must be projected on the yield surface to satisfy the flow rule. $F(\sigma)$ is compared to a maximum value $F(W_p)$ varying in function of the plastic work W_p during work hardening phase:

$$F(\sigma) = F(W_p) = 1 + bW_p^n \tag{873}$$

Where,

b	Hardening parameter
n	Hardening exponent

Therefore, the plasticity hardening is isotropic as illustrated in Figure 199.

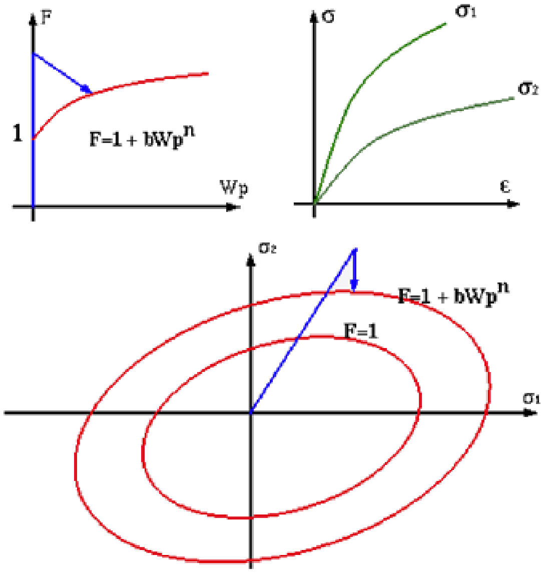

Figure 199: Isotropic Plasticity Hardening

Failure Behavior

The Tsai-Wu flow surface is also used to estimate the material rupture by means of two variables:

- plastic work limit $W_p^{\max}$,
- maximum value of yield function $F_{\max}$

If one of the two conditions is satisfied, the material is ruptured. The evolution of yield surface during work hardening of the material is shown in Figure 200.

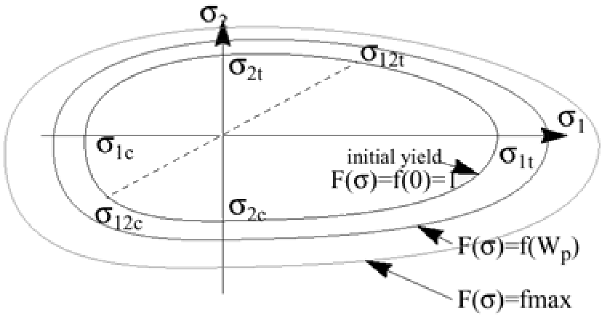

Figure 200: Evolution of Tsai-Wu Yield Surface

The model will allow the simulation of the brittle failure by formation of cracks. The cracks can either be oriented parallel or perpendicular to the orthotropic reference frame (or fiber direction), as shown in Figure 201. For plastic failure, if the plastic work W_p is larger than the maximum value $W_p^{\max}$ for a given

[99] Tsai S.W. and Wu E.M., "A general theory of strength for anisotropic materials", Journal of Composite Materials, 58-80, 1971.

element, then the element is considered to be ruptured. However, for a multi-layer shell, several criteria may be considered to model a total failure. The failure may happen:

- If $W_p > W_p^{\max}$ for one layer,
- If $W_p > W_p^{\max}$ for all layers,
- If $W_p > W_p^{\max}$ or tensile failure in direction 1 for each layer,
- If $W_p > W_p^{\max}$ or tensile failure in direction 2 for each layer,
- If $W_p > W_p^{\max}$ or tensile failure in directions 1 and 2 for each layer,
- If $W_p > W_p^{\max}$ or tensile failure in direction 1 for all layers,
- If $W_p > W_p^{\max}$ or tensile failure in direction 2 for all layers,
- If $W_p > W_p^{\max}$ or tensile failure in directions 1 and 2 for each layer.

The last two cases are the most physical behaviors; but the use of failure criteria depends, at first, to the analyst’s choice. In Radioss the flag I_{off} defines the used failure criteria in the computation.

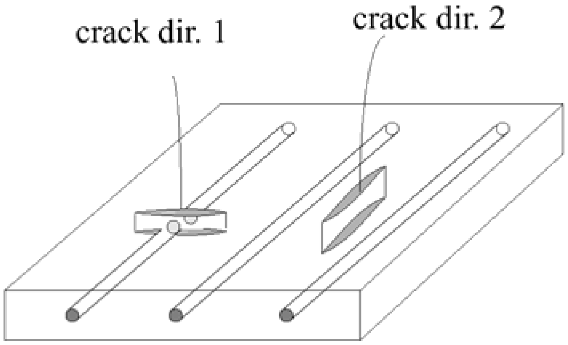

Figure 201: Crack Orientation

In practice, the use of brittle failure model allows to estimate correctly the physical behavior of a large rang of composites. But on the other hand, some numerical oscillations may be generated due to the high sensibility of the model. In this case, the introduction of an artificial material viscosity is recommended to stabilize results. In addition, in brittle failure model, only tension stresses are considered in cracking procedure.

The ductile failure model allows plasticity to absorb energy during a large deformation phase. Therefore, the model is numerically more stable. This is represented by CRASURV model in Radioss. The model makes also possible to take into account the failure in tension, compression and shear directions.

Strain Rate Effect

The strain rate is taken into account within the modification of Plastic Behavior, Equation 873 which acts through a scale factor:

$$F(W_p, \dot{\varepsilon}) = \left(1 + b\left(\frac{W_p}{W_p^{ref}}\right)^n\right) * \left(1 + c\ln\left(\frac{\dot{\varepsilon}}{\dot{\varepsilon}_0}\right)\right) \tag{874}$$

Where,

W_p	Plastic work
W_{pref}	Reference plastic work
b	Plastic hardening parameter
n	Plastic hardening exponent
c	Strain rate coefficient (equal to zero for static loading)

The last equation implies the growing of the Tsai-Wu yield surface when the dynamic effects are increasing. The effects of strain rate are illustrated in Figure 202.

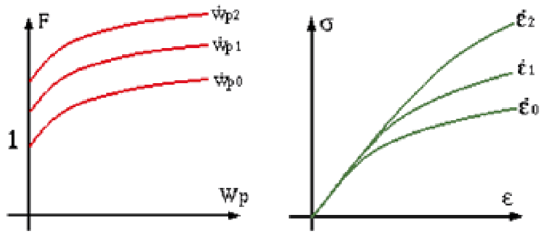

Figure 202: Strain Rate Effect in Work Hardening

CRASURV Model

The CRASURV model is an improved version of the former law based on the standard Tsai-Wu criteria. The main changes concern the expression of the yield surface before plastification and during work hardening. First, in CRASURV model the coefficient F_{44} in Plastic Behavior, Equation 865 depends only on one input parameter:

$$F_{44}\left(W_p^*, \dot{\varepsilon}\right) = \frac{1}{\sigma_{12}\left(W_p^*, \dot{\varepsilon}\right) \cdot \sigma_{12}\left(W_p^*, \dot{\varepsilon}\right)} \tag{875}$$

With $\sigma_{12}\left(W_p^*, \dot{\varepsilon}\right) = \sigma_{12y}\left(1 + b_{12}\left(W_p^*\right)^{n_{12}}\right)\left(1 + c_{12}\ln\left(\frac{\dot{\varepsilon}}{\dot{\varepsilon}_0}\right)\right)$

Another modification concerns the parameters F_{ij} in Plastic Behavior, Equation 865 which are expressed now in function of plastic work and plastic work rate as in Strain Rate Effect, Equation 874:

$$\begin{aligned} F\left(W_p^*\right) = {} & F_1\left(W_p^*, \dot{\varepsilon}\right)\sigma_1 + F_2\left(W_p^*, \dot{\varepsilon}\right)\sigma_2 + F_{11}\left(W_p^*, \dot{\varepsilon}\right)\sigma_1^2 + F_{22}\left(W_p^*, \dot{\varepsilon}\right)\sigma_2^2 \\ & + 2F_{12}\left(W_p^*, \dot{\varepsilon}\right)\sigma_1\sigma_2 + F_{44}\left(W_p^*, \dot{\varepsilon}\right)\sigma_{12}^2 \end{aligned} \tag{876}$$

With

$$F_i\left(W_p^*, \dot{\varepsilon}\right) = -\frac{1}{\sigma_i^c\left(W_p^*, \dot{\varepsilon}\right)} + \frac{1}{\sigma_i^t\left(W_p^*, \dot{\varepsilon}\right)} \quad (i{=}12)$$

$$F_{ii}\left(W_p^*,\ \dot{\varepsilon}\right)=\frac{1}{\sigma_i^c\left(W_p^*,\ \dot{\varepsilon}\right)\cdot\sigma_i^t\left(W_p^*,\ \dot{\varepsilon}\right)}\ (i=12)$$

$$F_{12}\left(W_p^*,\dot{\varepsilon}\right)=-\frac{\alpha}{2}\sqrt{F_{11}\left(W_p^*,\dot{\varepsilon}\right)F_{22}\left(W_p^*,\dot{\varepsilon}\right)}$$

$$F_{44}\left(W_p^*,\dot{\varepsilon}\right)=\frac{1}{\sigma_{12}\left(W_p^*,\dot{\varepsilon}\right)\cdot\sigma_{12}\left(W_p^*,\dot{\varepsilon}\right)}$$

And

$$\sigma_i^t\left(W_p^*,\dot{\varepsilon}\right)=\sigma_{iy}^t\left(1+b_i^t\left(W_p^*\right)^{n_i^t}\right)\left(1+c_i^t\ln\left(\frac{\dot{\varepsilon}}{\dot{\varepsilon}_0}\right)\right) \tag{877}$$

$$\sigma_i^c\left(W_p^*,\dot{\varepsilon}\right)=\sigma_{iy}^c\left(1+b_i^c\left(W_p^*\right)^{n_i^c}\right)\left(1+c_i^c\ln\left(\frac{\dot{\varepsilon}}{\dot{\varepsilon}_0}\right)\right) \tag{878}$$

$$\sigma_{12}\left(W_p^*,\dot{\varepsilon}\right)=\sigma_{12y}\left(1+b_{12}\left(W_p^*\right)^{n_{12}}\right)\left(1+c_{12}\ln\left(\frac{\dot{\varepsilon}}{\dot{\varepsilon}_0}\right)\right) \tag{879}$$

And $W_p^*=\frac{W_p}{W_p^{ref}}$

Where the five sets of coefficients b, n and c should be obtained by experience. The work hardening is shown in Figure 203.

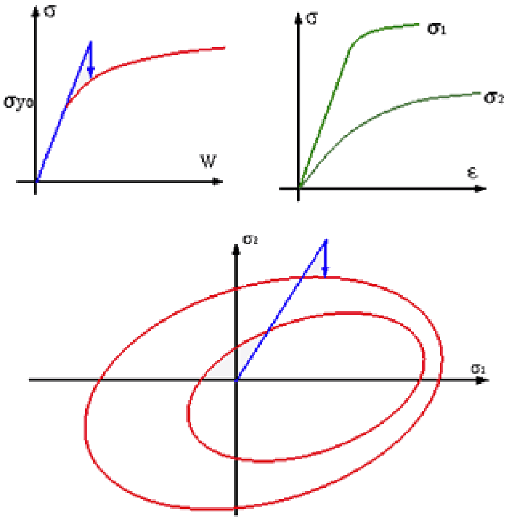

Figure 203: CRASURV Plasticity Hardening

The CRASURV model will allow the simulation of the ductile failure of orthotropic shells. The plastic and failure behaviors are different in tension and in compression. The stress softening may also be introduced in the model to take into account the residual Tsai-Wu stresses. The evolution of CRASURV criteria with hardening and softening works is illustrated in Figure 204.

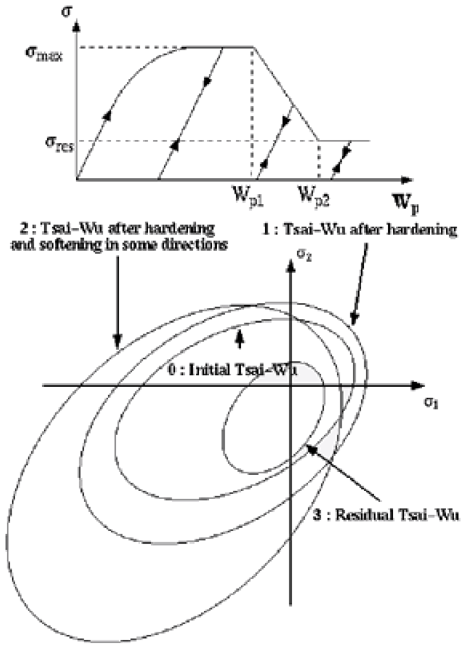
σ
σmax
σres
Wp1
Wp2
Wp
2 : Tsai–Wu after hardening and softening in some directions
1 : Tsai–Wu after hardening
σ2
0 : Initial Tsai–Wu
σ1
3 : Residual Tsai–Wu

Figure 204: Flow Surface in CRASURV Model

Chang Chang Model

Chang-Chang law [100], [101] incorporated in Radioss is a combination of the standard Tsai-Wu elastic-plastic law and a modified Chang-Chang failure criteria. [102] The affects of damage are taken into account by decreasing stress components using a relaxation technique to avoid numerical instabilities.

Six material parameters are used in the failure criteria:

S_1	Longitudinal tensile strength
S_2	Transverse tensile strength
S_{12}	Shear strength
C_1	Longitudinal compressive strength
C_2	Transverse compressive strength
β	Shear scaling factor

Where,

1	Fiber direction

The failure criterion for fiber breakage is written as:

- Tensile fiber mode: $\sigma_{11} > 0$

$$e_f^2 = \left(\frac{\sigma_{11}}{S_1}\right)^2 + \beta\left(\frac{\sigma_{12}}{S_{12}}\right)^2 - 1.0 \qquad \begin{cases} \geq 0 \; failed \\ < 0 \; elastic - plastic \end{cases} \tag{880}$$

- Compressive fiber mode: $\sigma_{11} < 0$

$$e_c^2 = \left(\frac{\sigma_{11}}{C_1}\right)^2 - 1.0 \qquad \begin{cases} \geq 0 \; failed \\ < 0 \; elastic - plastic \end{cases} \tag{881}$$

For matrix cracking, the failure criterion is:

- Tensile matrix mode: $\sigma_{22} > 0$

$$e_m^2 = \left(\frac{\sigma_{22}}{S_2}\right)^2 + \beta\left(\frac{\sigma_{12}}{S_{12}}\right) - 1.0 \qquad \begin{cases} \geq 0 \; failed \\ < 0 \; elastic - plastic \end{cases} \tag{882}$$

- Compressive matrix mode: $\sigma_{22} < 0$

$$e_d^2 = \left(\frac{\sigma_{22}}{2S_{12}}\right)^2 + \left[\left(\frac{C_2}{2S_{12}}\right)^2 - 1\right]\frac{\sigma_{22}}{C_2 +}\left(\frac{\sigma_{12}}{S_{12}}\right)^2 - 1.0 \qquad \begin{cases} \geq 0 \; failed \\ < 0 \; elastic - plastic \end{cases} \tag{883}$$

If the damage parameter is equal to or greater than 1.0, the stresses are decreased by using an exponential function to avoid numerical instabilities. A relaxation technique is used by gradually decreasing the stress:

$$[\sigma(t)] = f(t) * [\sigma_d(t_r)] \tag{884}$$

With: $f(t) = \exp\left(\frac{t - t_r}{T}\right)$ and $t \geq t_4$

Where,

t Time

t_r Start time of relaxation when the damage criteria are assumed

τ Time of dynamic relaxation

$[\sigma_d(t_r)]$ is the stress components at the beginning of damage (for matrix cracking $[\sigma_d(t_r)] = \begin{pmatrix} \sigma_{d22} \\ \sigma_{d12} \end{pmatrix}$).

[100] Chang, F.K. and Chang, K.Y., "A Progressive Damage Model For Laminated Composites Containing Stress Concentrations", Journal of Composite Materials, Vol 21, 834-855, 1987.

[101] Chang, F.K. and Chang K.Y., "Post-Failure Analysis of Bolted Composites Joints in Tension or Shear-Out Mode Failure", Journal of Composite Materials, Vol 21, 809-833, 1987.

[102] Matzenmiller A. and Schweizerhof K., "Crashworthiness Simulation of composite Structures-a first step with explicit time integration", Nonlinear Computational Mechanics-State of the Art Ed. p. Wriggers and W. Wagner, 1991.

Elastic-Plastic Orthotropic Composite Solids

The material LAW14 (COMPSO) in Radioss allows to simulate orthotropic elasticity, Tsai-Wu plasticity with damage, brittle rupture and strain rate effects. The constitutive law applies to only one layer of lamina. Therefore, each layer needs to be modeled by a solid mesh. A layer is characterized by one direction of the fiber or material. The overall behavior is assumed to be elasto-plastic orthotropic.

Direction 1 is the fiber direction, defined with respect to the local reference frame $\vec{r}, \vec{s}, \vec{t}$ as shown in Figure 205.

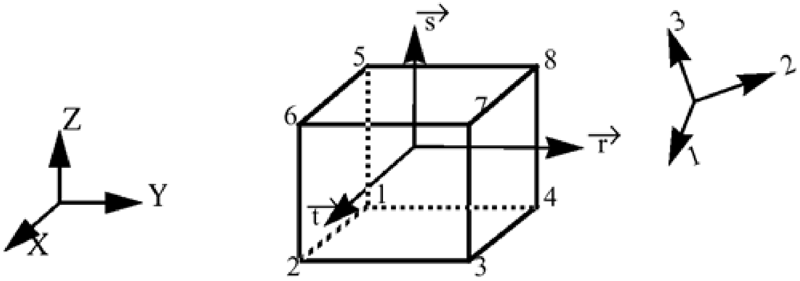

Figure 205: Local Reference Frame

For the case of unidirectional orthotropy (that is, $E_{33} = E_{22}$ and $G_{31} = G_{12}$) the material LAW53 in Radioss allows to simulate an orthotropic elastic-plastic behavior by using a modified Tsai-Wu criteria.

Linear Elasticity

When the lamina has a purely linear elastic behavior, the stress calculation algorithm:

- Transform the lamina stress, $\sigma_{ij}(t)$, and strain rate, d_{ij}, from global reference frame to fiber reference frame.
- Compute lamina stress at time $t + \Delta t$ by explicit time integration:

$$\sigma_{ij}(t + \Delta t) = \sigma_{ij}(t) + D_{ijkl} d_{kl} \Delta t \quad (885)$$

- Transform the lamina stress, $\sigma_{ij}(t + \Delta t)$, back to global reference frame.

The elastic constitutive matrix C of the lamina relates the non-null components of the stress tensor to those of strain tensor:

$$\{\sigma\} = [D]\{\varepsilon\} \quad (886)$$

The inverse relation is generally developed in term of the local material axes and nine independent elastic constants:

$$\begin{Bmatrix} \varepsilon_{11} \\ \varepsilon_{22} \\ \varepsilon_{33} \\ \gamma_{12} \\ \gamma_{23} \\ \gamma_{31} \end{Bmatrix} = \begin{bmatrix} \frac{1}{E_{11}} & -\frac{v_{21}}{E_{22}} & -\frac{v_{31}}{E_{33}} & 0 & 0 & 0 \\ & \frac{1}{E_{22}} & -\frac{v_{32}}{E_{33}} & 0 & 0 & 0 \\ & & \frac{1}{E_{33}} & 0 & 0 & 0 \\ & & & \frac{1}{2G_{12}} & 0 & 0 \\ & Symm. & & & \frac{1}{2G_{23}} & 0 \\ & & & & & \frac{1}{2G_{31}} \end{bmatrix} \begin{Bmatrix} \sigma_{11} \\ \sigma_{22} \\ \sigma_{33} \\ \sigma_{12} \\ \sigma_{23} \\ \sigma_{31} \end{Bmatrix} \tag{887}$$

Where,

E_{ij}	Young's modulus
G_{ij}	Shear modulus
v_{ij}	Poisson's ratios
γ_{ij}	Strain components due to the distortion

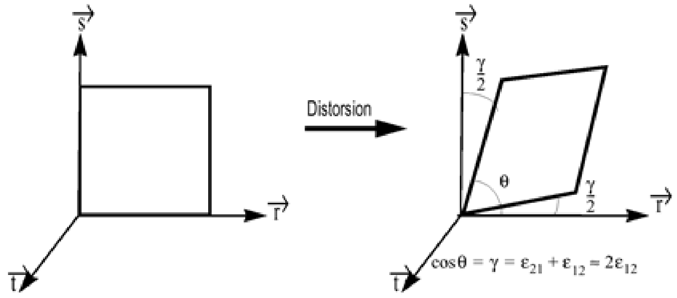

Figure 206: Strain Components and Distortion

Orthotropic Plasticity

Lamina yield surface defined by Tsai-Wu yield criteria is used for each layer:

$$\begin{aligned} F = f(W_p) = F_1\sigma_1 + F_2\sigma_2 + F_3\sigma_3 + F_{11}\sigma_1^2 + F_{22}\sigma_2^2 + F_{33}\sigma_3^2 + F_{44}\sigma_{12}^2 \\ + F_{55}\sigma_{23}^2 + F_{66}\sigma_{31}^2 + 2F_{12}\sigma_1\sigma_2 + 2F_{23}\sigma_2\sigma_3 + 2F_{13}\sigma_1\sigma_3 \end{aligned} \tag{888}$$

with:

$F_i = -\frac{1}{\sigma_{iy}^c} + \frac{1}{\sigma_{iy}^t}$ (i=1,2,3);

$F_{11} = \frac{1}{\sigma_{1y}^c \sigma_{1y}^t}$; $F_{22} = \frac{1}{\sigma_{2y}^c \sigma_{2y}^t}$; $F_{33} = \frac{1}{\sigma_{3y}^c \sigma_{3y}^t}$;

$$F_{44} = \frac{1}{\sigma^c_{12y}\sigma^t_{12y}};\ F_{55} = \frac{1}{\sigma^c_{23y}\sigma^t_{23y}};\ F_{66} = \frac{1}{\sigma^c_{31y}\sigma^t_{31y}};$$

$$F_{12} = -\frac{1}{2}\sqrt{(F_{11}F_{22})}\ ;\ F_{23} = -\frac{1}{2}F_{22}$$

Where, σ_i is the yield stress in direction i, c and t denote respectively for compression and tension.

$f(W_p)$ represents the yield envelope evolution during work hardening with respect to strain rate effects:

$$f(W_p) = \left(1 + B \cdot W_p^n\right)\left(1 + c.\ln\left(\frac{\dot{\varepsilon}}{\dot{\varepsilon}_0}\right)\right) \tag{889}$$

Where,

W_p	Plastic work
B	Hardening parameter
n	Hardening exponent
c	Strain rate coefficient

$f(W_p)$ is limited by a maximum value $f_{\max}$:

$$f(W_p) \le f_{\max} = \left(\frac{\sigma_{\max}}{\sigma_y}\right)^2 \tag{890}$$

If the maximum value is reached the material is failed.

In Equation 889, the strain rate effects on the evolution of yield envelope. However, it is also possible to take into account the strain rate $\dot{\varepsilon}$ effects on the maximum stress $\sigma_{\max}$ as shown in Figure 207.

(a) Strain rate effect on $\sigma_{\max}$	**(b) No strain rate effect on $\sigma_{\max}$**
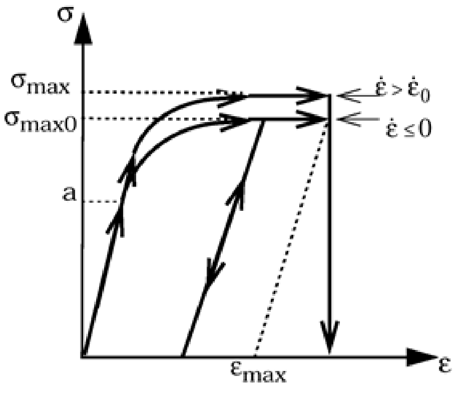	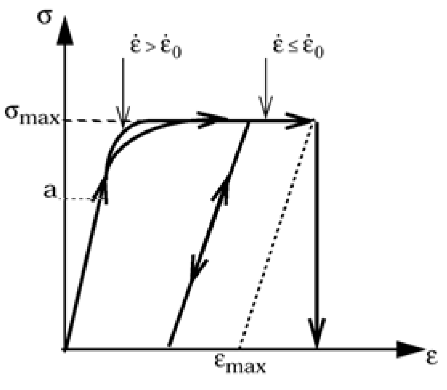
$\sigma = \sigma_y\left(1 + c.\ln\left(\frac{\dot{\varepsilon}}{\dot{\varepsilon}_0}\right)\right)$ $\sigma_{\max} = \sigma^0_{\max}\left(1 + c.\ln\left(\frac{\dot{\varepsilon}}{\dot{\varepsilon}_0}\right)\right)$	$\sigma = \sigma_y\left(1 + c.\ln\left(\frac{\dot{\varepsilon}}{\dot{\varepsilon}_0}\right)\right)$ $\sigma_{\max} = \sigma^0_{\max}$

(a) Strain rate effect on $\sigma_{\max}$	(b) No strain rate effect on $\sigma_{\max}$
$f_{\max} = \left(\frac{\sigma_{\max}}{\sigma_y}\right)^2$	

Figure 207: Strain Rate Dependency

Unidirectional Orthotropy

LAW 53 in Radioss provides a simple model for unidirectional orthotropic solids with plasticity. The unidirectional orthotropy condition implies:

$$E_{33} = E_{22} \quad \text{(891)}$$
$$G_{31} = G_{12}$$

The orthotropic plasticity behavior is modeled by a modified Tsai-Wu criterion (Orthotropic Plasticity, Equation 888) in which:

$$F_{12} = \frac{2}{\left(\sigma_y^{45c}\right)^2} - \frac{1}{2}\left(F_{11} + F_{22} + F_{44}\right) + \frac{F_1 + F_2}{\sigma_y^{45c}} \quad \text{(892)}$$

Where, σ_y^{45c} is yield stress in 45° unidirectional test. The yield stresses in direction 11, 22, 12, 13 and 45° are defined by independent curves obtained by unidirectional tests (Figure 208). The curves give the stress variation in function of a so-called strain ε_v:

$$\varepsilon_v = 1 - (Trace[\varepsilon]) \quad \text{(893)}$$

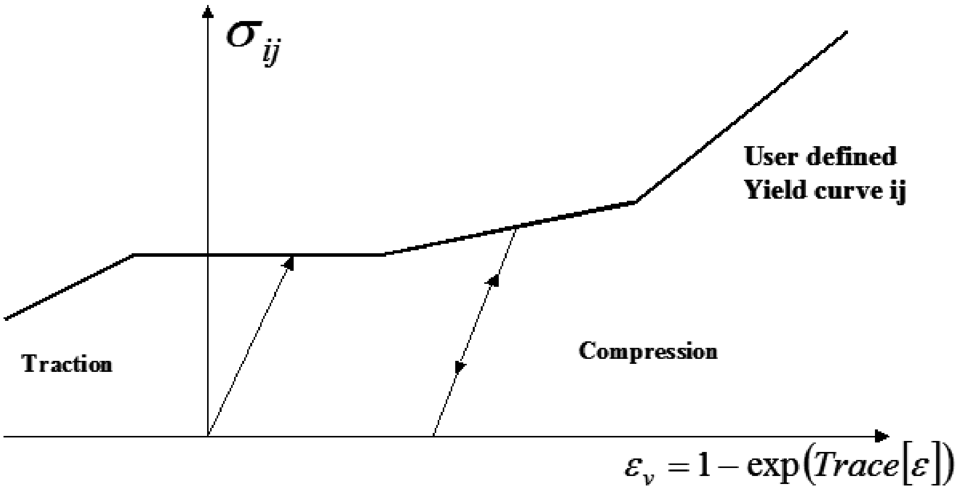

Figure 208: Yield Stress Curve for a Unidirectional Orthotropic Material

Elastic-plastic Anisotropic Shells (Barlat's Law)

Barlat's 3- parameter plasticity model is developed in F. Barlat, J. Lian [103] for modeling of sheet under plane stress assumption with an anisotropic plasticity model. The anisotropic yield stress criterion for plane stress is defined as:

$$F = a\left|K_1 + K_2\right|^m + a\left|K_1 - K_2\right|^m + c\left|2K_2\right|^m - 2\left(\sigma_e\right)^m \tag{894}$$

Where, σ_e is the yield stress, a and c are anisotropic material constants, m exponent and K_1 and K_2 are defined by:

$$\begin{aligned} K_1 &= \frac{\sigma_{xx} - h\sigma_{yy}}{2} \\ K_2 &= \sqrt{\left(\frac{\sigma_{xx} - h\sigma_{yy}}{2}\right)^2 + p^2\left(\sigma_{xy}\right)^2} \end{aligned} \tag{895}$$

Where, h and p are additional anisotropic material constants. All anisotropic material constants, except for p which is obtained implicitly, are determined from Barlat width to thickness strain ratio R from:

$$\begin{aligned} a &= 2 - 2\sqrt{\left(\frac{R_{00}}{1+R_{00}}\right)\left(\frac{R_{90}}{1+R_{90}}\right)} \\ c &= 2 - a \\ h &= \sqrt{\left(\frac{R_{00}}{1+R_{00}}\right)\left(\frac{1+R_{90}}{R_{90}}\right)} \end{aligned} \tag{896}$$

The width to thickness ratio for any angle ϕ can be calculated: [103]

$$R_\phi = \frac{2m\left(\sigma_e\right)^m}{\left(\frac{\partial F}{\partial \sigma_{xx}} + \frac{\partial F}{\partial \sigma_{yy}}\right)\sigma_\phi} - 1 \tag{897}$$

Where, σ_ϕ is the uniaxial tension in the ϕ direction. Let ϕ = 45°, Equation 897 gives an equation from which the anisotropy parameter p can be computed implicitly by using an iterative procedure:

$$\frac{2m\left(\sigma_e\right)^m}{\left(\frac{\partial F}{\partial \sigma_{xx}} + \frac{\partial F}{\partial \sigma_{yy}}\right)\sigma_{45}} - 1 - R_{45} = 0 \tag{898}$$

Note: Barlat's law reduces to Hill's law when using m=2

[103] Barlat F. and Lian J., "Plastic behavior and stretchability of sheet metals, Part I: A yield function for orthoropic sheets under plane stress conditions", International Journal of Plasticity, Vol. 5, pp. 51-66, 1989.

Elastic-plasticity of Isotropic Materials

The strain hardening behavior of materials is a major factor in structural response as metal working processes or plastic instability problems. A proper description of strain hardening at large plastic strains is generally imperative. For many plasticity problems, the hardening behavior of the material is simply characterized by the strain-stress curve of the material. For the proportional loading this is generally true. However, if the loading path is combined, the characterization by a simple strain-stress curve is no longer adequate.

The incremental plasticity theory is generally used in computational methods. Plasticity models are written as rate-dependent or independent. A rate-dependent model is a one in which the strain rate does affect the constitutive law. This is true for a large range of metals at low temperature relative to their melting temperature.

Most isotropic elastic-plastic material laws in Radioss use von Mises yield criteria as given in Stresses in Solids. Several kinds of models are integrated. The models involve damage for ductile or brittle failures with or without dislocation. The cumulative damage law can be used to access failure. The next few paragraphs describe theoretical bases of the integrated models.

Johnson-Cook Plasticity Model (LAW2)

In this law the material behaves as linear elastic when the equivalent stress is lower than the yield stress.

For higher value of stress, the material behavior is plastic. This law is valid for brick, shell, truss and beam elements. The relation between describing stress during plastic deformation is given in a closed form:

$$\sigma = \left(a + b\varepsilon_p^n\right)\left(1 + c\ln\frac{\dot{\varepsilon}}{\dot{\varepsilon}_0}\right)\left(1 - T^{*m}\right) \tag{899}$$

Where,

σ
: Flow stress (Elastic + Plastic Components)

ε_p
: Plastic strain (True strain)

a
: Yield stress

b
: Hardening modulus

n
: Hardening exponent

c
: Strain rate coefficient

$\dot{\varepsilon}$
: Strain rate

$\dot{\varepsilon}_0$
: Reference strain rate

m
: Temperature exponent

$$\mathrm{T}^* = \frac{\mathrm{T} - 298}{\mathrm{T}_{melt} - 298}$$

T

T_{melt}

Melting temperature in Kelvin degrees. The adiabatic conditions are assumed for temperature computation:

$$\mathrm{T} = \mathrm{T}_i + \frac{E_{\mathrm{int}}}{\rho C_\rho (Volume)} \tag{900}$$

Where,

ρC_p

Specific heat per unit of volume

T_i

Initial temperature (in degrees Kelvin)

E_{int}

Internal energy

Two optional additional inputs are:

σ_{max0}

Maximum flow stress

$\varepsilon_{\mathrm{max}}$

Plastic strain at rupture

Figure 209 shows a typical stress-strain curve in the plastic region. When the maximum stress is reached during computation, the stress remains constant and material undergoes deformation until the maximum plastic strain. Element rupture occurs if the plastic strain is larger than $\varepsilon_{\mathrm{max}}$. If the element is a shell, the ruptured element is deleted. If the element is a solid element, the ruptured element has its deviatoric stress tensor permanently set to zero, but the element is not deleted. Therefore, the material rupture is modeled without any damage effect.

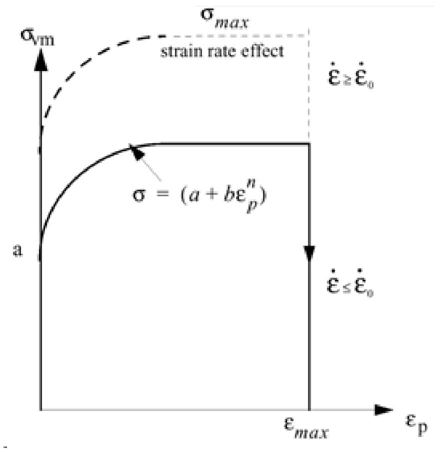
σ_{max}
σ_{vm}
strain rate effect
$\dot{\varepsilon} \geq \dot{\varepsilon}_0$
$\sigma = (a + b\varepsilon_p^n)$
a
$\dot{\varepsilon} \leq \dot{\varepsilon}_0$
ε_{max}
ε_p

Figure 209: Stress - Plastic Strain Curve

C

C_{hard} in this material law is same like in `/MAT/LAW44`. For more details on C_{hard}, refer to Cowper-Symonds Plasticity Model (LAW44).

Strain Rate Definition

Regarding to the plastification method used, the strain rate expression is different. If the progressive plastification method is used (that is, integration points through the thickness for thin-walled structured), the strain rate is:

$$\frac{d\varepsilon}{dt}=\max\left(\frac{d\varepsilon_x}{dt},\frac{d\varepsilon_y}{dt},2\frac{d}{dt}\left(\varepsilon_{xy}\right)\right) \tag{901}$$

$$\varepsilon_{xy}=\frac{1}{2}\gamma_{xy} \tag{902}$$

With global plastification method:

$$\frac{d\varepsilon}{dt}=\left(\frac{dE_i/dt}{\sigma_{VM}}\right) \tag{903}$$

Where, E_i is the internal energy.

For solid elements, the maximum value of the strain rate components is used:

$$\dot{\varepsilon}=\max\left(\dot{\varepsilon}_x,\ \dot{\varepsilon}_y,\ \dot{\varepsilon}_z,\ 2\dot{\varepsilon}_{xy},\ 2\dot{\varepsilon}_{yz},\ 2\dot{\varepsilon}_{xz}\right) \tag{904}$$

Strain Rate Filtering

The strain rates exhibit very high frequency vibrations which are not physical. The strain rate filtering option will enable to damp those oscillations and; therefore obtain more physical strain rate values.

If there is no strain rate filtering, the equivalent strain rate is the maximum value of the strain rate components:

$$\dot{\varepsilon}_{eq}=\max\left(\dot{\varepsilon}_{x,}\dot{\varepsilon}_{y,}\dot{\varepsilon}_{z,}\,2\dot{\varepsilon}_{xy,}\,2\dot{\varepsilon}_{yz,}\,2\dot{\varepsilon}_{XZ}\right) \tag{905}$$

For thin-walled structures, the equivalent strain is computed by the following approach. If ε is the main component of strain tensor, the kinematic assumptions of thin-walled structures allows to decompose the in-plane strain into membrane and flexural deformations:

$$\varepsilon=KZ=\varepsilon_m \tag{906}$$

Then, the expression of internal energy can by written as:

$$E_i=\int_{-\frac{t}{2}}^{\frac{t}{2}}\sigma\varepsilon dz=\int_{-\frac{t}{2}}^{\frac{t}{2}}E\varepsilon^2dz=\int_{-\frac{t}{2}}^{\frac{t}{2}}E\left(\kappa z+\varepsilon_m\right)^2dz \tag{907}$$

Therefore:

$$E_i=\int_{-\frac{t}{2}}^{\frac{t}{2}}E(\kappa^2z^2+\varepsilon_m^2+2\kappa\varepsilon_m z)\,dz=E\left(\frac{1}{3}\kappa^2z^3+\varepsilon_m^2z+\kappa\varepsilon_m z^2\right)_{-\frac{t}{2}}^{\frac{t}{2}} \tag{908}$$

The expression can be simplified to:

$$E_i=E\left[\frac{1}{12}\kappa^2t^3+\varepsilon_m^2t\right]=E\varepsilon_{eq}^2t \tag{909}$$

$$\varepsilon_{eq} = \sqrt{\frac{1}{12}\kappa^2 t^2 + \varepsilon_m^2} \tag{910}$$

The expression of the strain rate is derived from Equation 906:

$$\dot{\varepsilon} = \dot{K}Z + \dot{\varepsilon}_m \tag{911}$$

Admitting the assumption that the strain rate is proportional to the strain, that is:

$$\dot{\varepsilon}_m = \alpha\varepsilon_m \tag{912}$$

$$\dot{K} = \alpha K \tag{913}$$

Therefore:

$$\dot{\varepsilon} = \alpha\varepsilon \tag{914}$$

Referring to Equation 910, it can be seen that an equivalent strain rate can be defined using a similar expression to the equivalent strain:

$$\dot{\varepsilon}_{eq} = \alpha\varepsilon_{eq} \tag{915}$$

$$\dot{\varepsilon}_{eq} = \sqrt{\frac{1}{12}\kappa^2 t^2 + \dot{\varepsilon}_m^2} \tag{916}$$

For solid elements, the strain rate is computed using the maximum element stretch:

$$\dot{\varepsilon}_{eq} = \dot{\lambda}_{\max} \tag{917}$$

The strain rate at integration point, i in `/ANIM/TENS/EPSDOT`/i $(1 < i < n)$ is calculated by:

$$\dot{\varepsilon}_i = \dot{\varepsilon}_{\mathrm{m}} - \frac{1}{2}\left(\frac{(2i-1)}{n} - 1\right)t\dot{\varepsilon}_b \tag{918}$$

Where,

$\dot{\varepsilon}_m$
Membrane strain rate `/ANIM/TENS/EPSDOT/MEMB`

$\dot{\varepsilon}_b$
Bending strain rate `/ANIM/TENS/EPSDOT/BEND`.

The strain rate in upper and lower layers is computed by:

$$\dot{\varepsilon}_u = \varepsilon_m + \frac{1}{2}t\dot{\varepsilon}_b \tag{919}$$

`/ANIM/TENS/EPSDOT/UPPER`

$$\dot{\varepsilon}_1 = \dot{\varepsilon}_m - \frac{1}{2}t\dot{\varepsilon}_b \tag{920}$$

`/ANIM/TENS/EPSDOT/LOWER`

The strain rate is filtered by using:

$$\dot{\varepsilon}_f(t) = \mathrm{a}\dot{\varepsilon}(t) + (1 - \mathrm{a})\dot{\varepsilon}_f(t-1) \tag{921}$$

Where,

$a=2\pi \, dt \, F_{cut}$

dt	Time interval
$\boldsymbol{F_{cut}}$	Cutting frequency
$\dot{\varepsilon}_f$	Filtered strain rate

Strain Rate Filtering Example

An example of material characterization for a simple tensile test RD-E: 1100 Tensile Test is given in *Radioss Example Guide*. For the same example, a strain rate filtering allows to remove high frequency vibrations and obtain smoothed the results. This is shown in Figure 210 and Figure 211 where the cut frequency F_{cut} = 10 KHz is used.

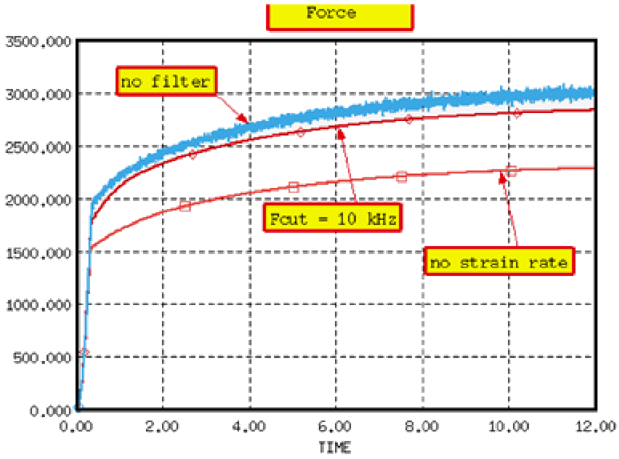

Figure 210: Force Comparison

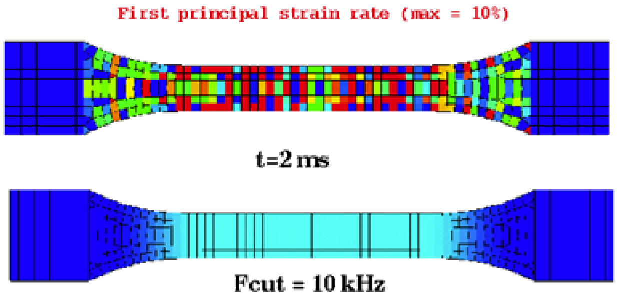

Figure 211: First Principal Strain Rate Comparison (max = 10%)

Zerilli-Armstrong Plasticity Model (LAW2)

This law is similar to the Johnson-Cook plasticity model. The same parameters are used to define the work hardening curve.

However, the equation that describes stress during plastic deformation is:

$$\sigma = C_0 + \left(C_1 \exp\left(\left(-C_3 \mathrm{T} + C_4 \mathrm{T}\,\mathrm{In}\left(\frac{\dot{\varepsilon}}{\dot{\varepsilon}_0}\right)\right)\right)\right) + C_5 \varepsilon_p^n \tag{922}$$

Where,

σ	Stress (Elastic + Plastic Components)
ε_p	Plastic strain
τ	Temperature (computed as in Johnson-Cook plasticity)
C_0	Yield stress
n	Hardening exponent
$\dot{\varepsilon}$	Strain rate, must be 1 s^{-1} converted into user's time unit
$\dot{\varepsilon}_0$	Reference strain rate

Additional inputs are:

$\sigma_{\max 0}$	Maximum flow stress
$\varepsilon_{\max}$	Plastic strain at rupture

The $\varepsilon_{\max}$ enables to define element rupture as in the former law. The theoretical aspects related to strain rate computation and filtering are also the same.

Cowper-Symonds Plasticity Model (LAW44)

This law models an elasto-plastic material with:

- Isotropic and kinematic hardening
- Tensile rupture criteria

The damage is neglected in the model. The work hardening model is similar to the Johnson-Cook model (LAW2) without temperature effect where the only difference is in the strain rate dependent formulation. The equation that describes the stress during plastic deformation is:

$$\sigma = \left(a + b\varepsilon_{pn}\right)\left(1 + \left(\frac{\dot{\varepsilon}}{c}\right)^{1/p}\right) \tag{923}$$

Where,

σ	Flow stress (Elastic + Plastic Components)
ε_p	Plastic strain (True strain)

a	Yield stress
b	Hardening modulus
n	Hardening exponent
c	Strain rate coefficient
$\dot{\varepsilon}$	Strain rate
$1/p$	Strain rate exponent

The implanted model in Radioss allows the cyclic hardening with a combined isotropic-kinematic approach.

The coefficient C_{hard} varying between zero and unity is introduced to regulate the weight between isotropic and kinematic hardening models.

In isotropic hardening model, the yield surface inflates without moving in the space of principle stresses. The evolution of the equivalent stress defines the size of the yield surface, as a function of the equivalent plastic strain. The model can be represented in one dimensional case as shown in Table 7. When the loading direction is changed, the material is unloaded and the strain reduces. A new hardening starts when the absolute value of the stress reaches the last maximum value (Table 7(a)).

Table 7: Isotropic and Kinematic Hardening Models for Deformation Decrease

(a) Isotropic hardening	**(b) Prager-Ziegler kinematic hardening**
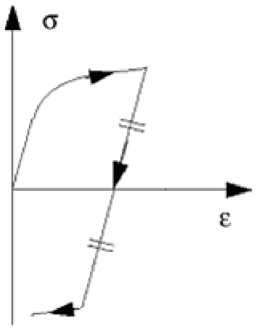	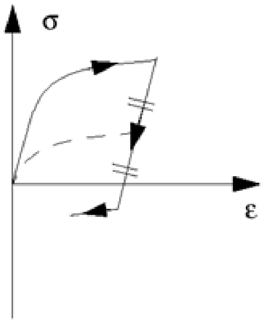

This law is available for solids and shells. Refer to the *Radioss Reference Guide* for more information about element/material compatibilities.

Zhao Plasticity Model (LAW48)

The elasto-plastic behavior of material with strain rate dependence is given by Zhao formula: [104] [105]

$$\sigma = \left(A + B\varepsilon_p^n\right) + \left(C - D\varepsilon_p^m\right).\mathrm{In}\frac{\ddot{\varepsilon}}{\dot{\varepsilon}_0} + E\dot{\varepsilon}^k \tag{924}$$

Where,

ε_p	Plastic strain
$\dot{\varepsilon}$	Strain rate
A	Yield stress
B	Hardening parameter
n	Hardening exponent
C	Relative strain rate coefficient
D	Strain rate plasticity factor
m	Relative strain rate exponent
E	Strain rate coefficient
k	Strain rate exponent

In the case of material without strain rate effect, the hardening curve given by Equation 924 is identical to those of Johnson-Cook. However, Zhao law allows a better approximation of strain rate dependent materials by introducing a nonlinear dependency.

As described for Johnson-Cook law, a strain rate filtering can be introduced to smooth the results. The plastic flow with isotropic or kinematic hardening can be modeled as described in Cowper-Symonds Plasticity Model (LAW44). The material failure happens when the plastic strain reaches a maximum value as in Johnson-Cook model. However, two tensile strain limits are defined to reduce stress when rupture starts:

$$\sigma_{n+1} = \sigma_n \left(\frac{\varepsilon_{t2} - \varepsilon_1}{\varepsilon_{t2} - \varepsilon_{t1}} \right) \tag{925}$$

Where,

ε_1	Largest principal strain
ε_{t1} **and** ε_{t2}	Rupture strain limits

If $\varepsilon_1 > \varepsilon_{f1}$, the stress is reduced by Equation 925. When $\varepsilon_1 > \varepsilon_{t2}$ the stress is reduced to zero.

[104] Zhao Han, "A Constitutive Model for Metals over a Large Range of Strain Rates", Materials Science & Engineering, A230, 1997.

[105] Zhao Han and Gerard Gary, "The Testing and Behavior Modelling of Sheet Metals at Strain Rates from 10.e-4 to 10e+4 s-1", Materials Science & Engineering" A207, 1996.

Tabulated Piecewise Linear and Quadratic Elasto-plastic Laws (LAW36 and LAW60)

The elastic-plastic behavior of isotropic material is modeled with user-defined functions for work hardening curve.

The elastic portion of the material stress-strain curve is modeled using the elastic modulus, E, and Poisson's ratio, υ. The hardening behavior of the material is defined in function of plastic strain for a given strain rate (Figure 212). An arbitrary number of material plasticity curves can be defined for different strain rates. For a given strain rate, a linear interpolation of stress for plastic strain change, can be used. This is the case of LAW36 in Radioss. However, in LAW60 a quadratic interpolation of the functions allows to better simulate the strain rate effects on the behavior of material as it is developed in LAW60. For a given plastic strain, a linear interpolation of stress for strain rate change is used. Compared to Johnson-Cook model (LAW2), there is no maximum value for the stress. The curves are extrapolated if the plastic deformation is larger than the maximum plastic strain. The hardening model may be isotropic, kinematic or a combination of the two models as described in Cowper-Symonds Plasticity Model (LAW44). The material failure model is the same as in Zhao law.

For some kinds of steels the yield stress dependence to pressure has to be incorporated especially for massive structures. The yield stress variation is then given by:

$$\sigma_\gamma = \sigma_\gamma^0(\varepsilon_p) \times f(p) \tag{926}$$

Where, p is the pressure defined by Stresses in Solids, Equation 84. Drücker-Prager model described in Drücker-Prager (LAW10 and LAW21) gives a nonlinear function for $f(p)$. However, for steel type materials where the dependence to pressure is low, a simple linear function may be considered:

$$\sigma_y = \sigma_y^0(\varepsilon_p) \times C \times p(\varepsilon_p) \tag{927}$$

Where,

C
User-defined constant

p
Computed pressure for a given deformed configuration

C_{hard} in `/MAT/LAW36` is same like in `/MAT/LAW44`. For more detail on C_{hard}, see Cowper-Symonds Plasticity Model (LAW44).

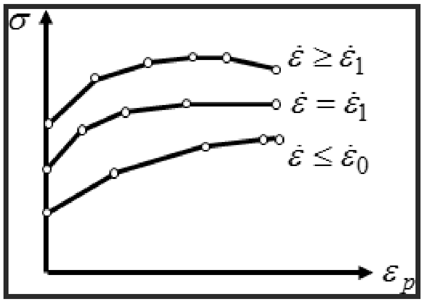

Figure 212: Piecewise Linear Stress-Strain Curves

The principal strain rate is used for the strain rate definition:

$$\frac{d\varepsilon}{dt}=\frac{1}{2}\left(\frac{d\varepsilon_x}{dt}+\frac{d\varepsilon_y}{dt}+\sqrt{\left(\frac{d\varepsilon_x}{dt}-\frac{d\varepsilon_y}{dt}\right)^2+\left(\frac{d\gamma_{xy}}{dt}\right)^2}\right) \tag{928}$$

For strain rate filtering, refer to Strain Rate Filtering.

Drücker-Prager Constitutive Model (LAWS 10, 21 and 81)

Drücker-Prager (LAW10 and LAW21)

For materials, like soils and rocks, the frictional and dilatational effects are significant. In these materials, the plastic behavior depends on the pressure as the internal friction is proportional to the normal force.

Furthermore, for frictional materials, associative plasticity laws, in which the plastic flow is normal to the yield surface, are often inappropriate. Drücker-Prager [106] yield criterion uses a modified von Mises yield criteria to incorporate the effects of pressure for massive structures:

$$F=J_2-\left(A_0+A_1P+A_2P^2\right) \tag{929}$$

Where,

J_2	Second invariant of deviatoric stress $J_2=\frac{1}{2}s_{ij}s_{ij}$
P	Pressure
A_0, A_1, A_2	Material coefficients

Figure 213 shows Equation 929 in the plane of $\sqrt{J_2}$ and P. The criterion expressed in the space of principal stresses represents a revolutionary surface with an axis parallel to the trisecting of the space as shown in Figure 214. This representation is in contrast with the von Mises criteria where yield criterion has a cylindrical shape. Drücker-Prager criterion is a simple approach to model the materials with internal friction because of the symmetry of the revolution surface and the continuity in variation of normal to the yield surface.

For LAW10 pressure evaluation for EOS is described with `/EOS/COMPATION`.

The pressure in the material is determined in function of volumetric strain for loading phase:

$$P=f(\mu) \tag{930}$$

for loading $d\mu>0$

Where, f is a user-defined (LAW21) or a cubic polynomial function (LAW10). For unloading phase, if the volumetric strain has a negative value, a linear relation is defined as:

$$P=C_1\mu \tag{931}$$

for unloading $d\mu<0$ and $\mu<0$

For unloading with a positive volumetric strain, another linear function may be used:

$$P = B\mu \tag{932}$$

for unloading $d\mu < 0$ and$\mu > 0$

In Radioss extended Drücker-Prager model is used in LAW10 and LAW21. Neither of these laws can reproduce the mono-dimensional behavior. In addition, no viscous effect is taken into account.

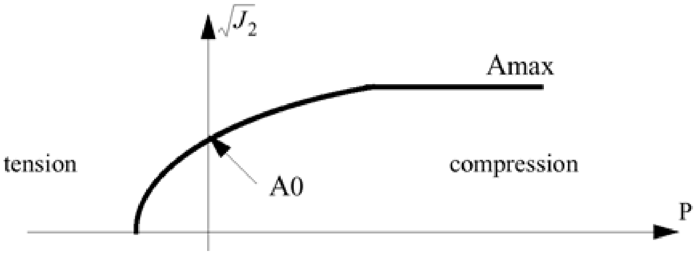

Figure 213: Yield Criteria in the Plane of $\sqrt{J_2}$ *and P*

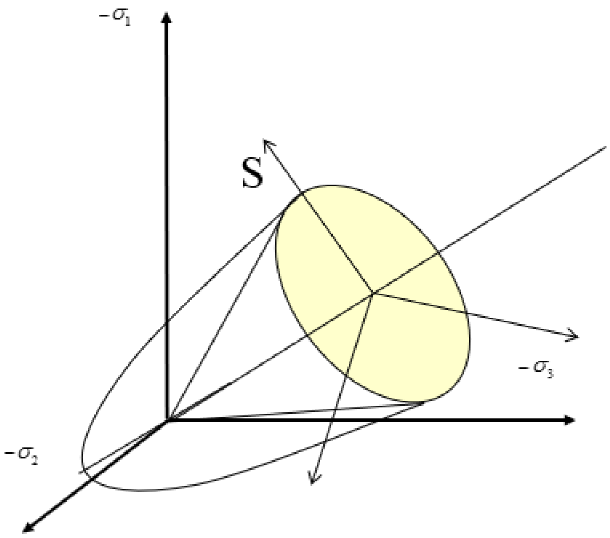

Figure 214: Drücker-Prager Yield Criteria in Space of Principal Stresses

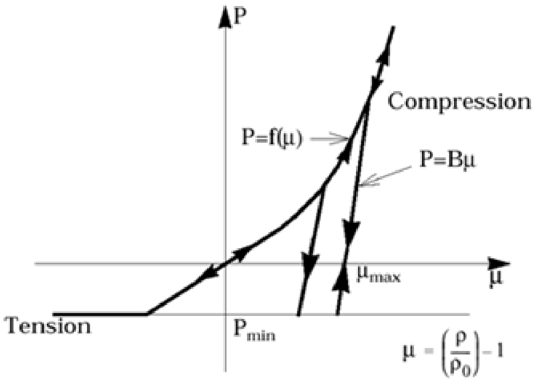

Figure 215: Material Pressure Variation in Function of Volumetric Strain

Drücker-Prager Constitutive Model with Cap (LAW81)

Yield Surface

The Drücker-Prager yield surface is:

$$F = q - \mathrm{r}_c(p) \cdot (p \tan\beta + c) = 0 \tag{933}$$

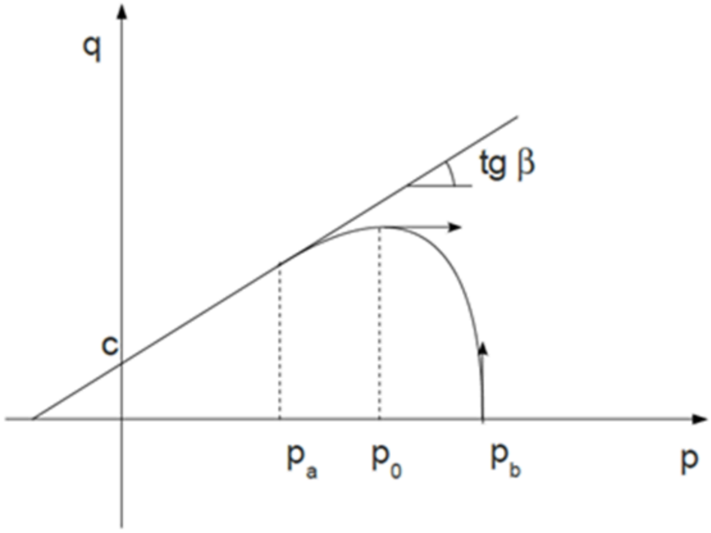

Figure 216:

Cap hardening considered in this material law in $p_a < p < p_b$ is described with:

[106] Drücker D. and Prager W., "Soil mechanics and plastic analysis of limit design", Quart. Appl. Math., Vol. 10, 157-165, 1952.

$$r_c(p) = \sqrt{1 - \left(\frac{p - p_a}{p_b - p_a}\right)^2} \tag{934}$$

In lower compression or tension $p \leq p_a$, then linear yield surface will be considered with:

$$r_c(p) = 1 \tag{935}$$

Where,

q	von Mises stress $q^2 = 3J_2 = \frac{3}{2}s_{ij}^2$
p	Pressure $p = -\frac{1}{3}\sigma_{ij} = -\frac{1}{3}I_1$
s_{ij}	Deviatoric stress $s_{ij} = \sigma_{ij} + p\delta_i^j$
c	Cohesion
β	Friction angle
p_0	Pressure value $\frac{\partial F}{\partial p}(p_0) = 0$

Plastic Flow

Plastic flow is governed by the non-associated flow potential G defined as:

If $p \leq p_a$

$$G = q - p \cdot \tan\psi = 0 \tag{936}$$

If $p_a < p \leq p_0$

$$G = q - \tan\psi\left(p - \frac{(p - p_a)^2}{2(p_0 - p_a)}\right) = 0 \tag{937}$$

If $p > p_0$ (example, the flow becomes associated on the cap)

$$G = F \tag{938}$$

The plastic potential is continuous as you have $\frac{\partial G}{\partial p}(p_0) = \frac{\partial F}{\partial p}(p_0) = 0$.

By definition the plastic flow is normal to the flow potential.

$$d\varepsilon_{ij}^{p} = d\Lambda \cdot \frac{\partial G}{\partial \sigma_{ij}} \tag{939}$$

The scalar $d\Lambda$ will be determined in order to satisfy consistency and experimental hardening/softening.

Hardening/Softening

The cap is defined by only one parameter p_b, assume that p_a evolves according to:

$$\frac{p_a}{p_b} = \frac{p_{a0}}{p_{b0}} = \alpha \tag{940}$$

Where,

p_{a0} and p_{b0} Initial value of p_a and p_b

The evolution of p_b depends on $\varepsilon_v^p = -\varepsilon_{ii}^p$ via a curve given in input *fct_ID*$_{pb}$.

Note: The same sign conversion for ε_v^p and p_b, which is positive in compression is considered.

- Shear yielding has an effect on p_b, which depends on the possible dilantancy imposed by the flow rule. An option to prevent this phenomenon is provided, for example, for rocks (cap softening deactivation flag I_{soft}).
- p_a is derived from p_b via Equation 940
- If softening is allowed, the condition $p_a > 0$ is imposed, otherwise, $d\varepsilon_v^p \geq 0$

Derive Stress-Strain Relationships

Considering bulk and shear moduli K and μ, write the relationship between stress and elastic strain deviatoric tensors and and between pressure and volumetric strain and its plastic component.

$$ds_{ij} = 2\mu\left(de_{ij} - de_{ij}^{p}\right) \tag{941}$$

$$dp = -K\left(d\varepsilon_{ii} - d\varepsilon_{ii}^{p}\right) = -K\left(d\varepsilon_{ii} - d\varepsilon_{ii}^{p}\right) \tag{942}$$

Note that,

$$\frac{\partial G}{\partial \sigma_{ij}} = -\frac{1}{3}\frac{\partial G}{\partial p}\delta_i^j + \frac{3}{2q}s_{ij} \tag{943}$$

$$\frac{\partial F}{\partial s_{ij}} = \frac{\partial G}{\partial s_{ij}} = \frac{3}{2q}s_{ij} \tag{944}$$

You can relate the increment of the plastic volumetric strain $d\varepsilon_v^p$ and the equivalent plastic strain $d\varepsilon_d^p$ and $d\Lambda$.

$$d\varepsilon_v^p = d\Lambda \frac{\partial G}{\partial p} \tag{945}$$

and $d\varepsilon_d^p = d\Lambda \frac{\partial G}{\partial q}$ with $\frac{\partial G}{\partial q} = 1.$

and solving for $d\Lambda$ from Equation 939, Equation 942, Equation 944 and Equation 945, you obtain,

$$d\Lambda = \frac{1}{h}\left(\frac{\partial F}{\partial s_{ij}} 2\mu de_{ij} - \frac{\partial F}{\partial p} K d\varepsilon_{ii}\right) \tag{946}$$

With $h = 3\mu + K \frac{\partial F}{\partial p}\frac{\partial G}{\partial p} - \frac{\partial F}{\partial c}\frac{dc}{d\varepsilon_d^p} - \frac{\partial G}{\partial p}\frac{\partial F}{\partial p_b}\frac{dp_b}{d\varepsilon_v^p}$

You can then compute all terms in Equation 946.

If $p \le p_a$, then $\frac{\partial F}{\partial p} = -\tan\beta$, $\frac{\partial F}{\partial c} = -1$, $\frac{\partial F}{\partial p_b} = 0.$

If $p \ge p_a$, then

$$\frac{\partial F}{\partial p} = -\left(\tan\beta r_c + \frac{dr_c}{dp}(p\tan\beta + c)\right) \tag{947}$$

$\frac{\partial F}{\partial c} = -r_c(p)$

and $\frac{\partial F}{\partial p_b} = \frac{-p(p - p_a)}{r_c p_b (p_b - p_a)^2}(p\tan\beta + c)$

If $p \le p_a$, then $\frac{\partial G}{\partial p} = -\tan\psi$

If $p_a \le p \le p_0$, then

$$\frac{\partial G}{\partial p} = -\tan\psi \frac{(p_0 - p)}{(p_0 - p_a)} \tag{948}$$

If $p \ge p_0$, then $\frac{\partial F}{\partial p} = \frac{\partial G}{\partial p}$

Finally, $\frac{dq}{dp} = 0$ gives

$$p_0 = p_a + \frac{-(p_a\tan\beta + c) + \sqrt{(p_a\tan\beta + c)^2 + 8[\tan\beta(p_b - p_a)]^2}}{4\tan\beta} \tag{949}$$

When $p < p_0$ and $\frac{\partial G}{\partial p} < 0$ leads to softening of the cap. If the no-softening cap flag is set, the last term in Equation 942 is irrelevant. To achieve this, set $\frac{\partial F}{\partial p_b} = 0$ and impose on the hardening parameter $d\varepsilon_v^p$ not decrease, although there is some volumetric plastic flow $d\varepsilon_v^p$.

For $p \to p_b$, $\frac{dr_c}{dp} \to \infty$, $d\Lambda \to \infty$, so that $d\varepsilon_v^p$ is undetermined in Equation 945.

In this case, a special treatment needs to be performed; at first order, the deviatoric terms are neglected.

(950)

$$d\varepsilon_v^p = -d\varepsilon_v \left(\frac{K}{K + \frac{dp_b}{d\varepsilon_v^p}} \right)$$

$$de_{ij}^p = 0$$

Elastic Properties

Yielding the cap actually models the compaction process. The elastic properties should thus increase when the porosity decreases, that is, ε_v^p increases.

The variation of K and μ with ε_v^p are determined by two functions given in input.

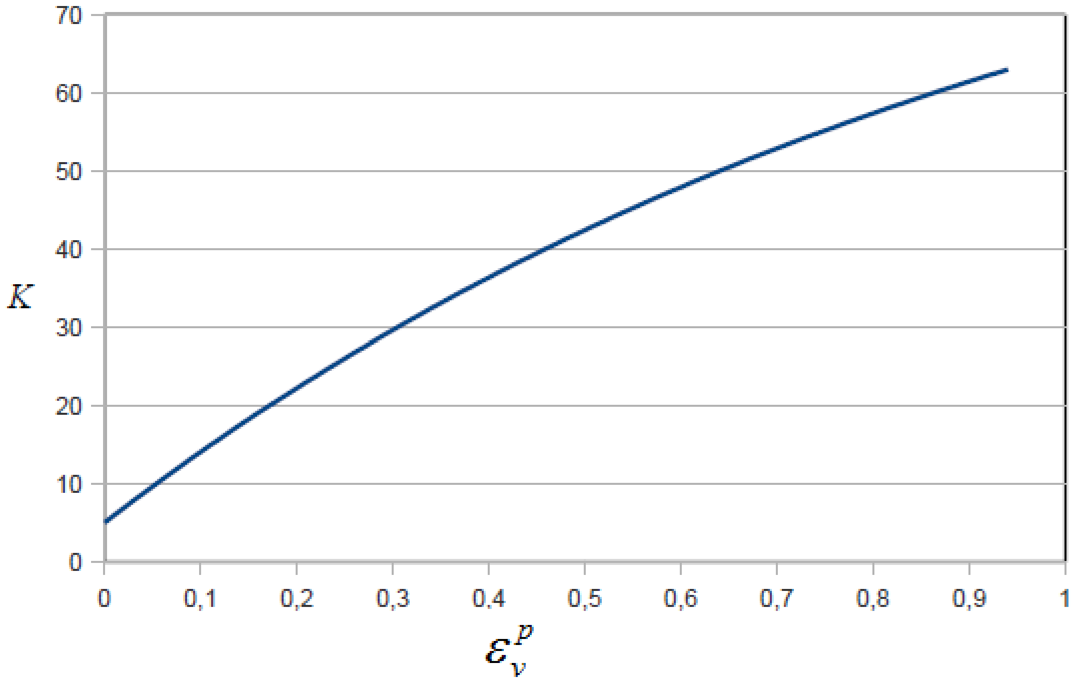

Figure 217:

Note: Typically, when variable elastic properties are used, the hardening parameter $\varepsilon_v^p = \int d\varepsilon_v^p$ and the volumetric deformation after full unloading are not consistent.

Porosity Model

The porosity model is inspired by [107] and assumes the soils are made of elastic grains with voids and is for low energies when the soil is not fully compacted. For a fully compacted soil at high energy, an equation of state should be used. In this material law, the variation of the volume of voids has an elastic part due to the elastic deformation of the skeleton and a plastic part which corresponds to the rearrangement of grains which induces compaction upon pressure loadings and dilatancy when undergoing shear loadings.

Note: The presence of air is not part of this model. The porosity is defined so that it represents the volume fraction of voids, with respect to the total reference volume.

$$n = \frac{V_{void}}{V_{total}} \tag{951}$$

In the elastic case, the void volume does not change. However, in the plastic case, the porosity change is defined by:

$$n = 1 - (1 - n_0) e^{\varepsilon_v^p - \varepsilon_{v0}^p} \tag{952}$$

The initial state of the pores is defined by the initial porosity, initial saturation, and initial pore pressure. The saturation is defined as the ratio of the volume of the water to the volume in the void:

$$S = \frac{V_{water}}{V_{void}} \tag{953}$$

The above voids can be partly or totally filled with water. In soil mechanics, when the soil is not saturated $S < 1$ the only effect of water is its weight and mass so the water pressure $u = 0$; the mechanical properties are then the same as the drained soil. When the soil is saturated $S \geq 1$, the water pressure u is taken into account using Terzaghi's assumption. [108] The total pressure is $p = p' + u$, where p is the effective pressure in the structure that has the voids. Also, assume the initial water pressure does not exceed the initial pressure in the skeleton.

The average density of the void can be calculated as the mass of the water divided by the volume of the void:

$$\rho_{void} = \frac{m_{water}}{V_{void}} \tag{954}$$

Next, define:

$$\mu_w = \frac{\rho_{void}}{\rho_{w0}} - 1 \tag{955}$$

Where, ρ_{w0} is the initial density of the water.

For stability reasons, a viscousity term is added.

If $\mu_w > -\quad tol$ then $u_{vis} = \quad -\alpha_v\sqrt{K_w \quad \rho} \quad (Vol)^{\frac{1}{3}} \quad \varepsilon_v$ and is added to u^*.

For a smoother transition, define:

$$\begin{aligned} &\text{If } \mu_w < -tol : u^* = \quad 0 \\ &\text{If } |\mu_w| < tol : u^* = \quad \frac{K_w}{4tol} \quad (\mu_w + tol)^2 \\ &\text{If } \mu_w > tol : u^* = \quad K_w \quad \mu_w \end{aligned} \tag{956}$$

Where, K_w is the water bulk modulus.

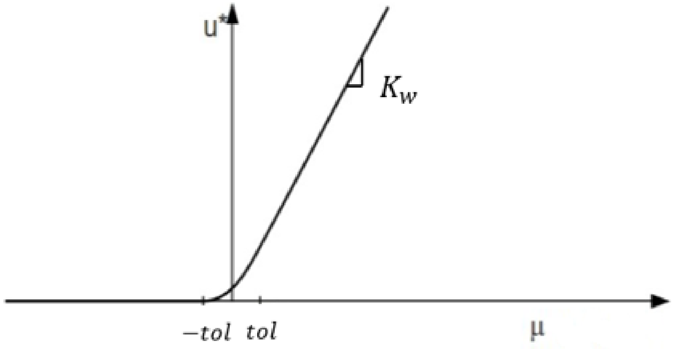

Figure 218: Pressure, due to Porosity

The cap is then modified by adding a purely von Mises region for $p_0 \leq p' \leq p_0 + u^*$.

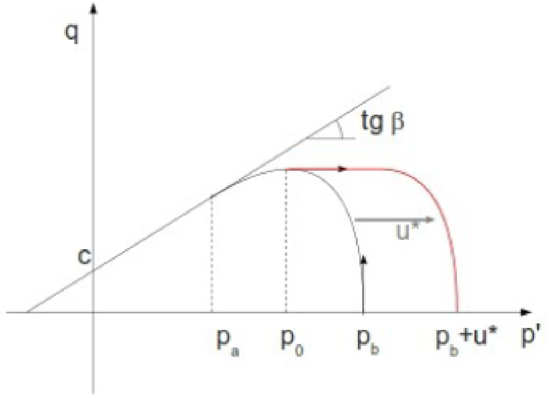

Figure 219: Modification to the Cap

[107] R. Kohler and G. Hofstetter, *A cap model for partially saturated soils*, Wiley & Sons, 2007

[108] Karl Terzaghi, *Theoretical Soil Mechanics*, Wiley & Sons, 1943

Brittle Damage: Johnson-Cook Plasticity Model (LAW27)

Johnson-Cook plasticity model is presented in Johnson-Cook Plasticity Model (LAW2). For shell applications, a simple damage model can be associated to this law to take into account the brittle failure. The crack propagation occurs in the plan of shell in the case of mono-layer property and through the thickness if a multi-layer property is defined (Figure 220).

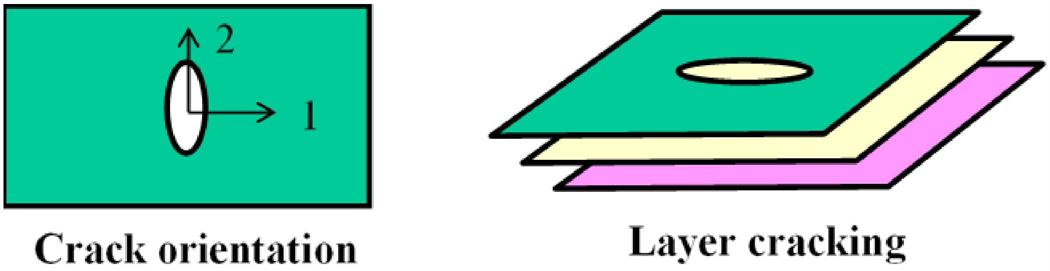

Figure 220: Damage Affected Material

The elastic-plastic behavior of the material is defined by Johnson-Cook model. However, the stress-strain curve for the material incorporates a last part related to damage phase as shown in Figure 221. The damage parameters are:

ε_{t1}	Tensile rupture strain in direction 1
ε_{m1}	Maximum strain in direction 1
d	

The element is removed if one layer of element reaches the failure tensile strain, ε_{f1}. The nominal and effective stresses developed in an element are related by:

$$\sigma_n = \sigma_{eff}(1 - d) \tag{957}$$

Where,

$0 < \mathrm{d} < 1$	Damage factor

The strains and the stresses in each direction are given by:

$$\varepsilon_1 = \frac{\sigma_1}{(1 - d_1)E} - \frac{\nu\sigma_2}{E} \tag{958}$$

$$\varepsilon_2 = \frac{\sigma_2}{E} - \frac{\nu\sigma_1}{E} \tag{959}$$

$$\gamma_{12} = \frac{\sigma_{12}}{(1 - d_1)G} \tag{960}$$

$$\sigma_1 = \frac{E(1 - d_1)}{\left[1 - (1 - d_1)\nu 2\right]}(\varepsilon_1 + \nu\varepsilon_2) \tag{961}$$

$$\sigma_2 = \frac{E}{\left[1-(1-d_1)\nu^2\right]}\left(\varepsilon_2 + (1-d_1)\nu\varepsilon_1\right) \tag{962}$$

The conditions for these equations are:

$0 < d < 1$

$\varepsilon = \varepsilon_t$; d = 0

$\varepsilon = \varepsilon_m$; d = 1

A linear damage model is used to compute the damage factor in function of material strain.

$$d = \frac{\varepsilon - \varepsilon_t}{\varepsilon_m - \varepsilon_t} \tag{963}$$

The stress-strain curve is then modified to take into account the damage by Equation 957. Therefore:

$$\sigma = E\frac{\varepsilon_m - \varepsilon}{\varepsilon_m - \varepsilon_t}\left(\varepsilon - \varepsilon_t^p\right) \tag{964}$$

The softening condition is given by:

$$\varepsilon_m - \varepsilon_t \le \varepsilon_t - \varepsilon_t^p \tag{965}$$

The mathematical approach described here can be applied to the modeling of rivets. Predit law in Radioss allows achievement of this end by a simple model where for the elastic-plastic behavior a Johnson-Cook model or a tabulated law (LAW36) may be used.

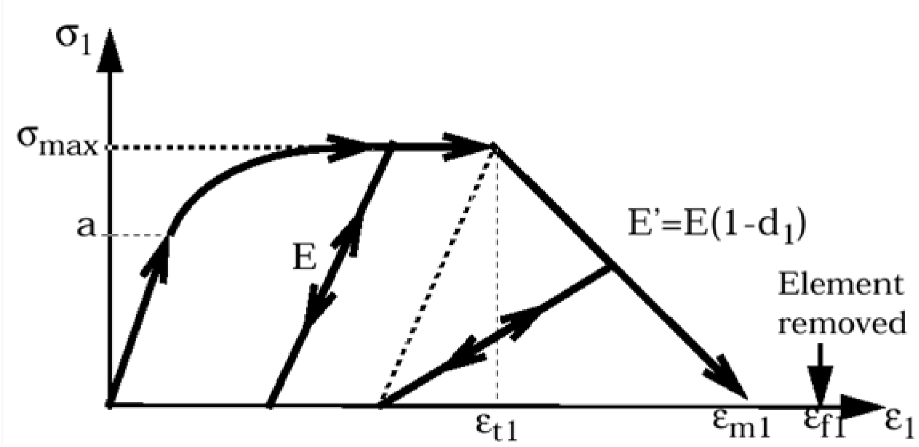

Figure 221: Stress-strain Curve for Damage Affected Material

Brittle Damage: Reinforced Concrete Material (LAW24)

The model is a continuum, plasticity-based, damage model for concrete. It assumes that the main two failure mechanisms are tensile cracking and compressive crushing of the concrete material.

The material law will enable to formulate the brittle elastic - plastic behavior of the reinforced concrete.

The input data for concrete are:

E $_c$ Young's modulus

32000 MPa

V$_c$ Poisson's ratio

0.2

f$_c$ Uniaxial compressive strength

32 $[\mathrm{MPa}]$

f$_i$**/f**$_c$ Tensile strength ratio

Default = 0.1

f$_b$**/f**$_c$ Biaxial strength ratio

Default = 1.2

f$_2$**/f**$_c$ Confined strength ratio

Default = 4.0

s$_0$**/f**$_c$ Confining stress ratio

Default = 1.25

Experimental results enable to determine the material parameters. This can be done by in-plane unidirectional and bi-axial tests as shown in Figure 223. The expression of the failure surface is in a general form as:

$$f = r - \mathrm{k}(\sigma_m, k_0) \cdot r_f = 0 \tag{966}$$

Where,

J_2 Second invariant of stress

Where, $r = \sqrt{2J_2} = \sqrt{\frac{2}{3}}\sigma_{VM}$

$\sigma_m = \frac{I_1}{3}$ Mean stress

A schematic representation of the failure surface in the principal stress space is given in Figure 223. The yield surface is derived from the failure envelope by introducing a scale factor $\mathrm{k}(\sigma_m, k_0)$. The meridian planes are presented in Figure 224.

The steel directions are defined identically to material LAW14 by a TYPE6 property set. If a property set is not given in the element input data, r, s, θ are taken respectively as direction 1, 2, 3. For quad elements, direction 3 is taken as the θ direction.

Steel data properties are:

E Young's modulus

σ_y	Yield strength
E t	Tangent modulus
α_1	Ratio of reinforcement in direction 1
α_2	Ratio of reinforcement in direction 2
α_3	Ratio of reinforcement in direction 3

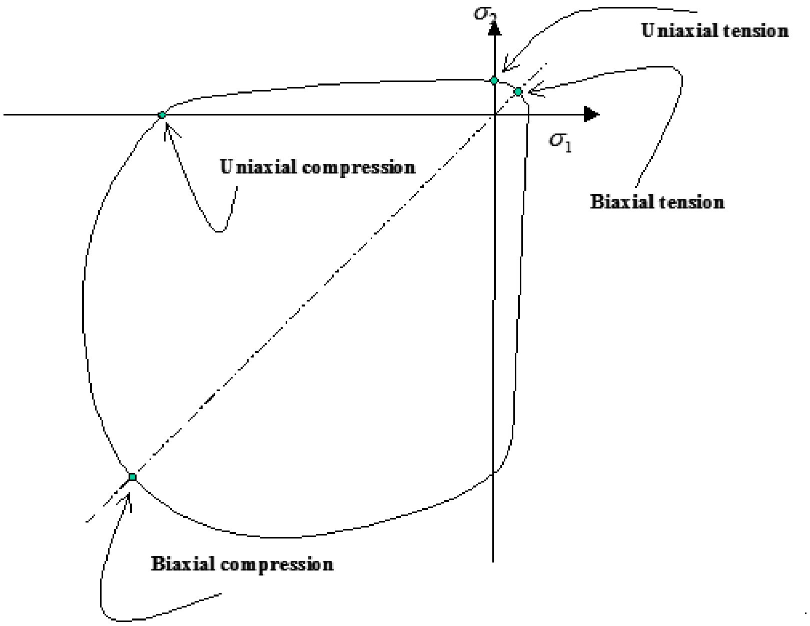

Figure 222: Failure Surface in Plane Stress

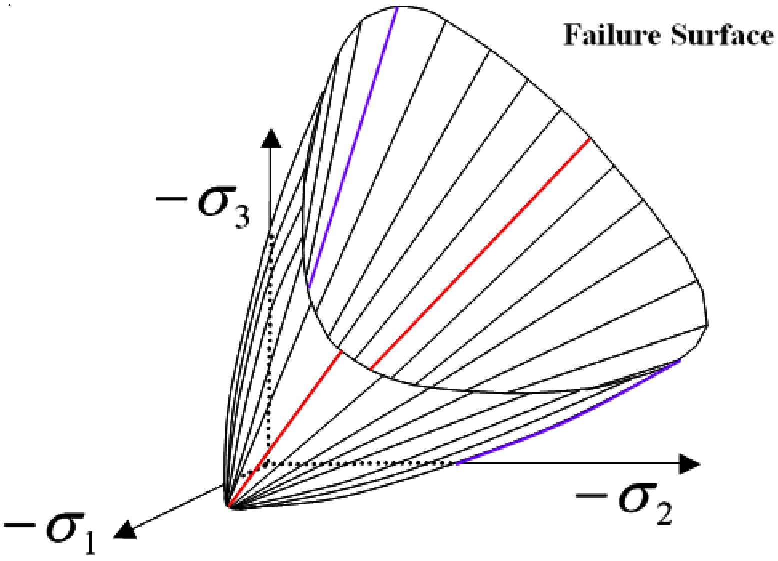

Figure 223: Failure Surface in Principal Stress Space

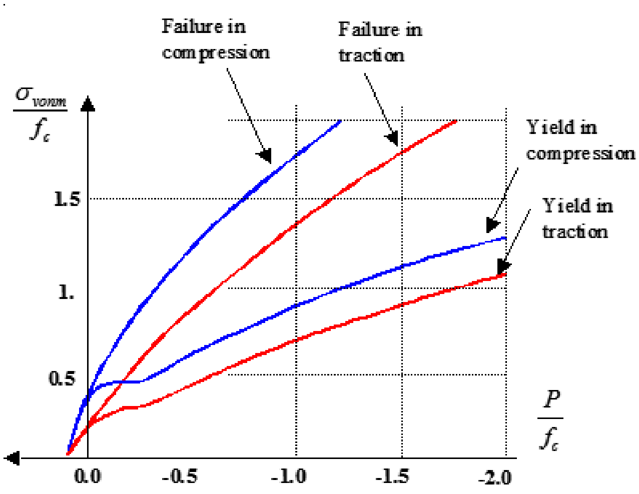

Figure 224: Meridians of Failure and Yield Surfaces

Ductile Damage Model

In Brittle Damage: Johnson-Cook Plasticity Model (LAW27), a damage model for brittle materials is presented. It is used in Radioss LAW27 valid for shell meshes. The damage is generated when the shell works in traction only. A generalized damage model for ductile materials is incorporated in Radioss LAW22 and LAW23. The damage is not only generated in traction but also in compression and shear. It is valid for solids and shells. The elastic-plastic behavior is formulated by Johnson-Cook model. The damage is introduced by the use of damage parameter, δ. The damage appears in the material when the strain is larger than a maximum value, ε_{dam}:

$$0 \le \delta \le 1$$

- If $\varepsilon < \varepsilon_{dam} \Rightarrow \delta = 0$ LAW 22 is identical to LAW2.
- If $\varepsilon \ge \varepsilon_{dam} \Rightarrow \varepsilon_{dam} = (1-\delta)E$ and $v_{dam} = \frac{1}{2}\delta + (1-\delta)v$

This implies an isotropic damage with the same effects in tension and compression. The inputs of the model are the starting damage strain ε_{dam} and the slope of the softening curve E_t as shown in Figure 225.

For brick elements the damage law can be only applied to the deviatoric part of stress tensor s_{ij} and $G_{dam} = \frac{E_{dam}}{2(1+v_{dam})}$. This is the case of LAW22 in Radioss. However, if the application of damage law to stress tensor σ_{ij} is expected, Radioss LAW23 may be used.

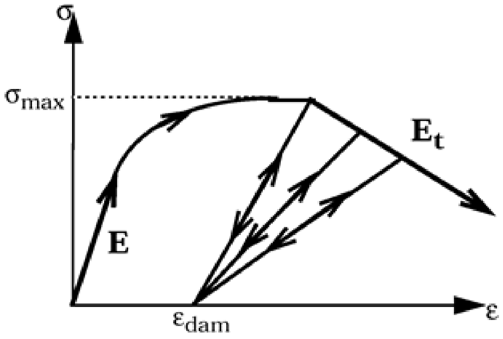

Figure 225: Ductile Damage Model

The strain rate definition and filtering for these laws are explained in Johnson-Cook Plasticity Model (LAW2). The strain rate $\dot{\varepsilon}$ may or may not affect the maximum stress value $\sigma_{\max}$ according to the user's choice, as shown in Figure 226.

(a) Strain rate effect on $\sigma_{\max}$	**(b) No strain rate effect on $\sigma_{\max}$**
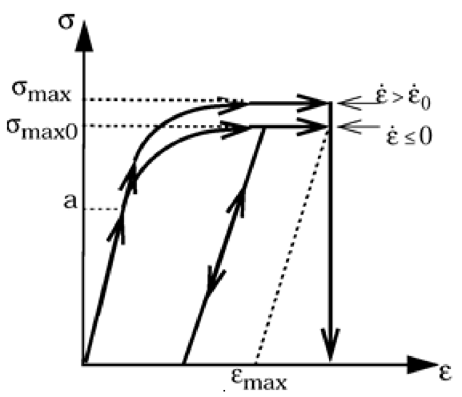	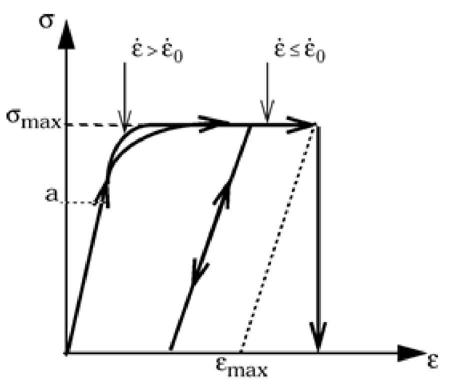
$\sigma = \sigma_y\left(1+c\ln\left(\frac{\dot{\varepsilon}}{\dot{\varepsilon}_o}\right)\right)$ $\sigma_{\max} = \sigma^0_{\max}\left(1+c.\ln\left(\frac{\dot{\varepsilon}}{\dot{\varepsilon}_0}\right)\right)$	$\sigma = \sigma_y\left(1+c\ln\left(\frac{\dot{\varepsilon}}{\dot{\varepsilon}_o}\right)\right)$ $\sigma_{\max} = \sigma^0_{\max}$

Figure 226: Strain Rate Dependency

Ductile Damage Model for Porous Materials (LAW52)

The Gurson constitutive law [109] models progressive microrupture through void nucleation and growth. It is dedicated to high strain rate elasto-viscoplastic porous metals. A coupled damage mechanical model for strain rate dependent voided material is used. The material undergoes several phases in the damage process as described in Figure 227.

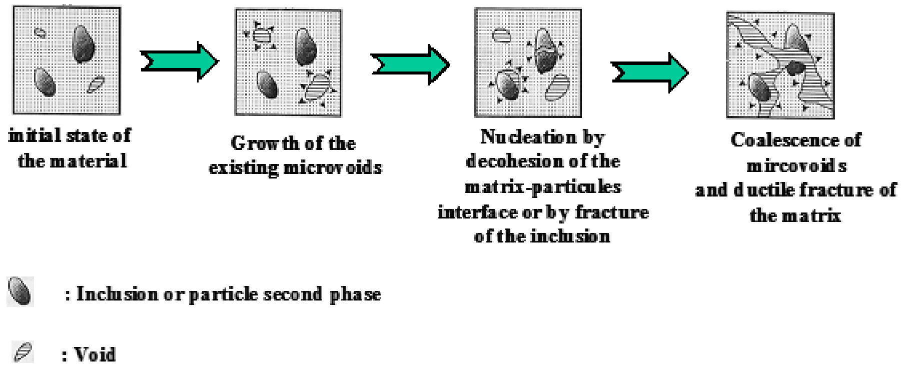
initial state of the material
Growth of the existing microvoids
Nucleation by decohesion of the matrix-particules interface or by fracture of the inclusion
Coalescence of mircovoids and ductile fracture of the matrix
: Inclusion or particle second phase
: Void

Figure 227: Damage Process for Visco-elastic-plastic Voided Materials

The constitutive law takes into account the void growth, nucleation and coalescence under dynamic loading. The evolution of the damage is represented by the void volume fraction, defined by:

$$f = \frac{V_a - V_m}{V_a} \tag{967}$$

Where,

V_a, V_m
: Respectively, are the elementary apparent volume of the material and the corresponding elementary volume of the matrix.

The rate of increase of the void volume fraction is given by:

$$f = f_g + f_n \tag{968}$$

The growth rate of voids is calculated by:

$$f_g = (1 - f)Trace[D^p] \tag{969}$$

Where, $Trace[D^p]$ is the trace of the macroscopic plastic strain rate tensor. The nucleation rate of voids is given by:

$$\dot{f}_n = \frac{f_N}{S_N\sqrt{2\pi}} e^{-\frac{1}{2}\left(\frac{\varepsilon_M - \varepsilon_N}{S_N}\right)^2} \dot{\varepsilon}_M \tag{970}$$

Where,

f_N	Nucleated void volume fraction
S_N	Gaussian standard deviation
ε_N	Nucleated effective plastic strain
ε_M	Admissible plastic strain

The viscoplastic flow of the porous material is described by:

$$\begin{cases} \Omega_{evp} = \frac{\sigma_{eq}^2}{\sigma_M^2} + 2q_1 f^* \cosh\left(\frac{3}{2} q_2 \frac{\sigma_m}{\sigma_M}\right) - \left(1 + q_3 f^{*2}\right) \quad if \ \sigma_m > 0 \\ \Omega_{evp} = \frac{\sigma_{eq}^2}{\sigma_M^2} + 2q_1 f^* - \left(1 + q_3 f^{*2}\right) \qquad if \ \sigma_m \leq 0 \end{cases} \tag{971}$$

Where,

σ_{eq}
: von Mises is effective stress

σ_M
: Admissible elasto-viscoplastic stress

σ_m
: Hydrostatic stress

f^*
: Specific coalescence function which can be written as:

$$\begin{cases} \Omega_{evp} = \frac{\sigma_{eq}^2}{\sigma_M^2} + 2q_1 f^* \cosh\left(\frac{3}{2} q_2 \frac{\sigma_m}{\sigma_M}\right) - \left(1 + q_3 f^{*2}\right) \text{ if } \sigma_m > 0 \\ \Omega_{evp} = \frac{\sigma_{eq}^2}{\sigma_M^2} + 2q_1 f^* - \left(1 + q_3 f^{*2}\right) \text{ if } \sigma_m \leq 0 \end{cases} \tag{972}$$

Where,

f_c
: Critical void volume fraction at coalescence

f_F
: Critical void volume fraction at ductile fracture

f_u
: Corresponding value of the coalescence function $f_u = \frac{1}{q_1}$, $f^*\left(f_F\right) = f_u$

The variation of the specific coalescence function is shown in Figure 228.

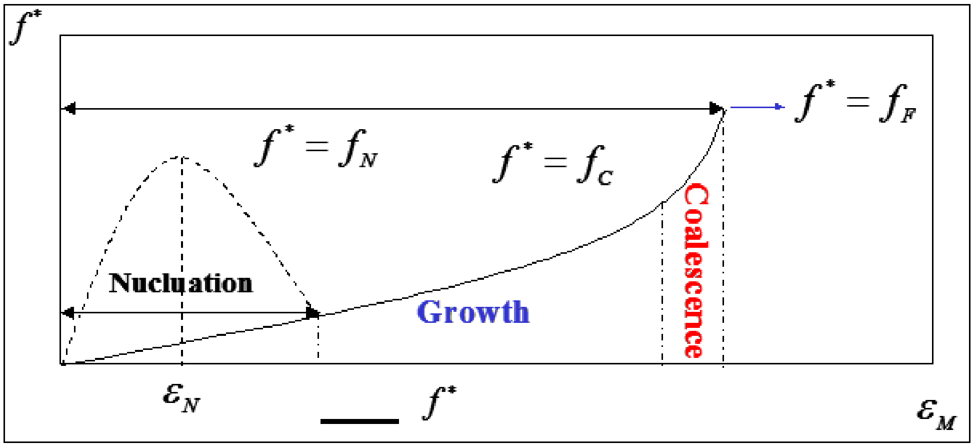

Figure 228: Variation of Specific Coalescence Function

The admissible plastic strain rate is computed as:

$$\dot{\varepsilon}_M = \frac{\sigma : D^p}{(1-f)\sigma_M} \tag{973}$$

Where,

σ
Cauchy stress tensor

σ_M
Admissible plastic stress

D^p
Macroscopic plastic strain rate tensor which can be written in the case of the associated plasticity as:

$$D^p = \dot{\lambda}\frac{\partial \Omega_{evp}}{\partial \sigma} \tag{974}$$

with Ω_{evp} the yield surface envelope. The viscoplastic multiplier is deduced from the consistency condition:

$$\Omega_{evp} = \dot{\Omega}_{evp} = 0 \tag{975}$$

From this last expression we deduce that:

$$\dot{\lambda} = \frac{\Omega_{evp}}{\frac{\partial\Omega_{evp}}{2\partial} : C^e : \frac{\partial\Omega_{evp}}{\partial\sigma} - \frac{\partial\Omega_{evp}}{\partial\sigma_M}\frac{\partial\sigma_M}{\partial\varepsilon_M}A_2 - \frac{\partial\Omega_{evp}}{\partial f}\left[(1-f)\frac{\partial\Omega_{evp}}{\partial\sigma} : I + A_1A_2\right]} \tag{976}$$

Where,

$$A_2 = \frac{\sigma : \frac{\delta\Omega_{evp}}{\delta\sigma}}{(1-f)\sigma_M}; A_1 = \frac{f_N}{S_N\sqrt{2\pi}}e^{-\frac{1}{2}\left(\frac{\varepsilon_M-\varepsilon_N}{S_N}\right)^2} \tag{977}$$

Connect Materials (LAW59)

For the moment `/MAT/LAW59` is only compatible with `/PROP/TYPE43` and `/FAIL/CONNECT`.

Solid Connection Element and Material

These materials and properties are only compatible with each other; `/FAIL/CONNECT`, and the designated failure model.

They are designed for spotweld, welding line or glue type connections.

The property is only compatible with standard 8 node brick elements. The element orientation with respect to the connected surfaces is important, and must be defined, as:

[109] Gurson A. L. “Continuum theory of ductile rupture by void nucleation and growth: Part I - Yield criteria and flow rules for porous ductile media”, Journal of Engineering Materials and Technology, Vol. 99, 2-15, 1977.

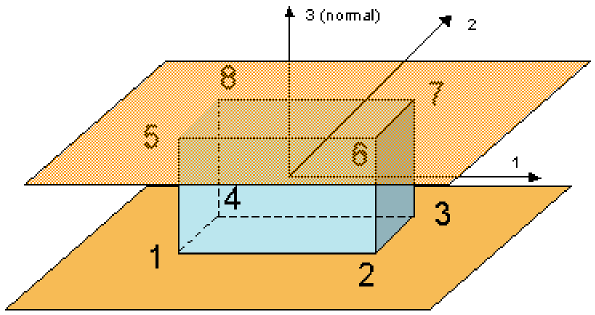

Figure 229: Solid connect element

The main characteristic of CONNECT property is the time step is independent on the element height, only on the section surface area. Hence, it can be used for glue or spotweld connections, with null height distance.

Element Definition

The element local coordinate system is constructed in the mid-plane section between the bottom and top faces. The orientation is the same as in Radioss shell elements:

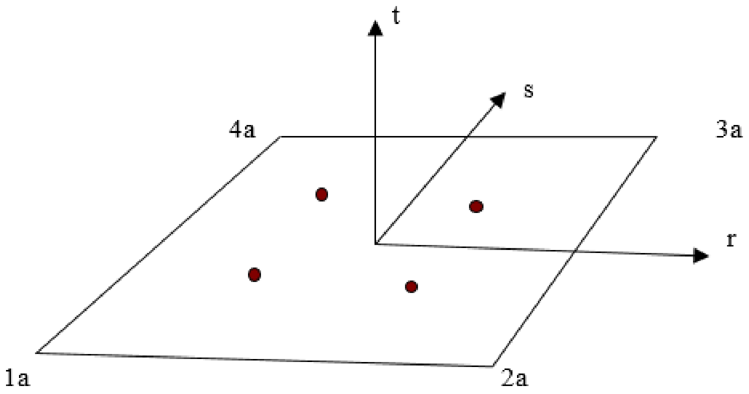

Figure 230: Points 1a, 2a, 3a and 4a are in the mid-distance between bottom and top face nodes

The local element system is fully corotational (not only convected), local deformations are thus independent on rigid element rotations.

The element has four Gauss integration points placed in the mid plane section. Element deformation in each point is constructed using nodal displacements and linear function forms in the following way:

```
Dzz = sum(Ni*Vzi)i=5,6,7,8 - sum(Nj*Vzj)j=1,2,3,4
Dxz = sum(Ni*Vxi)i=5,6,7,8 - sum(Nj*Vxj)j=1,2,3,4
Dyz = sum(Ni*Vyi)i=5,6,7,8 - sum(Nj*Vyj)j=1,2,3,4
```

Where,

Vx, Vy, and Vz
    Nodal velocities in local corotational system

Ni

Function forms

Note: These independent variables are not deformations but relative displacements (velocities).

The element has only three "strain" components - traction/compression in normal (Z) direction and both transverse shears XZ and YZ. Actually, in-plane shear, as well as lateral tractions/compressions does not give any resistance forces. It's a pure "connection" element and is not intended to be used in independent way. Both upper and bottom faces have to be tied to different structural parts.

Material Law

The elastic-plastic behavior is modeled independently in normal and tangent (in-plane) directions in each Gauss integration points, using user-defined functions for work hardening curve. There is no coupling between normal and shear direction in the material law. The hardening model is purely isotropic. Different number of hardening curves may be defined in each direction, for different values of deformation rate.

For a given strain rate, a linear interpolation between corresponding curves is used to find the value of the yield stress for the actual plastic displacement.

Deformation rates may be optionally filtered. In this regard, the law is similar to the classical elastic-plastic tabulated approach.

Nodal forces are assembled using stress components calculated in each Gauss integration point, and additional treatment is performed to assure global force and moment balance at every time step.

Input Parameters

The material stiffness parameters are input as total element rigidity per section area, which is equivalent to the Young and shear modulus per height unit $\left[\frac{Pa}{m}\right]$ $(\left[\frac{Kg}{m^2s^2}\right])$.

The hardening functions are expressed as engineering stress relative to plastic displacements.

Element Stability

The element does not have its own elementary time step. Corresponding nodal time step is calculated using nodal masses and stiffness to assure the numerical stability. In Radioss v12.0, the nodal time step is imposed to the whole model, in the next releases the elementary time step is option is maintained if chosen in the Engine input file, only the connection material elements will use nodal time step.

Viscous Materials

General case of viscous materials represents a time-dependent inelastic behavior.

However, special attention is paid to the viscoelastic materials such as polymers exhibiting a rate- and time-dependent behavior. The viscoelasticity can be represented by a recoverable instantaneous elastic deformation and a non-recoverable viscous part occurring over the time. The characteristic feature of viscoelastic material is its fading memory. In a perfectly elastic material, the deformation is proportional to the applied load. In a perfectly viscous material, the rate of change of the deformation over time is proportional to the load. When an instantaneous constant tensile stress σ_0 is applied to a viscoelastic material, a slow continuous deformation of the material is observed. When the resulting time dependent strain $\varepsilon(t)$, is measured, the tensile creep compliance is defined as:

$$D(t) = \frac{\varepsilon(t)}{\sigma_0} \tag{978}$$

The creep behavior is mainly composed of three phases:

- Primary creep with fast decrease in creep strain rate
- Secondary creep with slow decrease in creep strain rate
- Tertiary creep with fast increase in creep strain rate.

The creep strain rate is the slope of creep strain to time curve.

Another kind of loading concerns viscoelastic materials subjected to a constant tensile strain, ε_0. In this case, the stress, $\sigma(t)$ which is called stress relaxation, gradually decreases. The tensile relaxation modulus is then defined as:

$$E(t) = \frac{\sigma(t)}{\varepsilon_0} \tag{979}$$

Because viscoelastic response is a combination of elastic and viscous responses, the creep compliance and the relaxation modulus are often modeled by combinations of springs and dashpots. A simple schematic model of viscoelastic material is given by the Maxwell model shown in Figure 231. The model is composed of an elastic spring with the stiffness E and a dashpot assigned a viscosity μ. It is assumed that the total strain is the sum of the elastic and viscous strains:

$$\varepsilon = \varepsilon^e + \varepsilon^v \tag{980}$$

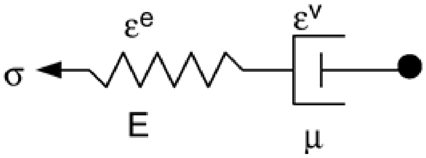

Figure 231: Maxwell Model

The time derivation of the last expression gives the expression of the total strain rate:

$$\dot{\varepsilon} = \dot{\varepsilon}^e + \dot{\varepsilon}^v \tag{981}$$

As the dashpot and the spring are in series, the stress is the same in the two parts:

$$\sigma^e = \sigma^v = \sigma \tag{982}$$

The constitutive relations for linear spring and dashpot are written as:

$$\sigma = E\varepsilon^e \text{ then } \dot{\sigma} = E\dot{\varepsilon}^e \tag{983}$$

$$\sigma = \mu\dot{\varepsilon}^v \tag{984}$$

Combining Equation 981, Equation 983 and Equation 984, an ordinary differential equation for stress is obtained:

$$\dot{\sigma} = E\left(\dot{\varepsilon} - \frac{\sigma}{\mu}\right) \text{ or } \dot{\sigma} = E\dot{\varepsilon} - \frac{\sigma}{\tau} \tag{985}$$

Where, $\tau = \frac{\mu}{E}$ is the relaxation time. A solution to the differential equation is given by the convolution integral:

$$\sigma(t) = \int_{-\infty}^{t} Ee^{\frac{-(t-t')}{\tau}} \frac{d\varepsilon(t')}{dt'} dt' = \int_{-\infty}^{t} R(t-t') \frac{d\varepsilon(t')}{dt'} dt' \tag{986}$$

Where, $R(t)$ is the relaxation modulus. The last equation is valid for the special case of Maxwell one-dimensional model. It can be extended to the multi-axial case by:

$$\sigma(t) = \int_{-\infty}^{t} C_{ijkl}(t-t') \frac{d\varepsilon(t')}{dt'} dt' \tag{987}$$

Where, C_{ijkl} are the relaxation moduli. The Maxwell model represents reasonably the material relaxation. But it is only accurate for secondary creep as the viscous strains after unloading are not taken into account.

Another simple schematic model for viscoelastic materials is given by Kelvin-Voigt solid. The model is represented by a simple spring-dashpot system working in parallel as shown in Figure 232.

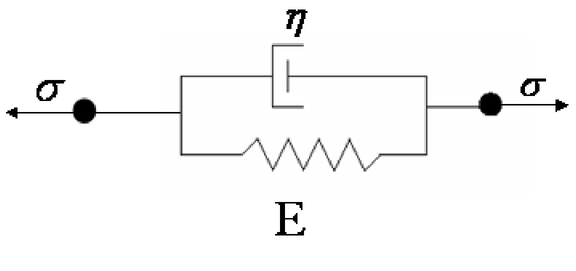

Figure 232: Kelvin-Voigt Model

The mathematical relation of Kelvin-Voigt solid is written as:

$$\sigma = E\varepsilon + \eta\dot{\varepsilon} \tag{988}$$

When $\eta = 0$ (no dashpot), the system is a linearly elastic system. When E=0 (no spring), the material behavior is expressed by Newton's equation for viscous fluids. In the above relation, a one-dimensional model is considered. For multiaxial situations, the equations can be generalized and rewritten in tensor form.

The Maxwell and Kelvin-Voigt models are appropriate for ideal stress relaxation and creep behaviors. They are not adequate for most of physical materials. A generalization of these laws can be obtained by adding other springs to the initial models as shown in Figure 233 and Figure 234. The equations related to the generalized Maxwell model are given as:

$$\sigma = \sigma_i = \sigma_1 \tag{989}$$

$$\varepsilon = \frac{\sigma_i}{E_i} \tag{990}$$

$$\dot{\varepsilon} = \frac{\dot{\sigma}_1}{E_1} + \frac{\sigma_1}{\eta_1} \tag{991}$$

The mathematical relations which hold the generalized Kelvin-Voigt model are:

$$\varepsilon = \varepsilon^e + \varepsilon^k \tag{992}$$

$$\sigma = \sigma^e + \sigma^k$$

$$\varepsilon^e = \frac{\sigma}{E};\ \varepsilon^k = \frac{\sigma^V}{E_t};\ \dot{\varepsilon}^k = \frac{\sigma^V}{\eta}$$

The combination of these equations enables to obtain the expression of stress and strain rates:

$$\dot{\varepsilon} = \dot{\varepsilon}^e + \dot{\varepsilon}^k = \frac{\dot{\sigma}}{E} + \dot{\varepsilon}^k \tag{993}$$

$$\sigma = \eta\dot{\varepsilon}^k + E_t\varepsilon^k \tag{994}$$

$$\dot{\sigma} = E\dot{\varepsilon} - \frac{(E - E_t)\sigma}{\eta} + \frac{EE_t\varepsilon}{\eta} \tag{995}$$

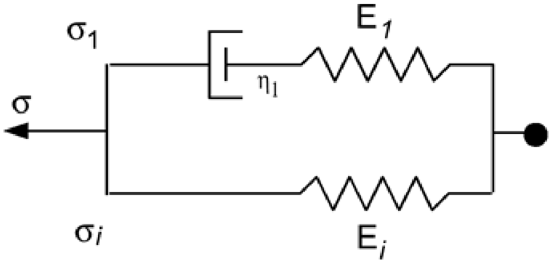

Figure 233: Generalized Maxwell Model

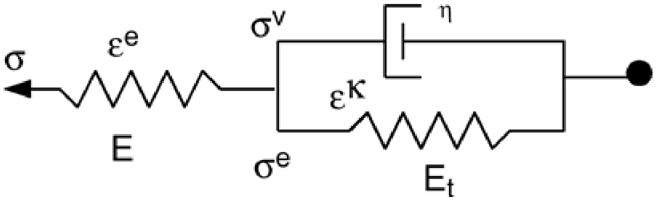

Figure 234: Generalized Kelvin-Voigt Model

The models described above concern the viscoelastic materials. The plasticity can be introduced in the models by using a plastic spring. The plastic element is inactive when the stress is less than the yield value. The modified model is able to reproduce creep and plasticity behaviors. The viscoplasticity law (LAW33) in Radioss will enable to implement very general constitutive laws useful for a large range of applications as low density closed cells polyurethane foam, honeycomb, impactors and impact limiters.

The behavior of viscoelastic materials can be generalized to three dimensions by separating the stress and strain tensors into deviatoric and pressure components:

$$s_{ij} = \int_0^t 2\Psi(t-\tau)\frac{\partial e_{ij}}{\partial \tau}d\tau \tag{996}$$

$$\sigma_{kk}(t) = \int_0^t 3K(t-\tau)\frac{\partial \varepsilon_{kk}}{\partial \tau}d\tau \tag{997}$$

Where, s_{ij} and e_{ij} are the stress and strain deviators. ε_{kk}, $\Psi(t)$ and $K(t)$ are respectively the dilatation and the shear and bulk relaxation moduli.

Boltzmann Viscoelastic Model (LAW34)

This law valid for solid elements can be used for viscoelastic materials like polymers, elastomers, glass and fluids.

Elastic bulk behavior is assumed. Air pressure may be taken into account for closed cell foams:

$$P = -K\varepsilon_{kk} + P_{air} \tag{998}$$

with:

$$P_{air} = -\frac{P_0\gamma}{1+\gamma-\Phi} \quad ; \quad \gamma = \frac{V}{V_0} - 1 + \gamma_0 \tag{999}$$

and:

$$\varepsilon_{kk} = \ln\left(\frac{V}{V_0}\right) \tag{1000}$$

Where,

γ	Volumetric strain
Φ	Porosity
P_0	Initial air pressure
γ_0	Initial volumetric strain
K	Bulk modulus

For deviatoric behavior, the generalized Maxwell model is used. The shear relaxation moduli in Viscous Materials, Equation 996 is then defined as:

$$\Psi(t) = G_l + G_s e^{-\beta t} \tag{1001}$$

$$G_s = G_0 - G_l \tag{1002}$$

Where,

G_0
: Short time shear modulus

G_l
: Long time shear modulus

β
: Decay constant, defined as the inverse of relaxation time τ_s:

$$\beta = \frac{1}{\tau_s}; \text{ with } \tau_s = \frac{\eta_s}{G_s} \tag{1003}$$

The coefficients η_s, G_s and G_l are defined for the generalized Maxwell model, as shown in Figure 235.

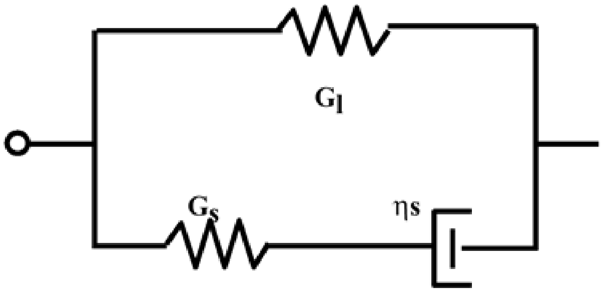

Figure 235: Generalized Maxwell Model for Boltzmann Law

From Equation 1001, the value of β governs the transition from the initial modulus G_0 to the final modulus G_l. For t=0, you obtain $\Psi(t) \to G_0$ and when $t \to \infty$, then $\Psi(t) \to G_l$. For a linear response, put $G_0 = G_l$.

Generalized Kelvin-Voigt Model (LAW35)

This law uses a generalized viscoelastic Kelvin-Voigt model whereas the viscosity is based on the Navier equations.

The effect of the enclosed air is taken into account via a separate pressure versus compression function. For open cell foam, this function may be replaced by an equivalent "removed air pressure" function. The model takes into account the relaxation (zero strain rate), creep (zero stress rate), and unloading. It may be used for open cell foams, polymers, elastomers, seat cushions, dummy paddings, etc. In Radioss the law is compatible with shell and solid meshes.

The simple schematic model in Figure 236 describes the generalized Kelvin-Voigt material model where a time-dependent spring working in parallel with a Navier dashpot is put in series with a nonlinear rate-dependent spring. If $\sigma_m = \frac{I_1}{3}$ is the mean stress, the deviatoric stresses s_{ij} at steps n and $n+1$ are computed by the expressions:

$$s_{ij}^n = \sigma_{ij}^n - \delta_{ij}\sigma_m^n \tag{1004}$$

for $i = j$ else, $\delta_{ij} = 0$

$$s_{ij}^{n+1} = s_{ij}^n + \dot{s}_{ij}dt \tag{1005}$$

with:

$$\dot{s}_{ij} = 2G\dot{e}_{ij} - \left(\frac{G+G_t}{\eta_0} s_{ij}(t)\right) + \frac{2G \cdot G_t}{\eta_0} e_{ij} \tag{1006}$$

for $i \neq j$

$$\dot{s}_{ij} = G\dot{e}_{ii} - \left(\frac{G+G_t}{\eta_0} s_{ii}(t)\right) + \frac{G \cdot G_t}{\eta_0} e_{ii} \tag{1007}$$

for $i = j$

Where, G and G_t are defined as:

$$G = \max\left(\frac{E}{2(1+v)}, \frac{A\dot{e} + B}{2(1+v)}\right) \tag{1008}$$

$$G_t = \frac{E_t}{2(1+v_t)} \tag{1009}$$

In Equation 1008 the coefficients A and B are defined for Young's modulus updates ($E = E_1\dot{\varepsilon} + E_2$).

.

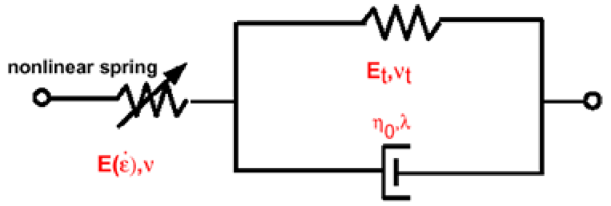

Figure 236: Generalized Kelvin-Voigt Model

The expressions used by default to compute the pressure is:

$$\frac{dP}{dt} = C_1 K\dot{\varepsilon}_{kk} - C_2\left[\frac{K+K_t}{3\lambda + 2\eta_0}\sigma_{kk}\right] + C_3\left[\frac{KK_t}{3\lambda + 2\eta_0}\varepsilon_{kk}\right] \tag{1010}$$

Where,

$$K = \frac{E}{3(1-2v)} \tag{1011}$$

$$K_t = \frac{E_t}{3(1-2v_t)} \tag{1012}$$

$$P = -\frac{1}{3}\sigma_{kk} \tag{1013}$$

$$\varepsilon_{kk} = \ln\left(\frac{V}{V_0}\right) \tag{1014}$$

λ and η_0 are the Navier Stokes viscosity coefficients which can be compared to Lame constants in elasticity. $\lambda + \frac{2\eta_0}{3}$ is called the volumetric coefficient of viscosity. For incompressible model, $\varepsilon_{kk}^{v} = 0$ and $\lambda \to \infty$ and $\mu_0 = \frac{\mu}{3}$. In Equation 1014, C_1, C_2 and C_3 are Boolean multipliers used to define different responses. For example, C_1=1, C_2=C_3=0 refers to a linear bulk model. Similarly, C_1=C_2=C_3=1 corresponds to a visco-elastic bulk model.

For polyurethane foams with closed cells, the skeletal spherical stresses may be increased by:

$$P_{air} = -\frac{P_0 \cdot \gamma}{1+\gamma-\Phi} \tag{1015}$$

Where,

γ	Volumetric strain
Φ	Porosity
P_0	Initial air pressure

In Radioss, the pressure may also be computed with the P versus $\mu = \frac{\rho}{\rho_0} - 1$, by a user-defined function. Air pressure may be assumed as an "equivalent air pressure" versus μ. You can define this function used for open cell foams or for closed cell by defining a model identical to material `LAW 33 (FOAM_PLAS)`.

Tabulated Strain Rate Dependent Law for Viscoelastic Materials (LAW38)

The law incorporated in Radioss can only be used with solid elements.

It can be used to model:

- polymers
- elastomers
- foam seat cushions
- dummy paddings
- hyperfoams
- hypoelastic materials

In compression, the nominal stress-strain curves for different strain rates are defined by you (Figure 237). Up to 5 curves may be input. The curves represent nominal stresses versus engineering strains.

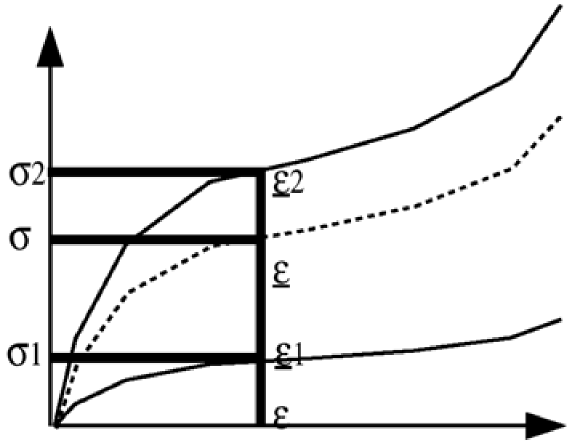

Figure 237: Nominal Stress-strain Curves Defined by User Input Functions

The first curve is considered to represent the static loading. All values of the strain rate lower than the assumed static curve are replaced by the strain rate of the static curve. It is reasonable to set the strain rate corresponding to the first curve equal to zero. For strain rates higher than the last curve, values of the last curve are used. For a given value of $\varepsilon\dot{\varepsilon}$, two values of function at for the two immediately lower $\dot{\varepsilon}_1$ and higher $\dot{\varepsilon}_2$ strain rates are read. The related stress is then computed as:

$$\sigma = \sigma_2 + (\sigma_1 - \sigma_2)\left[1 - \left(\frac{\dot{\varepsilon} - \dot{\varepsilon}_1}{\dot{\varepsilon}_2 - \dot{\varepsilon}_1}\right)^a\right]^b \tag{1016}$$

Parameters a and b define the shape of the interpolation functions. If $a = b = 1$, then the interpolation is linear.

Figure 238 shows the influence of a and b parameters.

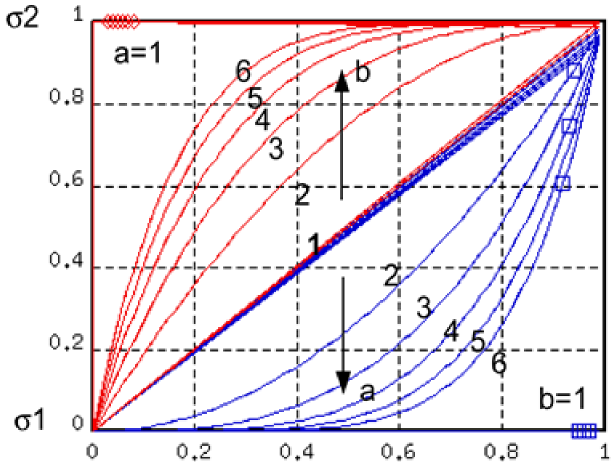

Figure 238: Influence of a and b Parameters

The coupling between the principal nominal stresses in tension is computed using anisotropic Poisson's ratio:

$$\nu_{ij} = \nu_c + (\nu_t - \nu_c)(1 - \exp(-R_\nu|\varepsilon_{ij}|)) \tag{1017}$$

Where, ν_t is the maximum Poisson's ratio in tension, ν_c being the maximum Poisson's ratio in compression, and R_ν, the exponent for the Poisson's ratio computation (in compression, Poisson's ratio is always equal to ν_c).

In compression, material behavior is given by nominal stress versus nominal strain curves as defined by you for different strain rates. Up to 5 curves may be input.

The algorithm of the formulation follows several steps:

1. Compute principal nominal strains and strain rates.
2. Find corresponding stress value from the curve network for each principal direction.
3. Compute principal Cauchy stress.
4. Compute global Cauchy stress.
5. Compute instantaneous modulus, viscosity and stable time step.

Stress, strain and strain rates must be positive in compression. Unloading may be either defined with an unloading curve, or else computed using the "static" curve, corresponding to the lowest strain rate (Figure 239 and Figure 240).

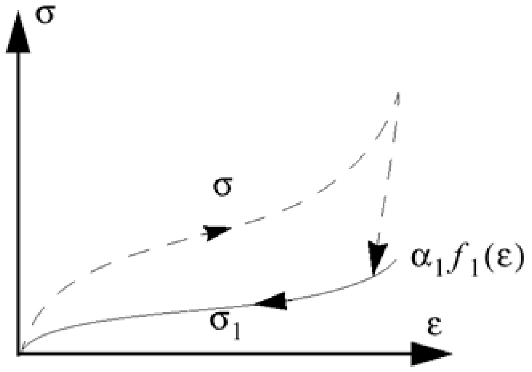

Figure 239: Unloading Behavior (No Unloading Curve Defined)

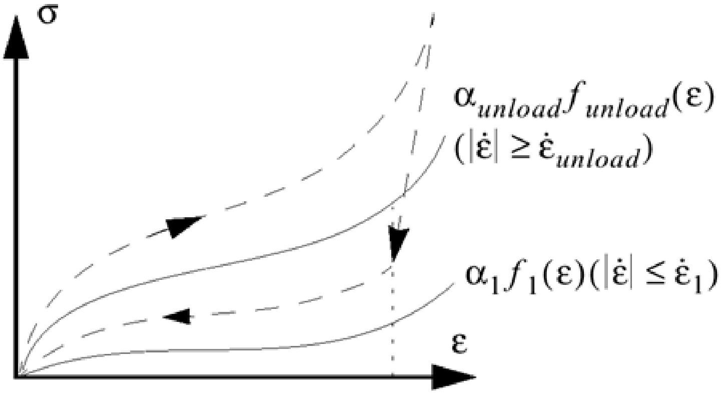
σ
$\alpha_{unload} f_{unload}(\varepsilon)$
$(|\dot{\varepsilon}| \geq \dot{\varepsilon}_{unload})$
$\alpha_1 f_1(\varepsilon)(|\dot{\varepsilon}| \leq \dot{\varepsilon}_1)$
ε

Figure 240: Unloading Behavior (Unloading Curve Defined)

It should be noted that for stability reasons, damping is applied to strain rates with a damping factor:

$$\dot{\varepsilon}^{n-1} + R_D\left(\dot{\varepsilon}^{n} - \dot{\varepsilon}^{n-1}\right) \tag{1018}$$

The stress recovery may be applied to the model in order to ensure that the stress tensor is equal to zero, in an undeformed state.

An hysteresis decay may be applied when loading, unloading or in both phases by:

$$\sigma = \sigma \cdot H \cdot \min\left(1, \left(1 - e^{-\beta \varepsilon(t)}\right)\right) \tag{1019}$$

Where,

H
: Hysteresis coefficient

β
: Relaxation parameter

Confined air content may be taken into account, either by using a user-defined function, or using the following relation:

$$P_{air} = P_0 \frac{\left(1 - \frac{V}{V_0}\right)}{\left(\frac{V}{V_0} - \Phi\right)} \tag{1020}$$

The relaxation may be applied to air pressure:

$$P_{air} = \min(P_{air}, P_{\max})\exp(-R_p t) \tag{1021}$$

Generalized Maxwell-Kelvin Model for Viscoelastic Materials (LAW40)

This law may only be applied to solid elements.

Bulk behavior is assumed to be linear:

$$\frac{dp}{dt} = K\dot{\varepsilon}_{kk} \tag{1022}$$

Shear behavior is computed using a shear factor as:

$$\mathrm{G}(t) = \mathrm{G}_\infty + \sum_1^5 G_i e^{-\beta_i t} \tag{1023}$$

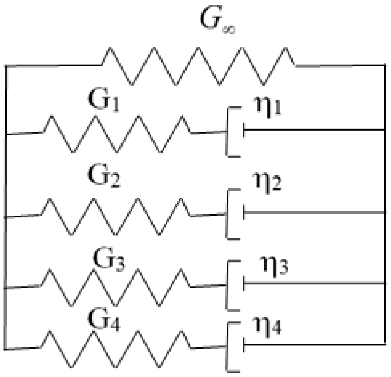

Figure 241: Maxwell-Kelvin Model

β_{i} are time decays, $\beta_{\mathrm{i}} = \frac{G_i}{\eta_i} = \frac{1}{\tau_i}$ with τ_i being relaxation time.

Visco-elasto Materials for Foams (LAW33)

This material law can be used to model low density closed cell polyurethane foams, impactors, impact limiters. It can only be used with solid elements.

The main assumptions in this law are:

- The components of the stress tensor are uncoupled until full volumetric compaction is achieved (Poisson's ratio = 0.0).
- The material is isotropic.
- The effect of the enclosed air is considered via a separate Pressure versus Volumetric Strain relation:

$$P_{air} = -\frac{P_0 \cdot \gamma}{1 + \gamma - \Phi} \tag{1024}$$

with:

$$\gamma = \frac{V}{V_0} - 1 + \gamma_0 \quad (1025)$$

Where,

γ	Volumetric strain
Φ	Porosity
P_0	Initial air pressure
γ_0	Initial volumetric strain

- The structural stresses σ follow the Maxwell-Kelvin-Voight viscoelastic model (Generalized Kelvin-Voigt Model (LAW35), Equation 1015 before the limiting yield curve is reached):

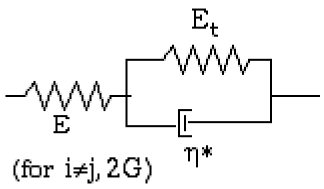

Figure 242: Maxwell-Kelvin-Voight Model

$$\sigma_{ij}(t+\Delta t) = \sigma_{ij}(t) + \left[E\dot{\varepsilon}_{ij} - \left(\frac{E+E_t}{\eta} \sigma^{s}_{ij}(t) \right) + \frac{E \cdot E_t}{\eta} \varepsilon_{ij} \right] \cdot \Delta t \quad (1026)$$

- The Young's modulus used in the calculation is: $E = \max(E, E_1\dot{\varepsilon} + E_2)$
- Yield is defined by a user-defined curve versus volumetric strain, γ, or $\sigma = A + B(1 + C\gamma)$
- Yield is applied to the principal structural stresses.
- Unloading follows Young's modulus, which results in viscous unloading.
- The full stress tensor is obtained by adding air pressure to the structual stresses:

$$\sigma^{total}{}_{ij}(t) = \sigma_{ij}(t) - P_{air}\delta_{ij} \quad (1027)$$

Hyper Visco-elastic Law for Foams (LAW62)

Experimental tests on foam specimens working in compression illustrate that the material behavior is highly nonlinear. The general behavior can be subdivided into three parts related to particular deformation modes of material cells. When the strain is small, the cells working in compression deform in membrane without causing buckling in its lateral thin-walls. In the second step, the lateral thin-walls of the cells buckle while the material undergoes large deformation. Finally, in the last step the cells are completely collapsed and the contact between the lateral thin-walled cells increases the global stiffness of the material.

As the viscous behavior of foams is demonstrated by various tests, it is worthwhile to elaborate a material law including the viscous and hyper elasticity effects. This is developed in [110] where a decoupling between viscous and elastic parts is introduced by using finite transformations. Only the deviatoric part of the stress tensor is concerned by viscous effects.

Material LAW62 corresponds to a hyper-elastic solid material using the Ogden formulation for rubber material. The strain energy functional [111] is given by:

$$\mathrm{W}(\mathbf{C})=\sum_{i=1}^{N}\frac{2\mu_i}{\alpha_i^2}\left(\lambda_1^{\alpha_i}+\lambda_2^{\alpha_i}+\lambda_3^{\alpha_i}-3+\frac{1}{\beta}\left(J^{-\alpha_i\beta}-1\right)\right) \tag{1028}$$

Where, $\mathbf{C}$ is the right Cauchy Green Tensor, $C=F^tF$ with F the deformation gradient matrix, λ_i are the eigenvalues of F, $J=\det F,\beta=\frac{v}{(1-2v)}$, $v\neq 0$ and $v\neq\frac{1}{2}$

> **Note:** For rubber materials which are almost incompressible, the bulk modulus is very large compared to the shear modulus.

The ground shear modulus is given by:

$$\mu=\sum_{i=1}^{N}\mu_i \tag{1029}$$

W can be written as:

$$W(C)=\overline{W}(\overline{C})+U(J) \tag{1030}$$

Where,

$\overline{C}=\overline{F}^t\overline{F}$

$\overline{F}=J^{-1/3}F$

$\overline{C}$
Deviatoric part of the right Cauchy Green Tensor

U **and** $\overline{W}$
Volumetric and deviatoric parts of the stored energy functions and S_0 the second Piola-Kirchhoff stress tensor given by:

$$S_0=\frac{\partial W}{\partial E}=2\frac{\partial W}{\partial C}=2\frac{\partial\overline{W}}{\partial C}+2\frac{\partial U}{\partial C}=S_0^{dev}+S_0^{vol} \tag{1031}$$

With $E=\frac{1}{2}(C-I)$

The Green-Lagrange strain tensor:

$S_0^{dev}=2\frac{\partial\overline{W}}{\partial C}$ and $S_0^{vol}=2\frac{\partial U}{\partial C}$ are the deviatoric and volumetric parts of the second Piola-Kirchhoff stress tensor S_0.

Rate effects are modeled through visco-elasticity using a convolution integral using Prony series. This corresponds to an extension of small strain theory or finite deformation to large strain. The rate effect is applied only to the deviatoric stress. The deviatoric stress is computed as:

$$S^{dev}(t)=\gamma_{\infty}S_0^{dev}(t)-J^{-2/3}DEV[\sum_{i=1}^{M_i}Q_i(t)] \tag{1032}$$

Where, Q_i is the internal variable given by the following rate equations:

$$\dot{Q}_i(t)+\frac{1}{\tau_i}Q_i(t)=\frac{\gamma_i}{\tau_i}DEV[2\frac{\partial\overline{W}}{\partial\overline{C}}(t)] \tag{1033}$$

$\lim Q_i(t)=0,\ t\rightarrow-\infty$

$\gamma_i\in[0,\ 1],\ \tau_i>0$

Q_i is given by the following convolution integral:

$$Q_i(t)=\frac{\gamma_i}{\tau_i}\int_{-\infty}^{t}\exp[-(t-s)/\tau_i]\frac{d[DEV\{2\partial_{\overline{C}}\overline{W}^0[\overline{C}(s)]\}]}{ds}ds \tag{1034}$$

Where,

$\gamma_{\infty}=G_{\infty}/G_0$

$1=\gamma_{\infty}+\sum_{i=1}^{M_i}\gamma_i$

$\gamma_i=G_i/G_0$

$G_0=G_{\infty}+\sum_{i=1}^{M_i}G_i$

$dev(\bullet)=\bullet-\frac{1}{3}(\bullet:C)C^{-1}$

Where, G_0 is the initial shear modulus; G_0 should be exactly the same as the ground shear modulus μ. G_{∞} is the long-term shear modulus that can be obtained from long-term material testing. τ_i are the relaxation times.

The relation between the second Piola-Kirchhoff stress tensor $S=S^{dev}+S_0^{vol}$ and Cauchy stress tensor $\boldsymbol{\sigma}$ is:

$$\boldsymbol{\sigma}=\frac{1}{\det\mathbf{F}}\mathbf{F}\mathbf{S}\mathbf{F}^t \tag{1035}$$

[110] Simo J.C., “On a fully three-dimensional finite strain viscoelastic damage model: Formulation and Computational Aspects”, Computer Methods in Applied Mechanics and Engineering, Vol. 60, pp. 153-173, 1987.

[111] Ogden R.W., “Nonlinear Elastic Deformations”, Ellis Horwood, 1984.

Hydrodynamic Analysis Materials

The following material laws are commonly used for fluid simulations:

- Johnson-Cook model for strain rate and temperature dependence on yield stress (LAW4),
- Hydrodynamic viscous material for Newtonian or turbulent fluids (LAW6),
- Elasto-plastic hydrodynamic materials with von Mises isotropic hardening and polynomial pressure (LAW3),
- Steinberg-Guinan elasto-plastic hydrodynamic law with thermal softening (LAW49),
- Boundary element materials (LAW11),
- Purely thermal materials (LAW18)

Radioss provides a material database incorporated in the installation. Many parameters are already defined by default and give accurate results.

Johnson-Cook Law for Hydrodynamics (LAW4)

This law enables to model hydrodynamic behavior of an elastic-plastic material using Johnson-Cook Yield criteria and any equation of state available with `/EOS` card. It based on `/MAT/LAW3` and adds strain rate and temperature dependency. The advantage of material LAW04 regarding classical `LAW02 (/MAT/JCOOK)` is that you can choose any available EOS from `/EOS` card.

The equation describing yield stress (scale value) is:

$$\sigma_y = \left(A + B\,\varepsilon_{pn}\right)\left(1 + C\ln\frac{\dot{\varepsilon}}{\dot{\varepsilon}_0}\right)\left(1 - T^{*}{}_{m}\right) \tag{1036}$$

Where, $T^{*} = \dfrac{T - T_r}{T_{melt} - T_r}$

The pressure and energy values are obtained by solving equation of state $P(\mu, E)$ related to the material (`/EOS`).

Material parameters are the same as in LAW3.

The parameters are:

C	Strain rate coefficient
$\dot{\varepsilon}_0$	Reference strain rate
m	Temperature exponent
T T_{melt}	Melting temperature
T_{max}	Maximum temperature For $T > T_{\max}$, then m=1 is used.
$\rho_0 C_p$	Specific heat per unit volume

For an explanation about strain rate filtering, refer to Strain Rate Filtering.

Hydrodynamic Viscous Fluid Materials (LAW6)

This law is specifically designed to model liquids and gases.

The equations used to describe the material are:

$$S_{ij} = 2\rho v \dot{e}_{ij} \tag{1037}$$

$$p = C_0 + C_1\mu + C_2\mu^2 + C_3\mu^3 + \left(C_4 + C_5\mu\right)E_n \tag{1038}$$

Where,

S_{ij}	Deviatoric stress tensor
$\vec{V}$	Kinematic viscosity
$\dot{e}_{ij}$	Deviatoric strain rate tensor

The kinematic viscosity $\vec{V}$ is related to the dynamic viscosity, η by:

$$v = \frac{\eta}{\rho} \tag{1039}$$

Perfect Gas Model

To model a perfect gas, all coefficients C_0, C_1, C_2, C_3 must be set to equal zero. Also:

$$C_4 = C_5 = \gamma - 1 \tag{1040}$$

$$E_{n0} = \frac{P_0}{\gamma - 1} \tag{1041}$$

A perfect gas allows compressibility and expansion and contraction with a rise in temperature. However, for many situations, especially very slow subsonic flows, an incompressible gas gives accurate and reliable results with less computation.

Incompressible Gas Model

To model an incompressible gas, the coefficients should be set to:

$$C_0 = C_1 = C_2 = C_3 = C_4 = C_5 = E_0 = 0 \tag{1042}$$

$$C_1 = \rho_0 \cdot c^2 \tag{1043}$$

Where,

c	Speed of sound

Incompressibility is achieved via a penalty method. The sound speed is set to at least 10 times the maximum velocity.

This classical assumption is not valid when fluid and structures are coupled. In this case, set the sound speed in the fluid so that the first eigen frequency is at least 10 times higher in the fluid than in the structure.

Elasto-plastic Hydrodynamic Materials (LAW3)

This law is only used with solid brick and quadrilateral elements.

It models the elastic and plastic regions, similar to LAW2, with a nonlinear behavior of pressure and without strain rate effect. The law is designed to simulate materials in compression.

The stress-strain relationship for the material under tension is:

$$\sigma = \left(a + b\varepsilon_{pn}\right) \tag{1044}$$

The pressure and energy values are obtained by solving equation of state $P(\mu, E)$ related to the material (`/EOS`).

Input requires Young's or the elastic modulus, E, and Poisson's ratio, υ. These quantities are used only for the deviatoric part. The plasticity material parameters are:

a	Yield stress
b	Hardening modulus
n	Hardening exponent
$\sigma_{\max}$	Maximum flow stress
ε_p^{max}	Plastic strain at rupture

A pressure cut off, *P_{min}*, can be given to limit the pressure in tension. The pressure cut off must be lower or equal to zero. Figure 243 shows a typical curve of the hydrodynamic pressure.

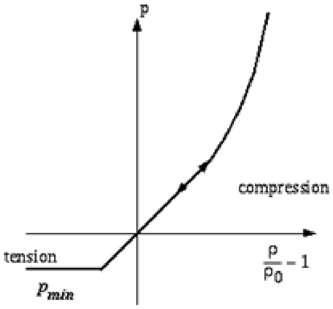

Figure 243: Hydrodynamic Pressure Relationship

Steinberg-Guinan Material (LAW49)

This law defines as elastic-plastic material with thermal softening. When material approaches melting point, the yield strength and shear modulus reduces to zero.

The melting energy is defined as:

$$E_m = E_c + \rho c_p T_m \tag{1045}$$

Where, E_c is cold compression energy and T_m melting temperature is supposed to be constant. If the internal energy E is less than E_m, the shear modulus and the yield strength are defined by:

$$G = G_0\left[1 + b_1 p V^{1/3} - h\left(T - T_0\right)\right] e^{-\frac{fE}{E - E_m}} \tag{1046}$$

$$\sigma_y = \sigma'_0\left[1 + b_2 p V^{1/3} - h\left(T - T_0\right)\right] e^{-\frac{fE}{E - E_m}} \tag{1047}$$

Where, b_1, b_2, h and f are the material parameters. σ'_0 is given by a hardening rule:

$$\sigma'_0 = \sigma_0\left[1 + \beta\varepsilon_p\right]^n \tag{1048}$$

The value of σ'_0 is limited by $\sigma_{\max}$.

The material pressure p is obtained by solving equation of state $P(\mu, E)$ related to the material (`/EOS`) as in LAW3.

Void Materials (LAW0)

This material can be used to define elements to act as a void, or empty space.

Shape Memory Superelastic Material (LAW71)

This material can be used to define elements to act as a void, or empty space.

The constitutive model that is used in LAW71 to describe the shape memory alloy superelastic behavior is based on the work of Auricchio.[112]

Phase Transformation Conditions

Two phase transformations are considered:

- Transformation from austenite to martensite denoted AS $(\mathrm{A} \rightarrow \mathrm{S})$
- Transformation from martensite to austenite denoted SA $(\mathrm{S} \rightarrow \mathrm{A})$

A transformation strain is introduced dependent on the evolution of the fraction of martensite:

$$\dot{\varepsilon}^{tr} = \varepsilon_L \dot{X}_m \mathbf{n} \tag{1049}$$

The stress deviator and pressure are updated using the fraction of martensite and transformation strain:

$$s = 2G(e - \varepsilon_L X_m \mathbf{n}) \tag{1050}$$

$$p = K(tr(\varepsilon) - 3\alpha\varepsilon_L X_m) \tag{1051}$$

G and K are the shear and the bulk modulus, respectively. It is possible to define these parameters dependent on the martensite fraction. In this case, A and M subscripts refer to austenite and martensite, respectively. The two moduli are calculated as:

$$G = G_A + X_m(G_M - G_A) \tag{1052}$$

(1053)

Where,

e	Deviator of the strain
tr	Denotes the trace of the tensor
Xm	Martensite fraction
ε_L **and** a	Constant material parameters
$\mathbf{n}$	Unit vector is defined as $\mathbf{n} = \frac{e}{\lVert e \rVert}$

Transformation from Austenite to Martensite

Two functions are defined for the start and the final point of transformation. These functions are expressed as:

$$F_S^{SA} = F^{SA} - R_S^{SA} \tag{1054}$$

$$F_F^{SA} = F^{SA} - R_F^{SA} \tag{1055}$$

Where,

$$R_S^{SA} = \sigma_S^{SA}\left(\sqrt{\frac{2}{3}} + \alpha\right) - C^{SA}T_S^{SA} \tag{1056}$$

$$R_F^{SA} = \sigma_F^{SA}\left(\sqrt{\frac{2}{3}} + \alpha\right) - C^{SA}T_F^{SA} \tag{1057}$$

The loading function F^{SA} is computed using the stress deviator s, the pressure p, and the temperature:

$$F^{SA} = \lVert s \rVert + 3\alpha p - C^{SA}T \tag{1058}$$

Where, a, σ_S^{SA}, σ_F^{SA}, T_S^{SA}, T_F^{SA}, and C^{SA} are the material parameters.

The conversion of austenite to martensite takes place when the following conditions are verified:

$$F_S^{SA} < 0 \tag{1059}$$

$$F_F^{SAS} > 0 \tag{1060}$$

$$\dot{F}^{SAS} < 0 \tag{1061}$$

[112] F. Auricchio, R.L. Taylor. Shape memory alloys: modeling and numerical simulations of the finite-strain superelastic behavior. Comput. Methods Appl. Mech. Engrg. 143 (1997) 175-194.

Failure Models

In addition to the possibility to define user's material failure models, Radioss integrates several failure models. These models use generally a global notion of cumulative damage to compute failure. They are mostly independent to constitutive law and the hardening model and can be linked to several available material laws. A compatibility table is given in the *Radioss Reference Guide*. Table 8 provides a brief description of available models.

Table 8: Failure Model Description

Failure Model	Type	Description
BIQUAD	Strain failure model	Direct input on effective plastic strain to failure
CHANG	Chang-Chang model	Failure criteria for composites
CONNECT	Failure	Normal and Tangential failure model
EMC	Extended Mohr Coulomb failure model	Failure dependent on effective plastic strain
ENERGY	Energy isotrop	Energy density
FABRIC	Traction	Strain failure
FLD	Forming limit diagram	Introduction of the experimental failure data in the simulation
HASHIN [115] [116]	Composite model	Hashin model
HC_DSSE	Extended Mohr Coulomb failure model	Strain based Ductile Failure Model: Hosford-Coulomb with Domain of Shell-to-Solid Equivalence
JOHNSON	Ductile failure model	Cumulative damage law based on the plastic strain accumulation
LAD_DAMA	Composite delamination	Ladeveze delamination model
NXT	NXT failure criteria	Similar to FLD, but based on stresses
PUCK	Composite model	Puck model
SNCONNECT	Failure	Failure criteria for plastic strain
SPALLING	Ductile + Spalling	Johnson-Cook failure model with Spalling effect
TAB1	Strain failure model	Based on damage accumulation using user-defined functions

Failure Model	Type	Description
TBUTCHER	Failure due to fatigue	Fracture appears when time integration of a stress expression becomes true
TENSSTRAIN	Traction	Strain failure
WIERZBICKI	Ductile material	3D failure model for solid and shells
WILKINS	Ductile Failure model	Cumulative damage law

Johnson-Cook Failure Model

High-rate tests in both compression and tension using the Hopkinson bar generally demonstrate the stress-strain response is highly isotropic for a large scale of metallic materials. The Johnson-Cook model is very popular as it includes a simple form of the constitutive equations. In addition, it also has a cumulative damage law that can be accesses failure:

$$D=\sum\frac{\Delta\varepsilon}{\varepsilon_f} \tag{1062}$$

with:

$$\varepsilon_f=\left[D_1+D_2\exp\left(D_3\sigma^*\right)\right]\left[1+D_4\ln\left(\frac{\dot{\varepsilon}}{\dot{\varepsilon}_0}\right)\right]\left[1+D_5T^*\right] \tag{1063}$$

Where $\Delta\varepsilon$ is the increment of plastic strain during a loading increment, $\sigma^*=\frac{\sigma_m}{\sigma_{VM}}$ the normalized mean stress and the parameters D_i the material constants. Failure is assumed to occur when D=1.

Wilkins Failure Criteria

An early continuum model for void nucleation is presented in [113]. The model proposes that the decohesion (failure) stress σ_c is a critical combination of the hydrostatic stress σ_m and the equivalent von Mises stress σ_{VM}:

$$\sigma_c=\sigma_m+\sigma_{VM} \tag{1064}$$

In a similar approach, a failure criteria based on a cumulative equivalent plastic strain was proposed by Wilkins. Two weight functions are introduced to control the combination of damage due to the hydrostatic and deviatoric loading components. The failure is assumed when the cumulative reaches a critical value D_c. The cumulative damage is obtained by:

$$D_c=\int W_1W_2\,d\bar{\varepsilon}_p\approx\sum_{i=1}^{n}W_1W_2\,\Delta\bar{\varepsilon}_p^i \tag{1065}$$

Where,

$$W_1=\left(\frac{1}{1+aP}\right)^{\alpha}$$

$$P = \frac{1}{3}\sum_{j=1}^{3}\sigma_{jj}$$

$$W_2 = (2 - A)^{\beta}$$

$$A = \max\left(\frac{s_2}{s_3}, \frac{s_2}{s_1}\right)$$

$$s_1 \geq s_2 \geq s_3$$

Where,

$\Delta\bar{\varepsilon}_p$	An increment of the equivalent plastic strain
W_1	Hydrostatic pressure weighting factor
W_2	Deviatoric weighting factor
s_{i}	Deviatoric principal stresses
a, α **and** β	The material constants

Tuler-Butcher Failure Criteria

A solid may break owning to fatigue due to Tuler-Butcher criteria: [114]

$$D = \int_0^t \max\left(0, (\sigma - \sigma_r)^{\lambda}\right)dt \tag{1066}$$

Where,

σ_r	Fracture stress
σ	Maximum principal stress
λ	Material constant
t	Time when solid cracks
D	Another material constant, called damage integral

Forming Limit Diagram for Failure (FLD)

In this method the failure zone is defined in the plane of principal strains (Figure 244). The method usable for shell elements allows introducing the experimental results in the simulation.

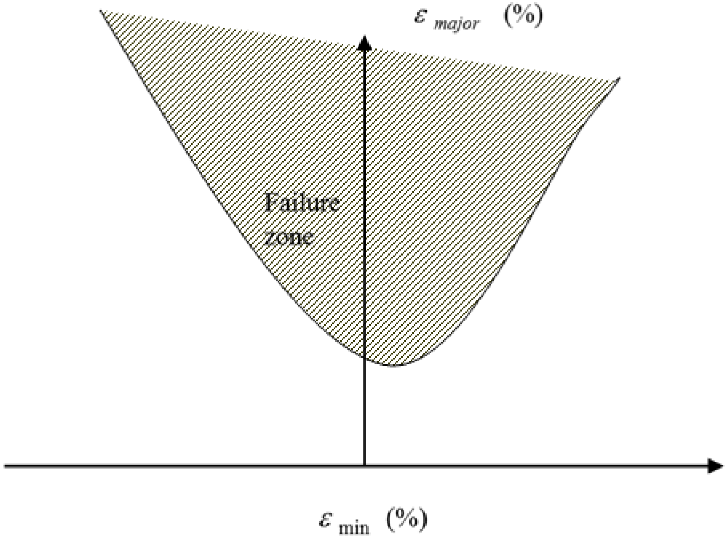

Figure 244: Generic Forming Limit Diagram (FLD)

Spalling with Johnson-Cook Failure Model

In this model, the Johnson-Cook failure model is combined to a Spalling model where we take into account the spall of the material when the pressure achieves a minimum value P_{min}. The deviatoric stresses are set to zero for compressive pressure. If the hydrostatic tension is computed, then the pressure is set to zero. The failure equations are the same as in Johnson-Cook model.

Bao-Xue Wierzbicki Failure Model

Bao-Xue-Wierzbicki model [117] represents a 3D fracture criterion which can be expressed by:

$$\bar{\varepsilon}_f{}^n = \bar{\varepsilon}_{\max}{}^n - \left[\bar{\varepsilon}_{\max}{}^n - \bar{\varepsilon}_{\min}{}^n\right]\left(1-\bar{\xi}^m\right)^{1/m} \tag{1067}$$

$$\bar{\varepsilon}_{\max} = C_1 e^{-C_2\bar{\eta}} \tag{1068}$$

$$\bar{\varepsilon}_{\min} = C_3 e^{-C_4\bar{\eta}} \tag{1069}$$

Where, C_1, C_2, C_3 , C_4, γ and m are the material constants, n is the hardening parameter and $\bar{\eta}$ and $\bar{\xi}$ are defined as:

- for solids:

  If I_{moy}=0:

  $$\bar{\eta} = \frac{\sigma_m}{\sigma_{VM}}; \; \bar{\xi} = \frac{27}{2}\frac{J_3}{\sigma_{VM}{}^3}$$

  If I_{moy}=1:

$$\overline{\eta} = \frac{\int_0^{\varepsilon p} \frac{\sigma_m}{\sigma_{VM}} d\varepsilon p}{\varepsilon p} \quad \overline{\xi} = \frac{\int_0^{\varepsilon p} \frac{27 J_3}{2\sigma_{VM}^3} d\varepsilon p}{\varepsilon p}$$

- for shells:

$$\overline{\eta} = \frac{\sigma_m}{\sigma_{VM}}; \ \overline{\xi} = -\frac{27}{2}\overline{\eta}\left(\overline{\eta}^2 - \frac{1}{3}\right)$$

Where,

σ_m
Hydrostatic stress

σ_{VM}
The von Mises stress

$J_3 = s_1 s_2 s_3$
Third invariant of principal deviatoric stresses

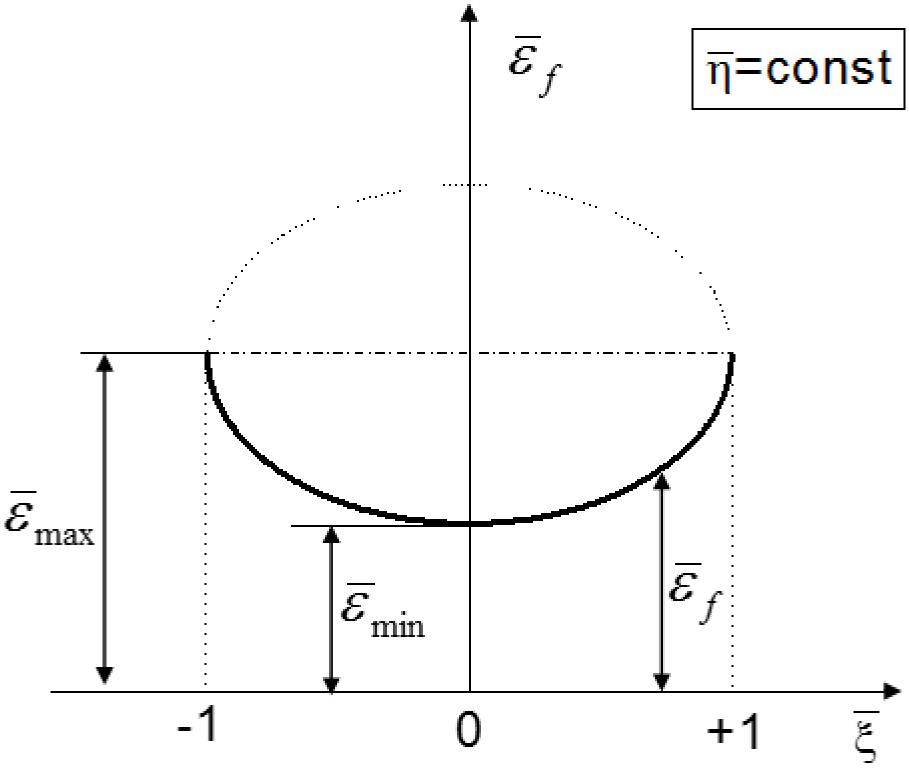
$\overline{\varepsilon}_f$
$\overline{\eta}$=const
$\overline{\varepsilon}_{max}$
$\overline{\varepsilon}_{min}$
$\overline{\varepsilon}_f$
-1
0
+1
$\overline{\xi}$

Figure 245: Graphical Representation of Bao-Xue-Wierzbicki Failure Criteria

Strain Failure Model

This failure model can be compared to the damage model in LAW27. When the principal tension strain ε_1 reaches ε_{t1}, a damage factor D is applied to reduce the stress, as shown in Figure 246. The element is ruptured when D=1. In addition, the maximum strains ε_{t1} and ε_{t2} may depend on the strain rate by defining a scale function.

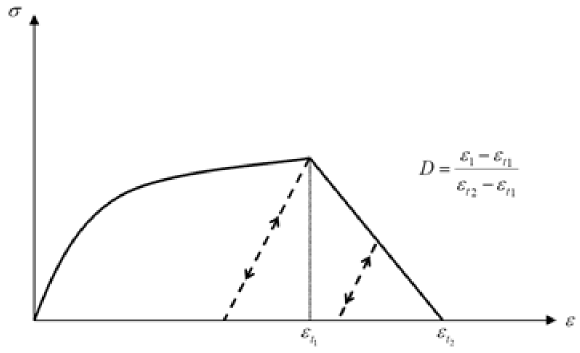
σ
ε
ε_{f_1}
ε_{f_2}
$D = \frac{\varepsilon_1 - \varepsilon_{f1}}{\varepsilon_{f2} - \varepsilon_{f1}}$

Figure 246: Strain Failure Model

Energy Density Failure Model

When the energy per unit volume achieves the value E_1, then the damage factor D is introduced to reduce the stress. For the limit value E_2, the element is ruptured. In addition, the energy values E_1 and E_2 may depend on the strain rate by defining a scale function.

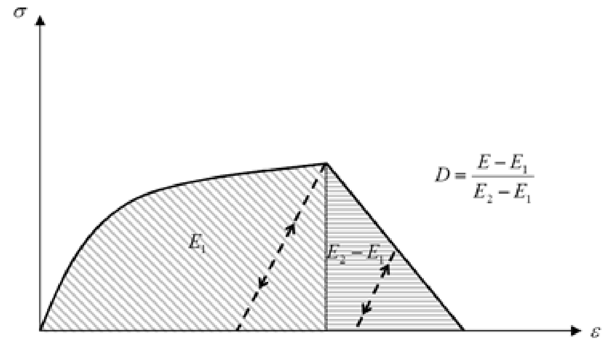

Figure 247: Strain Failure Model

XFEM Crack Initialization Failure Model

This failure model is available for Shell only.

In `/FAIL/TBUTCHER`, the failure mode criteria are written as:

For ductile materials, the cumulative damage parameter is:

$$D = \int_0^t \max\left(0, (\sigma - \sigma_r)^{\lambda}\right) dt \tag{1070}$$

Where,

σ_r	Fracture stress
σ	Maximum principal stress
λ	Material constant

t
Time when shell cracks for initiation of a new crack within the structure

D
Another material constant called damage integral

For brittle materials, the damage parameter is:

$$\dot{D} = \frac{1}{K}\left(\sigma - \sigma_r\right)^a \tag{1071}$$

$$\sigma_r = \sigma_0\left(1 - D\right)^b \tag{1072}$$

$$D = D + \dot{D}\Delta t \tag{1073}$$

[113] Argon A.S., J. Im, and Safoglu R., “Cavity formation from inclusions in ductile fracture”, Metallurgical Transactions, Vol. 6A, pp. 825-837, 1975.

[114] Tuler F.R. and Butcher B.M., “A criteria for time dependence of dynamic fracture”, International Journal of Fracture Mechanics, Vol. 4, N°4, 1968.

[115] Hashin, Z. and Rotem, A., “A Fatigue Criterion for Fiber Reinforced Materials”, Journal of Composite Materials, Vol. 7, 1973, pp. 448-464. 9.

[116] Hashin, Z., “Failure Criteria for Unidirectional Fiber Composites”, Journal of Applied Mechanics, Vol. 47, 1980, pp. 329-334.

[117] Wierzbicki T., “From crash worthiness to fracture; Ten years of research at MIT”, International Radioss User's Conference, Nice, June 2006.

Monitored Volume

An airbag is defined as a monitored volume. A monitored volume is defined as having one or more 3 or 4 node shell property sets.

The defined surface must be closed (the normal to shell elements must be all oriented outward, as shown in Figure 248. The shell normal must be oriented outside the volume. It is possible to reverse the

shell normals for a given property set (by entering a negative property number). Dummy properties (`/PROP/TYPE0`) and materials (`/MAT/TYPE0`) can be used.

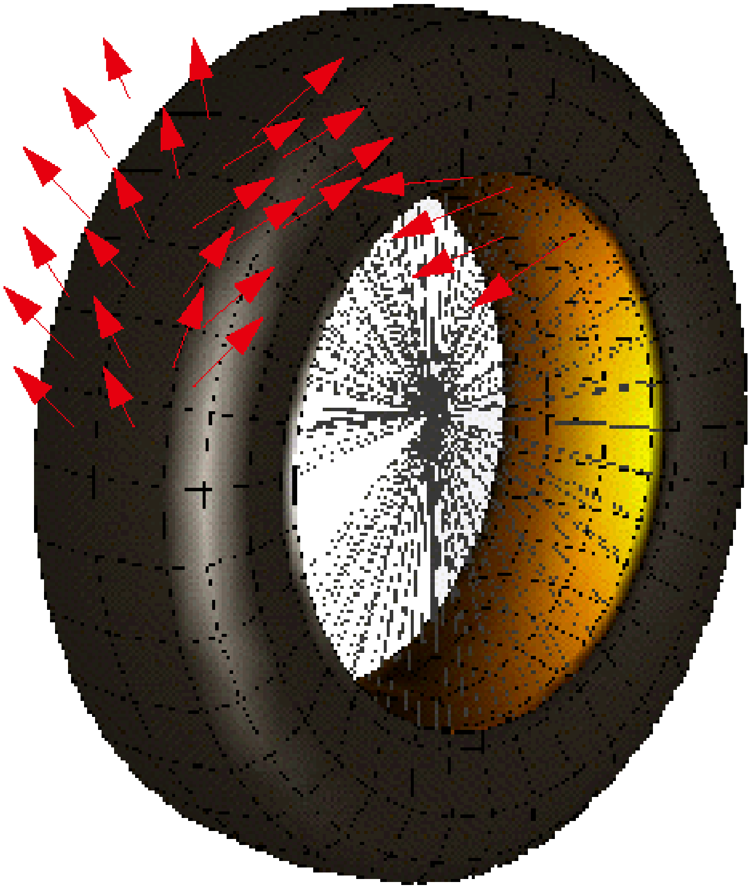

Figure 248: Tire Model: Volume Closed

There are five types of MONITORED VOLUME:

1. AREA Type: volume and surface output (post processing option, no pressure)
2. PRES Type: user function defining pressure versus relative volume
3. GAS Type: adiabatic pressure volume relation. $P(V - V_{inc})^{\gamma} = Cst$ with $\gamma = \frac{c_p}{c_v}$
4. AIRBAG Type: Single airbag $PV = nRT = mrT$

   $P = \rho rT = \rho(c_p - c_v)T = (\gamma - 1)\rho c_v T = (\gamma - 1)\frac{E}{V}$
5. COMMU1 Type: Chambered, communicating, folded airbag (airbag with communications)

Same basic equations:

Typical use of monitored volume is for tire, fuel tank, airbag.

- For tire use PRES or GAS type monitored volume.
- For fuel tank use PRES or GAS type monitored volume.
- For simple unfolded airbag use AIRBAG type monitored volume.
- For chambered airbag use two ore more COMMU1 type monitored volumes.
- For folded airbag use a set of COMMU1 type monitored volumes.

AREA Type

This type is only a post processing option. It allows plotting of the Time History of volume and area of a closed surface.

No pressure is applied with this option.

No specific input is needed for this type.

PRES Type

With this type the pressure is defined versus relative volume with a tabulated function:

$$P = F\left(\frac{V_0}{V}\right) \tag{1074}$$

Where,

F(x)	Function
V_0	Initial volume

No external pressure is defined.

Only the load curve number is needed as specific input.

GAS Type

This option gives an adiabatic pressure volume relation. With γ = 1 an isothermal condition can also be applied.

It is possible to define an incompressible sub-volume to model a volume partially filled with a liquid.

The general equation is:

$$P = \left(V - V_i\right)^{\gamma} = P_0\left(V_0 - V_i\right)^{\gamma} \tag{1075}$$

With

V_0	Initial volume
V_i	Incompressible volume $V_i < V_0$

A viscosity μ can be used to reduce numerical oscillations.

If μ = 1 a critical damping (shell mass and volume stiffness) is used. The viscous pressure q is:

$$q = \mu \frac{1}{A} \sqrt{\frac{\gamma P m_{fabric}}{V}} \frac{dV}{dt} \tag{1076}$$

Where,

$m_{fabric} = A\rho t$	Mass of fabric
A	Its surface

The applied pressure is $P - P_{ext} + q$.

The specific inputs for this type are:

- γ
- μ
- P_{ext}
- P_0
- V_i

If the deflation is considered (isenthalpic outflow computation), the initial mass of gas, must also be input.

This monitored volume is typically used to model tire pressure or simple fuel tank. For tire model V_i is zero and for fuel tank V_i is the fuel volume.

Thermodynamical Equations

The basic energy equation of the monitored volume can be written as:

$$dE_{Monitored\ Volume} = -Pd(V - V_i) - dH_{out} \tag{1077}$$

Where,

E	Internal energy
P	Pressure
V	Monitored volume
V_i	Incompressible volume
H_{out}	Outgoing enthalpy

When the adiabatic condition is applied and assuming a perfect gas:

$$P = \frac{(\gamma - 1)E}{V - V_i} \tag{1078}$$

Where, γ is the gas constant. For air, γ = 1.4.

The two equations above allow the current volume to be determined. The energy and pressure can then be found.

External Work Variation

At the current time step, t, assume we know:

- $P(t-dt)$
- $E(t-dt)$
- $\widetilde{V}=V-V_i$

$\delta W(t),\ E(t),\ P(t)$ will be obtained as:

$$\delta W=\frac{P(t)+P(t-dt)}{2}\left(\widetilde{V}(t)-\widetilde{V}(t-dt)\right) \tag{1079}$$

be the variation of external work and from the adiabatic condition:

$$P=\frac{(\gamma-1)E}{\widetilde{V}} \tag{1080}$$

we have:

$$\delta W=\frac{(\gamma-1)\Delta\widetilde{V}}{2}\left[\frac{E(t)}{\widetilde{V}(t)}+\frac{E(t-dt)}{\widetilde{V}(t-dt)}\right] \tag{1081}$$

Let:

$E=E(t-dt)$

$\widetilde{V}=\left(\widetilde{V}(t)-\widetilde{V}(t-dt)\right)/2$

$\Delta E=E(t)-E(t-dt)$

$$\delta W=\frac{(\gamma-1)}{2}\frac{\Delta\widetilde{V}}{\widetilde{V}}\left[\frac{1+\frac{\Delta E}{E}}{1+\frac{\Delta\widetilde{V}}{2\widetilde{V}}}+\frac{1}{1-\frac{\Delta\widetilde{V}}{2\widetilde{V}}}\right] \tag{1082}$$

Hence, the external work is given by:

$$\delta W\approx(\gamma-1)E\frac{\Delta\widetilde{V}}{\widetilde{V}}\left[1+\frac{\Delta E}{2E}\right] \tag{1083}$$

Computing the energy from basic principles:

$$\Delta E=-(\gamma-1)E\frac{\Delta\widetilde{V}}{\widetilde{V}}\left[1+\frac{\Delta E}{2E}\right]-\Delta H_{out} \tag{1084}$$

ΔH_{out} can be estimated from, $u(t-dt)$, the velocity at vent hole; this estimation will be described hereafter.

The variation of internal energy ΔE can be given by:

$$\Delta E = \left[-(\gamma - 1)E\frac{\Delta \widetilde{V}}{\widetilde{V}} - \Delta H_{out} \right]\left[1 - (\gamma - 1)E\frac{\Delta \widetilde{V}}{2\widetilde{V}} \right] \tag{1085}$$

Therefore:

$$E(t) = E(t - dt) + \Delta E \tag{1086}$$

$$P(t) = (\gamma - 1)\frac{E(t)}{\widetilde{V}(t)} \tag{1087}$$

This pressure is then applied to the monitored volume to get:

1. New accelerations
2. New velocities
3. New geometry
4. New volume
5. Ready for next step evaluation

Venting

Venting, or the expulsion of gas from the volume, is assumed to be *isenthalpic*.

The flow is also assumed to be unshocked, coming from a large reservoir and through a small orifice with effective surface area, A.

Conservation of enthalpy leads to velocity, u, at the vent hole. The Bernouilli equation is then written as:

$$(\text{monitored volume})\frac{\gamma}{\gamma - 1}\frac{P}{\rho} = \frac{\gamma}{\gamma - 1}\frac{P_{ext}}{\rho_{vent}} + \frac{u^2}{2}\ (\text{vent hole}) \tag{1088}$$

Applying the adiabatic conditions:

$$\frac{P}{\rho^{\gamma}} = \frac{P_{ext}}{{\rho_{vent}}^{\gamma}} \tag{1089}$$

Therefore, the exit velocity is given by:

$$u^2 = \frac{2\gamma}{\gamma - 1}\frac{P}{\rho}\left(1 - \left(\frac{P_{ext}}{P} \right)^{\frac{\gamma - 1}{\gamma}} \right) \tag{1090}$$

The mass flow rate is given by:

$$\dot{m}_{out} = \rho_{vent}A_{vent}u = \rho\left(\frac{P_{ext}}{P} \right)^{1/\gamma}A_{vent}u \tag{1091}$$

The energy flow rate is given by:

$$\dot{E}_{out} = \dot{m}\frac{E}{\rho\widetilde{V}} = \left(\frac{P_{ext}}{P} \right)^{1/\gamma}A_{vent}u\frac{E}{\widetilde{V}} \tag{1092}$$

The vent hole area or scale factor area, A_{vent}, can be defined in these ways:

- a constant area taking into account a discharge coefficient
- a variable area equal to the area of a specified surface, multiplied by a discharge coefficient
- a variable area equal to the area of the deleted elements within a specified surface, multiplied by a discharge coefficient

Supersonic Outlet Flow

Vent pressure P_{vent} is equal to external pressure P_{ext} for unshocked flow. For shocked flow, P_{vent} is equal to critical pressure P_{crit} and U is bounded to critical sound speed:

$$u^2 < \frac{2}{\gamma+1}c^2 = \frac{2}{\gamma+1}\frac{P}{\rho} \tag{1093}$$

And,

$$P_{crit} = P\left(\frac{2}{\gamma+1}\right)^{\frac{\gamma}{\gamma-1}} \tag{1094}$$

$$P_{vent} = \max\left(P_{crit}\right),\ P_{ext})$$

Example: GAS Type

Some applications in Radioss:

- A tire model:

  The inputs are:

  - γ = 1.4
  - μ
  - P_{ext}= 10^5 Pa
  - P_{ini} = initial tire pressure

    Then, the pressure in the tire is $P_{tire} = P_{ini} - P_{ext}$
  - $V_{inc} = 0$
- A fuel tank model if the sloshing effect is neglected

  Only if the sloshing effect is neglected, pressure in a partial filled fuel tank can be modeled with a type GAS monitored volume. Use the following input:

  - γ = 1.4
  - μ
  - P_{ext} = 10^5 Pa
  - P_{ini} = 10^5 Pa
  - V_{inc} = volume of fuel

AIRBAG Type

The airbag simulation used by Radioss uses a special uniform pressure airbag. Hence, regardless of state of inflation or shape, the pressure remains uniform.

Perfect gas law and adiabatic conditions are assumed. Injected mass and temperature are defined as a time function. A sensor can define the inflater starting time.

Deflation of vent hole is available after reaching a pressure (P_{def}) for a given duration $\Delta t\, P_{def}$ or at time (T_{def}) criteria. $\Delta t\, P_{def}$ prevents deflation due to initial peak of pressure corresponding to the jetting activation.

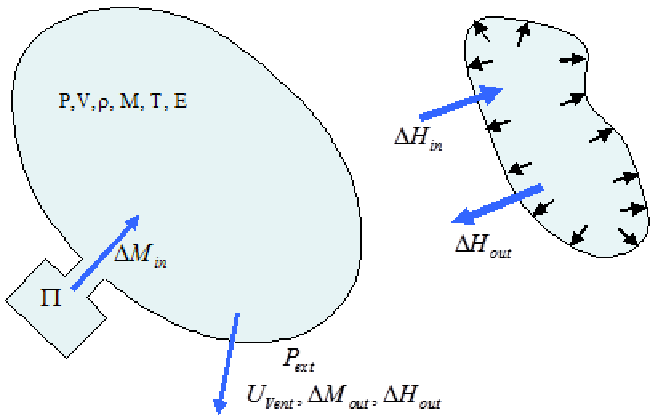

Figure 249: Uniform Pressure Airbag

The key assumptions are:

- Uniform airbag pressure ⇔ kinetic energy is negligible
- Adiabatic conditions

The airbag simulation must include:

- Injection of energy and mass
- Bag mechanics (that is, unfolding, expansion, membrane tension, impacts, ...)
- Exhaust through vent holes

Thermodynamical Equations

The basic energy equation of the airbag can be written as:

$$dE_{airbag} = -PdV + dH_{in} = dH_{out} \tag{1095}$$

Where,

E	Internal energy
P	Pressure
V	Airbag volume

H_{in}	Incoming enthalpy
H_{out}	Outgoing enthalpy

When the adiabatic condition is applied and assuming a perfect gas:

$$P = \frac{(\gamma - 1)E}{V} \tag{1096}$$

Where, γ is the gas constant. For air, γ = 1.4.

The two equations above allow the current airbag volume to be determined. The energy and pressure can then be found. To know the current airbag volume, derive energy and thus pressure.

Considering a gas such that the constant pressure and the constant volume heat capacities per mass unit (respectively, c_p and c_v) vary in temperature T.

The following temperature dependency of the constant pressure heat capacity is assumed:

$$c_p = a + bT + cT^2 \tag{1097}$$

Where, a, b and c are the constants depending to characteristics of the gas.

The c_p and c_v satisfy the Mayer relation:

$$\mathrm{c_p(T)\text{-}c_v(T)} = \frac{R}{M} \tag{1098}$$

With R is the universal gas constant depending to the unit system ($R = 8.3144\,Jmol^{-1}K^{-1}$):

$$\begin{gathered} c_v(T) = \frac{de}{dT}(T) \\ h(t) = e(t) + \frac{P}{\rho} \end{gathered} \tag{1099}$$

Where,

e	Specific energy
h	Specific enthalpy per mass unit of the gas at temperature T

You can then obtain:

$$e(T) = e_{cold} + \int_{T_{cold}}^{T} c_v(T)dT \tag{1100}$$

and

$$h(T) = e_{cold} + \int_{T_{cold}}^{T} c_v(T)dT + \frac{R}{M}T \tag{1101}$$

Where, the lower index $cold$ refers to the reference temperature T_{cold}.

Now, assuming an ideal mixture of gas:

$$PV = nRT \tag{1102}$$

with n the total number of moles:

$$n = \sum_i n^{(i)} = \sum_i \frac{m^{(i)}}{M^{(i)}} \tag{1103}$$

Where,

$M^{(i)}$
Mass of gas i

$M^{(i)}$
Molar weight of gas$i$

It follows:

$$P = \frac{nRT}{V} \tag{1104}$$

With $n = \sum_i \frac{m^{(i)}}{M^{(i)}}$.

Energy Variation Within a Time Step

Let $T(t-\delta t)$ the temperature, $P(t-\delta t)$ the pressure, and $V(t-\delta t)$ the volume of the airbag at time$t-\delta t$, and $\mathrm{m}^{(i)}$ the mass of gas i at time $t-\delta t$. $T(t)$, $P(t)$, $V(t)$ are respectively temperature, pressure and volume of the airbag at time t, and $\mathrm{m}^{(i)} + \delta \mathrm{m}_{\mathrm{in}}^{(i)} - \delta \mathrm{m}_{\mathrm{out}}^{(i)}$ the mass of gas i at time t.

Using , the variation of total gas energy can be written as:

$$\Delta E = \left[\sum_i (\mathrm{m}^{(i)} + \delta m^{(i)}{}_{\mathrm{in}} - \delta m^{(i)}{}_{\mathrm{out}}) \left(e^{(i)}{}_{cold} + \int_{T_{cold}}^{T(t)} c_{v}{}^{(i)}(T) dT \right) \right] - \left[\sum_i \mathrm{m}^{(i)} \left(e^{(i)}{}_{cold} + \int_{T_{cold}}^{T(t-\delta t)} c_{v}{}^{(i)}(T) dT \right) \right] \tag{1105}$$

which can be written as:

$$\Delta E = \left[\sum_i (\mathrm{m}^{(i)} + \delta m^{(i)}{}_{\mathrm{in}} - \delta m^{(i)}{}_{\mathrm{out}}) \left(\int_{T(t-\delta t)}^{T(t)} c_{v}{}^{(i)}(T) dT \right) \right] + \left[\sum_i \left(\delta m^{(i)}{}_{\mathrm{in}} - \delta m^{(i)}{}_{\mathrm{out}} \right) \left(e^{(i)}{}_{cold} + \int_{T_{cold}}^{T(t-\delta t)} c_{v}{}^{(i)}(T) dT \right) \right] \tag{1106}$$

On the other hand, the basic energy equation Thermodynamical Equations, Equation 1095 of the airbag and the expression of enthalpy in Thermodynamical Equations, Equation 1099 gives:

$$\Delta E = \left[\sum_i \delta m^{(i)}_{in} \left(e^{(i)}_{cold} + \frac{R}{M^{(i)}} T^{(i)}_{in} + \int_{T_{cold}}^{T^{(i)}_{in}} c_{v(i)}(T) dT \right) \right] - \left[\sum_i \delta m^{(i)}_{out} \left(e^{(i)}_{cold} + \frac{R}{M^{(i)}} T^{(i)}_{out} + \int_{T_{cold}}^{T^{(i)}_{out}} c_{v(i)}(T) dT \right) \right] - \delta W \tag{1107}$$

Where, $\delta \mathrm{m}_{\mathrm{in}}^{(\mathrm{i})}$ and $T^{(i)}_{in}$ are characteristics of the inflator and are considered as input to the problem. $\delta \mathrm{m}_{\mathrm{out}}^{(\mathrm{i})}$ and $T^{(i)}_{out}$ can be estimated from the velocity at vent hole $u(t)$. δW is the variation of the external work. This estimation will be described hereafter.

It comes from Equation 1105 and Equation 1106:

$$\sum_i \left(m^{(i)} + \delta m^{(i)}_{in} - \delta m^{(i)}_{out} \right) \int_{T(t-\delta t)}^{T(t)} c_{v(i)}(T) dT = \left[\sum_i \delta m^{(i)}_{in} \left(\frac{R}{M^{(i)}} T^{(i)}_{in} + \int_{T(t-\delta t)}^{T^{(i)}_{in}} c_{v(i)}(T) dT \right) \right] - \left[\sum_i \delta m^{(i)}_{out} \left(\frac{R}{M^{(i)}} T^{(i)}_{out} + \int_{T(t-\delta t)}^{T^{(i)}_{out}} c_{v(i)}(T) dT \right) \right] - \delta W \tag{1108}$$

The variation of the external work can be written as:

$$\delta W = \frac{\left(P(t) + P(t-\delta t) \right)}{2} \left(V(t) - V(t-\delta t) \right) \tag{1109}$$

Using Thermodynamical Equations, Equation 1103, the last expression can be written as:

$$\delta W = \frac{1}{2} \left(\frac{\left[\sum_i \frac{m^{(i)} + \delta m^{(i)}_{in} - \delta m^{(i)}_{out}}{M^{(i)}} \right] RT(t)}{V(t)} + \frac{\left[\sum_i \frac{m^{(i)}}{M^{(i)}} \right] RT(t-\delta t)}{V(t-\delta t)} \right) \left(V(t) - V(t-\delta t) \right) \tag{1110}$$

The last equation can be introduced to Equation 1108:

$$\left[\sum_i (m^{(i)}+\delta m^{(i)}_{in}-\delta m^{(i)}_{out})\int_{T(t-\delta t)}^{T(t)} c_{v(i)}(T)dT\right]+\left[\sum_i \frac{m^{(i)}+\delta m^{(i)}_{in}-\delta m^{(i)}_{out}}{M^{(i)}}\right]RT(t)\frac{V(t)-V(t-\delta t)}{2V(t)}$$
$$=\left[\sum_i \delta m^{(i)}_{in}\left(\frac{R}{M^{(i)}}T^{(i)}_{in}+\int_{T(t-\delta t)}^{T^{(i)}_{in}} c_{v(i)}(T)dT\right)\right]-\left[\sum_i \delta m^{(i)}_{out}\left(\frac{R}{M^{(i)}}T^{(i)}_{out}+\int_{T(t-\delta t)}^{T^{(i)}_{out}} c_{v(i)}(T)dT\right)\right]-$$
$$\left[\sum_i \frac{m^{(i)}}{M^{(i)}}\right]RT(t-\delta t)\frac{V(t)-V(t-\delta t)}{2V(t-\delta t)} \tag{1111}$$

The first order approximation $\int_{T(t-\delta t)}^{T(t)} c_{v(i)}(T) \approx c_{v(i)}(T|_{t-\delta t})(T(t)-T(t-\delta t))$ for each gas, which allows rewrite Equation 1111 as:

$$\left[\sum_i (m^{(i)}+\delta m^{(i)}_{in}-\delta m^{(i)}_{out})c_{v(i)}(T|_{t-\delta t})(T(t)-T(t-\delta t))\right]+$$
$$\left[\sum_i \frac{m^{(i)}+\delta m^{(i)}_{in}-\delta m^{(i)}_{out}}{M^{(i)}}\right]RT(t)\frac{V(t)-V(t-\delta t)}{2V(t)}$$
$$=\left[\sum_i \delta m^{(i)}_{in}\left(\frac{R}{M^{(i)}}T^{(i)}_{in}+\int_{T(t-\delta t)}^{T^{(i)}_{in}} c_{v(i)}(T)dT\right)\right]-\left[\sum_i \delta m^{(i)}_{out}\left(\frac{R}{M^{(i)}}T_{out}+\int_{T(t-\delta t)}^{T^{(i)}_{out}} c_{v(i)}(T)dT\right)\right]-$$
$$\left[\sum_i \frac{m^{(i)}}{M^{(i)}}\right]RT(t-\delta t)\frac{V(t)-V(t-\delta t)}{2V(t-\delta t)} \tag{1112}$$

Which allows to determine the actual temperature $T(t)$. The actual pressure then computed from the equation of perfect gas (Thermodynamical Equations, Equation 1103).

Mass Injection

The amount of mass injected into the airbag needs to be defined with respect to time. This is required as a function.

The specific heat, c_p, along with a function defining the change in temperature with time is required.

The data can be obtained by two methods:

1. Possibly from the airbag manufacturer
2. From a tank experiment

A diagram of a tank experiment can be seen in Figure 250.

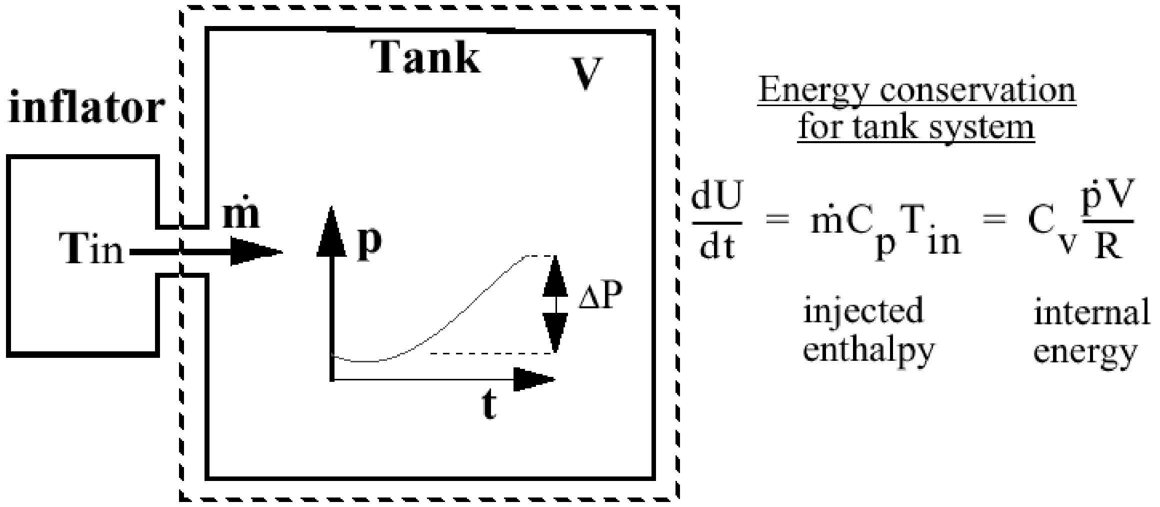
inflator
Tin
ṁ
Tank
V
p
ΔP
t
Energy conservation for tank system
$\frac{dU}{dt} = \dot{m} C_p T_{in} = C_v \frac{\dot{p}V}{R}$
injected enthalpy
internal energy

Figure 250: Tank Experiment

The mass versus time curve can be derived from the pressure curve if T_{in} is known:

$$\dot{m} = \frac{\dot{P} V M}{\gamma R T_{in}} \tag{1113}$$

Where, M is the molecular weight of the injected gas. R is the perfect gas constant: $\frac{R}{M} = c_p - c_v$; $\gamma = \frac{c_p}{c_v}$.

The average estimate for temperature of injection is:

$$T_{in} = \frac{\Delta P}{\Delta m} \frac{V M}{\gamma R} \tag{1114}$$

Where,

ΔP
: Total pressure variation during the experiment

Δm
: Total injected mass, which can be derived from the mass of propellant in the pyrotechnic inflator and the chemical reaction; 40% is a typical value for the ratio of the produced mass of gas to the solid propellant mass.

Venting Outgoing Mass Determination

Venting, or the expulsion of gas from the airbag, is assumed to be isenthalpic.

The flow is also assumed to be unshocked, coming from a large reservoir and through a small orifice with effective surface area, T.

Conservation of enthalpy leads to velocity, u, at the vent hole. The Bernouilli equation is then written as:

$$\text{(airbag)}\ \frac{\gamma}{\gamma-1}\frac{P}{\rho}=\frac{\gamma}{\gamma-1}\frac{P_{ext}}{\rho_{vent}}+\frac{u^2}{2}\ \text{(vent hole)} \tag{1115}$$

Applying the adiabatic conditions:

$$\text{(airbag)}\ \frac{P}{\rho^{\gamma}}=\frac{P_{ext}}{\rho_{vent}{}^{\gamma}}\ \text{(vent hole)} \tag{1116}$$

Therefore, the exit velocity is given by:

$$u^2=\frac{2\gamma}{\gamma-1}\frac{P}{\rho}\left(1-\left(\frac{P_{ext}}{P}\right)^{\frac{\gamma-1}{\gamma}}\right) \tag{1117}$$

with $\rho=\frac{\sum_i m^{(i)}}{V}$ the averaged density of the gas and $\gamma=\frac{\left[\sum_i m^{(i)}c_{p(i)}\right]/\left[\sum_i m^{(i)}\right]}{\left[\sum_i m^{(i)}c_{v(i)}\right]/\left[\sum_i m^{(i)}\right]}$ the fraction of massic averages of heat capacities at constant pressure and constant volume.

The mass flow rate is given by:

$$\dot{m}_{out}=\rho_{vent}A_{vent}u=\rho\left(\frac{P_{ext}}{P}\right)^{1/\gamma}A_{vent}u \tag{1118}$$

The energy flow rate is given by:

$$\dot{E}_{out}=\dot{m}\frac{E}{\rho V}=\left(\frac{P_{ext}}{P}\right)^{1/\gamma}A_{vent}u\frac{E}{V} \tag{1119}$$

The total mass flow rate is given by:

$$dm_{out}=\rho\left(\frac{P_{ext}}{P}\right)^{1/\gamma}A_{vent}u \tag{1120}$$

Where,

A_{vent} Vent hole surface.

The vent hole area or scale factor area, A_{vent}, can be defined in two ways:

- a constant area taking into account a discharge coefficient
- a variable area equal to the area of a specified surface multiplied by a discharge coefficient.

Supersonic Outlet Flow

Vent pressure P_{vent} is equal to external pressure P_{ext} for unshocked flow. For shocked flow, P_{vent} is equal to critical pressure P_{crit} and u is bounded to critical sound speed:

$$u^2 < \frac{2}{\gamma+1} c^2 = \frac{2*\gamma}{\gamma+1} \frac{P}{\rho} \tag{1121}$$

And,

$$P_{crit} = P\left(\frac{2}{\gamma+1}\right)^{\frac{\gamma}{\gamma-1}}$$

$$P_{vent} = \max\left(P_{crit}, P_{ext}\right)$$

Outgoing Mass per Gas

The mass flow of gas i is $dm^{(i)}{}_{out} = \frac{V^{(i)}}{V} dm_{out}$, where $V^{(i)}$ is the volume occupied by gas i and satisfies:

$V^{(i)} = \frac{n^{(i)}}{n} V$ (from $PV^{(i)} = n^{(i)}RT$ and $PV = \left[\sum_i n^{(i)}\right]RT$).

It comes finally

$$dm^{(i)}{}_{out} = \frac{n^{(i)}}{\sum_i n^{(i)}} dm_{out} \tag{1122}$$

Porosity

The isenthalpic model is also used for porosity. In this case, one can define the outgoing surface by:

$$A_{OUT} = \lambda\, f(A)\, g(P)\, h(t) \tag{1123}$$

Where,

A	Area of the specified surface
λ	Scale factor
P	Pressure of the gas
t	Time

It is also possible to define closure of the porous surface in the case of contact.

The second model integrated in Radioss is called the Chemkin model, in which the mass flow due to the porosity is computed by:

$$\dot{m} = A_{vent}\, u\, \rho_{airbag} \tag{1124}$$

Where, u is the user-defined function, represented as:

$$u = f\left(P - P_{ext}\right) \tag{1125}$$

Initial Conditions

To avoid initial disequilibrium and mathematical discontinuity for zero mass or zero volume, following initial conditions are set:

- $P_{ini} = P_{ext}$
- T_{ini}

If the initial volume is less than $10^{-4}A^{\frac{3}{2}}$ a constant small volume is added to obtain an initial volume:

- $V_{ini} = 10^{-4}A^{\frac{3}{2}}$

Initial mass energy density is defined from the above values.

There is no need to define an injected mass at time zero.

Jetting Effect

The jetting effect is modeled as an overpressure applied to each element of the airbag (Figure 251).

$$\Delta P_{jet} = \Delta P_1(t).\Delta P_2(\theta).\Delta P_3(\delta).\max(\vec{n}.\vec{n}_1, 0) \tag{1126}$$

with:

$\vec{n}_1$
: Being the normalized vector between the projection of the center of the element upon segment (N_1, N_3) and the center of element as shown in Figure 251.

θ
: The angle between the vector $\vec{MN}_2$ and the vector $\vec{n}_1$.

δ
: The distance between the center of the element and its projection of a point upon segment (N_1, N_3).

The projection upon the segment (N_1, N_3) is defined as the projection of the point in direction $\vec{MN}_2$ upon the line (N_1, N_3) if it lies inside the segment (N_1, N_3). If this is not the case, the projection of the point upon segment (N_1, N_3) is defined as the closest node N_1 or N_3. If N_3 coincides to N_1, the dihedral shape of the jet is reduced to a conical shape.

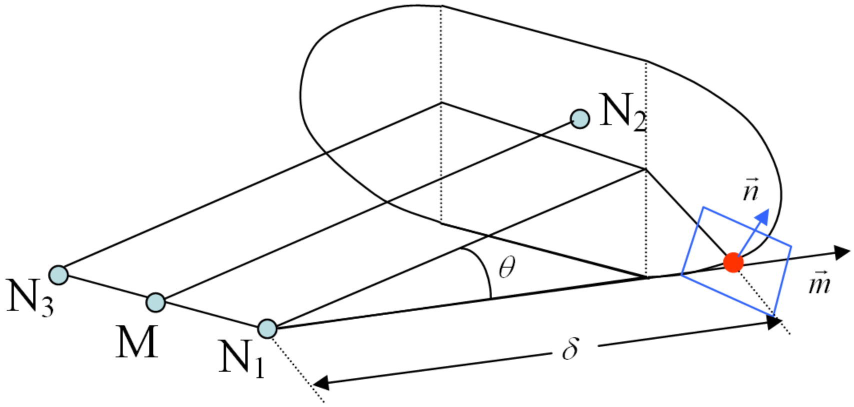

Figure 251: Jetting Effect Schema

Reference Metric

This option can be used to inflate an airbag instead of simulating the real unfolding which is difficult numerically. A jetting effect can be added in order to set a preferential direction for the unfolding.

An initial State (airbag geometry input by the user in the initial deck `D00`) is given.

Reference Metric is a reference state with no strains. This state is defined from a file containing the nodal coordinates, the connectivities of the airbag being the same as in the Initial State. The format of this file is the same as the format of Nodal Coordinates of a Radioss Starter input. The file is read according to `/XREF` keyword of a Radioss Starter input deck. The default name is `RunNameRS0`.

The Reference Metric method consists in the calculation for the Initial State of the initial strains, stresses and energy.

Compatible with:

- 4-node shells
- 3-node shells
- large strain option
- small strain option
- material LAW1
- material LAW19

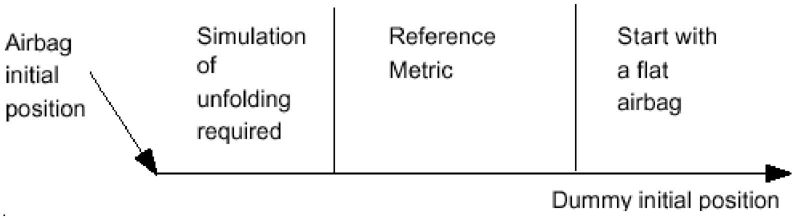

Figure 252: Reference Metric Schema

Tank Experiment

Injected mass curve and injection temperature can be obtained from:

- the airbag manufacturer
- a tank test

With a tank test it is possible to measure temperature at injection point or in the middle of the tank. For pressure the two values are equal.

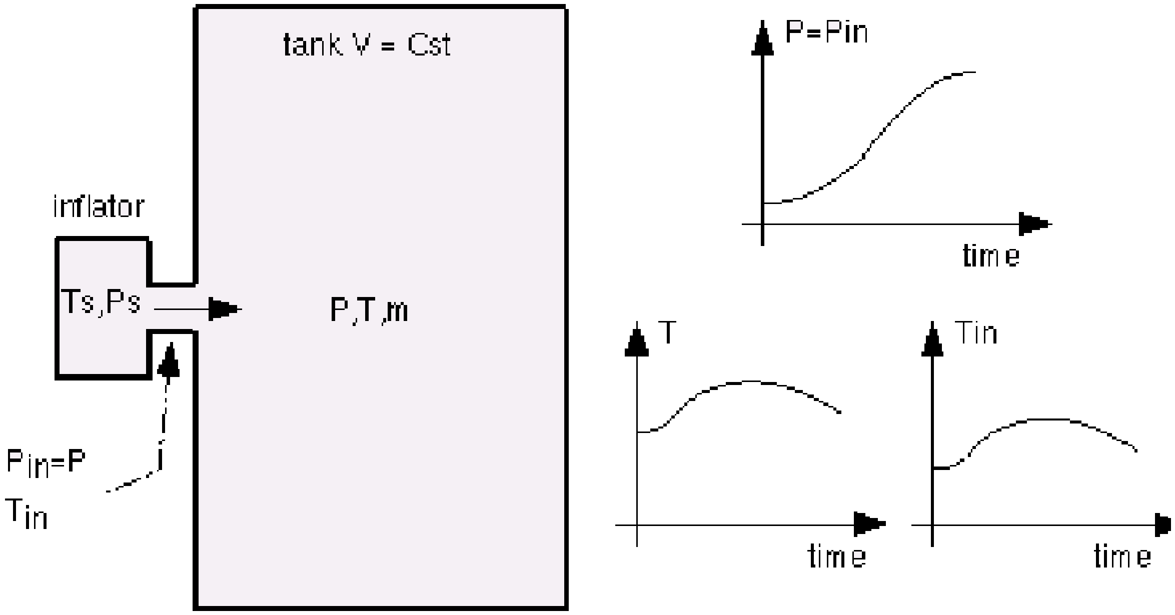

Figure 253: Tank Experiment Schema

T_{in} and P are known

$$\dot{m} = \frac{\frac{dP}{dt}V}{\gamma(\gamma-1)C_V T_{in}} \tag{1127}$$

T and P are known

$$\dot{m} = \frac{\left(T\frac{dP}{dt} - P\frac{dT}{dt}\right)V}{\gamma(\gamma-1)C_V T^2} \tag{1128}$$

Or,

$$m = \frac{PV}{(\gamma-1)C_V T} \tag{1129}$$

$$T_{in} = \frac{T^2\frac{dP}{dt}}{\gamma\left(T\frac{dP}{dt} - P\frac{dT}{dt}\right)} \tag{1130}$$

Or,

$$T_{in} = \frac{T}{\gamma} + \frac{m\frac{dT}{dt}}{\gamma m} \qquad (1131)$$

And if T is constant: $T_{in} = T/\gamma$.

COMMU1 Type

The airbag simulation used by Radioss adopts a special uniform pressure airbag. Hence, regardless of the state of inflation or shape, the pressure is uniform.

Perfect gas law and adiabatic conditions are assumed. Injected mass and temperature are defined as a time function. A sensor can define the inflate start time.

Deflation of vent hole is available after reaching a pressure (P_{def}) or time (T_{def}) criteria.

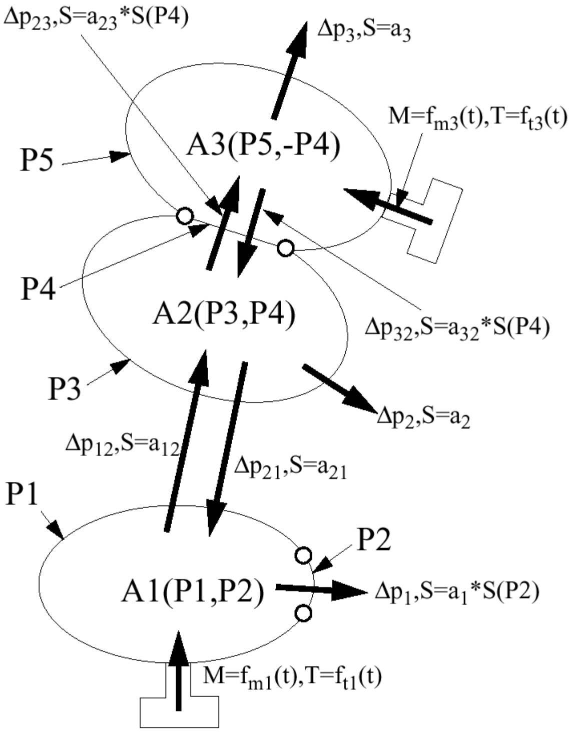

Figure 254: Chambered Airbag Schema

The key assumptions are:

- Uniform airbag pressure ⇔ kinetic energy is negligible
- Adiabatic conditions

The airbag simulation must include:

- Injection of energy and mass
- Bag mechanics (that is, unfolding, expansion, membrane tension, impacts, ...)
- Exhaust through vent holes

This option is used to simulate chambered airbags and may be used to unfold an airbag.

Each COMMU1 type monitored volume works like an AIRBAG type monitored volume with possible vent communication with some other monitored volume of COMMU1 type. A chambered airbag is therefore modeled with two or more COMMU1 type monitored volumes.

Each monitored volume can have an inflater and an atmospheric vent hole.

Monitored volume 1 can communicate with monitored volume 2 with or without communication from 2 to 1. Communicating area, deflation pressure or time from 1 to 2 can be different from corresponding values from 2 to 1. It is thereby possible to model a valve communication.

Thermodynamical Equations

Same equations as for AIRBAG type monitored volume are used. Refer to Thermodynamical Equations.

External Work Variation

Same equations as for AIRBAG type monitored volume are used. Refer to Energy Variation Within a Time Step.

Mass Injection

Same equations as for AIRBAG type monitored volume are used. Refer to Mass Injection.

Venting

Same equations as for AIRBAG type monitored volume are used. Refer to Venting Outgoing Mass Determination.

The mass flow rate is given by:

$$\dot{m}_{out} = \rho_{vent} A_{vent} u = \rho \left(\frac{P_{ext}}{P}\right)^{1/\gamma} A_{vent} u \tag{1132}$$

The energy flow rate is given by:

$$\dot{E}_{out} = \dot{m}\frac{E}{\rho V} = \left(\frac{P_{ext}}{P}\right)^{1/\gamma} A_{vent} u \frac{E}{V} \tag{1133}$$

These mass and energy flux are removed from the current volume and added to the communicating volume at next cycle.

Supersonic Outlet Flow

Same equations as for AIRBAG type monitored volume is used. Refer to Supersonic Outlet Flow.

Jetting Effect

Same explanation as for AIRBAG type monitored volume is used. Refer to Jetting Effect.

Reference Metric

Same explanation as for AIRBAG type monitored volume is used. Refer to Reference Metric.

COMMU1 Type Examples

Example: Communication between the 2 Volumes

Volume 1 communicates with volume 2 and vice-versa.

Monitored volume 1 communicates with monitored volume 2 with or without communication from 2 to 1. The communicating area, deflation pressure or time from 1 to 2 can be different from the corresponding values from 2 to 1. It is thereby possible to model a valve communication.

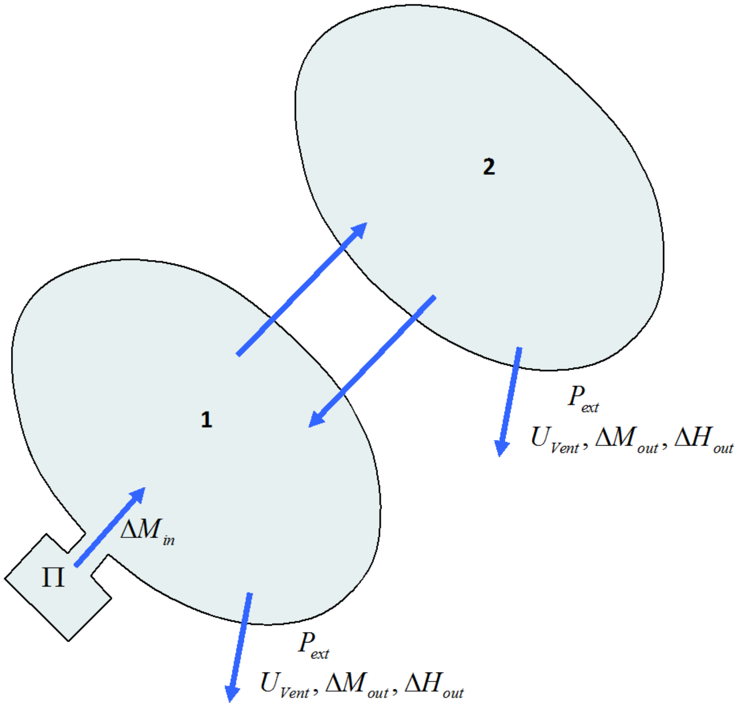
2
1
P_{ext}
$U_{Vent}, \Delta M_{out}, \Delta H_{out}$
ΔM_{in}
Π
P_{ext}
$U_{Vent}, \Delta M_{out}, \Delta H_{out}$

Figure 255: Communication between the 2 Volumes

Example: No Communication between 2 and 3

Volume 1 communicates with volume 2 and volume 2 with volumes 1 and 3, but there is no communication from 3 to 2.

Two COMMU1 type monitored volume communications can have common nodes or common shell property sets but this is optional.

To model a folded airbag, one COMMU1 type monitored volume is used for each folded part. The boundary between two folded parts is closed with a dummy property set (fictitious property). The pressure in each folded part will be different and the area of communication will increase during inflation. With this model, the volume with inflater will inflate first and before than folded parts (better than "jetting" model).

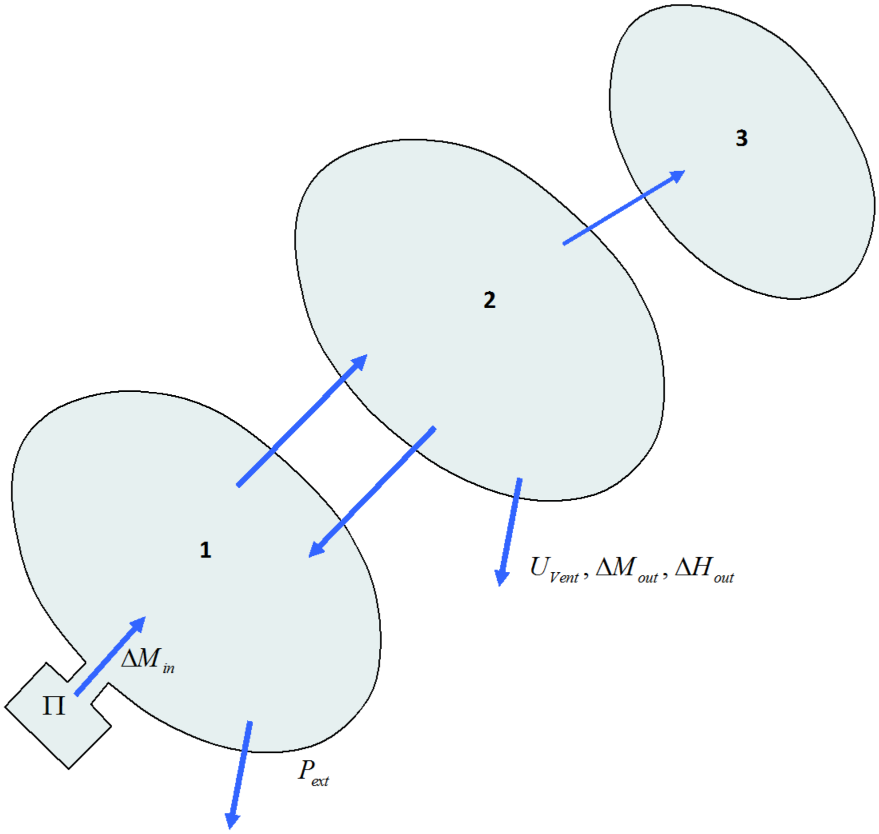

Figure 256: No Communication between 2 and 3

Example: Monitored Volume with Communication Coefficient

Volume 1 and volume 2 with common property set.

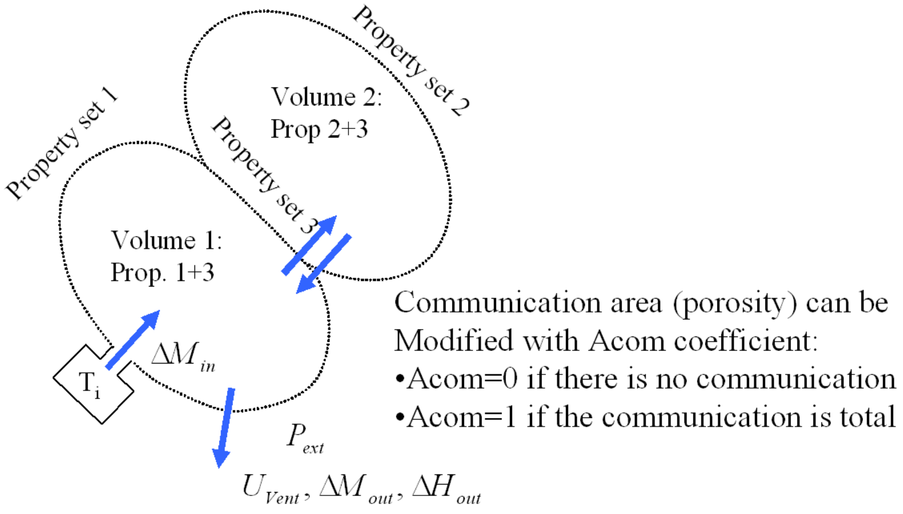
Property set 2
Volume 2:
Prop 2+3
Property set 1
Property set 3
Volume 1:
Prop. 1+3
ΔM_{in}
T_i
P_{ext}
$U_{Vent}, \Delta M_{out}, \Delta H_{out}$
Communication area (porosity) can be
Modified with Acom coefficient:
•Acom=0 if there is no communication
•Acom=1 if the communication is total

Figure 257: Monitored Volume with Communication Coefficient

Example: Folded Airbag

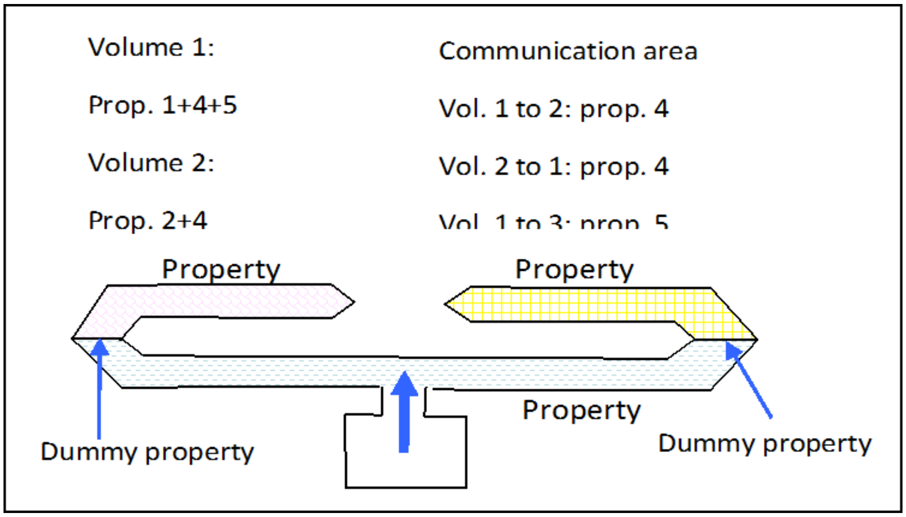

Static

Explicit scheme is generally used for time integration in Radioss, in which velocities and displacements are obtained by direct integration of nodal accelerations.

With this approach, the time step is often small due to stability condition. For the static solution of structural mechanical problems as the steady state is a part of the transient response for a temporal-step load, the use of explicit scheme is usually possible if the computation time remains reasonable. However, in static or slow dynamic computations as duration of the study is large, many cycles are necessary to carry out the simulation.

To resolve static problems, an alternative to explicit method is the implicit time-integration scheme. In this method, a system of nonlinear equations is obtained and then resolved by Newton-Raphson method. It can be shown that the implicit scheme is always stable. That results in a large time step with the explicit method. However, as a global stiffness matrix should be assembled and inverted, the method is relatively high cost per loading step.

The primary difference between the explicit and implicit methods is that an explicit algorithm obtains the next value from known previous values. An implicit method assumes a solution to a problem and solves the equations simultaneously. As the global equilibrium equation is generally nonlinear, an iterative numerical resolution is generally used.

The implicit method might fail when:

- The material law is highly nonlinear. Complicated material behavior is easier to accommodate using an explicit method.
- The number of elements is too large.
- Explicit method does not require large matrix inversion, the I/O is less important and the memory required is also less.
- Matrices must be re-evaluated at each time step and for most of the iterations.

In such cases the CPU time of an explicit solution becomes competitive:

- The problem includes several contacts. Contact algorithms are very efficient in explicit programs.
- The static analysis is a pre-loading case before a fully dynamic behavior phase. In this case, the coupling of two phases is very common.
- Explicit approaches furnish an alternative to the previous cases.

As of Radioss V5 both implicit and explicit methods are available to study the static behavior of systems. The choice a method depends on the nature of the problem and the engineer's feeling. The explicit approach is especially attractive for problems with highly nonlinear geometric and material behavior as all quantities may be treated as vectors, resulting in low storage requirements. The number of cycles to achieve convergence may be quite large, but global efficiency is generally observed. The implicit method is introduced to study efficiently static applications such as spring back in sheet metal forming or gravity loading or other initial state computations before/after dynamic simulations.

Static Solution by Explicit Time Integration

Explicit algorithms are very useful for modeling a dynamic simulation. However, they cannot model a quasi-static or static simulation as easily. This is due to the fact that in an explicit approach, first the nodal accelerations are found by resolving the equilibrium equation at time t_n. Other DOFs are then computed by explicit time integration. This procedure implies that the nodal acceleration must exist; however, some numerical methods may be employed for the simulation of a static process.

Slow Dynamic Computation

The loading is applied at a rate sufficiently slow to minimize the dynamic effects. The final solution is obtained by smoothing the curves.

In case of elasto-plastic problems, one must minimize dynamic overshooting because of the irreversibility of the plastic flow.

Dynamic Relaxation or Nodal Damping (/DYREL)

This method was first introduced by Otter [118] and has been used in several hydrodynamic codes. A nodal damping Cv is added to the momentum equation:

$$M\frac{dv}{dt} + Cv = f_{ext} - f^{\text{int}} \tag{1134}$$

The dashpot force is calculated by:

$$F_c = -CV \tag{1135}$$

The internal force is calculated by:

$$F_k = -KX = F_{kt-\Delta t/2} + KV\Delta t \tag{1136}$$

$$\gamma_0 = \frac{F_k}{M} \tag{1137}$$

The total acceleration is given by:

$$\gamma_1 = \gamma_0 + \frac{F_c}{M} = \gamma_0 - \frac{CV}{M} \tag{1138}$$

$$V_{t+\Delta t/2} = V_{t-\Delta t/2} + \gamma_1\Delta t \tag{1139}$$

$$V = V_{t-\Delta t/2} + \frac{1}{2}\gamma_1\Delta t \tag{1140}$$

$$V_{t+\Delta t/2} = V_{t-\Delta t/2} + \gamma_0\Delta t - \frac{CV}{M}\Delta t \tag{1141}$$

You have:

$$V_{t+\Delta t/2} = V_{t-\Delta t/2} + \gamma_0\Delta t - \frac{C}{M}\left(V_{t-\Delta t/2} + \frac{1}{2}\gamma_1\Delta t\right)\Delta t \tag{1142}$$

$$V_{t+\Delta t/2} = \left(1 - \frac{C\Delta t}{M}\right)V_{t-\Delta t/2} + \left(\gamma_0 - \frac{1}{2}\gamma_1\Delta t\frac{C}{M}\right)\Delta t \tag{1143}$$

$$V_{t+\Delta t/2} = \left(1 - \frac{C\Delta t}{M}\right) V_{t-\Delta t/2} + \left(1 - \Delta t \frac{C\gamma_1}{M\gamma_0}\right)\gamma_0 \Delta t \tag{1144}$$

Approximation $\frac{\gamma_1}{\gamma_0} = 1$ after the variable is changed, $\omega = C\frac{\Delta t}{2M}$, you obtain:

$$V_{t+\Delta t/2} = (1 - 2\omega) V_{t-\Delta t/2} + (1 - \omega)\gamma_0 \Delta t \tag{1145}$$

$$\omega = C\frac{\Delta t}{2M} \rightarrow C = \frac{2M\omega}{\Delta t} \tag{1146}$$

Which gives the expression of C as a proportional matrix to M with:

$$C = AM \text{ and } A = \frac{2\omega}{\Delta t} \tag{1147}$$

or

$$A = \frac{2\beta}{T} \tag{1148}$$

$$\omega = \beta\frac{\Delta t}{T} \tag{1149}$$

Combining Equation 1147 and Equation 1148, and you obtain:

$$C = \frac{2\beta M}{T} \tag{1150}$$

Where, β is the relaxation coefficient whose recommended value is 1. T is less than or equal to the highest period of the system. These are the input parameters used in `/DYREL` option.
The explicit time integration scheme is changed to compute the new velocities. The explicit time integration in Dynamic Analysis gives (Central Difference Algorithm, Equation 192):

$$V_{t+\Delta t/2} = V_{t-\Delta t/2} + \gamma_t \Delta t \tag{1151}$$

which is now written as:

$$V_{t+\Delta t/2} = (1 - 2\omega) V_{t-\Delta t/2} + (1 - \omega)\gamma_t \Delta t \tag{1152}$$

Where,

$$\omega = \beta\frac{\Delta t}{T} \tag{1153}$$

[118] Otter J.R.H., Mechanical Engineering and Design 3, 1965.

Energy Discrete Relaxation

This empirical methodology consists in setting to zero the nodal velocities each time the Kinetic Energy reaches a maximum.

The loading is applied at a rate sufficiently slow to minimize the dynamic effects. The final solution is obtained by smoothing the curves.

In case of elasto-plastic problems, one must minimize dynamic overshooting because of the irreversibility of the plastic flow.

Rayleigh Damping (/DAMP)

In this method a proportional damping matrix is defined as:

$$[C]=\alpha[M]+\beta[K] \tag{1154}$$

Where, α and β are the pre-defined constants. In modal analysis, the use of a proportional damping matrix allows to reduce the global equilibrium equation to n-uncoupled equations by using an orthogonal transformation.

If the global equilibrium equation is expressed as:

$$[M]\{\ddot{X}\}+[C]\{\dot{X}\}+[K]\{X\}=\{F_t\} \tag{1155}$$

The transformed uncoupled system of equations can be written as:

$$[\phi]^T[M][\phi]\{\ddot{\xi}\}+[\phi]^T[C][\phi]\{\dot{\xi}\}+[\phi]^T[K][\phi]\{\xi\}=[\phi]^T\{F_T\} \tag{1156}$$

With

$$[\varphi]^T[C][\varphi]=\begin{bmatrix} \alpha+\beta\omega_1 2 & 0 & . \; . & 0 \\ 0 & \alpha+\beta\omega_2 2 & . \; . & 0 \\ \vdots & \vdots & \vdots \; \vdots & \vdots \\ 0 & . & . \; . & \alpha+\beta\omega_n 2 \end{bmatrix} \tag{1157}$$

Each uncoupled equation is written as:

$$\ddot{\xi}_i+2\omega_i\zeta_i\dot{\xi}_i+\omega_i 2\xi_i=f_i^t \tag{1158}$$

With

$$2\zeta_i\omega_i=\alpha+\beta\omega_i 2 \tag{1159}$$

Where,

ω_i	The i^th natural frequency of the system
ζ_i	The i^th damping ratio

This leads to a system of n equations with two unknown variables α and β. Regarding to the range of the dominant frequencies of system, two frequencies are chosen. Using the pair of the most significant frequencies, two equations with two unknown variables can be resolved to obtain values for α and β. For high frequencies the role of β is more significant. However, for lower frequencies α plays an important role (Figure 258).

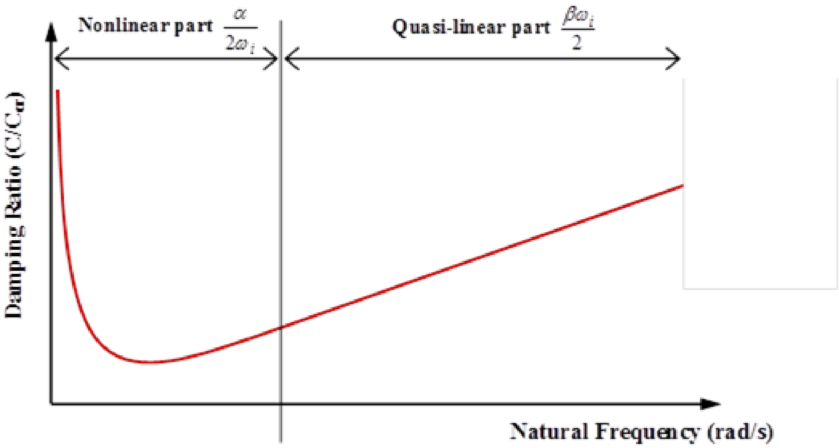

Figure 258: Rayleigh Damping Variation for Natural Frequencies

The Rayleigh damping method applied to explicit time-integration method leads to the following equations:

$$M\gamma^t + Cv^t = F^t_{ext} - F^t_{\mathrm{int}} \tag{1160}$$

With $C = \alpha M + \beta K$

$$F^t_{\mathrm{int}} = F^{t-dt}_{\mathrm{int}} + Kv^{t-\frac{dt}{2}}dt \tag{1161}$$

$$v^t = v^{t-\frac{dt}{2}} + \gamma^t\frac{dt}{2} \tag{1162}$$

$$M\gamma^t_0 = F^t_{ext} - F^t_{\mathrm{int}} \tag{1163}$$

Neglecting $F^t_{ext} - F^{t-dt}_{ext}$ and $v^t - v^{t-\frac{dt}{2}}$, in βKv^t evaluation you have:

$$Kv^t = Kv^{t-\frac{dt}{2}} = \frac{F^t_{\mathrm{int}} - F^{t-dt}_{\mathrm{int}}}{dt} \approx M\frac{\left(\gamma^t_0 - \gamma^{t-dt}_0\right)}{dt} \tag{1164}$$

And finally:

$$\gamma^t_0 = M^{-1}\left(F^t_{ext} - F^t_{\mathrm{int}}\right) \tag{1165}$$

$$\gamma^t = \frac{\gamma_0 - \alpha v^{t-\frac{dt}{2}} - \frac{\beta}{dt}\left(\gamma^t_0 - \gamma^{t-dt}_0\right)}{1+\alpha\frac{dt}{2}} \tag{1166}$$

$$v^{t+\frac{dt}{2}} = v^{t-\frac{dt}{2}} + \gamma^t dt \tag{1167}$$

The three approaches available in Radioss are Dynamic Relaxation (`/DYREL`), Energy Discrete Relaxation (`/KEREL`) and Rayleigh Damping (`/DAMP`). Refer to Example Guide for application examples.

The loading is applied at a rate sufficiently slow to minimize the dynamic effects. The final solution is obtained by smoothing the curves.

In case of elasto-plastic problems, one must minimize dynamic overshooting because of the irreversibility of the plastic flow.

Acceleration Convergence

For every method, an acceleration of the convergence to the static solution is desirable. The constant time step is one of the more usual methods. In fact, in quasi-static analysis, the duration of the study is proportional to the maximum period of the structure. The total number of computation cycles is then proportional to the ratio $\frac{T}{dt}$.

Where,

T	Largest period of the structure
dt	Time step

The number of time steps necessary to reach the static solution is minimal if all the elements have the same time step. An initial given time step Δt_0 can be obtained by increasing or decreasing the density of each element. The constant nodal time step option ensures a homogenous time step over the structure. However, in usual static problems the change is expected to be small, but one may think of increasing the density of the element which gives the critical time step in such a way that $\Delta t = \Delta t_0$.

Static Solution by Implicit Time-Integration

The static behavior of many structures can be characterized by a load-deflection or force-displacement response. If the response plot is nonlinear, the structure behavior is nonlinear. From computational point of view the resolution of a nonlinear problem is much more complex with respect to the linear case. However, the use of relatively recent resolution methods based on sparse iterative techniques allows saving substantially in memory.

Linear Static Solver

A linear structure is a mathematical model characterized by a linear fundamental equilibrium path for all possible choices of load and deflection variables.

This implies that:

- The response to different load systems can be obtained by superposition,
- Removing all loads returns the structure to the reference position.

The requirements for such a model to be applicable are:

- Perfect linear elasticity for any deformation,
- Infinitesimal deformation,

- Infinite strength.

Despite of obvious physically unrealistic limitations, the linear model can be a good approximation of portions of nonlinear response. As the computational methods for linear problems are efficient and low cost, Radioss linear solvers can be used to find equilibrium of quasi-linear systems. The Preconditioned Conjugate Gradient method is the iterative linear solver available in Radioss. The algorithm enables saving a lot of memory for usual application of Radioss as a sparse storage method is used. This means that only the non-zero terms of the global stiffness matrix are saved. In addition, the symmetry property of both stiffness and preconditioning matrices is worthwhile to save memory.

The performance of conjugate gradient method depends highly to the preconditioning method. Several options are available in Radioss using the card `/IMPL/SOLV/1`. The simplest method is a so-called Jacobi method in which only the diagonal terms are taken into account. This choice allows saving considerable memory space; however, the performance may be poor. The incomplete Choleski is one of the best known effective preconditioning methods. However, it can result in negative pivots in some special cases even if the stiffness matrix is definite positive. This results a low convergence of PCG algorithm. The problem can be resolved by using a stabilization method. [119] Finally, the Factored Approximate Inverse method may be the best choice which is used by default in Radioss.

Nonlinear Static Solver

As explained in the beginning of this chapter, a nonlinear behavior is characterized by a nonlinear load-deflection diagram called *path*. The tangent to an equilibrium path may be formally viewed as the limit of the ratio force increment on displacement increment. This is the definition of a stiffness or more precisely the tangent stiffness related to a given equilibrium state. The reciprocal ratio is called flexibility. The sign of the tangent stiffness is closely associated with the stability of an equilibrium state. A negative stiffness is necessary associated with unstable equilibrium. A positive stiffness is necessary but not sufficient for stability.

The problem of nonlinear analysis can be viewed as that of minimising the total potential energy Π which is a function of the total displacement $\mathbf{X}$. A truncated Taylor series then leads to:

$$\Pi_n(\mathrm{X}+\delta\mathrm{X}) = \Pi_0(\mathrm{X}) + \frac{\partial\Pi}{\partial\mathrm{X}}\delta\mathrm{X} + \frac{1}{2}\delta\mathrm{X}^{\mathrm{T}}\frac{\partial^2\Pi}{\partial\mathrm{X}^2}\delta\mathrm{X} + \ldots \tag{1168}$$

Where the subscripts n and 0 denote respectively final and initial configurations. The term $\frac{\partial\Pi}{\partial\mathrm{X}}$ can be identified as the out-of-balance forces or gradient $\mathbf{F}$, of the total potential energy which is the difference between the internal force vector $\mathbf{F}_{\mathrm{int}}$ and the external force vector $\mathbf{F}_{\mathrm{ext}}$. The term $\frac{\partial^2\Pi}{\partial\mathrm{X}^2}$ describes the tangent stiffness matrix $\mathbf{K}_T$. The principle of minimum energy and the equilibrium of stable state give:

$$\delta\Pi = \Pi_n(\mathrm{X}+\delta\mathrm{X}) - \Pi_0(\mathrm{X}) = 0 \tag{1169}$$

Which is implied in Equation 1168:

[119] Ajiz M.A. and Jennings A., "A robust incomplete Choleski-conjugate gradient algorithm", Int. J. Method Eng., Vol. 20, pp. 949-966, 1984.

$$K_T \delta X = F_{ext}(X)\text{-}F_{int}(X) \tag{1170}$$

The tangent matrix $\mathbf{K}_T$ should be defined positive at the equilibrium point for stable case:

$$\delta X^T K_T \delta X > 0 \tag{1171}$$

Equation 1170 can handle the solution of the nonlinear problem when an incremental method is used. The solution methods are generally based on continuous incremental and corrective phases. The most important class of corrective methods concerns the Newton-Raphson method and its numerous variants as modified, modified-delayed, damped, quasi and so forth. All of these Newton-like methods require access to the past solution. In the following section the conventional and modified Newton methods under general increment control are studied.

Newton and Modified New Methods

As you will often prefer to trace the complete load/deflection response or in other words, the equilibrium path, it is useful to combine the incremental and iterative solution procedures. You can recall that the purpose is to solve Nonlinear Static Solver, Equation 1170 which can be written in residual form:

$$R(X,\lambda) = F_{ext}(X,\lambda)\text{-}F_{int}(X) = 0 \tag{1172}$$

with $F_{ext}(X,\lambda) = F_C + \lambda F_{ext}(X)$. This equation represents a system of n algebraic nonlinear equations depending on only one loading parameter λ. If the loading depends to only one loading variable independent to the state of deflection, you have:

$$F_{ext}(X,\lambda) = \lambda F_{ext}(X) \tag{1173}$$

Several techniques are available to resolve Equation 1172. In some situations, the parameter λ is fixed, and the equations are resolved to determine n components of $\mathbf{X}$ in order to verify Equation 1172. In this case, the technique is called *load control method*. Another technique called *displacement control* consists in fixing a component of $\mathbf{X}$ and searching for λ and 'n-1' other components of displacement vector $\mathbf{X}$. A generalization of displacement control technique will enable to imply several components of displacement vector by using an Euclidian norm. The method is called *arc-length control* and intended to enable solution algorithms to pass limit points (that is, maximum and minimum loads). The techniques making possible to obtain the load-deflection curve by finding point by point the solution are called *piloting techniques*.

When the piloting technique is chosen for a given step, the associated solution is obtained by an iterative resolution of so-called Newton-Raphson methods. At iteration i, the residual vector $\mathbf{R}^i$ is:

$$R^i = F_{ext}(X^i,\lambda^i),\text{-}F_{int}(X^i) \tag{1174}$$

A correction ΔX and $\Delta\lambda$ can be considered with:

$$R^{i+1} = R^i + \left[\frac{\partial R}{\partial X}\right]^i \Delta X + \left[\frac{\partial R}{\partial \lambda}\right]^i \Delta\lambda \tag{1175}$$

Combining Equation 1175 with Equation 1174, you obtain:

$$K_T^i \Delta X\text{-}F_{ext}^i \Delta\lambda = R^i \tag{1176}$$

as $R^{i+1} = 0$ and:

$X^{i+1} = X^i + \Delta X$

$$\lambda^{i+1} = \lambda^i + \Delta\lambda \tag{1177}$$

The tangent matrix K_{T^i} is obtained by assembling the elementary matrices k_{T^i}. It corresponds to:

$$K_{T^i} = \frac{\partial F_{int}}{\partial X} - \frac{\partial F_{ext}}{\partial X} \tag{1178}$$

Using load control technique, the standard Newton-Raphson method resolves Equation 1176 to Equation 1178 by applying a known load increment $\Delta\lambda$ as illustrated in Figure 259. The tangent matrix is updated and triangulized at each iteration. This insures a quadratic convergence to exact solution.

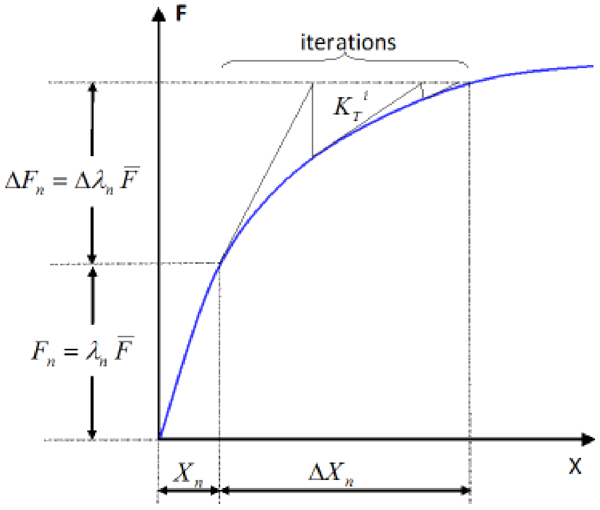
F
iterations
K_T^i
$\Delta F_n = \Delta\lambda_n \bar{F}$
$F_n = \lambda_n \bar{F}$
X_n
ΔX_n
X

Figure 259: Standard Newton-Raphson Resolution in the Case of Load Control Technique

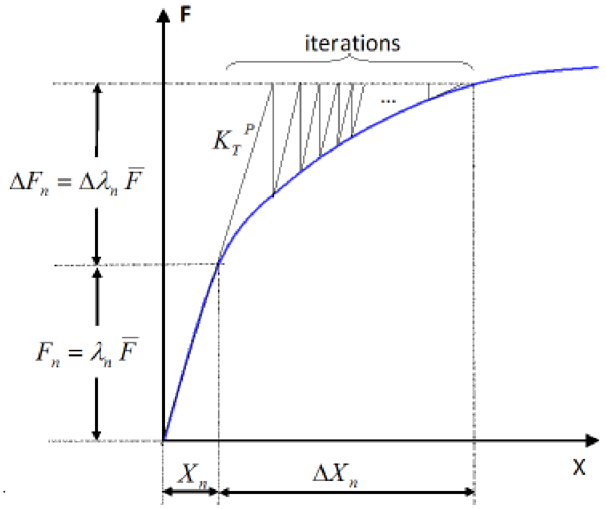

Figure 260: Modified Newton-Raphson Resolution in the Case of Load Control Technique

However, it is possible to save computation time which depends on the size of the problem and on the degree of the nonlinearity of the problem. The method is called *modified Newton-Raphson* which is based on the conservation of the tangent matrix for all iterations (Figure 260). This method can also be combined with the acceleration techniques as *line-search* explained in Line Search Method to Optimize the Resolution.

The convergence criteria may be based on Euclidian norm of residual forces, residual displacements or energy where an allowable tolerance is defined.

Line Search Method to Optimize the Resolution

The Newton-Raphson resolution of Newton and Modified New Methods, Equation 1176 implies updating the variables at each iteration with Newton and Modified New Methods, Equation 1177. The new estimation of X^{i+1}does not satisfy Newton and Modified New Methods, Equation 1176 only if $R^{i+1} = 0$. In order to reduce the number of iterations the line-search method is used. The line-search technique is an important feature of most numerical techniques used in optimization problems. [120] The method consists in introducing a parameter α, such as:

$$\mathrm{X}^{i+1} = \mathrm{X}^{\mathrm{i}} + \alpha \Delta \mathrm{X} \tag{1179}$$

Where, α is obtained to minimize the total potential energy or to satisfy the principle of virtual works. The techniques to determine α use often a Raleigh-Ritz procedure with only one unknown parameter.

The principle of virtual work can be written in the general form:

$$\mathrm{W}(\mathrm{X},\delta\mathrm{X}) = \delta\mathrm{X} \bullet \mathrm{R}(\mathrm{X}) = 0 \text{ For all kinematical acceptable } \delta\mathrm{X} \tag{1180}$$

Considering Equation 1179, write:

$$\delta\mathrm{X} = \alpha \Delta \mathrm{X} \tag{1181}$$

and:

$$\delta W = \delta\alpha\,\Delta X \bullet R(X^i + \alpha\Delta X) = 0 \text{ for all } \alpha \tag{1182}$$

Then, α is determined from:

$$\Delta X \bullet R(X^i + \alpha\Delta X) = 0 \tag{1183}$$

which leads to a three-order polynomial equation in α for elastic materials:

$$C_1 + C_2\alpha + C_3\alpha 2 + C_4\alpha^3 = 0 \tag{1184}$$

The coefficients C_1, C_2, C_3 and C_4 can be expressed in terms of displacements X^i and the increment of displacements ΔX.

Arc Length Method

To obtain the load-deflection behavior of a structure, the load or the displacement of a given point of the structure must be parameterized. Up to now, you have parameterized the load by the time t. However, a single parameter is not always sufficient to control in an optimum way the time step. On the other hand, it is not possible to pass limit points with "snap-through" and "snap-back" when using load-controlled or displacement-controlled techniques. This is due to the fact that the increase in load or in a given displacement component may result a dynamic response losing a part of load-deflection curve as shown in Table 9 (a) and (b).

Table 9: Various Load-deflection Curves and Step-by-Step Solution by Arc-length Method

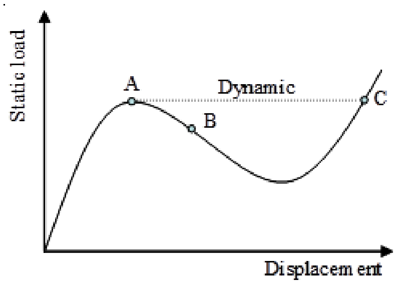 (a) Snap-through	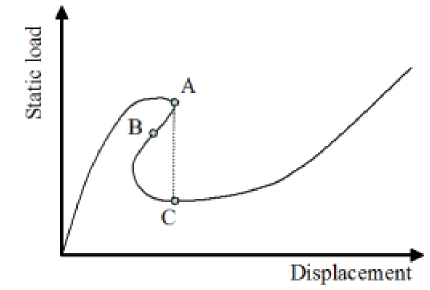 (b) Snap-backs

[120] Flectcher R., “Practical methods of optimization”, 2nd edition, Wiley, 1987.

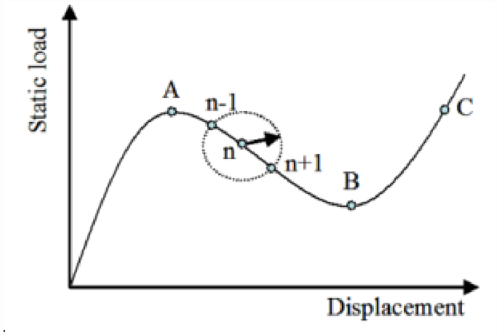

(c) Arc-length method: intersection of the equilibrium branch with the circle about the last solution

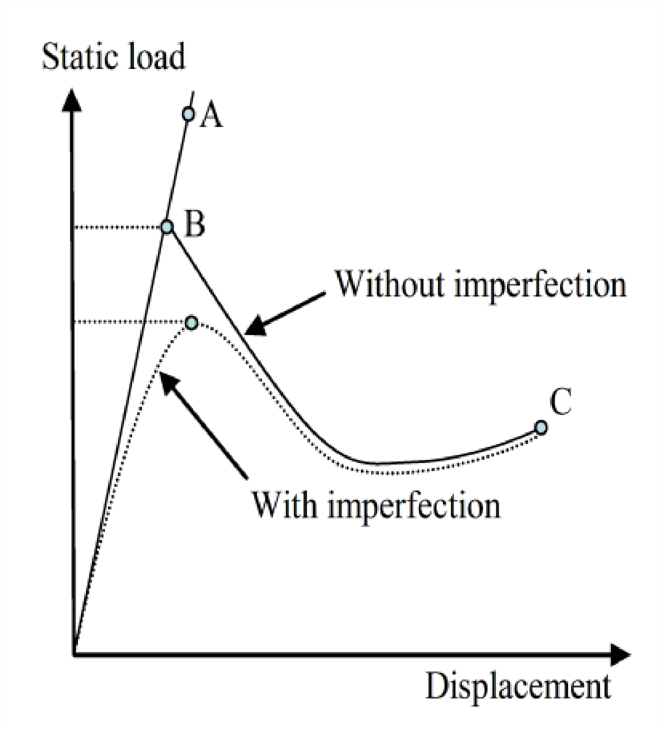

(d) Buckling with or without imperfections

The tracing of equilibrium branches are quite difficult. In arc-length method, instead of incrementing the load parameter, a measure of the arc length in the displacement-load parameter space is incremented. This is accomplished by adding a controlling parameter to the equilibrium equations.

The arc-length method was originally introduced by Riks [121] and Wempner. [122] Considering a function f implying several components of the displacement vector X, the arc-length method consists in determining in each step the Euclidian norm of the increase in X:

$$f = \langle X^{i+1} - X^{n} \rangle \{X^{i+1} - X^{n}\} - (\Delta S_n)^2 = 0 \tag{1185}$$

This leads to:

$$\langle X^{i+1} - X^{n} \rangle \{X^{i+1} - X^{n}\} = (\Delta S_n)^2 \tag{1186}$$

And

$$a(\Delta\lambda)^2 + b(\Delta\lambda) + c = 0 \tag{1187}$$

With:

$$a = \langle \Delta X_F \rangle \{\Delta X_F\};\ \{\Delta X_F\} = [K_T^n]^{-1} \{F_{ext}\}$$

$$b = 2\langle \Delta X_F \rangle \{Y\};\ \{Y\} = \{\Delta X_F\} + \{X^{i} - X^{n}\}$$

$$c = \langle Y \rangle \{Y\} - (\Delta S_n)^2$$

In each of the Newton-Raphson iterations, Equation 1187 must be resolved to select a real root. If there is no root, ΔS_n should be reduced. The most closed root to the last solution is retained in the case of two real roots.

Table 9(c) illustrates the intersection of the equilibrium branch with the circle about the last solution.

[121] Riks E., "An incremental approach to the solution of snapping and buckling problems", Int. J. Solids & Structs, Vol. 15, pp. 529-551, 1979.

[122] Wempner G.A., "Discrete approximations related to nonlinear theories of solids", Int. J. Solids & Structs, Vol. 7, pp. 1581-1599, 1971.

Radioss Parallelization

The performance criterion in the computation was always an essential point in the architectural conception of Radioss. At first, the program has been largely optimized for the vectored super-calculators like CRAY. Then, a first parallel version SMP made possible the exploration of shared memory on processors.

In the case of analysis of systems with high number of DOFs, the use of shared memory parallel machine architectures is common. In Radioss, there are two models of parallel programming:

- SMP: Shared Memory Processors,
- SPMD: Single Program Multiple Data.

In this section, the principle of Radioss parallelization is described.

Measure of Performance

The Speed-Up is the ratio of sequential time $T(1)$ and the parallel time on P processors $T(P)$:

$$S(P) = T(1) / T(P) \tag{1188}$$

The efficiency is defined as:

$$E(P) = S(P) / P;\ E(P) \leq 1 \tag{1189}$$

The Amdahl’s law for multitasking is used to determine the speed-up:

$$S(P) = \frac{\left(T_{Seq} + T_{Par}\right)}{\left(T_{Seq} + T_{Par}/P\right)} \tag{1190}$$

Where, T_{Par} and T_{Seq} are the computation times respectively related to parallel and non-parallel parts. As $T_{Seq} + T_{Par} = 1$, write:

$$S(P) = \frac{1}{\left(T_{Seq} + T_{Par}/P\right)} \tag{1191}$$

The limit value can be obtained when the process number tends to infinite:

$$S(\infty) = \frac{1}{T_{Seq}} \tag{1192}$$

Table 10 provides the Speed-Up in function of number of processors and the rate of parallelization in the program. It can be seen that if the rate of parallelization is less 95%, the computation acceleration will not be greater than 20; however, the number of processors. This means that to obtain a good scalability of a code, at least 99% of the program must be parallel.

Table 10: Speed-up in Function of Process Number and Parallelization

Process Number **Seq / P**	**2**	**4**	**8**	**16**	**32**	**64**	**128**	∞
100%	2.0	4.0	8.0	16.0	32.0	64.0	128.	∞
99%	2.0	3.9	7.5	13.9	24.4	39.3	56.4	100.
98%	2.0	3.8	7.0	12.3	19.8	28.3	36.2	50.0
97%	1.9	3.7	6.6	11.0	16.5	22.1	26.6	33.3
96%	1.9	3.6	6.3	10.0	14.3	18.2	21.1	25.0
95%	1.9	3.5	5.9	9.1	12.5	15.4	17.4	20.0
90%	1.8	3.0	4.7	6.4	7.8	8.7	9.3	10.0
50%	1.3	1.6	1.8	1.9	1.9	2.0	2.0	2.0

Shared Memory Processors (SMP)

Radioss SMP version is based on the concept of computers with shared memory as the architecture is described in Figure 261.

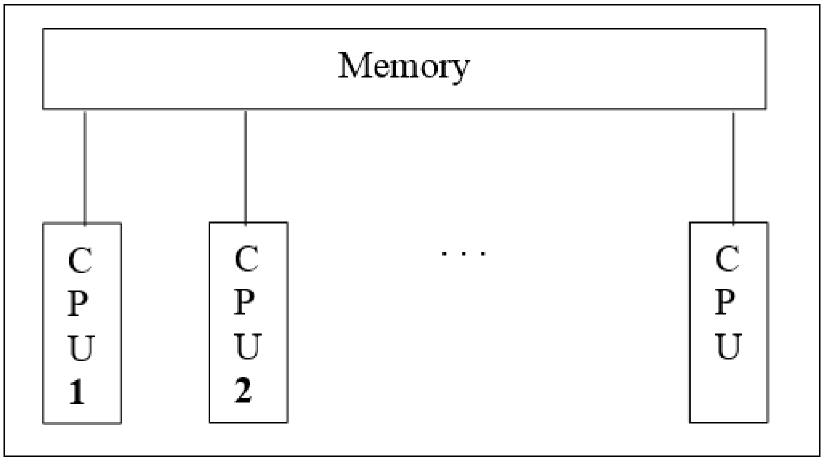

Figure 261: Architecture of Shared Memory

In this case, all processors can access to a common memory space. From programming point of view, each process called *parallel task*, reach to the entire memory space allocated by the program. It is necessary to manage properly the access to this shared memory by introducing barriers and locking mechanisms. The SMP model programming has the advantage to be managed easily. However, the performance of the method depends on the ratio between the memory access speed and the CPU speed.

The parallelism approach used in Radioss SMP is a multi-task programming type. The tasks are explicitly managed by the programmer. The computation tasks are attributed to the processors by a dynamic procedure as they are available. This approach is especially adapted to the super-computers used as computation server where the load of a given processor varies with respect to others. The SMP version is developed for computers with shared memory architecture and cannot be used efficiently on the super-computers with distributed memory or cluster structures.

The Radioss SMP version is constantly improved since the first release. However, the efficiency of SMP version has to be updated to take into account the evolution of computer architecture in memory management and CPU speed.

Single Program Multiple Data (SPMD)

The development of the first SPMD version of Radioss is started in 1994. The version became a real alternative to SMP version after a long period of parallelization and optimization of the code. In fact, the scalability of the version is much better than the SPM version. The SPMD version allows using more processors with a better efficiency. It makes possible to use up to 64 processors. In addition, all Radioss Crash options are available in this version including "*Arithmetic Parallel*" option.

The principle of program is based on Single Program Multiple Data, where the same program runs with different data. Radioss Starter carries out domain decomposition. Then, Radioss Engine has just to send data to different processors in an initialization step. Thereafter, each program runs over each sub domain. It is necessary to communicate information between processors to manage data on the border of domains. This is carried out in Radioss using MPI (Message Passing Interface) library.

Figure 262 illustrates the architecture of multi-processor computers with distributed memory. The Radioss SPMD version runs independently to architecture of memory as well on the computers with shared memory or distributed memory or a set of work stations in a network.

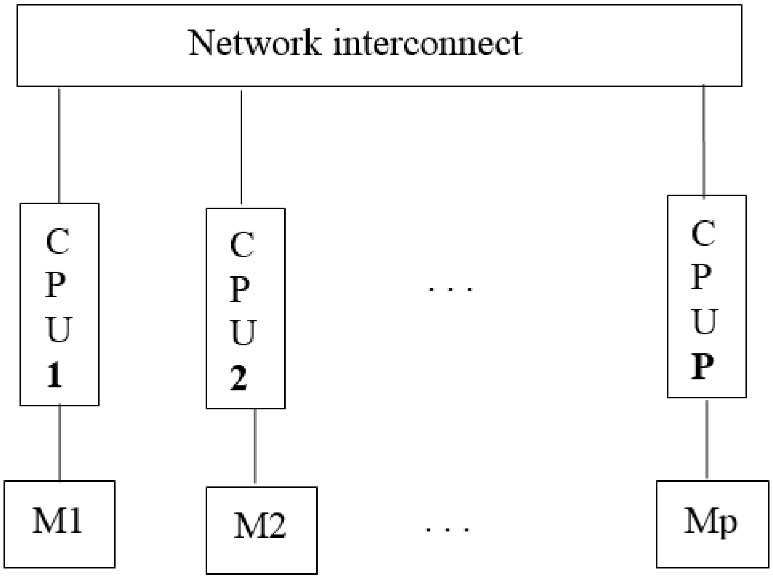

Figure 262: Architecture with Distributed Memory

Hybrid Massively Parallel Program (HMPP)

The Hybrid MPP combines the best of the SMP and SPMD parallel versions inside a unique code.

Benefits

This new approach allows reaching an impressive level of scalability. Radioss HMPP can scale up to 512 cores and more for a real performance breakthrough.

Radioss HMPP is independent of the computer architecture, more flexible and efficiently adapted to any hardware resources. It can run on distributed memory machines, shared memory machines, workstation cluster, or a high performance computation cluster. It can better exploit the inside power of highly multi-core machine and optimize the software according to the hardware.

It decreases installation and maintenance costs by having a unique parallel version instead of two types of executables.

It improves the quality of the code in term of numerical results by having a full convergence between SMP and SPMD results. `/PARITH/ON` provides a unique answer independent of the number of SPMD domains and the number of SMP threads used.

Hybrid Usage Example

In the example below, the hardware is composed of N nodes of a cluster. Each node is a dual processor machine and each processor is a dual core. On each node the memory is shared between processors but the memory is distributed between the nodes.

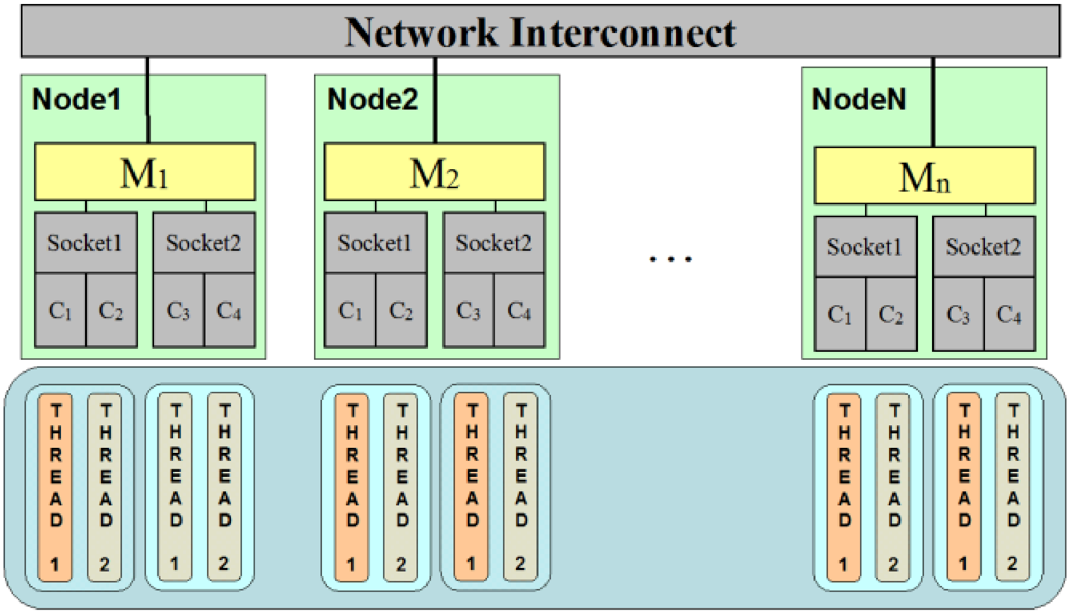

Figure 263: Hybrid Version Run with 2 SMP Threads per SPMD Domains

With the Hybrid version, it is easy to optimize the software to run on such complex architecture. Figure 263 shows that each SPMD domain is computed by a different processor. The number of threads per domain is set to the number of cores per processor (two).

So, each processor computes a SPMD domain using two SMP threads, one per core.

Making it Work

For SPMD version, Radioss Starter divides the model into several SPMD domains and writes multiple RESTART files.

Then, `mpirun` command is used to start all the SPMD programs. Each program computes a SPMD domain using the number of SMP threads set. Indeed, each MPI program is a SMP parallel program. The management of computation at the frontiers of the domains remains and it is necessary to communicate some information between programs using MPI.

Execution Example

Radioss Starter is run from the command line. Here, the number of SPMD domains (`Nspmd`) with option `-nspmd` 16 is specified:

```
./s_11.0_linux64 -nspmd 16 -i ROOTNAME_0000.rad
```

The number of SMP threads (`Nthread`) is set through the use of environment variable `OMP_NUM_THREADS`:

```
setenv OMP_NUM_THREADS 2
```

Then, Radioss Engine is run using `mpirun` command:

```
mpirun -np 16 ./e_11.0_linux64_impi -i ROOTNAME_0001.rad
```

Note:

- `-np` value of `mpirun` must match `-nspmd` value
- The total number of processes is equal to `Nspmd*Nthread` (32 in this example)

Recommended Setup

As seen in the example above, a good rule is to set the number of SPMD domains equal to the number of sockets and to set the number of SMP threads equal to the number of cores per socket.

With a low number of cores (below 32), a pure SPMD run might be more effective but the performance gap should be small if the setup explained above is respected.

With a very high number of cores (1024), it is possible to increase the number of SMP threads up to the number of cores per node and set only one SPMD domain per node to maximize performance if the limit of scalability of the interconnect network is reached.

ALE, CFD and SPH Theory Manual

ALE Formulation

ALE or Arbitrary Lagrangian Eulerian formulation is used to model the interaction between fluids and solids; in particular, the fluid loading on structures. It can also be used to model fluid-like behavior, as seen in plastic deformation of materials.

ALE derives its name from a combination of two different finite element modeling techniques.

- Lagrangian Formulation - where the observer follows material points.
- Eulerian Formulation - where the observer looks at fixed points in space.
- Arbitrary Lagrangian Eulerian Formulation - where the observer follows moving points in space.

Referential Domain

At any location in space x and time t, there is one material point, identified by its space coordinates x at time t=0, and one grid point identified by its coordinates ξ at time t=0. Figure 264 provides a pictorial representation and defines the velocities in each formulation.

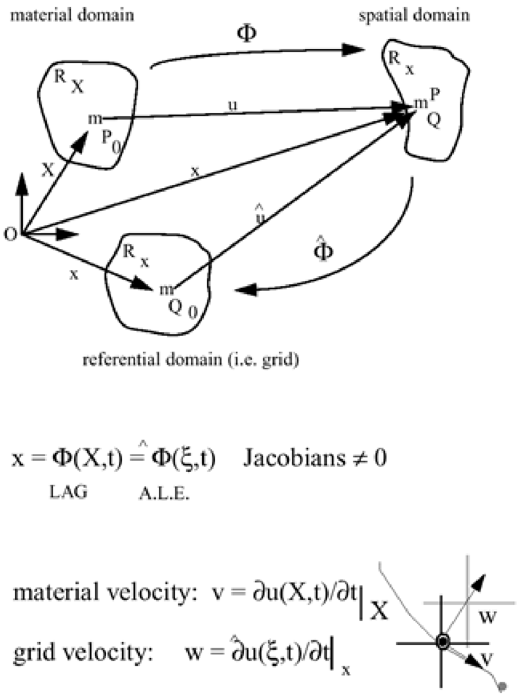
material domain
spatial domain
Φ
R X
m
P 0
u
R x
m P
Q
X
x
O
û
Φ̂
R x
x
m
Q 0
referential domain (i.e. grid)
x = Φ(X,t) =^ Φ(ξ,t) Jacobians ≠ 0
LAG
A.L.E.
material velocity: v = ∂u(X,t)/∂t | X
grid velocity: w = ∂u(ξ,t)/∂t | x
w
v

Figure 264: ALE Formulation

The derivative of any physical quantity can be computed either following the material point or following the grid point. They can then be related to each other.

Given that F is a function f of space and time representing a physical property:

- The spatial domain is given by $f(x, t)$
- The material domain is given by $f^{*}(X, t)$
- The mixed domain is given by $f^{**}(\xi, t)$

Therefore,

$$\frac{\partial f^{*}}{\partial t}|_{X} = \frac{\partial f}{\partial t}|_{x} + \frac{\partial f}{\partial x_j} \times \frac{\partial x_j}{\partial t}|_{X} = \frac{\partial f}{\partial t}|_{x} + V_j(x_k, t)\frac{\partial f(x, t)}{\partial x_j}|_{t} \quad (1193)$$

Also:

$$\frac{\partial f^{*}}{\partial t}|_{X} = \frac{\partial f^{**}}{\partial t}|_{\xi} + \left(V_j - W_j\right)\frac{\partial f(x, t)}{\partial x_j} \quad (1194)$$

This relates to acceleration by:

$$\vec{\gamma} = \frac{d\vec{v}}{\partial t}|_{X} = \frac{\partial}{\partial t}\vec{v}|_{\xi} + \left(v_j - w_j\right)\frac{\partial}{\partial x}\vec{v}|_{t} \quad (1195)$$

Where,

v	Material velocity
w	Grid velocity

Conservation of Momentum

Conservation of momentum, expressed in terms of a finite element formulation, is given by:

$$\int_{V} \Phi_I \left(\rho\frac{\partial v_i}{\partial t} - \frac{\partial \sigma_{ij}}{\partial x_j} - \rho b_i\right) dV = 0 \quad (1196)$$

Where,

Φ_I	Weight functions
ρ	Material density
v	Velocity
σ_{ij}	Stress matrix
b_i	Body acceleration vector
V	Volume

This can be rewritten in a form similar to the explicit Lagrangian formulation with the addition of a new nodal force F^{trm}, accounting for transport of momentum:

$$M\frac{\partial}{\partial t}v = \left\{F^{ext}\right\} - \left\{F^{\text{int}}\right\} + \left\{F^{bod}\right\} + \left\{F^{hgr}\right\} + \left\{F^{trm}\right\} \quad (1197)$$

Where,

$\{F^{trm}\} = \sum f^{trm}$
Transport of momentum forces

Momentum Transport Force

By default, since version 2018.0 a streamline upwind technique is used to computed transportation forces (SUPG). This formulation enables to get rid of false diffusion (numerical issue with classical upwind technique). Nevertheless, SUPG method can be disabled in order to retrieve numerical solution obtained with classical upwind technique from versions prior to 2017. For this purpose, Engine keyword must be define: `/ALE/SUPG/OFF`. Using this keyword, momentum transport forces are computed using the classical upwind technique which was the default method up to version 2017.

$$F_{iI}^{trm} = \left(1 + \eta_I\right)\rho\Phi_I\left(w_j - v_j\right)\frac{\partial v_i}{\partial x_j}V \tag{1198}$$

The classical upwinding technique is introduced to add numerical diffusion to the scheme, which otherwise is generally under diffuse and thus unstable.

$$\eta_I = \eta sign\left[\frac{\partial \Phi_I}{\partial x_j}\left(v_j - w_j\right)\right] \tag{1199}$$

$0 \le \eta \le 1$ Upwind coefficient, given in input.

Full upwind $\eta = 1$ (default value) is generally used and can be tuned with η_1 parameter from `/UPWIND` keyword (now obsolete with SUPG formulation).

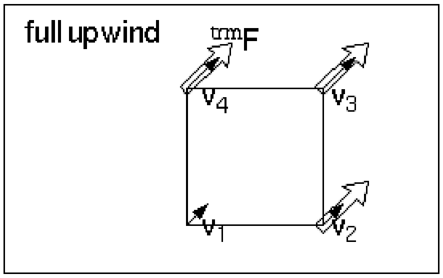

Figure 265:

Conservation of Mass

The finite element formulation of the Lagrangian form of the mass conservation equation is given by:

$$\frac{d\rho}{dt}\Big|x = -\left(\rho / V\right)\frac{dV}{dt}\Big|x \tag{1200}$$

When transformed into the ALE formulation it gives:

$$\frac{\partial \rho}{\partial t}\Big|_{\xi} - \left(\left(w_i - v_i\right) \cdot \frac{\partial \rho}{\partial x_i}\Big|_t\right) + \rho\frac{\partial v_K}{\partial x_K}\Big|_t = 0 \tag{1201}$$

Applying a Galerkin variation form for the solution of Equation 1201:

$$\int_V \psi \left(\frac{\partial \rho}{\partial t}\Big|_{\xi} - \left((w_i - v_i) \cdot \frac{\partial \rho}{\partial x_i}\Big|_t \right) + \rho \frac{\partial v_K}{\partial x_K}\Big|_t \right) = 0 \tag{1202}$$

Where, ψ is the Weighting function.

Using a finite volume formulation

Where, ψ=1

ρ = constant density over control volume V.

Therefore:

$$\int_V \frac{\partial \rho}{\partial t} dV + \int_V \rho \frac{\partial v_K}{\partial x_K} dV = 0 \tag{1203}$$

Using the divergence theorem leads to:

$$\int_V \frac{\partial \rho}{\partial t} dV + \int_S \rho (v_j \cdot n_j) dS = 0 \tag{1204}$$

Further expansion gives:

$$\frac{d}{dt} \int_v \rho dV = \int_s \underbrace{\rho (w_j - v_j) n_j dS}_{mass\ flux} \tag{1205}$$

This formula is still valid if density ρ is not assumed uniform over volume V.

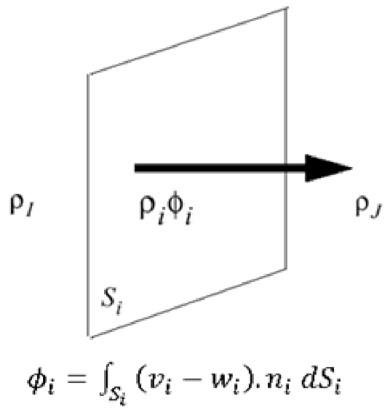

Figure 266: Mass Flux Across a Surface

The density, ρ_i, is given computed:

$$\rho_i = \frac{1}{2} \rho_I \{1 + \eta \quad sign(\phi_i)\} + \frac{1}{2} \rho_J \{1 - \eta \quad sign(\phi_i)\} \tag{1206}$$

Where, $0 \leq \eta \leq 1$ is the upwind coefficient given on the input card.

If η=0, there is no upwind.

Therefore, $\rho_i = \frac{\rho_I + \rho_J}{2}$.

If η=1, there is full upwind.

The smaller the upwind factor, the faster the solution; however, the solution is more stable with a large upwind factor. This upwind coefficient can be tuned with parameter from `/UPWIND` keyword (not recommended, this keyword has been obsolete as of version 2018).

For a free surface: $\rho_J = \rho_I$

Conservation of Internal Energy

Conservation of internal energy is used to model temperature dependent material behavior. It also allows an energy balance evaluation.

However, internal energy is only calculated if it is turned on, to reduce computation time in problems not involving heat transfer.

The conservation of energy is given by:

$$\frac{\partial \rho e}{\partial t} - \left((w_i - v_i) \cdot \frac{\partial \rho e}{\partial x_i} \right) + (\rho e + P) \frac{\partial v_K}{\partial x_K} = 0 \tag{1207}$$

Where,

e	Internal energy in Joules (Nm)
P	Fluid pressure

Applying a Galerkin variation form for the solution gives:

$$\int^{V} \psi \left(\frac{\partial \rho e}{\partial t} - \left((w_i - v_i) \cdot \frac{\partial \rho e}{\partial x_i} \right) + (\rho e + P) \frac{\partial v_K}{\partial x_K} \right) = 0 \tag{1208}$$

Making the following assumptions:

ψ=1

ρ_e = constant over control volume V

Equation 1208 reduces to:

$$\int_V \frac{\partial \rho e}{\partial t} dV + \int_V (\rho e + P) \frac{\partial v_K}{\partial x_K} dV = 0 \tag{1209}$$

Applying the divergence theorem gives:

$$\int^{V} \frac{\partial \rho e}{\partial t} dV + \int^{S} \left(\rho e (v_j \cdot n_j) dS \right) + \int^{V} P \frac{\partial v_K}{\partial x_K} dV = 0 \tag{1210}$$

Hence:

$$\frac{d}{dt}\int_V \rho e dV = \int_S \rho e\left(w_j - v_j\right)n_j dS - \int_V P\frac{\partial v_K}{\partial x_K}dV \tag{1211}$$

This formula is still valid if e is not assumed uniform over volume V.

New formulation based on total energy conservation are under investigation.

Rezoned Quantities

The deviatoric stress tensor and the equivalent plastic strain must be rezoned and recalculated after every time step due to the ability of one element to contain a different amount of material.

ALE Materials

The following materials may be used with the ALE formulation.

Law Number	Description
2	Elasto-plastic - `/MAT/PLAS_JOHN`
3	Elasto-plastic-Hydrodynamic - `/MAT/HYDPLA`
4	Johnson-Cook - `/MAT/HYD_JCOOK`
6	Hydrodynamic Viscous - `/MAT/HYD_VISC`
10 and 21	Rock Concrete Foam - `/MAT/LAW10` or `/MAT/DPRAG`
22 and 23	Elasto-plastic with Damage - `/MAT/DAMA` or `/MAT/LAW23`
20	Bimaterial - `/MAT/BIMAT`
37	Hydrodynamic - Bi-phase liquid gas - `/MAT/BIPHAS`
11	Boundary - Stagnation conditions in flow calculations - `/MAT/BOUND`
16	Gray Model - Multiphase Gray E.O.S + Johnson's shear law - `/MAT/GRAY`
18	Thermal Conductivity, purely thermal material - `/MAT/THERM`

Numerical Integration

The numerical integration techniques used are the same as those used for any other analysis type.

The flow chart of calculations can be seen in Figure 267.

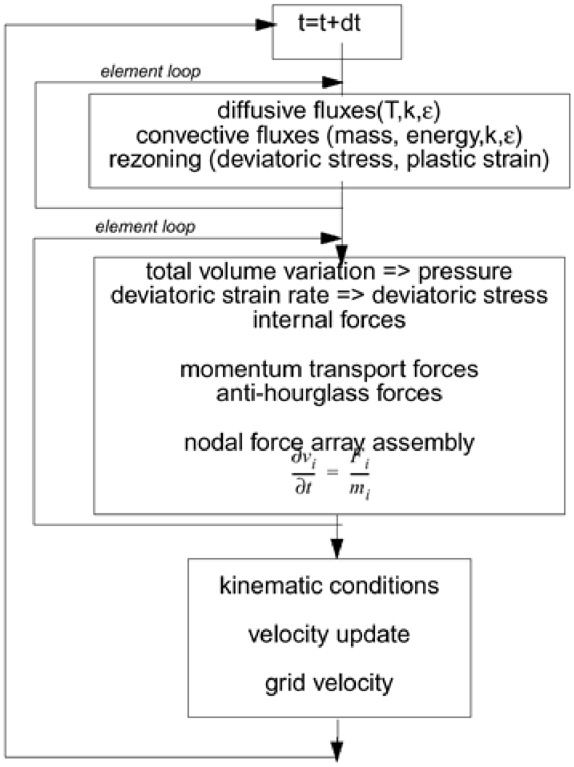
t=t+dt
element loop
diffusive fluxes(T,k,ε)
convective fluxes (mass, energy,k,ε)
rezoning (deviatoric stress, plastic strain)
element loop
total volume variation => pressure
deviatoric strain rate => deviatoric stress
internal forces
momentum transport forces
anti-hourglass forces
nodal force array assembly
$\frac{\partial v_i}{\partial t} = \frac{F_i}{m_i}$
kinematic conditions
velocity update
grid velocity

Figure 267: Flow Chart

Improved Integration Method

This method can only be used with the CFD version of Radioss, and only available in Eulerian formulation. An eight Gauss point integration scheme is used to determine the shape functions. The shape functions are condensed to one point. This gives an eight point integration scheme with constant stress.

Momentum Transport Force

This scheme is only used with the ALE formulation (Arbitrary Lagrangian Eulerian) and in the CFD version of Radioss. The force is calculated using the relation:

$${}^{trm}F_i^I = \left(1+\eta_I\right)\rho\Phi_I\left(w_j - v_j\right)\frac{\partial v_i}{\partial X_j}\,V \qquad (1212)$$

Where,

w	Grid velocity
v	Material velocity
V	Element volume

η	Upwind coefficient (user-defined, default = 1 for full upwind)

When a Lagrangian formulation is used, the values of w_j and v_j are equal. Thus, Equation 1212 is equal to zero.

Upwinding Technique

An upwinding technique is introduced to add numerical diffusion to the scheme; otherwise it is generally under diffusive and thus unstable. The upwind coefficient used in Equation 1212 is calculated by:

$$\eta_I = \eta sign\left(\frac{\partial \Phi_I}{\partial X_j}\left(v_j - w_j\right)\right) \tag{1213}$$

Development of a less diffusive flux calculation is currently under investigation.

$$F_i^I = \sigma_{ij} \int_V \frac{\partial \Phi_I}{\partial X_j} dV \tag{1214}$$

This option is activated with the flag *INTEG* (only in the CFD version).

Stability

The Courant condition (neglecting viscosity effects) is used to determine the stability of an ALE process.

The maximum time step is calculated by:

$$\Delta t \le k \frac{\Delta l}{c + v - w} \tag{1215}$$

Where,

k	Coefficient
Δl	Smallest characteristic length of an element
c	Material speed of sound
v	Material velocity
w	Grid velocity

The speed of sound is determined by:

$$c = \sqrt{\frac{1}{\rho}\frac{\partial p}{\partial \rho} + \frac{4}{3}\frac{\mu}{\rho}} \tag{1216}$$

Where,

ρ	Density
μ	Dynamic viscosity

p Pressure

The relative velocity between the material and grid motion (v-w) is computed by:

$$v - w = \sqrt{\frac{1}{N}\sum_{i=1}^{3}\sum_{I=1}^{N}\left(v_i^I - w_i^I\right)^2} \tag{1217}$$

Where,

N Number of nodes of the considered element (usually N=8)

ALE Kinematic Conditions

Boundary Conditions

Boundaries with Lagrangian materials are declared automatically Lagrangian.

Nodes can be declared Lagrangian.

Constraints can be applied separately or simultaneously on:

- Material velocity
- Grid velocity

These constraints can be applied in one or several directions of a skew reference frame.

When the flag is set to 1, boundary condition is activated with global reference frame or skew reference frame.

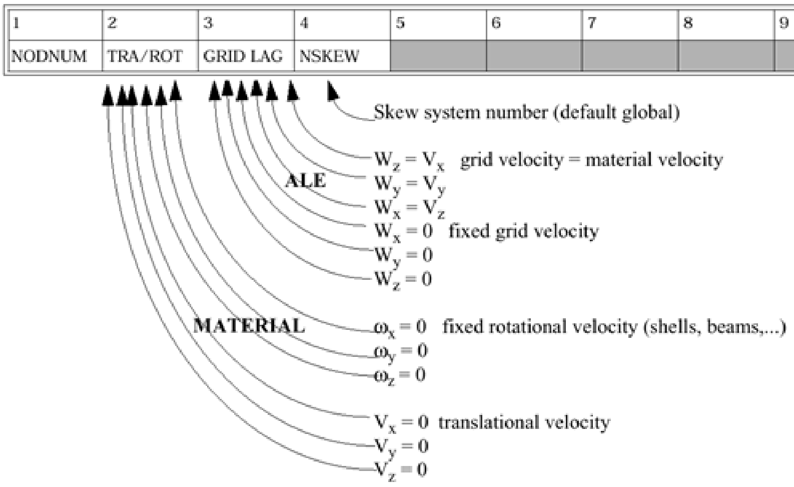

1	2	3	4	5	6	7	8	9	10
NODNUM	TRA/ROT	GRID LAG	NSKEW						

Skew system number (default global)
$W_z = V_x$ grid velocity = material velocity
$W_y = V_y$
$W_x = V_z$
ALE
$W_x = 0$ fixed grid velocity
$W_y = 0$
$W_z = 0$
MATERIAL
$\omega_x = 0$ fixed rotational velocity (shells, beams,...)
$\omega_y = 0$
$\omega_z = 0$
$V_x = 0$ translational velocity
$V_y = 0$
$V_z = 0$

Figure 268:

i = DOF with respect to global reference frame or skew reference frame

VELOCITY: Vi = 0

ACCELERATION: п i = 0

The boundary conditions can be changed during Engine runs with `/BCS` or `/BCSR` Engine options.

ALE Links

An ALE link is identical to a rigid link. The secondary node sets' grid velocity can be controlled by two main nodes, M1 and M2.

There are three options to choose from:

Option 0

Velocity is linearly interpolated with respect to order of input.

$$W_{NI} = W_{M1} + \left(W_{M2} - W_{M12}\right)\frac{I}{N+1} \tag{1218}$$

Option 1

Velocity is set to maximum absolute velocity of main nodes.

$$W_{NI} = W_{M1} \quad \text{if} \quad \left|W_{M1}\right| < \left|W_{M2}\right| \tag{1219}$$

Option 2

Velocity is set to minimum absolute velocity of main nodes.

$$W_{NI} = W_{M1} \quad \text{if} \quad \left|W_{M1}\right| < \left|W_{M2}\right| \tag{1220}$$

The input data is specified at each restart run.

Automatic Grid Computation

There are three different grid velocity formulations that can be used in an ALE simulation. New keywords define the type of method used. The different formulations are:

- 0 - J. Donea Grid Formulation: use keyword `/DONEA`

  (NWALE =0 for version < 4.1)
- 1 - Average Displacement Formulation: use keyword `/DISP`

  (NWALE =1 for version < 4.1)
- 2 - Nonlinear Spring Formulation: use keyword `/SPRING`

  (NWALE =2 for version < 4.1)

J. Donea Grid Formulation (/DONEA)

This formulation [123] [124] computes grid velocity using:

$$W_I(t+\Delta t/2) = \frac{1}{N}\sum_J W_j(t-\Delta t/2) + \frac{1}{N^2}\frac{a}{\Delta t}\sum_J L_{IJ}(t)\sum_J \frac{u_J(t)-u_I(t)}{L_{IJ}(t)} \tag{1221}$$

Where,

$$1-\gamma \le \frac{w}{v} \le 1+\gamma$$

N	Number of nodes connected to node I
L_{IJ}	Distance between node I and node J

$\boldsymbol{\alpha}$, γ adimensional factors given in input

Therefore, the grid displacement is given by:

$$u(t+\Delta t)=u(t)+w(t+\Delta t/2)\Delta 2 \tag{1222}$$

Average Displacement Formulation (/DISP)

The average displacement formulation calculates average velocity to determine average displacement.

$$u(t+\Delta t)=\frac{1}{N}\sum_{J} w_j(t) \tag{1223}$$

Nonlinear Spring Formulation (/SPRING)

Each grid node is connected to neighboring grid nodes through a nonlinear viscous spring, similar to that shown in Figure 269.

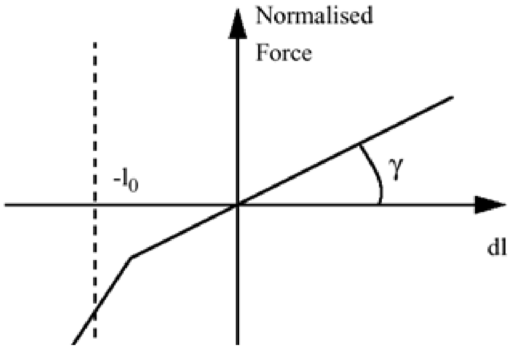

Figure 269: Spring Force Graph

The input parameters required are:

ΔT_0 Typical time step (Must be greater than the time step of the current run.)

$0<\gamma<1$ Nonlinearity factor

η Damping coefficient

V Shear factor (stiffness ratio between diagonal springs and springs along connectivities)

This formulation is the best of the three, but it is the most computationally expensive.

[123] Donea J., "An Arbitary Lagrangian-Eulerian finite element method for transient dynamic fluid-structure interactions", Computer methods in applied mechanics, 1982.

[124] Brooks A.N. and Hughes T.J.R., "Streamline Upwind /Petrov-Galerkin Formulations for Convection Dominated Flows with particular Emphasis on the Incompressible Navier-Stokes Equations", Computer Methods in Applied Mechanics and Engineering, Vol. 32, 1982.

Fluid-Structure Interaction (TYPE 1 Interface)

TYPE1 interface is used to model fluid-structure interactions, as shown in Figure 270.

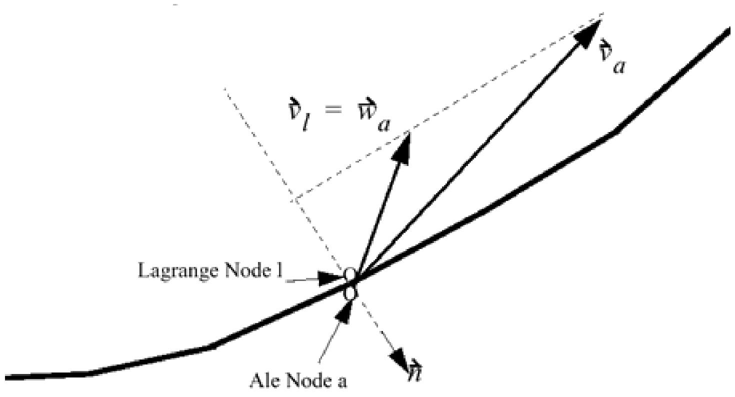

Figure 270: Fluid-Structure Interaction

This interface allows Lagrangian elements (structure) to interact with ALE (Arbitrary Lagrangian Eulerian) elements, which model a viscous fluid. Full slip conditions are applied at the boundary between the two domains.

The acceleration of the Lagrange node is computed by:

$$\vec{\gamma}_i = \frac{\vec{F}_i + \vec{F}_a}{m_i + m_a} \tag{1224}$$

The acceleration of the ALE node is computed by:

$$\vec{\gamma}_a = \frac{\vec{F}_a}{m_a} \tag{1225}$$

The grid velocity of the ALE node is equal to the material velocity of the Lagrange node:

$$\vec{w}_a = \vec{v}_i \tag{1226}$$

The normal material velocities of Lagrange and ALE nodes are equal. Therefore:

$$\vec{v}_a \cdot \vec{n} = \vec{v}_i \cdot \vec{n} \tag{1227}$$

Example: High Velocity Impacts

A typical application of the ALE method is using high velocity impacts.

Here a cylinder, moving at 227 m/s, impacts with a rigid wall. The material is copper, with a yield stress of 400 MPa. The initial diameter is 6.4 mm and initial length is 32.4 mm. The simulation was performed using two different methods: ALE and standard Lagrangian. The results can be seen in Figure 271.

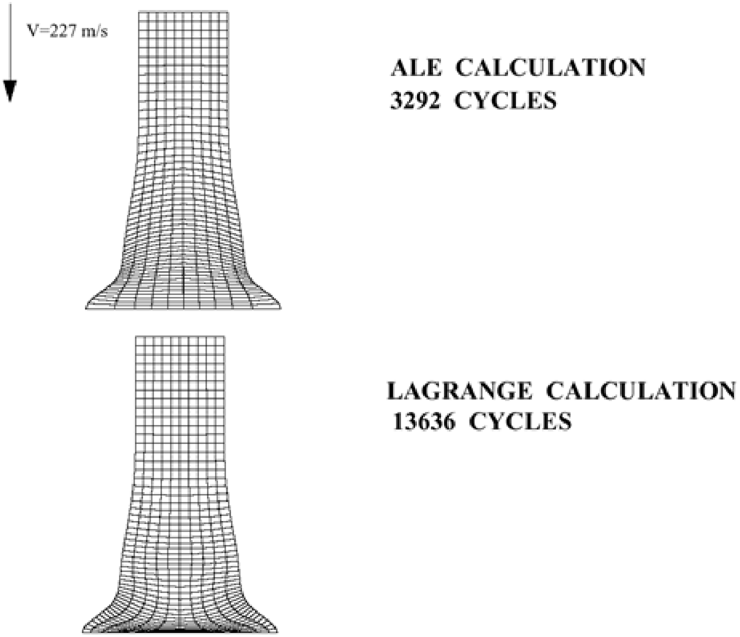

Figure 271: Cylinder Impact Deformation

It can be seen that the cylinder mesh using ALE remains regular, unlike the Lagrange method, where large element deformation creates very small and skewed elements. This reduces the time step, leading to more time step cycles. However, each ALE cycle takes longer than a Lagrangian.

Computational Aero-Acoustic

This section presents a resumed state-of-the-art of simulation in aero-acoustic domain. [125] Aero-Acoustics is the engineering field dealing with noise generated generally (but not necessarily) by a turbulent fluid flow interacting with a vibrating structure. This field differs from the pure acoustic domain where the object is the propagation of acoustic pressure waves, including reflections, diffractions and absorptions, in a medium at rest. Aero-Acoustic questions arise in many industrial design problems and are heavily represented in the noise nuisances related to the transportation industry.

A classification of Aero-Acoustic problems can be made using the following categories:

External wind noise transmitted to the inside through a structure
In the automotive industry, a pillar, side mirror and windshield wipers noise are typical problems of this category.

Internal flow noise transmitted to the outside through a structure
Examples of this class of problems are exhaust, HVAC and Intakes noises.

Rotating machine noise
Axial and centrifugal fans are noisy components that bring with them many interesting Aero-Acoustic problems.

Most of the Aero-Acoustic R&D works are performed experimentally but this method has some critical pitfalls. Although it is relatively simple to setup a microphone, measure a noise level and derive a spectrum at any given location in space, the correct analysis of an Aero Acoustic problem involves the use of advanced experimental techniques and is complex to use. The Aero Acoustic engineering community seeks more and more the help of CAE tools as they become available. Those tools complement the experimentations and allow a thorough visualization and understanding of the pressure and velocity fields as well as the structural vibrations. Furthermore, parametric studies can be carried out with little added cost since a numerical model modification is often straightforward and the CPU time is becoming cheaper and cheaper.

CFD codes are available since over several years, able to predict with a reasonable precision steady state flows (drag and lift) and slow transient flows like heating and defrosting. Highly transient flows involved in the Aero-Acoustic phenomena have not been treated since they were not in the bulk of the needs and they required way too much CPU to be industrially feasible. Acoustic Propagation numerical tools have also been industrially available since quite a few years. These tools operate in the frequency domain and are able to propagate a given boundary condition signal in a fluid at rest, including the noise reflections, diffractions, transmissions and attenuations thanks to the various geometrical obstacles and different materials.

Attempts have been made to combine existing CFD and Acoustic propagation tools to predict Aero-Acoustic problems. Most methodologies are based on the Lighthill and Curle method, developed in the mid 1950's and Ffowcs Williams and Hawkings contributions made in the late 1960's. [126] [127] [128] [129] The ideas underlying these methods are to decouple the flow pressure field and the acoustic pressure field. The fluid flow can then be computed by a standard CFD code and the noise derived from the curvature and turbulent intensities of the flow. A propagation tool is then used to compute the noise on a sub grid of the CFD computational domain loosing therefore quite some local information and high frequency content. First attempts were made with incompressible steady state CFD simulations and were not able to deliver valuable result in many cases. A good example of these limitations is highlighted by the study of the noise generated by a simple *side mirror* shape written by R. Siegert. [130] Recent developments of this family of techniques require the use of transient simulations and filtering to avoid loosing to much information on the coarser acoustic mesh. Reasonable success has been met in specific areas involving low frequencies (up to a couple hundred Hz) and considerable CPU time is needed.

An alternative methodology is to incorporate in a single numerical tool, right from the beginning, the ingredients that are necessary to perform direct Aero-Acoustic numerical simulation. They are:

Compressible Navier Stokes
To be able to propagate pressure waves and therefore take into account in a single simulation the flow and the noise, including all possible cavity modes.

Fluid structure coupling
To be able to treat the problems involving a turbulent flow on one side of the structure and the noise radiation on the other side.

Small time step
To be able to deal accurately with frequencies going up to several thousand Hertz.

Transient turbulence modeling
Unlike the Reynolds Averaged Navier Stokes (RANS) methods that makes the assumption that the flow is a combination of a steady state and turbulent fluctuations. Aero-Acoustic noise is directly linked to the small scale turbulence fluctuations and strongly time dependant.

Acoustic boundaries with prescribed impedance
This is a critical point of a good Aero-Acoustic simulation. Boundaries need to be able to perform tasks such as giving a free field impedance to an inlet with fixed velocity, prescribing a specific impedance at the outlet of a duct to make sure long wavelength stay trapped inside, treat exterior air impedance effect on a vibrating structure and be used to model absorbing materials (carpet, foams,and so on) that are used to coat many components.

These ingredients have been implemented in a single numerical code. The outcome is Radioss solver which is different from the existing CFD codes in its capabilities and particularly well suited to short time transient analysis.

[125] Nicolopoulos D., Périé F., and Jacques A., "Direct numerical simulation of Aero-Acoustic phenomena", M-CUBE, Internal Report, February 2004.

[126] Lighthill M.J., "On Sound Generated Aerodynamically, Part I: General Theory", Proc. Roy. Soc., A211, 564-587, 1952.

[127] Lighthill M.J., "On Sound Generated Aerodynamically, Part II: Turbulence as a source of sound", Proc. Roy. Soc., A222, 1-32, 1954.

[128] Curle N., "The influence of solid boundaries upon aerodynamic sound", Proc. Roy. Soc. Lond., A23, 505-514, 1955.

Modeling Methodology

The process of defining a numerical model for a given CAA application unfolds in four consecutive phases. The quality of the results is directly tight to the quality of the numerical model developed in the points 1 and 2 below. It is, therefore, critical to define precisely the questions the model is supposed to answer to before starting any development:

1. Mesh definition: Targeting specific answers to engineering questions and constrained by the available computer resources.
2. Numerical model construction, including material, boundary conditions and desired output.
3. Run monitoring.
4. Post-processing of the time domain data. Including 3D visualization, time history and frequency content analysis.

Mesh Definition

The mesh building process is the art of building models able to solve the CFD and the CAA problem for a given set of boundary conditions and range of frequencies while keeping the model as small as possible to minimize the compute time. To do so, a set of practical rules have been developed. These rules should be used as initial guidelines to get started on a given problem.

However each class of problems has its own requirements and subtleties and a good knowledge of the problem physics through experimental data and/or numerical simulations will be necessary to refine these rules and get the best possible results.

Post-processing

Post-processing of the numerical simulation is very similar to the post-processing of a detailed experimental study of the same problem. The analysis will be carried out by using:

- FFT's of recorded time domain signal to access the frequency domain content at any given location of the computational domain.
- Visualization and analysis of intensities on the structures
- Propagation in the far field (if and when needed) of the pressure signal. Typically, this is required for simulations where the measurement locations are not located in the computational domain. In most of the internal flow problems for instance the limit of the domain is the structure and a boundary elements layer to represent the outside air impedance (exhaust, HVAC, and so on). The noise is often measured at a given distance outside the ducts in still air where there is no reason to have an expensive CAA solution. This propagation can be performed by a simple monopolar approximation that gives satisfactory results in the free conditions or by more sophisticated tools such as BEM methods.

[129] Ffowcs Williams, J.E. and Hawkings D.L., “Sound Generation by Turbulence and Surfaces in Arbitrary Motion”, Phil.Trans.Roy.Soc., A, Vol. 264, No. 1151, pp. 321-344, 1969.

[130] Siegert R., “Numerical simulation of aero-acoustic sound generated by a simplified side mirror model.”, SIA, 1999.

Application and Validation

As the aim of this manual is not to describe the modeling techniques, the readers are invited to consult the available publications (for example [131] [132] [133] [134] and the proceeding of International Radioss User Conference).

Conclusion

Along the whole development process, the CAA orientation has been kept in mind for all the decisions and lead to the choice of the following methods:

- Compressible 3D Navier stokes solver
- Transient explicit time integration
- LES Turbulence
- Acoustic boundary conditions
- Fluid Structure coupling

These ingredients are needed to perform CAA simulations with no particular assumptions on the flow (except for the use of a turbulence model), the fluid structures coupling or the vibrations, making Radioss a fairly general code.

Further developments are considered among which can cite the ability to deal with bent flows. In the real world, in many interesting cases, the object to be studied is not positioned on a flat ground but embedded within a complex geometrical shape (for example a side mirror on a car). The flow, which hits the component, is distorted by this geometry. Simulation of the whole vehicle with a CAA method is not practical beyond a few hundred Hertz because of the huge number of elements needed in the propagation zone. Therefore, a method mixing a steady state simulation of the far field to get proper bent boundary conditions and Radioss close to the component and the acoustic sources zones is currently under development to perform CAA analysis of this kind of problem well beyond 1000 Hz.

[131] Sakurai M., Endo M., and Périé F., “Development of the exhaust systems radiation noise technology”, Proceedings of Insert ASMEFEDSM'03, ASME 2003 Fluids Engineering Division Summer Meeting, Honolulu, Hawaii, USA, July 6-11, 2003.

[132] Vergne S., Auger J.M., G'Styr N., and Périé F., “Simulation of cavity Aero-Elastic Noise induced by an external turbulent flow perturbed by a small ruler”, Workshop on LES for Acoustics October 2002, DLR Goettingen, Germany 2002.

[133] Obrist D., Nicolopoulos D., and Jacques A., “Aero Acoustic Simulation of a side mirror compared with experimental results”, The 2002 International Congress and Exposition on Noise Control Engineering, Dearborn, 2002.

[134] Fukui Y. and Périé F., “Methodological developments for vibrating pipes noise prediction”, The 2002 International Congress and Exposition on Noise Control Engineering, Dearborn, 2002.

Smooth Particle Hydrodynamics

Smooth Particle Hydrodynamics (SPH) is a meshless numerical method based on interpolation theory. It allows any function to be expressed in terms of its values at a set of disordered point's so-called particles.

SPH is not based on the particle physics theory. The conservation laws of continuum dynamics, in the form of partial differential equations, are transformed into integral equations through the use of kernel approximation. A comprehensive state-of-the-art of the method. [135] [136] [137] These techniques were initially developed in astrophysics. [138] [139] During the 1991-1995 periods, SPH has become widely recognized and has been used extensively for fluid and solid mechanics type of applications. SPH method is implemented in Radioss in Lagrangian approach whereby the motion of a discrete number of particles is followed in time.

SPH is a complementary approach with respect to ALE method. When the ALE mesh is too distorted to handle good results (for example in the case of vortex creation), SPH method allows getting a sufficiently accurate solution.

SPH Approximation of a Function

Let $\prod f(x)$ the integral approximation of a scalar function f in space:

$$\prod f(x) = \int_{\Omega} f(y) W(x-y, h) dy \tag{1228}$$

with h the so-called smoothing length and W a kernel approximation such that:

$$\forall\, x, \int_{\Omega} W(x-y, h) dy = 1 \tag{1229}$$

and in a suitable sense

$$\forall\, x, \lim_{h \to 0} W(x-y, h) = \delta(x-y) \tag{1230}$$

δ denotes the Dirac function.

[135] Bonet J., TSL Lok, “Variational and Momentum Preservation Aspects of Smooth Particle Hydrodynamic Formulations”, Computer Methods in Applied Mechanics and Engineering, Vol. 180, pp. 97-115 (1999).

[136] Randles P.W. and Libersky L.D., “Smoothed Particle Hydrodynamics: Some recent improvements and applications”, Computer Methods Appl. Mech. Engrg. Vol. 139, pp. 375-408, 1996.

[137] Balsara D.S., “Von Neumann Stability Analysis of Smoothed Particle Hydrodynamics Suggestions for Optimal Algorithms”, Journal of Computational Physics, Vol. 121, pp. 357-372, 1995.

[138] Lucy L.B., “A numerical approach to the testing of the fission hypothesis”, Astro. J., Vol. 82, 1013, 1977.

[139] Gingold R.A. and Monaghan J.J., “SPH: Theory and application to non-spherical stars”, Mon. Not. R. Astron. Soc., Vol. 181, 375, 1977.

Let a set of particles i=1, n at positions x_i (i=1,n) with mass m_i and density ρ_i. The smoothed approximation of the function f is (summation over neighboring particles and the particle i itself):

$$\prod_s f(x) = \sum_{i=1,n} \frac{m_i}{\rho_i} f(x_i) W(x-y,\, h) \tag{1231}$$

The derivatives of the smoothed approximation are obtained by ordinary differentiation.

$$\nabla f(x) = \sum_{i=1,n} \frac{m_i}{\rho_i} f(x_i) \nabla W(x-y,\, h) \tag{1232}$$

The following kernel [140] which is an approximation of Gaussian kernel by cubic splines was chosen (Figure 272):

$$r \le h \Rightarrow W(r,\, h) = \frac{3}{2\pi h^3}\left[\frac{2}{3} - \left(\frac{r}{h}\right)^2 + \frac{1}{2}\left(\frac{r}{h}\right)^3\right] \tag{1233}$$

$$h \le r \le 2h \Rightarrow W(r,\, h) = \frac{1}{4\pi h^3}\left(2 - \frac{r}{h}\right)^3 \tag{1234}$$

and

$$2h \le r \Rightarrow W(r,\, h) = 0 \tag{1235}$$

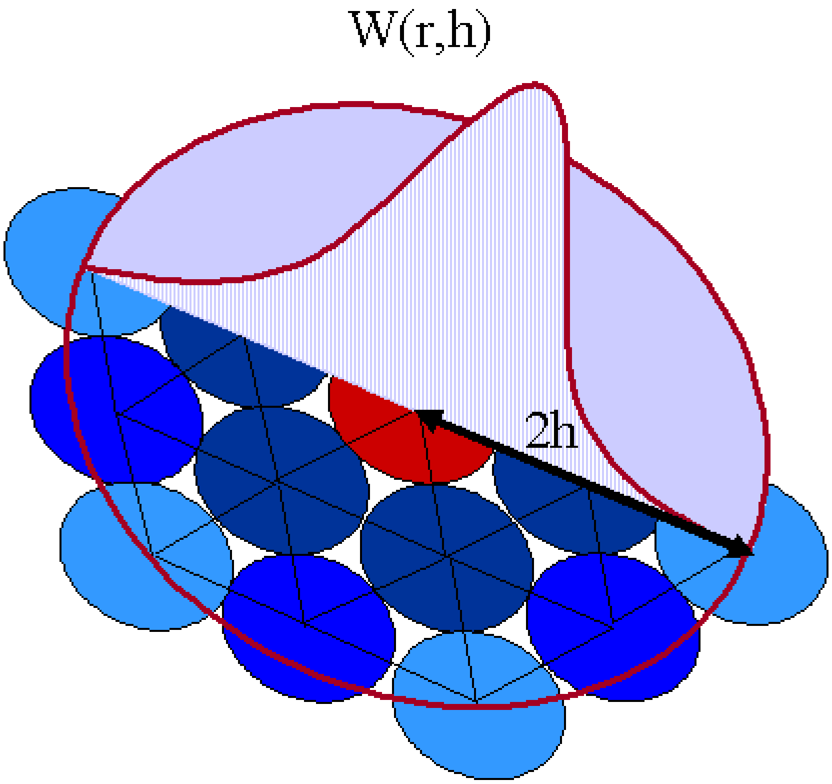

Figure 272: Kernel Based on Spline Functions

This kernel has compact support, so that for each particle i, only the closest particles contribute to approximations at i (this feature is computationally efficient). The accuracy of approximating Equation 1228 by Equation 1231 depends on the order of the particles.

Corrected SPH Approximation of a Function

Corrected SPH formulation [141] [142] has been introduced in order to satisfy the so-called consistency conditions:

$$\int_{\Omega} W(y-x,h)=1,\ \forall\ x \tag{1236}$$

$$\int_{\Omega} (y-x)W(y-x,h)=0,\ \forall\ x \tag{1237}$$

These equations insure that the integral approximation of a function f coincides with f for constant and linear functions of space.

CSPH is a correction of the kernel functions:

$$\hat{W}_j(x,h)=W_j(x,h)\alpha(x)\left[1+\beta(x)\bullet(x-x_j)\right] \text{ with } W_j(x,h)=W(x-x_j,h) \tag{1238}$$

Where the parameters $\alpha(x)$ and $\beta(x)$ are evaluated by enforcing the consistency condition, now given by the point wise integration as:

$$\sum_j V_j\hat{W}_j(x,h)=1,\ \forall\ x \tag{1239}$$

$$\sum_j V_j(x-x_j)\hat{W}_j(x,h)=0,\ \forall\ x \tag{1240}$$

These equations enable the explicit evaluation of the correction parameters $\alpha(x)$ and $\beta(x)$ as:

$$\beta(x)=\left[\sum_j V_j(x-x_j)\otimes(x-x_j)W_j(x,h)\right]^{-1}\sum_j V_j(x_j-x)W_j(x,h) \tag{1241}$$

$$\alpha(x)=\frac{1}{\sum_j V_jW_j(x,h)\left[1+\beta(x)\bullet(x-x_j)\right]} \tag{1242}$$

Since the evaluation of gradients of corrected kernel (which are used for the SPH integration of continuum equations) becomes very expensive, corrected SPH limited to order 0 consistency has been introduced. Therefore, the kernel correction reduces to the following equations:

[140] Monaghan J.J., “Smoothed Particle Hydrodynamics”, Annu.Rev.Astron.Astro-phys; Vol. 30; pp. 543-574, 1992.

$$\hat{W}_j(x, h) = W_j(x, h)\alpha(x) \tag{1243}$$

that is

$$\alpha(x) = \frac{1}{\sum_j V_j W_j(x, h)} \tag{1244}$$

$$\sum_j V_j \hat{W}_j(x, h) = 1, \forall\, x \tag{1245}$$

Note: SPH corrections generally insure a better representation even if the particles are not organized into a hexagonal compact net, especially close to the integration domain frontiers. SPH corrections also allow the smoothing length h to values different to the net size Δx to be set.

SPH Integration of Continuum Equations

In order to keep an almost constant number of neighbors contributing at each particle, use smoothing length varying in time and in space.

Consider d_i the smoothing length related to particle i;

$$W_j(i) = \widehat{W}\left(x_i - x_j, \frac{d_i + d_j}{2}\right) \text{ and } \nabla W_j(i) = grad\Big|_{x_i}\left[\widehat{W}\left(x - x_j, \frac{d_i + d_j}{2}\right)\right] \text{ if kernel correction} \tag{1246}$$

or

$$W_j(i) = W\left(x_i - x_j, \frac{d_i + d_j}{2}\right) \text{ and } \nabla W_j(i) = grad\Big|_{x_i}\left[W\left(x - x_j, \frac{d_i + d_j}{2}\right)\right] \text{ without kernel correction} \tag{1247}$$

At each time step, density is updated for each particle i, according to:

$$\left.\frac{d\rho}{dt}\right|_i = -\rho_i \nabla \cdot v\Big|_i \tag{1248}$$

with

141. Bonet J., TSL Lok, "Variational and Momentum Preservation Aspects of Smooth Particle Hydrodynamic Formulations", Computer Methods in Applied Mechanics and Engineering, Vol. 180, pp. 97-115 (1999).

142. Bonet J. and Kulasegram S., "Correction and Stabilization of Smooth Particle Hydrodynamics Methods with Applications in Metal Forming Simulations", Int. Journal Num. Methods in Engineering, Vol. 47, pp. 1189-1214, 2000.

$$\nabla \cdot v\big|_i = \sum \frac{m_j}{\rho_j}\left(v_i - v_j\right)\cdot \nabla W_j(i) \tag{1249}$$

Where,

m_j	Mass of a particle i
ρ_i	Density
v_j	Velocity

Strain tensor is obtained by the same way when non pure hydrodynamic laws are used or in the other words when law uses deviatoric terms of the strain tensor:

$$\frac{dv^\alpha}{dx^\beta}\bigg|_i = \sum \frac{m_j}{\rho_j}\left(v_i^\alpha - v_j^\alpha\right)\frac{dW_j}{dx^\beta}(i),\ \alpha = 1 \ldots 3,\ \beta = 1 \ldots 3. \tag{1250}$$

Next the constitutive law is integrated for each particle. Then Forces are computed according to:

$$m_i \frac{dv}{dt}\bigg|_i = -\sum_j V_i V_j\left[p_i \nabla W_j(i) - p_j \nabla W_i(j)\right] - \sum_j m_i m_j \pi_{ij} \frac{\left[\nabla W_j(i) - \nabla W_i(j)\right]}{2} \tag{1251}$$

Where ρ_i and p_j are pressures at particles i and j, and π_{ij} is a term for artificial viscosity. The expression is more complex for non pure hydrodynamic laws.

> **Note:** The previous equation reduces to the following one when there is no kernel correction:

$$m_i \frac{dv}{dt}\bigg|_i = -\sum_j V_i V_j\left[p_i + p_j\right]\nabla W_j(i) - \sum_j m_i m_j \pi_{ij} \nabla W_j(i), \tag{1252}$$

since $\nabla W_i(j) = -\nabla W_j(i)$

Then, in order particles to keep almost a constant number of neighbors into their kernels (ρd^3 is kept constant), search distances are updated according to:

$$\frac{d(d_i)}{dt} = d_i \frac{\nabla \cdot v|_i}{3} \tag{1253}$$

Artificial Viscosity

As usual in SPH [143] implementations, viscosity is rather an inter-particles pressure than a bulk pressure. It was shown that the use of Equation 1254 and Equation 1255 generates a substantial amount of entropy in regions of strong shear even if there is no compression.

$$\pi_{ij} = \frac{-q_b \frac{c_i + c_j}{2} \mu_{ij} + q_\alpha \mu_{ij}^2}{\frac{\left(\rho_i + \rho_j\right)}{2}} \tag{1254}$$

with

$$\mu_{ij} = \frac{d_{ij}\left(v_i - v_j\right) \bullet \left(X_i - X_j\right)}{\| X_i - X_j \|^2 + \varepsilon d_{ij}^2} \tag{1255}$$

Where, X_i (resp. X_j) indicates the position of particle I (resp. j) and c_i (resp c_j) is the sound speed at location i (resp. j), and q_a and q_b are constants. This leads us to introduce Equation 1256 and Equation 1257. [144] The artificial viscosity is decreased in regions where vorticity is high with respect to velocity divergence.

$$\pi_{ij} = \frac{-q_b \frac{c_i + c_j}{2} \mu_{ij} + q_\alpha \mu_{ij}^2}{\frac{\left(\rho_i + \rho_j\right)}{2}} \tag{1256}$$

with

$$\mu_{ij} = \frac{d_{ij}\left(v_i - v_j\right) \bullet \left(X_i - X_j\right)}{\| X_i - X_j \|^2 + \varepsilon d_{ij}^2} \frac{\left(f_i + f_j\right)}{2}, \; f_k = \frac{\| \nabla \cdot v|_k \|}{\| \nabla \cdot v|_k \| + \| \nabla \times v|_k \| + \varepsilon' \frac{c_k}{d_k}} \tag{1257}$$

Default values for q_a and q_b are respectively set to 2 and 1.

Time Step Control Stability

The stability conditions of explicit scheme in SPH formulation can be written over cells or on nodes.

Cell Time Step

In case of cell stability computation (when no nodal time step is used), the stable time step is computed as:

$$\Delta t = \Delta t_{sca} \cdot \min_i \left(\frac{d_i}{c_i\left(\alpha_i + \sqrt{\alpha_i^2 + 1}\right)} \right), \; with \quad \alpha_i = \left(q_b + \frac{q_a \cdot \bar{\mu}_i \cdot d_i}{c_i} \right), \; and \quad \bar{\mu}_i = \max_j \left(\mu_{ij} \right) \tag{1258}$$

[143] Monaghan J.J., "Smoothed Particle Hydrodynamics", Annu.Rev.Astron.Astro-phys; Vol. 30; pp. 543-574, 1992.

[144] Balsara D.S., "Von Neumann Stability Analysis of Smoothed Particle Hydrodynamics Suggestions for Optimal Algorithms", Journal of Computational Physics, Vol. 121, pp. 357-372, 1995.

Δt_{sca} is the user-defined coefficient (Radioss option `/DT` or `/DT/SPHCEL`). The value of ΔT_{sca} =0.3 is recommended. [145]

Nodal Time Step

In case of nodal time step, stability time step is computed in a more robust way:

$$\Delta t_i = \sqrt{\frac{2m_i}{K_i}} \text{ at particle } i \tag{1259}$$

Use the following notations, if kernel correction:

$$W_j(i) = \widehat{W}\left(x_i - x_j, \frac{d_i + d_j}{2}\right) \; and \, \nabla W_j(i) = grad|_{xi}\left[\widehat{W}\left(x - x_j, \frac{d_i + d_j}{2}\right)\right] \tag{1260}$$

Or, if no kernel correction:

$$W_j(i) = W\left(x_i - x_j, \frac{d_i + d_j}{2}\right) \; and \, \nabla W_j(i) = grad|_{xi}\left[W\left(x - x_j, \frac{d_i + d_j}{2}\right)\right] \tag{1261}$$

Recalling that apart from the artificial viscosity terms:

$$F_i = \sum_j F_{ij}, \; F_{ij} = V_i V_j \left[p_i \nabla W_j(i) - p_j \nabla W_j(j)\right] \tag{1262}$$

write

$$|K_{ij}| = \left\| \frac{dF_{ij}}{d(u_i - u_j)} \right\| \le \frac{d}{d(u_i - u_j)} \left(V_i V_j \left[p_i \| \nabla W_j(i) \| + p_j \| \nabla W_i(j) \| \right] \right) \tag{1263}$$

Where, $u_i - u_j$ is the relative displacement of particles i and j. Keeping the only first order terms leads to:

$$|K_{ij}| \le V_i V_j \left[\frac{dp_i}{d(u_i - u_j)} \| \nabla W_j(i) \| + \frac{dp_j}{d(u_i - u_j)} \| \nabla W_i(j) \| \right] \tag{1264}$$

Where,

$$V_i V_j \frac{dp_i}{d(u_i - u_j)} \| \nabla W_j(i) \| = V_i V_j \frac{dp_i}{d\rho_i} \cdot \frac{d\rho_i}{d(u_i - u_j)} \| \nabla W_j(i) \| = V_i V_j c_i^2 \frac{d\rho_i}{d(u_i - u_j)} \| \nabla W_j(i) \| \tag{1265}$$

that is

$$V_i V_j \frac{dp_i}{d(u_i - u_j)} \| \nabla W_j(i) \| = m_i c_i^2 V_j^2 \| \nabla W_j(i) \|^2 \tag{1266}$$

Same reasoning leads to:

$$V_i V_j \frac{dp_j}{d(u_i - u_j)} \| \nabla W_i(j) \| = m_j c_j^2 \dot{V}_i^2 \| \nabla W_i(j) \|^2 \tag{1267}$$

So that

$$|K_{ij}| \leq m_i c_i^2 \dot{V}_j^2 \| \nabla W_j(i) \|^2 + m_j c_j^2 \dot{V}_i^2 \| \nabla W_i(j) \|^2 \tag{1268}$$

Stiffness around node i is then estimated as:

$$|K_i| \leq \sum_j |K_{ij}| \tag{1269}$$

Conservative Smoothing of Velocities

It can be shown that the SPH method is unstable in tension. The instability is shown to result from an effective stress with a negative modulus (imaginary sound speed) being produced by the interaction between the constitutive relation and the kernel function, and is not caused by the numerical time integration algorithm. [146] D.S Balsara [147] states, use special filtering of velocities (so called *conservative smoothing*, because momentum quantities are not modified):

$$V_i(smoothed) = v_i + \alpha_{cs} \sum_j \frac{2m_j}{\rho_i + \rho_j} (v_j - v_i) \frac{W_i(j) + W_j(i)}{2} \tag{1270}$$

SPH Cell Distribution

It is recommended to distribute the particles through a hexagonal compact or a cubic net.

Hexagonal Compact Net

A cubic centered faces net realizes a hexagonal compact distribution and this can be useful to build the net (Figure 273). The nominal value h_0 is the distance between any particle and its closest neighbor. The mass of the particle m_p may be related to the density of the material ρ and to the size h_0 of the hexagonal compact net, with respect to:

[145] Monaghan J.J., "Smoothed Particle Hydrodynamics", Annu.Rev.Astron.Astro-phys; Vol. 30; pp. 543-574, 1992.

[146] Swegle J.W., Hicks D.L., and Attaway S.W., "Smoothed Particle Hydrodynamics: Stability Analysis", Journal of Computational Physics, Vol. 116, pp. 123-134, 1995.

[147] Balsara D.S., "Von Neumann Stability Analysis of Smoothed Particle Hydrodynamics Suggestions for Optimal Algorithms", Journal of Computational Physics, Vol. 121, pp. 357-372, 1995.

$$m_p \approx \frac{h_0^3}{\sqrt{2}}\rho \tag{1271}$$

Since the space can be partitioned into polyhedras surrounding each particle of the net, each one with a volume:

$$V_p \approx \frac{h_0^3}{\sqrt{2}} \tag{1272}$$

But, due to discretization error at the frontiers of the domain, mass consistency better corresponds to $m_P = \frac{\rho V}{n}$.

Where,

V
: Total volume of the domain and n the number of particles distributed in the domain

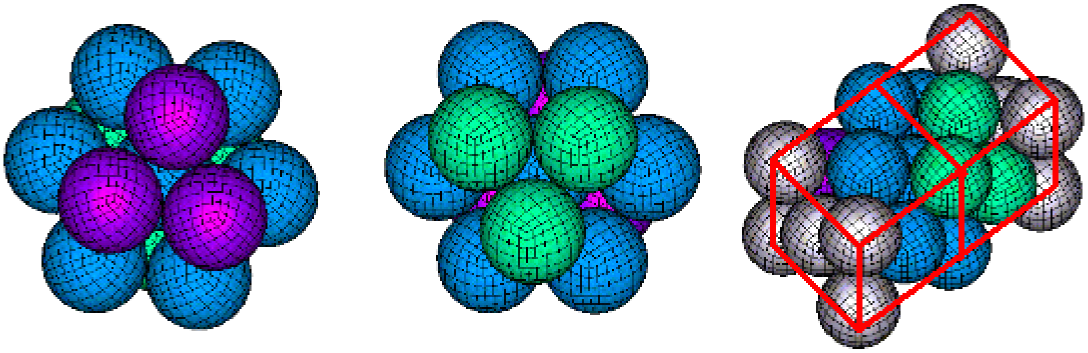

Figure 273: Local View of Hexagonal Compact Net and Perspective View of Cubic Centered Faces Net

> **Note:** Choosing h_0 for the smoothing length insures naturally consistency up to order 1 if the previous equation is satisfied.

Weight functions vanish at distance $2h$ where h is the smoothing length. In an hexagonal compact net with size h_0, each particle has exactly 54 neighbors within the distance $2\mathrm{h}_0$ (Table 11).

Table 11: Number of Neighbors in a Hexagonal Compact Net

Distance d	Number of Particles at Distance d	Number of Particles within Distance d
h_0	12	12
$\sqrt{2}\,h_0$	6	18

Distance d	Number of Particles at Distance d	Number of Particles within Distance d
$\sqrt{3}\,h_0$	24	42
$2h_0$	12	54
$\sqrt{5}\,h_0$	24	78

Cubic Net

Let c the side length of each elementary cube into the net. The mass of the particles m_p should be related to the density of the material ρ and to the size c of the net, with respect to the following equation:

$$m_p \approx c^3\rho \tag{1273}$$

By experience, a larger number of neighbors must be taken into account with the hexagonal compact net, in order to solve the tension instability as explained in following sections. A value of the smoothing length between 1.25c and 1.5c seems to be suitable. In the case of smoothing length h=1.5c, each particle has 98 neighbors within the distance $2h$.

Table 12: Number of Neighbors in a Cubic Net

Distance d	Number of Particles at Distance d	Number of Particles within Distance d
c	6	6
$\sqrt{2}\,c$	12	18
$\sqrt{3}\,c$	8	26
2c	6	32
$\sqrt{5}\,c$	24	56
$\sqrt{6}\,c$	24	80
$2\sqrt{2}\,c$	12	92
3c	6	98

Appendix A: Basic Relations of Elasticity

Isotropic Material

Hooke Law 3D (Principal Stress and Strain)

$$\{\sigma\} = [D]\{\varepsilon\}$$

$$\sigma_1 = D_{11}\varepsilon_1 + D_{12}\varepsilon_2 + D_{13}\varepsilon_3$$

$$\sigma_1 = (\lambda + 2\mu)\varepsilon_1 + \lambda(\varepsilon_2 + \varepsilon_3)$$

$$\sigma_1 = \lambda(\varepsilon_1 + \varepsilon_2 + \varepsilon_3) + 2\mu\varepsilon_1$$

$$\sigma_1 = K\varepsilon_{kk} + 2\mu e_1 \qquad \text{with } \varepsilon_{kk} = (\varepsilon_1 + \varepsilon_2 + \varepsilon_3) \text{and } \mathrm{e}_1 = \varepsilon_1 - 1$$

$$\{\sigma\} = [D]\{\varepsilon\} \quad ; \quad [D] = \frac{E}{(1+v)(1-2v)} \begin{bmatrix} 1-v & v & v & 0 & 0 & 0 \\ & 1-v & v & 0 & 0 & 0 \\ & & 1-v & 0 & 0 & 0 \\ & & & \frac{1-2v}{2} & 0 & 0 \\ & Symm. & & & \frac{1-2v}{2} & 0 \\ & & & & & \frac{1-2v}{2} \end{bmatrix}$$

$$\{\varepsilon\} = [C]\{\sigma\} \quad ; \quad [C] = \begin{bmatrix} \frac{1}{E} & \frac{-v}{E} & \frac{-v}{E} & 0 & 0 & 0 \\ & \frac{1}{E} & \frac{-v}{E} & 0 & 0 & 0 \\ & & \frac{1}{E} & 0 & 0 & 0 \\ & & & \frac{2(1+v)}{E} & 0 & 0 \\ & Symm. & & & \frac{2(1+v)}{E} & 0 \\ & & & & & \frac{2(1+v)}{E} \end{bmatrix}$$

Hooke Law for 2D Plan Stress

$$\{\sigma\} = [H]\{\varepsilon\}$$

$$\sigma_1 = H_{11}\varepsilon_1 + H_{12}\varepsilon_2$$

$$\{\sigma\} = [H]\{\varepsilon\};\ [H] = \frac{E}{1-v^2} \begin{bmatrix} 1 & v & 0 & 0 & 0 \\ v & 1 & 0 & 0 & 0 \\ 0 & 0 & \frac{1-v}{2} & 0 & 0 \\ 0 & 0 & 0 & \frac{1-v}{2} & 0 \\ 0 & 0 & 0 & 0 & \frac{1-v}{2} \end{bmatrix}$$

$$\{\varepsilon\}=[C]\{\sigma\};\ [C]=\frac{1}{E}\begin{bmatrix} 1 & -v & 0 & 0 & 0 \\ -v & 1 & 0 & 0 & 0 \\ 0 & 0 & 2(1+v) & 0 & 0 \\ 0 & 0 & 0 & 2(1+v) & 0 \\ 0 & 0 & 0 & 0 & 2(1+v) \end{bmatrix}$$

Hooke Law for 2D Plane Strain

$$\{\sigma\}=[H]\{\varepsilon\};\ [H]=\frac{E}{(1+v)(1-2v)}\begin{bmatrix} 1-v & v & 0 \\ v & 1-v & 0 \\ 0 & 0 & \frac{1-2v}{2} \end{bmatrix}$$

$$\{\varepsilon\}=[C]\{\sigma\};\ [C]=\frac{1+v}{E}\begin{bmatrix} 1-v & -v & 0 \\ -v & 1-v & 0 \\ 0 & 0 & 2 \end{bmatrix}$$

Table 13: Material Constants Relations

	E, v	**E,G**	**E,B**	**G,** v	**G, B**	**B,** v	λ,μ
E	E	E	E	2(1+v)G	$\frac{9BG}{3B+G}$	3(1-2v)B	$\frac{(3\lambda+2\mu)\mu}{\lambda+\mu}$
$G=\mu$	$\frac{E}{2(1+v)}$	G	$\frac{3EB}{9B-E}$	G	G	$\frac{3(1-2v)B}{2(1+v)}$	μ
B=K	$\frac{E}{3(1-2v)}$	$\frac{EG}{9G-3E}$	B	$\frac{2(1+v)G}{3(1-2v)}$	B	B	$\frac{3\lambda+2\mu}{3}$
v	v	$\frac{E-2G}{2G}$	$\frac{3B-E}{6B}$	v	$\frac{3B-2G}{6B+2G}$	v	$\frac{\lambda}{2(\lambda+\mu)}$
λ	$\frac{Ev}{(1+v)(1-2v)}$	$\frac{(E-2G)G}{3G-E}$	$\frac{(3B-E)3B}{9B-E}$	$\frac{2Gv}{1-2v}$	$\frac{3B-2G}{3}$	$\frac{3Bv}{(1+v)}$	λ

Orthotropic Material

General 3D Orthotropic Case

The strain-stress relations are defined using 9 material constants:

- Three Young's modulus in orthotropic directions 1, 2 and 3: E_1, E_2, E_3
- Three shear modulus in planes 12, 13 and 23: G_{12}, G_{13}, G_{23}
- Three Poisson ratio's satisfying the relations:

$$\frac{\nu_{12}}{E_1}=\frac{\nu_{21}}{E_2} \quad ; \quad \frac{\nu_{13}}{E_1}=\frac{\nu_{31}}{E_3} \quad ; \quad \frac{\nu_{23}}{E_2}=\frac{\nu_{32}}{E_3}$$

$$1-\nu_{12}\nu_{21}>0;1-\nu_{13}\nu_{31}>0;\ 1-\nu_{23}\nu_{32}>0$$

$$1-\nu_{12}\nu_{21}-\nu_{13}\nu_{31}-\nu_{23}\nu_{32}-\nu_{12}\nu_{23}\nu_{31}-\nu_{21}\nu_{13}\nu_{32}>0$$

$$\{\varepsilon\}=[C]\{\sigma\};[C]=\begin{bmatrix} \frac{1}{E_1} & \frac{-\nu_{21}}{E_2} & \frac{-\nu_{31}}{E_3} & 0 & 0 & 0 \\ \frac{-\nu_{12}}{E_1} & \frac{1}{E_2} & \frac{-\nu_{32}}{E} & 0 & 0 & 0 \\ \frac{-\nu_{13}}{E_1} & \frac{-\nu_{23}}{E_2} & \frac{1}{E_3} & 0 & 0 & 0 \\ 0 & 0 & 0 & \frac{1}{G_{12}} & 0 & 0 \\ 0 & 0 & 0 & 0 & \frac{1}{G_{13}} & 0 \\ 0 & 0 & 0 & 0 & 0 & \frac{1}{G_{23}} \end{bmatrix}$$

2D In-plane Orthotropic Material

- Orthotropic plane 1-2, isotropic plane 2-3
  - Orthotropy coefficients in the plane 1-2: $E_1,\ E_2,\ \nu_{12},\ G_{12}$
  - Isotropy coefficients in plane 2-3: $E_2,\ \nu$
- Five independent coefficients

$$\{\varepsilon\}=[C]\{\sigma\};\ [C]=\begin{bmatrix} \frac{1}{E_1} & \frac{-\nu_{12}}{E_1} & \frac{-\nu_{12}}{E_1} & 0 & 0 & 0 \\ \frac{-\nu_{12}}{E_1} & \frac{1}{E_2} & \frac{-\nu}{E_2} & 0 & 0 & 0 \\ \frac{-\nu_{12}}{E_1} & \frac{-\nu}{E_2} & \frac{1}{E_2} & 0 & 0 & 0 \\ 0 & 0 & 0 & \frac{1}{G_{12}} & 0 & 0 \\ 0 & 0 & 0 & 0 & \frac{1}{G_{12}} & 0 \\ 0 & 0 & 0 & 0 & 0 & \frac{2(1+\nu)}{E_2} \end{bmatrix}$$

Stiffness Matrix of Beam Element

Terms of the stiffness matrix:

$$[k]=\left[\begin{array}{cccccccccccc}
\frac{EA}{L} & 0 & 0 & 0 & 0 & 0 & -K_{11} & 0 & 0 & 0 & 0 & 0 \\
 & \frac{12EI_3}{L^3(1+\phi_2)} & 0 & 0 & 0 & \frac{L}{2}K_{22} & 0 & -K_{22} & 0 & 0 & 0 & K_{26} \\
 & & \frac{12EI_2}{L^3(1+\phi_2)} & 0 & -\frac{L}{2}K_{33} & 0 & 0 & 0 & -K_{33} & 0 & K_{35} & 0 \\
 & & & \frac{GJ}{L} & 0 & 0 & 0 & 0 & 0 & -K_{44} & 0 & 0 \\
 & & & & \frac{(4+\phi_3)EI_2}{L(1+\phi_3)} & 0 & 0 & 0 & -K_{35} & 0 & \frac{2-\phi_3}{4+\phi_3}K_{55} & 0 \\
 & & & & & \frac{(4+\phi_2)EI_3}{L(1+\phi_2)} & 0 & -K_{26} & 0 & 0 & 0 & \frac{2-\phi_2}{4+\phi_2}K_{66} \\
 & & & & & & K_{11} & 0 & 0 & 0 & 0 & 0 \\
 & & & & & & & K_{22} & 0 & 0 & 0 & -K_{26} \\
 & & Symm. & & & & & & K_{33} & 0 & -K_{35} & 0 \\
 & & & & & & & & & K_{44} & 0 & 0 \\
 & & & & & & & & & & K_{55} & 0 \\
 & & & & & & & & & & & K_{66}
\end{array}\right]$$

For a rectangle cross-section:

$$\phi_2=\frac{144(1+v)I_3}{5AL^2}$$

$$\phi_3=\frac{144(1+v)I_2}{5AL^2}$$

$$I=\frac{bh^3}{12}$$

Index

Numerics

10-node solid tetrahedron *101*
3-node shell elements *150*
3-node triangle without rotational DOF *159*

A

acceleration convergence, theory manual *409*
advanced elasto-plastic hourglass control *149*
AIRBAG type monitored volume *388*
ALE formulation *423*
ALE kinematic conditions *431*
ALE materials, theory manual *428*
algorithm flow chart *51*
appendix A
    isotropic material *450*
    orthotropic material *451*
    stiffness matrix of beam element *452*
application and validation *439*
arc length method, theory manual *414*
AREA type monitored volume *383*
Arruda-Boyce material (LAW92) *298*
artificial viscosity *444*
assumed strain rate, theory manual *83*
auto contacts, theory manual *237*
automatic grid computation *432*

B

basic equations - theory manual *18*
beam element behavior *171*
beam element geometry *170*
beam elements, TYPE3 *170*
beam type spring elements (TYPE13) *194*
bend y axis, theory manual *201*
bend z axis, theory manual *201*
bilinear mindlin plate element *109*
bilinear shape functions *111*
body drop example, theory manual *52*
Boltzmann viscoelastic model (LAW34) *358*
brittle damage
    Johnson--Cook plasticity model (LAW27) *344*
    reinforced concrete material (LAW24) *345*

C

central difference algorithm *50*

Chang Chang model, elastic-plastic orthotropic composite shells *319*

closest main segment formulation *219*

combine modal reduction *72*

COMMU1 type examples, theory manual *401*

composite and anisotropic materials, theory manual *301*

composite modeling *155*

composite shell elements *154*

composite shell elements limitations *159*

composite shells *158*

composite shells with variable layers *158*

computation aero-acoustic *436*

computation algorithm, theory manual *250*, *257*

computational aero-acoustic conclusion *439*

connect materials, theory manual *352*

conservation

- internal energy, theory manual *427*
- mass, theory manual *425*
- momentum, theory manual *424*

conservative smoothing of velocities *447*

contact detection, theory manual *247*

contact processing, theory manual *246*

contacts modeling, theory manual *238*

courant condition stability *64*

Cowper-Symonds plasticity model (LAW44) *331*

CRASURV model, elastic-plastic orthotropic composite shells *317*

D

delamination, theory manual *312*

deviatoric stress calculation *98*

direct integration method: explicit scheme *48*

discrete equations *39*

Drücker-Prager constitutive model (laws 10, 21 and 81) *335*

ductile damage model

- for porous materials (LAW52) *349*

dynamic analysis, theory manual *48*

dynamic relaxation or nodal damping (/DYREL) *405*

E

elastic-plastic anisotropic shells (Barlat's law) *325*

elastic-plastic orthotropic composite shells, Chang Chang model *319*

elastic-plastic orthotropic composite shells, CRASURV model *317*

elastic-plastic orthotropic composite shells, failure behavior *315*

elastic-plastic orthotropic composite shells, strain rate effect *316*

elastic-plastic orthotropic composite solids *321*, *321*
elastic-plastic orthotropic composite solids - orthotropic plasticity *322*
elastic-plastic orthtropic composite shells *310*
elastic-plasticity of isotropic materials *326*
elasto-plastic hydrodynamics materials (LAW3) *372*
element coordinates *41*
element degeneration, theory manual *92*
element library *80*
element orientation *156*
ellipsoidal surface to node contact (TYPE14) *278*
ellipsoidal surface to segment contact (TYPE15) *279*
energy discrete relaxation, theory manual *407*
energy variation, theory manual *390*
equation of motion
  angular velocities *40*
  translational velocities *39*
equilibrium equations *29*
explicit integration of the nodal internal force vector *146*
explicit scheme stability *54*
external work variation, COMMU *400*

F

fabric law for elastic orthotropic shells (LAW19 and LAW58) *301*
failure behavior, elastic-plastic orthotropic composite shells *315*
failure models, theory manual *375*
finite element approximation *37*
finite element formulation *37*
fluid structure interaction, theory manual *434*
forces and moments calculation *132*
friction effects, theory manual *192*
fully-integrated shell element QBAT *142*
function derivatives *43*

G

GAS type monitored volume *383*
general degenerated 4-node shell formulations *138*
general purpose contact
  detection and gap size *272*
  force orientation *276*
  gap correction *273*
  interface algorithm *260*
  interface hints *276*
  penetration reaction *274*
  time step *271*
  TYPE 5 interface friction *259*
  TYPE 5 interface gap *260*

- TYPE 5 limitations *257*
- TYPE 7 interface friction *268*
- TYPE 7 interface stiffness *267*
- TYPE5 *256*
- TYPE5 interface stiffness *258*
- TYPE7 *266*
- TYPE7 interface gap *270*
- TYPE7 limitations *267*
- variable gap *272*

general spring elements (TYPE8) *185*
general surface to surface contact (TYPE17) *281*
generalized Kelvin-Voigt model (LAW35) *359*
generalized Maxwell-Kelvin model for viscoelastic materials (LAW40) *365*

H

high velocity impacts example *434*
Hill's law for orthotropic plastic shells *307*
hourglass modes, theory manual *86*, *117*
hourglass resistance, theory manual *120*
hybrid massively parallel program, theory manual *420*
hydrodynamic analysis materials - theory manual *370*
hydrodynamics viscous fluid materials (LAW6) *371*
hyper visco-elastic materials for foams (LAW62) *366*

I

impact candidates, algorithms *241*
in-plane strain-rate construction *143*
inertia computation *176*
initial conditions, AIRBAG *396*
integration and nodal forces, theory manual *42*
integration method, theory manual *429*
interface failure examples *255*
interface friction, theory manual *253*
interface gap, theory manual *255*
interface overview, theory manual *234*
interface stiffness, theory manual *251*
interfaces

- theory manual *231*

interfaces common problems *282*
internal and external nodal forces *38*
internal force calculation *85*
internal forces *116*
internal forces computation *205*
internal stress calculation *93*
isotropic elastic material *292*

J

jetting effect
- AIRBAG *396*
- COMMU *401*

Johnson-Cook law for hydrodynamics (LAW4) *370*
Johnson-Cook plasticity model (LAW2) *326*

K

kinematic approximation *142*
kinematic constraints *210*
kinematic description *21*
kinetic description *24*

L

Lagrange multiplier method *232*
lagrangian and corotational formulations *27*
large scale eigen value computation *71*
line search method to optimize the resolution *413*
linear brick shape functions, theory manual *81*
linear elastic material (LAW1) *292*
linear spring - beam type spring (theory manual) *195*
linear spring - pulley type spring (theory manual) *192*
linear stability
- general theory *228*
- theory manual *227*

linear static solver, theory manual *409*
local coordinate system *170*
local reference frame *110*

M

mass injection
- AIRBAG *392*
- COMMU *400*
- monitored volume COMMU1 *399*

mass matrix and inertial forces *39*
material and spatial coordinates *18*
material laws, theory manual *288*
material properties *175*
mechanical properties *113*
mesh definitions *19*
minimum time step, theory manual *171*
modeling methodology *438*
momentum transport force *429*
monitored volume, theory manual *382*
multidirectional failure criteria, theory manual *202*

multistrand elements (TYPE28) *203*

N

Newark's method, theory manual *48*
Newton and modified new methods, theory manual *411*
node to curved surface contact (TYPE16) *281*
nonlinear dashpot *192*
nonlinear dashpot, theory manual *196*
nonlinear elastic spring *192*, *195*
nonlinear elasto-plastic spring
- decoupled hardening *195*
- isotropic hardening *195*
- kinematic hardening *195*
- nonlinear unloading *196*

nonlinear elasto-plastic spring - decoupled hardening *192*
nonlinear elasto-plastic spring - isotropic hardening *192*
nonlinear pseudo-plastic orthotropic solids (laws 28, 50 and 68) *304*
nonlinear static solver, theory manual *410*
nonlinear visco-elastic spring *196*
notation *11*
numerical integration, theory manual *428*
numerical procedures *45*
numerical quadrature: reduced integration, theory manual *44*
numerical stability *53*
numerical starting procedure *51*

O

Ogden materials (LAW42, LAW69 and LAW82) *292*
one degree of freedom spring elements (TYPE4) *177*
one-point quadrature shell elements *142*
orthotropic plasticity - elastic-plastic orthotropic composite solids *322*
orthotropic shells *157*
out-plane strain-rate construction *146*

P

parallelization, measure of performance *417*
particle kinematics *12*
penalty method, theory manual *233*
plastic behavior, theory manual *312*
porosity, AIRBAG *395*
PRES type monitored volume *383*
pretensioner model, theory manual *208*
pulley type spring elements (TYPE12) *191*

R

Radioss parallelization, theory manual *417*

Rayleigh damping, theory manual *407*

reference metric

- AIRBAG *397*
- COMMU *401*

referential domain, theory manual *423*

rezoned quantities, theory manual *428*

rigid body contact (TYPE6) *264*

rigid body, theory manual *210*

rigid link, theory manual *224*

rigid wall, theory manual *221*

S

section definition, theory manual *225*

shape memory superelastic material (LAW71) *373*

shared memory processors, theory manual *418*

shear XY, theory manual *198*

shear XZ, theory manual *199*

shell elements

- overview, theory manual *106*

shell formulations *137*

shock waves, theory manual *91*

sign conventions *197*

single program multiple data, theory manual *419*

skew frame properties *196*

slow dynamic computation *405*

small strain formulation *32*

smooth particle hydrodynamics *440*

solid and shell element contact (TYPE3) *249*

solid and shell elements contact limitations *249*

solid hexahedron elements *80*

solid hexahedron elements strain rate, theory manual *82*

solid tetrahedron elements *101*

solid-shell elements *164*

SPH approximation of a function *440*, *442*

SPH cell distribution *447*

SPH integration of continuum equations *443*

spotweld formulation *214*

spring type pretensioners (TYPE32) *208*

stability time step *110*

stability, ALE formulation *430*

stability, theory manual *90*

static solution

- explicit time integration *404*
- implicit time-integration *409*

static, theory manual *404*
Steinberg-Guinan material (LAW49) *372*
strain rate
  definition *327*
  filtering *328*
  filtering example *330*
strain rate effect, elastic-plastic orthotropic composite shells *316*
stress and strain calculation *124*
stress rates, theory manual *25*
stresses in solids, theory manual *26*
supersonic outlet flow, COMMU *401*

T

tabulated piecewise linear and quadratic elasto-plastic (LAW36 and LAW60 *334*
tabulated strain rate dependent law for viscoelastic materials (LAW38) *361*
tank experiment, AIRBAG *398*
tensile behavior, theory manual *311*
tension, theory manual *198*
theory manual introduction *10*
thermodynamical equations
  AIRBAG *388*
  COMMU *400*
tied interface (TYPE2) *213*, *237*
time step - beam type spring (theory manual) *194*
time step - pulley type spring (theory manual) *191*
time step control *66*
time step control limitations *69*
time step control stability *445*
time step example *70*
torsion, theory manual *200*
transformation matrix: global to orthotropic skew *154*
truss elements, TYPE2 *167*

U

unidirectional orthotropy - theory manual *324*

V

venting outgoing mass determination - theory manual *393*
venting, COMMU *400*
vicinity transformations *20*
virtual power principle *30*
virtual power term names *31*
visco-elasto materials for foamS (LAW33) *365*
viscous materials *355*
void materials (LAW0) *373*

Y

Yeoh material (LAW94) *300*

Z

Zerilli-Armstrong plasticity model (LAW2) *331*
Zhao plasticity model (LAW48) *332*